

Biofuels and Biorefineries 4

Zhen Fang  
Richard L. Smith, Jr.  
Xinhua Qi *Editors*

---

# Production of Biofuels and Chemicals with Ultrasound

 Springer

# **Biofuels and Biorefineries**

Volume 4

## **Editor-in-Chief**

Professor Zhen Fang, Chinese Academy of Sciences, Kunming, China

## **Editorial Board Members**

Professor Liang-shih Fan, Ohio State University, USA;

Professor John R. Grace, University of British Columbia, Canada;

Professor Yonghao Ni, University of New Brunswick, Canada;

Professor Norman R. Scott, Cornell University, USA;

Professor Richard L. Smith, Jr., Tohoku University, Japan

## Aims and Scope of the Series

---

The Biofuels and Biorefineries Series aims at being a comprehensive and integrated reference for biomass, bioenergy, biofuels, and bioproducts. The Series provides leading global research advances and critical evaluations of methods for converting biomass into biofuels and chemicals. Scientific and engineering challenges in biomass production and conversion are covered that show technological advances and approaches for creating new bio-economies in a format that is suitable for both industrialists and environmental policy decision-makers.

The Biofuels and Biorefineries Series provides readers with clear and concisely-written chapters that are peer-reviewed on significant topics in biomass production, biofuels, bio-products, chemicals, catalysts, energy policy, economics and processing technologies. The text covers major fields in plant science, green chemistry, economics and economy, biotechnology, microbiology, chemical engineering, mechanical engineering and energy.

## Series Description

Annual global biomass production is about 220 billion dry tons or 4,500 EJ, equivalent to 8.5 times the world's energy consumption in 2008 (532 EJ). On the other hand, world-proven oil reserves at the end of 2011 reached 1652.6 billion barrels, which can only meet 54.2 years of global production. Therefore, alternative resources are needed to both supplement and replace fossil oils as the raw material for transportation fuels, chemicals and materials in petroleum-based industries. Renewable biomass is a likely candidate, because it is prevalent over the Earth and is readily converted to other products. Compared with coal, some of the advantages of biomass are: (i) its carbon-neutral and sustainable nature when properly managed; (ii) its reactivity in biological conversion processes; (iii) its potential to produce bio-oil (ca. yields of 75%) by fast pyrolysis because of its high oxygen content; (iv) its low sulphur and lack of undesirable contaminants (e.g. metals, nitrogen content) (v) its wide geographical distribution and (vi) its potential for creating jobs and industries in energy crop productions and conversion plants. Many researchers, governments, research institutions and industries are developing projects for converting biomass including forest woody and herbaceous biomass into chemicals, biofuels and materials and the race is on for creating new "biorefinery" processes needed for future economies. The development of biorefineries will create remarkable opportunities for the forestry sector, biotechnology, materials, chemical processing industry, and stimulate advances in agriculture. It will help to create a sustainable society and industries that use renewable and carbon-neutral resources.

More information about this series at <http://www.springer.com/series/11687>

Zhen Fang · Richard L. Smith, Jr. · Xinhua Qi  
Editors

# Production of Biofuels and Chemicals with Ultrasound

 Springer



*Editors*

Zhen Fang  
Biomass Group, Key Laboratory  
of Tropical Plant Resources  
and Sustainable Use  
Xishuangbanna Tropical Botanical Garden  
Chinese Academy of Sciences  
Kunming  
China

Xinhua Qi  
Nankai University  
Tianjin  
China

Richard L. Smith, Jr.  
Tohoku University  
Sendai  
Japan

ISSN 2214-1537

ISBN 978-94-017-9623-1

DOI 10.1007/978-94-017-9624-8

ISSN 2214-1545 (electronic)

ISBN 978-94-017-9624-8 (eBook)

Library of Congress Control Number: 2014953925

Springer Dordrecht Heidelberg New York London

© Springer Science+Business Media Dordrecht 2015

This work is subject to copyright. All rights are reserved by the Publisher, whether the whole or part of the material is concerned, specifically the rights of translation, reprinting, reuse of illustrations, recitation, broadcasting, reproduction on microfilms or in any other physical way, and transmission or information storage and retrieval, electronic adaptation, computer software, or by similar or dissimilar methodology now known or hereafter developed. Exempted from this legal reservation are brief excerpts in connection with reviews or scholarly analysis or material supplied specifically for the purpose of being entered and executed on a computer system, for exclusive use by the purchaser of the work. Duplication of this publication or parts thereof is permitted only under the provisions of the Copyright Law of the Publisher's location, in its current version, and permission for use must always be obtained from Springer. Permissions for use may be obtained through RightsLink at the Copyright Clearance Center. Violations are liable to prosecution under the respective Copyright Law.

The use of general descriptive names, registered names, trademarks, service marks, etc. in this publication does not imply, even in the absence of a specific statement, that such names are exempt from the relevant protective laws and regulations and therefore free for general use.

While the advice and information in this book are believed to be true and accurate at the date of publication, neither the authors nor the editors nor the publisher can accept any legal responsibility for any errors or omissions that may be made. The publisher makes no warranty, express or implied, with respect to the material contained herein.

Printed on acid-free paper

Springer is part of Springer Science+Business Media ([www.springer.com](http://www.springer.com))

# Preface

As a renewable resource and substitute of traditional fossil resources, conversion of biomass into chemicals, materials, biofuels and energy is one of the most important research topics today. The application of process intensification techniques such as ultrasound irradiation in biorefineries has been proved to be able to increase energy efficiency, shorten reaction time and improve product yields. The present text provides up-to-date fundamentals, state-of-the-art reviews, current assessments and prospects in this area that includes aspects of reactors design, ultrasound assisted pretreatment, extraction and transformation of lignocellulose, microalgae and the other wastes to materials, chemicals and biofuels. The techno-economic analysis of the processes and some other auxiliary methods such as catalysis and mechanochemical techniques used in the pretreatment and transformations are also covered.

This book is the fourth book of the series entitled, *Biofuels and Biorefineries*, and it consists of 12 chapters contributed by leading experts in the field around the world. The chapters are categorized into three parts:

Part I: Fundamentals and Reactors (Chaps. 1–3)

Part II: Biodiesel: Extraction and Production (Chaps. 4–6)

Part III: Lignocellulose and Industrial Waste: Pretreatment and Conversions (Chaps. 7–12).

Chapter 1 provides an overview of the dynamics, mechanisms and theories of acoustic cavitation in sonochemistry. Chapter 2 illustrates physical and chemical mechanisms of ultrasound-assisted processes involved in the synthesis of biofuels. Chapter 3 describes reactor configurations for both transesterification and esterification for the production of methyl esters from vegetable oils. Chapter 4 reviews ultrasound applications in lipid extractions from algal biomass and challenges associated with the processes. Chapter 5 covers microalgae lipid extraction by the ultrasound-assisted method accompanied with solvents and the characteristics of the obtained fuel. Chapter 6 describes the synthesis of biodiesel and bioethanol by employing microwave and sonochemistry. Chapter 7 gives an overview of the technology associated with the conversion of biomass into biofuels. Chapter 8 focuses

on the production of biogas through ultrasound pretreatment of lignocellulosic materials, manures, sludges and microalgae. Chapter 9 shows methods for the ultrasonic vibration-assisted pelleting of cellulosic biomass for biofuel production and includes topics on pellet quality, pellet sugar yield, pelleting energy consumption and pelleting conditions. Chapter 10 focuses on the treatment of biomass with mechanical and combined chemical and mechanical techniques. Chapter 11 deals with the valorization of starch-based industrial waste into sugars employing ultrasound and microwave technologies. Chapter 12 provides a methodology for performing a techno-economic assessment during the development process and a framework for its application for the ultrasonic production of biofuels and chemicals.

This book covers a wide range of scientific and technical aspects of ultrasound that are used in conversion of biomass to bioenergy, biofuels, bio-based chemicals and materials. The reactor design techniques and techno-economic assessment necessary for the process are also included. The text will be of interest to students, researchers, academicians and industrialists in the areas of biomass processing, sonochemistry technique, and bioenergy and bioproduct development.

# Acknowledgments

First and foremost, we would like to cordially thank all the contributing authors for their great efforts in writing the chapters and ensuring the reliability of the information given in their chapters. Their contributions have really made this project realizable.

Apart from the efforts of authors, we would also like to acknowledge the individuals listed below for carefully reading the book chapters and giving constructive comments that significantly improved the quality of many aspects of the chapters:

Dr. Daria C. Boffito, Polytechnique Montréal, Université de Montréal, Canada;  
Prof. Chieh-Ming Chang, National Chung Hsing University, Taiwan, ROC;  
Dr. Shih-Yuan Chen, National Institute of Advanced Industrial Science and Technology (AIST), Japan;  
Prof. Giancarlo Cravotto, University of Turin, Italy;  
Dr. Veera Gnanaswar Gude, Mississippi State University, USA;  
Dr. Tamara Hamilton, Barry University, USA;  
Dr. Hanwu Lei, Washington State University, USA;  
Dr. Lin Li, University of Illinois at Chicago, USA;  
Dr. Carol S.K. Lin, City University of Hong Kong, China;  
Dr. Huang-Mu Lo, Chaoyang University of Technology, Taiwan, ROC;  
Dr. Jia Luo, Chinese Academy of Sciences, China;  
Prof. Sivakumar Manickam, University of Nottingham Malaysia Campus, Malaysia;  
Prof. Vijayanand Suryakant Moholkar, Indian Institute of Technology Guwahati, India;  
Dr. Melissa Montalbo-Lomboy, Iowa State University, USA;  
Prof. Dmitry Yu. Murzin, Åbo Akademi University, Finland;  
Prof. A.B. Pandit, University of Mumbai, India;  
Dr. Binod Parameswaran, National Institute for Interdisciplinary Science and Technology, India;  
Dr. Virendra K. Rathod, Institute of Chemical Technology, India;

Dr. Muhammad Saif Ur Rehman, Korea Advanced Institute of Science and Technology, Korea;  
Dr. Sebastian Schwede, Mälardalen University, Sweden;  
Dr. Achim Stolle, Friedrich-Schiller University of Jena, Germany;  
Prof. Jochen Strube, Clausthal University of Technology, Germany;  
Dr. Shuntaro Tsubaki, Kochi University, Japan;  
Dr. Maobing Tu, Auburn University, USA;  
Dr. Maryline Abert Vian, University of Avignon, France;  
Dr. Hui Wang, Florida A&M University—Florida State University, USA;  
Prof. Jianli Wang, Zhejiang University of Technology, China;  
Prof. Yo-ping Greg Wu, National Ilan University, Taiwan, ROC;  
Dr. Chengying “Cheryl” Xu, Florida State University, USA;  
Prof. Yang Zhang, the University of Sheffield, UK.

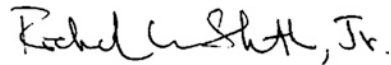
We are also grateful to Ms. Becky Zhao (senior editor) and Ms. Abbey Huang (editorial assistant) for their encouragement, assistance and guidance during the preparation of the book.

Finally, we would like to express our deepest gratitude towards our families for their love, understanding and encouragement, which helped us in completion of this project.

Kunming, September 2014  
Sendai  
Tianjin



Zhen Fang



Richard L. Smith, Jr.



Xinhua Qi

# Contents

## Part I Fundamentals and Reactors

- 1 Fundamentals of Acoustic Cavitation in Sonochemistry** . . . . . 3  
Jia Luo, Zhen Fang, Richard L. Smith, Jr. and Xinhua Qi
- 2 Physical and Chemical Mechanisms of Ultrasound  
in Biofuel Synthesis** . . . . . 35  
V.S. Moholkar, Hanif A. Choudhury, Shuchi Singh, Swati Khanna,  
Amrita Ranjan, Sankar Chakma and Jaykumar Bhasarkar
- 3 Batch and Continuous Ultrasonic Reactors for the Production  
of Methyl Esters from Vegetable Oils** . . . . . 87  
D.C. Boffito, J.-M. Leveque, C. Pirola, C.L. Bianchi, R. Vibert,  
A. Perrier and G.S. Patience

## Part II Biodiesel: Extraction and Production

- 4 Ultrasound Applications in Lipid Extractions from Microalgae** . . . . . 117  
Ramya Natarajan, Xue Chen and Raymond Lau
- 5 Microalgae Lipid Extraction Methods and the Fuel  
Characteristics of *Isochrysis galbana*  
by Ultrasound-Assisted Extraction** . . . . . 141  
Cherng-Yuan Lin, Li-Wei Chen and Bo-Yu Lin
- 6 Employing Novel Techniques (Microwave and Sonochemistry)  
in the Synthesis of Biodiesel and Bioethanol** . . . . . 159  
Indra Neel Pulidindi and Aharon Gedanken

**Part III Lignocellulose and Industrial Waste: Pretreatment and Conversions**

**7 Ultrasound as a Green Processing Technology for Pretreatment and Conversion of Biomass into Biofuels** . . . . . 189  
 Siah Ying Tang and Manickam Sivakumar

**8 Ultrasound-Enhanced Biogas Production from Different Substrates.** . . . . 209  
 Cristina Gonzalez-Fernandez, Rudolphus Antonius Timmers,  
 Begoña Ruiz and Beatriz Molinuevo-Salces

**9 Ultrasonic Vibration-Assisted Pelleting of Cellulosic Biomass for Biofuel Production** . . . . . 243  
 Meng Zhang, Xiaoxu Song, Z.J. Pei and Donghai Wang

**10 Mechanical and Combined Chemical and Mechanical Treatment of Biomass** . . . . . 269  
 Richard G. Blair

**11 Production of Glucose from Starch-Based Waste Employing Ultrasound and/or Microwave Irradiation** . . . . . 289  
 Audrey Villière, Giancarlo Cravotto, Raphaël Vibert, Arnaud Perrier,  
 Ulla Lassi and Jean-Marc Lévêque

**12 Techno-economic Assessment Methodology for Ultrasonic Production of Biofuels** . . . . . 317  
 Miet Van Dael, Tom Kuppens, Sebastien Lizin and Steven Van Passel

**Index** . . . . . 347

# Contributors

**Jaykumar Bhasarkar** Department of Chemical Engineering, Indian Institute of Technology Guwahati, Guwahati, Assam, India

**C.L. Bianchi** Dipartimento Di Chimica, Università Degli Studi Di Milano, Milan, Italy

**Richard G. Blair** Department of Physics, Mechanical and Aerospace Engineering, University of Central Florida, Orlando, FL, USA

**D.C. Boffito** Polytechnique Montréal—Département de Génie Chimique, Montreal, Canada

**Sankar Chakma** Department of Chemical Engineering, Indian Institute of Technology Guwahati, Guwahati, Assam, India

**Li-Wei Chen** Department of Mechanical and Computer-Aided Engineering, National Formosa University, Yunlin, Taiwan, ROC

**Xue Chen** School of Chemical and Biomedical Engineering, Nanyang Technological University, Singapore, Singapore

**Hanif A. Choudhury** Center for Energy, Indian Institute of Technology Guwahati, Guwahati, Assam, India

**Giancarlo Cravotto** Dipartimento di Scienza e Tecnologia del Farmaco, University of Turin, Turin, Italy

**Miet Van Dael** Centre for Environmental Sciences, Hasselt University, Hasselt, Belgium; VITO, Mol, Belgium

**Zhen Fang** Biomass Group, Key Laboratory of Tropical Plant Resources and Sustainable Use, Xishuangbanna Tropical Botanical Garden, Chinese Academy of Sciences, Kunming, China



**Aharon Gedanken** Department of Chemistry, Center for Advanced Materials and Nanotechnology, Bar-Ilan University, Ramat Gan, Israel; Department of Materials Science and Engineering, National Cheng Kung University, Tainan, Taiwan, ROC

**Cristina Gonzalez-Fernandez** IMDEA Energy, Móstoles, Spain

**Swati Khanna** Center for Energy, Indian Institute of Technology Guwahati, Guwahati, Assam, India

**Tom Kuppens** Centre for Environmental Sciences, Hasselt University, Hasselt, Belgium

**Ulla Lassi** Kokkola University Consortium Chydenius, Kokkola, Finland; Department of Chemistry, University of Oulu, Oulu, Finland

**Raymond Lau** School of Chemical and Biomedical Engineering, Nanyang Technological University, Singapore, Singapore

**Jean-Marc Lévêque** Laboratoire de Chimie Moléculaire et Environnement, Université de Savoie, Le Bourget du Lac Cedex, France; Department of Fundamental and Applied Sciences, Universiti Teknologi Petronas, Tronoh, Perak, Malaysia

**Bo-Yu Lin** Department of Marine Engineering, National Taiwan Ocean University, Keelung, Taiwan, ROC

**Cherng-Yuan Lin** Department of Marine Engineering, National Taiwan Ocean University, Keelung, Taiwan, ROC

**Sebastien Lizin** Centre for Environmental Sciences, Hasselt University, Hasselt, Belgium

**Jia Luo** Biomass Group, Key Laboratory of Tropical Plant Resources and Sustainable Use, Xishuangbanna Tropical Botanical Garden, Chinese Academy of Sciences, Kunming, China

**V.S. Moholkar** Department of Chemical Engineering, Indian Institute of Technology Guwahati, Guwahati, Assam, India; Center for Energy, Indian Institute of Technology Guwahati, Guwahati, Assam, India

**Beatriz Molinuevo-Salces** Section for Sustainable Biotechnology, Aalborg University Copenhagen, København SV, Denmark

**Ramya Natarajan** Department of Biology, Indiana University, Bloomington, IN, USA

**Steven Van Passel** Centre for Environmental Sciences, Hasselt University, Hasselt, Belgium

**G.S. Patience** Polytechnique Montréal—Département de Génie Chimique, Montreal, Canada

**Z.J. Pei** Department of Industrial and Manufacturing Systems Engineering, Kansas State University, Manhattan, KS, USA

**Arnaud Perrier** Synetude, Chambéry, France

**C. Pirola** Dipartimento Di Chimica, Università Degli Studi Di Milano, Milan, Italy

**Indra Neel Pulidindi** Department of Chemistry, Center for Advanced Materials and Nanotechnology, Bar-Ilan University, Ramat Gan, Israel

**Xinhua Qi** College of Environmental Science and Engineering, Nankai University, Tianjin, China

**Amrita Ranjan** Center for Energy, Indian Institute of Technology Guwahati, Guwahati, Assam, India

**Begoña Ruiz** ainia Technology Centre, Valencia Technology Park, Paterna, Valencia, Spain

**Shuchi Singh** Center for Energy, Indian Institute of Technology Guwahati, Guwahati, Assam, India

**Manickam Sivakumar** Manufacturing and Industrial Processes Research Division, Faculty of Engineering, University of Nottingham Malaysia Campus, Semenyih, Selangor, Malaysia

**Richard L. Smith, Jr.** Research Center of Supercritical Fluid Technology, Tohoku University, Sendai, Japan

**Xiaoxu Song** Department of Industrial and Manufacturing Systems Engineering, Kansas State University, Manhattan, KS, USA

**Siah Ying Tang** Chemical Engineering Discipline, School of Engineering, Monash University Malaysia, Bandar Sunway, Selangor, Malaysia

**Rudolphus Antonius Timmers** Department of Chemical and Energy Technology, Rey Juan Carlos University, Móstoles, Spain

**Raphaël Vibert** Synetude, Chambéry, France

**Audrey Villière** Kokkola University Consortium Chydenius, Kokkola, Finland; Laboratoire de Chimie Moléculaire et Environnement, Université de Savoie, Le Bourget du Lac Cedex, France

**Donghai Wang** Department of Biological and Agricultural Engineering, Kansas State University, Manhattan, KS, USA

**Meng Zhang** Department of Industrial and Manufacturing Systems Engineering, Kansas State University, Manhattan, KS, USA

## Editors' Biography



**Dr. Zhen Fang** is leader and founder of biomass group, Xishuangbanna Tropical Botanical Garden, Chinese Academy of Sciences. He is also an adjunct full Professor of Life Sciences, University of Science and Technology of China. He is the inventor of “fast hydrolysis” process. He specializes in thermal/biochemical conversion of biomass, nanocatalyst synthesis and its applications, pretreatment of biomass for biorefineries. He obtained his Ph.Ds from China Agricultural University (Biological and Agricultural Engineering, 1991, Beijing) and McGill University (Materials Engineering, 2003, Montreal). Prof. Fang is Associate

Editor of Biotechnology for Biofuels and is serving on editorial boards of major international Journals in energy.



**Richard L. Smith, Jr.** is Professor of Chemical Engineering, Graduate School of Environmental Studies, Research Center of Supercritical Fluid Technology, Tohoku University, Japan. Professor Smith has a strong background in physical properties and separations and obtained his Ph.D. in Chemical Engineering from the Georgia Institute of Technology (USA). His research focuses on developing green chemical processes, especially those that use water and carbon dioxide as solvents in their supercritical state. He has expertise in physical property measurements and in separation techniques with ionic liquids

and has more than 200 scientific papers, patents and reports in the field of chemical engineering. Professor Smith is the Asia Regional Editor for the Journal of Supercritical Fluids and has served on editorial boards of major international journals associated with properties and energy.



**Xinhua Qi** is Professor of Environmental Science, Nankai University, China. Professor Qi obtained his Ph.D. from the department of environmental science, Nankai University, China. Professor Qi has a strong background in environmental treatment techniques in water and in chemical transformations in ionic liquids. His research focuses on the catalytic conversion of biomass into chemicals and biofuels with ionic liquids. Professor Qi had published more than 60 scientific papers, books and reports with a number of papers being in top-ranked international journals.

**Part I**  
**Fundamentals and Reactors**

# Chapter 1

## Fundamentals of Acoustic Cavitation in Sonochemistry

Jia Luo, Zhen Fang, Richard L. Smith, Jr. and Xinhua Qi

**Abstract** Acoustic cavitation is the main mechanism for reaction intensification in sonochemistry. This chapter provides an overview of the dynamics, mechanisms and theories of acoustic cavitation. Through mathematical simulation and experimental observation, single bubble cavitation theory describes the radial growth, oscillation and energy behavior of a single bubble in a low frequency acoustic field. In multibubble cavitation, the bubble dynamics and energy are greatly influenced by neighboring bubbles. Many hypotheses, such as rectified diffusion, bubble coalescence, concerted collapse and bubble cloud theory, and experiment methods, are used to describe multibubble behavior and energy intensity. Factors such as liquid properties, acoustic field parameters and heterogeneous characteristics of reaction system influence acoustic cavitation. Adverse effects from heterogeneous characteristics on acoustic cavitation can be analyzed to improve the efficiency of sonochemical reactors. The introduction of sonication into a chemical system allows intensification of many reactions, however, proper design of acoustic equipment is needed to obtain reliable results.

**Keywords** Ultrasonic auxiliary · Acoustic cavitation · Bubble dynamics · Heterogeneous chemical system

---

J. Luo · Z. Fang (✉)

Biomass Group, Key Laboratory of Tropical Plant Resources and Sustainable Use,  
Xishuangbanna Tropical Botanical Garden, Chinese Academy of Sciences,  
Kunming, China  
e-mail: zhenfang@xtbg.ac.cn

R.L. Smith, Jr.

Research Center of Supercritical Fluid Technology, Tohoku University, Sendai, Japan

X. Qi

College of Environmental Science and Engineering, Nankai University, Tianjin, China

## 1.1 Ultrasound and Acoustic Cavitation

Ultrasound is a longitudinal pressure wave that has a wave frequency higher than normal human hearing range. In acoustic science, the classification of a sound wave is according to its oscillating frequency. Waves that have oscillating frequencies from 0.001 to 10 Hz are referred to as infrasonic sound, and waves with oscillating frequencies from 16 kHz and higher are referred to as ultrasonic sound or ultrasound [1]. Table 1.1 lists some key parameters including the wavelength, speed, frequency, amplitude, power, pressure, intensity of acoustic wave, acoustic characteristic impedance of medium material and their typical values in sonochemistry [1].

Compared with audible sound and other wave phenomena, ultrasound causes many special physical or chemical effects in materials. Because of the high oscillating frequency of liquid molecules in an ultrasonic field and the high viscosity of the liquid medium compared with a gas, molecules absorb a large number of energy from the propagating ultrasonic wave. As shown in Table 1.1 for the acoustic pressure, liquid reactants in ultrasonic field can have a high pressure difference relative to the hydrostatic pressure of fluid [2]. The high energy absorption and high acoustic pressure make it possible for ultrasonic auxiliary to overcome intermolecular interactions in a solvent, and produce numerous cavities, which is referred to as acoustic cavitation. The formed cavities drain and accumulate ultrasonic energy, and explosively release their energy by the collapse of cavities. Therefore, there are two main routes that ultrasound provides energy to liquid reactants: (i) ultrasonic microstreaming (mechanical force) and (ii) acoustic cavitation. However, only acoustic cavitation is believed to activate chemical reactions with high energy intensity.

As shown in Table 1.1, ultrasound is used in power applications at low frequencies of 20–40 kHz and at high acoustic power (>50 W), or it can be used in nondestructive detection or measurement at frequencies above 1 MHz and low acoustic power as commonly used in diagnostics, clinical medicine and biological processing.

In this chapter, the fundamentals in ultrasound and acoustic cavitation are introduced. The dynamics and influencing factors of cavitation bubbles are summarized. The secondary effects of acoustic cavitation are introduced and discussed. The knowledge may be useful in studying the intensification mechanism of sonochemical reaction of biomass materials. The authors would like to emphasize the relationship between energy intensity and energy efficiency with sonication. The ability of cavitating bubbles to focus and concentrate energy, forces and stresses is the basic of phenomena for ultrasonic auxiliary of biomass-related reactions [3], while the development of bioenergy requires attentions to special energy intensity that could activate chemical species and possibly lower energy cost.

**Table 1.1** Key parameters in acoustic science and typical parameter values for studies in sonochemistry [1]

Parameters ( <i>symbol</i> , unit)	Physical definition	Typical values
Acoustic wavelength ( $\lambda$ , m)	Distance between two neighboring points that have the same phase position in an acoustic wave	3.0–7.5 cm for power ultrasound in liquids
		0.015–0.075 cm for measurement
Acoustic speed ( $c$ , m/s)	Acoustic propagation distance per unit time	Air, 340 m/s
		Liquid, 1,000–2,000 m/s
		Solids, 3,000–6,000 m/s
Acoustic frequency ( $f$ , Hz)	Vibration number per unit time	20–40 kHz for power ultrasound in liquids
		1–20 MHz for measurement
Acoustic amplitude ( $P_A$ , m)	Maximum distance of mass point at the ultrasonic field from its balance position	
Acoustic power ( $P$ , W)	Acoustic energy that passes through one surface perpendicular to the propagating direction per unit time	Extremely high power (>1,000 W) for cavitation erosion of solids and metal working
	Optimum acoustic power depends on sample, reactor volume and processing needs	High power (50–1,000 W) for ultrasound-assisted conventional thermochemical and biochemical reactions
		Low power (1–10 W) for stimulating biological cells or for promoting particle aggregation with low cavitation
Acoustic pressure ( $P_a$ , Pa)	Difference of dynamic force per area from its static value, as the result of the compressed zone and rarefacted zone of fluid formed with sound transport	0.1–1 MPa for ultrasonic cleaner
	$P_a = P_A \sin(2\pi ft)$ , where $t$ refers to the propagating time	
Acoustic intensity ( $I$ , W/m <sup>2</sup> )	Average acoustic energy that passes through a unit surface perpendicular to the propagating direction per unit time	
	Vector $I = P_A^2 / (2\rho c)$ , where $\rho$ is the medium density	
Acoustic characteristic impedance ( $Z$ , kg/(m <sup>2</sup> s))	Ratio of acoustic pressure to acoustic velocity at one mass point in the medium	Gases, $1.1\text{--}5.5 \times 10^2$ kg/(m <sup>2</sup> s)
		Liquids, $0.7\text{--}3.2 \times 10^6$ kg/(m <sup>2</sup> s)
	Characteristic of the transmitting medium. $Z = \rho c$ , where $\rho$ is the medium density	Nonmetals, $0.1\text{--}1.5 \times 10^7$ kg/(m <sup>2</sup> s) Metals, $1.0\text{--}10.4 \times 10^7$ kg/(m <sup>2</sup> s)



## 1.2 Acoustic Cavitation

The energy content of ultrasonic microstreaming is relatively low due to the small amplitude of the oscillation of fluid elements and it is generally insufficient to induce chemical reaction in the medium. The wavenumber of ultrasound in liquid is much larger than ultraviolet light, and the excitation of electrons in compound molecules is not possible with sonication. Sonication does not result in the resonance of chemical molecules or atoms like other methods such as microwave or infrared radiation, because the oscillating frequency of ultrasound is on the order of  $10^4$ – $10^5$  Hz. As a result, acoustic cavitation, which could concentrate and explosively release acoustic energy, is believed to be the dominant mechanism for process intensification and chemical activation in sonochemical systems.

### 1.2.1 Dynamics and Energy of Single Bubble Cavitation

The complete process of acoustic cavitation consists of three steps [4, 5]:

1. Formation of cavitation nuclei. Figure 1.1 shows bubble formation, growth and collapse phenomena for transient and steady cavitation. Negative and positive acoustic pressure act alternately on one point in the liquid medium in an ultrasonic cycle with the propagation of ultrasound wave (Fig. 1.1). The negative acoustic pressure stretches the liquid medium apart to make a relatively rarefacted zone. If the acoustic pressure is increased to a value that is higher than certain intensity, the microscopic distance between the liquid molecules becomes far enough to initiate cavity formation that contains solvent vapors or dissolved gases. The minimum requirement for acoustic pressure to form a cavity is called the Blake threshold,  $P_B$ . If the vapor pressure in a bubble can be ignored, then Eq. 1.1 results [5]:

$$P_B = P_0 + \frac{2}{3} \left[ \frac{(2\sigma/R_0)^3}{3(P_0 + 2\sigma/R_0)} \right]^{1/2} \quad (1.1)$$

where  $P_0$  is the static pressure on the liquid,  $R_0$  is the initial radius of the formed bubble, and  $2\sigma/R_0$  is the surface tension of the assumed bubble when it forms. Low surface tension and low static pressure on a liquid favors the formation and growth of cavitation nuclei. The existence of impurities and heterogeneous crevices in liquids decrease the actual pressure threshold of cavitation by reducing the surface tension. The Blake threshold value for untreated solvents is about 1–10 % of that in ultrapure solvents [4]. The influence of impurities and heterogeneous crevices on nucleation is kinetic. Similarly to a catalyst, the presence of surface defects lowers the free energy barriers separating the metastable liquid state from the vapor phase, and modifies the nucleation

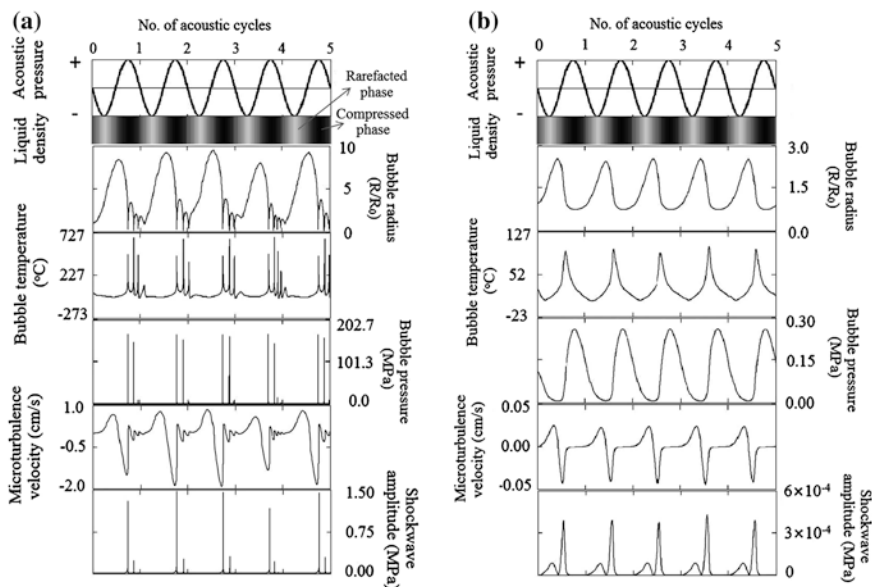


**Fig. 1.1** Calculation results of bubble dynamics: **a** transient cavitation and **b** steady cavitation: acoustic pressure, bubble temperature, microturbulence velocity, bubble radius, bubble pressure, and shockwave amplitude (adapted with permission from [8], Copyright © 2012 Elsevier)

mechanism [6]. As a result, the nucleation rate on surface defects with simple geometries can be increased by up to five orders of magnitude compared with that of a flat hydrophobic surface [6]. The presence of surface defects has also been found to affect the nucleation rate for non-condensable gas as dissolved in liquids [6]. For bubble nucleation in solutions containing solid substances, the contact angle of gas bubbles on the solid surface is a critical index to evaluate the possibility of bubble nucleation. A small contact angle means a low energy barrier for the nucleation. In recent research by Zhang et al. [7], it was pointed out that the contact angle of gas bubbles on spherical surfaces could be remarkably reduced by several methods such as decreasing the surface tension of the solution, by reducing the size of solid particles, or by changing the hydrophilic surface of solid particles to that of a hydrophobic surface.

2. Growth (radial motion) of cavitation bubbles. The formed microbubble continually grows to a maximum bubble radius of about 2–150  $\mu\text{m}$  until the end of the negative acoustic pressure phase. The oscillating motion of cavitation bubble can be described with the Rayleigh-Plesset equation [5]:

$$R \frac{d^2R}{dt^2} + \frac{3}{2} \left( \frac{dR}{dt} \right)^2 = \frac{1}{\rho} \left[ \left( P_0 + \frac{2\sigma}{R_0} \right) \left( \frac{R_0}{R} \right)^{3\gamma} - \frac{2\sigma}{R} - \frac{4\mu}{R} \left( \frac{dR}{dt} \right) - P_\infty \right] \quad (1.2)$$

where  $R$  is the radius of bubble in motion,  $dR/dt$  is the velocity item of bubble wall away from the bubble center,  $R_0$  is the initial radius of bubble,  $\rho$  and  $\mu$  are the density and viscosity of the liquid,  $\gamma$  refers to the specific heat ratio of gas in bubble and the  $P_0$  and  $P_\infty$  are the static pressure nearby bubble and at infinite distance in the liquid. The terms on the left-hand side of the equation represent the radial motion (expansion or compression) of the bubble wall. On the right-hand side of the equation, the first term shows the pressure variation in the bubble, while the second and third terms are the surface tension and the viscous stresses at the bubble surface, respectively. Equation 1.2 is based on the assumption that the motion of a bubble is adiabatic and that the liquid is incompressible [4]. The mass and heat transfer between the bubble and the surroundings is not considered in Eq. 1.2. It is assumed that no chemical reaction or physical changes occur and that there are no temperature, density or pressure gradients in cavitating bubble.

3. Collapse or the next oscillation of bubbles. Positive acoustic pressure phase comes after the negative pressure phase (Fig. 1.1), and under its influence, the cavitation bubble undergoes contraction. The time required for the bubble to contract is about 25–0.5  $\mu\text{s}$ , which is half of the reciprocal of ultrasound frequency. According to the literature [9], the oscillating frequency of a bubble in a liquid,  $f_b$ , increases with contraction of the bubble radius,  $R$ :

$$f_b = \frac{1}{2\pi R} \left[ \frac{3\gamma}{\rho} \left( P_0 + \frac{2\sigma}{R} \right) \right]^{1/2} \quad (1.3)$$

where  $\rho$  is liquid density,  $\gamma$  and  $2\sigma/R$  are the gas specific heat ratio and surface tension in the bubble and  $P_0$  is the static pressure. If the resonant frequency of a bubble,  $f_b$ , is smaller than the frequency of ultrasonic field,  $f_a$ , at the end of the positive acoustic pressure phase, the bubble survives and turns to growth in a new ultrasonic cycle. The radial motion of the cavitation bubble can be repeated for several acoustic cycles, and is called as steady cavitation (Fig. 1.1b). However, if  $f_b \geq f_a$ , the bubbles will collapse quickly in several nanoseconds, and this is called as transient cavitation (Fig. 1.1a). Fragments generated during the collapse of the parent bubble may become new nuclei for subsequent cavitation phenomena. Steady and transient cavitation are both present in most sonochemical systems, although the properties of the liquid may favor one type of cavitation.

During the transient collapse of a bubble, work is done by the liquid such that fluid elements impart energy to the bubble, thus raising its temperature and pressure. The energy intensity of the cavitation bubble collapse is proportional to the compression ratio of the bubble at the point of minimum radius during radial motion. At the instance of bubble collapse, energy is released that does not have time to be transferred to the surroundings and therefore local hotspots are produced [10, 11]. These local hotspots have extremely high temperatures (ca. 5,000 °C) and

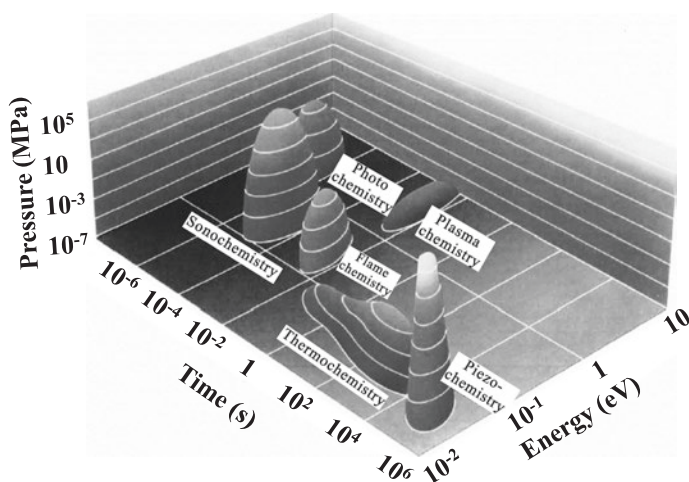


**Fig. 1.2** Range of duration time, pressure and energy for various energy chemistries (reprinted with permission from [11], Copyright © 2010 WILEY-VCH Verlag GmbH & Co. KGaA, Weinheim)

pressures (ca. 100 MPa) in its interior, and causes very high rates of local heating and cooling ( $>10^9$  °C/s). The energy density of acoustic cavitation can be on the order of  $10^{15}$  W/cm<sup>3</sup>, while the rated acoustic power density used in common sonochemical reactors is  $10^{-2}$ – $10$  W/cm<sup>3</sup> [12]. Acoustic cavitation also produces high intensity shockwave and violent flowing of localized liquid.

In Fig. 1.2, the average energy of acoustic cavitation (about 0.1–1 eV) is much higher than that in conventional heating, so that breaking most of chemical bonds is possible. However, this energy is not enough for plasma ionization of volatile molecules and photon production in bubbles. Suslick et al. [13, 14] observed very strong Ar atomic excitation in the sonication of 95 wt% sulfuric acid solution at 20 kHz at ambient temperature under an Ar atmosphere. The emission temperature of Ar excitation in bubble was estimated at about 8,000 °C. However, the thermal excitation of Ar atom needed very high energy of  $>13$  eV, and thus Ar atom could not be thermally excited at 8,000 °C, which shows that the distribution of temperature and pressure in a bubble is not uniform. Figure 1.3 shows the physical structure of a bubble and the active zones for sonochemistry. Optically opaque plasma probably exists at the core of a collapsing bubble at extreme conditions, and the collision of higher energy electrons in this plasma zone is believed to result in the excitation of an Ar atom. Spectral lines of Ar excitation are emitted just on the outer zone of the plasma ionization (emissive shell) and can be detected by ultraviolet-visible spectroscopy [14]. The emissive shell is optically transparent and has a temperature that is much lower than the plasma zone.

On the other hand, the energy intensity of bubbles is also influenced by the mass and heat transfer of the surrounding liquid. It is believed that the vapor or gas

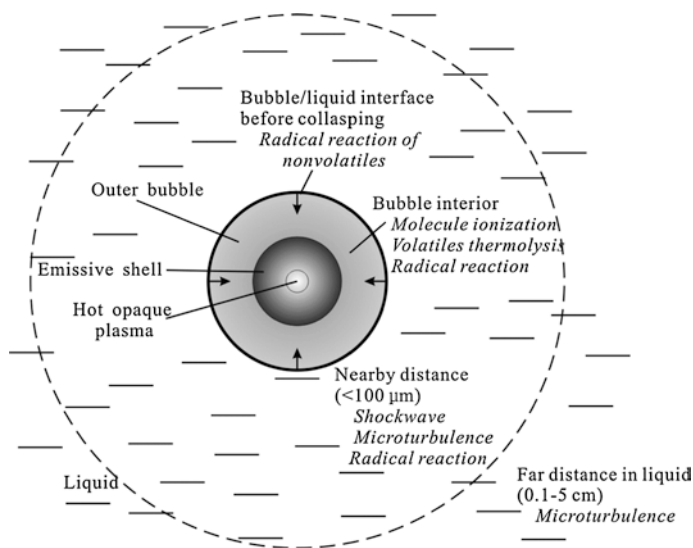


**Fig. 1.3** Physical structure of collapsing bubble and active zones for sonochemistry (adapted with permission from [14], Copyright © 2011 Elsevier)

in the cavity can not escape into the surroundings before bubble collapse occurs. However, the evaporation of liquid molecules at the interface between bubbles and surroundings is possible and materials flowing into the bubbles can change the vapor composition in a bubble. Dissociation and chemical reactions of volatile molecules in the bubble can occur and this will consume the energy of the bubble and reduce its energy release when it collapses. For example, sonication in alcohol solution under Ar atmosphere at the frequencies of 20, 363 and 1,056 kHz gives contradictory results [15]. Much less energy is released in a high frequency acoustic field of 1,056 kHz than at low frequencies, which is determined by the volume change of bubbles when bubbles collapse. However, the calculated temperature of the cavitation bubbles has the following order of high to low according to frequencies of  $1,056 > 363 > 20$  kHz. It is highly possible that the evaporation of solvent in the acoustic field of 20 kHz is more than that at 1,056 kHz, because of the longer acoustic cycle and larger bubble size during the radial motion of bubbles under sonication at 20 kHz.

Therefore, it is necessary to modify the Rayleigh-Plesset equation (Eq. 1.2), because Eq. 1.2 deals with slow bubble motions, and many of the assumptions on which Eq. 1.2 is based are invalid at the time of rapid collapse of bubbles [16]. Equation 1.2 does not take mass transfer, heat transfer, chemical reactions, non-equilibrium phase changes and non-uniform pressures in the bubble interior into account, so that modeling results have large deviations from their true values. Boundary layer approximation on the basis of physical observations allows simplification of the theory.

For example, considering the compressibility of liquid and the acoustic attenuation, the bubble motion can be described by the Keller-Miksis equation (Eq. 1.4) [17, 18]:

$$\begin{aligned} & \left(1 - \frac{dR/dt}{c}\right)R \frac{d^2R}{dt^2} + \frac{3}{2}\left(1 - \frac{dR/dt}{3c}\right)\left(\frac{dR}{dt}\right)^2 \\ & = \frac{1}{\rho} \left\{ \left(1 + \frac{dR/dt}{c}\right)[P_b - (P_{\text{am}} - P_A \sin 2\pi ft)] + \frac{R}{c} \frac{dP_b}{dt} - \frac{2\sigma}{R} - \frac{4\mu}{R} \left(\frac{dR}{dt}\right) \right\} \end{aligned} \quad (1.4)$$

where  $R$  is the radius of bubble in motion,  $dR/dt$  is the velocity item of bubble wall away from the bubble center,  $\rho$  is the liquid density,  $\mu$  is the dynamic viscosity of the liquid ( $\mu = \rho\nu$ ,  $\nu$  is kinematic viscosity), and the  $c$ ,  $f$  and  $P_A$  are the speed, frequency and pressure amplitude of the sound wave in liquid, respectively. In Eq. 1.4,  $2\sigma/R$  is the surface tension of the bubble according to the liquid temperature,  $P_{\text{am}}$  is the ambient pressure (1 atm),  $P_b$  is the pressure inside the bubble, and its time derivative is given by a van der Waals type equation of state as Eq. 1.5 [17, 18]:

$$P_g(t) = \frac{N_{\text{tot}}(t)kT_b}{\frac{4\pi}{3} \left[ (R(t))^3 - (R_{\text{eq}}(t)/8.86)^3 \right]} \quad (1.5)$$

In Eq. 1.5,  $k$  is the Boltzmann constant,  $N_{\text{tot}}$  is the total number of vapor molecules in the bubble due to the condensation and evaporation,  $T_b$  is the temperature of bubble contents and  $R_{\text{eq}}$  is the equilibrium radius of the bubble.

Other important parameters for numerical simulation of bubble motion are the mass diffusion and non-equilibrium phase change of water vapor during the sonication in water. In 2000, Storey and Szeri [16, 19] proposed a two-step process that consisted of the diffusion of vapor molecule to the bubble wall and the condensation of vapor at the bubble wall, along with three important time scales, namely, the time scale of bubble dynamics ( $t_{\text{osc}}$ ), the time scale of mass diffusion ( $t_{\text{dif}}$ ) and the time scale of condensation ( $t_{\text{cond}}$ ) as follows:

$$\begin{aligned} t_{\text{osc}} &= \frac{R}{|dR/dt|} \\ t_{\text{dif}} &= ReSc \frac{R^2}{D_{\text{H}_2\text{O}}^M} \approx ReSc \frac{1}{R\sqrt{T_b}}, \quad Re = \rho_0 R_0 v_0 / \mu_0, \quad Sc = \mu_0 / \rho_0 D_{\text{avg}} \\ t_{\text{cond}} &= \frac{R}{\sigma} \sqrt{\frac{2\pi M_{\text{H}_2\text{O}}}{9M_0 T_0}} \end{aligned} \quad (1.6)$$

where  $T_b$  is the temperature of the bubble,  $D_{\text{H}_2\text{O}}^M$  is the diffusion coefficient of water vapor in the gas mixture,  $Re$  and  $Sc$  are Reynolds number and Schmidt number, respectively. In Eq. 1.6,  $\rho_0$ ,  $R_0$ ,  $v_0$  and  $\mu_0$  are the initial values of liquid density, bubble radius, bubble wall velocity and gas viscosity, respectively.  $D_{\text{avg}}$  is the

average binary coefficient matrix of the diffusion coefficients of vapor mixture, which is dimensionless.  $T_0$  is the temperature of the bubble interface and the  $M_{\text{H}_2\text{O}}$  and  $M_0$  are the molecular mass of water and the initial molecular mass of the bubble contents, respectively.

For mass diffusion of water vapor, in the earlier phase of bubble collapse,  $t_{\text{osc}} \gg t_{\text{dif}}, t_{\text{cond}}$ , so that bubble motion is slow enough to allow the completion of one cycle of mass transfer between liquid and bubble interior, which results in uniform bubble composition [18, 19]. Then, with the acceleration of the bubble wall,  $t_{\text{osc}} \ll t_{\text{dif}}$ , the bubble motion is so rapid that the water vapor has insufficient time to diffuse to the bubble wall that results in nearly unchanged composition of vapor content in the bubble [18, 19].

For condensation of water vapor, if  $t_{\text{osc}} \gg t_{\text{cond}}$ , the condensation is in quasi-equilibrium with respect to the bubble motion. If  $t_{\text{osc}} \ll t_{\text{cond}}$ , the phase change will be non-equilibrium, which results in the entrapment of water molecules in the bubble [18, 19]. However, Storey and Szeri [19] demonstrated that the condition  $t_{\text{osc}} \ll t_{\text{dif}}$  is reached well before  $t_{\text{osc}} \ll t_{\text{cond}}$  during bubble collapse and so the slow mass diffusion is responsible for trapping water vapor in the bubble.

Actually, during bubble oscillation, the surface temperature of the bubble exceeds the temperature of bulk water only for a very brief moment [17, 18]. Therefore, the bubble is divided into two parts, a ‘‘cold’’ boundary layer in thermal equilibrium with liquid and an eventually hot homogeneous core. Based on this assumption, the instantaneous diffusive penetration depth  $l_{\text{dif}}$  is taken to be Eq. 1.7 [17, 18]:

$$l_{\text{dif}} = \sqrt{Dt_{\text{osc}}} \quad (1.7)$$

where  $D$  is the diffusion coefficient.

The analysis [17] shows that the penetration depth exceeds the bubble radius ( $l_{\text{dif}} \geq R$ ) during the expansion and a major part of the afterbounce in bubble motion, and the total volume of bubble interior is in equilibrium with the liquid. Since  $l_{\text{dif}}$  is only  $0.01R$  during bubble collapse, this implies that the thickness of the boundary layer is negligible compared with the total bubble volume. Therefore, the bubble can be regarded as being homogeneous in both cases, and then the rate of change of water molecules in the bubble ( $N_{\text{H}_2\text{O}}$ ) when the velocity of the bubble wall is non-zero is given by Eq. 1.8 as:

$$\frac{dN_{\text{H}_2\text{O}}}{dt} = 4\pi R^2 D \frac{\partial C_{\text{H}_2\text{O}}}{\partial r} \Big|_{r=R} \approx 4\pi R^2 D \left( \frac{C_{\text{H}_2\text{O},eq} - C_{\text{H}_2\text{O}}}{l_{\text{dif}}} \right) \quad (1.8)$$

where  $C_{\text{H}_2\text{O}}$  and  $C_{\text{H}_2\text{O},eq}$  are the actual concentrations of water molecules in the bubble core and the equilibrium concentration of water molecules at bubble wall, respectively. The  $C_{\text{H}_2\text{O},eq}$  is calculated from the vapor pressure of water at bulk temperature ( $T_1$ ).

At the instant that the bubble stops growing, the velocity of the bubble wall is zero, and the upper limit of the diffusion length can be calculated [17, 18]:

$$l_{dif} = \min(\sqrt{Dt_{osc}}, \frac{R}{\pi}) \quad (1.9)$$

For diffusion of heat in analogy with diffusion of mass, in the earlier phases of bubble collapse when the time scale of bubble oscillation is longer than that for heat transfer, sufficient heat transfer helps to keep the bubble interior at ambient liquid temperature, while during bubble collapse, the bubble motion is so rapid that bubble collapse behaves nearly adiabatically with negligible outflow of bubble energy [19]. Equation 1.10 provides a method to estimate the rate of heat loss across a bubble wall during its motion [17, 18]:

$$\begin{aligned} \frac{dQ}{dt} &= 4\pi R^2 \lambda_{tc} \left( \frac{T_0 - T}{l_{th}} \right), \quad l_{th} = \min\left(\frac{R}{\pi}, \sqrt{\frac{R\kappa}{|dR/dt|}}\right), \\ \kappa &= \frac{\lambda_{tc}}{\rho_{mix} C_{p,mix}}, \quad \rho_{mix} C_{p,mix} = \sum_{i=1}^n \rho_i C_{pi} \end{aligned} \quad (1.10)$$

where  $\lambda_{tc}$  is the thermal conductivity of bubble contents and  $T_0$  is the temperature of the cold bubble surface that is nearly the same with the temperature in the liquid. In Eq. 1.10,  $l_{th}$  is the thermal diffusion length,  $\kappa$  is the thermal diffusivity and terms  $\rho_i$  and  $C_{pi}$  are the density and molecular specific heat of compound  $i$ , respectively. The  $\rho_{mix}$  and  $C_{p,mix}$  in Eq. 1.10 are the density and molecular specific heat of the vapor mixture in the bubble, respectively.

The overall energy balance for the bubble as an open system can be written as Eq. 1.11 [18]:

$$\frac{dE}{dt} = \frac{dQ}{dt} - \frac{dW}{dt} + h_{H_2O} \frac{dN_{H_2O}}{dt} \quad (1.11)$$

where  $dW/dt$  refers to the work done by the bubble. The enthalpy per water molecule that condenses at the cold bubble surface is given by  $h_{H_2O} = 4kT_0$ , where  $k$  is the Boltzmann constant. Equation 1.11 can be rewritten as [17, 18]:

$$\begin{aligned} C_{v,mix} \frac{dT}{dt} &= \frac{dQ}{dt} - P_i \frac{dV}{dt} + (h_{H_2O} - U_{H_2O}) \frac{dN_{H_2O}}{dt} \\ U_{H_2O} &= \frac{\partial E}{\partial N_{H_2O}} = N_{H_2O} kT \left( 3 + \sum \frac{\theta_i T}{\exp(\theta_i/T) - 1} \right) \\ C_{v,mix} &= \sum_{i=1}^n C_{v,i} N_i \end{aligned} \quad (1.12)$$

where  $U_{H_2O}$  is the internal energy, namely, the specific energy of water molecules in the bubble,  $P_i$  is the pressure in the bubble interior,  $\theta_i$  is the characteristic vibrational temperature of species  $i$ ,  $N_i$  is the number of molecules of component  $i$  and  $C_{v,i}$  and  $C_{v,mix}$  are the specific heats of individual component  $i$  and the mixture, respectively.



Equation 1.12 can be used to estimate the temperature change of a bubble during its motion, and it gives better results in the numerical simulation of the sonochemical phenomena [17].

In summary, cavitation behavior of a single bubble under a high intensity ultrasonic field has been discussed along with fundamental relationships. Information on the formation, growth, collapse and energy change of single bubble as the result of certain ultrasonic field parameters in a sonochemical reactor has been highlighted. By solving related mathematical equations, the motion and energy behavior of a single bubble can be estimated theoretically. By trapping a single bubble of gas in partially degassed liquid by a standing acoustic wave and then driving it into highly nonlinear oscillation, single bubble cavitation can be realized and studied in the laboratory [20], which demonstrates that cavitation takes place when the acoustic intensity is higher than the Blake threshold, and it provides much higher energy intensity than conventional acoustic streaming. The energy intensity of cavitation bubble depends on the compression ratio of bubble radius and also the net heat capacity of the bubble content. However, the entrapment of solvent vapor in the bubble at the moment of collapse consumes the heat capacity of the bubble through evaporation, which lowers the temperature attained at the moment of minimum radius during collapse. Moreover, dissociation of solvent vapor mainly involves endothermic reactions that further consume energy and contribute to the lowering of the peak temperature attained at collapse.

### 1.2.2 *Multibubble Cavitation*

In an actual sonochemical reaction, there are numerous active bubbles (ca.  $10^4$  bubbles/1 mL water) for sonication at 20 kHz [2]. Bubbles at different positions of acoustic field follow different cavitation behavior and have different cavitation energy due to spatial diversity of the acoustic pressure intensity. Bubble behavior is influenced not only by the acoustic field, but also by the cavitation behavior of neighboring bubbles. As a result, multibubble cavitation shows statistical results of cavitation behavior and gives rise to the interactions between bubbles.

In multibubble cavitation, the intensity and efficiency of acoustic cavitation is determined by the number density of effective bubbles in the liquid. Rectified diffusion, bubble coalescence and concerted collapse influence the behavior of bubbles.

**Rectified diffusion.** In acoustic cavitation, two possibilities exist for the newly formed bubble nuclei—dissolution in the liquid phase if the ultrasonic intensity is below a threshold value, or growth to a larger size under the action of negative acoustic pressure. If the size of the bubble expands to over a critical (resonance) size, the bubbles will quickly collapse in the following positive acoustic pressure stage, which initiates sonochemical reactions. However, several or tens of acoustic cycles may be necessary for a significant number of bubbles to reach the critical size (Fig. 1.4) [21]. Rectified diffusion is the main way to enlarge the sizes

of bubbles to a critical size, whether in single bubble cavitation or in multibubble cavitation. Rectified diffusion refers to the unequal mass transfer through the cavitation bubble wall in an acoustic cycle. In the expansion phase of bubbles, gas concentration in the bubbles decrease, which drives the mass transfer from bulk liquid to bubble interior. During the shrinkage of bubbles, materials in the bubbles diffuse out of the bubbles. The expansion process of bubbles is relatively slow, while shrinkage of bubbles is rapid. In bubble expansion, the surface area of the bubble is much higher than that during shrinkage. Volumetric work done by the shrinkage of bubble is converted to the evaporation heat of liquid molecules at the bubble/liquid boundary, namely more liquid molecules transform into vapor content of the bubble. Since materials flowing into the bubble are more than materials flowing out in the acoustic cycles, net growth of cavitation bubbles occurs [21].

**Bubble coalescence.** Compared with the slow progress of rectified diffusion, bubble coalescence can be regarded as a rapid progress in which bubbles grow to the critical size. Bremond et al. [22] used photography that showed the coalescence of two bubbles subjected to a negative pressure of  $-2$  MPa. The work demonstrated that if the distance of two bubbles is in the range for weak interaction ( $400\ \mu\text{m}$  for instance), collapse of the two bubbles will be delayed due to the partially shielding of acoustic pressure by each other, but the coalescence would not occur. However, if the two bubbles are initially closer to each other (ca.  $200\ \mu\text{m}$ ), or if the intensity of negative pressure increases, the two bubbles will lose their spherical shape and join to form a single bubble. The significant interaction of cavitating bubbles with their neighbors is governed by secondary Bjerknes forces derived from the nonlinear oscillations of bubbles [23, 24]. A threshold distance exists for the merging of bubbles. The secondary Bjerknes forces become dominant and attract two bubbles to move towards each other only when the distance of the two bubbles is within a threshold value [23]. High acoustic pressure accelerates the approach and merging of bubbles. The threshold distance is  $200\ \mu\text{m}$  when the acoustic pressure is  $10\ \text{kPa}$ , while it increases to  $500\ \mu\text{m}$  when the acoustic pressure is  $40\ \text{kPa}$  [23]. Bubble interactions reversely affect the nonlinear motions of each bubble and thus influences cavitation phenomena and sonochemical yields [24].

An interesting work on the experimentally observation and control of bubble coalescence was performed by Ashokkumar [15] and Ashokkumar et al. [21]. They used pulse ultrasound instead of continuous ultrasound. The growth of bubbles in the measuring system was stimulated when the ultrasound was applied, however, during the off time, some small bubbles became dissolved in the liquid, while others that had sizes large enough to live through the pulse off period, continued to grow in the next acoustic pulse. As mentioned before, most bubbles need several or tens of acoustic cycles to reach the critical size, which is also referred to as an “induction period” for the achievement of steady cavitation. As shown in Fig. 1.4b, the number of acoustic pulses required for steady cavitation in water under a pulse ultrasonic field at  $515\ \text{kHz}$  is about 10, while with the addition of surfactants—methanol (Fig. 1.4c) and sodium dodecyl sulfonate (SDS, Fig. 1.4d), the number of acoustic pulses increases to about 20 and 40, respectively. The addition of surfactants seems to change the surface properties of the bubbles, and

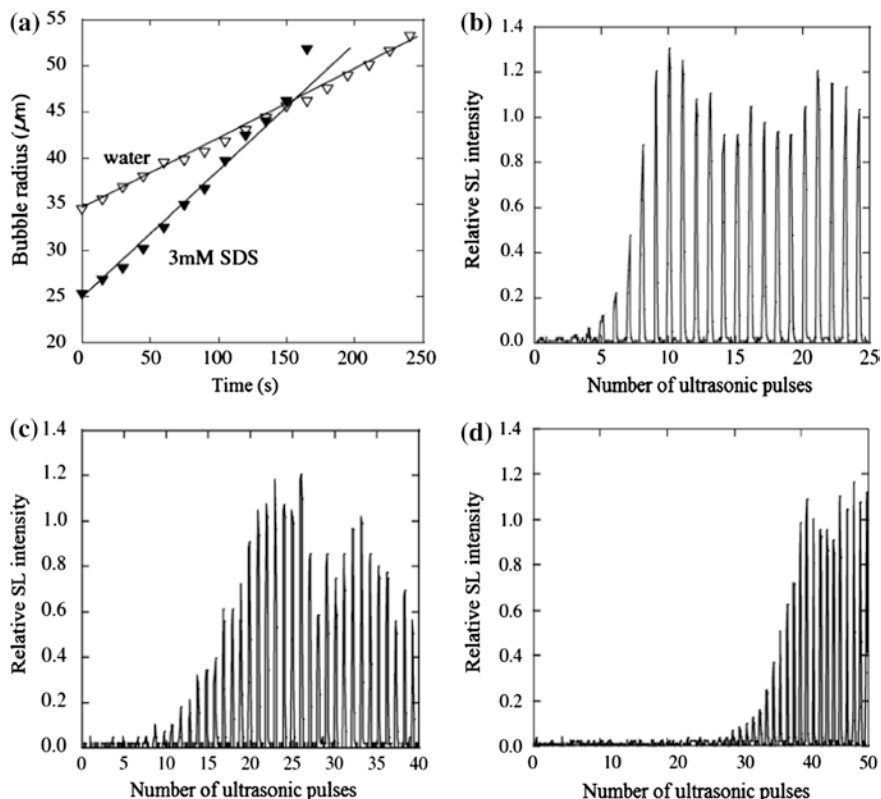


**Fig. 1.4** Bubble growth in surfactant solution under sonication: **a** bubble growth as the function of time in water and sodium dodecyl sulfonate (*SDS*) solution at acoustic pressure of  $\sim 0.022$  MPa and frequency of  $\sim 22$  kHz; **b** sonoluminescence (*SL*) intensity as the function of acoustic pulse number in water under pulse ultrasonic field at 515 kHz; **c** *SL* intensity as the function of acoustic pulse number in 1 M aqueous methanol solution under pulse ultrasonic field at 515 kHz; **d** *SL* intensity as the function of acoustic pulse number in 0.75 mM aqueous *SDS* solution under pulse ultrasonic field at 515 kHz (adapted with permission from [21], Copyright © 2007 Elsevier)

hinders coalescence of small bubbles to larger ones. As a result, the growth of bubbles through bubble coalescence requires more sonication time or more acoustic pulses in surfactant solutions. On the other hand, for high concentration of *SDS*, the adsorption of *SDS* at the bubble/liquid interface is thought to restrict outflow of chemical matters in the bubbles during bubble shrinkage. Therefore, the growth of bubbles via rectified diffusion route is promoted and accelerated with the addition of surfactants.

**Concerted collapse.** In a bubble cloud, the collapse of a bubble emits strong shockwaves. The produced shockwave elevates the ambient pressure or external energy intensity on neighboring bubbles, and accelerates the collapse of neighboring bubbles and other bubbles in the cloud. This assumption is referred to as

concerted collapse [2, 25]. Concerted collapse starts at the boundary of a bubble cloud and proceeds until collapse of bubbles at the cloud center occurs. As a result, shockwaves from multiple bubbles converge together and form a single shockwave directing towards the solid surface with much higher shockwave intensity (several hundreds of kPa) than the collapse of multiple single bubbles.

In a practical sonochemical reactor, the behavior of bubbles is influenced by the pattern of ultrasonic streaming. Some sonochemical systems show interference characteristics in ultrasonic wave propagating in the whole reactor space, which means numerous alternate or fixed regions with strong or weak ultrasonic intensity. An example is the common ultrasonic bath with special depths (integral multiples of quarter-wavelength of ultrasound wave) from the bath bottom to the liquid surface. For this type of sonochemical reactor, the collapse of bubbles are generally concentrated at points that have high ultrasonic intensity (antinodes) in the reactor space, which gives high cavitation activities as shown in Fig. 1.5 [26, 27]. Regions with long-term low or even zero ultrasonic intensity (nodes) may favor the growth of bubbles via rectified diffusion and coalescence. At these nodes, the size of the bubbles may increase beyond the critical size. The bubbles possibly survive even for long time after the ultrasound is shut off [21]. The behavior of bubbles at antinodes or nodes is also used in distinguishing the intensification mechanism of cavitation from that of ultrasonic streaming [28].

Because of the uncertainties in the spatial distribution of bubble size and bubble density as well as the complex interaction between bubbles, the determination of cavitation in a multibubble system is more involved than that for a single bubble system [15, 20]. Several effective methods have been developed for analyzing cavitation in multibubble systems [14, 15, 29, 30]. These methods are summarized in Table 1.2. Acoustic frequency spectroscopy (AFS, Fig. 1.6) is

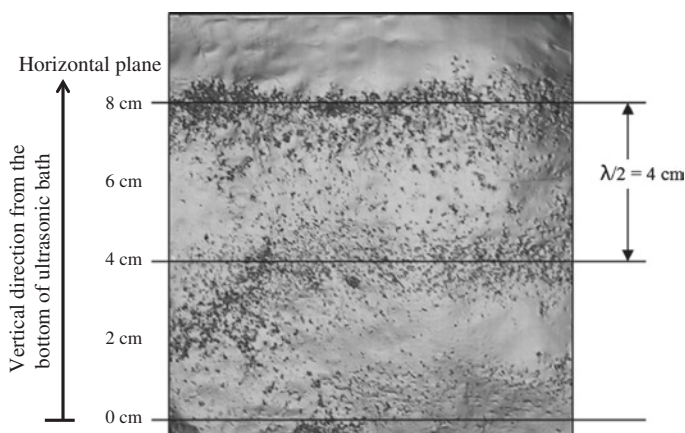
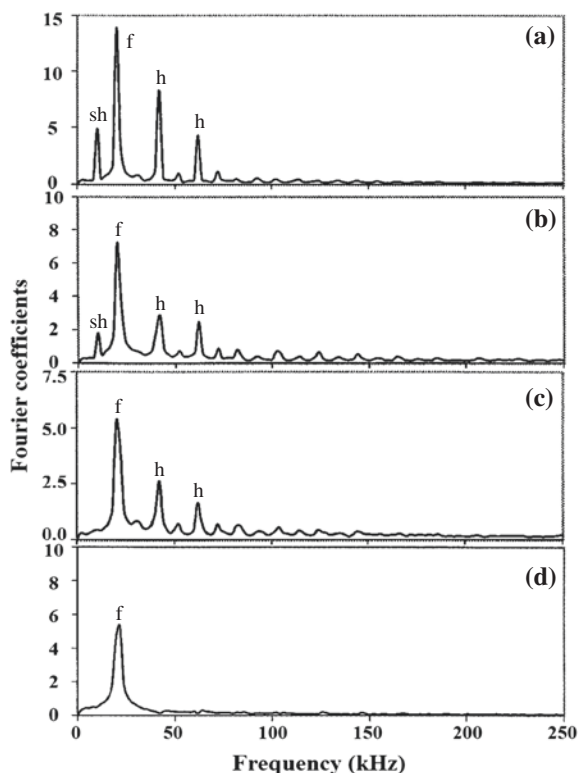


**Fig. 1.5** Cavitation erosion pattern on aluminum foil vertically positioned in ultrasonic bath (water depth of 10 cm) at 20 kHz (adapted with permission from [27], Copyright © 2009 Elsevier)

**Table 1.2** Qualitative and quantitative approaches for measuring ultrasonic cavitation and secondary effects

Method	Sensor	Principle of measurement	Reference
<i>Spectroscopic</i>			
Acoustic frequency	Hydrophone	Steady and transient bubbles oscillating at subharmonics, harmonics and ultraharmonics frequencies produce variation of local acoustic pressure	[27, 31]
Sonoluminescence	Light intensity	Light intensity is detected and plotted as the function of scanning wavelength from 300–900 nm (ultraviolet-visible range)	[14, 15, 29]
<i>Chemical</i>			
Iodine method	$\cdot\text{OH}$ radical	$\text{H}_2\text{O} \rightarrow \cdot\text{OH} + \cdot\text{H}$ , $\text{I}^- + \cdot\text{OH} \rightarrow \text{I}_2^- \rightarrow \text{I}_3^-$ $\text{I}_3^-$ concentration determined by ultraviolet spectroscopy	[30]
Fricke method		$\text{H}_2\text{O} \rightarrow \cdot\text{OH} + \cdot\text{H}$ , $\text{Fe}^{2+} + \cdot\text{OH} \rightarrow \text{Fe}^{3+} + \text{OH}^-$ $\text{Fe}^{3+}$ concentration determined by ultraviolet spectroscopy	
Salicylic acid method		Hydroxylation of salicylic acid by $\cdot\text{OH}$ radical Salicylic acid concentration determined by high performance liquid chromatography	
Terephthalic acid method		$p\text{-C}_6\text{H}_4(\text{COOH})_2 + \cdot\text{OH} \rightarrow \text{C}_6\text{H}_3\text{OH}(\text{COOH})_2$ Hydroxyterephthalic acid concentration determined by fluorescence spectroscopy	
Sonochemiluminescence		3-Aminophthalhydrazide (luminol) + $\cdot\text{OH} \rightarrow$ 3-aminophthalate, in alkaline solution Blue light emission of 3-aminophthalate proportional to concentration	
<i>Physical</i>			
Aluminum foil erosion	Al foil	Indentations on foil and weight loss	[27, 30]
Laser scattering	Light attenuation	Volumetric concentration of bubbles from Beer-Lambert law	[32, 33]
Laser phase-Doppler	Frequency variation	Velocity of bubbles from frequency variation between scattering and incident waves while bubble size by phase displacement between scattering and reflected waves	[33, 34]

**Fig. 1.6** Average acoustic frequency spectra under sonication of 22 kHz: **a** strong cavitation intensity in water; **b** medium cavitation intensity in water; **c** weak cavitation intensity in water; **d** no cavitation intensity in silicon oil. *f* fundamental frequency (22 kHz); *h* harmonic frequencies; *sh* subharmonic frequencies (adapted with permission from [31], Copyright © 2000 American Institute of Chemical Engineers [AIChE])



a direct but approximate way for measuring the occurrence of acoustic cavitation. Hydrophones are placed in liquid under sonication, and record the intensity of pressure pulse at local place as the function of scanning frequency. AFS results reflect the change of acoustic parameters as the result of acoustic activation. Since it uses hydrophones for detection of sound waves, AFS needs complex mathematical transformation and processing to obtain useful information from the as-received spectra [27]. AFS spectrum with high intensity peaks at the harmonic, higher harmonic, or even subharmonic frequencies proved the occurrence of cavitation [27, 31]. Chemical measurements are normally used in the quantitative determination of cavitation yield and cavitation efficiency [12, 30]. In common horn- and bath-type reactors, the cavitation yields are determined as  $3.5 \times 10^{-9}$  and  $5.8 \times 10^{-7}$  g/J, respectively, which give relatively low energy efficiency (5–20 %) of acoustic cavitation [12]. Because of less energy requirement, the results from chemical measurement represent the less violent energy characteristics in bubble dynamics than that from sonoluminescence [15]. Erosion analysis of aluminum foil of several micrometer thickness is used to evaluate the cavitation number (punching number on foil) and cavitation intensity (weight loss of foil).

Results from chemical methods and erosion analysis describe the intensity of  $\cdot\text{OH}$  radical and shockwave, secondary effects of cavitation, respectively.

Advanced technologies such as pulsed multibubble sonoluminescence (MBSL), laser diffraction [32, 33], laser phase-Doppler [33, 34], methyl radical recombination and others are widely used in analyzing multibubble cavitation in recent years, and these methods give the scale or distribution of energy, number, size, velocity of bubble clusters. For MBSL, light emitted at certain wavelength relates to the formation of special plasma. Light intensity is proportional to the energy intensity of bubbles. By fitting the emission spectra of special plasma, the emission temperature of plasma in bubbles can be estimated, which indicates the energy level of bubble cavitation. However, the analysis of multibubble cavitation is still challenging. In fact, as the time for bubble collapse is short, cavitation bubbles analyzed by various methods are mainly in growth or in oscillating, which does not apply to the bubbles before collapse. For laser phase-Doppler, the number and volume fractions of bubbles are plotted against to the motion velocity and size of bubbles at certain plane in acoustic field. Velocity of bubbles is determined by frequency variation between scattering and incident waves, while bubble size is determined by phase displacement between scattering and reflected waves. Laser scattering and laser phase-Doppler are both direct methods to determine the cavitation number.

In multibubble cavitation, the production of cavitation bubbles means the formation of another immiscible phase besides the liquid medium. The intensity of ultrasonic energy is scattered and weakened for a heterogeneous liquid containing high concentrations of insoluble solid particles or gas microbubbles. High acoustic intensity produces high number density of bubbles (bubble cloud) in the liquid phase, while high number density of bubbles greatly influence the delivery of acoustic intensity to the entire reactor space. These two opposing effects have contradictory consequences [26]. For example, in a horn type sonochemical reactor, a high density of bubble cloud gathers at the region near the tip of the transducer, and results in inefficient cavitation in sonochemical processing [35]. Thus, the system with a controlled concentration of cavitation nuclei gives much higher cavitation intensity than the system with too many nuclei and the system suffering completely denucleation [26]. Appropriate number of cavitation nuclei uses energy efficiently.

The formation and distribution of cavitating bubbles in the whole space of a sonochemical reactor is not uniform and is greatly influenced by ultrasonic streaming. Ultrasonic streaming occurs according to the geometry of the reactor and the variation of its ultrasonic parameters. By using high-speed photography [36] and chemical methods such as the iodine method [37] and sonochemiluminescence [38], it is possible to observe and record the spatial distribution of active bubbles. Bubbles are forced to migrate directionally in the acoustic field due to primary Bjerknes forces. The primary Bjerknes force is defined as the translational force on a cavitating bubble in a liquid when the nonlinear oscillation of the cavitating bubble is interacting with the acoustic pressure field [39]. Parlitz et al. [40] demonstrated that when the amplitude of the acoustic pressure was not high, cavitating bubbles tended to move along the direction of pressure rise (pressure antinode). This deduction is consistent with the phenomenon that is described in the



section dealing with concerted collapse (Fig. 1.5). However, when the amplitude is further increased, the primary Bjerknes force may change, and the high pressure amplitude region may become repulsive for the bubbles because of nonlinear oscillation of bubbles [36, 40]. As a result, in an acoustic field near a sonotrode with the pressure amplitude of greater than 190 kPa [36], cavitation bubbles tend to move along the direction of pressure drop. This creates different spatial distributions and migration features of bubbles in a reactor that is commonly referred to as acoustic cavitation structure.

Typical acoustic cavitation structures can be conical bubble structure (CBS), smoker bubble structure, tailing bubble structure (TBS), jet-induced bubble structure (JBS) and acoustic Lichtenberg figure (ALF). Acoustic cavitation structure CBS (Fig. 1.7a) [36] and smoker (Fig. 1.7b) [41] are two common forms that

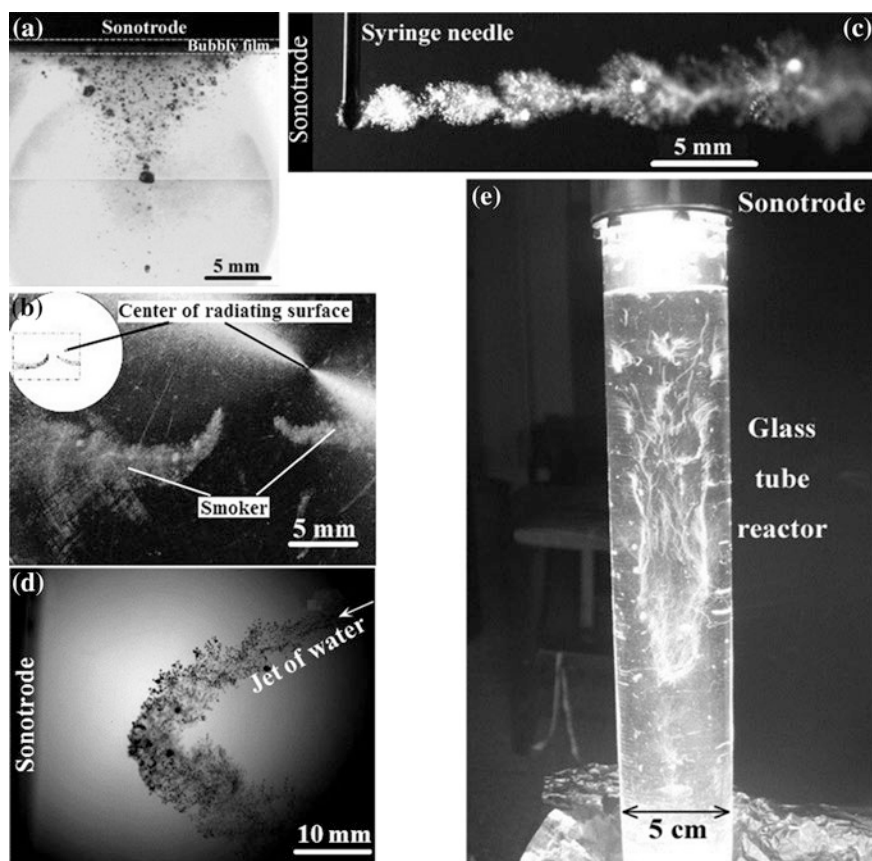


**Fig. 1.7** Acoustic cavitation structures: **a** conical bubble structure; **b** smoker bubble structure; **c** tailing bubble structure; **d** jet-induced bubble structure; **e** acoustic Lichtenberg figure (**a**, **b**, **d** and **e** are reprinted with permission from [36], Copyright © 2014 Elsevier. **c** is reprinted with permission from [42], Copyright © 2014 Elsevier)



occur in a relatively strong acoustic field. CBS is produced by sonotrode. When the sonotrode vibrates with moderate amplitude, the radiating surface is covered by bubbly web structures and the CBS is composed of filament structures, while as the vibrating amplitude of the sonotrode increases, the CBS becomes a homogeneous distribution of bubbles and the radiating surface is covered by a bubbly film [36]. Smoker, which only appears on a radiating surface such as the bottom of a cleaning bath or on the surface of transducer submerged in liquid, is bound to the surface with a small tip and a big tail [41]. TBS (Fig. 1.7c) and JBS (Fig. 1.7d) are two new acoustic cavitation structures produced by artificially implanting nuclei in a strong acoustic field [42]. For TBS, acoustic radiation forces make the cavitation bubbles move away from the radiating surface to form a cloud tail [42]. For JBS, the submerged liquid jet and acoustic radiation forces both determine the direction of the bubble translation [42]. ALF (Fig. 1.7e) occurs in an ultrasonic field with relatively weak intensity [40, 43]. Bubbles in ALF translate towards the pressure antinodes one after another that causes a dendritic bubble structure and self-organization. The nuclei sources of CBS and smoker are mainly small air bubbles trapped within crevices or non-condensed air microbubbles in the liquid. The nuclei sources of TBS and JBS are small air bubbles that originate from foreign impurities or the submerged liquid jet [36]. The above acoustic cavitation structures are closely interrelated to each other and can be interchanged under special conditions. By artificially implanting nuclei, one can create controllable distributions of cavitation bubbles over an entire reactor space that is favorable for promoting sonochemical reaction [42].

In summary, this section has discussed statistical cavitation behavior of bubbles formed under the application of ultrasound to a reactor. The spatial characteristics in number density or volume fraction of bubbles with certain sizes or velocities in the uneven acoustic intensity field have been mainly considered. The number and size distribution of bubbles greatly influence cavitation behavior of neighboring bubbles and thus it strongly affects the product yields in sonochemical reactions.

### ***1.2.3 Physical and Chemical Effects of Cavitation***

The oscillation and transient collapse of cavitation bubbles produce many special secondary physicochemical phenomena, including shockwave, microturbulence, microjet, radical effects and sonoluminescence, which can have great influence on the dynamics and process equilibrium in a system. Mass and heat transfer coefficients of a reacting system can be multiplied by sonication with the predominant reason for enhancement being related to acoustic cavitation and its secondary effects [28, 44]. The collapse of transient bubbles produces local hot spots with temperature and pressure that is much higher than that of the surrounding liquid. The huge temperature and pressure drop generates strong shockwaves towards bubble outsides [45]. The shrinkage and transient collapse of bubbles creates large voids in the liquid, while the quick influx of liquid stream to the voids forms

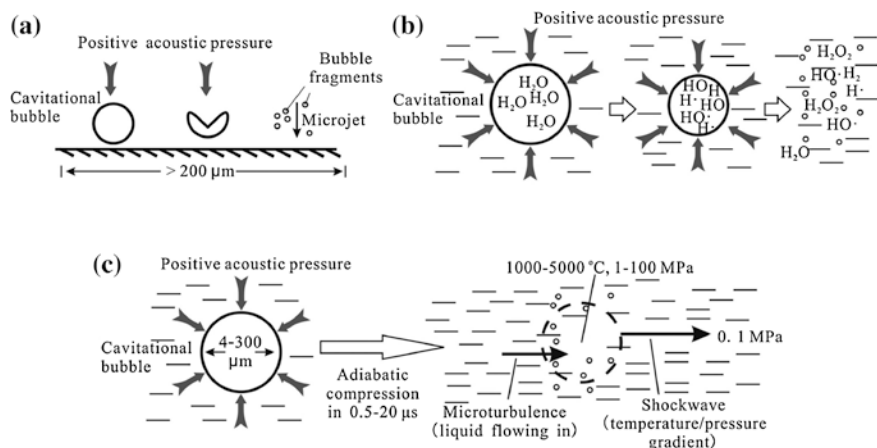


**Fig. 1.8** Schematic representations of secondary effects: **a** microjet, **b** radical formation and **c** shockwave and microturbulence in ultrasonic cavitation

violent microturbulence in local liquid. Microjet refers to the unsymmetrical collapse of bubbles at a broad solid/solvent interface (>200 μm) that produces high speed impact (>100 m/s) oriented towards the solid surface [2]. Schematic representation of several secondary effects is given in Fig. 1.8. As shown in Fig. 1.1, the collapse of transient bubbles produces secondary effects that have a much higher intensity than the oscillating motion from steady bubbles [8]. Transient bubbles have a more violent change in bubble size during the acoustic cycle. Therefore, the intensities of shockwave and microturbulence emitted by transient bubbles become about 3,000 and 40 times, respectively, of that from steady bubbles (Fig. 1.1).

During cavitation, high-temperature dissociation of gaseous water molecules generates radical  $\cdot\text{OH}$ , while the burning of gaseous  $\text{N}_2$  with gaseous  $\text{O}_2$  generates ion  $\text{NO}_2^-$  in bubbles as bubbles shrink or collapse. And light is emitted from the emissive shell (sonoluminescence). In the sonication of water at 22 °C and 52 kHz, a single cavitating bubble with a maximum radius of 28.9 μm produces  $6.1 \times 10^{-18}$  mol  $\text{NO}_2^-$ ,  $1.1 \times 10^{-18}$  mol  $\cdot\text{OH}$  and  $1.3 \times 10^{-20}$  mol photons in an acoustic cycle [20]. However, the negligible amounts of these spontaneous species has less influence on the performance of general sonochemistry [46].

It should be clarified that ultrasound wave, acoustic cavitation and these secondary effects have their action range. Most cavitation activity and high sonochemical yields appear within the distance of about one wavelength, namely several centimeters, away from the sound-emitting surface such as the ultrasonic horn [47, 48]. In some texts [1], according to the distance  $X$  away from the sound-emitting surface, the action zone for ultrasound in sonochemical reactor is divided as near-surface zone ( $X < \text{wavelength } \lambda$ ), streaming zone ( $X \sim \lambda$ ) and far-field zone ( $X > \lambda$ ). Only the near-surface zone is suitable for effective cavitation and sonochemical reactions, while the streaming zone is suitable for particle aggregation

and emulsion separation under low intensity ultrasound by standing wave principle. The action ranges of acoustic cavitation and relevant secondary effects are much shorter. The surrounding liquid absorbs much of the cavitation energy, while the reactive radicals generated by cavitation are easily quenched and cannot migrate far from the location of the collapsed bubble. The attenuation of the pressure pulse for the bubbles is greater than 5  $\mu\text{m}$ , which makes the pressure amplitude measured at 1 mm from the bubble center only  $10^{-3}$  of its actual value [31]. In a heterogeneous system, such as in systems containing a high concentration of small-size solid particles, the absorption of cavitation energy by the surroundings become significant due to the scattering effects. Near the surface of the solid materials, the shockwave that has high temperature and high pressure from bubble collapse, impacts the solid surface and changes the morphology and properties of solid surface. The high energy shockwave lasts for short time of about 200 ns and this happens within a short distance of only tens of nanometers from the solid surface [2]. However, the energy from many shockwaves can be concentrated and enhanced due to concerted collapse. Therefore, it is possibly for ultrasound wave to make indentations of 10–100  $\mu\text{m}$  on solid surface even if the solid surface is exposed under acoustic cavitation for a short period of time [2].

As shown in Fig. 1.3, the active zones for acoustic cavitation and most of the derived physicochemical effects can be divided into four parts—bubble interior, bubble/liquid interface, nearby zone and far-distance zone. The bubble interior allows the access of volatile chemicals and dissolved gases. The bubble generates high temperatures and pressures in its interior during the nearly adiabatic compression process, and initiates ionization, thermolysis and violent radical reactions of vapor molecules. Radical reactions not only occur in the bubble interior, but also at the bubble/liquid interface and in the nearby liquid, especially for nonvolatile compounds. In the sonochemical degradation of phenol in water, the increase of relative concentration of nonvolatile phenol at the bubble/liquid interface promotes the degradation efficiency of phenol multiply even though the concentration of phenol in the bulk liquid remains almost unchanged [49]. This demonstrates that the bubble/liquid interface plays a vital role in radical-induced chemical reactions of nonvolatile compounds under sonication. However, it does not mean that the chemical reactions of nonvolatile compounds cannot take place in the bubble interior. In the study of sonoluminescence in concentrated  $\text{H}_3\text{PO}_4$  solution, peaks assigned to radicals  $\cdot\text{OH}$  and  $\text{PO}\cdot$  are both significantly visible in the ultraviolet spectrum [29]. In the sonoluminescence of  $\text{H}_3\text{PO}_4$ , radical  $\text{PO}\cdot$  must be produced from nonvolatile  $\text{H}_3\text{PO}_4$  in the plasma zone, namely the deepest core in the bubble structure. There are probably two different types of cavitating bubbles that exist in sonicated  $\text{H}_3\text{PO}_4$  solution [29]: (1) stationary bubbles that undergo highly symmetrical collapse and produce radical  $\cdot\text{OH}$  and (2) rapidly moving bubbles that have less symmetrical collapse. In the second type of bubbles, nanodroplets of liquid containing  $\text{H}_3\text{PO}_4$  might be injected into the bubble interior due to capillary wave action, microjetting, or bubble coalescence in the asymmetry collapse of bubbles [29]. However, the ratio of chemical reactions of nonvolatile species in bubbles is not large. As the collapse of transient bubble occurs, numerous active

radicals are released into the nearby liquid which initiate radical reactions such as the oxidative degradation of chemical materials in wastewater or are captured by chemical reagent in determining cavitation activity. For the nearby zone which is within 100  $\mu\text{m}$  from the bubble boundary, the dominant ultrasound-intensification mechanism is physical, such as shockwave and microturbulence. High impact and high temperatures that result from shockwave and high-speed microjet are responsible for the modification of solid surfaces under high-energy ultrasound, such as surface erosion, particle breakage, metal melting and peeling of surface oxide coating [2, 50]. Microturbulence promotes dispersion and fine emulsification in immiscible liquid mixtures and helps to dislodge substances that adhere onto solid surfaces (ultrasonic cleaning). In the far-distance zone, cavitation and shockwaves lose their strength, while microturbulence may be the main mechanism for ultrasonic intensification of chemical processing such as emulsification [48].

Most sonochemical reactions do not occur in the interior of active bubbles. The intensification of these sonochemical reactions is through the action of secondary effects, but not the cavitation behavior of bubbles themselves. However, the energy intensity of secondary effects greatly depends on the behavior of the bubbles, as well as the liquid properties and heterogeneous characteristics of the reaction system. For chemical reactions that are related to biomass conversion, the effective intensification/activation zones are mainly the zones that are nearby the bubbles and the zones that have distance within one wavelength from the bubbles. Therefore, the physical mechanism should be applicable to the discussion of ultrasound-enhanced biomass processing, and intensification of the mass transfer.

### *1.2.4 Factors that Influences the Energy of Acoustic Cavitation*

For most practical sonochemical reactions, it is necessary to know the factors that could influence acoustic cavitation, and these factors include the physicochemical properties of liquids, acoustic operation and heterogeneous characteristics of reaction system [4, 5, 51, 52]. The selection and optimization of those factors allows proper energy intensity to be applied and gives higher energy efficiency. Table 1.3 describes some important factors and their effects on cavitation. Energy efficiency for cavitation is related to the proper design of sonochemical reactors that provide a uniform acoustic energy field for bubble cavitation. Generally, the influence of the factors shown in Table 1.3 can be divided into four categories:

1. **Influence on acoustic environment for the occurrence of cavitation.** Factors such as heterogeneous characteristics, acoustic frequency and liquid temperature influence the propagation and attenuation of acoustic energy in the liquid and thus affect the intensity and uniformity of the acoustic field. The characteristics of acoustic streaming in different reactors also influences the spatial distribution of acoustic energy [54].

- Influence on the occurrence of cavitation, namely cavitation threshold and cavitation density.** Dissolved gases and volatile liquids provide cavitation nuclei, which lower cavitation threshold and make the occurrence of cavitation easier. Relatively high acoustic frequency increases the number of useful cavitation events in per unit of time by shortening the duration of an acoustic cycle.
- Influence on growth and energy accumulation of bubbles.** High acoustic frequency reduces time for the expansion and compression of bubbles, and influences the work done onto the bubble during compression and the energy concentration generated thereby. The properties of liquids such as surface tension and viscosity limit the growth and maximum size of bubbles. The concentration of organic liquids and surfactants influences the growth of bubbles through rectified diffusion and bubble coalescence.
- Influence on the release of bubble energy during their shrinkage and collapse.** The evaporation of liquid in bubbles and the chemical reactivity of liquid and dissolved gases both consume the energy obtained during bubble growth and these buffer the released intensity of cavitation and the secondary effects [53]. Heterogeneous characteristics and high viscosity in liquid absorb the intensity of secondary effects and result in their rapid reduction.

Many factors may promote acoustic cavitation in one aspect but may have adverse effects on another aspect. Representative cases appear in the discussion of acoustic frequency [51] and bubble cloud effects [26], which are mentioned in Table 1.3 and Sect. 1.2.3, respectively. Thus comprehensive analysis and evaluation of the factors influencing acoustic cavitation (Table 1.3) is needed. For practical sonochemical processes, the purpose of chemical treatment often determines the selection and optimization of ultrasonic parameters [51]. High ultrasonic frequency of >100 kHz weakens the physical or mechanical effects generated by acoustic cavitation [55], however, it promotes advanced oxidation reactions through radical reaction pathways [56]. Furthermore, the conditions with the highest cavitation efficiency are not necessarily the optimal conditions for achieving highest product yields in sonochemical reactions. The best of reaction temperature must be appropriate for both cavitation effects and the chemical dynamics [51].

The heterogeneous characteristics in cavitating systems are especially important. Strictly speaking, no cavitation happens in an absolutely single phase. Even for acoustic cavitation mediums such as concentrated  $\text{H}_2\text{SO}_4$  or  $\text{H}_3\text{PO}_4$  solution or ionic liquids that have a very low vapor pressure, the cavitating system is heterogeneous [29, 57–59]. Much of the literature has demonstrated that high cavitation intensity can be obtained with only very small numbers of bubble nuclei. More importantly, compared with water and common organic liquids that have high volatility, cavitation in low-vapor-pressure and nonpolyatomic vapor liquids such as concentrated  $\text{H}_3\text{PO}_4$  solutions reduces excessive energy consumption due to solvent evaporation, polyatomic vibrations, rotations, and especially endothermic bond dissociations. As a result, high cavitation intensity is obtained in concentrated  $\text{H}_3\text{PO}_4$  solutions, which emits bright MBSL intensity that could be visible under fluorescent lamp [29].

**Table 1.3** Factors influencing acoustic cavitation [4, 5, 51–53]

Factor	Direct effect	Remarks
1. Liquid properties		
Compressibility	Cavitation bubble dynamics	High compressibility reduces cavitation intensity
Vapor pressure	1. Cavitation threshold 2. Vapor composition in bubble 3. Intensity of bubble collapse	High vapor pressure makes cavitation easier, but decreases energy intensity of bubble collapse due to liquid evaporation during acoustic cycles
Surface tension	1. Cavitation threshold 2. Bubble size	High surface tension increases cavitation threshold, but gives bubble collapse with high energy intensity
Viscosity	1. Cavitation threshold 2. Bubble oscillation	1. Cavitation occurring in low viscosity is mainly transient 2. High viscosity induces steady or no cavitation. High cavitation energy in single bubble and high attenuation of acoustic energy, shockwave and microturbulence
Chemical reactivity	1. Radical formation 2. Intensity of bubble collapse	Reaction of active compounds consumes the energy released by cavitation
Pretreatment	Cavitation threshold	Degassing and nucleation influence acoustic cavitation
2. Properties of gas in liquid		
Gas solubility	1. Number of cavitation events 2. Vapor composition in bubble	1. Dissolved gas acts as cavitation nuclei facilitating cavitation 2. Cavitation intensity is inversely proportional to amount of dissolved gas
Specific heat, thermal diffusivity	1. Heat transfer between bubble and liquid 2. Energy of cavitation bubbles	Low thermal conductivity of gas leads to high local heating during bubble collapse
Chemical reactivity	1. Radical formation 2. Intensity of bubble collapse	Reaction of compounds decreases the energy intensity of bubble collapse
3. Liquid temperature		
	1. Bubble dynamics 2. Liquid properties, gas solubility 3. Sound propagation	1. Complex influences. Liquid temperature increases cavitation intensity due to volatility effect in most cases 2. Chemical reactions need appropriate temperature for efficient coupling of cavitation effects with chemical dynamics
4. Static pressure		
	1. Cavitation threshold 2. Bubble dynamics	High cavitation threshold and violent bubble collapse occur at high static pressure Increasing static pressure allows one to distinguish between acoustic microstreaming and cavitation mechanism
5. Existence of solid particles		
	1. Spatial distribution of acoustic intensity 2. Intensity of secondary effects	High concentration of solid microparticles decreases cavitation efficiency and intensity of secondary effects due to acoustic scattering

(continued)

**Table 1.3** (continued)

Factor	Direct effect	Remarks
6. Acoustic intensity		
	<ol style="list-style-type: none"> <li>1. Bubble dynamics</li> <li>2. Number of cavitation events</li> </ol>	<ol style="list-style-type: none"> <li>1. High acoustic intensity promotes cavitation</li> <li>2. Capacity for indefinite increase of acoustic intensity depends on material stability of transducer and the properties of liquid medium. Acoustic intensity is determined according to reaction requirement</li> <li>3. Bubble cloud effect seriously decreases cavitation efficiency at high acoustic intensity. Additional auxiliaries such as mechanical agitation avoid bubble clouds gathering in zones that have high acoustic intensity</li> </ol>
7. Acoustic frequency		
	<ol style="list-style-type: none"> <li>1. Acoustic cycle</li> <li>2. Bubble dynamics</li> <li>3. Cavitation threshold</li> <li>4. Sound attenuation</li> </ol>	<ol style="list-style-type: none"> <li>1. Cavitation threshold increases with acoustic frequency</li> <li>2. High acoustic frequency of &gt;1 MHz means short acoustic cycle and insufficient time for the generation, growth and collapse of bubbles</li> <li>3. High frequency increases attenuation of ultrasonic energy in liquid</li> <li>4. Number of useful cavitation events per unit time increases for acoustic frequency of &lt;200 kHz. This increases cavitation efficiency</li> <li>5. Longer duration of bubble motion and larger bubble size exist with low frequency. This increases the evaporation of liquid at the bubble surface and chemical reaction of vapor content in bubble, which consumes energy in cavitation bubble, and decreases the energy intensity of transient collapse</li> </ol>

It can be concluded that in “homogeneous” liquids, the concentration of microbubbles that are artificially produced by researchers determines the cavitation intensity in sonochemical reactors. This conclusion is obtained for microbubbles from vapor that is produced by solvent volatilization, but the conclusion is also applicable to liquid containing noncondensable gases. In the latter case, noncondensable gases displace vapor molecules as the main source of microbubble nuclei, while the content of noncondensable gases in liquids can be controlled by properly degassing and removal of gas microbubbles trapped in crevice (denucleation) [26]. Aqueous solutions that are not degassed give relatively poor cavitation intensity according to acoustic emission spectrum results, and this is due to the acoustic attenuation and acoustic energy scattering in the bubble-rich liquid. Aqueous solutions that are completely pre-denucleated show no cavitation intensity as no microbubble is available as cavitation nuclei. As a result, the highest



acoustic emission intensity is observed in the liquid that is degassed but not denucleated which contains a controlled concentration of noncondensable air [26]. In most cases, degassing before sonochemical treatment enhances the intensity of cavitation and dramatically improves cavitation distribution. Cavitation is concentrated more closely to transducers when sonication is performed in tap water, while it is highly dispersed and evenly in the whole reactor space when sonication is performed in boiled water [60]. Nuclei concentration effects seem to artificially regulate cavitation intensity in homogeneous liquids.

For solid-liquid heterogeneous systems, especially patterned geometry of defects on solid surfaces, the size and concentration of the solid micro-/nanoparticles are important for selective production or control of cavitation intensity [6, 7]. As mentioned in Sect. 1.2.1, smart design of surface defects can enhance the nucleation rate by several orders of magnitude [6]. In biomass reactions handling lignocellulose particles, appropriate particle size (several tens to several hundreds of micrometers) [61, 62] and solid concentration (<5 wt%) [51] seems to promote efficient reaction.

Another interesting heterogeneous system is the hot-pressed solvents such as subcritical CO<sub>2</sub> [63]. Acoustic cavitation only occurs below the critical point of liquid, because no phase boundary exists above the critical point. Compared to ambient water, acoustic cavitation in subcritical CO<sub>2</sub> requires a lower threshold pressure, as the high vapor pressure of CO<sub>2</sub> counteracts the hydrostatic pressure. The Blake threshold for subcritical CO<sub>2</sub> at 20 °C and 5.82 MPa is only 0.1 MPa, while water needs 5.9 MPa for the same conditions [63]. Theoretical calculations show that with stimulation of ultrasound at 20 kHz, liquid CO<sub>2</sub> at 20 °C and 5.82 MPa gives high cavitation intensity, with the maximum bubble radius comparable to that in water at 20 °C and ambient pressure [63]. The acoustic cavitation in subcritical CO<sub>2</sub> is already used in radical-induced chemical reactions, such as polymer synthesis.

### 1.3 Conclusions and Future Outlook

Ultrasound can be an effective technology for process intensification by acoustic cavitation in many chemical reactions. Acoustic cavitation accumulates and explosively releases energy through the growth, radial motion and collapse of bubbles. The intensity of released energy is enough to break chemical bonds and even to generate plasma and photons. However, in many practical reactions, secondary effects generated by cavitation become the primary and direct cause for process intensification under sonication, while the intensity of secondary effects also depend on the behavior of bubbles themselves and the influence from the properties of the sonication medium. The analysis of influencing factors must be comprehensive and be directed towards specific situations. Ultrasonic streaming and heterogeneous characteristics of sonochemical systems have great influence on the efficiency of acoustic cavitation, namely the transformation ratio of ultrasonic



energy to cavitation energy. Some qualitative and quantitative approaches are recommended for measuring ultrasonic cavitation and secondary effects, which will help to understand the regularity of cavitation energy and its distribution in specific reactors. Optimization of chemical reactions under sonication can be achieved through combined knowledge of the regularities in cavitation energy, ultrasonic operation and reaction requirement.

Acoustic cavitation can vary greatly between reactor types and different sonochemical systems. Mechanics and fluid dynamics help to develop mathematical models for acoustic cavitation and provide some possible theoretical frameworks. However, experimental methods are needed to examine many hypotheses that are used in the design of practical reactors. In the last decade, new technologies such as multibubble sonoluminescence and advanced photography have greatly elevated the progress of experimental acoustics, and advanced application of ultrasound in biomass conversion. However, new studies are still needed to help many of the intrinsic characteristics and nature of acoustic cavitation. Research areas that are probably fruitful for exploration are: (1) acoustic cavitation in multibubble systems, (2) cavitation in special liquid mediums such as viscous liquid, ionic liquids and near-critical fluids, (3) acoustic cavitation occurring on the solid/liquid interface both on experimental and theoretical level, (4) characteristic analysis of acoustic fields in new sonochemical reactors with different geometric arrangements and (5) mechanisms of sonochemistry for special reactions.

Especially, the experimental mapping and theoretical study of the spatial distribution of active cavitation in reactor space needs more attention. Further, the combination of sonochemistry with general chemistry methods should be given attention within educational environments.

In practical chemical processes that are enhanced by ultrasonic energy, the most important consideration will be the system performance and energy efficiency of the applied ultrasound. New advances in the statistic analysis and purposeful design of the energy of cavitation bubbles will allow the design of efficient systems.

## References

1. Ensminger D, Bond LJ (2011) *Ultrasonics: fundamentals, technologies, and applications*, 3rd edn. CRC Press, Boca Raton
2. Shchukin DG, Skorb E, Belova V, Möhwald H (2011) Ultrasonic cavitation at solid surfaces. *Adv Mater* 23(17):1922–1934
3. Marmottant P, Hilgenfeldt S (2003) Controlled vesicle deformation and lysis by single oscillating bubbles. *Nature* 423(6936):153–156
4. Shah YT, Pandit AB, Moholkar VS (1999) *Cavitation reaction engineering*. Kluwer Academic/Plenum Press, New York
5. Thompson LH, Doraiswamy LK (1999) *Sonochemistry: science and engineering*. *Ind Eng Chem Res* 38(4):1215–1249
6. Giacomello A, Chinappi M, Meloni S, Casciola CM (2013) Geometry as a catalyst: how vapor cavities nucleate from defects. *Langmuir* 29(48):14873–14884

7. Zhang L, Belova V, Wang HQ, Dong WF, Möhwald H (2014) Controlled cavitation at nano/microparticle surfaces. *Chem Mater* 26(7):2244–2248
8. Parkar PA, Choudhary HA, Moholkar VS (2012) Mechanistic and kinetic investigations in ultrasound assisted acid catalyzed biodiesel synthesis. *Chem Eng J* 187:248–260
9. Minnaert M (1933) On musical air bubbles and the sounds of running water. *Philos Mag* 16(104):235–248
10. Suslick KS (1990) Sonochemistry. *Science* 247(4949):1439–1445
11. Bang JH, Suslick KS (2010) Applications of ultrasound to the synthesis of nanostructured materials. *Adv Mater* 22(10):1039–1059
12. Gogate PR, Tayal RK, Pandit AB (2006) Cavitation: a technology on the horizon. *Curr Sci* 91(1):35–46
13. Flannigan DJ, Suslick KS (2005) Plasma formation and temperature measurement during single-bubble cavitation. *Nature* 434(7029):52–55
14. Suslick KS, Eddingsaas NC, Flannigan DJ, Hopkins SD, Xu H (2011) Extreme conditions during multibubble cavitation: sonoluminescence as a spectroscopic probe. *Ultrason Sonochem* 18(4):842–846
15. Ashokkumar M (2011) The characterization of acoustic cavitation bubbles—An overview. *Ultrason Sonochem* 18(4):864–872
16. Storey BD, Szeri AJ (2001) A reduced model of cavitation physics for use in sonochemistry. *Proc R Soc Lond A* 457(2011):1685–1700
17. Toegel R, Gompf B, Pecha R, Lohse D (2000) Does water vapor prevent upscaling sonoluminescence? *Phys Rev Lett* 85(15):3165–3168
18. Sivasankar T, Paunikar AW, Moholkar VS (2007) Mechanistic approach to enhancement of the yield of a sonochemical reaction. *AIChE J* 53(5):1132–1143
19. Storey BD, Szeri AJ (2000) Water vapour, sonoluminescence and sonochemistry. *Proc R Soc Lond A* 456(1999):1685–1709
20. Didenko YT, Suslick KS (2002) The energy efficiency of formation of photons, radicals and ions during single-bubble cavitation. *Nature* 418(6896):394–397
21. Ashokkumar M, Lee J, Kentish S, Grieser F (2007) Bubbles in an acoustic field: an overview. *Ultrason Sonochem* 14(4):470–475
22. Bremond N, Arora M, Dammer SM, Lohse D (2006) Interaction of cavitation bubbles on a wall. *Phys Fluids* 18(12):121505
23. Jiao JJ, He Y, Leong T, Kentish SE, Ashokkumar M, Manasseh R, Lee J (2013) Experimental and theoretical studies on the movements of two bubbles in an acoustic standing wave field. *J Phys Chem B* 117(41):12549–12555
24. Stricker L, Dollet B, Fernández Rivas D, Lohse D (2013) Interacting bubble clouds and their sonochemical production. *J Acoust Soc Am* 134(3):1854–1862
25. Hansson I, Mörch KA (1980) The dynamics of cavity clusters in ultrasonic (vibratory) cavitation erosion. *J Appl Phys* 51(9):4651–4658
26. Moholkar VS, Warmoeskerken MMCG (2003) Integrated approach to optimization of an ultrasonic processor. *AIChE J* 49(11):2918–2932
27. Avvaru B, Pandit AB (2009) Oscillating bubble concentration and its size distribution using acoustic emission spectra. *Ultrason Sonochem* 16(1):105–115
28. Moholkar VS, Warmoeskerken MMCG, Ohl CD, Prosperetti A (2004) Mechanism of mass-transfer enhancement in textiles by ultrasound. *AIChE J* 50(1):58–64
29. Xu HX, Glumac NG, Suslick KS (2010) Temperature inhomogeneity during multibubble sonoluminescence. *Angew Chem Int Ed* 49(6):1079–1082
30. Sutkar VS, Gogate PR (2009) Design aspects of sonochemical reactors: techniques for understanding cavitation activity distribution and effect of operating parameters. *Chem Eng J* 155(1–2):26–36
31. Moholkar VS, Sable SP, Pandit AB (2000) Mapping the cavitation intensity in an ultrasonic bath using the acoustic emission. *AIChE J* 46(4):684–694
32. Tuziuti T, Yasui K, Iida Y (2005) Spatial study on a multibubble system for sonochemistry by laser-light scattering. *Ultrason Sonochem* 12(1–2):73–77

33. Burdin F, Tsochatzidis NA, Guiraud P, Wilhelm AM, Delmas H (1999) Characterisation of the acoustic cavitation cloud by two laser techniques. *Ultrason Sonochem* 6(1–2):43–51
34. Tsochatzidis NA, Guiraud P, Wilhelm AM, Delmas H (2001) Determination of velocity, size and concentration of ultrasonic cavitation bubbles by the phase-Doppler technique. *Chem Eng Sci* 56(5):1831–1840
35. Kadkhodae R, Povey MJW (2008) Ultrasonic inactivation of *Bacillus*  $\alpha$ -amylase. I. Effect of gas content and emitting face of probe. *Ultrason Sonochem* 15(2):133–142
36. Bai LX, Xu WL, Deng JJ, Li C, Xu DL, Gao YD (2014) Generation and control of acoustic cavitation structure. *Ultrason Sonochem* 21(5):1696–1706
37. Gogate PR, Tatake PA, Kanthale PM, Pandit AB (2002) Mapping of sonochemical reactors: review, analysis, and experimental verification. *AIChE J* 48(7):1542–1560
38. Yin H, Qiao YZ, Cao H, Li ZP, Wan MX (2014) Cavitation mapping by sonochemiluminescence with less bubble displacement induced by acoustic radiation force in a 1.2 MHz HIFU. *Ultrason Sonochem* 21(2):559–565
39. Louisnard O (2012) A simple model of ultrasound propagation in a cavitating liquid. Part II: primary Bjerknes force and bubble structures. *Ultrason Sonochem* 19(1):66–76
40. Parlitz U, Mettin R, Luther S, Akhatov I, Voss M, Lauterborn W (1999) Spatio-temporal dynamics of acoustic cavitation bubble clouds. *Philos Trans R Soc London, Ser A* 357(1751):313–334
41. Bai LX, Ying CF, Li C, Deng JJ (2012) The structures and evolution of Smoker in an ultrasonic field. *Ultrason Sonochem* 19(4):762–766
42. Bai LX, Deng JJ, Li C, Xu DL, Xu WL (2014) Acoustic cavitation structures produced by artificial implants of nuclei. *Ultrason Sonochem* 21(1):121–128
43. Mettin R, Luther S, Ohl CD, Lauterborn W (1999) Acoustic cavitation structures and simulations by a particle model. *Ultrason Sonochem* 6(1–2):25–29
44. Legay M, Gondrexon N, Le Person S, Boldo P, Bontemps A (2011) Enhancement of heat transfer by ultrasound: review and recent advances. *Int J Chem Eng* 2011:17
45. Ohl CD, Kurz T, Geisler R, Lindau O, Lauterborn W (1999) Bubble dynamics, shock waves and sonoluminescence. *Philos Trans R Soc London Ser A* 357(1751):269–294
46. Kalva A, Sivasankar T, Moholkar VS (2009) Physical mechanism of ultrasound-assisted synthesis of biodiesel. *Ind Eng Chem Res* 48(1):534–544
47. Sutkar VS, Gogate PR, Csoka L (2010) Theoretical prediction of cavitation activity distribution in sonochemical reactors. *Chem Eng J* 158(2):290–295
48. Cuheval A, Chow RCY (2008) A study on the emulsification of oil by power ultrasound. *Ultrason Sonochem* 15(5):916–920
49. Sivasankar T, Moholkar VS (2008) Mechanistic features of the sonochemical degradation of organic pollutants. *AIChE J* 54(8):2206–2219
50. Suslick KS, Skrabalak SE (2008) Sonocatalysis. In: Ertl G, Knözinger H, Schüth F, Weitkamp J (eds) *Handbook of heterogeneous catalysis*, 2nd edn. Wiley-VCH Verlag GmbH & Co. KGaA, Weinheim, pp 2007–2017
51. Luo J, Fang Z, Smith RL Jr (2014) Ultrasound-enhanced conversion of biomass to biofuels. *Prog Energy Combust Sci* 41:56–93
52. Vichare NP, Senthilkumar P, Moholkar VS, Gogate PR, Pandit AB (2000) Energy analysis in acoustic cavitation. *Ind Eng Chem Res* 39(5):1480–1486
53. Rooze J, Rebrov EV, Schouten JC, Keurentjes JTF (2013) Dissolved gas and ultrasonic cavitation—A review. *Ultrason Sonochem* 20(1):1–11
54. Gogate PR, Sutkar VS, Pandit AB (2011) Sonochemical reactors: important design and scale up considerations with a special emphasis on heterogeneous systems. *Chem Eng J* 166(3):1066–1082
55. Tran KVB, Kimura T, Kondo T, Koda S (2014) Quantification of frequency dependence of mechanical effects induced by ultrasound. *Ultrason Sonochem* 21(2):716–721
56. Hua I, Hoffmann MR (1997) Optimization of ultrasonic irradiation as an advanced oxidation technology. *Environ Sci Technol* 31(8):2237–2243

57. Eddingsaas NC, Suslick KS (2007) Evidence for a plasma core during multibubble sonoluminescence in sulfuric acid. *J Am Chem Soc* 129(13):3838–3839
58. Oxley JD, Prozorov T, Suslick KS (2003) Sonochemistry and sonoluminescence of room-temperature ionic liquids. *J Am Chem Soc* 125(37):11138–11139
59. Bradley M, Ashokkumar M, Grieser F (2013) Multibubble sonoluminescence in ethylene glycol/water mixtures. *J Phys Chem B* 118(1):337–343
60. Liu LY, Yang Y, Liu PH, Tan W (2014) The influence of air content in water on ultrasonic cavitation field. *Ultrason Sonochem* 21(2):566–571
61. Bussemaker MJ, Xu F, Zhang DK (2013) Manipulation of ultrasonic effects on lignocellulose by varying the frequency, particle size, loading and stirring. *Bioresour Technol* 148:15–23
62. Rezaia S, Ye ZL, Berson RE (2009) Enzymatic saccharification and viscosity of sawdust slurries following ultrasonic particle size reduction. *Appl Biochem Biotechnol* 153(1–3):103–115
63. Kuijpers MWA, van Eck D, Kemmere MF, Keurentjes JTF (2002) Cavitation-induced reactions in high-pressure carbon dioxide. *Science* 298(5600):1969–1971

## Chapter 2

# Physical and Chemical Mechanisms of Ultrasound in Biofuel Synthesis

V.S. Moholkar, Hanif A. Choudhury, Shuchi Singh, Swati Khanna, Amrita Ranjan, Sankar Chakma and Jaykumar Bhasarkar

**Abstract** Physical and chemical mechanisms ultrasound-assisted processes as related to the synthesis of biofuels are reviewed. Ultrasound and its secondary effect of cavitation have physical and chemical effects on a reaction system, which can contribute to enhancement of the kinetics and yield. In this chapter, a mechanistic insight into the ultrasound assisted biofuels synthesis is given by coupling simulations of cavitation bubble dynamics with experimental data. The physical effect of ultrasound and cavitation is through intense micro-convection in the system that gives marked improvements in the mass transfer of the system. The chemical effect is through generation of highly reactive radicals through transient cavitation that induce or accelerate chemical reactions. Chemical effects include thermal decomposition of the solvent vapor molecules in the cavitation bubble resulting in generation of smaller molecular species that also affect chemistry of the process. Raising the static pressure of the reaction system above ultrasound pressure amplitude in the system helps to discriminate between physical and chemical effects of ultrasound and cavitation. Biofuels systems considered in this chapter are the pretreatment of biomass, biodiesel synthesis with acid/base and homogeneous/heterogeneous catalysts, extraction of microalgal lipids, bioconversion of crude glycerol from biodiesel industry to value added products and desulfurization of the fuel. Among the physical effects of ultrasound and cavitation, micro-streaming by ultrasound has a greater influence on reactions than shock waves generated by cavitation bubbles. In some cases, chemical effects of transient cavitation are revealed to have adverse influence on a reaction. Many biofuels systems are limited by their intrinsic characteristics that restrict the effect of ultrasound and cavitation on the reaction system.

---

V.S. Moholkar (✉) · S. Chakma · J. Bhasarkar  
Department of Chemical Engineering, Indian Institute of Technology Guwahati, Guwahati  
781 039, Assam, India  
e-mail: vmoholkar@iitg.ernet.in

V.S. Moholkar · H.A. Choudhury · S. Singh · S. Khanna · A. Ranjan  
Center for Energy, Indian Institute of Technology Guwahati, Guwahati 781 039, Assam, India

**Keywords** Biofuel • Sonochemistry • Bubble dynamics • Ultrasound • Biodiesel • Biomass

## 2.1 Introduction

Fast depletion of global fossil fuel reserves, sparking an almost four fold increase in international prices of crude oil has made energy security a daunting issue for developing economies. A related issue is that of climate change due to enormous rise in emissions of greenhouse gases from vehicular exhaust. Both of these issues have triggered immense research in alternate renewable energy sources (mainly the biofuels) in the past two decades. With growing economies, the energy demands in all sectors of a developing nation are rising fast, with major sectors being domestic, industry and agriculture. The main energy demand in these sectors is in two forms, viz. electricity and liquid transportation fuel. Numerous ways have been explored to fulfill these energy needs from renewable and carbon neutral bio-sources. The major routes for electricity are either biogas digestion or biomass gasification. Biogas digestion produces methane which could be used in engine generator sets. Biomass gasification produces a mixture of carbon monoxide and hydrogen, which also can be used in engine generator sets. Other alternate carbon neutral sources for electricity are solar (either photovoltaics or solar-thermal) and wind energy. As far as liquid transportation fuels are concerned, there are two main options, viz. alcoholic biofuels through fermentation and biodiesel. Alcoholic biofuels such as methanol, ethanol and butanol have been widely used for blending with gasoline (replacing the conventional methyl *t*-butyl ether, MTBE, as oxygenate). Biodiesel is essentially alkyl esters of fatty acids. These are produced by the process of esterification/transesterification of free fatty acids/triglycerides using short chain alcohols like methanol and ethanol. Like alcoholic biofuels, biodiesel can be blended with petro-diesel. Up to 20 % blends of diesel/biodiesel can be used in the vehicles without requiring modifications of engine.

Despite promise of these biofuels for mitigating the threats of energy security and climate change risk, large scale commercial production of these biofuels has been hampered by economic non-feasibility. For example, the total production cost of biodiesel is almost at par with petroleum-diesel. This is due to high cost of the feedstock (i.e. vegetable oil) coupled with large processing cost. For bio-diesel, use of low-cost non-edible oils like *Jatropha curcas* and *Karanja* offer a possible solution, but the processes based on these feedstocks have been largely unsuccessful due to non-availability of oil seeds for regular supply. There are three possible means of enhancing the economy of biodiesel production: (1) use of low-cost feedstock than non-edible oils such as microalgal lipids and animal fats which have high contents of free fatty acids (FFA); (2) use of efficient processing techniques that give high yield with faster kinetics for esterification (thus lowering the cost of recycle with simultaneous increase in the throughputs); (3) forward integration of the biodiesel process by conversion of byproducts such as glycerol to value-added products.

As far as alcoholic biofuels are concerned, the most popular fuel is ethanol, which is a major byproduct of the sugar industry. However, the substrate for ethanol, i.e. molasses, has numerous other outlets that fetch attractive revenue. This essentially increases the production cost of ethanol, as a result of which the producer is compelled to sell it for potable use, which fetches high price unless a sufficiently high minimum support price (MSP) is provided by Government for ethanol purchase by petroleum industry. Thus, the ethanol from sugar industry is largely unavailable for blending with gasoline. This necessitates exploration of alternate sources of cheaper ethanol. Fermentation of lignocellulosic biomass as substrate is a potential solution to this issue. The biomass available in the form of agro-residue or forest-residue or waste biomasses like invasive weeds and grasses have been extensively explored in lab-scale investigations for bioethanol production. The major bottleneck of bioalcohol production from this route is the high cost of biomass pretreatment. A simple, energy efficient and low-cost technology for effective biomass pretreatment can boost economy of alcoholic biofuels products several fold.

The efficiency of physical, chemical or biological process depends on the method of introduction of energy into the system to bring about the required transformation. Numerous new techniques have been invented in recent years that offer efficient and effective means of introduction of energy into the system, which gives higher yield as well as kinetics of desired transformation. One such technique is ultrasound irradiation or sonication. Ultrasound is essentially a longitudinal acoustic wave with frequency equal to or higher than 20 kHz—which is the upper limit of human hearing range. The propagation of ultrasound gives sinusoidal variation in the static pressure in the liquid medium. This phenomenon gives rise to cavitation in the medium. Cavitation can be defined as nucleation, volumetric oscillations and implosive collapse of tiny gas or vapor bubbles driven by ultrasound wave. Transient cavitation causes extreme energy concentration in the medium at an incredibly small temporal (~50 ns) and spatial scale (~100 nm) [1]. The transient implosive collapse of the bubble is adiabatic and the temperature and pressure inside the bubble reaches extremely high (~5,000 K and ~50 MPa) [2, 3]. Transient cavitation has both physical and chemical effects on the reaction system. The physical effect is generation of intense local convection in the medium that enhances the mass transfer characteristics of the system. The chemical effect includes generation of highly reactive radicals inside the cavitation bubble at the moment of transient collapse, when the temperature and pressure in the bubble reach extrema. The radicals generated inside the bubble get released into the medium with fragmentation of the bubble where they can induce/accelerate chemical reactions. This is the well known sonochemical effect. Use of ultrasound for intensification of synthesis of biofuels has been attempted by many researchers and a voluminous literature (more than 300 papers) has been published in this area in the past few years. An excellent and comprehensive review of this literature has been recently published by Luo et al. [4]. Ultrasound has mainly been applied for the pretreatment of biomass (delignification/acid hydrolysis), enzymatic hydrolysis of pretreated biomass (or saccharification), fermentation of the hydrolyzates from acid/enzymatic hydrolysis,



microalgal lipid extraction, biodiesel synthesis and biogas digestion. Literature published in these area reports beneficial effects of ultrasound and cavitation on the process in terms of higher yield, faster kinetics, reduction in the number of process steps, use of cruder chemicals and substrates etc. However, very little effort has been dedicated to deduce the exact physical mechanism underlying the observed enhancement. The relative contribution of physical and chemical effects towards enhancement has not been discerned. For achieving effective design and scale-up of ultrasound based biofuels synthesis, the establishing exact physical mechanism of the ultrasound-induced enhancement is crucial.

In this chapter, critical analysis of our research in this area is given as applied to different biofuels systems. Review of general literature published in the area of ultrasound assisted biofuels synthesis is beyond the scope of this chapter. The focus of this chapter is to bring together all results of our research in linking the chemistry of biofuels synthesis with the physics of ultrasound and cavitation. Biofuel systems that are treated in this chapter are: (1) biomass pretreatment and hydrolysis, (2) biodiesel synthesis with homogeneous/heterogeneous acid/alkali catalyst, (3) microalgal lipid extraction, (4) bioethanol synthesis from lignocellulosic biomass with either separate hydrolysis and fermentation or simultaneous saccharification and fermentation and (5) bioconversion of crude glycerol from biodiesel industry to value-added products. Finally, a coherent mechanistic picture of ultrasound enhanced biofuels synthesis is proposed that gives research directions.

## 2.2 Physics of Ultrasound and Cavitation: A Brief Overview

Before proceeding to discussions on effects of ultrasound and cavitation on different biofuels systems mentioned in previous section, we briefly ponder over some basic physical aspects of ultrasound and cavitation. Greater details on this subject can be found in standard textbooks and monographs [5–12] and popular reviews [13–18].

### 2.2.1 *Ultrasound Wave Phenomenon*

Sound wave passes through a compressible medium, such as air and water, in the form of a longitudinal wave comprising of alternate compression and rarefaction phases. The pressure as well as density of the medium undergoes periodic variation with passage of the wave. The fluid elements in the medium undergo an oscillatory motion around a mean position. The sound wave is characterized on the basis of its frequency, velocity and pressure amplitude. Some basic relations between ultrasound frequency ( $f$ ), velocity ( $c$ ), pressure amplitude ( $P_A$ ) oscillatory velocity of fluid elements ( $u$ ), density of the medium ( $\rho$ ), and the acoustic intensity



( $I$ ) are as follows:  $u = 2\pi fa$  (where  $a$  is the amplitude of oscillation);  $P_A = u\rho c$ ;  $I = P_A^2/\rho c = 2\pi^2 f^2 a^2 \rho c$  [5, 6]. During its passage through the medium, the sound wave suffers from attenuation due to energy loss through several mechanisms like frictional (or viscous) loss, thermal loss and acoustic damping due to bubbles. The momentum of the wave is absorbed by the medium due to finite viscosity and this loss is manifested in terms of unidirectional circulatory currents set up in the medium (known as acoustic streaming). Bubbles present in the medium scatter the ultrasound waves causing severe attenuation. Presence of gas bubbles in the liquid also alters the compressibility of the medium, as a result of which the speed of sound in the medium reduces. The properties of the sound wave are also a function of the static pressure in the medium. As far as sound wave propagation in liquids is concerned, the static pressure in the medium is of insignificant importance, as the liquid properties are relatively insensitive to static pressures of moderate values. Thus, the properties of sound wave propagating in a liquid medium do not alter with static pressure of the medium for moderate rise in pressure levels.

### 2.2.2 Cavitation Bubble Dynamics

Cavitation is generally known to be a fluid transportation problem that damages the transport machineries. However, recent research has proven that controlled cavitation is a highly effective tool for intensification of physical and chemical processes. As noted earlier, the principal cause behind cavitation, which is nucleation, growth, oscillations and transient collapse of small gas bubbles due to pressure variation or in general, energy dissipation in the system. On the basis of this criterion, cavitation can be categorized as: *Acoustic cavitation*—which results due to pressure variation generated due to passage of an acoustic wave, and *Hydrodynamic cavitation*—which results due to pressure variation in the liquid flow due to change in the flow geometry. Theoretically, cavitation refers to creation of voids in the liquid medium by overcoming the Laplace pressure ( $2\sigma/R$ ), which would require extremely high acoustic pressure amplitudes exceeding  $\sim 100$  MPa. Practically, actual cavitation occurs at low pressure amplitudes that are attributed to phenomenon of nucleation. Nucleation occurs due to presence of solid particles or tiny free-floating bubbles present in the liquid that act as nuclei. Another source of nuclei is the gas pockets trapped in the crevices of the solid boundaries in the liquid medium. These gas pockets can grow in response to reduction in ambient pressure with passage of acoustic wave [19].

### 2.2.3 Radial Motion of Cavitation Bubbles

The periodic pressure variation caused by propagation of ultrasound wave gives rise to volume oscillations of cavitation bubbles. The amplitude of the volume

oscillations of the cavitation bubbles is a function of amplitude of the acoustic wave. For relatively small acoustic pressure amplitudes, the volume oscillations of the bubble are small-driven mainly by the pressure forces, and essentially in phase with the acoustic wave. For larger pressure amplitudes (typically greater than static pressure in the medium), the volumetric oscillations of the cavitation bubble become non-linear—comprising of an initial explosive growth followed by a transient collapse and few after-bounces. In this case, the volume oscillations (or radial motion) of the bubble are governed by pressure as well as inertial forces [20]. The model for radial motion of cavitation bubbles has been a subject of investigation for more than 100 years. The first-ever mathematical analysis of an empty cavity collapsing under constant static pressure was given by Rayleigh [21]. This analysis was improved in later years by several researchers to include the effects of surface tension and viscosity of liquid. Presence of non-condensable gas and solvent vapor inside the bubble was also accounted for. The popular Rayleigh–Plesset–Noltingk–Neppiras–Poritsky [22–24] equation for radial motion of bubble is as follows (Eq. 2.1):

$$R \frac{d^2 R}{dt^2} + \frac{3}{2} \left( \frac{dR}{dt} \right)^2 = \frac{1}{\rho} \left[ \left( P_o + \frac{2\sigma}{R_o} - P_v \right) \left( \frac{R_o}{R} \right)^{3\gamma} + P_v - \frac{2\sigma}{R} - \frac{4\mu}{R} \frac{dR}{dt} - (P_o + P(t)) \right] \quad (2.1)$$

The above equation did not account for liquid compressibility, which becomes a dominant factor as the bubble wall velocity ( $dR/dt$ ) becomes closer or even exceeds the sonic velocity in the medium. Later research in this area addressed this facet of bubble dynamics. The first model for cavitation bubble dynamics accounting for liquid compressibility effect was proposed by Gilmore [25] using Kirkwood–Bethe hypothesis [26] and Tait equation of state for liquid medium. Major developments occurred in this area during the subsequent years by Keller and Kolodoner [27], Keller and Miksis [28] and Prosperetti and Lezzi [29] have resulted in more rigorous forms of models for radial motion of cavitation bubbles. Two most popular equations for cavitation bubble dynamics among scientific community in bubble dynamics and sonoluminescence are:

1. Keller and Miksis equation [28, 30]:

$$\left( 1 - \frac{\dot{R}}{c} \right) R \ddot{R} + \left( 1 - \frac{3\dot{R}}{c} \right) \frac{3}{2} \dot{R}^2 = \frac{1}{\rho} \left( 1 + \frac{\dot{R}}{c} \right) [p_g - P_o - P(t)] + \frac{\dot{R}}{\rho c} \frac{dp_g}{dt} - 4v \frac{\dot{R}}{R} - \frac{2\sigma}{\rho R} \quad (2.2)$$

In this equation the term  $d^2(R^2\dot{R})/dt^2$  is calculated using Rayleigh–Plesset equation itself for the condition  $\dot{R}/c \sim 1$ , when the sound radiation by the bubble becomes important.

2. Another important variant of the bubble dynamics equation is the model proposed by Lofstedt et al. [31] and Barber et al. [32], in which all prefactors in the parantheses containing  $\dot{R}/c$  are deleted. This leads to the equation:

$$R\ddot{R} + \frac{3}{2}\dot{R}^2 = \frac{1}{\rho}[p_g - P_o - P(t)] + \frac{\dot{R}}{\rho c} \frac{dp_g}{dt} - 4v\frac{\dot{R}}{R} - \frac{2\sigma}{\rho R} \quad (2.3)$$

### 2.2.4 Modeling of the Sonochemical and Sonophysical Effects

The passage of ultrasound wave through the medium gives rise to sinusoidal pressure variation in the medium. The cavitation bubbles grow from the nuclei in the medium during the rarefaction half cycle of ultrasound, when the pressure in the medium falls sufficiently below the ambient or static pressure. If the pressure amplitude of the ultrasound wave is sufficiently high, the bubble undergoes an explosive growth to several times its original size in the rarefaction half cycle of ultrasound. This expansion is accompanied by large evaporation of water at the bubble interface. The vapor molecules diffuse towards the core of the bubble after evaporation into the bubble. The vapor transport in the bubble is a crucial aspect of the cavitation bubble dynamics. This matter has been treated by numerous authors with different approaches [13, 33–41]. A review of literature treating vapor transport across bubble interface during radial motion and the entrapment of vapor in the bubble during transient collapse has been provided in our earlier paper [42].

The general treatment of the vapor transport and entrapment in the cavitation bubble was given by Storey and Szeri [43] in a landmark paper published in 2000. Storey and Szeri coupled the Navier–Stokes equations for gas mixtures in the bubble to the reaction mechanism between species in the bubble. The transport properties (thermal and mass diffusion and viscosity) were calculated from equations based on Chapman–Enskog theory and the equation of state was Redlich–Kwong–Soave type. Storey and Szeri [43] showed that in the compression phase of radial bubble motion, counter diffusion of the vapor molecules occurs with condensation at the bubble wall. The rate of transport of vapor molecules is proportional to the difference between partial pressure of liquid in the bubble and the saturation (or vapor) pressure at the bubble interface. However, not all of the vapor molecules that approach the bubble interface stick to it, giving rise to non-equilibrium phase change. The fraction of vapor molecules that stick to the bubble interface is the accommodation coefficient. The lower the value of this parameter, the greater the resistance to condensation and the higher the amount of vapor entrapped. The principal result of the study of Storey and Szeri was that water vapor transport in the bubble is a two-step process, i.e. diffusion to the bubble wall and condensation at the wall. Thus, it is influenced by two time scales, viz. time scale of diffusion ( $t_{\text{dif}}$ ) and time scale of condensation ( $t_{\text{cond}}$ ) [44], and their magnitudes relative

to the time scale of bubble dynamics,  $t_{\text{osc}}$ . In the initial phase of bubble collapse  $t_{\text{osc}} \gg t_{\text{diff}}, t_{\text{cond}}$ , due to which the phase change at the bubble interface is in equilibrium, and the concentration of vapor molecules at the bubble interface is essentially same as that in the bubble core. As the bubble wall acceleration increases during collapse, the time scales of bubbles dynamics and vapor diffusion becomes equal. At this stage, the rate of reduction of vapor molecules in the central region of the bubble is less than that at the bubble wall. With further acceleration of the bubble wall,  $t_{\text{osc}} \ll t_{\text{diff}}$  condition is reached, and the vapor molecules have insufficient time to diffuse to the bubble wall, which results in a fixed and uneven distribution of vapor molecules in the bubble. At this condition, the bubble composition is “frozen” and the vapor present inside the bubble is essentially “trapped” in the bubble.

Another mechanism which traps vapor molecules inside the bubble is the non-equilibrium phase change at the bubble wall. In the final moments of bubble collapse, when  $t_{\text{osc}} \ll t_{\text{cond}}$ , the condensation or phase change at the bubble wall is non-equilibrium in that not all vapor molecules that approach the bubble wall can escape the bubble by undergoing phase change, and get trapped in the bubble. The exact mechanism by which water vapor gets trapped in the bubble is determined by relative magnitudes of  $t_{\text{osc}}, t_{\text{cond}}$  and  $t_{\text{diff}}$ . When the bubble dynamics time scale is smaller than either diffusion or condensation time scale, it leads to entrapment of the vapor. Storey and Szeri [43] showed that the condition  $t_{\text{osc}} \ll t_{\text{diff}}$  is reached well before the condition of  $t_{\text{osc}} \ll t_{\text{cond}}$ . Thus, the contribution to vapor entrapment from diffusion mechanism is more than the condensation mechanism or in other words, vapor transport in the bubble is a diffusion limited process. The entrapped vapor and gas molecules in the bubble are subjected to extreme conditions generated during transient collapse due to which they undergo thermal dissociation to several chemical species—some of which are radical species which induce the sonochemical effect.

In view of the results of Storey and Szeri [43, 45], Toegel et al. [46] developed a simple diffusion limited model using boundary layer approximation, which has become immensely popular among the sonochemical community. This model, based on ordinary differential equations, has distinct merits of being simple yet physically realistic. This model has been validated against the full partial differential equation (PDE) model of Storey and Szeri [43, 45]. This model does not take into account the rectified diffusion of non-condensable gas across the bubble during radial motion, as the time scale of this diffusion, approximated by ratio  $R_0^2/D$ , is of the order of milliseconds (100 ms for typical values of  $R_0 \sim 10 \mu\text{m}$  and  $D = 10^{-9} \text{m}^2/\text{s}$ ), while the bubble motion time scale is of the order of microseconds (50  $\mu\text{s}$  for 20 kHz). As a result of large difference in the two time scales, practically no diffusion of gas occurs across bubble interface for the radial motion of few hundreds of acoustic cycles, and hence, the approximation of neglecting gas diffusion is good [47]. Another important assumption made while estimation of the sonochemical effect is that of prevalence of chemical equilibrium in the bubble all through radial motion. This assumption is again based on the relative time scales of reactions occurring inside the bubble and the timescale of bubble

dynamics. As the temperature and the pressure in the bubble at the point of maximum compression is extreme ( $\sim 5,000$  K and  $\sim 50$  MPa), and also that the concentration of different chemical species is very high due to extremely small volume. The rates of various reactions occurring between these species are also very high. As a result, chemical equilibrium prevails in bubbles all along during the radial motion [14, 42].

The essential equations and thermodynamic data of the diffusion limited ordinary differential equation (ODE) model are given in Tables 2.1 and 2.2 [48]. The main components of this model are: (1) Keller-Miksis equation for radical motion of cavitation bubbles, (2) Equation for the diffusive flux of solvent vapor through the bubble wall, (3) Equation for heat conduction across bubble wall and (4) Overall energy balance treating the cavitation bubble as an open system. The transport parameters for the heat and mass transfer are determined using Chapman–Enskog theory with Lennard–Jones 12–6 potential at the bulk temperature of the liquid [49–52]. The thermal and diffusive penetration depths are estimated using dimensional analysis from the radial motion of cavitation bubbles assuming that the condensation of vapor molecules at bubble interface is fast enough to maintain equilibrium. Thus the instantaneous diffusive penetration depth for mass transfer is given by Eq. 2.4:

$$l_{diff} = \sqrt{D_{ij}t_{osc}} \quad (2.4)$$

where  $D_{ij}$  is the binary diffusion coefficient and  $t_{osc}$  is the time scale of bubble oscillation taken as  $R/|dR/dt|$ . At the instance of maximum compression or minimum radius, the bubble wall velocity  $|dR/dt| = 0$ , and the above equation has a singularity. However, at the instance of minimum radius, the bubble is essentially a stagnant sphere, and the mass transfer is a purely diffusional process. Using the series solution for mass transfer through sphere [53], the upper limit for the diffusive penetration depth is found to be  $R/\pi$ . Thus, the mass diffusive penetration depth is given by Eq. 2.5:

$$l_{diff} = \min\left(R/\pi, \sqrt{RD_{ij}/|dR/dt|}\right) \quad (2.5)$$

Similar analysis can also be given for thermal diffusion, and the thermal diffusive length is given by Eq. 2.6:

$$l_{th} = \min\left(R/\pi, \sqrt{R\kappa/|dR/dt|}\right) \quad (2.6)$$

### 2.2.5 Numerical Solution

The set of 4 simultaneous ODEs in Table 2.1 can be solved using Range–Kutta 4th order–5th order adaptive step size method [54]. The cavitation bubble reaches extremely energetic and highly unstable state at the instance of maximum compression (or minimum radius) and may collapse. The word “collapse” essentially

**Table 2.1 a** The diffusion-limited model for the radial motion of cavitation bubble. **b** Thermodynamic properties of various species

Model component	Equation	Initial value
1. Radial motion of the cavitation bubble	$\left(1 - \frac{dR/dt}{c}\right) R \frac{d^2R}{dt^2} + \frac{3}{2} \left(1 - \frac{dR/dt}{3c}\right) \left(\frac{dR}{dt}\right)^2$ $= \frac{1}{\rho_L} \left(1 + \frac{dR/dt}{c}\right) (P_i - P_l) + \frac{R}{\rho_L c} \frac{dP_i}{dt} - 4v \frac{dR/dt}{R} - \frac{2\sigma}{\rho_L R}$	At $t = 0$ , $R = R_0$ , $dR/dt = 0$
2. Diffusive flux of solvent (methanol) molecules	<p>Internal pressure in the bubble: <math>P_i = \frac{N_i \mu_i(t) kT}{[4\pi(R^3(t) - R_0^3)/3]}</math></p> <p>Pressure in bulk liquid medium: <math>P_l = P_0 - P_A \sin(2\pi f t)</math></p> $\frac{dN_S}{dt} = 4\pi R^2 D_S \left. \frac{\partial C_S}{\partial r} \right _{r=R} \approx 4\pi R^2 D_S \left( \frac{C_{S,R} - C_S}{l_{diff}} \right)$	At $t = 0$ , $N_S = 0$
3. Heat conduction across bubble wall	<p>Instantaneous diffusive penetration depth: <math>l_{diff} = \min\left(\sqrt{\frac{RD_S}{ dR/dt }}, \frac{R}{\pi}\right)</math></p> $\frac{dQ}{dt} = 4\pi R^2 \lambda \left. \frac{\partial T}{\partial r} \right _{r=R} \approx 4\pi R^2 \lambda \left(\frac{T_0 - T}{l_h}\right)$ <p>Thermal diffusion length: <math>l_h = \min\left(\sqrt{\frac{R\kappa}{ dR/dt }}, \frac{R}{\pi}\right)</math></p>	At $t = 0$ , $Q = 0$
4. Overall energy balance	$C_{V,mix} dT/dt = dQ/dt - P_l dV/dt + (h_S - U_S) dN_S/dt$ <p>Mixture heat capacity: <math>C_{V,mix} = \sum C_{V,i} N_i</math> (<math>i = N_2/O_2/Solvent</math>)</p> <p>Molecular properties of solvent:</p> <p>Enthalpy: <math>h = \left(1 + \frac{f_i}{2}\right) kT_0</math></p> <p>Internal energy: <math>U_S = N_S kT \left(3 + \sum_{i=1}^3 \frac{\theta_i/T}{\exp(\theta_i/T) - 1}\right)</math></p> <p>Heat capacity of various species (<math>i = N_2/O_2/Solvent</math>):</p> $C_{V,i} = N_i k \left( \frac{f_i}{2} + 2 + \sum (\theta_i/T)^2 \exp(\theta_i/T) / (\exp(\theta_i/T) - 1)^2 \right)$	At $t = 0$ , $T = T_0$

(continued)

Table 2.1 (continued)

Species	Degrees of freedom (translational + rotational) ( $f$ )	Lennard-Jones force constants		Characteristic vibrational temperatures $\theta$ (K)
		$\sigma$ ( $10^{-10}$ m)	$\epsilon/k$ (K)	
N <sub>2</sub>	5	3.68	92	3,350
O <sub>2</sub>	5	3.43	113	2,273
CH <sub>3</sub> OH	6	3.626	481.8	500.59, 1,674.41, 1,708.94, 1,854.22, 2,169.26, 2,356.26, 2,376.4, 2,392.22, 4,581.62, 4,649.23, 4,752.8, 5,923.74
Ar	3	3.42	124	—
H <sub>2</sub> O	6	2.65	380	2,295, 5,255, 5,400

<sup>a</sup> Data taken from Toegel [48], Hirschfelder et al. [49], Reid et al. [50], Davis [51], Condon and Odishaw [52]

**Notations**  $R$ —radius of the bubble;  $dR/dt$ —bubble wall velocity;  $c$ —velocity of sound in bulk liquid medium;  $\rho_L$ —density of the liquid;  $\nu$ —kinematic viscosity of liquid;  $\sigma$ —surface tension of liquid;  $\lambda$ —thermal conductivity of bubble contents;  $\kappa$ —thermal diffusivity of bubble contents;  $\theta$ —characteristic vibrational temperature(s) of the species;  $N_S$ —number of solvent molecules in the bubble;  $N_{N_2}$ —number of nitrogen molecules in the bubble;  $N_{O_2}$ —number of oxygen molecules in the bubble;  $t$ —time;  $D_S$ —diffusion coefficient of solvent vapor;  $C_S$ —concentration of solvent molecules in the bubble;  $C_{S,R}$ —concentration of solvent molecules at the bubble wall or gas-liquid interface;  $Q$ —heat conducted across bubble wall;  $T$ —temperature of the bubble contents;  $T_\sigma$ —ambient (or bulk liquid medium) temperature;  $k$ —Boltzmann constant;  $h_S$ —molecular enthalpy of solvent;  $U_S$ —internal energy of solvent molecules;  $f$ —translational and rotational degrees of freedom;  $C_{V,i}$ —heat capacity at constant volume for species  $i$ ;  $N_{\text{tot}}$ —total number of molecules (gas + vapor) in the bubble;  $h$ —van der Waal's hard core radius;  $P_0$ —ambient (bulk) pressure in liquid;  $P_A$ —pressure amplitude of ultrasound wave;  $f$ —frequency of ultrasound wave

**Table 2.2 a** Summary of simulation results. Conditions at the first compression of the cavitation bubble. **b** Summary of simulation results. Equilibrium composition of the cavitation bubble contents in methanol at collapse conditions

<b>a</b>		
Parameter	Liquid medium	
	Methanol	Oil
$T_{\max}$ (K)	810	727
$P_{\max}$ (bar)	1,455	7.37
$N_{\text{MeOH}}$	3.88E+011	–
$V_{\text{turb}}$ (m/s)	0.0205	0.00277

<b>b</b>	
Species	Equilibrium composition (mole fraction)
CH <sub>4</sub>	7.3213E–01
H <sub>2</sub> O	2.2833E–01
H <sub>2</sub>	2.0609E–02
CO <sub>2</sub>	1.8203E–02
C <sub>2</sub> H <sub>6</sub>	3.1621E–04
CO	4.1087E–04
CH <sub>3</sub> OH	1.5522E–07
C <sub>2</sub> H <sub>4</sub>	1.2378E–07
CH <sub>3</sub> COOH	2.8683E–08
HCOOH	1.3946E–08
H <sub>2</sub> CO	2.4576E–08

Reprinted with permission from [70], Copyright © 2009, American Chemical Society

**Notations**  $T_{\max}$ —temperature peak reached in the bubble at the time of first collapse;  $P_{\max}$ —pressure peak reached in the bubble at the time of first collapse;  $N_{\text{MeOH}}$ —number of methanol molecules trapped in the bubble at the instance of first collapse;  $V_{\text{turb}}$ —bulk liquid velocity (or the microturbulence velocity) generated by the cavitation bubbles

means fragmentation of the bubble [55, 56]. For conditions of maximum shape and flow instability, the cavitation bubble fragmentation can occur at the first compression after an initial expansion. Thus, for determination of the chemical composition of the contents of cavitation bubble using thermodynamic equilibrium approximation, the temperature and pressure inside the bubble can be taken at the instance of first compression.

### 2.2.6 Physical Effects of Cavitation Bubble

Ultrasound and cavitation render several physical effects on a reaction system. The main manifestation of all of these results is generation of intense micro-convection and micro-mixing in the reaction system. A brief description of all physical effects of ultrasound and cavitation is given below [9–12]:



*Micro-streaming:* This is essentially small amplitude oscillatory motion of fluid elements around a mean position, which is induced by propagation of ultrasound wave. The velocity of micro-turbulence is given as:  $u = P_A/\rho C$ , where  $P_A$ —pressure amplitude of acoustic wave,  $\rho$  is the density of the medium and  $C$  is the velocity of sound in the medium. For a typical ultrasound wave with pressure amplitude of 120 kPa in water ( $\rho = 1,000 \text{ kg/m}^3$ ,  $C = 1,500 \text{ m/s}$ ), the micro-streaming velocity = 0.08 m/s.

*Acoustic streaming:* During propagation of ultrasound wave, the momentum of the wave is absorbed by the medium due to finite viscosity. This results in setting up of low velocity unidirectional currents of the fluid known as acoustic streaming [57, 58]. The phenomenon of acoustic streaming also occurs in the vicinity of solid boundaries in the medium, where the oscillatory motion of fluid elements is obstructed and results in setting up of unidirectional current parallel to the boundary.

*Microturbulence:* The oscillatory motion of fluid induced by an oscillatory bubble in its vicinity is called microturbulence. This phenomenon is explained as follows: in the expansion phase of radial motion of the cavitation bubble, the liquid is displaced away from bubble interface. During the collapse phase the liquid is pulled towards the bubble as it fills the vacuum created in the liquid with size reduction of bubble. The mean velocity of microturbulence depends on the amplitude of bubble oscillation. However, it was noted that phenomenon of microturbulence is restricted only in the region in close vicinity of the bubble. The microturbulence velocity diminishes very rapidly away from the bubble.

*Acoustic (or shock) waves:* During the compression phase of radial motion, as the bubble contracts void space is created in the liquid, and the fluid element spherically converge (or essentially “gush”) in this void space and work is done on the bubble. For a cavitation bubble containing non-condensable gas such as air, the adiabatic compression results in rapid rise of pressure inside the bubble. At the point of minimum radius (or maximum compression), the bubble wall comes to a sudden halt. At this instance, the fluid elements converging towards the bubble are reflected back from the interface. This reflection creates a high pressure shock wave that propagates through the medium. The pressure exerted by the non-condensable gas inside the bubble causes rebound of the bubble.

*Microjets:* During radial motion driven by ultrasound wave, the cavitation bubble maintains spherical geometry as long as the motion of liquid in its vicinity is symmetric and uniform, and thus there are no pressure gradients. If the bubble is located close to a phase boundary, either solid–liquid, gas–liquid or liquid–liquid, the motion of liquid in its vicinity is hindered, resulting in development of pressure gradient around it. This non-uniformity of pressure results in the loss of spherical geometry of the bubble. Numerous authors [59–67] have investigated this phenomenon in the past three decades—either theoretically (numerical simulations) or experimentally (high speed photography). During the asymmetric radial motion, the portion of bubble exposed to higher pressure collapses faster than rest of the bubble, which gives rise to the formation of a high speed liquid jet. However, the direction of this jet depends on the characteristics of the solid

boundary. Rigid boundaries such as metal surfaces are characterized by the boundary condition:  $\nabla \cdot \phi = 0$ , where  $\phi$  is velocity potential at the boundary, while free boundaries (or pressure release boundaries such as gas–liquid interface) are characterized by condition  $\phi = 0$ . For a rigid boundary, the microjet is directed towards the boundary, while for a free boundary, the microjet is directed away from the boundary. The velocity of these microjets has been estimated in the range of 120–150 m/s [59–67]. In case of rigid boundaries, these jets can cause severe damage at the point of impact and can erode the surface.

## 2.3 Discerning the Physical Mechanism of an Ultrasonic Process

### 2.3.1 Discriminating Between Physical and Chemical Effects

The bubble dynamics model described earlier (Sect. 2.2.4) offers an efficient tool to estimate the physical and chemical effects of cavitation, and also to discriminate between them. Sonophysical and sonochemical effects mentioned earlier are induced by transient cavitation. The radial bubble motion is governed by two forces: viz. pressure force and inertial force. For transient cavitation to occur, the pressure amplitude of the ultrasound wave driving has to exceed a minimum level or limit, known as transient cavitation threshold. For acoustic pressure amplitudes above this threshold value, the bulk pressure in the medium falls to sufficiently low values below the ambient pressure of 101.3 kPa in the rarefaction half cycle of the wave, and the radius of the cavitation bubble expands to more than double of its original size. Since the bubble motion is dominated by inertial force, the bubble keeps on expanding even after completion of rarefaction half period [13, 20]. The ensuing collapse phase is also dominated by inertial force. The spherical convergence of fluid elements imparts high kinetic energy to the bubble causing a transient collapse that generates extreme condition of temperature and pressure as mentioned earlier. The transient cavitation threshold is mainly a function of the frequency of the ultrasound wave and the initial size of the cavitation bubble [15]. However, if the size of the cavitation bubble is far smaller than the resonant size corresponding to the frequency, the transient cavitation threshold is essentially same as the static pressure in the medium [15]. This approximation applies to bubbles in the size range of 1–10  $\mu\text{m}$  and frequencies in the range of 20–100 kHz, which is the typical range of power ultrasound used in physical and chemical processing.

Discriminating between the physical and chemical effects of ultrasound and cavitation would essentially mean elimination of the transient cavitation, while leaving the ultrasound wave phenomenon unaltered. A simple technique to achieve this is to raise the static pressure of the medium, so that fall in the bulk pressure in the medium during rarefaction half cycle of the acoustic wave is reduced. The acoustic pressure amplitudes in commercial ultrasound equipment rarely exceed 200 kPa. Therefore, raising the static pressure of the medium to even moderate values of 400–500 kPa can help achieve complete elimination of the transient

cavitation [68] and the associated effects such as generation of radicals and shock-waves. However, since the liquid properties such as density, viscosity and surface tension remain practically same at 100 and 500 kPa, the ultrasound wave propagation is not influenced by elevated static pressure. Especially the phenomenon of strong micro-mixing induced by micro-streaming remains unchanged. Therefore, at elevated static pressure the ultrasonic system is essentially equivalent to mechanically stirred system, yet with mixing on micro-scale instead of bulk scale as in the case of conventional mechanical agitation.

We have extensively used the technique of elevated static pressure in our studies of different biofuels systems. The following sections of this chapter show application of elevated static pressure for many biofuel systems.

## 2.4 Mechanistic Insight into Ultrasound Enhanced Biofuels Processes

In this section, a summary of our studies in mechanistic investigations of different biofuels systems is given. The main approach in these studies has been to identify the exact role played by ultrasound and cavitation in the enhancement of process, and to identify and discriminate the contribution of physical and chemical effects of ultrasound and cavitation. Initially, we describe our major results and findings for different individual biofuels systems; and finally, we present a broad overview and analysis of these findings, which gives a cogent and coherent picture of the exact role of ultrasound and cavitation in the field of biofuels.

### 2.4.1 *Microalgal Lipid Extraction*

Microalgal route to biodiesel has been extensively investigated in the past one decade. The lipids produced by certain species of microalgae are potential feedstock for biodiesel that can be substituted for vegetable oil. Efficient extraction of these lipids is an important step in the biodiesel synthesis. Ranjan et al. [69] made a mechanistic assessment of this process. The relative contribution of two principal mechanisms of extraction of lipids, viz. cell disruption and diffusion across cell wall, to the overall lipid yield was determined. Three processes for extraction of lipids were assessed with three conventional methods, viz. Soxhlet extraction, Bligh and Dyer method and sonication. Two types of solvents were used for extraction, viz. n-hexane and mixture of chloroform and methanol. Sonication of the biomass mixture was carried out with both types of solvents. Simulations of cavitation bubble dynamics were carried out for both n-hexane and chloroform–methanol solvents. Microscopic analysis of the algal biomass after extraction was also done (Fig. 2.1). The trend in extent of lipid extraction was found as follows: Soxhlet extraction (n-hexane)  $\approx$  sonication with n-hexane < Bligh and Dyer method with chloroform–methanol  $\ll$  sonication with chloroform–methanol.

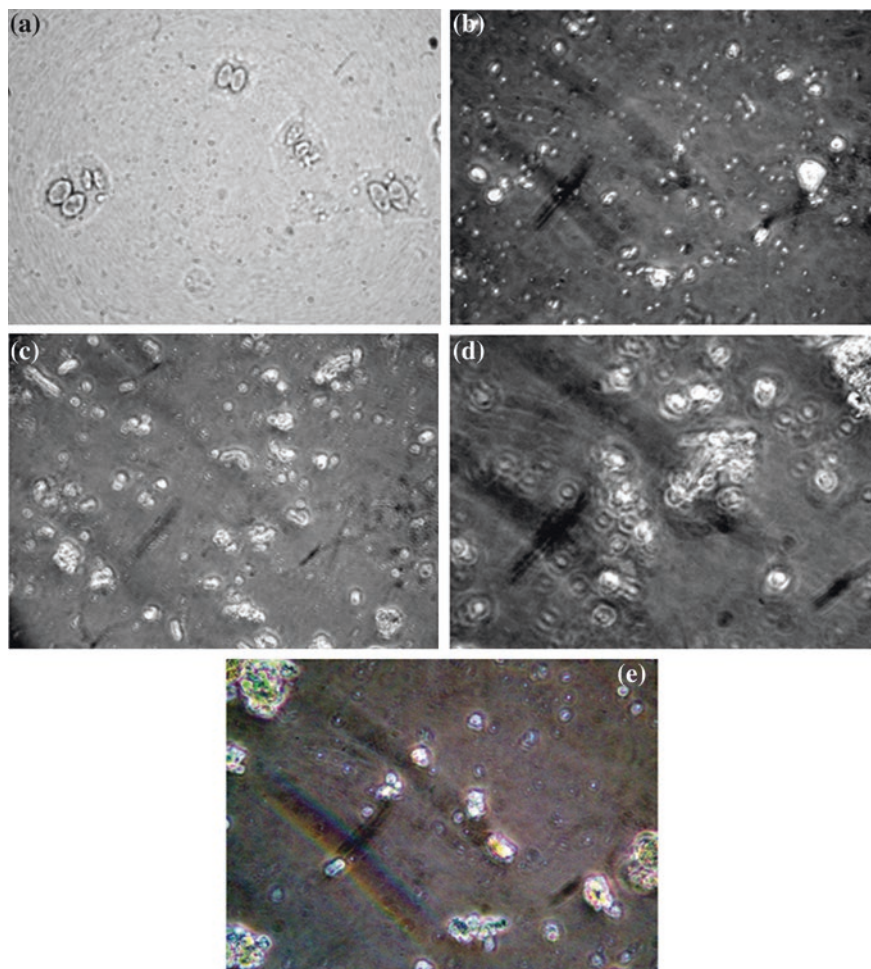
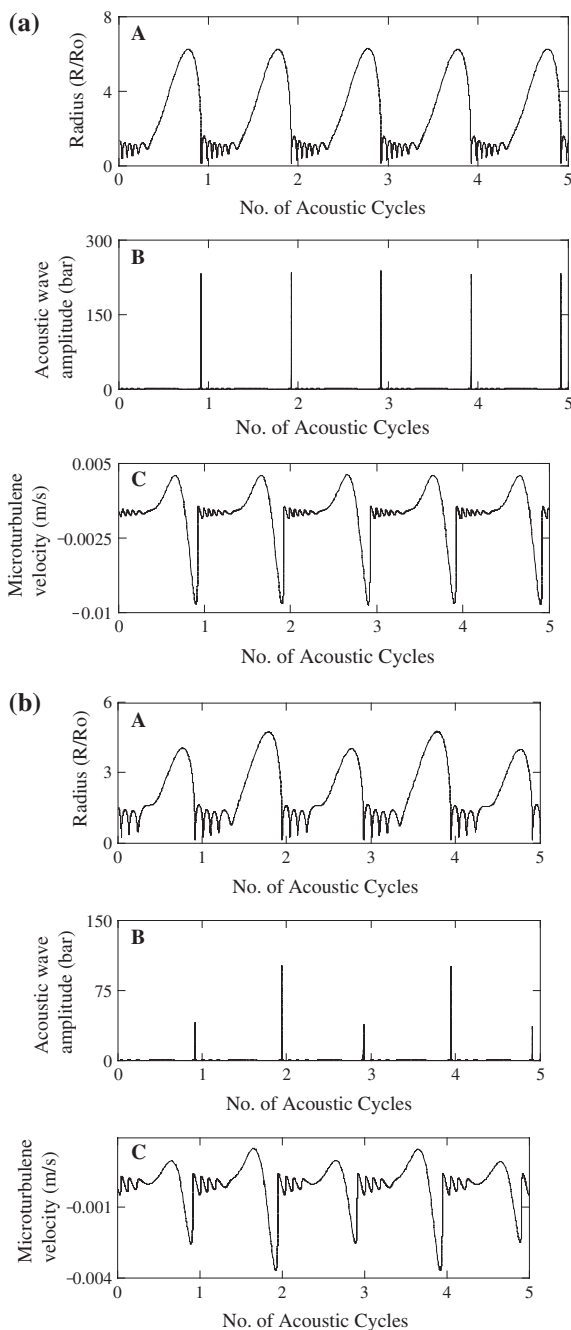


**Fig. 2.1** Representative micrographs of the algal biomass before and after extraction of lipids with various techniques. **a** Original algal cells of *Scenedesmus* sp.; **b** biomass after extraction with soxhlet apparatus; **c** biomass after extraction with Bligh and Dyer method; **d** biomass after extraction using sonication with n-hexane as solvent; **e** biomass after extraction using sonication with chloroform-methane mixture as solvent. Reprinted with permission from [69], Copyright © 2010, American Chemical Society

The micrographs of algal biomass revealed no disruption of biomass with Soxhlet extraction (indicating diffusion as the only mechanism of lipid extraction; while Bligh and Dyer method as well as sonication indicated disruption of biomass indicating both cell disruption and diffusion as the possible mechanisms.

Simulations of cavitation bubble dynamics indicated microturbulence as well as shock waves of much higher magnitude for n-hexane as solvent than chloroform-methanol (Fig. 2.2a, b). It was an interesting anomaly that despite stronger

**Fig. 2.2 a** Simulations of the radial bubble motion and its physical effects in *n*-hexane. Time history of (A) normalized bubble radius ( $R/R_0$ ); (B) acoustic waves emitted by bubble; (C) velocity of microturbulence generated by the bubble. Reprinted with permission from [69], Copyright © 2010, American Chemical Society. **b** Simulations of the radial bubble motion and its physical effects in chloroform-methanol. Time history of (A) normalized bubble radius ( $R/R_0$ ); (B) acoustic waves emitted by bubble; **c** velocity of microturbulence generated by the bubble. Reprinted with permission from [69], Copyright © 2010, American Chemical Society



turbulence generated in n-hexane, extraction of lipids with mixture of chloroform-methanol as solvent was higher. These results brought out following mechanistic facts of ultrasound-assisted microalgal lipid extraction: (1) shock waves originating from transient cavitation are capable of disrupting microalgal cells causing rapid release of lipids. However, the extent of disruption depended on the probability of interaction of cells with cavitation bubbles. This probability would depend on the density of microalgal cells in the medium.

Due to rather dilute solution of microalgal biomass, the probability of cell-bubble interaction was low, and hence, complete disruption of biomass was not achieved. This phenomenon put limitations on the contribution of disruption mechanism to overall extraction of lipids, and thus, diffusion across cell wall was a major factor. (2) The extent of lipid extraction by process of convective diffusion (which is far slower than lipid extraction by cell disruption) depends on the intensity of bulk convection in the medium.

In case of sonication, the convection in the medium is generated by microstreaming and microturbulence. The second governing factor is the selectivity of solvents. The chloroform-methanol mixture, being polar in nature, will have much higher selectivity and partition coefficient than the non-polar hexane. Despite higher convection in n-hexane, greater extraction of lipids in chloroform-methanol mixture clearly indicated that solvent selectivity or partition coefficient is the dominant factor in lipid extraction than the intensity of convection in the medium. The role of ultrasound in the extraction process seemed to be more of physical nature in that intense convection generated by ultrasound and cavitation sweeps away lipids diffused out of cell wall from the liquid-microalgae interfacial region, thus maintaining a constant concentration gradient for the continuous diffusion of lipids from the cells.

#### ***2.4.2 Ultrasonic Synthesis of Biodiesel***

Biodiesel, which essentially is alkyl esters of fatty acids, is synthesized by the esterification/transesterification reaction with either an acid or alkali catalyst. Our first investigation in ultrasound-assisted biodiesel synthesis aimed at discerning the individual contributions of physical and chemical effects of transient cavitation towards the transesterification reaction. Kalva et al. [70] conducted experiments in following categories to deduce the possible ultrasonic enhancement of transesterification: (1) no addition of external base catalyst so that the transesterification reaction would be initiated by methoxide radicals produced by reaction between OH radicals generated by transient cavitation and the methanol molecules; (2) addition of  $\text{Fe}^{2+}$  to methanol so that the Fenton reaction between  $\text{Fe}^{2+}$  and OH radicals generated by transient cavitation would result in in situ generation of  $\text{OH}^-$  ions, which would then react with methanol to generate methoxide ions for transesterification. No biodiesel was produced with these techniques showing that the influence of ultrasound on transesterification reaction system was determined to be of a physical nature. Simulations of cavitation bubble dynamics corroborated this conclusion.



Cavitation can occur both in the oil and methanol phase. Due to large vapor pressure of methanol, large evaporation of methanol molecules takes place inside the bubble. Accordingly, the peak temperature and pressure attained during at transient collapse is reduced. The radial motion of cavitation bubble in methanol and oil has been depicted in Figs. 2.3 and 2.4. The summary of the simulation results has been given in Table 2.2. Although thermal dissociation of methanol molecules occurs during collapse, the species resulting from this are molecular species such as  $\text{CH}_4$ ,  $\text{H}_2\text{O}$ ,  $\text{H}_2$  and  $\text{CO}_2$ . No formation of radical species was seen. This result basically confirmed that intensification of transesterification reaction by ultrasound was due to emulsification effect, which generated enormous interfacial area between oil and methanol phases.

With these results, further experiments were carried out with external addition of the base catalyst and the alcohol to oil molar ratio was varied in the range of 6:1, 12:1, 16:1 and 24:1. Higher yields were obtained in all the experiments at ambient temperature, but quite interestingly, the biodiesel yield passed through a maximum for an alcohol to oil ratio of 12:1. An explanation for this result is given as follows. Although cavitation and ultrasound wave phenomenon occurs in both oil and methanol phase, the velocities of micro-streaming and microturbulence are far higher in methanol due to its viscosity being lower than oil. For molar ratio of 6:1, the methanol phase forms the minor fraction of the reaction mixture, as compared with the oil phase. Thus, the dispersion of methanol in oil phase decides the interfacial area for reaction. Due to high level of microturbulence generated by cavitation bubbles in methanol, the dispersion of methanol in oil phase is uniform. However, the production of methoxy ( $\text{CH}_3\text{O}^-$ ) ions is limited due to smaller volume of methanol, which places a limit on biodiesel yield.

At a molar ratio of 12:1, the equilibrium of methoxide formation reaction shifts favorably towards  $\text{CH}_3\text{O}^-$  and higher concentration of  $\text{CH}_3\text{O}^-$  leads to faster reaction. Moreover, the volume of methanol is still smaller than the oil, making methanol as dispersed phase and oil as continuous phase. Due to stronger microturbulence and micro-streaming in methanol, the dispersion of methanol in oil is uniform, leading to high interfacial area. Combination of higher  $\text{CH}_3\text{O}^-$  concentration and high interfacial area leads to higher yield of biodiesel. As the molar ratio of alcohol to oil increases to 16:1, the volume of oil and methanol in the reaction mixture become comparable; and thus, interfacial area is determined by the dispersion of oil as well. Since the micro-streaming and microturbulence velocities in oil are very low, oil does not get dispersed properly in methanol, and hence, interfacial area reduces. At the highest molar ratio of 24:1, the problem of low dispersion of oil is even more pronounced leading to further reduction in interfacial area. Hence, the kinetics and yield of biodiesel reduces further. The study of Kalva et al. [70] clearly brought out the roles of physical and chemical effects of ultrasound and cavitation in transesterification reaction catalyzed by an alkali.

The experimental framework developed by Kalva et al. has been extended further to acid catalyzed transesterification process by Parker et al. [71]. Acid catalyzed ultrasonic transesterification revealed many interesting mechanistic features,

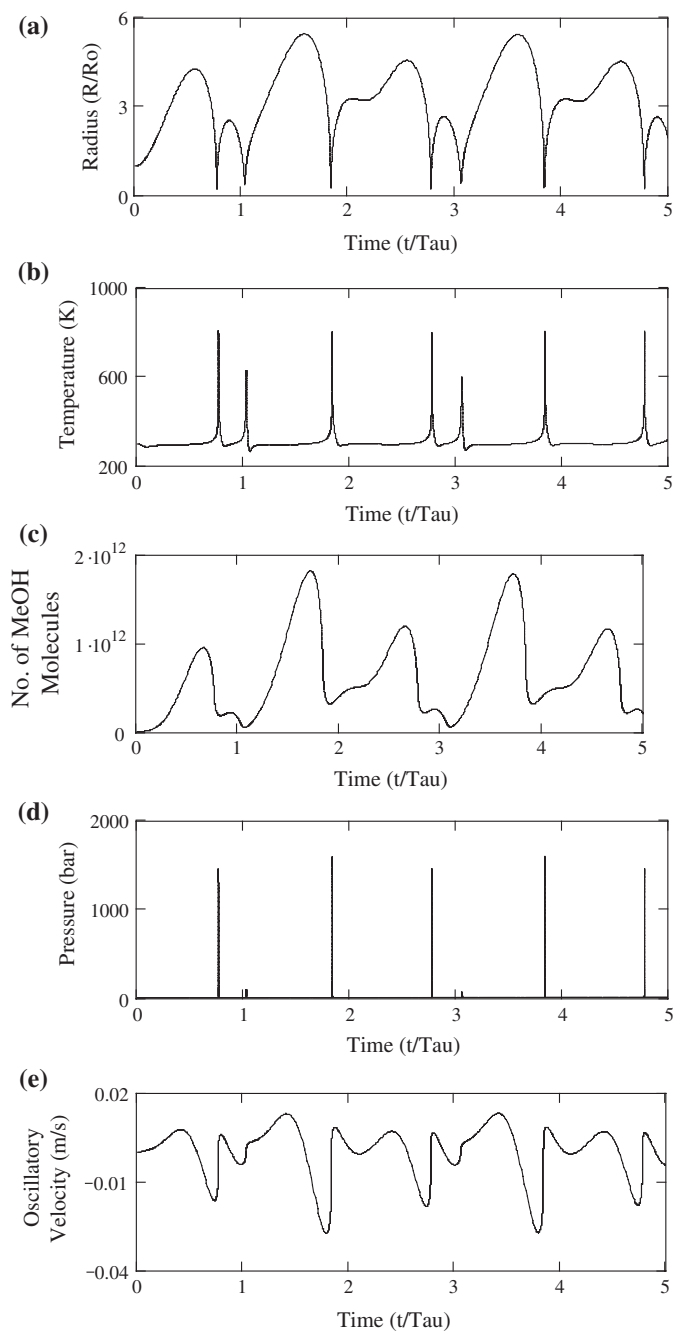


**Fig. 2.3** Simulation results of radial motion of a 10  $\mu\text{m}$  cavitation bubble in methanol medium. Reprinted with permission from [70], Copyright © 2009, American Chemical Society



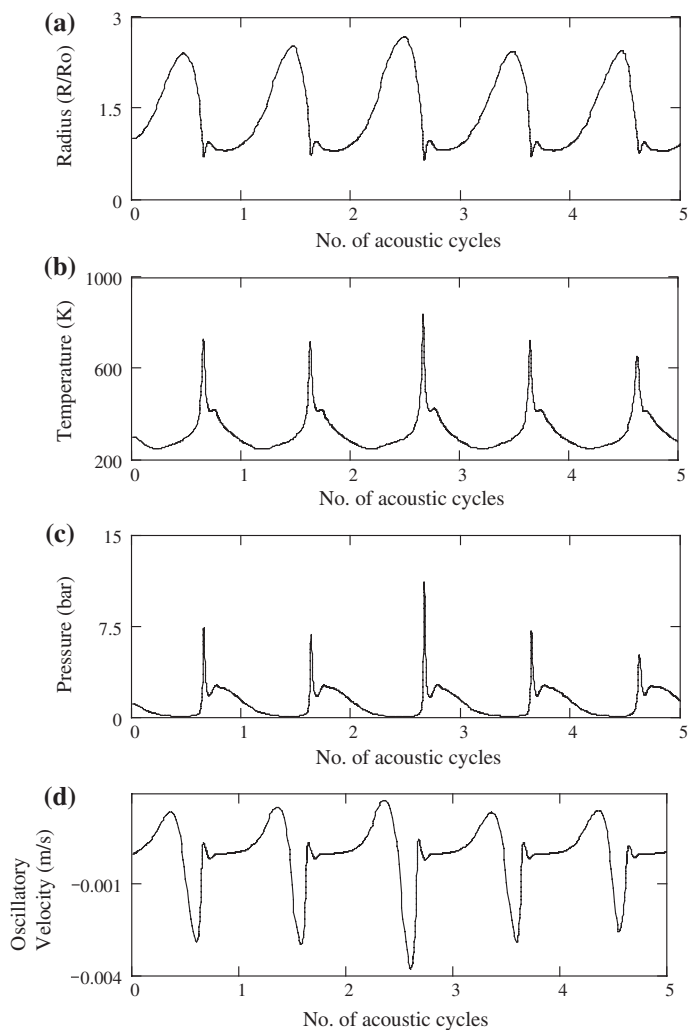
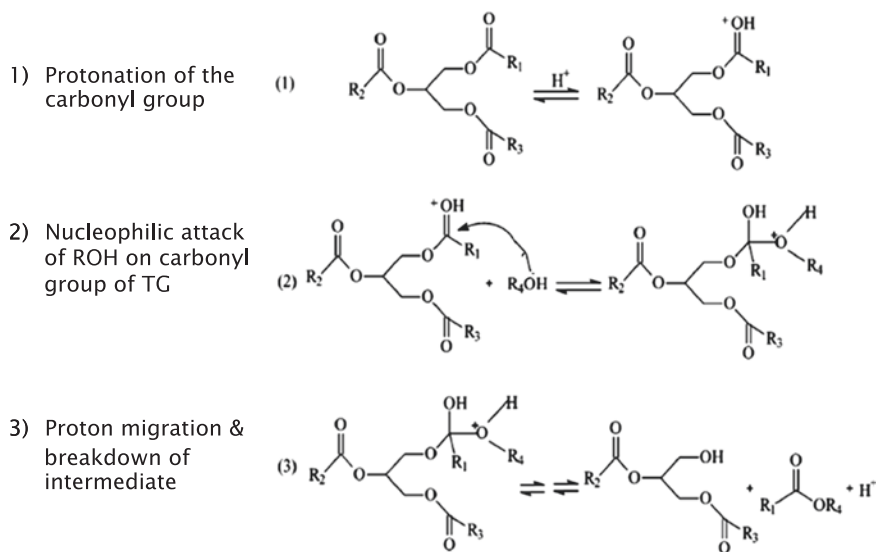


**Fig. 2.4** Simulation results of radial motion of a 10  $\mu\text{m}$  cavitation bubble in oil medium. Reprinted with permission from [70], Copyright © 2009, American Chemical Society

which were quite atypical of base catalyzed reaction. Compared to mechanically agitated systems, ultrasonic transesterification with acid catalyst showed several anomalies such as the occurrence of reaction at a low temperatures (15  $^{\circ}\text{C}$ ), high reaction rate constants for alcohol ratio of 6:1 despite the high activation energy, and a minimum in reaction rate constant at temperatures in the range of 15–65  $^{\circ}\text{C}$ . These results, when correlated with simulation of cavitation bubble dynamics, revealed interesting physical mechanistic facts of acid-catalyzed transesterification.



**Scheme 2.1** Chemical mechanism of acid catalyzed transesterification reaction

Before simulation can be discussed, it is important to note the basic difference in chemical mechanism of transesterification catalyzed by base [70] and acid [71]. Unlike alkoxide anion generated by reaction between alcohol and alkali catalyst in case of base-catalyzed transesterification; it is the direct protonation of triglycerides by acid catalyst that initiates the reaction (Scheme 2.1). Protonation of triglycerides generates electrophilic center on the carbonyl carbon making it susceptible to nucleophilic attack of methanol. Therefore, the rate controlling step for acid catalyzed transesterification is the probability of interaction between proton generated by acid catalyst that is in the methanol phase and the triglyceride that is in the organic phase. With increasing alcohol to oil molar ratio, the concentration of acid catalyst decreases, and so does the probability of interaction between proton and triglyceride—although the macroscopic equilibrium constant shift towards product. Reduction in the concentration of protons with increasing alcohol ratio causes reduction in macroscopic rate constant at any temperature. For the same reason, the highest rate constant and yield is obtained for an alcohol ratio of 6:1, as against 12:1 in case of base-catalyzed process. This result clearly indicates that intrinsic kinetics of acid catalyzed transesterification overwhelms the physical effect of emulsification and enhancement of interfacial area, which eliminate mass transfer effects. However, keeping the parameters for intrinsic kinetic constants the influence of physical effects of ultrasound and cavitation is evident from trends in kinetic constants and yield with temperature.

The numerical simulation of cavitation bubble dynamics in methanol (aqueous phase of reaction mixture) reveals that the intensity of the shock waves generated by cavitation bubble at 15 °C are much higher than those generated at 25 °C. Thus, greater emulsification is achieved at 15 °C resulting in greater interfacial area.

This physical effect overwhelms the intrinsic kinetics at lower temperature, and hence, higher rate constants are seen at 15 °C than at 25 °C. However, as the temperature of the reaction increases further to 45–65 °C the intrinsic kinetics dominates and higher rate constant than at 15 °C are obtained. These results have again demonstrated the physical or mechanistic features of ultrasonic biodiesel synthesis. Parkar et al. [71] also determined the activation energies for different alcohol to oil molar ratios. The least activation energy of 27.53 kJ/mol was obtained for molar ratio of 12:1. Despite the lowest activation energy (which would give the lowest specific rate constant at any temperature), the overall yield and kinetic constant was lower for the molar ratio of 12:1 at 15 °C.

Further mechanistic investigations in ultrasonic biodiesel synthesis were based on statistical design of experiments (DOE) that were coupled with simulation of cavitation bubble dynamics. The reaction systems studied in these investigations were: (1) biodiesel synthesis with heterogeneous base (CaO) catalyst [72]; (2) acid catalyzed (2 step) biodiesel synthesis of *Jatropha* oil; (3) heterogeneous base (CaO) catalysed biodiesel synthesis with *Jatropha curcus* oil; (4) single step ultrasonic and biodiesel synthesis from crude *Jatropha curcus* oil. We give below a brief description of the major results of these studies based on correlation with the simulation of cavitation bubble dynamics model.

1. In the first study, soybean oil was used as feedstock and Box–Behnken statistical design of experiments was employed to optimize the transesterification. The optimization parameters were temperature, alcohol to oil molar ratio and catalyst loading, with transesterification yield as the objective function. The optimum values of these parameters for the highest yield were identified through response surface methodology (RSM) using a quadratic model and analysis of variance (ANOVA). The response surface plots have been depicted in Fig. 2.5. The optimum values of the parameters were: Temperature = 62 °C, molar ratio = 10:1 and catalyst loading of 6 wt%. The activation energy was determined as 82.3 kJ/mol, which was higher than the value for homogenous catalyst (typically in the range of 20–30 kJ/mol). Analysis of experimental results vis-à-vis simulation of cavitation bubble dynamics revealed the mechanistic features of the process. The reaction system in the present case was three-phase heterogeneous, and hence, mass transfer resistance was more pronounced. The optimum temperature of the process was close to boiling point of methanol. Due to very large evaporation of methanol into the bubble, the transient collapse of the bubble was not much energetic. The peak temperature in the bubble reached ~700 K, which is not sufficient to generate radical species. The microturbulence induced by the bubble was accordingly less intense, and the contribution of micro-streaming to the overall convection in the medium was relatively much higher. The base catalyst CaO, being heterogeneous in nature, preferably stays in the aqueous (or methanol) phase. The methoxy ions in this case are generated by adsorption of methanol molecules on the catalyst surface. These methoxy ions are then transferred to organic phase at the interface between oil and methanol phase. Micro-streaming by ultrasound can enhance the rate of adsorption and enhance  $\text{CH}_3\text{O}^-$  production.

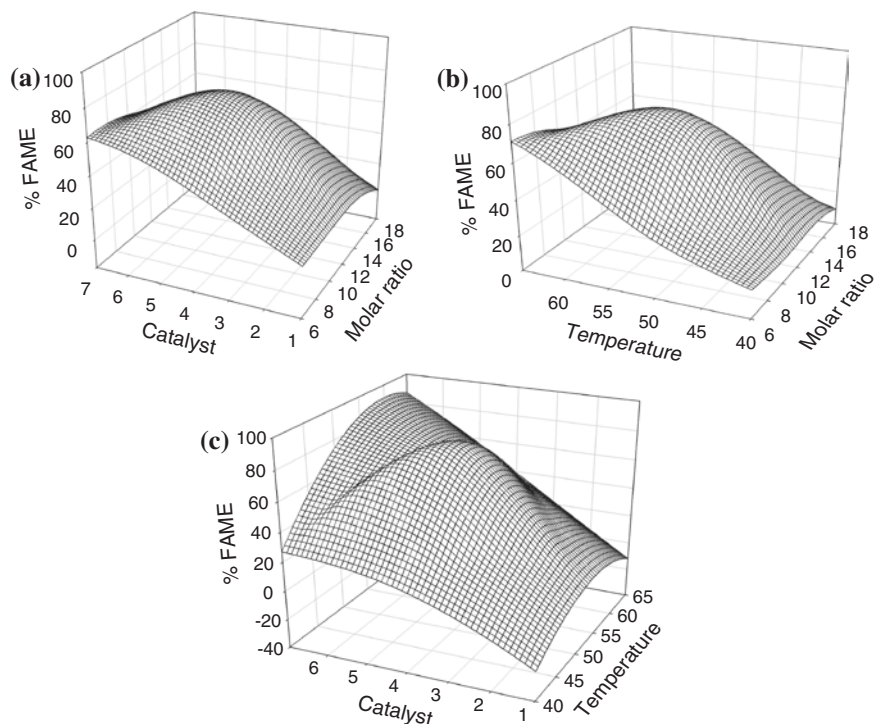


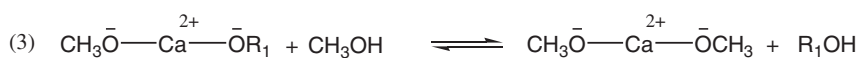
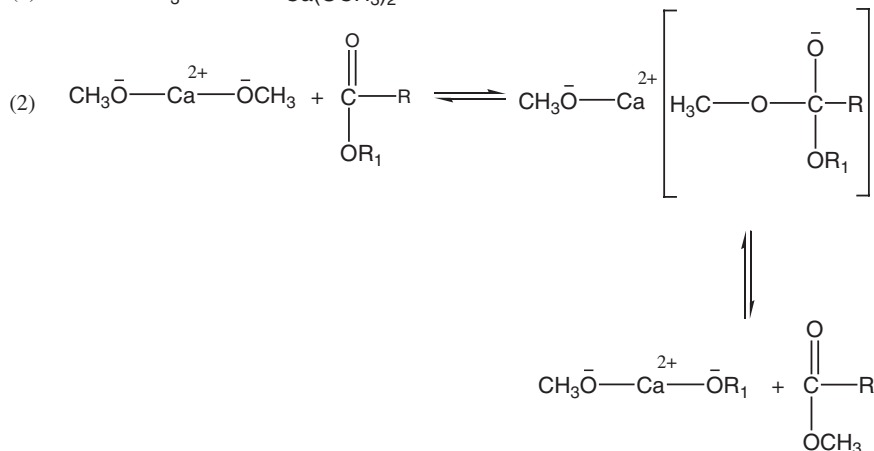
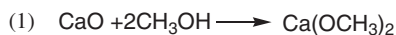
**Fig. 2.5** Response surface plots for percentage of fatty acid methyl ester (*FAME*) yield as a function of reaction temperature, catalyst loading and methanol-to-oil molar ratio. Reprinted with permission from [72], Copyright © 2014, Elsevier

However, unlike the homogenous base where reaction at ambient temperature gave high yield of biodiesel; the optimum temperature in the case of heterogeneous catalyst was 62 °C. This essentially means that enhancement of mass transfer due to ultrasound does not overcome the intrinsic kinetic limitations of the process, that can be attributed to the high activation energy of the system. However, the optimum alcohol ratio of 10:1 is almost similar to that for the homogenous system (12:1). The explanation for this can be given along similar lines as that for homogenous system. The statistical model predicted strong interaction between effects of all optimization parameters on the *FAME* yield. The parameters of catalyst loading and molar ratio and temperature and molar ratio are related through the variation in convection level in the medium, which in turn related to cavitation bubble dynamics and ultrasound wave phenomena. The parameters of catalyst loading and temperature are related through intrinsic kinetics of the process. Some carbonate impurity in the catalyst could have also contributed to a reduction in the yield.

- Choudhury et al. [73] have also done mechanistic investigations on acid catalyzed biodiesel synthesis from *Jatropha curcus* oil. This oil has much higher

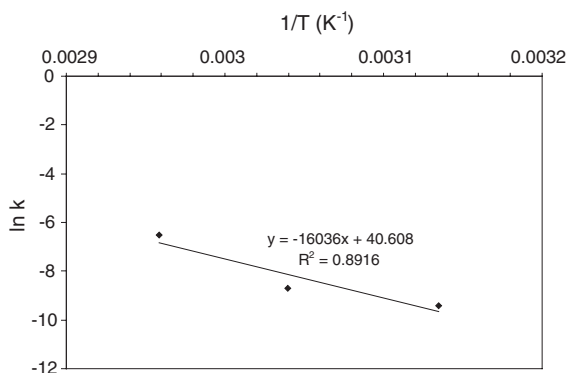
contents of free fatty acids than conventional refined oils. Therefore, the process was carried out in two stages, viz. esterification of free fatty acids followed by transesterification of triglycerides. Once again, a statistical design of experiments based on Box–Behnken method using response surface methodology was coupled with simulation of cavitation bubble dynamics. The acid catalyzed esterification was insensitive to ultrasound irradiation, while the beneficial effect of sonication on transesterification reaction was only through intense micro-mixing induced by ultrasound, as transient cavitation in methanol does not produce any radical species. Even at higher temperatures of 70 °C or 85 °C, and high catalyst concentration of 6 %w/w or 9 %w/w oil, the biodiesel yield was low for alcohol to oil molar ratio of 4:1. Low yield was attributed to low extent of emulsification that gives low interfacial area—as the transient cavitation in alcohol and not oil is responsible for emulsification effect. Reduced interfacial area between oil and methanol restricts the extent of protonation of carbonyl carbon of triglycerides. The biodiesel yield was also low at a temperature of 55 °C and an alcohol molar ratio of 10:1. The low yield was attributed to lower concentration of protons in aqueous phase at high alcohol ratios, due to which the probability of interaction between triglyceride and proton at interfacial area between phases is reduced. Raising of catalyst concentration to 9 wt% and temperature of 70 °C doubles this yield. The relative influence of mass transfer and intrinsic kinetics of the process is evident from these observations. The optimum set of process parameter as identified by the statistical design of experiments was alcohol to oil molar ratio = 7, catalyst concentration = 6 wt%, and temperature = 70 °C. The kinetics of the acid catalyzed transesterification was found to be much slower than base catalyzed process, which is attributed to basic difference in the chemical mechanism of acid and alkali catalyzed transesterification. The transesterification for acid catalyst is initiated by nucleophilic attack of methanol on the protonated carbonyl carbon of triglycerides. Since methanol is a poor nucleophile, its intrinsic reactivity is much less than the methoxide ( $\text{CH}_3\text{O}^-$ ) ion, which initiates the transesterification in base catalyzed process. This is essentially manifested in slower kinetics of the reactions. These experimental trends clearly show that enhanced mass transfer with ultrasound is not sufficient to boost the overall kinetics of the process leading to higher biodiesel yield. Therefore, for high yield of transesterification process an overall optimization in terms of all parameters is necessary.

3. Choudhury et al. [74] have extended the above theme of two-stage biodiesel synthesis from *Jatropha curcus* oil with acid catalyst in the transesterification step replaced by solid base catalyst. The chemical mechanism of CaO catalyzed transesterification reaction is depicted in Scheme 2.2. The results of experiments using ultrasound were compared with mechanically agitated system. The statistical design of experiments yielded optimum parameters as: alcohol to oil molar ratio ~11, catalyst concentration = 5.5 wt% and temperature = 64 °C. The XRD analysis of catalyst revealed formation of calcium methoxide  $\text{Ca}(\text{OMe})_2$  phase, which is the active catalyst for transesterification



**Scheme 2.2** Proposed chemical mechanism of calcium oxide catalyzed transesterification reaction. Reprinted with permission from [72], Copyright © 2014, Elsevier

**Fig. 2.6** Arrhenius plot of  $\ln(k)$  versus  $1/T$  for transesterification reaction considering 3rd order reaction kinetics (with respect to triglyceride) for optimum conditions of methanol to oil molar ratio (11:1) and catalyst concentration (5.5 wt%) as determined by statistical analysis. Reprinted with permission from [74], Copyright © 2014, Elsevier

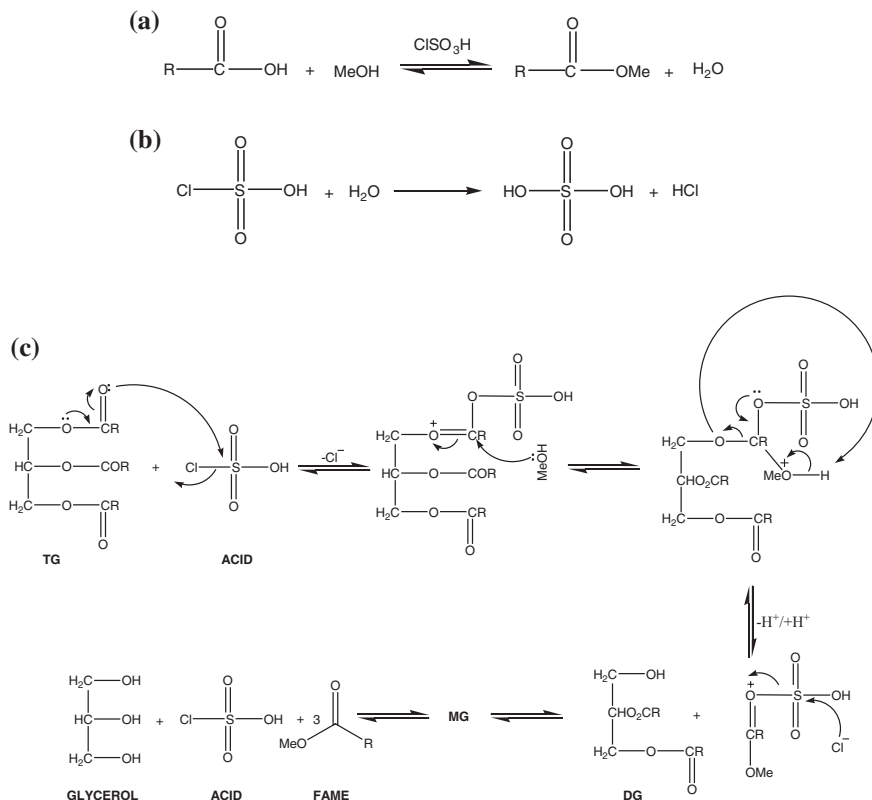


reaction. The activation energy of the ultrasonic process was found to be 133.5 kJ/mol, and this is attributed to 3 phase heterogeneity of the system. As compared to the previous study of Choudhury et al. [72] using refined soybean oil as a feedstock, which showed an activation energy of 82.3 kJ/mol (refer to the Arrhenius plot shown in Fig. 2.6), ~50 % higher activation energy for *Jatropha* could also be attributed to crudeness of oil. The impurities in the oil could poison the catalyst by adsorbing over it and reducing its activity. However, as compared to mechanically stirred system, the ultrasonic system showed ~30 % reduction in activation energy, which could be a consequence

of the mass transfer enhancement in the system. The optimum value of alcohol molar ratio of 11 could be justified as follows: For very low catalyst concentration (3 wt%), the amount of methoxy ions generated is low, resulting in smaller yields. Although stronger dispersion and emulsification between oil and methanol phases is achieved at high alcohol molar ratio, the mass transfer resistance for  $\text{CH}_3\text{O}^-$  ions increases. Higher mass transfer resistance can be explained as follows:  $\text{CH}_3\text{O}^-$  ions are generated at the surface of CaO catalyst. The CaO catalyst particles, being hydrophilic in nature, preferentially stay in the methanol phase. As the volume fraction of methanol in the total reaction mixture increases with molar ratio, these ions have to diffuse through larger volume so as to reach the interface and react with triglyceride. For low alcohol molar ratios, the volume fraction of oil in reaction mixture is high and some catalyst particles may also stay in oil phase. The oil can wet the catalyst surface, and hinder adsorption of methanol leading to formation of methoxy ions.

4. Choudhury et al. [75] have also reported a novel single step process for biodiesel synthesis using chlorosulphonic acid as catalyst. The previous process with  $\text{H}_2\text{SO}_4$  catalyst [73] requires a two stage approach with esterification and transesterification. However, with chlorosulfonic acid as the catalyst, two steps process is combined in a single step process. The chemical mechanism of this synthesis is shown in Scheme 2.3. The acid catalyzed esterification of the free fatty acids in *Jatropha* oil releases water, which has serious inhibition effects due to solvation of the protons as well as  $\text{CH}_3\text{OH}_2^+$  (methoxenium) ions. Solvation of the protons reduces their reactivity and accessibility leading to lowering of kinetics. The chlorosulphonic acid counteracts this inhibition by in situ removal of water formed during esterification. Water produced in the esterification process reacts with chlorosulfonic acid to produce  $\text{H}_2\text{SO}_4$ . Dissociation of this  $\text{H}_2\text{SO}_4$  can generate additional protons that catalyze esterification/transesterification reaction. However, generation of  $\text{H}_2\text{SO}_4$  is accompanied by in situ removal of water molecules that solvate the  $\text{H}_3\text{O}^+$  ion and reduce its activity. In this study as well, the statistical design of experiment was used to determine the optimum condition for the highest biodiesel yield. The optimum conditions are: catalyst concentration = 8.358 wt%, alcohol molar ratio = 18:1 and temperature = 60 °C.

The optimum temperature was close to boiling point of methanol, and also that the intensity of transient cavitation is minimal at this temperature, once again demonstrates that the beneficial effect of ultrasound and cavitation on reaction system was merely physical, that is emulsification of the phases. The activation energy for the single-step process was determined as 57.3 kJ/mol, which is more than three-fold lower than for  $\text{H}_2\text{SO}_4$  catalyzed process (i.e. 169 kJ/mol). Choudhury et al. [75] also carried out chlorosulfonic acid catalyzed transesterification in conventional two-step process comprising of esterification and tranesterification. Quite interestingly, the two-step process had 40 % less activation energy of 31 kJ/mol. This reduction has been attributed to complete removal of water from reaction system in the two-step process—as compared to single step process, in which some trace of water might be left in the system despite the in situ removal of chlorosulfonic acid, which reduces inhibition effect on the process.



**Scheme 2.3** **a** Reaction of chlorosulfonic acid induced esterification process, **b** removal of water formed during esterification by chlorosulfonic acid, and **c** mechanism of chlorosulfonic acid induced transesterification process. Reprinted with permission from [75], Copyright © 2014, Wiley

The six studies on ultrasonic synthesis of biodiesel published reviewed in this section clearly reveal that the beneficial effect of ultrasound and cavitation on the transesterification reaction system is mainly physical as the reaction system is governed by intrinsic kinetics, through the alcohol to oil molar ratio, catalyst concentration and temperature.

### 2.4.3 Bioconversion of Crude Glycerol

The transesterification reaction for biodiesel synthesis produces glycerol as the product. Transesterification of 1 mol of triglyceride with 3 mol of alcohol yields 3 mol of fatty acid alkyl ester (which is biodiesel) and 1 mol of glycerol. On a

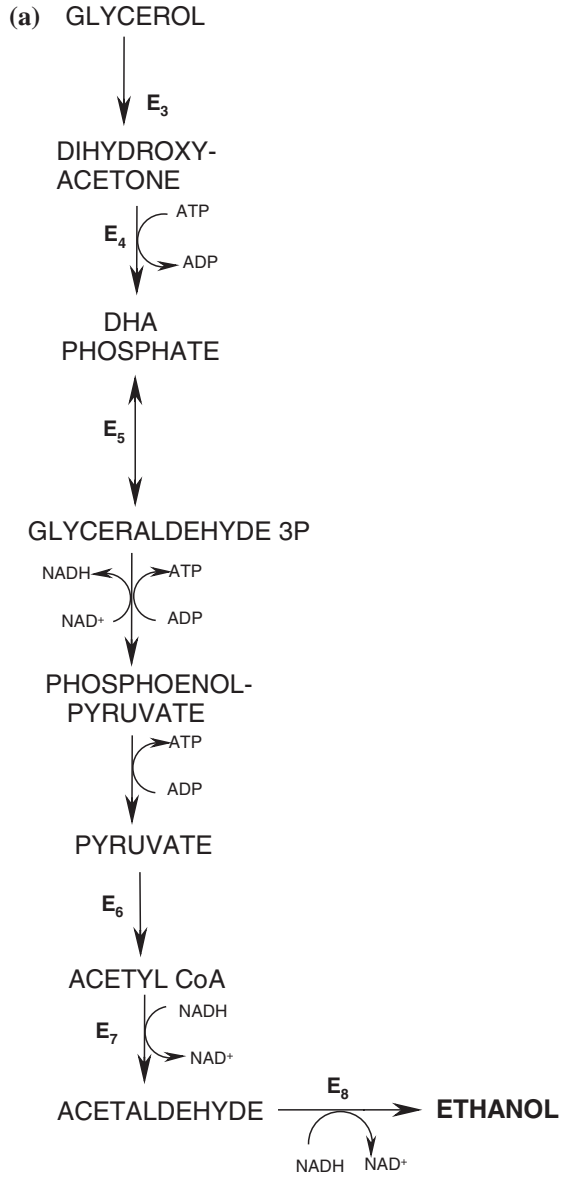


weight basis, 1 kg of crude glycerol is produced per 9 kg of biodiesel. However, this glycerol is contaminated with alkali and alcohol, and is not useful for conventional applications such as cosmetics. Purification costs of this glycerol are prohibitively high. With biodiesel industry growing at an unprecedented rate all over the world, effective and efficient utilization of billions of gallons of crude glycerol is a daunting challenge before biodiesel industry. Glycerol, however, is an excellent carbon source for fermentation. Catalytic conversion of glycerol to other value-added products has also been extensively investigated. Forward integration of the biodiesel industry to convert crude glycerol to value-added products is a potential means of effective utilization of glycerol, as well as improvement of the economy of biodiesel industry with additional revenue fetched by these products. We have conducted investigations in the bioconversion of glycerol to three products, viz. 1,3-propanediol, butanol and ethanol, using immobilized cultures of *Clostridium pasteurianum*. Our approach has been to develop a complete process for this conversion, including optimization and intensification with ultrasound. Below is the summary of our investigations in ultrasonic enhanced bioconversion of glycerol. After initial optimization of culture growth medium and physical parameters for fermentation [76–78], Khanna et al. [79] have carried out mechanistic investigations in ultrasound enhanced glycerol bioconversion using free cells of *Clostridium pasteurianum*. The experimental results were analyzed *vis-à-vis* the simulation of cavitation bubble dynamics. Experiments were carried out in a specially designed test tube with provision of raising the static pressure to eliminate the transient cavitation in the system, which is harmful for microbial cells. The control experiments were carried out in an incubator shaker. The morphological changes in the microbial cells in control (mechanical shaking) and test (sonication) were assessed using flow cytometry. The influence of ultrasound on glycerol bioconversion was assessed using enzyme kinetics. The metabolic pathway of glycerol bioconversion to 1,3-PDO and ethanol is shown in Schemes 2.4a and 2.5a, respectively. The metabolic pathway for 1,3-PDO involves only one intermediate, while ethanol pathway involves multiple intermediates. The enzymes in the pathway for 1,3-PDO are inhibited by substrate (glycerol) as well as 3-hydroxypropionaldehyde (the intermediate), while no such effect is seen for the metabolic pathway for ethanol. Therefore, influence of ultrasound on ethanol production was assessed using Michaelis–Menten model, while 1,3-PDO production was evaluated using substrate inhibition or Haldane kinetics model. Before proceeding to the results and discussion of study of Khanna et al. [79], we give herewith a description of these models for general readers. The equation for Michaelis–Menten model is given below (Eq. 2.7) with scheme depicted in Scheme 2.4b.

$$V = \frac{k_2 E_0 [S]}{K_m + [S]} = \frac{V_{\max} [S]}{K_m + [S]} \quad (2.7)$$

where  $k_1$ ,  $k_{-1}$  and  $k_2$  are kinetic constants,  $K_m$  is the Michaelis constant and is defined as  $(k_2 + k_{-1})/k_1$  and approximated as  $k_{-1}/k_1$  under rapid equilibrium conditions,  $k_{-1} \gg k_2$ .

**Scheme 2.4 a** Metabolic pathway for glycerol bioconversion to ethanol (Enzymes: E3 = Glycerol dehydrogenase Type I; E4 = Dihydroxyacetone kinase; E5 = Triose phosphate isomerase; E6 = Pyruvate dehydrogenase complex; E7 = Acetaldehyde dehydrogenase; E8 = Alcohol dehydrogenase), **b** Michaelis–Menten reaction scheme. Reprinted with permission from [79], Copyright © 2012, Elsevier





products. Comparative evaluation of these constants for the experiments with mechanical shaking and ultrasound gives a mechanistic account of the influence of ultrasound on bioconversion process. The kinetic data of glycerol conversion into 1,3-PDO and ethanol with different substrate concentrations was fitted to the enzyme kinetics models to get physical insight into the influence of ultrasound.

The major results of this study are summarized in Table 2.3, which shows the complete material balance for glycerol conversion for 3 different initial glycerol concentrations, viz. 5, 10 and 25 g/L, along with the yield and selectivity of products and the constants in enzyme kinetics models. Assessment of the morphology of microbial cells with flow cytometry and microscopic analysis (Figs. 2.7 and 2.8) revealed no adverse effect of sonication or elevated static pressure on cells. Moreover, the cell population in the medium as determined by the optical density was also found to stay constant during the test period. The typical trends of glycerol bioconversion are as follows.

1. Glycerol uptake by the microbial cells remained unaltered with sonication, while the glycerol utilization (product formation) showed significant rise with sonication.
2. Highest percentage of glycerol utilization was seen for an initial concentration of 10 g/L. Due to substrate inhibition, the amount of unutilized glycerol was the highest for an initial concentration of 25 g/L.
3. Production of both 1,3-PDO and ethanol increases with ultrasound. Percentage enhancement of yield for ethanol shows a monotonous increase with initial glycerol concentration, while enhancement of yield of 1,3-PDO shows a maximum for an initial concentration of 10 g/L. The yield was the lowest for 25 g/L glycerol, as large quantity of glycerol remained unutilized.

These experimental trends were analyzed *vis-à-vis* the simulation of bubble dynamics. In absence of transient cavitation, the rapid oscillatory motion of microbial cells due to micro-streaming may cause collisions among cells or with the walls of the reactor vessel. This phenomenon could help enhance the metabolism and utilization rate of glycerol. Moreover, ultrasound can also enhance desorption of the gaseous products of metabolism from medium, thus causing enhancement in the kinetics of the metabolic reactions.

Comparative evaluation of enzyme kinetic parameters for ethanol and 1,3-PDO in test and control experiments, and their manifestation on the yield and selectivity gives a physical insight into the influence of ultrasound on the bioconversion. Due to faster diffusivity of glycerol into microbial cells, the overall enzymatic reaction system or metabolic pathway is always expected to be substrate saturated, with enzyme being limiting reactant.

1. The Michaelis–Menten constant for ethanol formation reduces with ultrasound, which indicates higher substrates affinity and faster formation of  $E \cdot S$  complex. But the value of  $V_{\max}$  indicating splitting of the  $E \cdot S$  complex into products also getting reduced. Nonetheless, greater formation of the  $E \cdot S$  complex still drives enhancement in ethanol formation.

**Table 2.3** Material balance for glycerol bioconversion

Final concentrations (mM)	Initial glycerol concentration					
	5 g/L (54.4 mM)		10 g/L (108.7 mM)		25 g/L (271.7 mM)	
	Ultrasound	Without ultrasound	Ultrasound	Without ultrasound	Ultrasound	Without ultrasound
Ethanol	2.12 ± 0.13	1.74 ± 0.07	11.33 ± 0.22	7.29 ± 0.19	10.58 ± 0.32	5.78 ± 0.05
1,3 Propanediol	2.98 ± 0.01	2.33 ± 0.18	4.76 ± 0.15	3.19 ± 0.10	5.47 ± 0.26	4.18 ± 0.10
Glycerol uptake <sup>a</sup>	48.6	48.4	91	91.5	262	244
Glycerol consumption <sup>a</sup> (Stoichiometric)	5.1	4.07	16.09	10.48	16.05	9.96
Residual glycerol <sup>a</sup> in cells	43.5	44.33	74.91	81.02	245.95	234.04
Percentage enhancement in glycerol consumption with ultrasound <sup>a</sup>	25.3	N.A.	53.5	N.A.	61.1	N.A.
Percentage glycerol utilized <sup>a</sup>	10.5	8.4	17.7	11.5	6.1	4.1
Percentage glycerol remained unutilized <sup>a</sup>	89.5	91.6	82.3	88.5	93.9	95.9

N.A. not applicable

<sup>a</sup> Calculated using mean values of ethanol and 1,3-PDO production Reprinted with permission from [79]. Copyright © 2012, Elsevier

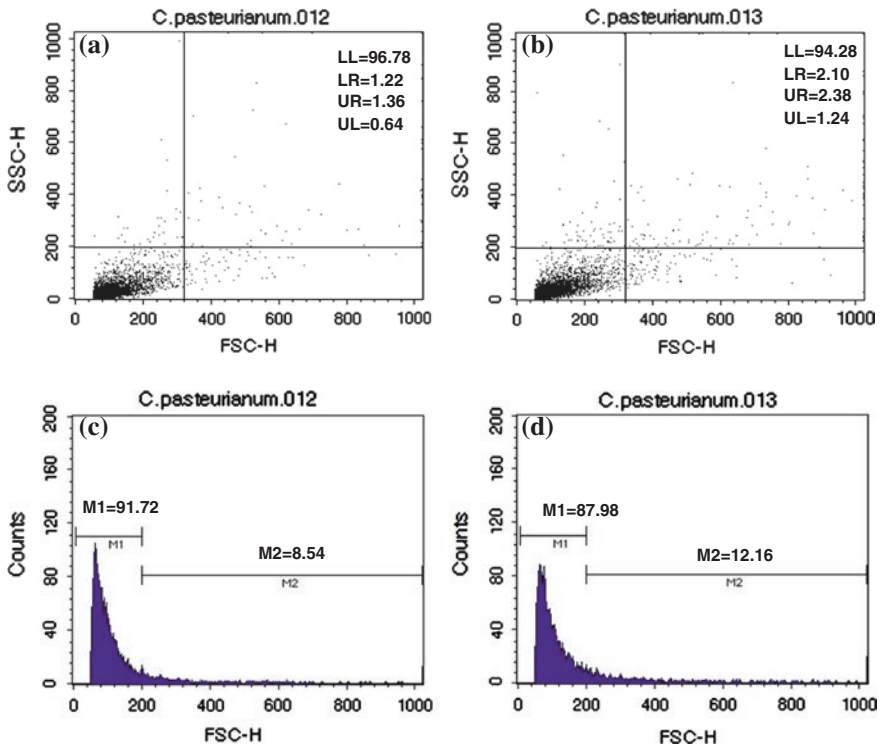


**Fig. 2.7** Flow cytometric analysis for estimation of morphological changes **a** and **b** acquisition *dot plots* (forward-scattered light vs. side-scattered light) of *C. pasteurianum* cells in control and test samples respectively. **c** and **d** Histogram plots (counts vs. FSC) of *C. pasteurianum* in control and test samples cells respectively. As there is no significant change in FSC after sonication as shown by both plots, therefore morphology of cells remains same. Reprinted with permission from [79], Copyright © 2012, Elsevier

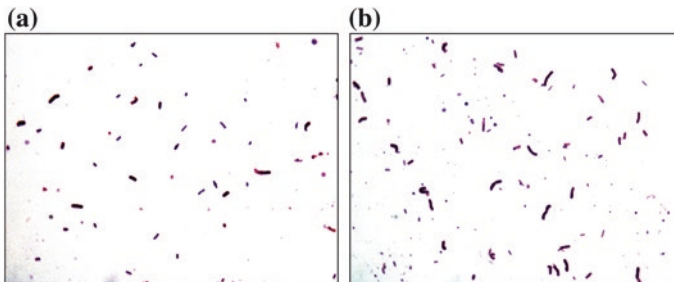


**Fig. 2.8** Morphology of cells of *Clostridium pasteurianum* **a** before sonication, and **b** after sonication. As there is no significant change in FSC after sonication as shown by both plots, therefore morphology of cells remains same

- For 1,3-PDO formation, the Michaelis–Menten constant increases with ultrasound indicating reduced substrate affinity and reduced formation of  $E \cdot S$  complex. Reduction in the inhibition constant  $K_I$  indicates greater tendency of binding of  $E \cdot S$  complex to non-catalytic site and formation of non-productive  $S \cdot E \cdot S$  complex. On the contrary, the reaction velocity increases with ultrasound, signifying higher rate of splitting of the  $E \cdot S$  complex into products. Despite these counter-productive variations in kinetic parameters, the overall rate of 1,3-PDO production increases—which is attributed to saturation of the cells with substrate due to its faster intrinsic diffusivity into the cells. However, due to greater substrate inhibition seen with ultrasound, the extent of percentage enhancement is much less than that seen for ethanol—where enzymes are not inhibited by the substrate.

All of these results pointed that convection generated by ultrasound and cavitation enhances the rates of enzymatic reactions in the pathway of glycerol conversion. However, the biochemistry of metabolic pathway of glycerol conversion is not affected by ultrasound, as the exactly same profiles in terms of absolute rate of production and yield are seen with ultrasound and mechanical shaking. Thus, the role of ultrasound and cavitation is found to be of physical nature.

Khanna et al. [81] extended the theme of ultrasonic enhancement of glycerol bioconversion with immobilized culture of *Clostridium pasteurianum* on silica support. A similar approach of assessing effect of ultrasound with enzyme kinetics models was adopted. The kinetic constants determined from Michaelis–Menten and Haldane kinetics model are listed in Table 2.4. The major conclusions of this study, which showed distinct differences from the results observed for free cells, are summarized below:

- The dominant product of glycerol bioconversion using immobilized cells was 1,3-PDO. This was a consequence of favorable change in kinetic parameters for immobilized cells under ultrasound as seen from Table 2.4. The inhibition constant  $K_I$  increased (indicating reduction in inhibition), while the Michaelis–Menten constant  $K_m$  reduced (indicating increase in substrate affinity) under sonication, which essentially promoted the glycerol conversion through metabolic pathway indicated in Scheme 2.5a, b. The total product concentration for immobilized cells was higher than free cells, which is attributed to greater tolerance of immobilized cells towards substrate inhibition. In this study, the individual enhancement effect of ultrasound for immobilized cells was lower, as the technique of immobilization itself counteracted inhibition to large extent.

**Table 2.4** Enzyme kinetics parameters for Ethanol dehydrogenase and 1,3-PDO dehydro-genase

Kinetic parameters	Ethanol dehydrogenase		1,3-PDO dehydrogenase	
	Test	Control	Test	Control
$V_{\max}$ (mM/min)	0.016	0.016	0.023	1.699
$K_m$ (mM)	1.1	1.1	16.56	3,691.90
$K_i$ (mM <sup>-1</sup> )	N.A	N.A	1,036.14	1.61

Reprinted with permission from [81], Copyright © 2013, Wiley

2. The immobilization of cells coupled with sonication caused a major shift of selectivity through predominant pathway of glycerol conversion. Although the metabolic pathway for ethanol was multi-step, involving several enzymes and intermediates, there was no limitation of inhibition (either substrate or product). On the other hand, although the metabolic pathway for 1,3-PDO was single step, it suffers from both substrate and product inhibition of the enzyme, 1,3-PDO dehydrogenase. Immobilization as well as sonication reduced the inhibition significantly, which essentially resulted in shift of preferable pathway to 1,3-PDO.
3. The enhancement effect of ultrasound for ethanol was rather negligible for immobilized cells as the same value of reaction velocity and Michaelis–Menten constant were observed with mechanical shaking and sonication.
4. Maximum percentage enhancement of glycerol bioconversion for immobilized cells was seen for the highest glycerol concentration of 25 g/L—as against moderate concentration of 10 g/L seen for free cells.

The investigations of Khanna et al. [79, 81] have corroborated the physical influence of ultrasound and cavitation on glycerol bioconversion system. Coupling of sonication with other process alternatives like immobilization of cultures can have great beneficial effects on glycerol bioconversion.

#### ***2.4.4 Ultrasonic Desulfurization***

Oxidative desulfurization is the new technology for the removal of sulfur compounds from liquid transportation fuels. The sulfur content of biofuels is relatively much less than petroleum fuels. Yet, in some cases where the feedstock for biofuels itself contains sulfur impurities, and hence, desulfurization becomes a necessary step in the downstream processing. In oxidative desulfurization, the sulfur containing compounds are initially oxidized to sulfones and the sulfones are extracted using suitable solvent like dimethyl sulfoxide (DMSO), dimethyl formamide (DMF), acetonitrile or methanol. Oxidative desulfurization has several distinct merits over conventional hydro-desulfurization in that it does not require expensive hydrogen. The treatment conditions of ambient temperature and pressure and effective desulfurization of substituted sulfur compounds can be achieved which is difficult with conventional hydro-desulfurization due to low reactivity of these compounds. The reaction system of oxidative desulfurization is liquid–liquid heterogeneous type in which the oxidant is in the form of peroxyorganic acids, hydroperoxides or peroxy salts and is in the aqueous phase, while the sulfur compounds are in the form of sulfides, thiols, thiophenes, benzothiophene, dibenzothiophene and their substituted derivatives and are in the organic phase. Several studies have been published in the recent past, which have reported the beneficial influence of ultrasound on the enhancement of oxidative desulfurization. We have conducted the same studies recently that have shed light on the exact physical mechanism of ultrasound enhanced oxidative desulfurization.

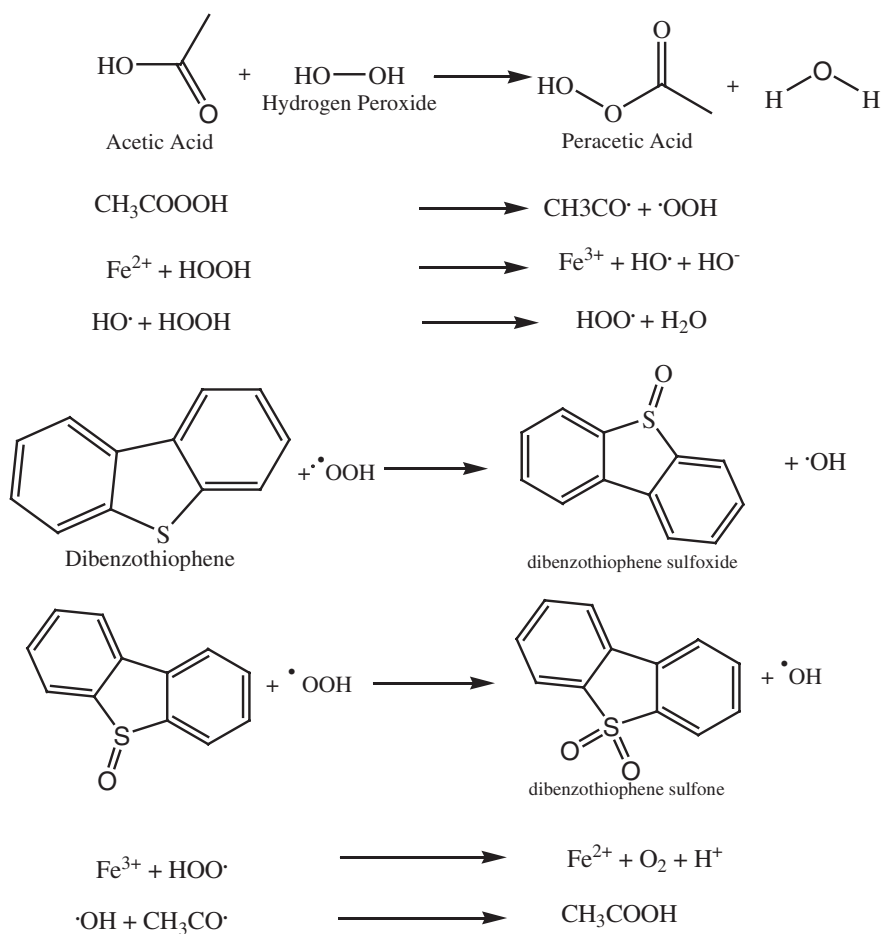


Bolla et al. [82] investigated oxidative desulfurization of three sulfur compounds, viz. thiophene, benzothiophene and 3-methyl thiophene with peroxy acetic acid and  $\text{FeSO}_4 \cdot 7\text{H}_2\text{O}$  as oxidants and n-hexane as model liquid fuel. The experiments were conducted in an ultrasound bath with frequency of 35 kHz and power of 35 W with pressure amplitude of the ultrasound wave being 150 kPa. The major experimental variable was system pressure. Experiments were conducted at two static pressures, viz. atmospheric (101.3 kPa) and elevated (250 kPa). Simulations of cavitation bubble dynamics in n-hexane were carried out to estimate the peak temperature and pressure conditions reached during transient collapse and the chemical species generated in the bubble during collapse. The major conclusions of this study were as follows:

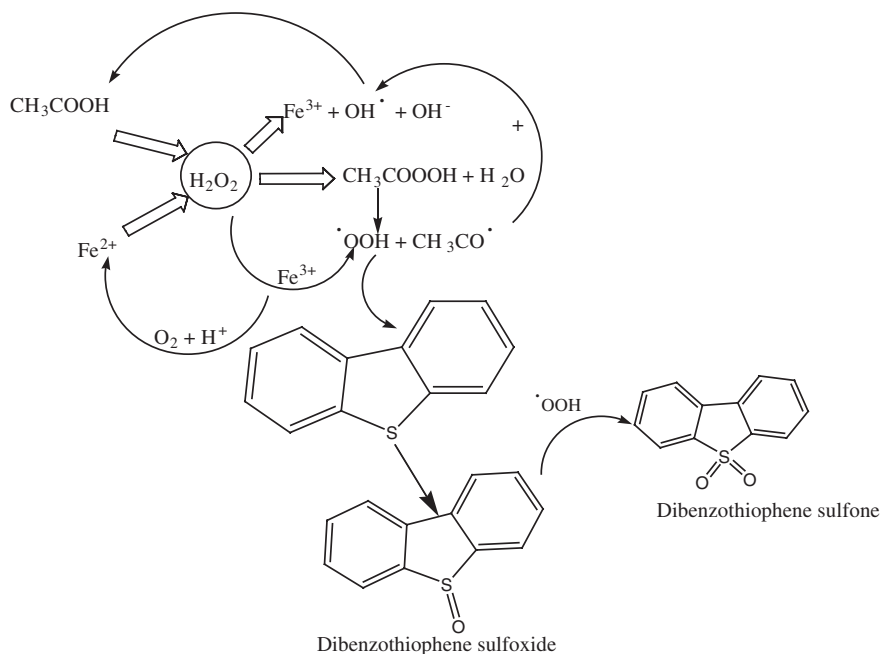
1. Time profile of oxidation for all sulfur compounds (and for all 3 levels of initial concentrations) followed first order kinetics;
2. Transient collapse of cavitation bubble in n-hexane was not intense enough to generate any radical species;
3. Higher rates of oxidation were obtained with peracetic acid coupled with  $\text{FeSO}_4 \cdot 7\text{H}_2\text{O}$ .
4. Most interestingly, higher kinetics as well as extent of oxidation was achieved for all sulfur compounds in experiments at elevated static pressure of 250 kPa.

An explanation for these results can be given along following lines: Large evaporation of n-hexane vapor in the bubble reduces the intensity of the transient collapse of the bubble. Due to lower temperature and pressure peaks reached during transient collapse, the main species generated from thermal dissociation of n-hexane were  $\text{H}_2$ , CO,  $\text{CH}_4$ . Higher oxidation rates in presence of peracetic acid and  $\text{FeSO}_4 \cdot 7\text{H}_2\text{O}$  mixture was attributed to additional generation of the oxidant species by reaction of  $\cdot\text{OH}$  radicals generated from Fenton's reactions with dissolved in the system ( $\cdot\text{OH} + \text{O}_2 \rightarrow \text{HO}_2\cdot + \text{O}\cdot$ ). This effect essentially is the conservation of radical species in the system, which leads to their effective utilization in the reaction. Higher kinetic and yield of oxidation at elevated static pressure could be explained on the basis of the simulation of cavitation bubble dynamics. The predominant species generated from thermal dissociation of n-hexane in the cavitation bubble at transient collapse are  $\text{H}_2$  and CO. These species can competitively consume  $\text{O}\cdot$  species generated by the oxidant. Thus, utilization of  $\text{O}\cdot$  species towards oxidation of sulfur compound is limited, which results in the reduction in the extent of oxidation. With application of elevated static pressure, the transient cavitation in the system is eliminated, and hence, the formation of  $\text{H}_2$  and CO. The oxidant species are thus effectively utilized for desulfurization. As far as the physical effect of intense micro-mixing and emulsification that facilitates interphase mass transfer is concerned, the contribution by micro-streaming due to ultrasound is more than microturbulence due to cavitation. The ultrasound wave phenomena is unaffected by the static pressure, and hence, the interfacial area between organic and aqueous phase at the two pressure levels stays practically unaltered. The results of Bolla et al. [82] clearly revealed the physical mechanism of ultrasonic oxidative desulfurization.

In a subsequent publication, Bhasarkar et al. [83] studied oxidative desulfurization with sono-Fenton–peracetic acid system as oxidant. The model fuel used in this work was toluene, which has significantly different physical properties than n-hexane used in the previous study. The overall reaction scheme for the oxidative desulfurization and the links between different chemical species are shown in Schemes 2.6 and 2.7, respectively. Simulations of cavitation bubble dynamics were carried out for both peracetic acid and toluene as the liquid medium. In addition to static pressure of the system, additional optimization parameters were: (1) acetic acid to  $\text{H}_2\text{O}_2$  molar ratio, (2) volume ratio of organic and aqueous phases, (3) loading of iron catalyst and (4) excess  $\text{H}_2\text{O}_2$ . This study, which spanned more process variables and alternatives, revealed further features of ultrasonic oxidative desulfurization. Simulation results revealed that transient collapse of bubble was

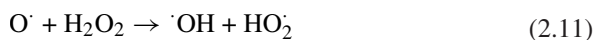
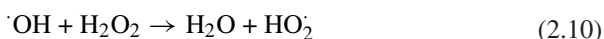
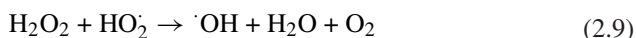


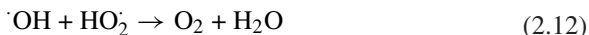
**Scheme 2.6** Reaction scheme for oxidative desulfurization. Reprinted with permission from [83], Copyright © 2013, American Chemical Society



**Scheme 2.7** Links or interactions between different chemical species in peracetic acid—Fenton process for oxidative desulfurization. Reprinted with permission from [83], Copyright © 2013, American Chemical Society

quite intense and peak temperature and pressure conditions reached in the bubble for both peracetic acid and toluene as the medium were sufficiently high to cause generation of radical oxidant species like  $\text{O}\cdot$  and  $\text{HO}_2\cdot$ . This result was attributed to low vapor pressure of toluene and peracetic acid. At elevated pressure, the intensity of transient collapse reduced sharply, but due to very low evaporation of toluene/peracetic acid in the bubble, the species were mainly  $\text{CO}_2$  and  $\text{H}_2\text{O}$ , which would not hinder the oxidative desulfurization. The chemistry of oxidative desulfurization in this case was complicated due to different sources of radicals (viz.  $\text{O}\cdot$ ,  $\text{HO}_2\cdot$  and  $\cdot\text{OH}$ ) in the process, i.e. cavitation bubbles, peracetic acid and Fenton reaction. The most effective radical species for oxidative desulfurization is  $\text{HO}_2\cdot$ . Different possible reactions between the radicals can result in scavenging of  $\text{HO}_2\cdot$  radicals before their utilization for oxidative desulfurization as follows (Eqs. 2.9–2.13):

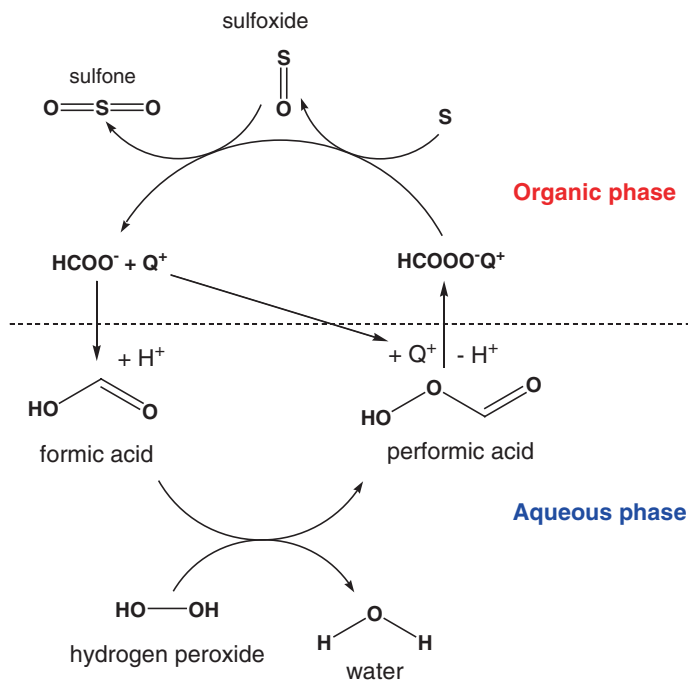




The major results of this study and their explanations on the basis of bubble dynamics simulations are as follows:

Addition of  $\text{Fe}^{2+}$  to reaction system showed greater enhancement for mechanically stirred system than sonicated system. This clearly indicated that mass transfer characteristics of the system have more influence on the reaction system than the chemical kinetics.  $\cdot\text{OH}$  radical production by Fenton process causes regeneration of acetic acid (by combining with  $\text{CH}_3\text{CO}\cdot$  radical), which further enhances  $\text{HO}_2$  radical production. However, less enhancement of oxidation with  $\text{Fe}^{2+}$  for ultrasonic system clearly indicates that effective interphase transfer of  $\text{HO}_2$  radicals is more important than mere generation of these radicals. Reduction of oxidation with excess  $\text{H}_2\text{O}_2$  was also an unexpected result of this study. This is attributed to scavenging of the  $\text{HO}_2$  radicals by  $\text{H}_2\text{O}_2$  through reactions mentioned earlier. The rise in oxidation yield at elevated static pressure is attributed to elimination of production of  $\cdot\text{OH}$  and  $\text{O}\cdot$  radical species, which scavenge the  $\text{HO}_2$  species.

Bhasarkar et al. [84] have also studied the influence of phase transfer agent on ultrasound enhanced oxidative desulfurization simultaneously. The model system used was toluene as the model fuel, dibenzothiophene as the model sulfur compound, tetra octyl ammonium bromide (TOAB) as the phase transfer agent, and two oxidation systems, viz. peracetic acid and performic acid. The results of different operational variables on ultrasonic oxidative desulfurization system were compared against mechanically agitated system. The beneficial action of PTA on the oxidative desulfurization system is shown in Scheme 2.8. The influence of PTA on the enhancement of oxidation was more pronounced for mechanically agitated system. This result has been attributed to faster mass transfer characteristics of sonicated system due to fine emulsification, due to which the additional effect of enhancement of interphase mass transfer by PTA is limited. Comparing between performic acid and peracetic acid, the extent of oxidation was higher for performic acid, and this result is attributed to relatively faster diffusion of performic acid-PTA complex due to smaller size. Addition of excess  $\text{H}_2\text{O}_2$  in this case caused reduction in the extent of oxidation. This effect was not only attributed to scavenging of radicals, but competitive formation of  $\text{H}_2\text{O}_2$ -PTA complex in addition to peracetic acid-PTA complex. Finally, the beneficial effect of elevated static pressure is reduced in the presence of PTA, as noted earlier. Elevation of static pressure eliminates transient cavitation responsible for the formation of molecular and radical species in the organic phase that competitively consume the oxidant. However, in the present situation, the PTA assists efficient transfer of oxidant species across interface, and thus, helps mitigate the adverse effect of reducing/scavenging species.



**Scheme 2.8** The cyclic mechanism of phase transfer agent (PTA) during oxidative desulfurization with perorganic acid (e.g. performic acid)

### 2.4.5 Biomass Pretreatment

Lignocellulosic biomass derived biofuels have been extensively investigated in the past few decades. Synthesis of alcoholic biofuels like ethanol, butanol requires pretreatment and hydrolysis of biomass to release fermentable sugar. The biomass is subjected to several physical and chemical treatments for pretreatment and sugar release. The physical treatments are grinding, milling, water bath treatment, steam explosion or autoclaving. These techniques are coupled with acid or alkali for the removal of hemicelluloses and lignin components, respectively. The lignocellulosic biomass comprises of lignin, hemicelluloses and cellulose. The dense layers of lignin prevent accessibility of cellulose during enzymatic hydrolysis to release hexose sugars. The hydrolysis of hemicellulose is carried out under acidic pretreatment, and this hydrolysis releases pentose sugars. The pretreated biomass after removal of lignin and hemicelluloses is hydrolyzed using enzymes. All three steps of pretreatment, viz. acid hydrolysis, alkaline delignification and enzymatic hydrolysis have been intensified using ultrasound. We have carried out mechanistic investigation of these systems that are summarized next.

Suresh et al. [85] have investigated the mechanics of hybrid techniques for treatment of rice straw prior to fermentation to alcohol liquid fuels. Two chemical techniques viz. dilute acid and dilute alkali treatment and two physical techniques viz. hot water bath and autoclaving were coupled with sonication. The efficacy of each sono-hybrid was assessed on the basis of total sugar and reducing sugar release. The total sugar released during acid and alkali hydrolysis consists of sugars in any form, viz. monomer sugars (i.e. pentose sugars like xylose and arabinose, and hexose sugars like glucose and mannose), oligomers (cellobiose) and dehydrated forms that form at low pH from xylose and glucose like furfural and hydroxy methyl furfural. The reducing sugar fractions of total sugar essentially are the monomeric sugars. During experiments, elevated static pressure was applied to discriminate between physical and chemical effects of ultrasound and cavitation. The mathematic model used in this study included not only the micro-streaming, microturbulence and shock wave effects, but also the acoustic streaming near the boundaries. Nyborg [57] presented the pioneering analysis of steady circulations induced by high amplitude sound fields near surfaces of obstacles and vibrating elements and bounding walls. Nyborg et al. [57] proposed that gas comes out of solution under influence of ultrasound at solid-liquid surfaces that leads to the formation of gas nuclei on the surface. The oscillatory velocities of liquid induced by volume oscillations of these gas bodies can be an effective source of highly localized streaming. The near boundary limiting velocity of micro-streaming flow over plain surfaces was determined as (Eq. 2.14):

$$U_L = (1/4\pi^2\omega)(Q^2/r^5) \quad (2.14)$$

where  $Q$  is the volumetric flow rate and  $r$  is the distance from boundary. Applying this analysis for the present situation of hydrolysis of biomass, a pulsating hemispherical bubble was taken as basis and the micro-streaming velocity was determined as follows (Eq. 2.15):

$$U_{ms} = (U^2/\omega R) \quad (2.15)$$

where  $U$  is the velocity amplitude of oscillations of fluid elements,  $\omega$  is the angular frequency of acoustic wave and  $R$  is the radius of the bubble. For acoustic pressure amplitude of 150 kPa, the velocity of fluid elements is 0.1 m/s. For an ultrasound frequency of 35 kHz as used by Suresh et al. [85] and 5  $\mu\text{m}$  size bubble trapped in the biomass matrix, the localized micro-streaming velocity is 0.09 m/s. The main results of the study of Suresh et al. [85] are summarized as below:

1. The physical technique of autoclaving alone did not give significant sugar release. However, coupled with sonication after autoclaving, the sugar release increased markedly.
2. Sonication after autoclaving in acidic environment results in doubling of the sugar release. However, raising the static pressure of the system is revealed to reduce the sugar release.

3. Highest sugar release (~54 %w/w rice straw) was obtained for autoclaving, stirring followed by sonication in an acidic environment. As per the composition of rice straw, this was the highest possible sugar yield from rice straw with hydrolysis of all cellulose and hemicelluloses components of biomass.

Before interpretations of the results, the chemical mechanism of different reactions occurring during biomass pretreatment needs to be considered. Autoclaving causes hydrolysis of hemicelluloses in biomass that results in the formation of organic acids like acetic acid and other acids that can form the acetyl and other functional groups released from biomass. Water itself promotes hydrolysis at elevated temperatures due to change in ion product that assists in reaction of hemicelluloses. Autoclaving also causes rapid thermal expansion of biomass that helps opening up of the biomass structure with an increase in pore volume. Hot water bath treatment enhances cellulose digestibility and sugar extraction. Dilute acid treatment results in the solubilization of hemicelluloses leaving lignin and cellulose intact, which helps in increasing the accessibility of cellulose for the further enzyme treatment. Under optimized conditions, oligomeric hemicelluloses saccharides can be completely hydrolyzed to monosaccharides giving high xylose yield.

Alkaline pretreatment is mainly aimed at delignification but it also causes partial hydrolysis of hemicelluloses. The main chemical mechanism of alkaline treatment is saponification of intermolecular ester bonds cross linking xylan hemicelluloses, other celluloses and lignin. Acetyl and uronic acid substitutions on hemicelluloses are removed during alkaline treatment. In addition to these, other effects of alkaline treatment are swelling of biomass resulting in reduction in the degree of polymerization as well as crystallinity, increase in the surface area, disruption of lignin structure and the structural linkages between lignin and carbohydrates.

Overall, the biomass hydrolysis system is mass transfer controlled. Jacobson and Wyman [86] have presented a hypothesis of mass transfer problem in biomass pretreatment. Long chain cellulose are less soluble in water than short chain oligomers formed as intermediates during hydrolysis, but solubility of both reduces with temperature. If liquid continuously flows through the reaction system, the oligomers are removed continuously from the biomass matrix, which facilitates dissolution of more oligomers. This process increases the recovery of sugar monomers and oligomers, before they can degrade at the reaction conditions. If this is not done, re-precipitation of oligomers back onto surface of biomass may occur, due to less solubility at reduced temperature. Reactive lignin and sugar degradation products can promote reattachment of cellulose, hemicelluloses, their oligomers and lignin in the solution back to solid biomass, and these may also form complexes with monomeric sugars. Strong micro-convection generated ultrasound and cavitation cause effective circulation of water through biomass matrix with regular removal of monomeric sugars and refreshment of medium, which facilitates effective removal of sugar monomers. The radicals generated by transient bubbles can also assist higher sugar release due to cleavage of lignin carbohydrate

components. With this preamble of pretreatment mechanics, the main findings of Suresh et al. [85] were as follows:

1. Increase in autoclaving period of biomass did not enhance sugar yield. The extent of hydrolysis increases with time of autoclaving, but due to low convection, sugar molecules are not transported out of biomass matrix. Therefore, sugar concentration in the bulk medium does not change with increasing autoclaving periods. Sonication of the solution after autoclaving helps effective transport of sugar molecules out of biomass matrix.
2. Stirring of biomass solution for 24 h after autoclaving of 30 min does not increase the sugar yield. This result indicates two things: first, most of the hydrolysis of cellulose and hemicelluloses is completed during autoclaving itself, due to high temperature and pressure; and secondly, mechanical stirring of solution does not produce strong currents to penetrate biomass matrix causing sugar transport as happens in case of sonication.
3. Only slight reduction in the sugar yield at elevated pressure indicates negligible contribution of both physical and chemical effects of cavitation bubbles to the overall process of pretreatment and sugar release. The contribution by micro-streaming due to ultrasound and acoustic streaming had greater contribution to enhancement of the transport of sugar molecules. Neither the microturbulence nor the shock waves were intense enough to cause opening up of the biomass matrix and create liquid flow through the matrix that would assist sugar release. The opening of biomass structure is found to occur only with autoclaving (a thermal effect) and ultrasonic micro-streaming enhances the transport of sugar molecules.

In a subsequent study, Singh et al. [87] studied the delignification of waste biomass *Parthenium hysterophorus* with ultrasound. Optimization of the delignification of pretreated biomass (after dilute acid hydrolysis + autoclaving) was carried out with NaOH as delignifying agent. The optimization parameters were temperature, NaOH concentration and biomass concentration. Assessment of delignification (based on the determination of cellulose, hemicelluloses and lignin content of original and treated biomass) was done according to standard TAPPI protocols [88]. Characterization of delignified biomass was carried out using FTIR, XRD and FESEM analysis. The optimization values of parameters for delignification were: temperature = 303 K, NaOH concentration = 1.5 %w/w and biomass concentration = 2 %w/w. The chemical mechanism of delignification is as follows: Lignin is derived from three monomer units, viz. trans-coniferyl, trans-sinapyl and trans-*p*-coumaryl alcohol. These units are linked randomly mostly via ester linkages at  $\alpha$ - and  $\beta$ -positions to construct the lignin macromolecules. The reactive sites in lignin are mainly the ester linkages and functional groups, since C–C are resistant to chemical attack. The areas of lignin susceptible to chemical attack are hydrolysable ester linkages, phenolic and aliphatic hydroxyl groups, methoxy groups, the unsaturated groups and uncondensed units. The major mechanism through which lignin degrades in alkaline environment is the cleavage of  $\alpha$ - and  $\beta$ -aryl ether linkages. Ultrasound can cause depolymerization and separation of



lignin, in addition to degradation of lignin components. Ultrasonic depolymerization of lignin occurs through hemolytic cleavages of phenyl ether  $\beta$ -O-4 and  $\alpha$ -O-4 bonds, while ultrasonic separation of lignin occurs through cleavage of lignin-hemicellulose linkages. The hydroxyl radical produced from transient cavitation bubbles can also contribute to degradation of lignin. The attack of  $\cdot$ OH radical occurs on the aromatic ring leading to the formation of hydroxylated, demethoxylated and side chain eliminated products. A relatively small extent of attack can also occur on the side chain leading to the formation of dimers and oxidation of aromatic aldehydes to carboxylic acids. Increase in number of non-conjugated carboxyl also indicates hydroxyl radical induced degradation. Lignin condensation and re-polymerization can also occur under ultrasonic treatment.

The major findings of Singh et al. [87] are as follows:

1. The kinetics of delignification is enhanced more than two fold with ultrasound.
2. The extent of delignification with ultrasound was practically same in the range of 30–80 °C. At higher biomass concentration, the extent of delignification reduced, while leveling-off of delignification was seen with respect to NaOH concentration above 2 %w/w. On the basis of bubble dynamics simulations, these results were explained as follows: Although the intensity of transient cavitation reduces drastically with temperature, the intrinsic reactivity of  $\text{OH}^-$  increases, which compensates the effect, and thus delignification stays practically same in the temperature range of 30–80 °C. At large biomass concentration, scattering of the ultrasound wave occurs due to which the extent of convection generated in the system reduces. Strong convection generated by ultrasound and cavitation eliminates mass transfer in the system making biomass accessible to  $\text{OH}^-$  ions. Thus, after a certain concentration of NaOH, leveling off of delignification is observed.

XRD analysis revealed reduction in the crystallinity index of biomass after delignification, which is attributed to depolymerization of cellulose with ultrasound with scission of  $\beta$ -1-4 glycosidic bonds that gives rise to short chains of glucose monomer units (Fig. 2.9). FTIR spectra of delignified biomass (Fig. 2.10) revealed reduction in the intensities of all bonds corresponding to lignin removal, rupture of cellulose bonds and carbohydrate-lignin linkages. Moreover, the bond intensities corresponding to aromatic ring stretching and cellulose band also reduced. Changes in the XRD and FTIR spectra of biomass after delignification are essentially manifestations of the physical and chemical effects of cavitation. Reduction in aromatic ring stretching and aromatic ring vibration bonds along with reduction in bonds corresponding to side chain removal are attributed to reactions induced by  $\cdot$ OH radicals from transient cavitation. Transient cavitation also generates high pressure amplitude shock waves. The biomass particles get drifted randomly in these waves at high velocities leading to collision between them. The energy released in such collisions is sufficient to cause hemolytic cleavage of phenyl esters  $\beta$ -1-4 and  $\alpha$ -1-4 bonds leading to depolymerization of lignin. Comparative analysis of FE-SEM pictures of delignified biomass with mechanical agitation and ultrasonication (Fig. 2.11) revealed more surface roughness of ultrasound treated

**Fig. 2.9** X-ray diffractograms of *P. hysterothorus* biomass after different treatments. The crystallinity index of biomasses was determined as: original biomass = 57.36 %; delignified biomass with mechanical agitation = 46.9 %, delignified biomass with ultrasound = 45.9 %. Reprinted with permission from [87], Copyright © 2014, American Chemical Society

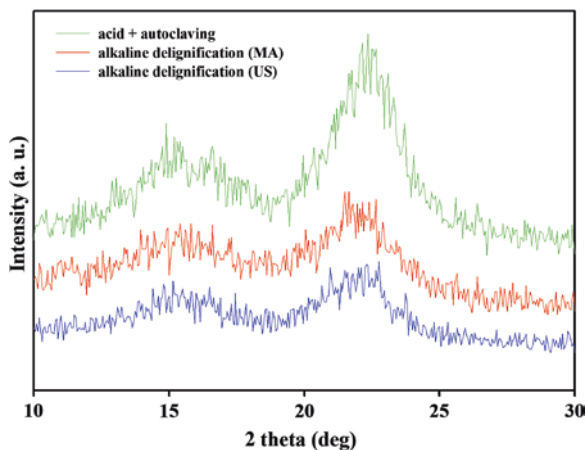
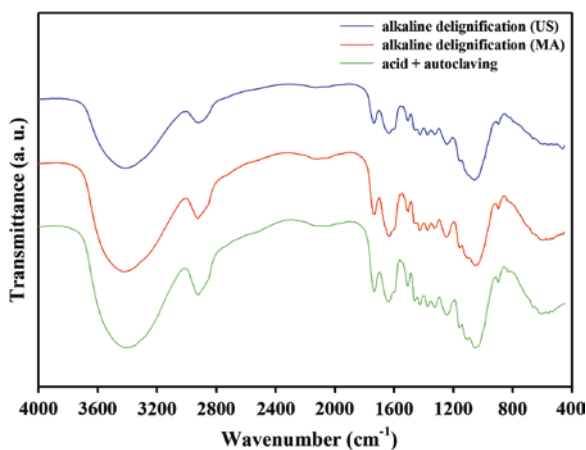


**Fig. 2.10** FTIR spectra of *P. hysterothorus* biomass after different treatments (viz. alkaline delignification with and without ultrasound and acid + autoclaving). Reprinted with permission from [87], Copyright © 2014, American Chemical Society



biomass due to erosion or attrition. Thus, the study of Singh et al. [87] portrays a vivid picture of mechanistic facets of ultrasonic delignification.

Bharadwaja [89] have assessed the effect of ultrasound on enzymatic hydrolysis of delignified biomass. Two commercial enzymes, viz. cellulase and cellobiase, were employed for hydrolysis. Initially, statistical optimization of the enzymatic hydrolysis with mechanical shaking was carried out using Central Composite Design (CCD) coupled with Response Surface Method (RSM) analysis. The optimization parameters were the concentrations of the two enzymes and the biomass concentration. The temperature of the reaction mixture was 50 °C. Later, mechanical shaking was replaced with ultrasound. However, the temperature of reaction mixture was reduced to 30 °C for ultrasonic treatment, as the physical

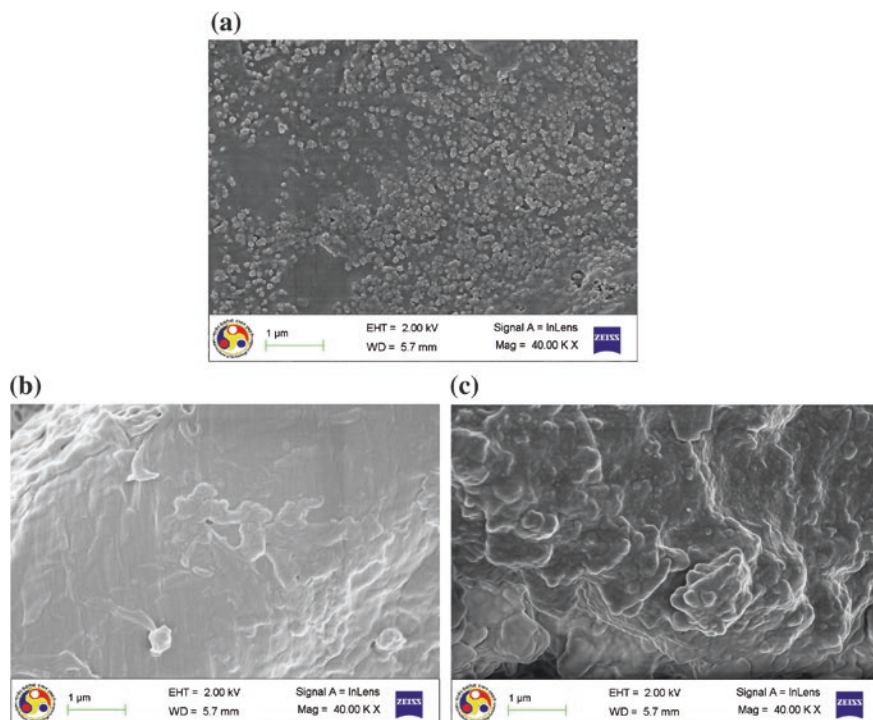


**Fig. 2.11** FESEM micrographs of *P. hysterothorus* biomass **a** original biomass, **b** delignified biomass with mechanical agitation, and **c** delignified biomass with ultrasound. Reprinted with permission from [87], Copyright © 2014, American Chemical Society

and mechanical effects of cavitation bubbles are known to reduce with temperature. The kinetics of enzymatic hydrolysis was found to increase 18-fold with ultrasound. To obtain mechanistic insight into ultrasound induced enhancement, experiments were carried out with varying substrate concentration and the reaction kinetics was analyzed using Michaelis–Menten Model and Lineweaver–Burk plots. The values of  $V_{\max}$  (reaction velocity) and  $K_m$  (substrate affinity constant) were compared for mechanical shaking and sonication. The value of reaction velocity showed an 18-fold increase, while the value of  $K_m$  stayed practically same with sonication. This result suggested that the enhancement effect of ultrasound on hydrolysis is in terms of increase in the reaction rate or velocity, which in turn could be a consequence of enhancement in convection in the medium that eliminates mass transfer, and increases the accessibility of substrate for the enzyme. The enzyme-substrate affinity, however, is an intrinsic property, which does not show any beneficial influence of ultrasound.

## 2.5 Conclusions and Future Outlook

In the preceding sections, we have put forth results of mechanistic investigations of several ultrasound assisted biofuels processes. A concurrent analysis of all of these results provides a coherent framework of the physics of ultrasound-induced enhancement. The physical effect of generation of strong micro-convection by ultrasound and transient cavitation seems to contribute to enhancement more than the chemical effect of radical generation. The technique of application of elevated static pressure provides a simple method for distinguishing between effects of ultrasound and cavitation. Among the individual contributions of ultrasound and transient cavitation, the physical effect of micro-streaming, i.e. rapid oscillatory motion of fluid elements is revealed to make greater impact than the microturbulence and shock waves generated by the transient cavitation. In some processes, such as oxidative desulfurization, transient cavitation is found to influence the system adversely. There are several reasons for some of the opposing trends that contribute to the overall effect of ultrasound on a reaction. In the first place, all biofuel systems are limited by the intrinsic characteristics of the system, which dominate the overall outcome of the process, and these intrinsic factors are relatively uninfluenced by physical and chemical effects of ultrasound. In addition, many chemical reactions actually occur in the bulk liquid and are catalyzed by ions, for example, methoxy radicals in transesterification and protons/hydroxyl ions in acid hydrolysis/delignification of biomass. Thus, the radicals generated by cavitation bubbles have no direct role in the reaction chemistry. In many systems, organic liquids are used as the liquid medium, for example, n-hexane or methanol/chloroform mixture for microalgal lipid extraction, or methanol for transesterification or toluene/n-hexane for oxidative desulfurization, which do not have intense transient radial motion of cavitation bubbles as in the case of when water is the reaction solvent. Accordingly, the physical and chemical effects induced by these bubbles are also not as intense as in water. This effect is attributed to the physical properties of the medium, i.e. large vapor pressure, low surface tension and low density. In addition, many secondary factors come into picture such as the probability of substrate-radical interaction. This factor is more pronounced for dilute systems such as extraction of lipids from microalgae. For microbial/enzymatic system, the transient cavitation has a sharp adverse effect in terms of the shock waves. These waves can cause disruption of microbial cells or denaturing of the enzymes. To understand the beneficial effects of ultrasound on chemical and biological systems, it is essential to isolate the effect of transient cavitation by application of elevated static pressure. An alternate solution is to keep the duty cycle of ultrasound irradiation sufficiently small so as to avoid continuous exposure of the microbial cells to ultrasound. However, the shock waves from transient cavitation have beneficial effects in case of heterogeneous reaction systems—examples of which are the liquid–liquid biphasic transesterification system or the solid–liquid delignification system. The heterogeneous systems have high mass transfer limitations, and thus, interphase transport is a dominant governing factor for kinetics as well as the

yield of these systems. Most of the biofuels systems described in this chapter have these limitations. The strong convection generated by ultrasound/cavitation helps overcome this mass transfer barrier, which helps in boosting the kinetics/yield of such systems. Fine emulsification generated by shock waves gives high interfacial area that boosts the kinetics of the process. Similarly, highly energetic collisions between biomass particles lead to breakage of lignin–hemicellulose bonds and also cause depolymerization of lignin.

Although, our studies have helped identify the physical mechanism of several biofuels system, one important facet of this system that has emerged from all results is the role of intrinsic characteristics of the system. These characteristics play a decisive role and place a limit on the ultrasonic enhancement of the process. For example, in case of microalgal lipid extraction, the selectivity of solvent is an intrinsic parameter. For acid catalyzed biodiesel synthesis, the intrinsic reactivity of the nucleophile attacking protonated carbonyl carbon is an intrinsic parameter. For oxidative desulfurization, diffusivity of PTA-oxidant complex is an intrinsic parameter. For an effective use of ultrasound energy input to the biofuels system, it is utmost essential that these intrinsic parameters be identified and studied in greater detail—as they form the limiting step of the process.

The results and analysis presented in this chapter give a typical framework for discerning the mechanistic issues of the biofuels system, which could be applied to many other biofuels systems not covered in this chapter. We believe that the review of research in physical mechanism of the ultrasound enhanced biofuels system will shed important light on the intricacies of these processes and will give crucial inputs for further research in this area.

## References

1. Suslick KS (1990) Sonochemistry. *Science* 247:1439–1445
2. Hart EJ, Henglein A (1985) Free radical and free atom reactions in the sonolysis of aqueous iodide and formate solutions. *J Phys Chem* 89(20):4342–4347
3. Hart EJ, Henglein A (1987) Sonochemistry of aqueous solutions: hydrogen-oxygen combustion in cavitation bubbles. *J Phys Chem* 91:3654–3656
4. Luo J, Fang Z, Smith RL Jr (2014) Ultrasound-enhanced conversion of biomass to biofuels. *Prog Energy Combust Sci* 41:56–93
5. Morse PM, Ingard KU (1986) *Theoretical acoustics*. Princeton University Press, Princeton
6. Pierce AD (1989) *Acoustics: an introduction to its physical principles and applications*. Acoustical Society of America, New York
7. Suslick KS (1988) *Ultrasound: its physical, chemical and biological effects*. VCH, New York
8. Ensminger D (1988) *Ultrasonics: fundamentals, technology, applications*. Marcel Dekker, New York
9. Young FR (1989) *Cavitation*. McGraw Hill, London
10. Leighton TG (1994) *The acoustic bubble*. Academic Press, San Diego
11. Mason TJ, Lorimer JP (2002) *Applied sonochemistry: the uses of power ultrasound in chemistry and processing*. Wiley-VCH, Coventry
12. Shah YT, Pandit AB, Moholkar VS (1999) *Cavitation reaction engineering*. Plenum Press, New York

13. Flynn HG (1964) Physics of acoustic cavitation in liquids. In: Mason WP (ed) *Physical acoustics*. Academic Press, New York, pp 57–172
14. Brenner M, Hilgenfeldt S, Lohse D (2002) Single-bubble sonoluminescence. *Rev Mod Phys* 74:425–484
15. Neppiras EA (1980) Acoustic cavitation. *Phys Rep* 61:159–251
16. Plesset MS, Prosperetti A (1977) Bubble dynamics and cavitation. *Ann Rev Fluid Mech* 9:145–185
17. Thompson LH, Doraiswamy LK (1999) Sonochemistry: science and engineering. *Ind Eng Chem Res* 38(4):1215–1249
18. Adewuyi YG (2001) Sonochemistry: environmental science and engineering application. *Ind Eng Chem Res* 40:4681–4715
19. Atchley AA, Prosperetti A (1989) The crevice model of bubble nucleation. *J Acoust Soc Am* 86:1065–1084
20. Flynn HG (1975) Cavitation dynamics I. A mathematical formulation. *J Acoust Soc Am* 57:1379–1396
21. Rayleigh L (1917) On the pressure developed in a liquid during the collapse of spherical cavity. *Phil Mag* 34:94–98
22. Plesset MS (1949) Dynamics of cavitation bubbles. *J Appl Mech (Trans ASME)* 16:277–282
23. Poritsky H (1952) The collapse or growth of a spherical bubble or cavity in a viscous fluid. In: Sternberg E (ed) *Proceedings of the 1st US national congress on applied mechanics*, pp 813–821
24. Noltingk BE, Neppiras EA (1950) Cavitation produced by ultrasonics. *Proc Phys Soc B* 63:674–685
25. Gilmore FR (1954) Hydrodynamic laboratory report, 26–4. California Institute of Technology, Pasadena
26. Kirkwood JG, Bethe HA (1942) The pressure wave produced by an under water explosion. Office of Science Research and Development, Report 558
27. Keller JB, Kolodner II (1956) Damping of underwater explosion bubble oscillations. *J Appl Phys* 27:1152–1161
28. Keller JB, Miksis MJ (1980) Bubble oscillations of large amplitude. *J Acoust Soc Am* 68:628–633
29. Prosperetti A, Lezzi A (1986) Bubble dynamics in a compressible liquid. Part 1. First order theory. *J Fluid Mech* 168:457–477
30. Brennen CE (1995) *Cavitation and bubble dynamics*. Oxford University Press, Oxford
31. Lofstedt R, Weninger K, Puttermann SJ, Barber BP (1995) Sonoluminescing bubbles and mass diffusion. *Phys Rev E* 51:4400–4410
32. Barber BP, Hiller RA, Lofstedt R, Putterman SJ, Weninger KR (1997) Defining the unknowns of sonoluminescence. *Phys Rep* 281:65–143
33. Colussi AJ, Weavers LK, Hoffmann MR (1998) Chemical bubble dynamics and quantitative sonochemistry. *J Phys Chem A* 102(35):6927–6934
34. Colussi AJ, Hoffmann MR (1999) Vapor supersaturation in collapsing bubbles: relevance to mechanisms of sonochemistry and sonoluminescence. *J Phys Chem A* 103:11336–11339
35. Kamath V, Prosperetti A, Egolfopoulos FN (1993) A theoretical study of sonoluminescence. *J Acoust Soc Am* 94:248–260
36. Prasad Naidu DV, Rajan R, Kumar R, Gandhi KS, Arakeri VH, Chandrasekaran S (1994) Modeling of a batch sonochemical reactor. *Chem Eng Sci* 49(6):877–888
37. Gong C, Hart DP (1998) Ultrasound induced cavitation and sonochemical yields. *J Acoust Soc Am* 104:2675–2682
38. Sochard S, Wilhelm AM, Delmas H (1997) Modeling of free radicals production in a collapsing gas-vapor bubble. *Ultrason Sonochem* 4:77–84
39. Moss WC, Young DA, Harte JA, Levalin JL, Rozsnyai BF, Zimmerman GB, Zimmerman IH (1999) Computed optical emissions from sonoluminescing bubbles. *Phys Rev E* 59:2986–2992



40. Yasui K (1997) Alternative model for single-bubble sonoluminescence. *Phys Rev E* 56:6750–6760
41. Yasui K (1997) Chemical reactions in a sonoluminescing bubble. *J Phys Soc Japan* 66:2911–2920
42. Krishnan SJ, Dwivedi P, Moholkar VS (2006) Numerical investigation into the chemistry induced by hydrodynamic cavitation. *Ind Eng Chem Res* 45:1493–1504
43. Storey BD, Szeri AJ (2000) Water vapor, sonoluminescence and sonochemistry. *Proc R Soc Lond Ser A* 456:1685–1709
44. Eames IW, Marr NJ, Sabir H (1997) The evaporation coefficient of water: a review. *Int J Heat Mass Transfer* 40:2963–2973
45. Storey BD, Szeri AJ (2001) A reduced model of cavitation physics for use in sonochemistry. *Proc R Soc Lond Ser A* 457:1685–1700
46. Toegel R, Gompf B, Pecha R, Lohse D (2000) Does water vapor prevent upscaling sonoluminescence? *Phys Rev Lett* 85:3165–3168
47. Hilgenfeldt S, Lohse D, Brenner MP (1996) Phase diagrams for sonoluminescing bubbles. *Phys Fluids* 8(11):2808–2826
48. Toegel R (2002) Reaction diffusion kinetics of a single sonoluminescing bubble. PhD dissertation, University of Twente, Netherlands
49. Hirschfelder JO, Curtiss CF, Bird RB (1954) *Molecular theory of gases and liquids*. Wiley, New York
50. Reid RC, Prausnitz JM, Poling BE (1987) *Properties of gases and liquids*. McGraw Hill, New York
51. Davis SL, Vibrational modes of methanol. (<http://classweb.gmu.edu/sdavis/research/modes.htm>)
52. Condon EU, Odishaw H (1958) *Handbook of physics*. McGraw Hill, New York
53. Crank J (1975) *The mathematics of diffusion*. Clarendon Press, Oxford
54. Press WH, Teukolsky SA, Flannery BP, Vetterling WT (1992) *Numerical recipes*, 2nd edn. Cambridge University Press, New York
55. Apfel RE (1981). In: Edmonds PD (ed) *Methods in experimental physics*, vol 19. Academic Press, New York, pp 355–413
56. Holland CK, Apfel RE (1989) An improved theory for prediction of microcavitation thresholds. *IEEE Trans Ultrason Ferroelectr Freq Control* 36:204–208
57. Nyborg WL (1958) Acoustic streaming near a boundary. *J Acoust Soc Am* 30:329–339
58. Kolb J, Nyborg WL (1956) Small scale acoustic streaming in liquids. *J Acoust Soc Am* 28:1237–1242
59. Lauterborn W, Hentschel W (1985) Cavitation bubble dynamics studied by high speed photography and holography: part one. *Ultrasonics* 23:260–268
60. Lauterborn W, Hentschel W (1986) Cavitation bubble dynamics studied by high speed photography and holography: part two. *Ultrasonics* 24:59–65
61. Pecha R, Gompf B (2000) Microimplosions: cavitation collapse and shock wave emission on a nanosecond time scale. *Phys Rev Lett* 84:1328–1330
62. Plesset MS, Chapman RB (1971) Collapse of an initially spherical vapour cavity in the neighbourhood of a solid boundary. *J Fluid Mech* 47:283–290
63. Blake JR, Taib BB, Doherty G (1986) Transient cavities near boundaries. Part I. Rigid boundary. *J Fluid Mech* 170:479–497
64. Blake JR, Taib BB, Doherty G (1987) Transient cavities near boundaries. Part II. Free surface. *J Fluid Mech* 181:197–212
65. Vogel A, Lauterborn W, Timm R (1989) Optical and acoustic investigations of the dynamics of laser-produced cavitation bubbles near a solid boundary. *J Fluid Mech* 206:299–338
66. Phillip A, Lauterborn W (1998) Cavitation erosion by single laser-produced bubbles. *J Fluid Mech* 361:75–116
67. Ilyichev VI, Koretz VL, Melnikov NP (1989) Spectral characteristics of acoustic cavitation. *Ultrasonics* 27:357–361

68. Moholkar VS, Warmoeskerken MMCG, Ohl CD, Prosperetti A (2004) The mechanism of mass transfer enhancement in textile with ultrasound. *AIChE J* 50:58–64
69. Ranjan A, Patil C, Moholkar VS (2010) Mechanistic assessment of microalgal lipid extraction. *Ind Eng Chem Res* 49:2979–2985
70. Kalva A, Sivasankar T, Moholkar VS (2009) Physical mechanism of ultrasound-assisted synthesis of biodiesel. *Ind Eng Chem Res* 48:534–544
71. Parkar PA, Choudhary HA, Moholkar VS (2012) Mechanistic and kinetic investigations in ultrasound assisted acid catalyzed biodiesel synthesis. *Chem Eng J* 187:248–260
72. Choudhury HA, Chakma S, Moholkar VS (2014) Mechanistic insight into sonochemical biodiesel synthesis using heterogeneous base catalyst. *Ultrason Sonochem* 21:169–181
73. Choudhury HA, Malani RS, Moholkar VS (2013) Acid catalyzed biodiesel synthesis from *Jatropha* oil: mechanistic aspects of ultrasonic intensification. *Chem Eng J* 231:262–272
74. Choudhury HA, Goswami PP, Malani RS, Moholkar VS (2014) Ultrasonic biodiesel synthesis from crude *Jatropha curcas* oil with heterogeneous base catalyst: mechanistic insight and statistical optimization. *Ultrason Sonochem* 21:1050–1064
75. Choudhury HA, Srivastava P, Moholkar VS (2014) Single-step ultrasonic synthesis of biodiesel from crude *Jatropha curcas* oil. *AIChE J* 60:1572–1581
76. Khanna S, Goyal A, Moholkar VS (2012) Bioconversion of biodiesel derived crude glycerol by immobilized *Clostridium pasteurianum*: effect of temperature. *Int J Chem Biol Eng* 6:301–304
77. Khanna S, Goyal A, Moholkar VS (2013) Effect of fermentation parameters on bio-alcohols production from glycerol using immobilized *Clostridium pasteurianum*: an optimization study. *Prep Biochem Biotechnol* 43:828–847
78. Khanna S, Ranjan A, Goyal A, Moholkar VS (2013) Medium optimization for mixed alcohols production by glycerol utilizing immobilized *Clostridium pasteurianum* MTCC 116. *Chem Biochem Eng Qtr* 27(3):319–325
79. Khanna S, Jaiswal S, Goyal A, Moholkar VS (2012) Ultrasound enhanced bioconversion of glycerol by *Clostridium pasteurianum*: a mechanistic investigation. *Chem Eng J* 200–202:416–425
80. Haldane J (1930) *Enzymes*. Longmans Green and Co., New York
81. Khanna S, Goyal A, Moholkar VS (2013) Mechanistic investigation of ultrasonic enhancement of glycerol bioconversion by immobilized *Clostridium pasteurianum* on silica support. *Biotechnol Bioeng* 110:1637–1645
82. Bolla MK, Choudhury HA, Moholkar VS (2012) Mechanistic features of ultrasound-assisted oxidative desulfurization of liquid fuels. *Ind Eng Chem Res* 51:9705–9712
83. Bhasarkar JB, Chakma S, Moholkar VS (2013) Mechanistic features of oxidative desulfurization using sono-Fenton–peracetic acid (ultrasound/ $\text{Fe}^{2+}$ – $\text{CH}_3\text{COOH}$ – $\text{H}_2\text{O}_2$ ) system. *Ind Eng Chem Res* 52:9038–9047
84. Bhasarkar JB, Chakma S, Moholkar VS (2014) Investigations in physical mechanism of the oxidative desulfurization process assisted simultaneously by phase transfer agent and ultrasound (communicated)
85. Suresh K, Ranjan A, Singh S, Moholkar VS (2014) Mechanistic investigations in sono-hybrid techniques for rice straw pretreatment. *Ultrason Sonochem* 21:200–207
86. Jacobsen SE, Wyman CE (2000) Cellulose and hemicellulose hydrolysis models for application to current and novel pretreatment processes. *Appl Biochem Biotechnol* 84–86:81–96
87. Singh S, Bharadwaja STP, Yadav P, Moholkar VS (2014) Mechanistic investigation in ultrasound-assisted (alkaline) delignification of *Parthenium hysterophorus* biomass. *Ind Eng Chem Res*. doi:10.1021/ie502339q
88. TAPPI (1992) Technical association of pulp and paper industry. Atlanta, Georgia, USA
89. STP Bharadwaja (2014) Mechanistic investigation in ultrasound assisted delignification and enzymatic hydrolysis of *Parthenium hysterophorus* for bioethanol production. M Tech dissertation, Indian Institute of Technology Guwahati, India



# Chapter 3

## Batch and Continuous Ultrasonic Reactors for the Production of Methyl Esters from Vegetable Oils

D.C. Boffito, J.-M. Leveque, C. Pirola, C.L. Bianchi, R. Vibert,  
A. Perrier and G.S. Patience

**Abstract** Mass transfer is a rate limiting step in biodiesel production. Ultrasound can accelerate tremendously the mass transfer in both triglycerides transesterification and free fatty acid esterification by finely emulsifying reagents that are poorly miscible. We describe reactor configurations for both transesterification and esterification, with emphasis on the work published by the authors. Ultrasound in the esterification increases the mass transfer in raw oils at temperatures below 40 °C. The Eley–Rideal kinetic model of the esterification including the mass transfer resistance between the phases is in excellent agreement with the experimental data.

---

D.C. Boffito (✉) · G.S. Patience  
Polytechnique Montréal—Département de Génie Chimique, 2900 Édouard-Montpetit,  
2500 Chemin Polytechnique, H3T 1J4 Montreal, Canada  
e-mail: daria-camilla.boffito@polymtl.ca

G.S. Patience  
e-mail: gregory-s.patience@polymtl.ca

J.-M. Leveque  
University of Savoie, LCME/CISM, 73376 Le Bourget du Lac Cedex, France  
e-mail: jm.leveque@petronas.com.my

J.-M. Leveque  
Department of Fundamental and Applied Sciences, Universiti Teknologi Petronas,  
Bandar Seri Iskandar, 31750 Tronoh, Perak, Malaysia

C. Pirola · C.L. Bianchi  
Università Degli Studi Di Milano—Dipartimento Di Chimica, via Golgi 19, 20133 Milan,  
Italy  
e-mail: carlo.pirola@unimi.it

C.L. Bianchi  
e-mail: claudia.bianchi@unimi.it

R. Vibert · A. Perrier  
Synetude, P.a. de Côte Rouse 180, Rue du Genevois, 73000 Chambéry, France  
e-mail: synetude@gmail.com

A. Perrier  
e-mail: synetude@gmail.com

The Rosett cell reactor combines acoustic cavitation and turbulence and transesterifies 90 % of the feedstock in 5 min, whereas it takes 90 min in a conventional batch reactor. Continuous and semi-continuous tubular reactors irradiated at a power density of 40 kW/cm<sup>3</sup> converts 90 % of the oil in 10 min. A Sonitube<sup>®</sup> (Synetude) converts 90 % of the oil after a single passage in a continuous reactor. This corresponds to 18 s and a rate 300 times faster than the conventional process. Sonitube<sup>®</sup> improves mass transfer substantially and is worthy of scaling up.

**Keywords** Biodiesel · Methyl esters · Esterification · Transesterification · Ultrasound · Tubular reactor · Acoustic cavitation · Sonitube<sup>®</sup>

### 3.1 Introduction

Process intensification techniques have a major role in biomass conversion. Biomass is a heterogeneous substrate, characterized by multiple phases, with different densities and viscosities. Therefore, biomass transformation processes are often mass-transfer limited and reaction rates are usually low [1, 2].

Vegetable oil, animal fat or waste oils and fats react with alcohol to yield biodiesel (BD), a liquid biofuel producible on a large scale [3] and used in compression ignition engines without major modifications [4]. Commercial plants usually consist of multiple stage reactors with separation steps in between (Scheme in Fig. 3.1). Commercial BD plants suffer from several drawbacks. The main issues are: very

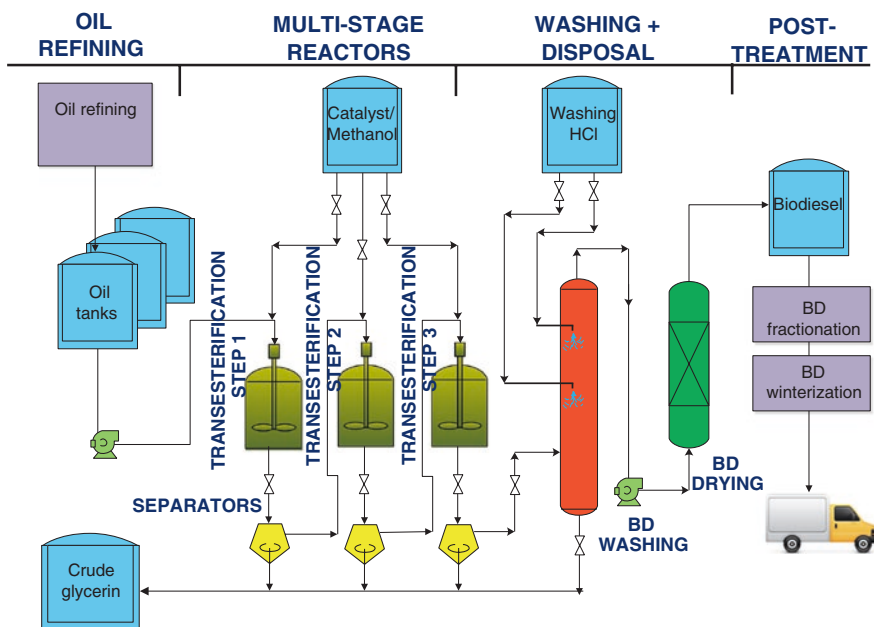
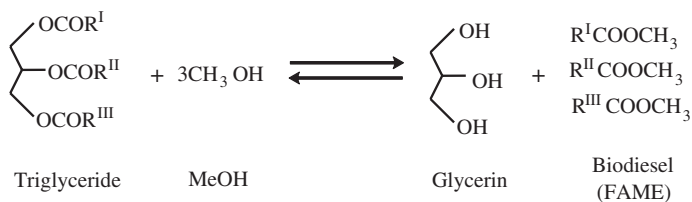
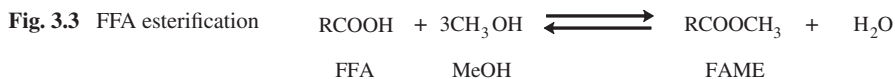


Fig. 3.1 Biodiesel production process schematic



**Fig. 3.2** Triglyceride transesterification



**Fig. 3.3** FFA esterification

long processing times (up to 8 h per batch), limited feedstock and disposal of the homogeneous (basic) catalyst [5]. Separation and purification of biodiesel is energy intensive [6, 7]. Radich estimated that 1 L of biodiesel from vegetable oils requires 3 kWh (production + separation + purification) [8].

Besides triglycerides transesterification, free fatty acid (FFA) esterification produces methyl esters. Oils contain triglycerides as well as FFA. Triglycerides hydrolyse to form FFA. In refined oils and fats, the amount of FFA is low (<0.2 wt%). In unrefined and, in particular, waste oils, FFA can exceed 0.5 wt%, which reacts with the alkaline transesterification catalyst to form soap [9–11]. The transesterification of triglycerides is the commercial process to convert oils and fats into BD. However, when the amount of FFA exceeds 0.5 wt%, the FFA must be esterified first. Acid catalysts transesterify triglycerides (Fig. 3.2) and esterify FFA (Fig. 3.3) simultaneously at temperatures above 120 °C [12], but operating temperatures in commercial plants approaches 65 °C [13]. Alkali-catalyzed transesterification is 4,000 times faster than the acid-catalyzed transesterification. Therefore, the two reactions are preferably carried out in separate reactors [14] or sequentially in the same reactor.

Various intensification methods have been tested to eliminate or minimize mass transfer limitations in BD production processes [15]. These include ultrasonic (US) and microwave (MW) irradiation [16, 17], design of the mixer [18, 19], hydrodynamic cavitation [20], micro-channel reactors [21, 22], adding co-solvents [23], operating at supercritical conditions [24], supercritical reaction extraction [25], and dividing wall technology [26]. US promote both FFA esterification [27, 28] and triglycerides transesterification, either homogeneously or heterogeneously-catalyzed [28, 29]. There are several reviews on BD process intensification that describe sonochemical techniques among other technologies [27, 30–34]. There are as well several reviews devoted exclusively to ultrasonic BD production [27, 35].

Veljković reviews the state of the art and perspectives of BD production by US-assisted transesterification and asserts that low frequency US (LFU) has several advantages over the classical synthesis process [15].

Sonochemical techniques and US in particular enhance the mass transfer between the two phases. US emulsifies immiscible liquids, such as oil and methanol, thereby increasing the available surface area to react the reagents of the two phases.

Sonication produces a more stable emulsion than those formed by conventional stirring [36]. Thomson and Doraiswamy [37] also highlight that cavitation

increases the localized temperature at the phase boundary and, as a consequence, accelerates the reaction rate. The amount of catalyst required for the US-assisted process is usually lower compared to mechanical stirring and energy savings can be higher than 60 % with respect to mechanical stirring [38].

The present chapter reviews several reactor configurations to produce BD with US. It includes energetic considerations and kinetic modelling of the FFA esterification in refined and raw oils. We examine both homogeneous and heterogeneous esterification and transesterification in ultrasonic reactors. Most of the data available in the literature concern batch and technologies based on continuous stirred tank reactors (CSTRs). This chapter also discusses continuous loop technologies.

## 3.2 Ultrasonic Batch Reactors and CSTRs

Batch reactors are widely used for both esterification and transesterification [15]. They are easy to operate and characterize at the laboratory scale but at the industrial scale there is less flexibility and mass transfer between the phases becomes problematic.

In general, commercial BD processes rely on either batch or CSTR technologies, in which a basic catalyst is solubilised in methanol [39, 40]. In these technologies, stirring vigorously decreases the mass transfer resistance between the reagents and the homogeneous catalyst contributes to increasing the reaction rates but still, methanol is poorly soluble in oil (6–8 % at 60 °C) and stirring is insufficient to form a fine MeOH-oil emulsion [14, 41].

US overcomes mass transfer limitations related to BD synthesis for both transesterification [15, 42, 43] and esterification [27–29, 44] in batch reactors and CSTRs, with either homogeneous or heterogeneous catalysts.

### 3.2.1 Homogeneously-Catalyzed Esterification

Sulfuric acid is widely used as a homogeneous catalyst for FFA esterification.  $\text{H}_2\text{SO}_4$  concentrations are typically lower than 2 wt% with respect to the system oil + methanol [27–29].

Ultrasonic baths are the most frequently cited equipment in the literature concerning the homogeneously-catalyzed esterification [15, 28, 29]. Santos et al. report the esterification of FFA from Nile tilapia oil in an ultrasonic bath with  $\text{H}_2\text{SO}_4$ . The ultrasonic system was a Unique model USC, operating at a constant low frequency of 40 kHz and 60 W. At 30 and 60 °C and at MeOH/FFA molar ratios higher than 9, in 30 min, over 90 % of the FFA esterifies to methyl esters (ME) [28]. The optimal operating conditions were MeOH/FFA molar ratio of 9.0 and  $\text{H}_2\text{SO}_4$ /FFA of 2.0 wt% at 30 °C.

**Table 3.1** References on the ultrasound (US)-assisted free fatty acids (FFA) esterification cited in this manuscript

Ultrasonic reactor	Catalyst	Ultrasound parameters	Oil type	FFA conv., T, time	Reference
US bath with 3 transducers in triangular arrangement	H <sub>2</sub> SO <sub>4</sub>	20 kHz 120 W (real 45 W)	Nagchampa oil	94 %, 40 °C, 15'	[27]
US bath	H <sub>2</sub> SO <sub>4</sub>	40 kHz 60 W/200 mL	Nila Tilapia oil	98 %, 30 °C, 90'	[28]
Batch US probe	Amberlyst®46	20 kHz 295 W (real 31.7 W)	Tobacco Canola Oleic acid	70 %, 20 °C, 6 h 90 %, 63 °C, 6 h 60 %, 63 °C, 6 h	[44]
Batch US probe	Immobilized lipase	20 kHz 50 W/40 mL	Nagchampa oil	97 %, 30 °C, 7 h	[45]
Continuous, with a static mixer and US homogenizer	H <sub>2</sub> SO <sub>4</sub>	18 kHz 10 W/mL	Palm	93 %, 60 °C, 18''	[46]

Gole and Gogate report the esterification of Nagchampa oil with H<sub>2</sub>SO<sub>4</sub> in an ultrasonic bath at 20 kHz. The bath was equipped with three transducers arranged in a triangular pitch at the bottom of the tank. The ultrasonication converts more than 90 % of the oil after 30 min, whereby the conventional stirring converted only 30 % of the oil [27].

All the references cited in this manuscript and concerning the US-assisted FFA esterification are listed in Table 3.1.

### 3.2.2 Heterogeneously-Catalyzed Esterification

Few studies report FFA esterification over solid catalysts with US. However, heterogeneous catalysts could overcome issues associated with homogeneous catalysts, i.e. corrosion, wastewater disposal and catalyst recovery-reuse.

Among the heterogeneously catalyzed-esterification technologies, US-assisted enzymatic FFA esterification is worth mentioning. An immobilized lipase converts 97 % of the FFA to methyl esters [46].

US together with solid catalysts increases reaction rates [44, 47]. Boffito et al. studied ultrasonic batch esterification of FFA in Canola, raw Tobacco oilseeds and pure oleic acid using Amberlyst® 46 (Dow Chemical) as a sulphonic ion exchange resin [44]. Amberlyst® 46 only has active –SO<sub>3</sub>H groups on the outer surface of the beads and not inside the pores. Internal diffusion of the reagents in the pores is therefore negligible and the system can be considered as pseudo-homogeneous.

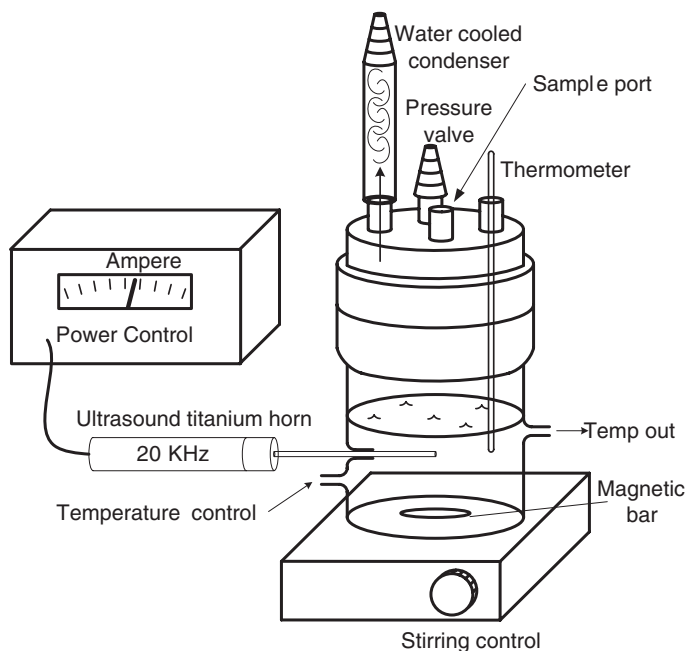


**Fig. 3.4** Batch ultrasonic reactor. Reprinted with permission from [44], Copyright © 2014, Elsevier

The batch ultrasonic reactor used by Boffito et al. [44] is illustrated in Fig. 3.4.

Ragaini et al. [48] describe the reactor system and highlight the special design features and energy considerations.

The maximum nominal power of the US horn (Bandelin, Mod. Sonoplus GM 2200 sonicator), was  $295 \pm 2$  W, with a frequency of 20 kHz and a tip diameter of 13 mm.

The fluid-catalyst slurry was continuously stirred either with a magnetic bar (in the case of the conventional process) or US. In the experiments, 10 g of catalyst was charged to the reactor followed by 16 g of methanol. The ratio of the oleic acid to MeOH was 1.4.

Boffito and coauthors describe the FFA esterification as a “doubly-heterogeneous system”: (i) oil-methanol liquid-liquid and (ii) oil/methanol-solid catalyst liquid–solid system. US is beneficial to both types of systems. In the case of liquid–liquid immiscible systems, as already mentioned in the introduction, US forms emulsions that are finer than those formed by conventional agitators [36, 44].

The collapse of the bubbles in the vicinity of the surface are responsible for the positive effects of acoustic cavitation. When a cavitation bubble collapses near a solid surface, it generates high speed liquid, which impact into the surface of a particle (due to asymmetric collapse of bubbles) [49], resulting in enhanced transport of the species towards the solid surface of the catalyst where the reagents are.

Boffito et al. [44] found that FFA reacts to methyl esters faster with US compared to conventional mechanical stirring in all of their experiments. US accelerates the reaction rates considerably more at lower temperatures (compare Figs. 3.5 and 3.6).

In the case of both Canola oil and Tobacco seed oil, the acidity dropped below 0.5 wt% in less than 6 h at 63 °C (Fig. 3.5) either with or without US. At 40 °C (Fig. 3.6), the difference between the US-assisted and the conventional process is more pronounced in the case of the Tobacco seed oil.

Sonochemically irradiating the Tobacco seed oil at 20 °C gave the same yield as at 40 °C (with US) but higher than the conventional process at 40 °C (Fig. 3.7).

**Fig. 3.5** Conversions with and without ultrasound at 63 °C in Ref. [44]. The lines represent the model. Reprinted with permission from [44], Copyright © 2014, Elsevier

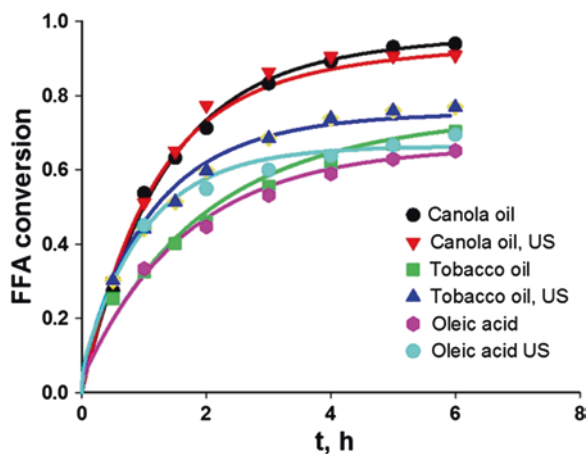


**Fig. 3.6** Conversions with and without ultrasound at 40 °C in Ref. [44]. The lines represent the model. Reprinted with permission from [44], Copyright © 2014, Elsevier

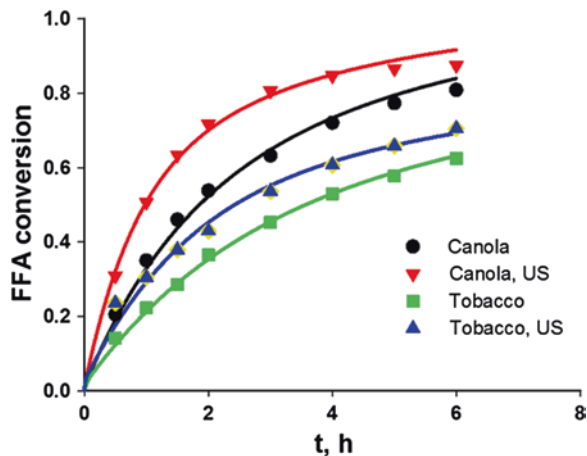
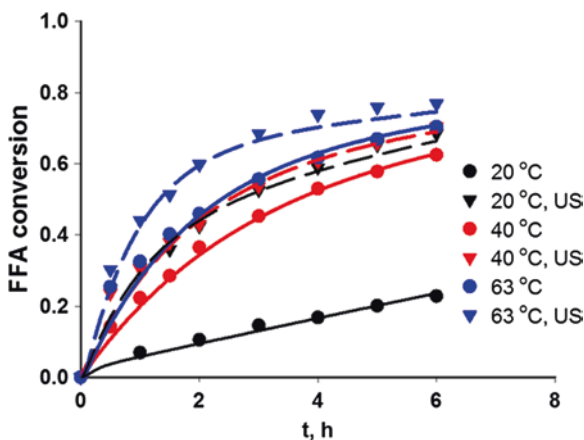


**Fig. 3.7** Conversions with and without ultrasound of the Tobacco seed oil in Ref. [44]. The lines represent the model. Reprinted with permission from [44], Copyright © 2014, Elsevier



At 63 °C and at 40 °C the difference in conversion after 6 h in the US and mechanical stirring are 6 and 8 % points, respectively. It is remarkable the FFA conversion is three times higher with US at 20 °C versus mechanical stirring.

The initial acidity in the Tobacco seed oil was 1.15 wt% and it dropped to the target of 0.5 wt% with US at all the temperatures but only at 63 °C with the mechanical stirring. After 6 h and at 63 °C, the US system reached equilibrium but the conversion was much lower compared to the Canola oil tests. The other conditions required more time to reach equilibrium. The lower conversion may be attributable either to water in the feedstock (as much as 4,000 ppm) or to the high viscosity of the oil. In fact, although Tobacco seed oil is expected to have a lower viscosity than Canola, because of the higher content of linoleic acid, the Tobacco seed oil appeared very thick and consequently viscous. The higher viscosity may be due to residues from the pressing or phospholipids that are usually present in the Tobacco seed oil.

The superior performance for the US with Tobacco seed oil and oleic acid might be due to the higher viscosity of the Tobacco seed oil and oleic acid with respect to Canola oil. In the case of highly viscous media, the contribution of US to mass transfer is expected to be more pronounced [49]. The lower difference in conversion at 63 °C compared to 40 °C (Fig. 3.7) may be accounted for by several phenomena. It is well known that acoustic cavitation is enhanced at low temperatures: more gas (air) is dissolved in liquids at lower temperature and this gas generates active nuclei for acoustic cavitation. Vapour pressure increases with temperature, which enhances bubble formation, however, when the vapour pressure is higher, the bubble collapse is less violent. This phenomenon is called “vapour cavitation”. The higher the temperature, the amount of methanol vapours in the cavitation bubbles is more likely to be higher and the collapse less violent [50]. Viscosity is lower at higher temperatures, and thus mass transfer resistance for the conventional process is lower. The kinetic model of Boffito and coauthors accounts for mass transfer at the phase boundaries in the reaction system methanol-oil (+FFA)-catalyst [44].



### 3.2.2.1 Kinetic Modelling

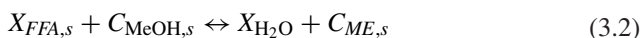
In a homogeneous system, equilibrium conversion depends on temperature and the initial concentration of reactants; the equilibrium constant depends solely on temperature. As noted above, the oil-methanol-catalyst is a doubly heterogeneous system. Thus, the bulk phase concentration may not be representative of the equilibrium conversion in the boundary phase of the catalyst. Furthermore, the equilibrium is shifted if one of the products or reactants is removed from the system like adsorption of a compound on the catalyst. Assuming that equilibrium is reached at 63 °C, the apparent equilibrium constant ( $K_{eq}$ ) equals 2, 0.3 and 0.02 for oleic acid, Canola oil and Tobacco seed oil, respectively. Boffito et al. [44] assessed the degree to which US accelerates mass transfer and to account for all of the phenomena described above (not necessarily comprehensively). Therefore, a mass balance equation was derived considering two phases—a bulk phase for which we measured the concentrations, and a boundary layer phase at the surface of the catalyst. We assumed that:

- The reaction rate in the absence of catalyst is negligible at all temperatures and for both the mechanically-stirred and the sonicated reactor.
- The temperature is uniform.
- The reaction starts only when the mechanical stirrer or sonicator is initiated.
- Catalyst deactivation is negligible during the course of the experiments.

Many recent studies hold that mass transfer resistance is negligible at high stirring rates [51–53] and substantiate this postulate by demonstrating that conversion remains constant beyond a certain stirring rate. We suggest that increasing the stirring rate may reduce mass transfer resistance in the bulk but may not affect the boundary layer mass transfer or the interface between the emulsion and the catalyst active sites.

Few studies report modelling US-assisted esterification kinetics. Several papers report that US increases mass transfer in the oil/MeOH systems [29], but their homogeneous kinetic models [54, 55] neglect it in the overall reaction rate.

Boffito et al.'s [44] model accounts for both surface reaction and mass transfer between the surface and the bulk phase. Initially, mass transfer limits the reaction rate as the system approaches equilibrium, the reaction kinetics become slower. FFA esterification follows an Eley-Rideal type mechanism: FFA adsorbs onto an acidic site (X) to form an adsorbed species  $X_{FFA,s}$  (1); this species reacts with methanol and releases ME to the liquid phase and forms an adsorbed water as species on the active sites  $X_{H_2O}$  (2).  $H_2O$  desorbs in the last step (3).



When FFA adsorption and water desorption are in equilibrium and the surface reaction (set 2) is the slow step, the rate equation becomes:

$$r = \frac{k \left( C_{FFA,s} \cdot C_{MeOH,s} - \frac{C_{H_2O,s} \cdot C_{ME,s}}{K_{eq}} \right)}{1 + K_1 C_{FFA,s} + K_3 C_{H_2O,s}} \quad (3.4)$$

The adsorption terms were small and thus neglected when deriving the rate constant,  $k$ , and equilibrium constant. This expression was combined with a mass balance between the boundary layer at the surface of the catalyst and bulk liquid:

$$\phi V \frac{d}{dt} C_i = -k_m (C_i - C_{i,s}) \quad (3.5)$$

where  $C_i$  and  $C_{i,s}$  represent the concentration of each of the four reacting species in the bulk and on the surface of the catalyst, respectively. Mass transfer between the catalyst surface and the bulk is represented by  $k_m$  and  $V$  is the total fluid volume,  $\phi$  is the fractional volume of the bulk phase and  $(1 - \phi)$  is the volume of the boundary layer around the catalyst.

The mass balance for water in the bulk phase becomes:

$$\phi V \frac{d}{dt} C_{H_2O} = -k_m (C_{H_2O} - C_{H_2O,s}) - k_{H_2O} C_{H_2O} (C_T - C_{H_2O,ads}) \quad (3.6)$$

The mass balance for the surface boundary layer phase is:

$$(1 - \phi) V \frac{d}{dt} C_{i,s} = k_m (C_i - C_{i,s}) - \nu_i r \quad (3.7)$$

where the stoichiometric coefficient,  $\nu_i$ , equals 1 for FFA and MeOH and is  $-1$  for ME and  $H_2O$ . Finally, the mass balance around the water adsorption by the catalyst is

$$W \frac{d}{dt} C_{H_2O,ads} = -k_{H_2O} C_{H_2O} (C_T - C_{H_2O,ads}) \quad (3.8)$$

where  $W$  is the weight of catalyst (g),  $C_T$ , is the capacity of the catalyst to absorb water (0.4 g/g catalyst) and  $C_{H_2O,ads}$  is the molar concentration of water on the surface. Note that the adsorbed water,  $C_{H_2O,ads}$ , is assumed to be independent of the reaction sites. The fitted parameters include the rate constant  $k$ , the mass transfer coefficient between the boundary layer and bulk fluid,  $k_m$ , as well as the equilibrium constants,  $K_{eq}$  and the absorption coefficient  $k_{H_2O}$ .

The boundary volume and mass transfer rate are coupled parameters such that an increase in one will decrease the other proportionately. Therefore, Boffito et al. [44] assumed a fixed boundary thickness and combined the two terms into a single coefficient  $k_m$ . The average particle diameter was 0.85 mm and the boundary layer was assumed to equal 30  $\mu\text{m}$ , which represents about 3 % of the total volume of the catalyst.

To assess the impact of the US on the reaction rate, they compared experiments with and without US maintaining the same temperature and 10 g of A46 for each 100 g of oil or oleic acid.

The conversion of FFA in the Tobacco seed oil is lower than for the Canola oil (Figs. 3.5 and 3.6). One of the major differences is the initial FFA concentration, that is about 1 % versus 4 % for Tobacco and Canola oil, respectively. However, this difference was insufficient to account for the lower conversion. US enhances the mass transfer rate considerably with the exception of the test with Canola oil at 63 °C. In this case, the conversion reached 94 % after 6 h, whereas it only reached 91 % with US. This lower conversion must be due to equilibrium considerations—perhaps water contamination, lower temperature or MeOH might have preferentially evaporated during this test, as already hypothesized by the authors in a previous study [42]. Vapour cavitation might have played a role, as already specified in the previous section. All other tests show a significant improvement in the mass transfer rate with US—typically greater than two times. Table 3.2 summarizes the relative improvement,  $k_{m,US}/k_m$ , and the best fit parameters.

Even if several papers report that external diffusion can be neglected [51–53], the reactive system has two boundaries. As a consequence, even considering that there are no diffusion limitations in the oil phase, there are still the diffusional considerations with respect to the oil/MeOH boundary in proximity of the catalyst surface.

The oleic acid/MeOH system is a single-phase solution. Therefore, we expect that the mass transfer should be due solely to the bulk phase. This test was made at the highest oleic acid concentration maintaining the same mass of MeOH as in the other experiments (100 g of oleic acid and 16 g of MeOH). However the mole fraction of MeOH is lower (0.585) compared to the tests with seed oils (0.800).

Oleic acid conversion was lower compared to most of the other experiments but its  $K_{eq}$  was the highest. We expected that all the tests conducted at 63 °C would have had the same or similar value of the  $K_{eq}$ . We attributed the higher value of the  $K_{eq}$  in the oleic acid tests to the presence of water. The catalyst A46 is well known to adsorb as much as 40 % of its weight of water [56]. Subtracting water from the system shifts the equilibrium towards products and thus alters the equilibrium constant based on the bulk concentration.

Each experiment was conducted as a pair, with and without US. The rate constant, equilibrium constant for each pair were given the same value and the data were fit allowing the mass transfer coefficient to vary.

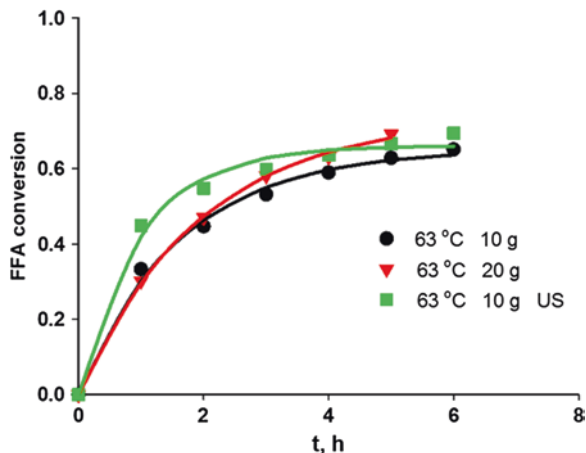
The model fits the experimental data very well with correlation coefficients greater than 0.97 and greater than 0.995 for the oleic acid tests. The activation energy was 85,000 kJ mol<sup>-1</sup> for the tests with Tobacco seed oil and Canola oil (derived for the experiments conducted at 40 and 63 °C). Nevertheless, the presence of water is problematic for the calculation of the reaction rate and the equilibrium. Any water originally present in the oil reduces the equilibrium conversion. While oleic acid is water free, Karl Fischer analysis confirmed that water originally present in Canola oil is on the order of 600 ppm and may increase with time under air exposure: in the Tobacco seed oil it is as much 2,000 ppm. At 63 °C the test fit value of the  $K_{eq}$  for oleic acid was 0.57 (assuming  $k_{H_2O} = 0.06$ ), 0.38 and 0.05 for Canola oil and Tobacco oil, respectively. The presence of water undoubtedly affects the conversion at equilibrium; however, the impact of US on the mass

**Table 3.2** Best fit parameters estimates with and without ultrasound (Eqs. 3.1–3.8). Reprinted with permission from [44], Copyright © 2014, Elsevier

Feedstock	H <sub>2</sub> O (ppm)	T (°C)	$k$ (L <sup>2</sup> mol <sup>-1</sup> min <sup>-1</sup> )	$K_{eq}$	$k_m$ (L min <sup>-1</sup> )	$k_{m,US}$ (L min <sup>-1</sup> )	$k_{m,US}/k_m$	$k_{H_2O}$ (L min <sup>-1</sup> )	R <sup>2</sup>	R <sup>2</sup> <sub>GS</sub>
Oleic acid	0	63	0.0050	0.57	0.0034	0.0064	1.9	0.06	1.00	1.00
Canola	600	40	0.0009	0.073	0.0015	0.0040	2.6	0.05	0.98	0.97
Canola	600	63	0.0088	0.380	0.0017	0.0020	1.2	0.02	0.99	0.99
Tobacco	2,000	20	0.0005	0.007	0.0004	0.0024	6.7	0.02	0.99	0.97
Tobacco	2,000	40	0.0003	0.027	0.0019	0.0080	4.1	0.02	1.00	0.98
Tobacco	2,000	63	0.0027	0.050	0.0013	0.0026	2.0	0.01	0.99	0.98

Reprinted with permission from [44], Copyright © 2014, Elsevier

**Fig. 3.8** Conversions with and without ultrasound of pure oleic acid. The lines represent the model



transfer rate is independent of the assumed initial concentration of water. For instance, increasing the initial concentration of water in the Tobacco seed oil from 600 to 4,000 and 10,000 ppm, increases the calculated  $K_{eq}$  to 0.026, 0.1 and 0.28, respectively (at 63 °C). However, the mass transfer coefficient for the conventional and US process,  $k_m$  and  $k_{m,US}$ , remains unchanged at 0.00162 and 0.05 regardless of the amount of water with  $R^2 > 0.98$ . More importantly, their ratio is constant as well. Thus, we may use the model to accurately characterize the change in mass transfer rate with US.

Figures 3.5, 3.6, 3.7 and 3.8 demonstrate excellent agreement between the model and experimental data at 63 and 40 °C for the A46 catalyst and various types of oils. The model confirms that mass transfer rates are higher with US at lower temperatures. It is six fold higher at 20 °C with Tobacco oil compared to four times higher at 40 °C and only two times at 63 °C. With the less viscous Canola oil, the increase in mass transfer with US versus conventional stirring is  $2.6\times$  at 40 °C and essentially the same at 63 °C.

### 3.2.2.2 Homogeneously-Catalyzed Transesterification

All the references cited in this manuscript and concerning the US-assisted FFA esterification are listed in Table 3.3.

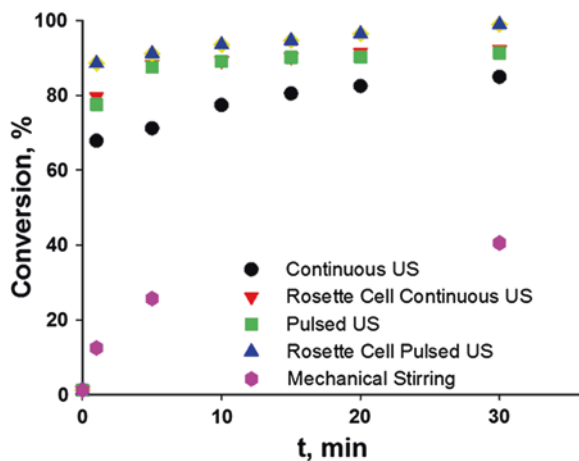
Various sonochemical reactor configurations have been used to transesterify triglycerides. Shape, kind and number of sonochemical applicators are all features that differentiate the design of a sonochemical reactor.

US applicators differ with respect to frequency, power and tip diameter. Velicković et al. [15] report that low frequency is beneficial for classical synthesis processes. Mahamuni and Adewuyi report the transesterification of soybean at high frequency (323, 581, 611 kHz, and 1.3 MHz) and at various powers in the range from 13 to 223 W. At 611 kHz and 139 W the conversion was 90 % after

**Table 3.3** References on the ultrasound (US)-assisted transesterification (triglycerides—TG conversion) mentioned in the manuscript

Ultrasonic reactor	Cat.	US parameters	Oil type	TG conv., T, time	Reference
Two-stage continuous loop system, US probes	KOH	20 kHz 1,000 W/120 L	Cooking oil	94 %, 30 °C, 56''	[6]
Recirculation loop system, US probe	KOH	20 kHz 1,000 W/0.8 L	Canola	99 %, 30 °C, 30'	[7]
US bath with 3 transducers in triangular arrangement	KOH	20 kHz 120 W (real 45 W)	Nagchampa oil	90 %, 40 °C, 40'	[27]
Semi-continuous loop system Sonitube®, US probe	KOH	35 kHz pulsed 400 W/0.07 L	Canola	91 %, 65 °C, 18''	[42]
Rosett cell, US probe	KOH	20 kHz pulsed 500 W/0.07 L	Canola	90 %, 40 °C, 5'	[42]
Multifrequency system with US probe	KOH	611 kHz 139 W (optimal)	Soybean	91 %, 26–45 °C, 10'	[43]
Continuous, with a static mixer and US homogenizer	KOH	18 kHz 10 W/mL	Palm	97 %, 30 °C, 18''	[46]
Ultrasonic bath	Lipase	43 kHz 80 W/	Coconut	92 %, 30 °C, 3 h	[57]
Continuous, US push–pull applicator	KOH	45 kHz 600 W/31.4–76.2 L	Palm	95 %, 40 °C, 10' (31.4 L) 90 %, 40 °C, 30' (76.2 L)	[58]
Us bath	CaO	35 kHz 35 W (real)	<i>J. curcas</i>	94 %, 65 °C, 2 h 40'	[59]
Continuous reactor high-efficiency pre-stressed piezoelectric rings	CH <sub>3</sub> ON <sub>a</sub>	21.5 kHz 600 W/1.6 L	Soybean	99 %, 45 °C, 1 h	[60]

**Fig. 3.9** Comparison between the ultrasound assisted transesterification in the Rosett cell and a classical cylindrical reactor (60 % of the maximum nominal power, 40 °C, 500 W) and the mechanically stirred process in Ref. [42]



10 min. All the other experimental conditions surpassed the 90 % conversion after 30 min [43].

It is worth mentioning the enzyme-catalyzed ultrasound-assisted transesterification. Lipase-catalyzed transesterification is slower than the alkali-catalyzed one. US accelerates the reaction rate of the enzyme-catalyzed reaction, as reported by Tupufia et al. [57].

Stavarache and coauthors use a push–pull US applicator in a CSTR [58]. Push–pull ultrasonic transducers have at least two ultrasonic wave emission points, usually in the form of driveheads, mounted at the bottom and at the end of the applicator. The power supplied to the driveheads provokes the longitudinal vibration of the entire applicator to produce a homogeneous sonic field.

In a recent study, Boffito et al. [42] compared the performance of mechanically stirred transesterification versus the ultrasonically-assisted process in a classical cylindrical vessel and in a Rosett cell reactor at low frequency (20 kHz). They tested various power levels, tip diameters and US pulses.

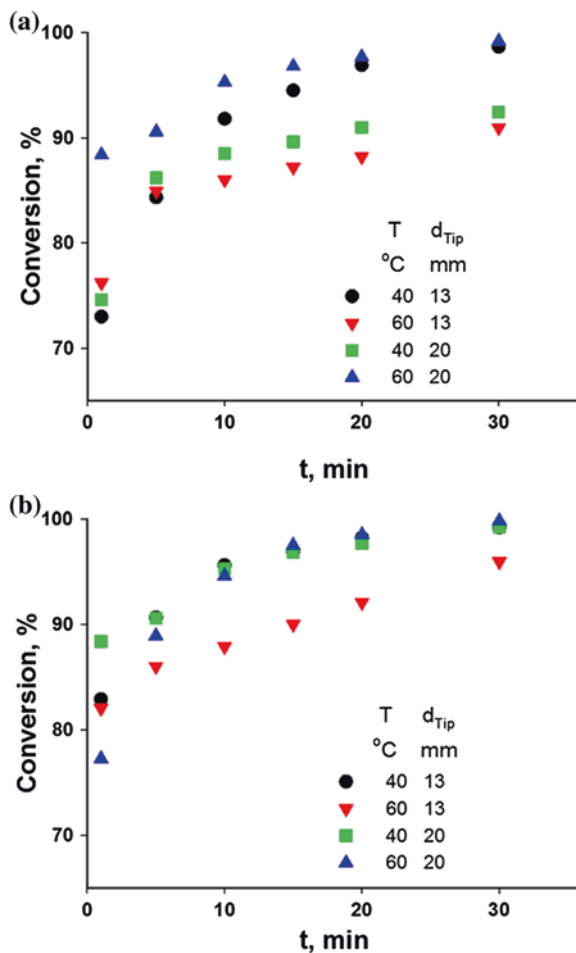
BD yield of the first sample, withdrawn after 1 min of sonication, ranged from 40 to 90 % in the case of the ultrasonically-assisted experiments. This level of performance was only reached after 90 min in the mechanically stirred reactor (Fig. 3.9).

In 10 min with US in the Rosett cell, oil conversion is the same as with the traditional process with 2 steps and 150 min. Moreover, ME yield was greater than 96.5 % (the minimum ME concentration required by the EN and ASTM standards) with less methanol and catalyst [42].

The results of this work regarding US pulses are consistent with data reported extensively in the literature for transesterification, i.e. increased BD yield [61–63].

Pulses heat the reaction medium less. The elution rate of gases from liquids is slower at lower temperatures resulting in higher concentrations of dissolved gases. The higher the amount of gases dissolved in a liquid system, the more numerous are the nuclei where acoustic cavitation initiate.

**Fig. 3.10** **a** Cylindrical vessel, **b** Rosett cell. Conversions at 80 % of the nominal power at different temperatures and ultrasonic tip diameter in Ref. [42] (13 mm = 400 W; 20 mm = 500 W)



Both Boffito et al. [42] and Chand et al. [61] report that the temperature rise in the reaction medium was lower with pulses. Excessive heating during transesterification might also evaporate methanol, which would decrease the reaction rate. High power heats the system excessively, which can also evaporate methanol.

In general, ME yield is related to power at low temperatures (Fig. 3.10a, b). When the intensity (i.e., ultrasonic power/irradiation area) increases, the acoustic amplitude increases and the cavitation bubbles collapse more violently [64]. Another factor is the design of the US applicator that accounts for the power delivery to the system. For instance, the tip diameter design determines how the power distributes in the reacting medium. At equal power, a smaller diameter ultrasonic tip delivers a higher power per surface area, affecting in a different way the reactivity of the system with respect to a larger diameter tip [42].

However, a too high power density decreases the reaction rate. There is an optimum power density (or acoustic intensity) at which an US process maximizes the



reaction rates [64] creasing it either does not bring. Singh et al. [65] have also observed an optimum energy input for BD production from soybean oil in the presence of US.

In general, at equivalent conditions, BD yields was higher with a 13 mm sonicator compared to a 20 mm tip. BD yield exceeded 96.5 % in 30 min with a 13 mm tip in both the Rosett cell and the classical reaction vessel.

The high temperatures inside the reaction medium with the 13 mm diameter tip (500 W) might have evaporated some methanol, thereby reducing the acoustic cavitation and, as a consequence, reducing the transesterification rate [42]. This phenomenon accounts for the lower reaction rates at higher power (Fig. 3.10b).

The optimal temperature was in most of cases 40 °C, as reported by Colucci et al. [66] for very similar reaction conditions in a classical reaction vessel.

Imploding cavitation bubbles are known to generate localized hot spots in the range of 1,000–15,000 K and pressures in the range of 500–5,000 bar.

Besides promoting turbulence, these conditions generate free radicals. In the case of transesterification, in situ generation of methoxy radicals might contribute to accelerating the reaction rates [67]. However, according to Kalva et al. [68], free radicals play a minor role, if any, in the base-catalysed methanolysis of soybean oil.

### 3.2.2.3 Rosett Cell Reactor

The cooling cell or Rosett cell reactor operates in batch mode and has several loops at the bottom (Fig. 3.11). US propels the liquid around the loops and hydrodynamic cavitation generates turbulence.

Passing a liquid through a constriction, such as an orifice plate generates hydrodynamic cavitation. The loops of the Rosett cell reactor act like a constriction [69]. The velocity in the arms vary which produce pressure waves that form vapour cavities [70]. Hydrodynamic cavitation generates flow energy at an intensity that is suitable for physical and chemical processing [69, 70].

Boffito et al. [42] report higher yields in the Rosett cell reactor than in a classical cylindrical reactor (Figs. 3.9 and 3.10). In particular, yields are significantly higher with US pulses (Fig. 3.9).

The Rosett cell reactor always perform better than the traditional vessel (other conditions being equal), resulting in higher BD yields. The Rosett cell is designed to sonically propel the reaction mixture from the tip of the ultrasonic probe around the loops of the vessel. The liquid pressure is very high at the entrance of the loops and propagates throughout their length generating turbulence inside the reactor, which promotes efficient mixing. Hydrodynamic cavitation might also occur but remains to be demonstrated. The Rosett cell provides both optimal temperature control within the reactor and enhances the mass transfer.

The combined effect of acoustic cavitation and turbulence due to the presence of the loops in the Rosett cell reactor increase yields. The extent of the hydrodynamic cavitation in contributing to the BD process intensification is already the

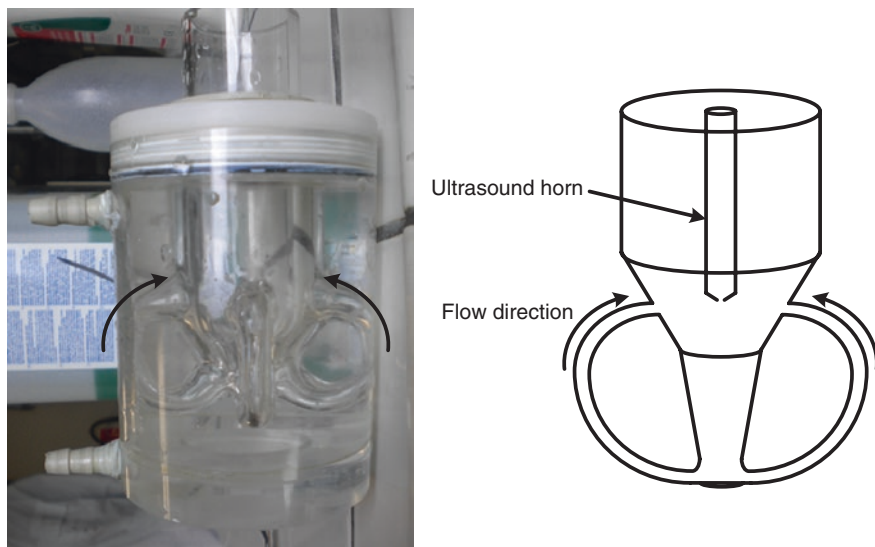


**Fig. 3.11** Rosett cell ultrasonic reactor. Reprinted with permission from [42], Copyright © 2014, ACS

subject of few papers [71, 72]. Kelkar et al. [71] reviewed ultrasonic and hydrodynamic cavitation for methyl esters production.

### 3.2.3 *Heterogeneously-Catalyzed Transesterification*

Ramachandran et al. review the literature on ultrasonic transesterification with basic heterogeneous catalysts. They conclude that ultrasonic transesterification requires lower methanol: oil molar ratios, lower temperatures and just one step compared to the mechanically stirred processes [73]. However, the reaction times are sensibly longer compared to the homogeneous ultrasonic transesterification and still in the range of 1–2 h. Deng et al. report the highest conversions to biodiesel: ultrasound at 20 kHz converted nearly 94 % of *Jatropha* oil to biodiesel in 30 min [74].

Choudhari et al. report activation energies four times higher for the heterogeneously-catalyzed transesterification of *Jatropha* oil versus the homogeneously-catalyzed one, even with sonification. The higher activation energy is ascribed to the presence of a third phase—the solid catalyst—besides the two liquid phases [59].

However most of the papers reviewed by Ramachandran et al. deal with batch technologies where the sonification delivers through ultrasonic baths or horns. Up to now, the highest conversion to methyl esters have been reported in continuous loop reactors, for both the esterification and transesterification [73].

### 3.3 Ultrasonic Continuous and Semi-continuous Loop Reactors

#### 3.3.1 Esterification

Somnuk et al. [46] describe a two-stage continuous process to produce methyl esters from a high free fatty acid crude Palm oil using a static mixer coupled with ultrasound. The two stages correspond to ultrasonic FFA esterification and ultrasonic transesterification, respectively. The flow of oil was  $20 \text{ L h}^{-1}$ . Oil, methanol and  $\text{H}_2\text{SO}_4$  were fed to a static mixer and sent to the first ultrasonic reactor to esterify the FFA. Water was removed from the mixture continuously in a separator. A second static mixer emulsified the oil, methanol and sodium methoxide before the second ultrasonic reactor (triglyceride transesterification). The working volume of both reactors was 1,000 mL. The power density was  $1.66 \text{ W mm}^{-2}$  and the acoustic power density  $10 \text{ W mL}^{-1}$ . The maximum nominal power was 1,000 W.

The residence time in both ultrasonic reactors was 18 s. The acid value of the oil was 28 and 0.29 FFA mg KOH  $\text{g}^{-1}$  before and after the ultrasonic FFA esterification, indicating almost complete conversion in very short times. The conversion of the triglycerides in the second ultrasonic reactor was as almost complete and the final product properties matched the biodiesel EN and ASTM norms [46].

#### 3.3.2 Transesterification

In general, BD processes rely on either batch or CSTR technologies in which the basic catalyst is mixed in one phase with the methanol [39, 40]. Both the transesterification and the FFA esterification process are labour intensive that generate a considerable amount of wastewater [5, 39]. The challenge to produce BD is undoubtedly to design a continuous system based on a heterogeneous catalyst and in which mass transfer limitations are reduced to those inherent to the homogeneously-catalyzed process.

It is widely believed that continuous reactors would increase the production of biofuels from vegetable oils [75–77]. In comparison to batch processes, continuous processes adapt to diverse production scales and needs, and are more adaptable to design-improvements [39]. As highlighted by Pirola et al. [14], when feeding oil and methanol to a plug flow reactor (PFR), they must remain as an emulsion over the whole length of the reactor, i.e. stable for at least the equivalent of the reactor residence time.

In BD synthesis, continuous and semi-continuous ultrasound processes in particular, can contribute to overcome both the drawbacks related to the batch processes (energy intensive, lack of flexibility) and the limitations of the continuous reactors (methanol-oil separation). Loop technologies, in which the reagents mixture is fed to an ultrasonic chamber and then either sent to a separator or

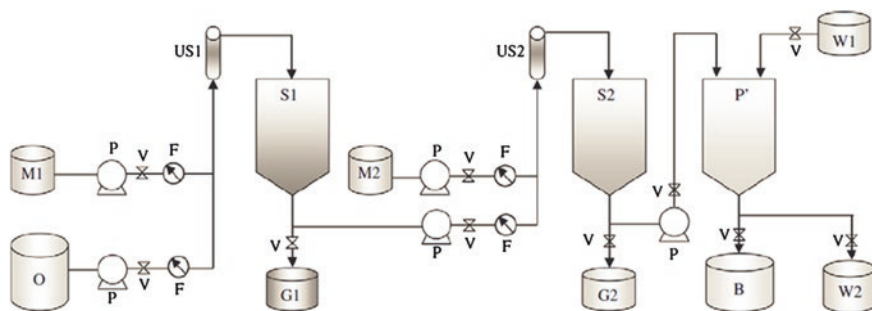


**Fig. 3.12** Schematic of the ultrasound assisted continuous process for biodiesel production. *O* oil tank; *M1*, *M2* methanol and catalyst tanks; *P* liquid pumps; *V* valves; *US1*, *US2* ultrasonic reactors; *S1*, *S2*: separation tanks; *G1*, *G2* glycerin tanks; *P* purification tank; *P* biodiesel product tank; *W1*, *W2* fresh and waste water tanks. Reprinted with permission from [7], Copyright © 2010, Elsevier

re-circulated to further ultrasonic treatment is a strategy to commercialize ultrasonic biodiesel process at a large scale.

Continuous processes exploiting ultrasound are a commercial reality. Tulsa Biofuels uses a Hielscher Ultrasonic device to accelerate the transesterification of oil: the oil/MeOH/catalyst mixture passes a flow cell, where it is exposed to ultrasonic cavitation for 5–30 s. The mixture then enters a reaction column where it remains for 1 h (<http://www.hielscher.com>).

Ultrasonic Power Corporation also provides ultrasonic reactors operating at high powers (from 0.5 to 2.0 kW) for continuous processing of oils (<http://www.upcorp.com>). INCBIO (<http://www.incbio.com>) applies ultrasound to promote both batch and continuous esterification and transesterification of acidic oils.

Thanh et al. [6] treated 54 L of Canola oil in a re-circulation ultrasonic reactor with a working volume of 0.8 L at 1 kW. The conversion was 99 % after 30 min. In a subsequent study [7] they report more than 93 % conversion of 120 L of waste cooking oil in a reactor similar to the previous one but with one more step under ultrasonic irradiation. The reaction times of the first and second steps were 1.5 and 1 h, respectively, plus the time required for the separation and purification of BD.

Figure 3.12 depicts the flow diagram of the pilot plant in described in Ref. [7].

However, there are little data available in the literature about continuous or semi-continuous processes in tubular reactors. The authors of this chapter have recently published some data about a new continuous ultrasonic reactor, Sonitube<sup>®</sup>, whereby very high biodiesel yields were achieved in times that had never been previously reported in literature. In the following sections details of the Sonitube<sup>®</sup> and the results of the Canola oil transesterification are summarized.

### 3.3.3 Sonitube<sup>®</sup>

The Sonitube<sup>®</sup> is an ultrasonic device patented by Syntetude (Chambery, France). The Sonitube<sup>®</sup> enables continuous on line process and features a very high ultrasonic power per volume unit.

**Table 3.4** Sonitube<sup>®</sup> features

Feature	SM20	SM35
Frequency (kHz)	20	35
Useful volume (L)	0.7	0.07
Length (m)	0.36	0.24
Inner diameter (mm)	50	20
Nominal power (W)	1,200	400
Power density (kW L <sup>-1</sup> )	0.8–1.7	2.8–5.7

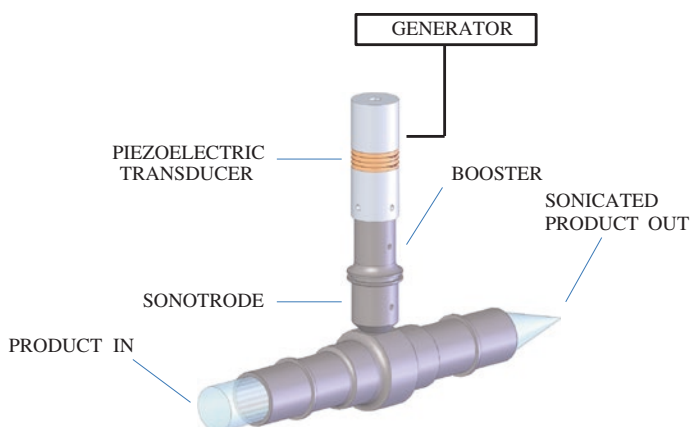
**Fig. 3.13** Sonitube<sup>®</sup> schematic

Table 3.4 lists the features of two models of Sonitube<sup>®</sup> (Fig. 3.13).

The electronic generator delivers a periodic electrical signal at an ultrasonic frequency. This signal is converted into mechanical vibration of the same frequency by the transducer. The shape and size of the Sonitube<sup>®</sup> are precisely computed to make the probe vibrate at the same frequency as the electronic generator. The entire experimental setup is shown in Fig. 3.14. The detailed description of the methods can be found in Ref. [42].

### 3.3.3.1 Results

Continuous experiments were performed using 0.700 L (SM20) and 0.070 L (SM35) tubular reactors, equipped with two different horns working at different powers as displayed in Table 3.2. First, the same total volume of reagents, corresponding to 2.40 L was fed to both reactors. Afterwards, for the sake of comparison, 0.68 L of reagents was fed to the smaller reactor, in order to have the same power density in the 0.700 L as in the 0.070 L reactor. This last experiment was performed using both continuous and pulsed ultrasound in the smaller reactor.

**Fig. 3.14** Schematic of the continuous ultrasonic reactors equipped with a Sonitube<sup>®</sup> device, as described in Ref. [42]

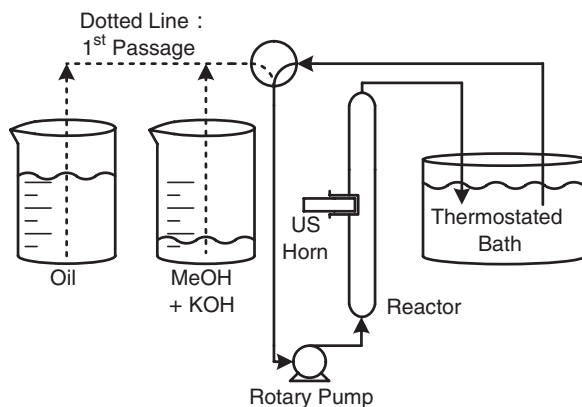
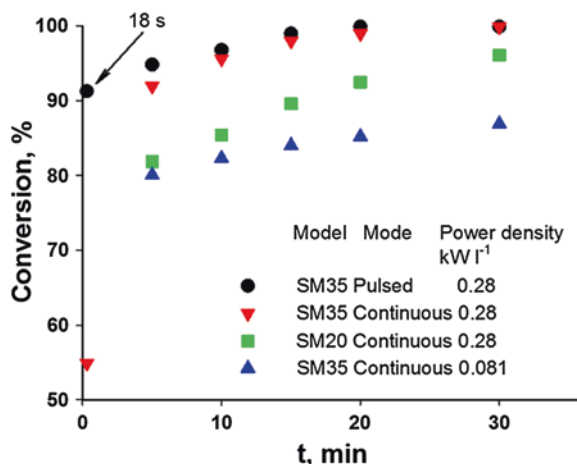


**Fig. 3.15** Conversion of Canola oil to biodiesel with Sonitube<sup>®</sup> reactors at 35 kHz (SM35) and 20 kHz (SM20). Reactor characteristics are given in Table 3.2. Reprinted with permissions from [42], Copyright © 2013, ACS



The reaction rates are extremely high in the continuous reactors. Within 10 min, BD yields exceeded 80 % at all the conditions tested (Fig. 3.15). High yields are achieved within very short times for experiments carried out in the smaller reactor and lowering the total volume of treated reagents. A remarkable result was achieved when pulses were adopted: BD yields surpassed 90 % after just one passage in the reactor, equivalent to 18 s and to a reaction time 300 times faster than the conventional process. Note that since pulses (2 s on and 2 s off) are adopted, the total time of sonication during one pass through the reactor equals just 9 s, which had never been reported previously. Somnuk et al. [46] report a TG conversion as high as 97 % in 18 s using a continuous reactor with a static mixer and US homogenizer. In our case we have used pulsed US (actual sonication time of 9 s) and no mixer.

The effect of pulses has been discussed previously for the ultrasound-assisted batch experiments in the conventional vessel and in the Rosett cell reactor. Another positive effect of pulses in the continuous reactors relates to reducing the

evaporation of methanol. Also, the gases remain dissolved with pulsed ultrasound versus continuous due to the lower heat generated.

### 3.4 Scale-Up Considerations

To compare alternative technologies to conventional technology two criteria must be considered: time and energy/power input. Reaction time has a direct impact on investment cost related to reactor size. Decreasing the reaction time by a factor 300 reduces the total investment by 30 times ( $300^{0.6}$  following the Chilton scale up factor criterion) [78, 79]. Power is more difficult to assess because of the combined effect of smaller equipment and scaling up heat losses and mixing. In the process of Cintas et al., 1 L of BD requires 0.28 kWh [60]. This excludes the power necessary to purify the BD. Thanh et al. [7] calculate that it takes 0.072 kWh to produce 1 L of BD including the purification steps.

In Ref. [42], the nominal power of the sonicator was 400 W. In the case of the pulsed US tests in the conventional vessel and the Rosett cell (2 s on 2 s off), to reach 90 % oil conversion required 10 min in the conventional vessel and 5 min in the Rosett cell, which corresponds to a total energy input of 120 kJ (0.1 kWh/L of BD produced) and 60 kJ (0.54 kWh/L of BD produced), respectively. For the continuous reactor, the power input was also 400 W (pulsed) but the reaction time was 18 s and the total energy input was 3.6 kJ. (Note that the temperature rise of the reagents was less than 40 °C and the reactor operated adiabatically.) This gives  $4.6 \times 10^{-4}$  kWh/L of BD produced in the Sonitube<sup>®</sup>, without taking into account the purification step and the power required by the pump.

At a small scale, the power consumption of the US is larger than in the conventional technology. The energy consumption of the impeller and heat losses are negligible compared to the energy required to heat the reagents (oil + MeOH) from 20 to 60 °C. The total energy to heat the reagents is 10 kJ ( $\rho C_p \Delta T$ ).

On scale-up, heat losses and impeller power constitute a significant fraction of operating costs in a conventional process. The mixing power (SHP—shaft horse power) input increases with 5<sup>th</sup> power of impeller diameter according to:

$$SHP = \frac{N_p N^3 D^5 g}{1.53 \times 10^{13}} \quad (3.9)$$

where  $N_p$  is the power number of the impeller,  $N$  is the impeller speed (rpm),  $D$  is the impeller diameter and  $g$  is specific gravity.

Radich estimated that 1 L of BD requires 3 kWh (production + purification).

The power calculated by Thanh et al. [7] (0.072 kWh) is 2 orders of magnitude lower than the conventional process. This would contribute to half the operating costs.

Another factor which contributes towards the economic viability of the US-assisted process is the reduced cost of the investment required due to time saving (Chilton relation) [78, 79]. The time saving would impact enormously the total plant investment. The time for the total conversion of triglycerides into methyl

esters depends on the characteristics and design of the sonochemical reactor, and in particular on the power density (W/L oil). Therefore, not only the operating costs would at least half, but also the investment would be lower.

The challenge for the Rosett cell and conventional reactor with US will be to maintain the energy density. This is also true for the continuous flow reactor, but since its size is 300 times smaller than conventional technology, it will be less challenging compared to the Rosett cell with US.

The results of the continuous Sonitube<sup>®</sup> reactor are tremendous and worthy of scaling up.

### 3.5 Conclusions and Future Outlook

Ultrasound increases the conversion rate of both free fatty acid esterification and triglyceride transesterification with respect to conventional mechanical stirring. The difference in conversion between the ultrasonic-assisted method and mechanical stirring is most evident at lower temperatures. Operating at low temperatures is particularly beneficial for manufacturers. Methanol fumes are a hazard and special precautions must be implemented to minimize the risk of exposure to operators as well to reduce the chance of forming flammable mixtures.

- Free fatty acid esterification can be characterized as a doubly-heterogeneous system with two phase boundaries: the catalyst-liquid boundary and the one between the methanol that surrounds the catalyst particle and the oil. Acoustic cavitation either shrinks the boundary layer or allows the bulk reactants to penetrate to the reacting surface more quickly: mass transfer coefficients are several times higher with US compared to mechanical stirring.
- Loop technologies, in which the mixture oil-methanol react in a ultrasonic chamber with high power/volume ratio ensure high conversion of free fatty acids and triglycerides in very short times. Boffito et al. [42] and Somnuk et al. [46] report transesterification conversion above 90 % under ultrasonic irradiation in 18 s at a nominal power density of 10 W mL<sup>-1</sup>. In particular, Boffito reports 91 % conversion using pulsed ultrasound (2 s off and 2 s on) and a nominal power density around 20 W mL<sup>-1</sup>. Somnuk also report the FFA esterification in the same loop system, where the acid value of a crude Palm oil dropped from 28 to 0.29 FFA mg<sub>KOH</sub> g<sup>-1</sup>.
- Ultrasonic free fatty acids esterification and triglycerides transesterification over heterogeneous catalysts in continuous reactors are subjects worthy of investigation that have not been explored, yet.

**Acknowledgments** The authors gratefully acknowledge \*/SYNETUDE/\* Company (Parc d'activités de Côte Rousse, 180 rue du Genevois, 73,000 Chambéry, France), for providing the ultrasound horns and Sonitube<sup>®</sup> devices.

The authors would like to thank Fonds de recherche du Québec—Nature et technologies (FRQNT) for the Programmes de bourses d'excellence pour étudiants étrangers (PBEEE) granted to Daria C. Boffito.



## References

1. Boffito DC, Neagoe C, Edake M et al (2014) Biofuel synthesis in a capillary fluidized bed. *Cat Today* 237:13–17
2. Luo J, Fang Z, Smith RL (2014) Ultrasound-enhanced conversion of biomass to biofuels. *Prog Energy Comb Sci* 41:56–93
3. Salvi BL, Panwar NL (2012) Biodiesel resources and production technologies—A review. *Renew Sustain Energy Rev* 16:3680–3689
4. Leung DYC, Wu X, Leung MKH (2010) A review on biodiesel production using catalysed transesterification. *Appl Energy* 87:1083–1095
5. Perego C, Ricci M (2012) Diesel fuel from biomass. *Catal Sci Technol* 2:1776–1786
6. Thanh LT, Okitsu K, Sadanga Y et al (2010) Ultrasound-assisted production of biodiesel fuel from vegetable oils in a small scale circulation process. *Biores Technol* 101:639–645
7. Thanh LT, Okitsu K, Sadanga Y et al (2010) A two-step continuous ultrasound assisted production of biodiesel fuel from waste cooking oils: a practical and economical approach to produce high quality biodiesel fuel. *Biores Technol* 101:5394–5401
8. Radich A (2004) Biodiesel performance, costs, and use. Energy Information Administration
9. Boffito DC, Pirola C, Galli F et al (2012) Free fatty acids esterification of waste cooking oil and its mixtures with rapeseed oil and diesel. *Fuel* 108:612–619
10. Boffito DC, Crocellà V, Pirola C et al (2012) Ultrasonic enhancement of the acidity, surface area and free fatty acids esterification catalytic activity of sulphated ZrO<sub>2</sub>–TiO<sub>2</sub> systems. *J Catal* 297:17–26
11. Bianchi CL, Boffito DC, Pirola C et al (2010) Low temperature de-acidification process of animal fat as a pre-step to biodiesel production. *Catal Lett* 134:179–183
12. Borges ME, Diaz L (2012) Recent developments on heterogeneous catalysts for biodiesel production by oil esterification and transesterification reactions: a review. *Renew Sustain Energy Rev* 16:2839–2849
13. Bianchi CL, Pirola C, Boffito DC et al (2011) Non edible oils: raw materials for sustainable biodiesel. In: Stoytcheva M, Montero G (eds) *Biodiesel feedstocks and processing technologies*. Intech, pp 3–22
14. Pirola C, Bianchi CL, Boffito DC et al (2010) Vegetable oil deacidification by Amberlyst: study of catalyst lifetime and a suitable reactor configuration. *Ind Eng Chem Res* 49:4601–4606
15. Veljković VB, Avramovi JM, Stamenkovi OS (2012) Biodiesel production by ultrasound assisted transesterification: state of art and the perspectives. *Renew Sustain Energy Rev* 16:1193–1209
16. Gole VL, Gogate PR (2013) Intensification of synthesis of biodiesel from non-edible oil using sequential combination of microwave and ultrasound. *Fuel Proc Technol* 10:62–69
17. Gole VL, Gogate PR (2014) Intensification of glycerolysis reaction of higher free fatty acid containing sustainable feedstock using microwave irradiation. *Fuel Proc Technol* 118:110–116
18. Eze VC, Phan AN, Pyrez C et al (2013) Heterogeneous catalysis in an oscillatory baffled flow reactor. *Catal Sci Technol* 3:273–2379
19. Santacesaria E, Turco R, Tortorelli M (2012) Biodiesel process intensification by using static mixers tubular reactors. *Ind Eng Chem Res* 51:8777–8787
20. Ghayal D, Pandit AB, Rathod VK (2013) Optimization of biodiesel production in a hydrodynamic cavitation reactor using used frying oil. *Ultrason Sonochem* 20:322–328
21. Santacesaria E, Di Serio M, Tesser R (2012) Biodiesel process intensification in a very simple microchannel device. *Chem Eng Proc* 52:47–54
22. Wen Z, Yu X, Tu S et al (2009) Intensification of biodiesel synthesis using zigzag microchannels reactors. *Biores Technol* 100:3054–3060
23. Dimian AC, Bildea CS, Omota F et al (2009) Innovative process for fatty acid esters by dual reactive distillation. *Comput Chem Eng* 33:743–750

24. Demirbas A (2008) Biodiesel from vegetable oils with MgO catalytic transesterification in supercritical methanol. *Energy Sources Part A* 30:1645–1651
25. Lim S, Lee KT (2013) Process intensification for biodiesel production from *Jatropha curcas* L. seeds: supercritical reactive extraction process parameters study. *Appl Energy* 103:712–720
26. Kiss AA (2013) Novel applications of dividing-wall column technology to biofuel production processes. *J Chem Technol Biotechnol* 88:1387–1404
27. Gole VL, Gogate PR (2012) Intensification of synthesis of biodiesel from nonedible oils using sonochemical reactors. *Ind Eng Chem Res* 51:11866–11874
28. Santos FFP, Malveira JQ, Cruz MGA et al (2010) Production of biodiesel by ultrasound assisted esterification of *Oreochromis niloticus* oil. *Fuel* 89:275–279
29. Gole VL, Gogate PR (2012) A review on intensification of synthesis of biodiesel from sustainable feedstock. *Ind Eng Chem Res* 53:1–9
30. Chakraborty R, Gupta AK, Chowdhury R (2014) Conversion of slaughterhouse and poultry farm animal fats and wastes to biodiesel: parametric sensitivity and fuel quality assessment. *Renew Sustain Energy Rev* 29:120–134
31. Maddikeri GL, Pandit AB, Gogate PR (2012) Intensification approaches for biodiesel synthesis from waste cooking oil: a review. *Ind Eng Chem Res* 51:14610–14628
32. Mazubert A, Poux M, Aubin J (2013) Intensified process for FAMR production from waste cooking oil: a technological review. *Chem Eng J* 223:201–223
33. Oh PP, Lau HLN, Chen J et al (2012) A review on conventional technologies and emerging process intensification (PI) methods for biodiesel production. *Renew Sustain Energy Rev* 16:5131–5145
34. Qiu Z, Zhao L, Weatherley L (2010) Process intensification technologies in continuous biodiesel production. *Chem Eng Proc* 49:323–330
35. Badday AS, Abdullah AZ, Lee KT, Khayoon MS (2012) Intensification of biodiesel production via ultrasonic-assisted process: a critical review on fundamentals and recent development. *Renew Sustain Energy Rev* 16:4574–4587
36. Kardos N, Luche JL (2001) Sonochemistry of carbohydrate compounds. *Carbohydr Res* 332:115–131
37. Thomson LH, Doraiswamy LK (1999) Sonochemistry: science and engineering. *Ind Eng Chem Res* 38:1215–1249
38. Abramovic JM, Stamenković OS, ZB Todorović et al (2010) The optimization of the ultrasound-assisted base-catalyzed sunflower oil methanolysis by a full factorial design. *Fuel Proc Technol* 91:1551–1557
39. Behzadi S, Farid MN (2009) Production of biodiesel using a continuous gas–liquid reactor. *Biores Technol* 100:683–689
40. Chen Y, Wang L, Tsai H et al (2010) Continuous-flow esterification of free fatty acids in a rotating packed bed. *Ind Eng Chem Res* 49:4117–4122
41. Pirola C, Galli F, Bianchi CL, Boffito DC, Manenti F (2014) Vegetable oils de-acidification by methanol heterogeneously catalyzed esterification in (monophasic liquid)/solid batch and continuous reactors. *Energy Fuels* 28:5236–5240
42. Boffito DC, Mansi S, Leveque JM et al (2013) Ultrafast biodiesel production using ultrasound in batch and continuous reactors. *Sustain Chem Eng* 1:1432–1439
43. Mahamuni NN, Adewuyi YG (2009) Optimization of the synthesis of biodiesel via ultrasound-enhanced base-catalyzed transesterification of soybean oil using a multifrequency ultrasonic reactor. *Energy Fuels* 23:2757–2766
44. Boffito DC, Galli F, Pirola C, Bianchi CL, Patience G (2014) Ultrasonic free fatty acids esterification in Tobacco and Canola oil. *Ultrason Sonochem*. <http://dx.doi.org/10.1016/j.ultsonch.2014.01.026>
45. Jadhav SH, Gogate PR (2014) Ultrasound assisted enzymatic conversion of non edible oil to methyl esters. *Ultrason Sonochem* 4:1374–1381
46. Somnuk K, Smithmaitrie P, Prateepchaikul G (2013) Two-stage continuous process of methyl ester from high free fatty acid mixed crude palm oil using static mixer coupled with high-intensity of ultrasound. *Energy Conv Manage* 75:302–310

47. Toukoniitty B, Mikkola JP, Murzin et al (2005) Utilization of electromagnetic and acoustic irradiation in enhancing heterogeneous catalytic reactions. *Appl Catal A* 279:1–22
48. Ragaini V, Pirola C, Borrelli S et al (2012) Simultaneous ultrasound and microwave new reactor: detailed description and energetic considerations. *Ultrason Sonochem* 19:872–876
49. Mason TJ, Lorimer JP (1988) *Sonochemistry, theory, applications and uses of ultrasound in chemistry*. Wiley, New York
50. Margulis MA (1992) *Fundamentals in sonochemistry*. Elsevier, Amsterdam
51. Liu Y, Lu H, Liu C et al (2009) Solubility measurements for the reaction systems in pre-esterification of high acid value *Jatropha curcas* L. *Oil J Chem Eng Data* 54:1421–1425
52. Tesser R, Casale L, Verde D et al (2010) Kinetics and modelling of fatty acids esterification on acid exchange resins. *Chem Eng J* 157:539–550
53. Tesser R, Casale L, Verde D et al (2009) Kinetics of free fatty acids esterification: batch and loop reactor modelling. *Chem Eng J* 154:25–33
54. Deshmane VG, Gogate PR, Pandit AB (2009) Ultrasound-assisted synthesis of biodiesel from palm fatty acid distillate. *Ind Eng Chem Res* 48:7923–7927
55. Deshmane VG, Gogate PR, Pandit AB (2009) Ultrasound assisted synthesis of isopropyl esters from palm fatty acid distillate. *Ultrason Sonochem* 16:345–350
56. Boffito DC, Pirola C, Bianchi CL (2012) Heterogeneous catalysis for free fatty acids esterification reaction as a first step towards biodiesel production. *Chem Today* 30:14–18
57. Tupufia SC, Jeon YJ, Marquis C et al (2010) Enzymatic conversion of coconut oil for biodiesel production. *Fuel Proc Technol* 106:721–726
58. Stavarache C, Vinatoru M, Maeda Y et al (2007) Ultrasonically driven continuous process for vegetable oil transesterification. *Ultrason Sonochem* 14:413–417
59. Choudhary HA, Goswami PP, Malani RS et al (2013) Ultrasonic biodiesel synthesis from crude *Jatropha curcas* oil with heterogeneous base catalyst: mechanistic insight and statistical optimization. *Ultrason Sonochem* 21:1050–1064
60. Cintas P, Mantegna S, Calcio Gaudino E, Cravotto G (2010) A new pilot flow reactor for high-intensity ultrasound irradiation, application to the synthesis of biodiesel. *Ultrason Sonochem* 17:985–989
61. Chand P, Chintareddy VR, Verkade JG et al (2010) Enhancing biodiesel production from soybean oil using ultrasonics. *Energy Fuels* 24:2010–2015
62. Kumar D, Kumar G, Singh CP et al (2010) Ultrasonic-assisted transesterification of *Jatropha curcas* oil using solid catalyst, Na/SiO<sub>2</sub>. *Ultrason Sonochem* 17:839–844
63. Kumar D, Kumar G, Singh CP (2010) Fast easy ethanolysis of coconut oil for biodiesel production assisted by ultrasonication. *Ultrason Sonochem* 17:555–559
64. Sivakumar M, Pandi AB (2001) Ultrasound enhanced degradation of Rhodamine B: optimization with power density. *Ultrason Sonochem* 8:233–240
65. Singh AK, Fernando SD, Hernandez R (2007) Base-catalyzed fast transesterification of soybean oil using ultrasonication. *Energy Fuels* 21:1161–1164
66. Colucci JA, Borrero EE, Alape F (2005) Biodiesel from an alkaline transesterification reaction of soybean oil using ultrasonic mixing. *J Am Oil Chem Soc* 82(7):525–530
67. Georgogianni KG, Kontominas MG, Pomonis PJ et al (2008) Conventional and in situ transesterification of sunflower seed oil for the production of biodiesel. *Fuel Process Technol* 89:503–509
68. Kalva A, Sivasankar T, Moholkar VS (2009) Physical mechanism of ultrasound-assisted synthesis of biodiesel. *Ind Eng Chem Res* 48:534–544
69. Gogate PR, Pandit AB (2001) Hydrodynamic cavitation: a state of the art review. *Rev Chem Eng* 17:1–85
70. Gogate PR (2008) Cavitation reactors for process intensification of chemical processing applications: a critical review. *Chem Eng Proc* 47:515–527
71. Kelkar MA, Gogate PR, Pandit AB (2008) Intensification of esterification of acids for synthesis of biodiesel using acoustic and hydrodynamic cavitation. *Ultrason Sonochem* 15:188–194
72. Ji J, Wang J, Li Y, Yu Y, Xu Z (2006) Preparation of biodiesel with the help of ultrasonic and hydrodynamic cavitation. *Ultrasonics* 44:411–414

73. Ramachandran K, Suganya T, Nagendra Gandhi N et al (2013) Recent developments for biodiesel production by ultrasonic assist transesterification using different heterogeneous catalyst: a review. *Renew Sustain Energy Rev* 22:410–418
74. Deng X, Fang Z, Hu Y, Zeng H et al (2009) Preparation of biodiesel on nano Ca–Mg–Al solid base catalyst under ultrasonic radiation in microaqueous media. *Petrochem Technol* 38:1071–1075
75. Knothe G, Van Gerpen JH, Krahl J (2005) *The biodiesel handbook*. AOCS Press, Champaign
76. Srivastava A, Prasad R (2000) Triglycerides-based diesel fuels. *Renew Sustain Energy Rev* 4:111–133
77. Van Gerpen J (2005) Biodiesel processing and production. *Fuel Proc Technol* 86:1097–1107
78. Chilton CH (1950) Six-tenths factor applies to complete plant costs. *Chem Eng* 57:112–114
79. Garnett DI, Patience GS (1993) Why do scale-up power laws work. *Chem Eng Progr* 89(8):76–78

**Part II**  
**Biodiesel: Extraction and Production**

# Chapter 4

## Ultrasound Applications in Lipid Extractions from Microalgae

Ramya Natarajan, Xue Chen and Raymond Lau

**Abstract** Microalgae have been identified as a promising next generation biofuel feedstock owing to their high lipid content and fast growth rate. Ultrasonication is one of the most effective methods of extracting the algal lipids for biofuel production. This chapter begins with a life cycle analysis of algal biofuel and the energy dynamics involved in the processing steps. A review of the ultrasound applications in lipid extractions from algal biomass and the challenges associated with the processes are described. The operation of continuous ultrasonication on wet algal culture is a good alternative to avoid the energy intensive drying step. The effect of operating parameters of continuous ultrasonication on extraction yield as well as the cell disruption and lipid releasing characteristics of two marine microalgal species—*Tetraselmis suecica* and *Nannochloropsis* sp., and one freshwater microalgal species—*Chlorella* sp. are presented. Marine microalgae are more susceptible to ultrasonic damage than freshwater microalgae. However, the soft marine microalgal cell membrane tends to roll up upon ultrasonic cell disruption and retain the membrane lipids. On the other hand, the rigid cell walls of freshwater microalgal cells can be shattered by ultrasonic cell disruption, which causes the release of their lipids. A mechanism for the temporal release of the lipid types is proposed.

**Keywords** Microalgae · Continuous ultrasonication · Cell disruption · Lipid extraction

---

R. Natarajan  
Department of Biology, Indiana University, 1001 East 3rd Street,  
Bloomington, IN 47405, USA

X. Chen · R. Lau (✉)  
School of Chemical and Biomedical Engineering, Nanyang Technological University,  
62 Nanyang Drive, Singapore 637459, Singapore  
e-mail: WMLau@ntu.edu.sg

## 4.1 Introduction

Microalgae have been considered as an excellent feedstock for biofuel production. Unlike other sources of biofuel such as corn, sugarcane, soybean or canola, microalgae do not require arable land to grow and therefore pose no threat to food crops [1]. Not only do they have high growth rates and produce biomass rapidly, they can also be grown in a wide range of aquatic environments, from freshwater through saline water and even wastewater. They use sunlight to convert CO<sub>2</sub> to glucose via photosynthetic machinery within each cell, thereby contributing to 40 % of the global carbon fixation [2].

Microalgae have the potential to accumulate oils as non-polar storage lipids like triacylglycerides within their cells while their thylakoid and cellular membranes contain polar lipids like phospholipids, glycolipids and sterols [3]. These oils can be converted into biodiesel through a process called transesterification, which requires three moles of methanol for each mole of triglyceride oil. Alkalis, acids or even enzymes can be used to catalyze the transesterification reaction [1]. It is also possible to eliminate the use of catalysts by hydrothermal liquefaction (HTL) that converts the cellular lipids into biodiesel under high temperature and pressure in the presence of water [4]. Gasoline can also be made from microalgal oil through distillation and cracking. Such energy rich oils can amount to 20–50 % of the dried microalgal biomass. Carbohydrates and proteins make up the remaining cellular content, which can be converted into bioethanol by fermentation or biogas by anaerobic digestion. The possible utilization of all cellular components as bioenergy feedstock can further improve the energy efficiency of the biofuel production process.

It has been well recognized that the current technologies for algal biofuel production require additional development and optimization to be a commercially viable biofuel alternative. Considering the incident solar radiation as the sole source of light and perfect efficiencies for all the processes involved, a maximum theoretical yield of algal oil is estimated to be 354,000 L ha<sup>-1</sup> year<sup>-1</sup> [5]. While the value is purely theoretical and unrealistic, it can provide a target for process development. A more reasonable and realistic yield was calculated to be 50,000 L ha<sup>-1</sup> year<sup>-1</sup> that conforms to other literature data [5].

This chapter begins with a review of the life-cycle analyses and the economic viability of algal biofuel production today. Focus will then be put on the use of ultrasonication in the lipid extraction step and the lipid releasing characteristics with the use of ultrasound-assisted extraction.

## 4.2 Life-Cycle Analyses of Microalgal Biofuels

Life-cycle analysis (LCA) is often known as a “cradle to grave” analysis of a product or service. In the case of biofuels, there are two main aspects to the LCA, namely the energy depletion potential and the global warming potential.

The energy depletion potential accounts for the fossil fuel energy used in the entire production process including raw materials, expressed in this chapter as megajoule (MJ) of energy required per MJ of biodiesel produced. The global warming potential determines the total amount of greenhouse gas emissions, mainly CO<sub>2</sub>, in the production processes and is expressed as kilogram (kg) of CO<sub>2</sub> emitted per MJ of biofuel produced.

There are four main steps involved in microalgal biofuel production: cultivation; harvesting; lipid extraction and biofuel conversion; and coproduction and recycling.

### 4.2.1 Cultivation

The first step in microalgal biofuel production is cultivation. The basic requirements for microalgal growth are sunlight, water, nutrients and CO<sub>2</sub>. The CO<sub>2</sub> can be provided from either direct injection of flue gas or monoethanolamine scrubbing. Direct injection of flue gas was reported to be the most economical method [6].

The cultivation system can vary from open ponds to closed photobioreactors (PBRs). There are different published reports comparing the various forms of microalgal cultivation systems. A study comparing open raceway ponds, annular PBR, flat panel PBR and tubular PBR found the biomass productivity of open raceway ponds to be significantly lower than closed PBRs [7]. The biomass concentration in ponds can reach a maximum of only 0.5 kg/m<sup>3</sup>, while up to 5 kg/m<sup>3</sup> of biomass can be achieved in closed PBRs. When energy requirements involving the PBR materials and fabrication as well as the lifetime of the PBRs are put into consideration, the energy depletion potentials for cultivation were estimated to be 0.22, 0.19, 4.9 and 15.8 MJ/MJ biodiesel for open raceway pond, flat panel PBR, annular PBR and tubular PBR, respectively. A similar comparison was done for open raceway pond, flat plate PBR and tubular PBR [8]. The energy depletion potentials were found to be 0.33, 0.61 and 14.3 MJ/MJ biodiesel for open raceway pond, flat plate PBR and tubular PBR, respectively. Another LCA study assumed that the microalgae takes CO<sub>2</sub> directly from the atmosphere in an open raceway pond and neglected the energy requirement for CO<sub>2</sub> pumping. In that case, the energy depletion potential becomes merely 0.015 MJ/MJ biodiesel with zero carbon emissions [9]. In another study that did not consider the energy requirements of the PBR materials used, the energy depletion potentials of open raceway pond and tubular PBR were found to be 0.62 and 5.77 MJ/MJ biodiesel, respectively [10]. It can be seen that the method incorporated in LCA and the design of the PBRs have significant impact on the energy depletion potentials obtained. It is also to note that the global warming potential for open raceway pond was found to be 0.05 kg CO<sub>2</sub>/MJ biodiesel while that for tubular PBR was found to be considerably higher at 0.37 kg CO<sub>2</sub>/MJ biodiesel [10]. In spite of having low biomass productivity, the open raceway pond has been preferred over PBRs in many LCA



studies due to its low energy depletion potential and low global warming potential [9, 11, 12]. However, it is accompanied with high water requirement due to significant evaporation. Therefore, the flat panel PBR is also considered as an ideal choice for microalgae cultivation [7]. Nonetheless, the search for the perfect microalgal cultivation system remains a continuous research effort.

### ***4.2.2 Harvesting***

After microalgal cultivation, the second step is to harvest the biomass for further processing. Depending on the lipid extraction method to be used, the harvesting procedure will differ. Conventional dry extraction methods require the biomass to have less than 10 % moisture content because the presence of water reduces the efficiency of the transesterification reaction [13]. The requirement for water removal makes harvesting the most energy intensive step. Typically, the harvesting step involves a liquid–solid separation step prior to the drying step. The use of centrifugation for primary harvesting followed by natural gas for drying was reported to have an energy depletion potential of 5.7 MJ/MJ biodiesel and a global warming potential of 0.4 kg CO<sub>2</sub>/MJ biodiesel [9]. By replacing centrifugation with filtration as the liquid–solid separation step, the energy depletion potential and the global warming potential can be reduced to 2.9 MJ/MJ biodiesel and 0.24 kg CO<sub>2</sub>/MJ biodiesel, respectively [9]. In fact, the drying step alone was reported to consume 2.4 MJ/MJ biodiesel [11]. The drying step is not sustainable if the energy needs to come from non-renewable sources. Solar drying has been considered as an alternative but the long processing time and high land requirement make the process not feasible at a large scale. Waste heat drying, the use of heat produced by burning the residual microalgal biomass after oil extraction, has also been suggested as a sustainable drying method [6]. The capability of “recycling” heat provides a good potential to significantly bring down the energy depletion potential of the harvesting process.

New processes have been developed to allow lipid extraction from microalgal biomass that has high water contents. Some of these processes can work with microalgae directly from the cultivation tank while others require prior liquid–solid separation during harvesting. Nonetheless, the elimination of the drying step makes these processes much less energy demanding. Three commonly used harvesting methods, centrifugation, filtration and flocculation were found to require 0.9, 0.8 and 0.09 MJ/MJ biodiesel, respectively [7].

### ***4.2.3 Lipid Extraction and Conversion to Biodiesel***

As mentioned in the previous section, lipid extraction can be performed on both dry and wet microalgal biomass. Dry extraction has been the traditional approach where dried biomass is used. The first step is to lyse the cells, and methods such

as homogenization, enzymatic lysis, bead beating, osmotic shock, grinding with liquid nitrogen, microwave heating, and ultrasonication have been introduced [14–16]. However, there is no consensus on the best cell disruption technique. The subsequent step after cell disruption is typically solvent extraction using hexane. A countercurrent cascade of mixer-settlers were developed by running the solvent countercurrent to the biomass for oil extraction, after which the oil is sent to industrial facilities to be treated with an alcohol to convert into biodiesel, via transesterification [10]. These processes require 114 g methanol and 7–15 g hexane per kg of biodiesel, and have an energy depletion potential of 0.3 MJ/MJ biodiesel and a global warming potential of 0.02 kg CO<sub>2</sub>/MJ biodiesel [9, 11]. Cultivation of algae under nitrogen starving conditions can enhance triacylglycerol (TAG) accumulation, thereby reducing the energy requirement of the downstream processing to 0.1 MJ/MJ biodiesel.

Wet extraction is a more recent process, developed in order to overcome the energy intensive drying step. The energy depletion potential for wet extraction and conversion to biodiesel was found to be 0.85 and 0.4 MJ/MJ biodiesel for the sufficient nitrogen and nitrogen starvation cases, respectively [11]. It was assumed that the same dry extraction process was employed on wet microalgal biomass for a simple estimation of the energy depletion potentials. A two step catalyst-free process for biodiesel production was developed to convert the lipids from wet microalgal biomass to biodiesel [4]. The lipids in wet microalgal culture were allowed to hydrolyze at subcritical water conditions. The cell aggregates rich in fatty acids were filtered and subsequently converted to fatty acid ethyl esters by supercritical in situ transesterification with ethanol. While no life cycle analysis has been performed for this process, the low biodiesel yield and high temperatures involved are likely to have high energy depletion potentials. Another form of wet extraction is hydrothermal liquefaction (HTL) [17]. The wet microalgal biomass slurry is heated to approximately 300 °C at 10–20 MPa. Under these conditions, microalgal cells can liquefy and the water catalyzes the conversion of biomass into oil, aqueous, gas and char-like solid fractions. HTL can be used on wet biomass containing 10–20 weight percent of solids. A portion of the proteins and carbohydrates in low-lipid microalgae can also be converted to oils. Cellular disruption and solvent recovery are also avoided. The energy depletion potential of HTL was estimated to be 0.4 MJ/MJ biodiesel while the same study has estimated the conventional lipid extraction method to have an energy depletion potential of 1.05 MJ/MJ biodiesel [17]. Though HTL has attractive energy depletion potential, the global warming potential was 30 % higher than the regular lipid extraction methods. Further studies to improve the efficiency are required to make this process feasible on an industrial scale.

#### ***4.2.4 Coproduction and Recycling***

After the lipid fraction of the biomass is used for biodiesel production, the remaining fractions can be either used for coproduction or disposed as waste.

Proper utilization of the remaining fractions to produce coproducts or electricity would allow the biodiesel production process to be more sustainable. It has been accepted that the only way in which biodiesel production from algae can be energy efficient is by coproduct allocation [9]. Residual microalgal biomass contains high carbohydrate content, which can be converted into simple sugars for ethanol fermentation, offsetting the currently used corn feedstock. Considering a 31 % carbohydrate and 37.5 % protein content in microalgal biomass, the energy depletion potential for coproduction allocation was offset by an energy credit of 10 MJ/MJ biodiesel produced. Replacing corn for ethanol fermentation estimated the microalgal biomass to reduce the overall global warming potential by 0.27 kg CO<sub>2</sub>/MJ biodiesel produced.

Using the residual microalgal biomass for anaerobic digestion to produce biomethane is one of the most commonly suggested waste management processes [18]. In fact, the energy produced in the form of methane is sometimes higher than that produced by the lipids. The energy depletion potential was therefore reduced by 1.35 MJ/MJ biodiesel produced and the global warming potential is reduced by 0.07 kg CO<sub>2</sub>/MJ biodiesel produced [10]. Some of the bottlenecks with this process are that the biodegradability of residual biomass depends on its constituents and the cell wall structure. For microalgae strains that have rigid cell walls, a pretreatment method such as homogenization or enzyme treatment is necessary and will increase the energy depletion potential.

The residual microalgal biomass can also be utilized via combined heat and power (CHP) to produce heat and electricity [6]. The electrical and thermal efficiency of the CHP plant were assumed to be 25 and 56.3 % respectively. Due to minimal downstream processing of microalgal biomass and high efficiency of CHP, it was found to reduce the energy depletion potential more than anaerobic digestion. Glycerol, being a common byproduct in biodiesel production process, can be recycled back to the cultivation unit. It has been reported that microalgae can grow mixotrophically to accumulate higher amounts of TAGs [19]. The water can also be recycled or used as liquid fertilizers due to its high nitrogen content.

A summary of the energy depletion and global warming potentials of the different steps involved in biodiesel production is presented in Table 4.1. The best-case scenario in terms of economic viability seems to involve the use of flat plate PBR for cultivation under nitrogen starving conditions, followed by flocculation for harvesting the biomass. For dry biomass lipid extraction process, solar drying or waste heat drying can be employed to reduce drying costs. However, the ideal choice would be wet biomass extraction as it completely eliminates the drying step.

**Table 4.1** Summary of the life cycle analysis

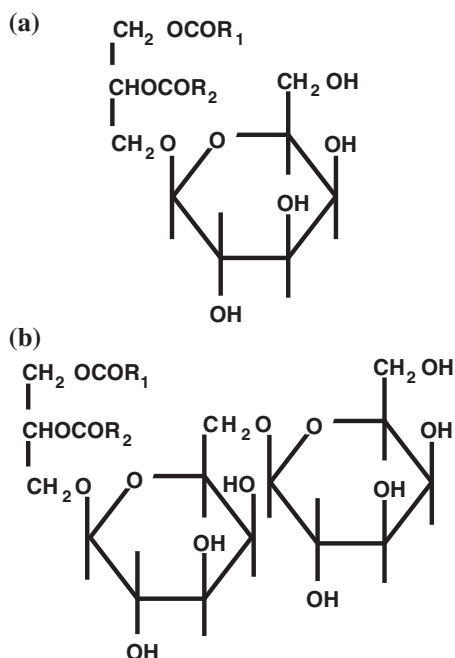
Steps involved in biodiesel production	Energy depletion potential (MJ/MJ biodiesel)	Global warming potential (kg CO <sub>2</sub> /MJ biodiesel)	Reference
1. Cultivation			
(a) Raceway ponds	0.22, 0.33	0.05	[7, 8, 10]
(b) Flat panel PBR	0.19	n.a	
(c) Annular PBR	4.9	n.a	
(d) Tubular PBR	15.8, 14.3	0.37	
2. Harvesting			
(a) Centrifugation	0.9	n.a	[7, 11]
(b) Filtration	0.8	n.a	
(c) Flocculation	0.09	n.a	
(d) Drying (natural gas)	2.4	n.a	
3. Lipid extraction and conversion to biodiesel			
(a) Dried biomass grown with sufficient nitrogen	0.3	0.02	[4, 9, 11]
(b) Dried biomass grown under nitrogen starvation	0.1	n.a	
(c) Wet biomass grown with sufficient nitrogen	0.85	n.a	
(d) Wet biomass grown under nitrogen starvation	0.4	n.a	
(e) Hydrothermal Liquefaction (HTL)	0.4	n.a	
4. Coproduction and recycling			
(a) Ethanol fermentation	-10	-0.27	[9, 10]
(b) Anaerobic digestion	-1.35	-0.07	

*n.a* not available

### 4.3 The Applications of Ultrasound in Microalgal Lipid Extraction

To understand the ultrasound applications in microalgal lipid extraction, it is first imperative to study the types and locations of the various lipids inside a microalgal cell. These lipids can be classified mainly into membrane lipids and cytoplasmic storage lipids. The membrane lipids are polar and are composed of phospholipids, glycolipids and betaine lipids. They are important structural components of cell membranes, intracellular thylakoid membranes and extra-chloroplast membranes. The thylakoid membranes are made up of 4 glycerolipids of which

**Fig. 4.1** Structures of **a** Monogalactosyl diacylglycerol (*MGDG*) and **b** Digalactosyl diacylglycerol (*DGDG*).  $R^1$  and  $R^2$  are the fatty acyl chains



monogalactosyl diacylglycerol (MGDG) and digalactosyl diacylglycerol (DGDG) are predominant. The structures of MGDG and DGDG are shown in Fig. 4.1, reproduced from Ref. [20].

In freshwater algae, MGDG and DGDG are mainly composed of  $\alpha$ -Linolenic acid (C18:3) and palmitic acid (C16:0), while in marine algae, long chain polyunsaturated fatty acids (PUFAs) like EPA are predominant in addition to C18:3 and C16:0. The extra-chloroplast membranes are composed of mostly phospholipids. Betaine lipids in freshwater algae are made up of mostly saturated fatty acids like C14:0 and C16:0, and C18 unsaturated fatty acids. On the other hand, a high PUFA content can be found among the betaine lipids in marine algae. Storage lipids are non-polar by nature and are made up of acylglycerols, sterols and free fatty acids. TAGs are the most common storage lipids and they exist as fat globules in the cytoplasm. The storage lipids contain a much lower percentage of PUFA than the betaine lipids and are made up of saturated and mono unsaturated fatty acids [20].

The lipid compositions in microalgae are highly dependent on environmental factors. Exposure to lower temperatures causes algae to increase their relative amount of fatty acid unsaturation. Alkaline pH stress leads to TAG accumulation and a proportional decrease in membrane lipids. Salinity induces an enzyme which is responsible for fatty acid chain elongation, and therefore algae exposed to saline water end up having a higher amount of long chain unsaturated fatty acids. Freshwater algae predominantly contain even chain fatty acids in the range

C14–C22, with C16 fatty acids forming the majority. In marine microalgae, C20 PUFAs were found to be predominant. A higher salinity can lead to longer chain fatty acids and more unsaturation [21].

Extraction of lipids from microalgal cells typically requires either the disruption of the cell wall to release the cellular contents; or the use of an appropriate solvent that has high selectivity and solubility for lipids to allow the diffusion of lipids through the cell walls [22]. Ultrasonication uses sound waves with a frequency of 20 kHz or above to irradiate the culture. The sound waves create alternating regions of compression and expansion and cause microbubbles to form. The microbubbles oscillate and grow in size as ultrasonic energy is absorbed. When the bubbles reach a critical size, they collapse powerfully causing a phenomenon called ultrasonic cavitation [23]. The cavitation gives rise to shock waves that lead to cell disruptions. It also increases the convection in the bulk medium by micro-turbulence that enhances the diffusion of lipids into the solvent [22, 24]. Therefore, ultrasound can either be used as a standalone mechanical cell disruption method or combined with solvents in lipid extraction processes.

Many microalgae have strong cell walls made up of various components like polysaccharides, uronic acid, mannose, xylan, algaenan, glycoproteins and minerals such as calcium and silicon [25]. Efficient extraction of lipids from inside the cells will require the cell walls to be either broken or made permeable. Various processes have been utilized for such purpose and they can generally be classified into four categories, namely mechanical (bead milling, homogenization, grinding with liquid nitrogen, ultrasonication, etc.); physical (osmotic shock, autoclave, microwave, freeze-drying, etc.); chemical (addition of antibiotics, chelators, detergents or solvents); and enzymatic (lysozyme, cellulase, snailase, autolytic phage, etc.). Factors such as scalability, costs, extraction times, lipid yields, toxicity and contamination of products govern the choice of extraction processes. While the search for the ideal process is still ongoing, it is generally accepted that addition of salts, chemicals or enzymes causes contamination of the products. It would increase the costs of downstream processing. The high temperatures involved in autoclave and microwave processes have the potential to decrease the quality of the lipids extracted. Overall, the mechanical processes look more promising among the rest.

The use of ultrasonication in particular has attracted increasing attention as it offers many advantages like high efficiency, low to moderate costs, low toxicity, increased yields, no external addition of chemicals or enzymes, low operation temperatures and is easily scalable from batch to continuous processing. The disadvantage, however, is that the long operation time may cause the formation of free radicals and degrade the oils [26, 27].

Most ultrasound applications in microalgal lipid extraction available in the literature are used in combination with solvent extractions. Several studies have shown that the use of ultrasound increases the yield of lipids extracted when compared to using solvent extraction methods like Soxhlet, Bligh and Dyer or Folch alone without ultrasound. Typically, the Folch and Bligh and Dyer methods use

**Table 4.2** Lipid yields of marine (M) and freshwater (F) microalgae with and without the use of ultrasonication

Strain of algae	Type	Extraction technique used	Ultrasonication parameters				Lipid yield (% weight of dry biomass)		Reference
			Frequency (kHz)	Power (W)	Time (min)	Without ultrasonication	After ultrasonication		
<i>Chlorella vulgaris</i>	M	Bligh and Dyer	20	600	20	3	15	[15]	
<i>Chlorella vulgaris</i>	F	Modified Bligh and Dyer	10	–	5	5	6	[14]	
<i>Chlorella</i> sp.	F	Bligh and Dyer	0.05	–	15	8	21	[16]	
<i>Nannochloropsis oculata</i>	M	Folch	30	100	–	7	24.3	[37]	
<i>Nannochloropsis</i> sp.	M	Bligh and Dyer with SrO catalyst	20	–	5	3	21	[38]	
<i>Scenedesmus</i> sp.	F	Modified Bligh and Dyer	10	–	5	2	7	[14]	
<i>Scenedesmus</i> sp.	F	Bligh and Dyer	20	100	30	2	6	[22]	
<i>Scenedesmus obliquus</i>	M	Modified Bligh and Dyer	35	80	90	1.7	3.5	[39]	
<i>Cryptocodinium colnii</i>	M	Soxhlet (n-hexane)	19	80	60	4.8	24.7	[40]	
Mixed culture	F	Soxhlet (n-hexane)	30	50	60	12	17.6	[32]	
Mixed culture	F	Bligh and Dyer	30	50	60	13.6	26.8	[32]	

a mixture of chloroform, methanol and water in different ratios for lipid extraction while Soxhlet extraction uses different solvents such as n-hexane, chloroform-methanol mixture and ethanol [28–31]. A comparison of lipid yields from solvent extractions with and without ultrasonication is shown in Table 4.2. It is obvious from the table that the use of ultrasound causes an increase in the amount of lipids extracted. The extent of increase depends on the solvents used and the ultrasonication operating parameters. When a mixture of chloroform, methanol and water is used as the solvent system, both polar and non-polar lipids are extracted but when n-hexane alone is used as the solvent, only non-polar lipids are extracted thereby lowering the lipid yield. In fact, ultrasonication is found to enhance the lipid yield much more greatly for the Bligh and Dyer method as compared to the Soxhlet extraction [22, 32]. Marine algae tend to have a high amount of PUFAs due to the effect of salinity on the chain elongation enzyme [20]. Since PUFAs are typically polar membrane fatty acids, an appropriate polar solvent is necessary to efficiently extract them out. Making the choice for a suitable solvent system is therefore very important.

The ultrasonication operating parameters are frequency, time, power, energy and cell concentration. From Table 4.2, it is evident that the frequency of the ultrasound wave does not play a crucial role in the total lipid yield. For example, a low frequency such as 50 Hz is able to give a three-fold increase in the lipid extracted but a 10 kHz frequency hardly increases the lipid yield by half. A frequency of 20 kHz, on the other hand, showed a five-fold increase in the lipid yield. While there is no clear trend observed in the effect of ultrasound frequency on the lipid yield, it has been reported that the ultrasound frequency can affect the purity of pigments extracted from microalgae [33]. It was found that phycocyanin was extracted at the highest purity at 28 kHz, which means that the purity of a desired cellular product can be controlled by the frequency of the ultrasound used. Ultrasonication time is one of the most important parameters controlling the lipid extraction. An increase in ultrasonication time increases the lipids yield linearly [34]. However, another study found that the lipid yield increases with an increase in ultrasonication time only until an optimum point, beyond which further ultrasonication can possibly degrade the lipids [35]. The lipid yield was also found to decrease with an increase in microalgae cell concentration and a weak function of ultrasound power [34]. Ultrasonication energy consumption per unit volume of sample was also introduced as a parameter to unify the effects of ultrasound power, time of ultrasonication and the volume of the treated sample. In the context of ultrasonication energy consumption, ultrasound power has been found to have negligible effect on the cell disruption efficiency [35]. Cell concentration is another important factor to be considered. Cell disruption efficiency increases with an increase in cell concentration up to an optimum beyond which there is no further change with increasing cell concentration. This is because the presence of highly concentrated cells increases the apparent liquid phase viscosity and subsequently reduces the efficiency of ultrasonic cavitation for cell disruption [35]. Marine microalgal species, *Tetraselmis suecica* and *Nannochloropsis* sp. were found to require lower ultrasound energy



for cell disruption compared to freshwater species, *Chlorella* sp. [35]. *Chlorella* sp. is known to have a rigid three-layered cell wall comprised of chitin, which can form a strong hydrogen-bonding matrix with the neighboring acetyl amine groups. The efficiency of ultrasonic cell disruption was reported to decrease with a decrease in cell size [36]. For a mixed microalgal culture, the optimum ultrasound energy for maximum release of intracellular substances was reported to be 0.4 kWh/L [32].

The choice of solvent extraction method also influences the efficiency of ultrasonication. A comparison of lipid extraction yields using Soxhlet extractor with acetone, ultrasound-assisted Bligh and Dyer and ultrasound-assisted Folch methods indicated that the Soxhlet extraction has the lowest lipid yield while ultrasound-assisted Bligh and Dyer has the highest lipid yield [41]. Diffusion is the main extraction mechanism for the Soxhlet extractor. The absence of shear stress on the cells makes the slow diffusion of lipids through the cell membrane the limiting condition and gives rise to a low lipid yield. The ultrasound-assisted Bligh and Dyer method, on the other hand, has a combined advantage of cell wall disruptions provided by the ultrasonic cavitation as well as the use of a solvent with high lipid selectivity. Therefore, ultrasound-assisted Bligh and Dyer method was found to be the most effective among the three methods studied [41].

Apart from the application of ultrasound in conjunction with solvent extraction, ultrasonication can also be applied as a standalone lipid extraction method. Almost all of the methods mentioned above use ultrasonication as a batch process to treat dried microalgal biomass followed by direct transesterification reaction, in which there is simultaneous solvent extraction of lipids and conversion to FAMES [42]. Dried biomass is used because the presence of water can decrease the efficiency of acid-catalyzed transesterification process and reduce the lipid yield [13]. However, based on the life cycle analysis of algal biofuel, drying is one of the most energy intensive processes. The application of ultrasonication as a standalone extraction method can be applied on microalgae culture without prior liquid–solid separation or drying. Wet microalgal culture can be added directly to a continuous flow cell ultrasonicator. In an industrial scale, considering that the amount of lipids released will be very high, the lipids released can form a separate layer on top of the aqueous phase and may be separated by using saline solution as a demulsifier [34]. The elimination of solvent usage makes the process ideal for commercialization. However, in lab scale studies, solvents are necessary for the extraction and analysis of lipids released. With the use of response surface methodology, the operating parameters of ultrasonication were optimized. However, the maximum oil yield was found to be only 0.21 % [34]. The cause of such a low oil yield can possibly be due to an inadequate recovery of lipids from the aqueous phase or that the lipids are still retained in the cell membranes. Therefore, it is necessary to study the lipid releasing characteristics for better understanding of ultrasound applications in microalgal lipid extractions.

## 4.4 Lipid Releasing Characteristics of Microalgae Through Continuous Ultrasonication

Analyzing the lipids present in the microalgal debris or in the aqueous phase after ultrasonication, and comparing it to the lipid content in the microalgae before ultrasonication can determine the lipid releasing characteristics. Investigation on the lipids present in the microalgal debris is preferred because it allows the use of dry extraction methods, which are more efficient compared to the wet extraction methods for small lipid amounts in the aqueous phase. The key assumption made is that the difference in lipid content before and after ultrasonication in the microalgal debris indicates the lipids that are released into the aqueous phase. As reported in Ref. [35], the microalgal culture at a concentration of 2 g/L was taken directly from the cultivation reactor and poured into the recirculation tank of the ultrasonication system (UIP1000HD, Hielscher Germany). It consists of an ultrasonic processor (20 kHz, 1,000 W) and a sonotrode (BS2d18, Hielscher, Germany) inside a 100 mL flow cell, a water cooling jacket for the flow cell, a recirculation tank for feed and processed sample storage, and a centrifugal pump for sample circulation. At set time intervals, ultrasonicated samples were collected at the flow cell exit before entering the recirculation tank, as shown in Fig. 4.2. Biomass was then harvested from these ultrasonicated samples by centrifugation and was subsequently freeze-dried. The fatty acids in the harvested and dried biomass were then subjected to *in situ* direct transesterification. 3.4 mL methanol, 4 mL chloroform,

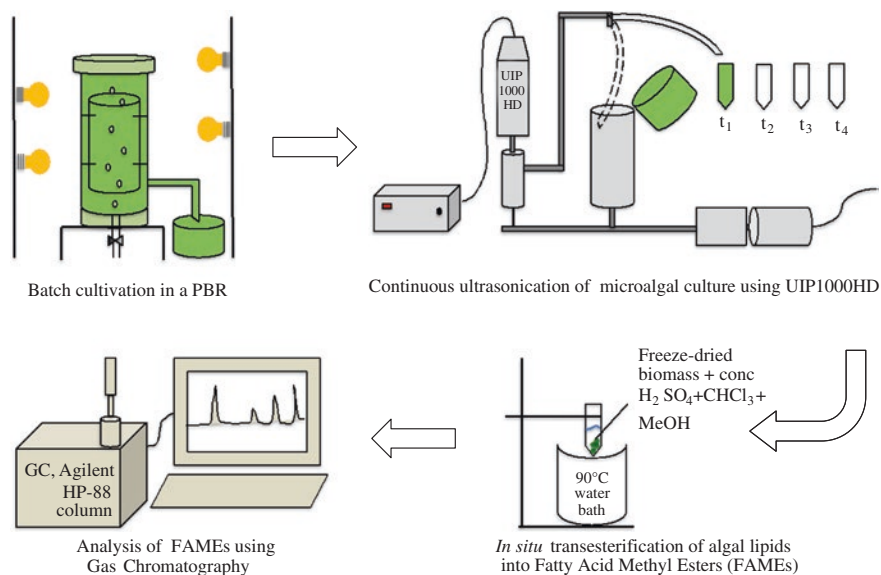


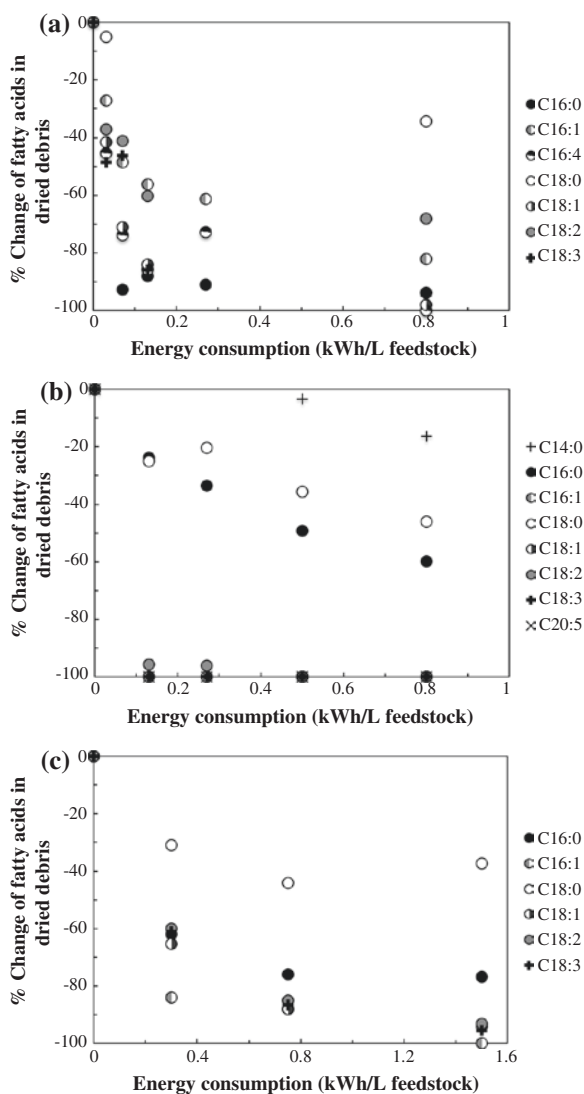
**Fig. 4.2** Experimental setup and measurement protocol

0.6 mL conc.  $H_2SO_4$  and 0.5 mL of 10 g/L internal standard (heptadecanoic acid Sigma Aldrich) were added to 1 g of freeze-dried microalgae and kept at 90 °C for 1 h. After allowing it to reach room temperature, 2 mL of deionised water was added to separate the organic and inorganic phases. The bottom organic layer was analyzed using a gas chromatograph (GC) (GC 6890N, Agilent, USA). It was installed with Agilent HP-88 capillary column (Agilent, USA) which is very effective for FAME analyses. The inlet temperature and the flame ionization detector (FID) temperature were set at 260 and 275 °C, respectively. The column inlet pressure was kept constant at 120 kPa and helium carrier gas was set at a flow rate of 44.3 mL/min. The oven temperature program is as follows—50 °C for 1 min, then raised to 150 °C at the rate of 10 °C/min and held for 2 min, then raised to 200 °C for 10 min at the rate of 8 °C/min and finally raised to 240 °C at the rate of 20 °C/min and held for 8 min. Supelco 37 Component FAME mix (Sigma Aldrich, Singapore) was used as the external standard for calibrating the peak areas. All measurements were performed in triplicate. A pictorial representation of the entire experimental setup is shown in Fig. 4.2.

The effects of ultrasonication on fatty acid content in the dried microalgal debris of *Tetraselmis suecica*, *Nannochloropsis* sp. and *Chlorella* sp. were reported in Ref. [35] and the results are presented in Fig. 4.3 as both the absolute and percentage changes relative to the original lipid content before ultrasonication. It can be seen from Fig. 4.3 that the fatty acid content in the microalgal debris reduces after ultrasonication for all the microalgae species. It indicates that the lipids retained in the cells reduce after ultrasonication and the reduction can be considered as being released into the aqueous phase after ultrasonic cell disruption. As shown in Fig. 4.3a, a majority of fatty acids in *Tetraselmis suecica*, except for C16:0, C16:1, C18:0 and C18:2, were released from the cells after an ultrasound energy consumption of 0.8 kWh/L. However, for the same ultrasound energy consumption, Fig. 4.3b indicates that the only fatty acids retained in the dry microalgal debris of *Nannochloropsis* sp. were C14:0, C16:0 and C18:0. For *Chlorella* sp., Fig. 4.3c shows that the fatty acids retained after an ultrasound energy consumption of 0.8 kWh/L were C16:0, C18:0 and C18:2. Palmitic acid (C16:0) is a constituent of both storage as well as membrane lipids. C18:0 is consistently found in all three species as a slow releasing fatty acid. C18:2 is found to be slow releasing in *Tetraselmis suecica* and *Chlorella* sp. but fast releasing in *Nannochloropsis* sp. A comparison of the lipid releasing behavior of all the three microalgal species in Fig. 4.3 indicates that the polar membrane lipids are easily released while the storage lipids require complete cell disruption to be released from *Nannochloropsis* sp. However, C18:2, being a part of polar membrane lipids, is not as easily released from *Tetraselmis suecica* and *Chlorella* sp.

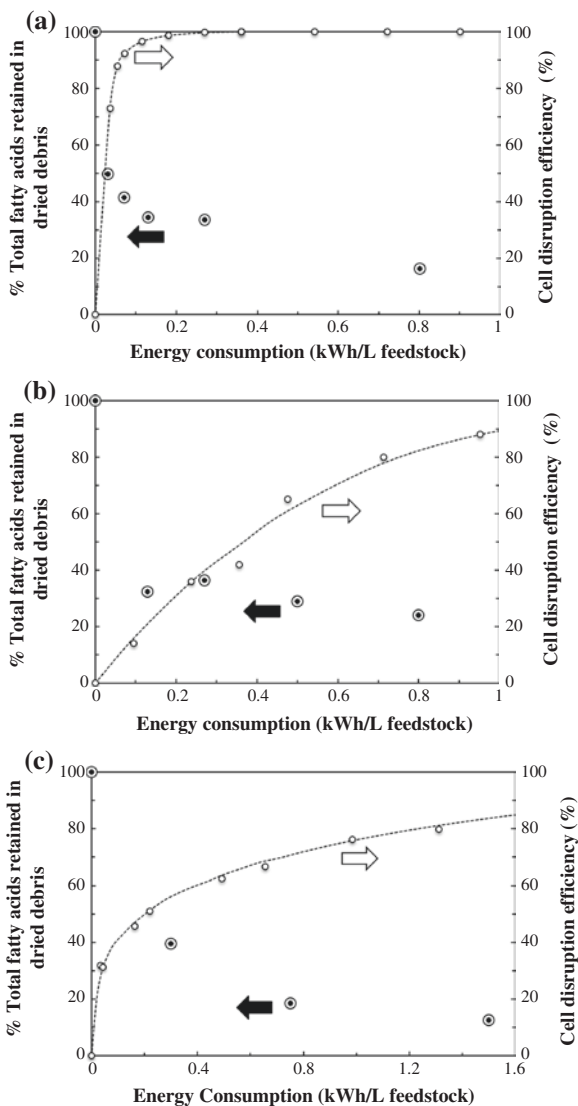
Comparisons of cell disruption efficiencies with the lipids retained in the dried microalgal debris for all the three microalgal species are shown in Fig. 4.4. It can be seen in Fig. 4.4a that for *Tetraselmis suecica*, the cell disruption efficiency reaches a 100 % at 0.25 kWh/L ultrasound energy but the lipids retained in the dried microalgal debris continue to decrease even beyond an ultrasound energy consumption of 0.8 kWh/L. Scanning electron microscopy (SEM) images

**Fig. 4.3** Percentage change in fatty acids in dried microalgal debris relative to the content before ultrasonication in **a** *Tetraselmis suecica*, **b** *Nannochloropsis* sp. and **c** *Chlorella* sp. Figure reproduced from data in [35]



of freeze-dried *Tetraselmis suecica* shown in Fig. 4.5a reveal that the cells become rod shaped after ultrasonication. It is believed that upon cell disruption by ultrasound, the fractured cell membrane coil up, thereby retaining the cellular lipids. Figure 4.4b indicates that the lipids retained in the dried microalgal debris of *Nannochloropsis* sp. reduced at a faster rate than the increase in cell disruption efficiency at low ultrasound energy consumption. However, a further increase in ultrasound energy consumption did not give a substantial reduction in the lipids retained in the dried microalgal debris. SEM images of *Nannochloropsis* sp. cells before and after ultrasonication in Fig. 4.5b show that the fractured cell

**Fig. 4.4** Comparison between percentage of total fatty acids retained in dried microalgal debris and cell disruption efficiency upon ultrasonication in **a** *Tetraselmis suecica*, **b** *Nannochloropsis* sp., and **c** *Chlorella* sp. Figure reproduced from data in [35]



membranes crumpled into small pellets. Similar to the coiled up membranes of fractured *Tetraselmis suecica*, the crumpled pellets also serve to retain the cellular lipids. On the other hand, Fig. 4.4c shows that the lipids retained in the dried *Chlorella* sp. debris had a positive correlation with the cell disruption efficiency. Figure 4.5c shows that the *Chlorella* sp. cells were completely shattered after ultrasonication and cannot retain the cellular lipids. It is possibly because of the rigid nature of the *Chlorella* sp. cell walls that are comprised of a chitin-like glycan [43].

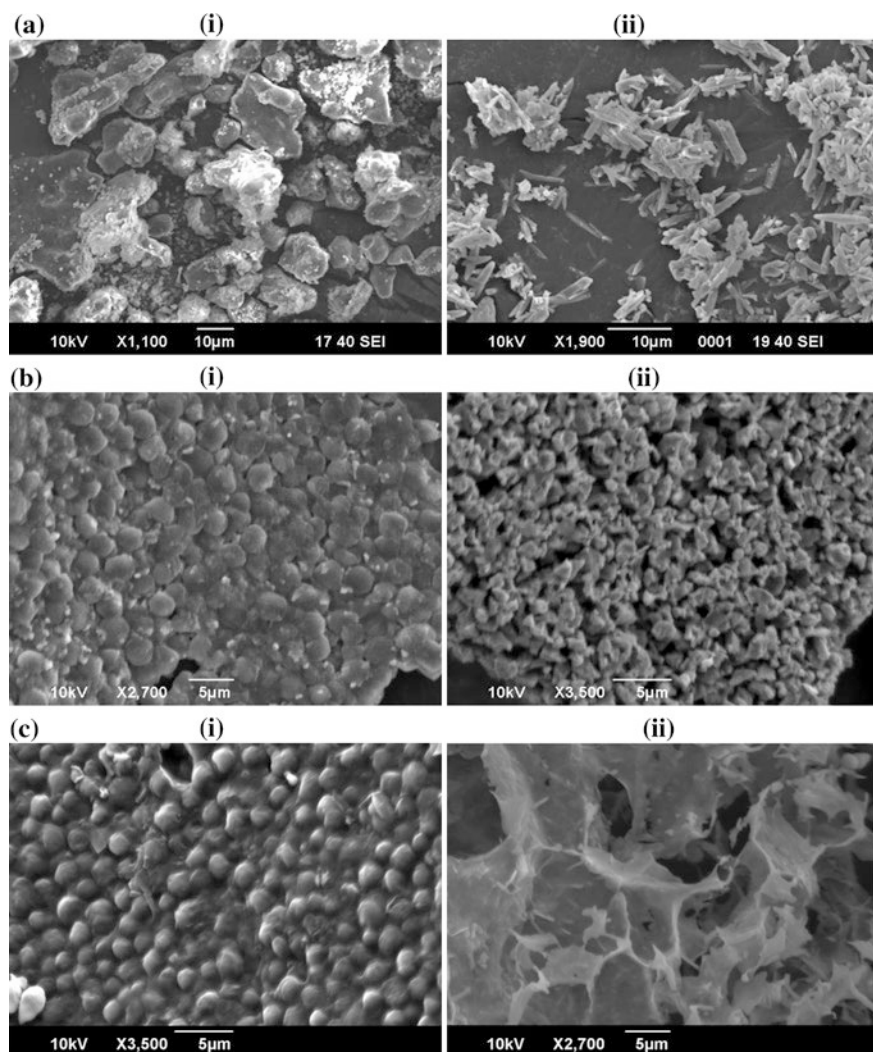


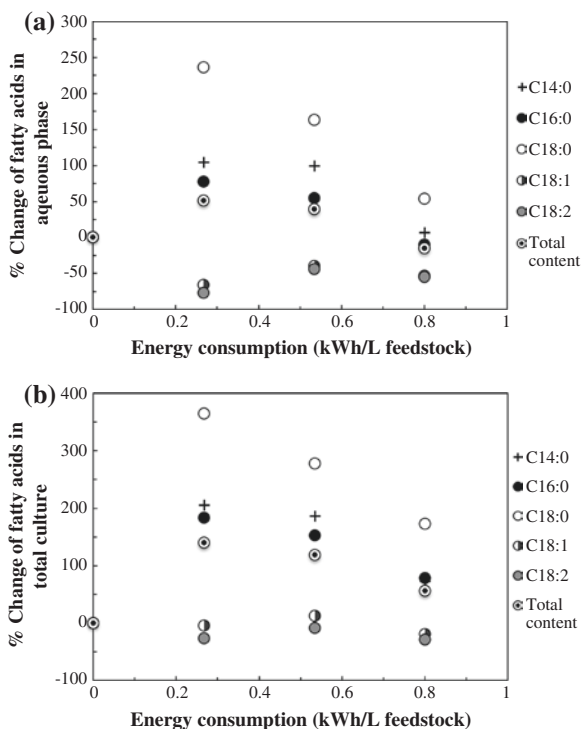
**Fig. 4.5** SEM images of freeze-dried microalgae (i) before ultrasonication, (ii) after ultrasonication for **a** *Tetraselmis suecica*, **b** *Nannochloropsis* sp., and **c** *Chlorella* sp.

To validate the release of lipids after ultrasonication, the lipids present in the aqueous phase were investigated. Although the wet extraction method is not as efficient as the dry extraction method, it can provide insights into the change in lipid content in the aqueous phase after ultrasonication. *Chlorella* sp. is chosen as the model microalgae species and it is cultivated and subjected to continuous ultrasonication in the same conditions as in Ref. [35]. After ultrasonication, the collected samples were centrifuged to separate the aqueous phase from the microalgal debris. The total culture (microalgal debris + aqueous phase) was also analyzed

separately. As the presence of water reduces the efficiency of transesterification, a two-step process was followed where the lipids were first extracted using solvents and then transesterified [44]. The lipids in both the aqueous phase (supernatant) and the total culture (microalgal debris + supernatant) were extracted with 2:2:1 (v/v) chloroform/methanol/(DI water + sample solution). Then the mixture was vortexed for 2 min and the layers were allowed to separate. The lower layer was collected in a clean tube and the procedure was repeated with the upper layer. The organic layer was evaporated by air at 40 °C. The residue containing the crude lipids was then used for transesterification. Transesterification reaction for all samples was performed by adding 2 ml of methanol (5 % H<sub>2</sub>SO<sub>4</sub>) at 95 °C for 1 h and cooled down to room temperature. Hexane (2 ml) was then added to separate the organic phases and inorganic phase. The upper layer was collected for gas GC analysis using the same temperature program and other conditions as in Natarajan et al. [35].

The fatty acid profiles in the aqueous phase and the total culture are shown in Fig. 4.6a, b, respectively. It can be seen in Fig. 4.6a that the maximum fatty acid content released to the aqueous phase was obtained at 0.3 kWh/L, which corresponds to 30 min of continuous ultrasonication. Figure 4.6b also shows that almost a three-fold increase in the total amount of fatty acids can be obtained at the same ultrasound energy consumption of 0.3 kWh/L. The result is consistent

**Fig. 4.6** Percentage change in fatty acid content upon ultrasonication in **a** aqueous phase, **b** entire culture for *Chlorella* sp.





to the ultrasonication improvement in lipid yield in the literature summarized in Table 4.2. The major increase in fatty acids was contributed by C16:0 and C18:0, both of which are part of the storage lipids (mostly TAGs). The other fatty acids do not show significant differences with or without ultrasonication. Extensive ultrasonication appears to have a negative effect on the extraction of lipids. It has been reported that long intervals of ultrasonication leads to free radical formation and degradation of cellular components including lipids [26, 27]. As indicated in Fig. 4.6b, most of the reduction is also attributed to C16:0 and C18:0. In microalgae, fatty acids are synthesized by de novo synthesis in chloroplasts and catabolized through beta-oxidation process. During ultrasonic cavitation, thermal and shear forces are likely to cause fatty acids oxidation [45]. Therefore, the decrease of C16:0 and C18:0 contents are likely because of oxidation.

A plausible mechanism for ultrasonic lipid extraction can be suggested by combining the results obtained in this study and the microalgal lipid extraction mechanism proposed by Ranjan et al. [22]. Membrane lipids can be released through diffusion across cell walls in the presence of proper solvents while the release of storage lipids depends on cell disruption. Based on cell geography, the storage lipids are typically found inside the cells while the membrane lipids are more likely to come in contact with the solvents. Non-polar solvents find it difficult to find their way into the cells because of the polar nature of the cell membranes, which act like a barrier. Cell disruption however exposes the storage lipids to the non-polar solvents and thereby contributes to the improvement in extraction efficiency. While membrane lipids can also be affected by cell disruption, the choice of a proper solvent extraction process plays a more important role. A graphical representation of the proposed ultrasonic lipid-releasing model for microalgae is demonstrated in Fig. 4.7. The cellular components when no solvent extraction or cell disruption is applied are shown in Fig. 4.7a. The membrane lipids are held both on the plasma membrane of the cell and in the thylakoid membranes present in the cytoplasm. The non-polar storage lipids are depicted as TAG molecules in the cytoplasm of the cell. Figure 4.7b shows that when a mixture of polar and non-polar solvents is added to the culture, some of the polar cell membrane lipids can be extracted through the cell wall. The non-polar storage lipids, on the other hand, cannot be extracted through the cell wall as easily because the polar nature of the plasma membrane barrier prevents the non-polar solvents to be in close proximity of the non-polar lipids that are located deep inside the cells. As shown in Fig. 4.7c, when ultrasound is applied, the plasma membranes are first broken and subsequently the thylakoid membranes are broken upon additional ultrasonication. Disruption of the thylakoid membranes releases the chloroplast inside and causes the aqueous phase to turn green. Upon complete cell disruption, the storage lipids and the thylakoid membrane lipids are easily accessible to the non-polar and polar solvents, respectively. As a result, a large enhancement in the rate of release for storage lipids and a slight enhancement in the rate of release for membrane lipids can be observed.



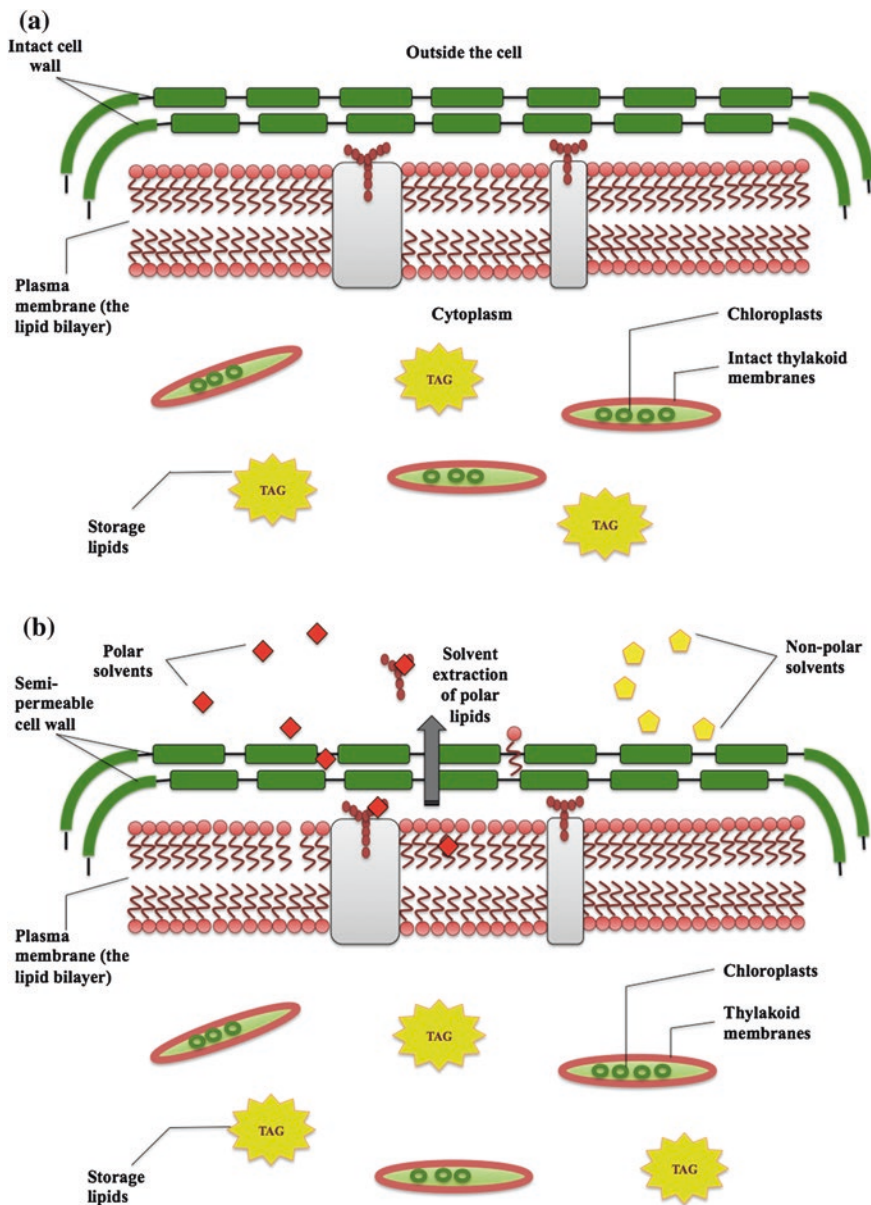


Fig. 4.7 Graphical representation of the proposed mechanism for ultrasonic lipid extraction: **a** undamaged microalgal cell, **b** solvent extraction, and **c** ultrasonic cell disruption followed by solvent extraction

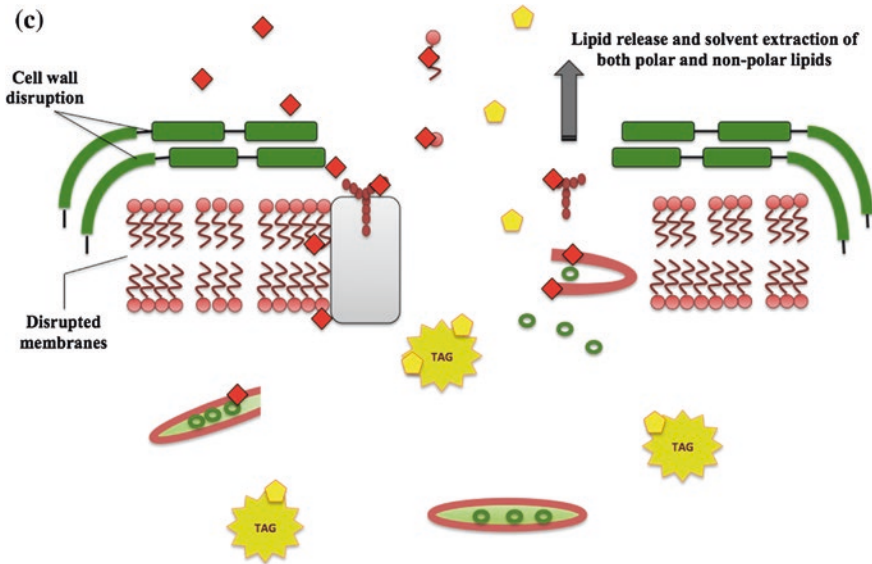


Fig. 4.7 (continued)

## 4.5 Conclusions and Future Outlook

A review of life cycle analysis showed that the drying of biomass contributes to one of the highest energy depletion potentials in microalgal biofuel production. Direct ultrasonication of the wet culture either in conjunction with solvent extraction or as a standalone method of extraction, can be a viable solution to eliminate the drying requirement. A mechanism of lipid extraction was proposed to demonstrate the interactions between lipids and solvents. While the use of ultrasonication with solvent extraction is promising, the involvement of organic solvent can raise environmental concerns and may not be suitable for commercial use. It is believed that development of environment friendly solvents and technologies for efficient separation of lipids in the aqueous phase can bring microalgal biofuel closer to commercial scale. Obviously, collective efforts should still be put on the development of ideal cultivation systems as it is most likely the key challenge to be faced.

## References

1. Chisti Y (2007) Biodiesel from microalgae. *Biotechnol Adv* 25:294–306
2. Hannon M, Gimpel J, Tran M, Rasala B, Mayfield S (2010) Biofuels from algae: challenges and potential. *Biofuels* 1:763–784
3. Harwood JL, Guschina IA (2009) The versatility of algae and their lipid metabolism. *Biochimie* 91:679–684

4. Levine RB, Pinnarat T, Savage PE (2010) Biodiesel production from wet algal biomass through in situ lipid hydrolysis and supercritical transesterification. *Energy Fuels* 24:5235–5243
5. Weyer K, Bush D, Darzins A, Willson B (2010) Theoretical maximum algal oil production. *Bioenergy Res* 3:204–213
6. Zaimes GG, Khanna V (2013) Environmental sustainability of emerging algal biofuels: a comparative life cycle evaluation of algal biodiesel and renewable diesel. *Environ Prog Sustain Energy* 32:926–936
7. Brentner LB, Eckelman MJ, Zimmerman JB (2011) Combinatorial life cycle assessment to inform process design of industrial production of algal biodiesel. *Environ Sci Technol* 45:7060–7067
8. Jorquera O, Kiperstok A, Sales EA, Embiruçu M, Ghirardi ML (2010) Comparative energy life-cycle analyses of microalgal biomass production in open ponds and photobioreactors. *Bioresour Technol* 101:1406–1413
9. Sander K, Murthy G (2010) Life cycle analysis of algae biodiesel. *Int J Life Cycle Assess* 15:704–714
10. Stephenson AL, Kazamia E, Dennis JS, Howe CJ, Scott SA, Smith AG (2010) Life-cycle assessment of potential algal biodiesel production in the United Kingdom: a comparison of raceways and air-lift tubular bioreactors. *Energy Fuels* 24:4062–4077
11. Lardon L, Hélias A, Sialve B, Steyer J-P, Bernard O (2009) Life-cycle assessment of biodiesel production from microalgae. *Environ Sci Technol* 43:6475–6481
12. Passell H, Dhaliwal H, Reno M, Wu B, Ben Amotz A, Ivry E, Gay M, Czartoski T, Laurin L, Ayer N (2013) Algae biodiesel life cycle assessment using current commercial data. *J Environ Manage* 129:103–111
13. Kusdiana D, Saka S (2004) Effects of water on biodiesel fuel production by supercritical methanol treatment. *Bioresour Technol* 91:289–295
14. Lee J-Y, Yoo C, Jun S-Y, Ahn C-Y, Oh H-M (2010) Comparison of several methods for effective lipid extraction from microalgae. *Bioresour Technol* 101:S75–S77
15. Zheng H, Yin J, Gao Z, Huang H, Ji X, Dou C (2011) Disruption of *Chlorella vulgaris* cells for the release of biodiesel-producing lipids: a comparison of grinding, ultrasonication, bead milling, enzymatic lysis, and microwaves. *Appl Biochem Biotechnol* 164:1215–1224
16. Prabakaran P, Ravindran AD (2011) A comparative study on effective cell disruption methods for lipid extraction from microalgae. *Lett Appl Microbiol* 53:150–154
17. Frank E, Elgowainy A, Han J, Wang Z (2013) Life cycle comparison of hydrothermal liquefaction and lipid extraction pathways to renewable diesel from algae. *Mitig Adapt Strat Glob Change* 18:137–158
18. Sialve B, Bernet N, Bernard O (2009) Anaerobic digestion of microalgae as a necessary step to make microalgal biodiesel sustainable. *Biotechnol Adv* 27:409–416
19. Scott SA, Davey MP, Dennis JS, Horst I, Howe CJ, Lea-Smith DJ, Smith AG (2010) Biodiesel from algae: challenges and prospects. *Curr Opin Biotechnol* 21:277–286
20. Guschina I, Harwood J (2009) Algal lipids and effect of the environment on their biochemistry. In: Kainz M, Brett MT, Arts MT (eds) *Lipids in aquatic ecosystems*. Springer, New York, pp 1–24
21. Harwood J (1998) Membrane lipids in algae. In: Paul-André S, Norio M (eds) *Lipids in photosynthesis: structure, function and genetics*, vol 6. *Advances in photosynthesis and respiration*. Springer Netherlands, pp 53–64
22. Ranjan A, Patil C, Moholkar VS (2010) Mechanistic assessment of microalgal lipid extraction. *Ind Eng Chem Res* 49:2979–2985
23. Mason TJ, Lorimer JP (1989) An introduction to sonochemistry. *Endeavour* 13:123–128
24. Wang L, Weller CL (2006) Recent advances in extraction of nutraceuticals from plants. *Trends Food Sci Technol* 17:300–312
25. Lee AK, Lewis DM, Ashman PJ (2012) Disruption of microalgal cells for the extraction of lipids for biofuels: processes and specific energy requirements. *Biomass Bioenergy* 46:89–101

26. Gerde JA, Montalbo-Lomboy M, Yao L, Grewell D, Wang T (2012) Evaluation of microalgae cell disruption by ultrasonic treatment. *Bioresour Technol* 125:175–181
27. Mercer P, Armenta RE (2011) Developments in oil extraction from microalgae. *Eur J Lipid Sci Technol* 113:539–547
28. Bligh EG, Dyer WJ (1959) A rapid method of total lipid extraction and purification. *Can J Biochem Physiol* 37:911–917
29. Folch J, Lees M, Sloane Stanley GH (1957) A simple method for the isolation and purification of total lipides from animal tissues. *J Bio Chem* 226:497–509
30. Prommuak C, Pavasant P, Quitain AT, Goto M, Shotipruk A (2012) Microalgal lipid extraction and evaluation of single-step biodiesel production. *Eng J* 16:157–166
31. McNichol J, MacDougall KM, Melanson JE, McGinn PJ (2012) Suitability of Soxhlet extraction to quantify microalgal fatty acids as determined by comparison with in situ transesterification. *Lipids* 47:195–207
32. Keris-Sen UD, Sen U, Soydemir G, Gurol MD (2014) An investigation of ultrasound effect on microalgal cell integrity and lipid extraction efficiency. *Bioresour Technol* 152:407–413
33. Furuki T, Maeda S, Imajo S, Hiroi T, Amaya T, Hirokawa T, Ito K, Nozawa H (2003) Rapid and selective extraction of phycocyanin from *Spirulina platensis* with ultrasonic cell disruption. *J Appl Phycol* 15:319–324
34. Adam F, Abert-Vian M, Peltier G, Chemat F (2012) “Solvent-free” ultrasound-assisted extraction of lipids from fresh microalgae cells: a green, clean and scalable process. *Bioresour Technol* 114:457–465
35. Natarajan R, Ang WMR, Chen X, Voigtmann M, Lau R (2014) Lipid releasing characteristics of microalgae species through continuous ultrasonication. *Bioresour Technol* 158:7–11
36. Alliger H (1975) Ultrasonic disruption. *Am Lab* 10:75–85
37. Converti A, Casazza AA, Ortiz EY, Perego P, Del Borghi M (2009) Effect of temperature and nitrogen concentration on the growth and lipid content of *Nannochloropsis oculata* and *Chlorella vulgaris* for biodiesel production. *Chem Eng Process* 48:1146–1151
38. Koberg M, Cohen M, Ben-Amotz A, Gedanken A (2011) Bio-diesel production directly from the microalgae biomass of *Nannochloropsis* by microwave and ultrasound radiation. *Bioresour Technol* 102:4265–4269
39. Wiltshire K, Boersma M, Möller A, Buhtz H (2000) Extraction of pigments and fatty acids from the green alga *Scenedesmus obliquus* (Chlorophyceae). *Aquat Ecol* 34:119–126
40. Cravotto G, Boffa L, Mantegna S, Perego P, Avogadro M, Cintas P (2008) Improved extraction of vegetable oils under high-intensity ultrasound and/or microwaves. *Ultrason Sonochem* 15:898–902
41. Araujo GS, Matos LJBL, Fernandes JO, Cartaxo SJM, Gonçalves LRB, Fernandes FAN, Farias WRL (2013) Extraction of lipids from microalgae by ultrasound application: prospection of the optimal extraction method. *Ultrason Sonochem* 20:95–98
42. Lewis T, Nichols PD, McMeekin TA (2000) Evaluation of extraction methods for recovery of fatty acids from lipid-producing microheterotrophs. *J Microbiol Methods* 43:107–116
43. Kapaun E, Reisser W (1995) A chitin-like glycan in the cell wall of a *Chlorella* sp. (Chlorococcales, Chlorophyceae). *Planta* 197:577–582
44. Gikonyo B (2013) *Advances in biofuel production: algae and aquatic plants*. CRC Press, Boca Raton
45. Metherel AH, Taha AY, Izadi H, Stark KD (2009) The application of ultrasound energy to increase lipid extraction throughput of solid matrix samples (flaxseed). *Prostaglandins Leukot Essent Fatty Acids* 81:417–423

# Chapter 5

## Microalgae Lipid Extraction Methods and the Fuel Characteristics of *Isochrysis galbana* by Ultrasound-Assisted Extraction

Cherng-Yuan Lin, Li-Wei Chen and Bo-Yu Lin

**Abstract** Fuel characteristics of microalgae lipid extracted by the ultrasound-assisted method accompanied with solvents are investigated. Successfully developed microalgae lipid separation methods include supercritical fluid extraction (SFE), Soxhlet extraction (SE), microwave-assisted extraction, ultrasound-assisted extraction, osmotic shock extraction, extraction by a high-pressure homogenizer, and accelerated solvent extraction. The effect of extraction solvent, lipid extraction time, and input extraction energy of the ultrasound cell breaker on the extracted quantity of crude *Isochrysis galbana* lipid, fatty acids compositions and elemental contents of *Isochrysis galbana* biodiesel, and typical fuel characteristics of the microalgae biodiesel are described. The experimental results show that the application of ultrasound-assisted extraction method together with iso-propanol solvent appears to give the largest quantity of crude lipid and methyl esters of *Isochrysis galbana* among the extraction solvents. The *Isochrysis galbana* lipid extracted by ultrasound-assisted solvents was found to have higher elemental content of C, H, and Si than by microwave-assisted extraction.

**Keywords** Ultrasound-assisted extraction · *Isochrysis galbana* · Crude lipid · Methyl esters · Fatty acids

---

C.-Y. Lin (✉) · B.-Y. Lin  
Department of Marine Engineering, National Taiwan Ocean University,  
Keelung 202, Taiwan ROC  
e-mail: Lin7108@ntou.edu.tw

L.-W. Chen  
Department of Mechanical and Computer-Aided Engineering, National Formosa University,  
Yunlin 632, Taiwan ROC

## 5.1 Introduction

### 5.1.1 *Microalgae Feedstock for Biodiesel Production*

Bioenergy includes biodiesel, bio-alcohol, bio-hydrogen, energy crops of agriculture and forestry, and biofuels produced from architecture wastes. Biodiesel is a green energy which is being developed in many countries. The chemical process which triglyceride contained in animal fat, vegetable oil, or algae reacts with a short-chain alcohol (frequently methanol) to form chemicals called long-chain mono alkyl esters or biodiesel is referred to transesterification. Biodiesel has several advantages, for example, relatively high lubricity, superior biodegradability, high combustion efficiency, low toxicity, low pollutant emission, and high flash point which allows it to be transported and stores safely [1].

Biofuels, produced from edible feedstock like soybean oil, corn, canola, tallow, lard, and sugarcane, are generally referred to the first-generation biofuels. However, growing those energy crops causes the controversy of food competing with fuel and sharp rise of human food price. Hence, the second-generation biofuels which use lignocelluloses and agricultural or architectural wastes such as miscanthus, wood chip, wheat straw, corn stalk, or sugarcane bagasse, as a main source are developing globally. Usage of those feedstock materials does not require large amounts of food crops so the development of the second-generation biofuel would reduce the impact of fuel production on human food supply [2].

Algae can generate higher lipid content through photosynthesis than other terrestrial plants and also has strong acclimation capability and is fast growing. These characteristics make algae as a potential feedstock for new-generation biofuels. Both quality and quantity of biofuels produced from algae are influenced by algae species, growing environment and extraction method. The techniques of algae culture and lipid extraction are considered the key factors towards successfully developing biofuel industry in which algae is used as the main feedstock.

Production techniques for biodiesel are rapidly developing in recent years. However, most feedstocks for more mature technologies of biodiesel production are obtained from animal fats or vegetable oils such as canola, corn, soybean, palm oil, lard, and tallow etc. Since those materials have been used for human consumption for thousands years, their supply is limited in the fuel market and large amounts of land for cultivating those plants is required. Furthermore, damage in forest resource is also a serious issue. Hence, the development of second generation biodiesel is actively required. Algae not only can produce high weight ratio of lipids, but also can be grown on infertile land [3]. Cultivation of microalgae can reduce carbon emissions from power plants through their photosynthesis process and provide lipid for production of biofuels. Lower greenhouse gas, such as CO<sub>2</sub> will be produced in comparison with fossil fuel when biofuel from algae is used as alternative fuel for engines or boilers.



### ***5.1.2 Potential Economic Extraction Methods for Microalgae Lipid***

There are various methods to extract microalgae liquid. For example, methods of supercritical fluid extraction, ultrasonic extraction, microwave extraction, extraction by a high-pressure homogenizer, and solvent extraction have been developed. However, most extraction methods require large amounts of organic solvents which will not only causes environmental pollution, but also waste large amounts of energy. Ultrasonic extraction method involves fewer amounts of both solvent and energy. The ultrasonic wave increases the contacting surface and frequency between the solvent and algae and creates penetrating force to break algae cell walls, making solvent extraction of the algae lipid efficient. However, the cost of microalgae lipid extraction for producing biodiesel is in general relatively high. As soon as the economic issues are resolved, algae lipid extraction technology will be one of the great potential options for biofuel production.

Microalgae belong to single-cell organisms. They absorb carbon dioxide from environment and transfer it into their constructing compounds such as carbohydrates, proteins, fats via photosynthesis [4]. A unit area of microalgae is able to produce lipid 10–150 times greater than other terrestrial plants including soybean, canola and oil palm, etc. As mentioned above, algae do not require as large area of land as terrestrial plants for cultivation so the food versus fuel issues incurred by the current first-generation biofuel can be minimized. The production procedures of microalgae biofuel include cultivation and harvest of algae, cell disruption, lipid extraction, and transesterification processes. Particularly, the process of microalgae cell disruption significantly affects the efficiency and percentage of later lipid extraction. Chloroform/methanol mixtures which are frequently used as the extraction solvent exhibit high toxicity and are costly. Hence, reduction in solvent consumption accompanied with improved extraction efficiency of lipid content will lead to low production cost of microalgae biofuel. Hexane is considered as a promising extraction solvent which has favorable characteristics of oil-solubility, low cost and low boiling point for ultrasonic extraction of lipids. After the microalgae lipid is extracted, the fatty acids methyl esters and elemental compositions of the biodiesel product are analyzed and discussed.

## **5.2 Types of Lipid-Contained Microalgae**

Algae are of prokaryotes, Protista and plant. In particular, algae belong to eukaryotic cell with cell wall and chlorophyll. Algae are also the single-cell organism which can undergo photosynthesis in the world. Certain bacteria, fungi and algae and other micro-organisms can contain over 20 wt% lipids within their cells.

Those organisms are generally referred to oleaginous microorganisms. In early centuries, algae were classified as plants by scientists since they are able to precede photosynthesis. Botanists have divided algae into ten phyla according to their pigment type, external structure, cell wall composition and cell structure. The algae which can only be observed through a microscopic are named microalgae.

Algae cells consist mainly of protein, carbohydrates and fats. Normally, all algae cells contain fat, but algae of different types contain various contents of fat. For example, *Chrysophyceae* and *Chlorophyceae* generally have high fat content within their cells which may reach as high as 60 wt%. Fat can be categorized as neutral lipids, phospholipids and glycolipids. Neutral lipids are known as triglycerides which have the highest fat content. Animal and vegetable fats are often stored in the form of triglyceride lipids which can be transesterified to form fatty acids methyl esters (FAME). In contrast, the phospholipids and glycolipids which do not have triglyceride content are unable to be chemically converted into biodiesel. The fat contained in *Cyanophyceae* and *Bacillariophyceae* mostly contains neutral lipids, which can reach up to 65 % [4].

### 5.3 Available Extraction Methods for Microalgae Lipid

#### 5.3.1 Supercritical Fluid Extraction (SFE)

Supercritical fluid technology has been widely used in industrial extraction and purification processes [5]. Supercritical fluid extraction has received special attention in the area of specific compound extraction and mixture separations [6]. Supercritical fluid extraction has been considered as an ideal lipid extraction method that can possibly replace organic solvent extraction methods. Supercritical fluid technology also fits into environmental protection requirements and has been applied to the fields of cosmetic, pharmaceutical, chemical, crops and food industries. Supercritical fluid technology is also regarded as an important separation technology.

Substances generally exhibit solid, liquid or gas phases. However, as the temperature and pressure reaches the corresponding critical point for some substance, a homogeneous phase will be formed. It has physical properties between a liquid phase and a gas phase and is referred to as a supercritical fluid state [7]. A supercritical fluid has density close to the liquid phase and viscosity close to the gas phase. A supercritical fluid frequently exhibits a superior mass transfer efficiency [8]. Due to the low viscosity of a supercritical fluid, the work required for its mass transport is lower than its corresponding liquid phase. Moreover, the diffusion coefficient of a supercritical fluid is 10–100 times higher than its corresponding liquid. Therefore, the supercritical fluid has superior capabilities of both permeability and solubility to extract a certain solute from some substance. Moreover, the low surface tension feature enables a supercritical fluid penetrate through pores



in substance, leading to a more efficient extraction than other solvent extraction method [9].

Carbon dioxide (CO<sub>2</sub>) has been commonly used as a solvent of supercritical fluid extraction. It is called a green solvent since it can replace traditional organic solvents. Carbon dioxide has critical temperature 31.1 °C which is close to room temperature, and critical pressure 72.8 atm. The critical condition of CO<sub>2</sub> can be easily achieved. CO<sub>2</sub> is an odorless, non-toxic, non-corrosive, non-flammable, low-cost, high-purity solvent and leaves no residual contaminant [10]. The residue of toxic solvents can be effectively avoided once a supercritical CO<sub>2</sub> extraction method is used instead of traditional organic solvent extraction ones. Therefore, supercritical carbon dioxide fluid is a natural solvent for extraction of lipid-soluble compounds.

Pressure and temperature are the key parameters for the extraction efficiency of a supercritical fluid extraction process. Around the critical point, only small change in temperature and pressure can affect the density of carbon dioxide significantly. Adequately controlling of both parameters of pressure and temperature can achieve the optimal extraction rate of plant lipids. Since carbon dioxide is a non-polar substance, some suitable chemical modifiers have been suggested to effectively promote extraction of polar compounds and increase the solubility of the extract mixture. Some typical chemical modifiers include methanol, ethanol, acetonitrile, diethyl ether, methylene chloride and acetone, etc. Methanol is one of potential chemical modifiers which can effectively break the binding compounds between plants and solute [11].

### 5.3.2 Soxhlet Extraction (SE) Method

Soxhlet extraction (SE) method is a traditional extraction method for extracting lipids. Reflux extraction accompanied with adequate organic solvent is used in this method. SE method is frequently used for analytical purposes through a batch process. The extraction steps begin with placing algae powder in a circular tube-shaped filter and then filling suitable organic solvent into a flask. The flask is thereafter heated up to produce vapor of organic solvent. The organic solvent vapor rises along the tube until being condensed in a condensing tube to form liquid drops. The condensed liquid drops of the organic solvent then trickle into algae powders to start lipid extracting. The solvent keep cycling in the Soxhlet extractor until the lipid extraction is complete [12].

Soxhlet extraction method has disadvantages such as long operation period and using large amount of organic solvent. Ordinary Soxhlet extraction may take as long as 12–18 h and uses as much as 100 ml organic solvent per 4 g sample with condensation for solvent recycle [13] so that this method is not economically beneficial. The long extraction period can be reduced by increasing the number of extraction, but the organic solvent will be lost during the process of solvent heating. Hence, this process needs to keep adding fresh organic solvent. However, this

will cause more serious environmental pollution so this extraction method is less applied recently. Conclusively, the disadvantages of Soxhlet extraction method include (1) use of hazardous, flammable organic liquid solvent, (2) possible emission of toxic gas, (3) long extraction period, (4) necessity of using costly high-purity organic solvent [12].

### ***5.3.3 Microwave Extraction Method***

Microwave exhibits frequency between 200 MHz and 300 GHz. Microwave extractions uses high-frequency electromagnetic wave to penetrate into substance. The substance which absorbs microwave energy can sharply increase the temperature inside its molecular cells and create a huge stress to break the cell wall. The intracellular material may then flow freely and dissolve into the surrounding solvents [14]. Microwave extraction presents fast and evenly heating, solvent consumption savings, short extraction period and environmentally friendly features. Microwave extraction requires polar solvents such as ethanol, acetonitrile, methylene chloride, water, acetone, etc. Normally, adding polar solvent into non-polar solvent can increase the extraction rate of non-polar compounds. The extraction temperature is required to be lower than the boiling point of the solvent when a polar solvent is used for the microwave extraction. The parameters which will affect the efficiency of microwave extraction include solvent type, extraction temperature, amount of solvent used, and extraction time. In addition, as the polarity between a polar solute and solvent increases, a higher extraction efficiency can be achieved [15].

### ***5.3.4 Ultrasound Extraction Method***

Ultrasound technology has been extensively applied in the fields of medical- and bio-technologies. For instance, ultrasound scalpel, ultrasound cleaning machines and the use of ultrasound wave to destroy cancer cells and tumors. Ultrasound technology also uses organic solvents, such as hexane, diethyl ether, isopropanol, methanol, ethanol, chloroform, to extract lipid of plants [16]. Ultrasound extraction generally has superior mass transfer efficiency, less usage of organic solvent and higher extraction rate than Soxhlet extraction method [17].

When ultrasonic wave is moving through the extraction solution, a large variation in pressure in the liquid medium occurs that create many tiny vacuum bubbles. Strong implosion forces then cause those vacuum bubbles to break, which is the cavitation effect. Plant cell walls can be broken by solvent molecules with high energy density, which are formed by cavitation of ultrasonic wave, allowing extraction solvents to penetrate more effectively into the cells to extract intracellular lipids [18]. Ultrasonic waves moving in the liquid not only creates cavitation, but

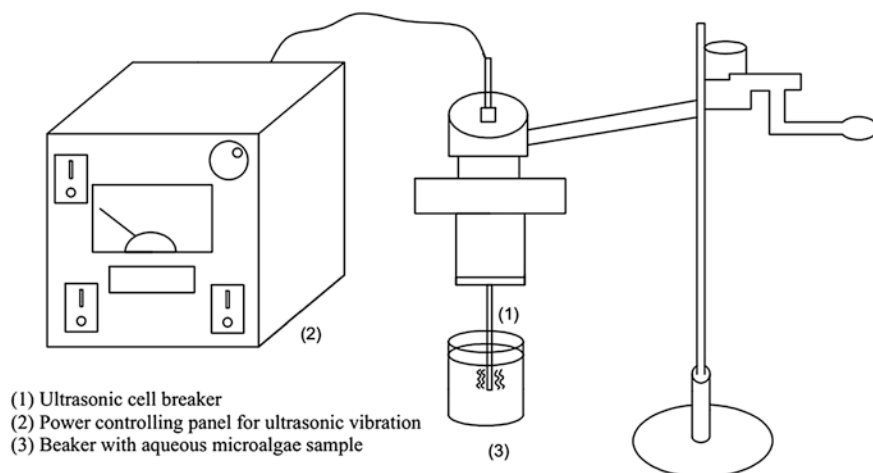


**Fig. 5.1** Scheme of the ultrasound-assisted lipid extraction from microalgae

also causes mechanical and thermal effects. Those combined effects of ultrasonic wave can be applied to effectively clip microorganisms and break cells [19, 20]. The scheme of the ultrasound-assisted extraction from microalgae is illustrated in Fig. 5.1.

### 5.3.5 Solvent Extraction Method

Solvent extraction is a common method for extracting lipids. The extraction solvent can be either polar or non-polar (e.g. ethanol, n-hexane, chloroform, methanol, isopropyl alcohol and water, etc.) [21]. Because of the tiny size of microalgae cells, the extraction method of mechanically squeezing the cells is not applicable. When using the Solvent extraction method, the mixture is placed in a separatory funnel and the solvent is evaporated from a still. The remaining weight is equal to the weight of extracted crude lipid [22]. However, some extraction solvents may be not completely removed and may remain in the still, resulting in an incorrect weight of the extracted lipid.

### 5.3.6 Osmotic Shock Extraction Method

Osmotic shock is a mild extraction method. This method applies a concentration difference between intracellular and surrounding solute to make plant cells expand rapidly and then to be self-broken. For example: plant cells are placed in a high osmolality solution such as a certain concentration of salt or sucrose solutions.

The solute inside the plant cells moves outward. The cells will then shrink until the concentration of the solute reaches equilibrium. The cells will thereafter be moved into a low-concentration solution to make sudden change of osmolality. After that, the surrounding solution then swiftly penetrates into the plant cells so that the cells are expanded rapidly and become self-broken [23].

### ***5.3.7 Accelerated Solvent Extraction Method***

The basic operating principle of accelerated solvent extraction method is controlling the temperature (50–200 °C) and pressure (10–15 MPa) of the extraction solvent to maintain the solvent in the liquid phase for susceptible extraction. This method leads to quick extraction and low amounts of solvent used in comparison with ordinary solvent extraction method. The operating parameters of accelerated solvent extraction method include extracting temperature and pressure, type of extraction solvent, and extraction time [24].

Extraction temperature affects the viscosity, solubility, diffusion efficiency of the solvent. Increasing extraction temperature decreases the surface tension and viscosity and raises the diffusion coefficient and permeability of the extraction solvent. High extraction temperature provides the extraction system with high dynamic energy that increases both the mutual fast motion and the solute diffusion rate among the extracting mixture. The solute concentration can therefore rapidly achieve equilibrium, leading to a decrease in the extraction time. However, an extraction temperature that is too high may also affect the solubility of interfering substances in the sample, resulting in lower selectivity of the extracts. In addition, too high of an extraction temperature may cause partial decomposition of the extracted substances and thus disturb the results of the extracted lipids [25].

### ***5.3.8 Extraction by a High-Pressure Homogenizer Method***

In the World's Fair in Paris in 1900, Gaulin displayed his invention of a high-pressure homogenizer. He used a piston to create high pressure to stabilize the properties of food and dairy. The early mold of such a device can only produce pressure under 50 MPa. Nowadays, a high-pressure homogenizer is able to produce pressure over 100 MPa [26].

The principle of high pressure homogenizer is to use a high-pressure pump to convert a high-pressure mixture into a high-speed mixture. The effect of high shear and impact forces, and large pressure drop is created by the high-speed mixture, leading to the formation of finely dispersed powder and an emulsion of water droplets in surrounding oil phase, and occurrence of cell disruption. The high-speed and high-pressure effects can improve the extent of miniaturization and homogenization of the fluid mixtures [27].

### ***5.3.9 Cell Explosion Method***

Cell explosion method applies an instantaneous increase of pressure and heat to make the intracellular solute reaches a critical point of vaporization. The large instantaneous pressure difference causes the plant cell walls to rupture. The intracellular substance such as lipids and nutrients remains un-damaged while the extraction efficiency is enhanced during the cell explosion process [28].

### ***5.3.10 Automatic Soxhlet Extraction Method***

The traditional Soxhlet extraction method requires long extraction time and consumes a large amount of solvent. Automatic Soxhlet extraction method requires only 1/3 of the extraction time or even shorter times and uses lower amounts of solvent than traditional extraction methods. This means that automatic Soxhlet extraction method has advantages of low lipid-extracting cost and less environmental pollution. The operation of automatic Soxhlet extraction method can be divided into five steps, which are (1) the sample is immersed in boiling solvent and the targeted ingredients of extraction are dissolved in the solvent; (2) when the solvent level reaches below the extraction filter barrel, the residual of dissolved solvent is collected at the rear of the recovery tank; (3) ingredients are extracted by circulating heated and concentrated solvent and collected in the bottom of the extraction beaker; (4) most of the solvent is distilled into the rear of the storage tank; (5) the extraction beaker automatically rises from the hotplate; some of the residual solvent is removed due to heat convection effect [29].

The advantages of automatic Soxhlet extraction method are (1) ability of heating the solvent up to 300 °C; (2) up to 80 % of extracting solvent can be recycled; (3) the solvent can be concentrated for repeated extraction; (4) the remaining solvent can be dried; (5) short extraction time period (90–120 min) [12, 30].

## **5.4 Microalgae-Harvesting Techniques**

Microalgae need to be harvested for forthcoming lipid extraction processes. There are many methods available for microalgae harvesting such as high-speed centrifugation, filtration, natural precipitation and pH precipitation, etc. [31]. Centrifugation method mainly separates the solid particles from liquid, or two insoluble fluids with different densities. Increasing the rotation speed of a centrifuge can increase the strength of force field on microalgae body, making the microalgae particles with lower density separate from the liquid phase.

Filtration method is also applied for microalgae harvesting which uses a filter with fine mesh size to separate solid particles from the liquid. Natural precipitation

method is similar to separation by gravity. The particles with higher density will collect at the bottom of the fluid that can be separated from the liquid. However, this method requires relatively a long period of time for microalgae harvesting. The method of pH precipitation changes the electric charge on the microalgae molecular surface by adjusting the pH value of water for culturing microalgae. The hydrophobicity of the microalgae surface will be enhanced as the charge on the surface of the microalgae is reduced. Microalgae biomass will aggregate because of the hydrophobic interactions and follow with precipitation. This method is commonly used in protein precipitation and has the advantage of low cost [32].

## 5.5 Experimental Study on Lipid Characteristics of *Isochrysis galbana* by Ultrasound-Assisted Extraction Method

In this experiment, Walne's medium is used as the nutrition source for growing *Isochrysis galbana*. Walne's medium generally consists of five compounds, which are nutrient solution, trace metal solution (TMS), vitamin solution, nitrogen source, and sterilized seawater [33]. The ultrasound-assisted extraction method accompanied with different organic solvents was used to extract lipid from microalgae. The crude *Isochrysis galbana* lipid was then transesterified to obtain fatty acid methyl esters (FAME). The properties of those lipid and biodiesel are analyzed.

The experimental steps in this study include: (1) microalgae cultivation and harvest; (2) algae separation from culturing seawater by a centrifuge; (3) freeze-drying the microalgae; (4) extraction of microalgae lipid by ultrasound-assisted method with various types of organic solvents; (5) transesterification of the microalgae lipid to obtain fatty acid methyl esters (FAME); and (6) analyzing the properties of the biofuels.

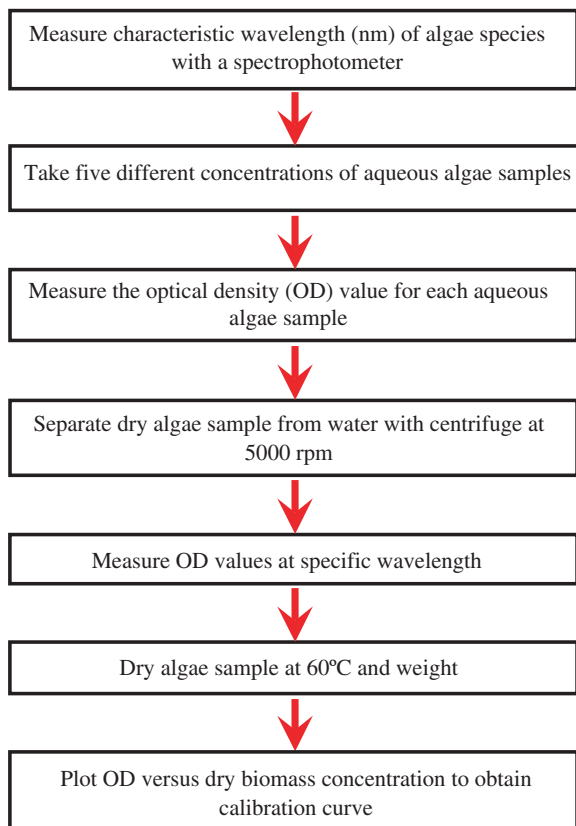
### 5.5.1 Analysis Methods for the Experiment

The analysis methods for crude microalgae lipid and products of microalgae biodiesel are described in this section.

#### (a) Analysis of microalgae concentration

A calibration curve which relates the optical density (OD) and concentration of microalgae biomass was used to obtain the microalgae concentration in culturing sea water in this study. Once the optical density of culturing algae medium is obtained by a spectrophotometer (Helios Beta model, Thermo Fisher Inc., U.S.A.), the *Isochrysis galbana* concentration in the culturing water can be readily

**Fig. 5.2** Process of plotting a calibration curve for microalage biomass



derived by referring to the calibration curve. The process of determining a calibration curve is illustrated in Fig. 5.2. The stages for obtaining the calibration curve include: (1) measuring the characteristic wavelength of the algae species by a spectrophotometer; (2) measuring the OD value of microalgae in culturing water; (3) taking five different concentrations of OD values at the specified characteristic wavelength; (4) plotting a calibration curve which relate the OD values with corresponding dry weights of the algae.

#### (b) Determination of crude lipid weight

Microalgae powder samples of 1 g was mixed with the organic solvent of hexane, isopropanol, or mixture of hexane/isopropanol (in volume ratio 2:1) separately. Ultrasound- or microwave-assisted methods are applied to break the microalgae cells and extract crude lipids. The weight difference of the microalgae sample before and after the lipid extraction process is used to calculate the weight percentage of the extracted crude lipid per gram of the dry microalgae powder sample.

(c) Analysis of fatty acid compositions of microalgae biodiesel

The compositions of fatty acid methyl esters (FAME) produced from *Isochrysis galbana* are analyzed by a Gas Chromatograph with Flame Ionization Detector (GC-FID). The size of the analysis columns is 30 m × 0.25 mm × 0.25 μm. Nitrogen with a flow rate of 45 ml/min is used as the carrier gas. An Elemental Analyzer (Heraeus varioIII-NCH, Germany) is used to analyze the elemental composition of the microalgae.

### 5.5.2 Fuel Characteristics of Microalgae Lipid by Ultrasound-Assisted Extraction

An ultrasound-assisted method with various organic solvents is applied to extract *Isochrysis galbana* in this study. The crude lipid characteristics and fuel properties of fatty acid methyl esters from *Isochrysis galbana* were analyzed and discussed below.

(a) Establishing the calibration curve for determining biomass of algae

The method for plotting a calibration curve for determining the biomass of aqueous algae was described in previous section. The characteristic wavelength of some microalgae strain is determined by spectrophotometer (Helios Beta model, Thermo Fisher Inc., U.S.A.). A calibration curve for the microalgae would be plotted. The correlation equation between the biomass of algae in the ordinate coordinate (i.e. y axis) and absorbance by algae biomass in sea water in terms of OD value (i.e. x axis) can thus be derived with a determination coefficient. The dry weight or biomass concentration of the algae strain corresponding to an OD value measured by a spectrophotometer under the characteristic wavelength can thereafter be determined by referring to this calibration curve.

(b) Comparison of lipids that extracted by ultrasound-assisted method with various organic solvents.

An ultrasound-assisted extraction method accompanied with various organic solvents including hexane, isopropanol, and a mixture of hexane/isopropanol (in volume ratio 2:1) were used to extract the lipid of algae. The power of ultrasound extraction was set between 7,500 and 45,000 kJ. The extracted crude lipid content is shown to increase with an increase in input ultrasound power for various solvents in Fig. 5.3. Moreover, the lipid extracted from *Isochrysis galbana* with isopropanol solvent appears to have the highest content while lipids extracted with hexane solvent have the lowest ones. High shear forces and cavitation effects were created due to mechanical agitation of ultrasound motion. Intensive micro-jets, heat production, and shock waves occurred due to the cavitation effect, leading to an increase in contacting surface between the organic solvent and microalgae biomass. Higher extent of microalgae cell wall breakage along with high lipid extraction efficiency was achieved.



**Fig. 5.3** Extracted crude lipid content from *Isochrysis galbana* for various organic solvents and ultrasound extraction power at 25 °C

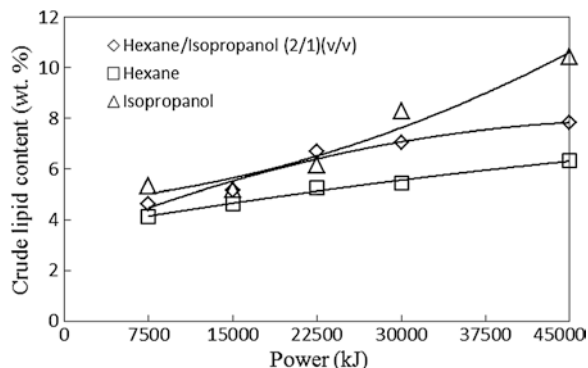
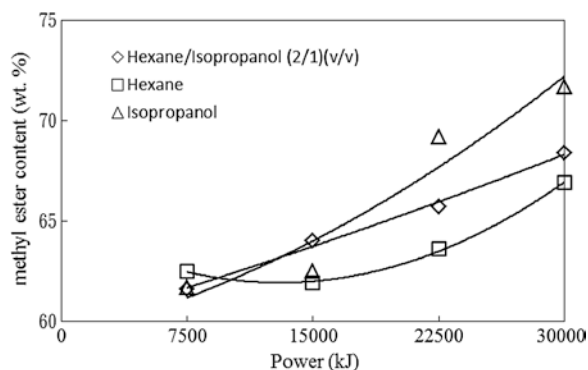


**Fig. 5.4** Content of fatty acid methyl esters produced from lipids extracted by ultrasound-assisted agitation with various organic solvents at 25 °C



(c) FAME characteristics produced from microalgae lipid extracted by ultrasound-assisted method.

The crude lipid extracted from *Isochrysis galbana* by ultrasound-assisted agitation with various organic solvents was further transesterified to produce fatty acid methyl esters (FAME). The lipid extracted with isopropanol solvent are shown to have the highest FAME content while with hexane solvent the lowest one among those three various solvents used in this study as shown in Fig. 5.4. The FAME content which was transesterified from the lipid extracted with isopropanol solvent reached 71.7 wt% in Fig. 5.4.

(d) Elemental compositions of *Isochrysis galbana* lipid extracted by different organic solvents.

An Elemental Analyzer (Heraeus varioIII-NCH, Germany) is used to analyze and compare the elemental compositions of the *Isochrysis galbana* lipid extracted by the ultrasound- and microwave-assisted methods with different organic solvents. Both C and H elemental contents of the crude *Isochrysis galbana* lipid by ultrasound-assisted method appear to be higher than those by microwave-assisted method for all solvents used in Figs. 5.5 and 5.6. No obvious variations

**Fig. 5.5** Comparison of elemental carbon content of *Isochrysis galbana* lipid by ultrasound- and microwave-assisted extraction method with different solvents at 25 °C

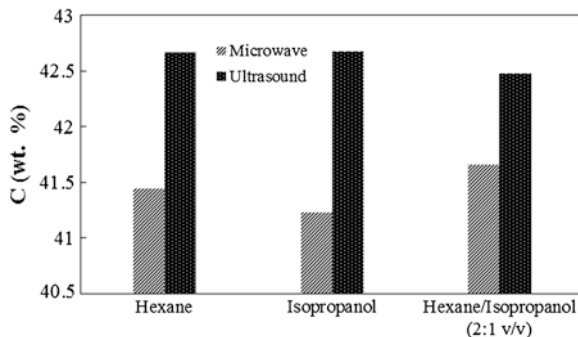


**Fig. 5.6** Comparison of elemental hydrogen content of *Isochrysis galbana* lipid by ultrasound- and microwave-assisted extraction method with different solvents at 25 °C

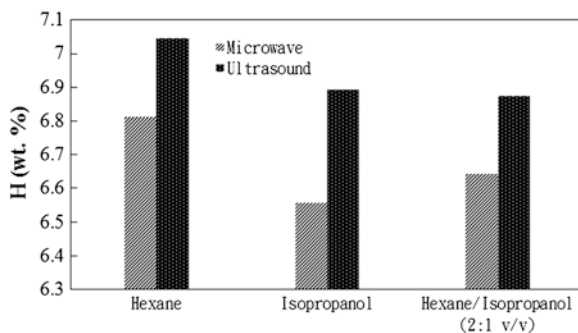
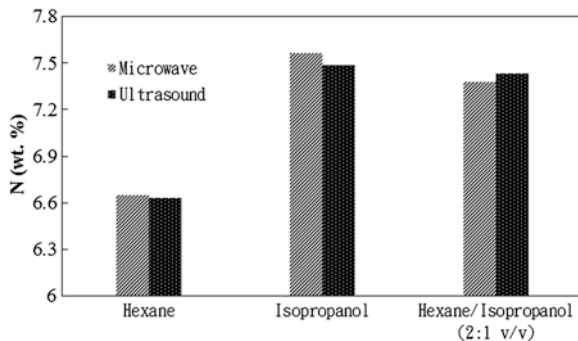


**Fig. 5.7** Comparison of elemental nitrogen content of *Isochrysis galbana* lipid by ultrasound- and microwave-assisted extraction method with different solvents at 25 °C



of elemental contents of N, Na, and P with the extraction methods were found in Figs. 5.7, 5.8 and 5.9. However, the elemental Si content of the lipid extracted by the ultrasound-assisted method appear to be significantly higher than that by the microwave-assisted method when hexane solvent was used in Fig. 5.10.

The intense cavitation effect by ultrasound agitation during the *Isochrysis galbana* lipid extraction period would raise the mixture temperature of liquid solvent and algae particles. Pyrolysis may thus occur in the mixture of isopropanol or hexane solvent molecules and the extracted lipids [34]. The chemical formula of isopropanol is  $C_3H_8O$  and hexane is  $C_6H_{14}$ . Hence, the C and H elements vary

**Fig. 5.8** Comparison of elemental sodium content of *Isochrysis galbana* lipid by ultrasound- and microwave-assisted extraction method with different solvents at 25 °C

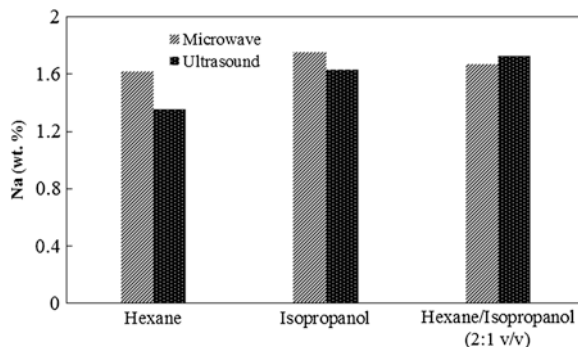


**Fig. 5.9** Comparison of elemental phosphorus content of *Isochrysis galbana* lipid by ultrasound- and microwave-assisted extraction method with different solvents at 25 °C

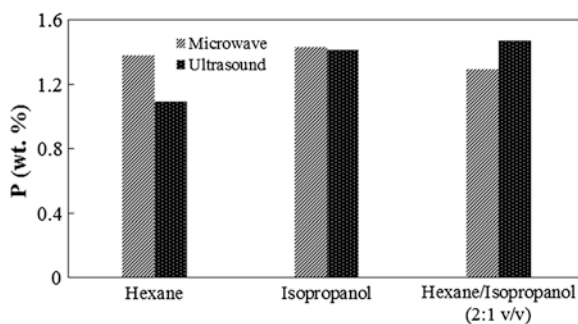
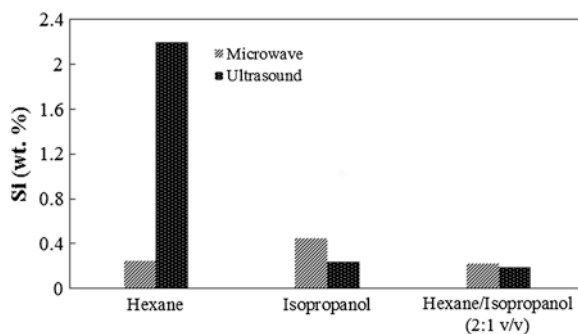


**Fig. 5.10** Comparison of elemental silicon content of *Isochrysis galbana* lipid by ultrasound- and microwave-assisted extraction method with different solvents at 25 °C



much more significantly with the extraction methods and solvent types than other elemental compositions such as N, P and Na.

## 5.6 Conclusions and Future Outlook

Microwave- and ultrasound-assisted extraction methods accompanied with various kinds of organic solvents [i.e. hexane, isopropanol, and mixture of hexane/isopropanol (with volume ratio 2:1)] for *Isochrysis galbana* lipids are considered in this section.

Analyses on fatty acids of crude microalgae lipid, elemental compositions, and methyl esters were carried out. As the input energy was 45,000 kJ for ultrasound-assisted extraction, *Isochrysis galbana* lipid extracted with isopropanol solvent appeared to have the highest crude lipid content among those three various solvents. The crude *Isochrysis galbana* lipid which was extracted by ultrasound-assisted method with isopropanol solvent was also found to have the highest content among various extraction solvents. The elemental compositions of C, H and Si of extracted crude lipid of *Isochrysis galbana* appeared to be higher by ultrasound-assisted extraction method than by microwave-assisted method. Elemental compositions of P, N and Na were not shown to have obvious relation with the extraction methods.

Traditional solvent-extraction methods commonly use chloroform/methanol solvent mixture to extract lipids. Those methods not only require large amounts of solvent that have various degrees of toxicity but also long extraction times. In contrast, hexane and isopropanol solvents which were used in the ultrasound-assisted extraction are found to have advantages of being more environmentally friendly and low cost. Lipid extraction is an important process for biodiesel production from microalgae. Ultrasound-assisted extraction is proven to be a rapid and efficient method to extract algae lipid. However, detailed design of microalgae lipid extraction assisted by ultrasound of industrial production scale needs further development to achieve large-scale efficient, rapid and economic extraction of microalgae lipid.

## References

1. Saydut A, Duz MZ, Kaya C, Kafadar AB, Hamamci C (2008) Transesterified sesame (*Sesamum indicum* L.) seed oil as a biodiesel fuel. *Bioresour Technol* 99:6656–6660
2. Scarlet N, Dallemand JF (2011) Recent developments of biofuels/bioenergy sustainability certification: a global overview. *Energy Policy* 39:1630–1646
3. Huang J, Yang J, Msangi S, Rozelle S, Weersink A (2012) Biofuels and the poor: global impact pathways of biofuels on agricultural markets. *Food Policy* 37:439–451
4. Ahmad AL, Yasin NHM, Derek CJC, Lim JK (2011) Microalgae as a sustainable energy source for biodiesel production: a review. *Renew Sustain Energy Rev* 15:584–593
5. Knutson B (2002) The use of a supercritical carbon dioxide-based solvent as a cost effective and environmentally sound alternative to current photoresist stripping solvents. Master Science thesis, The Graduate College, University of Wisconsin-Stout Menomonie, pp 1–25
6. Sahena F, Zaidul ISM, Jinap S, Karim AA, Abbas KA, Norulaini NAN, Omar AKM (2009) Application of supercritical CO<sub>2</sub> in lipid extraction—A review. *J Food Eng* 95:240–253
7. Madras G, Kolluru C, Kumar R (2004) Synthesis of biodiesel in supercritical fluids. *Fuel* 83:2029–2033
8. Herrero M, Cifuentes A, Ibañez E (2006) Sub- and supercritical fluid extraction of functional ingredients from different natural sources: plants, food-by-products, algae and microalgae: a review. *Food Chem* 98:136–148
9. Halim R, Danquah MK, Webley PA (2012) Extraction of oil from microalgae for biodiesel production: a review. *Biotechnol Adv* 30:709–732
10. Mitra P, Ramaswamy HS, Chang KS (2009) Pumpkin (*Cucurbita maxima*) seed oil extraction using supercritical carbon dioxide and physicochemical properties of the oil. *J Food Eng* 95:208–213

11. Lang Q, Wai CM (2001) Supercritical fluid extraction in herbal and natural product studies— A practical review. *Talanta* 53:771–782
12. Jensen WB (2007) The origin of the Soxhlet extractor. *J Chem Educ* 84:1913–1914
13. GarcõÂa-Ayuso LE, Castro MDL (1999) A multivariate study of the performance of a microwave-assisted Soxhlet extractor for olive seeds. *Anal Chim Acta* 382:309–316
14. Ganzler K, Salg A, Valk K (1986) Microwave extraction: a novel sample preparation method for chromatography. *J Chromatogr A* 371:299–306
15. Lew A, Krutzik PO, Hart ME, Chamberlin AR (2002) Microwave-assisted organic synthesis for combinatorial chemistry. *J Com Chem* 4:95–105
16. Vinatoru M, Toma M, Radu O, Filip PI, Lazurca D, Mason TJ (1997) The use of ultrasound for the extraction of bioactive principles from plant materials. *Ultrason Sonochem* 4:135–139
17. Toma M, Vinatoru M, Paniwnyk L, Mason TJ (2001) Investigation of the effects of ultrasound on vegetal tissues during solvent extraction. *Ultrason Sonochem* 8:137–142
18. Chua SC, Tan CP, Mirhosseini H, Lai OM, Long K, Baharin BS (2009) Optimization of ultrasound extraction condition of phospholipids from palm-pressed fiber. *J Food Eng* 92:403–409
19. Radel S, McLoughlin AJ, Gherardini L, Doblhoff-Dier O, Benes E (2000) Viability of yeast cells in well controlled propagating and standing ultrasonic plane waves. *Ultrasonics* 38:633–637
20. Yang SK, Huang YC (2000) The activation of growth in plant roots by ultrasound exposure. *Biomed Eng-App Bas C* 12:148–154
21. Aryee ANA, Simpson BK (2009) Comparative studies on the yield and quality of solvent-extracted oil from salmon skin. *J Food Eng* 92:325–358
22. Lee JY, Yoo C, Jun SY, Ahn CY, Oh HM (2010) Comparison of several methods for effective lipid extraction from microalgae. *Bioresour Technol* 101:s75–s77
23. Rastogi NK, Angersbach A, Knorr D (2000) Synergistic effect of high hydrostatic pressure pretreatment and osmotic stress on mass transfer during osmotic dehydration. *J Food Eng* 45:25–31
24. Wang L, Weller CL (2006) Recent advances in extraction of nutraceuticals from plants. *Trends Food Technol* 17:300–312
25. Hossain MB, Barry-Ryan C, Martin-Diana AB, Brunton NP (2011) Optimisation of accelerated solvent extraction of antioxidant compounds from rosemary (*Rosmarinus officinalis* L.), marjoram (*Origanum majorana* L.) and oregano (*Origanum vulgare* L.) using response surface methodology. *Food Chem* 126:339–346
26. Paquin P (1999) Technological properties of pressure homogenizers: the effect of fat globules, milk proteins, and polysaccharides. *Int Dairy J* 9:329–335
27. Barbosa-Canovas G, Mortimer A, Lineback D, Spiess W, Buckle K, Colonna P (2009) High-pressure homogenization for food sanitization. In: *Global issues in food science and technology*, Chap 19. Academic Press, San Diego, pp 309–352
28. Qun QZ (1998) Method for bursting cell wall. Taiwan Patent 087109822
29. Wu G, Bao X, Zhao S, Wu J, Han A, Ye Q (2011) Analysis of multi-pesticide residues in the foods of animal origin by GC-MS coupled with accelerated solvent extraction and gel permeation chromatography cleanup. *Food Chem* 126:646–654
30. Barreca S, Mazzola A, Orecchio S, Tuzzolino N (2014) Polychlorinated biphenyls in sediments from sicilian coastal area (Scoglitti) using automated Soxhlet, GC-MS, and principal component analysis. *Polycyclic Aromat Compd* 34:237–262
31. Mata TM, Martins AA, Caetano NS (2010) Microalgae for biodiesel production and other applications: a review. *Renew Sustain Energy Rev* 14:217–232
32. Pragma N, Pandey KK, Sahoo PK (2013) A review on harvesting, oil extraction and biofuels production technologies from microalgae. *Renew Sustain Energy Rev* 24:159–171
33. Batista IR, Kamermans P, Verdegem MCJ, Smaal AC (2014) Growth and fatty acid composition of juvenile *Cerastoderma edule* (L.) fed live microalgae diets with different fatty acid profiles. *Aquac Nutr* 20:132–142
34. Chen WS, Huang SC (2011) Sonophotocatalytic degradation of dinitrotoluenes and trinitrotoluene in industrial wastewater. *Chem Eng J* 172:944–951

# Chapter 6

## Employing Novel Techniques (Microwave and Sonochemistry) in the Synthesis of Biodiesel and Bioethanol

Indra Neel Pulidindi and Aharon Gedanken

**Abstract** Energy crisis and environmental deterioration are the twin problems facing the mankind. Alternate energy sources, especially, biofuels (biodiesel and bioethanol) produced from renewable sources like biomass would alleviate the problem to some extent. Fast and demand based production of biofuels is the need of the hour. Transesterification is the crucial chemical reaction for biodiesel production. Likewise, biomass pretreatment, hydrolysis of carbohydrates and fermentation of sugars are vital in bioethanol production. Interestingly, both the unconventional techniques, sonication and microwave irradiation were found to be extremely useful in accelerating the afore mentioned reactions holding a promise for making sustainable biorefinery possible. The present chapter fully covered the work on carrying out the biodiesel synthesis employing Sonochemistry, however, the use of MW radiation for the synthesis of biodiesel was limited to solid base catalysts. The second part of the chapter was devoted to the use of MW and sonochemistry for the synthesis of bioethanol.

**Keywords** Biofuels · Alternate energy · Biomass · Glucose · Biodiesel · Bioethanol · Ultrasound · Microwave irradiation · Fermentation · Transesterification

---

I.N. Pulidindi · A. Gedanken (✉)

Department of Chemistry, Center for Advanced Materials and Nanotechnology,  
Bar-Ilan University, 52900 Ramat Gan, Israel  
e-mail: [gedanken@mail.biu.ac.il](mailto:gedanken@mail.biu.ac.il)

A. Gedanken

Department of Materials Science and Engineering, National Cheng Kung University,  
Tainan 70101, Taiwan ROC

© Springer Science+Business Media Dordrecht 2015

Z. Fang et al. (eds.), *Production of Biofuels and Chemicals with Ultrasound*,  
Biofuels and Biorefineries 4, DOI 10.1007/978-94-017-9624-8\_6

159

## 6.1 Introduction

Microwave and sonochemical irradiations are known to accelerate chemical reactions [1–5]. Gedankent et al., found additional use of these techniques, namely, the synthesis of a large variety of nanomaterials [6–8].

Now-a-days, developing alternative fuels to replace gradually those produced from petroleum is necessary from economic and ecological points of view. Petroleum is considered as a major conventional resource of energy; unfortunately, it is on the verge of becoming extinct leading to increasing energy prices. Furthermore, constantly increasing CO<sub>2</sub> emissions are intensifying climate change [9]. As a result, there is increasing interest in developing alternative energy resources, which include hydrogen cells [10], solar energy [11], and wind power [12]. However, these technologies are still at the developing stage and the cost of applying them is high. Biodiesel and bioethanol have been identified as viable and reliable alternative fuels which could replace diesel in vehicles, with little or no modifications of their engines. When considering the pollution caused by the combustion of conventional petroleum-based diesel [13], a shift to non-conventional sources such as biodiesel and bioethanol is inevitable.

In a recent review on biofuels the authors outlined the following reasons for the interest in biofuels [14]. They explain that in the era of rising oil prices and growing concerns over climate change, biofuels are receiving increasing attention from governments worldwide as alternatives to fossil fuels [15]. Unlike gasoline and diesel, biofuels (derived from biological materials like carbohydrates and lipids) are renewable resources, and theoretically carbon-neutral, since greenhouse gases emitted when they are burned may be offset by those absorbed when growing bio-fuel crops [16, 17]. Biofuels thus offer the promise of energy security, and reduced greenhouse gas emissions. Additionally, biofuels could create jobs and promote economic diversification, especially in rural areas [18]. As a result, many governments have enthusiastically supported the development of the biofuel industry in recent years through financial subsidies, regulatory mandates, and research.

Many reviews have already been written on the research done in the field of bio-fuels, the scope of the current manuscript is limited to two synthetic methods which have not attracted much attention in the field of biofuels, they are Sonochemistry, and Microwave dielectric heating. Both techniques are known to accelerate chemical reactions and naturally they have found their application for converting biomass to bio-fuels. Since they are not well known to many researchers in the field, the review will briefly explain their principles and the reason they are so useful for producing biofuels.

## 6.2 Sonochemistry

In sonochemistry, molecules undergo chemical reaction due to the application of powerful ultrasound radiation (20 kHz to 10 MHz). The physical phenomenon responsible for the sonochemical process is acoustic cavitation. A number of theories have been developed in order to explain how 20 kHz sonic radiation can break



chemical bonds. The authors of this chapter adopt the hot spot mechanism proposed by Suslick. During the sonochemical reaction bubbles are created in the liquid. These bubbles grow and collapse when they reach a maximum size. The bubble collapses in an implosive mode and very high temperatures (5,000–25,000 K) [19] are obtained. Since this collapse occurs in less than a nanosecond [20, 21], very high cooling rates, in excess of  $10^{11}$  K/s, are also obtained. Sonochemistry is an excellent technique for the synthesis of NPs on the one hand and for coating surfaces by functional NPs on the other hand. These two aspects have been reviewed extensively in the last few years [22, 23]. The sonochemical immobilization of the nanoparticles and the strong adherence to the substrate can be the result of either the physical embedding of the particles into the surface layer, or, the nanoparticles could be anchored to the surface by forming chemical bonds or chemical interactions with the substrate and cannot be removed even by washing.

In short, in a sonochemical reaction very high temperatures were generated for a very short time in a very small volume while the solution around the hot spot is kept at around room temperature. In gas phase sonochemical processes, the vapor of the material (solvent or solute) fills the bubbles volume, the concentration of which in general is very low. It is therefore when the collapsing bubble contains the vapors of the solute (the solvent is usually not volatile), only the vapors of the solute will undergo the chemical reaction. When the solute is not volatile, the sonochemical reaction will occur in the liquid phase. The reacting non-volatile molecules will be found in a 200 nm ring around the bubble which will maintain a high temperature, but not as high as that in the center of the collapsing bubble, and it is in this ring the reaction will occur, in a faster rate than that of the reaction carried out at the same temperature as the bulk is kept, but without the application of ultrasound.

### 6.3 Microwave Dielectric Heating

The application of microwave radiation to chemical reactions and the understanding of why this technique accelerates chemical reactions have also been reviewed extensively [24–28].

The first review by Mingos and Bughurst [24] has attributed the effect of microwave (MW) dielectric heating to the ability of some liquids and solids to transform electromagnetic radiation into heat and thereby drive chemical reactions. MW will generally heat any material containing mobile electric charges, such as polar molecules in a solvent or conducting ions in a solid. Polar solvents are heated as their component molecules are forced to rotate with the field and lose energy in collisions. Semiconducting and conducting samples heat when ions or electrons within them form an electric current and energy is lost due to the electrical resistance of the material. Microwave heating is able to heat the target compounds without heating the entire furnace or oil bath, which saves time and energy. It is also able to heat sufficiently thin objects throughout their volume (rather than through the



outer surface), in theory, producing more uniform heating. However, due to the design of most microwave ovens and due to uneven absorption by the object being heated, the microwave field is usually non-uniform and localized superheating occurs.

There were attempts to attribute the similarity of sonochemistry and MW dielectric heating to the existence of hot spots in both the cases originating from the specific exciting molecules, or functional groups within molecules. However, the time within which thermal energy is repartitioned from such moieties is much shorter than the period of a microwave wave, thus precluding the presence of such ‘molecular hot spots’ under ordinary laboratory conditions. Processes with solid phases behave somewhat differently. In this case much higher heat transfer resistances are involved, and the possibility of the stationary presence of hot-spots should be contemplated. Some theoretical and experimental approaches have been published towards the clarification of the hot spot effect in heterogeneous catalysts. A review summarizing the effect of MW on solid state reactions has been published by Rao et al. [29].

## 6.4 Sonochemistry and Biodiesel Production

The authors of the current chapter consider Maeda as the originator of this field. Maeda is the pioneer in employing sonochemistry in the transesterification process [30]. He has described in a comprehensive series of papers the advantages of using ultrasound in obtaining biodiesel. It started in 2003 when Maeda and coworkers studied the influence of low frequency ultrasound (28 and 40 kHz), versus mechanical stirring, on the transesterification reaction of neat vegetable oil with methanol under base-catalysis. Maeda et al. found that the optimized variables of 6:1 methanol/oil (mol/mol), 0.5 % NaOH (wt/wt), and 40 kHz ultrasonic irradiation at 25 °C for 20 min gave a maximum isolated ester yield of 98 %. This early work was followed by another paper by Maeda and coworkers [31]. Maeda et al. performed the transesterification of vegetable oil with short-chain alcohols, in the presence of base-catalyst, by means of low frequency ultrasound (28 and 40 kHz) to obtain biodiesel. By using ultrasound the reaction time is much shorter (10–40 min) compared to mechanical stirring. The required quantity of catalyst is 2 or 3 times lower. The molar ratio of alcohol/oil used is only 6:1. Normal chain alcohols react fast, while secondary and tertiary alcohols show some or no conversion even after sonication for 60 min. Surprisingly, 40 kHz ultrasound is much more effective in the reduction of the reaction time (10–20 min). Use of 28 kHz ultrasound resulted in slightly better yields (98–99 %), but at a longer reaction time, while higher frequencies are not useful at all for the transesterification of fatty acids [32].

In their next paper [33] they describe a bench scale continuous system for the manufacture of biodiesel from neat vegetable oils under high power low frequency ultrasonic irradiation. The experimental studies explored variations in alcohol-oil stoichiometry and type of oil. Important parameters such as residence time and

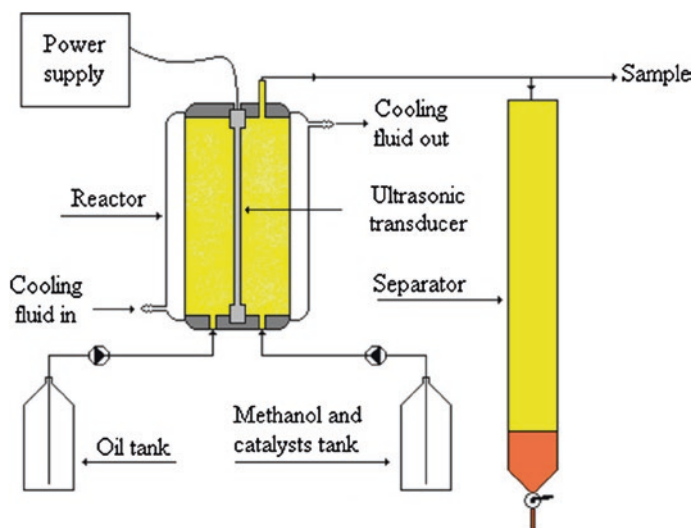


**Fig. 6.1** The experimental setup of the ultrasonic continuous transesterification of vegetable oil. Reprinted with permission from [33], Copyright © 2007, Elsevier

reaction volume were also considered. The highest conversion was achieved when short residence time was employed. The transesterification under ultrasonic irradiation is mainly influenced by the residence time in the reactor and alcohol-oil molar ratio. Figure 6.1 depicts the experimental setup of the continuous flow system.

The last two papers in Maedas' series were published in 2009. In their first paper biodiesel production through transesterification of triolein with various alcohols such as methanol, ethanol, propanol, butanol, hexanol, octanol and decanol was investigated [34]. The conditions of the reaction were: molar ratio 6:1 (alcohol:triolein) and 25 °C in the presence of base catalysts (NaOH and KOH) under ultrasonic irradiation (40 kHz) and mechanical stirring (1,800 rpm) conditions. It was found that the rate of the alkyl ester formation under the ultrasonic irradiation condition was higher than that under the stirring condition. In addition, it was confirmed that the rate depended upon the kind of alcohols; as the number of carbons in alcohol increased, the rate of the ester formation tended to decrease. On the other hand, the secondary alcohols such as 2-propanol, 2-butanol, 2-hexanol, and 2-octanol showed little ester conversion, suggesting that the steric hindrance strongly affected the transesterification of triolein. Their second paper dealt with the production of fatty acid ethyl ester (FAEE) from oleic acid (FFA) and short-chain alcohols (ethanol, propanol, and butanol) under ultrasonic irradiation [35]. Batch esterification of oleic acid was carried out to study the effect of: test temperatures of 10–60 °C, molar ratios of alcohol to oleic acid of 1:1–10:1, quantity of catalysts of 0.5–10 % (wt of sulfuric acid/wt of oleic acid) and irradiation times of 10 h. The optimum condition for the esterification process was molar ratio of alcohol to oleic acid at 3:1 with 5 wt% of H<sub>2</sub>SO<sub>4</sub> at 60 °C with an irradiation time of 2 h.

An early review on the application of ultrasound for enhancing the efficiency of transesterification reaction was published by Rokhina et al. [36]. The authors stressed firstly on the advantages of the biodiesel over petroleum-based fuels. Biodiesel is renewable, biodegradable and non-toxic and its contribution to greenhouse gases is minimal because the emitted CO<sub>2</sub> is equal to the CO<sub>2</sub> absorbed by the biomass. Rokhina et al., explained that the vegetable oil used for the biodiesel production cannot be used directly as a fuel engine because of engine problems such as injector fouling due to incomplete combustion and incorrect vaporization characteristics, and particle agglomeration due to their high viscosity, which is 10–20 times higher than that of petroleum fuel (Fig. 6.2).

The shortening of the transesterification time using sonication was attributed to that low-frequency ultrasound irradiation. Sonication is a highly efficient tool for emulsifying the immiscible liquids, oil and methanol. Rokhina et al. [36] quoted a large number of papers where in the use of ultrasound not only significantly reduced the reaction time, but also the amount of catalyst required, and eliminated saponification. Ultrasound could also be used to determine the completion of the transesterification reaction depending on the settling rates of by-products, such as glycerol which could be monitored with ultrasonic systems [37].

Pandit and coworkers [38] produced biodiesel by the esterification reaction. They illustrated the use of cavitation for intensification of biodiesel synthesis (esterification), which is mass transfer limited reaction considering the immiscible nature of the reactants, i.e., fatty acids and alcohol. Esterification of fatty acid (FA) odour cut (C<sub>8</sub>–C<sub>10</sub>) with methanol in the presence of concentrated H<sub>2</sub>SO<sub>4</sub> as a catalyst has been studied in hydrodynamic cavitation reactor as well as in the sonochemical reactor. The different reaction operating parameters such as molar ratio of acid to alcohol, catalyst quantity have been optimized under acoustic as well as hydrodynamic cavitating conditions. In addition they have optimized the geometry of the orifice plate in the case of hydrodynamic cavitation reactors. It has been observed that ambient operating conditions of temperature and pressure and reaction times of <3 h, for all the different combinations of acid (lower and higher)/methanol studied in the present work, was sufficient for giving >90 % conversion (mol%). They concluded that cavitation is an excellent way to achieve process intensification of the biodiesel synthesis process.

The mechanism of the sonochemical acceleration of the transesterification reaction was studied by Kalva et al. [39]. The mechanism was established by discriminating between physical and chemical effects of ultrasound. Experiments with different conditions have been coupled to a bubble dynamics model. It was revealed that the influence of ultrasound oil transesterification reaction is of purely physical in nature. Formation of fine emulsion between oil and alcohol due to microturbulence generated by cavitation bubbles resulting in enormous interfacial area, which accelerates the reaction. For the power input used in the present experiments, the temperature peak reached in transient collapse of cavitation bubble in methanol is found to be too low to produce any radical species, which can induce transesterification reaction. The yield of the reaction is found to have an optimum with respect to alcohol to oil molar ratio. This result is attributed to the

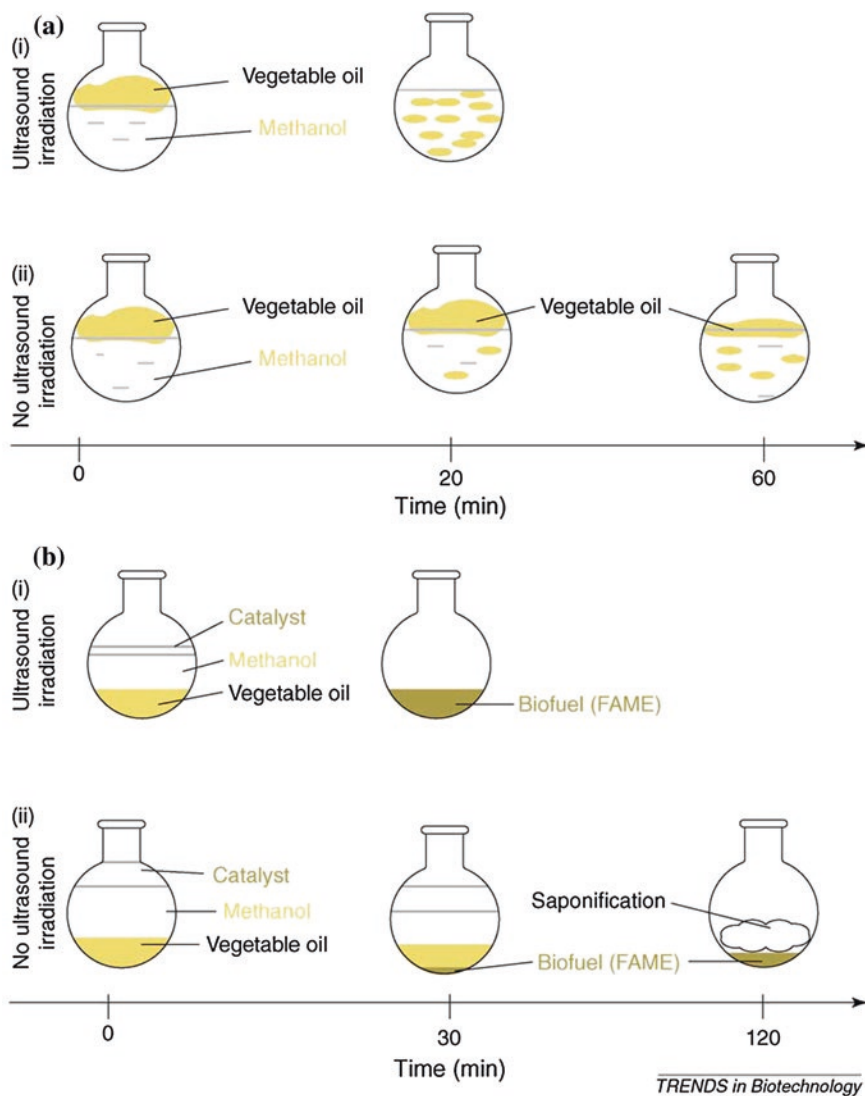


**Fig. 6.2** Schematic depiction of the advantageous effects of sonication for biodiesel production **a** improvement in emulsification, **b** increase of biodiesel yield, shortening of transesterification time and absence of saponification. Reprinted with permission from [36], Copyright © 2009, Elsevier

difference in intensity of microturbulence produced by cavitation bubbles in oil and methanol.

Adewuyi et al. published a few papers on the transesterification reaction carried out using ultrasonic waves. In their first article [40] Adewuyi discussed the two limiting factors for the base-catalyzed transesterification reaction. The first limit is

related to the formation of methoxide anions and the contact of the two reactants in the presence of methoxide anions. Adewuyi et al. explained that this limit is eliminated by dissolving the catalyst in methanol (leading to in situ formation of nucleophile methoxide ions) before the addition of the triglycerides. However, the second limitation of sufficient contact between the triglyceride and methanol molecules cannot be easily eliminated. High-speed stirring consumes a great deal of energy, and it is not an efficient way of contacting the two phases. The authors quote the Maeda's papers [30–35] and explained that the previous studies were carried out for the synthesis of biodiesel using ultrasound were performed at lower frequencies, such as 20, 28, 30, and 40 kHz. Hence, it was thought necessary therefore to further investigate the effect of ultrasound on the transesterification reaction at higher frequencies and power. This will provide a better alternative for biodiesel synthesis using ultrasound with lower amounts of catalysts, which in turn may reduce byproduct (soap) formation and, hence, the cost of separation. A higher rate of reaction also mean a lower residence time, lower amount of energy dissipation, and hence, higher throughput which may lead to lower cost of biodiesel production. The following parameters were changed in their study [40], (1) ultrasonic power and frequency, (2) catalyst loading, (3) oil/methanol ratio, and (4) temperature. In addition, the authors have evaluated the kinetics of the transesterification. The following were the main conclusions from their investigation on the formation of biodiesel from soybean oil (1) High-frequency ultrasound was found to be more effective in biodiesel formation than conventional magnetic stirring under similar conditions. (2) Use of optimum conditions (reaction time, energy consumed, oil/methanol molar ratio, catalyst loading, temperature, frequency of ultrasound, and power) conversions of more than 90 % FAME were achieved in less than 30 min. (3) The optimum catalyst loading was found to be 0.5 wt% KOH. (4) The optimum methanol/oil molar ratio was found to be 6:1. (5) The optimum frequency and power were found to be 611 kHz and 139 W, respectively.

In another paper [41] Adewuyi utilized the Taguchi optimization methodology (L-9 orthogonal array) to optimize various parameters for the ultrasound-assisted, KOH-catalyzed transesterification of soybean oil with methanol. The statistical tool used in the Taguchi method to analyze the results is the analysis of variance (ANOVA), which gives the relative contribution of the factors varied to the change in the dependent variable (i.e., FAME or biodiesel yield). It is observed that catalyst loading is the most influential parameter, with similar to 42.56 % contribution toward variation in biodiesel yield, followed by ultrasonic power with similar to 39.95 %, and oil/methanol molar ratio with 11.40 %. Ultrasonic frequency is found to have negligible influence on the biodiesel yield in the range of the present investigation. The optimum conditions are determined to be 581 kHz, 143 W, 0.75 % (w/w) KOH loading at 1:6 oil/methanol molar ratio, resulting in more than 92.5 % biodiesel yield in less than 30 min. Confirmation experiments have been performed to prove the effectiveness of the Taguchi technique after the optimum levels of process parameters are determined.

In the most recent paper of Deshmane and Adewuyi [42] the authors examined the transesterification of soybean oil using calcium methoxide as solid base

catalyst. The process parameters affecting the yield of biodiesel such as the catalyst concentration, methanol/oil molar ratio and the reaction temperature were investigated in detail. The calcium methoxide obtained from the supplier was in the form of flakes. It was grounded manually using mortar and pestle and passed through 100 mesh screen to obtain the fine powdered catalyst, which was stored in a dark, well closed, glass bottle in a desiccator containing silica gel. The results showed that the yield of biodiesel >90 % was achieved within 90 min using 1 % catalyst loading, 9:1 methanol/oil molar ratio and 65 °C reaction temperature. In addition, the effect of catalyst storage time on its activity and the effect of ultrasound at 20 and 611 kHz frequencies on the yield of biodiesel were also evaluated. TGA-DSC and BET studies showed that the catalyst has good thermal stability and high surface area, respectively. Furthermore, the mechanism of this heterogeneously catalyzed transesterification system with and without ultrasonication was demonstrated to be a two-step reaction in which mass-transfer controlled regime is accompanied by kinetically controlled regime with both regimes following pseudo first order reaction kinetics.

While the work reported so far concentrated on converting vegetable oils to biodiesel using sonochemistry two papers were found to employ other sources for this purpose.

Gedanken et al. [43] used sonochemistry and microwave radiation to convert harvested *Nannochloropsis* algae into biodiesel. The idea was to combine two novel techniques. The first is a unique biotechnology-based environmental system utilizing flue gas from coal burning power stations for microalgae cultivation. This method reduces considerably the cost of algae production. The second technique is the direct transesterification (a one-stage method) of the *Nannochloropsis* biomass to biodiesel production using microwave and ultrasound radiation with the aid of a SrO catalyst.

Sonochemistry and microwave were tested and compared to identify the most effective biodiesel production method. Crude dried *Nannochloropsis* (1 g) was mixed with methanol-chloroform (1:2 v/v) and a SrO catalyst (0.3 g). The reaction mixture was heated using the sonication and microwave irradiation, for 5 min. The yield of biodiesel was estimated by its weight relative to the weight of the microalgae biomass. The authors have used one and two-step processes for obtaining biodiesel. The results of the one-step process in which the transesterification was performed on the dry biomass are more important because they are faster and more cost effective. The direct transesterification reaction using microwave resulted in a biodiesel yield of 37.1 %. The direct transesterification by sonication resulted in a biodiesel yield of 20.9 %. The direct transesterification by reflux yielded 6.95 %. Based on these results, it is concluded that the microwave oven method appears to be the most simple and efficient method for the one-stage direct transesterification of the as-harvested *Nannochloropsis* algae.

In a series of three papers Moholkar have applied theoretical and experimental studies in the development of processes leading to biodiesel production. In their first paper [44], Moholkar et al. made a comparative assessment of three techniques, namely, soxhlet extraction, the Bligh and Dyer method, and sonication

for the extraction of lipids from microalgal biomass. The physical mechanism of extraction of lipids (cell disruption or diffusion across a cell wall) from microalgae was determined using microscopic analysis of extracted biomass. The relative influence of solvent (or extractant) selectivity and the intensity of convection in the oil medium and the overall lipid yield were assessed. None of the techniques used produced complete disruption of the cells, not even sonication. Thus, the prominent mechanism of lipid extraction was diffusion across a cell wall. Moreover, the selectivity of the solvent was found to be the most dominating factor in overall lipid extraction by diffusion than the intensity of bulk convection in the medium.

Moholkar and coworkers [45] have attempted to understand the physical mechanism and kinetic aspects of ultrasound irradiation on transesterification of soybean oil with methanol using sulfuric acid as catalyst. An approach of coupling experimental results with simulations of cavitation bubble dynamics was used.

Kinetic constants as well as activation energies of transesterification reaction were determined at different alcohol to oil molar ratios and reaction temperatures. The results of this study revealed the inter-relation between mechanics of ultrasound/cavitation, and the intrinsic behavior (represented by specific rate constant) of the transesterification reaction. The beneficial effect of ultrasound irradiation on transesterification is of physical nature. Several anomalies of ultrasound assisted acid catalyzed transesterification (as compared to conventional system) are: occurrence of reaction at low temperature of 15 °C (albeit with low conversions of 13.45 and 10.2 % for alcohol to oil molar ratios of 6:1 and 12:1, respectively); despite higher activation energy, higher rate constant at low alcohol to oil molar ratio of 6:1; and the minima shown by reaction rate constant with temperature. The major physical effect of sonication is the fine emulsification that generates enormous interfacial area for reaction that overwhelms the effect of specific rate constant. As revealed by simulations, physical effects of cavitation (viz, micro-convection and shock waves) are more pronounced at low temperature, which is the primary cause leading to these anomalies.

Jatropha is a plant grown on lands that cannot be agriculturally activated. Choudhury et al. [46] investigated the ultrasound assisted acid catalyzed transesterification of Jatropha oil. A statistical experimental design (Box-Behnken) is coupled to simulations of cavitation bubble dynamics. Acid catalyzed esterification was rather insensitive to ultrasound irradiation, while the beneficial effect of sonication on transesterification reaction was only through the intense micro-mixing induced by ultrasound. Transient cavitation in methanol did not render any impressive effect. The transesterification system was strongly controlled by the intrinsic kinetics and mass transfer resistance. The optimum values of experimental variables have been determined as: alcohol to oil molar ratio of 7, catalyst concentration of 6 % w/w oil and temperature of 70 °C. The influence of these variables was highly involved and interlinked, and any deviation from the optimum value lead to a sharp reduction in the FAME yield. Results of this study illustrated that sonication does not change the chemistry of acid-catalyzed transesterification but the beneficial effect is only of physical nature, which is further limited by the intrinsic kinetics and mass transfer.



Hobuss et al. [47] reported the use of sonochemistry for ester synthesis. The authors described the ultrasound-assisted synthesis of saturated aliphatic esters from synthetic aliphatic acids and alcohol (methanol or ethanol). The products were isolated in good yields after short reaction times under mild conditions.  $\text{H}_2\text{SO}_4$  was used as the catalyst and the reaction was followed by Gas Chromatograph. Ten esters were prepared in a duration of 15–30 min with the yields in the range of 50–95 %.

## 6.5 Use of Microwave and Sonication for Biomass Conversion to Bioethanol

Pretreatment of biomass, hydrolysis of biomass to fermentable sugars and conversion of fermentable sugars to bioethanol are the three important stages in the bioethanol production process.

### 6.5.1 *Role of Sonication and Microwave in the Pretreatment of Biomass*

Pretreatment is one of the vital and costly unit process involved in bioethanol production. The purpose of the pretreatment is to reduce the structural rigidity of the biomass and to make the reaction site (D-anhydro-glucopyranose linking in the cellulose) accessible to either enzymes or protons in the subsequent hydrolysis process. Moreover, the pretreatment method is biomass specific. Agricultural wastes (for instance, sugar cane bagasse, rice straw, wheat straw, barley straw) and hardwoods (like pine, oak, poplar) contain high pentose (hemicellulose) and low lignin content. For such biomass low temperature pretreatment is preferred. Such a pretreatment prevents the thermal degradation of pentoses [48]. Bioethanol production cost could be significantly reduced by the use of effective pretreatment processes that enhances the hydrolysis of biomass.

Ultrasound irradiation was more widely exploited as a promising pretreatment technique for lignocellulosic materials compared to microwave irradiation. Recently, Shewale et al., achieved 8 % enhancement in the saccharification (glucose yield) of sorghum slurry as a result of ultrasound (20 kHz, 750 W, 100 % amplitude, 1 min) pretreatment of the slurry. A reduction in the average particle size of the sorghum slurry from 302 to 115  $\mu\text{m}$  (38 %) is observed. The improvement in the glucose yield was attributed to the disruption of rigid hydrophobic protein matrix as well as the amylose-lipid complex surrounding the starch granules. Such a disruption is due to the physical effect of the acoustic cavitation (shock-wave propagation and microjet formation) occurring in a low frequency (16–100 kHz) ultrasound treatment [49]. Alvira et al. [50] reviewed the pros and cons of various (biological, chemical and physical) biomass pretreatment methods.



The authors attributed the enhancement of cellulose hydrolysis as a result of ultrasound pretreatment of biomass to the improved transport of the enzymes to the substrate surface. In addition, owing to the mechanical effects like the collapse of the cavitation bubbles, the interior of the solid substrate is made accessible to the action of the enzymes. More importantly, during the ultrasound irradiation majority of the cavitation effects arise at 50 °C which is the optimum temperature for the enzymatic saccharification.

Subhedar et al., made an indepth study and a critical review on the effect of ultrasound pretreatment on the enhancement of enzymatic hydrolysis of lignocellulose [51]. The superiority of ultrasound in reducing the mass transfer constraints, structural rigidity and enzyme agglomeration was depicted pictorially in Fig. 6.3.

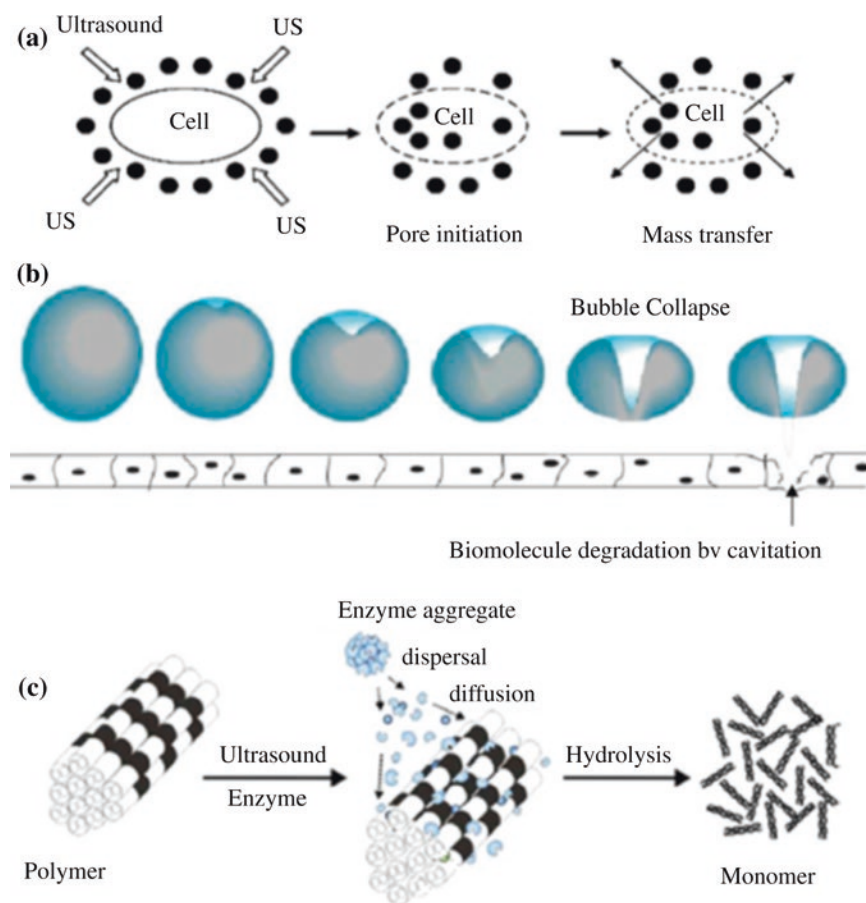


**Fig. 6.3** Depiction of **a** mass transfer of catalytic species into the interior of the substrate, **b** action of collapsing cavitation bubble in the degradation of structural rigidity of biomass and **c** improved transport of enzymes, as a result of ultrasound pretreatment. Reprinted with permission from [51], Copyright © 2013, ACS

Nikolic et al., used ultrasound pretreatment (40 kHz, 600 W, 5 min, 60 °C) of cornmeal which enhanced the glucose concentration in the hydrolyzate by 6.82 % and also a subsequent ethanol concentration in the fermentation (SSF) broth by 11.16 %. This indicates the vital role of sonication in degrading the starch granules (leading to the exposure of larger surface area of the substrate to the action of enzymes) by the action of cavitation and acoustic streaming. The main advantage of streaming is to cause mixing that facilitates even distribution of ultrasound energy within the medium and there by resulting in better mass transfer of catalytic species, and also the dissipation of the generated heat throughout the medium by convection [52]. The advantageous effects of ultrasound ( $28.0 \pm 1.4$  kHz, 50 W, 0 °C, 3 h) were further exploited by Goshadrou et al., for the pretreatment of sweet sorghum bagasse in the presence of alkali (NaOH). A  $\approx 27$  % enhancement in both the theoretical sugar yield and ethanol production were achieved as a result of such pretreatment. Partial delignification, reduction in cellulose crystallinity, distortion in structural rigidity and an increase in surface area and porosity were attributed to the enhanced sugar and ethanol yields. Moreover, the authors proposed *Mucor hiemalis* fungal strain as a substitute to the conventional Baker's yeast for sugar fermentation. Unlike Baker's yeast, *Mucor hiemalis* was found to metabolize even pentoses and also could grow even at relatively higher temperatures [53]. Bussemaker et al., made a comparative study on the effect of ultrasound frequency (40, 376 and 995 kHz) on biomass fractionation. Ultrasound assisted pretreatment at low frequency (40 kHz) enhanced delignification (7.2 %) whereas use of higher frequency ultrasound (995 kHz) improved carbohydrate solubilization (9.1 %). The mode of action of low and high frequency ultrasounds being mechanical and sonochemical respectively. Overall, biomass fractionation improved as a result of ultrasound pretreatment augmented with stirring [54]. Sindhu et al., achieved a high yield of 0.661 g reducing sugars per g of pretreated (sonication with Tween 40) sugar cane tops (SCT). Ultrasound pretreatment (for 1 min, 40 % amplitude, pulse 59 s on and 59 s off) in the presence of a surfactant (Tween 40, 1 wt%) with a loading of 10 wt% SCT lead to effective removal of lignin and hemicellulose. As a result of the removal of lignin and hemicellulose, the crystallinity index of the pretreated biomass increased from 37.7 to 48.8 % [55]. Lignin is the most rigid and recalcitrant component in the biomass and one of the objectives of pretreatment is effective delignification. Pretreatment of biomass with lime is known for effective delignification. But it is not industrially appealing owing to the slowness of the process. Sasmal et al. successfully accelerated the lime based delignification process of biomass using ultrasound pretreatment (30 kHz, 100 % amplitude, 100 W,  $35 \pm 2$  °C). Lignin removal of 65, 68 and 64 % were observed in the case of *Areca catechu*, *Ziziphus rugosa* and *Albizia lucida* respectively. Typical advantages of the process include overall ethanol yields in the range of 0.32–0.43 g/g of pretreated biomass in addition to the good recovery of the total solids and fermentable sugars [56]. Ramadoss et al., successfully utilized ultrasound (24 kHz, 400 W, 100 % amplitude, 45 min) assisted ammonia (10 wt%) pretreatment for the effective delignification (58.14 %) and cellulose recovery (95.78 %). Moreover, owing to such a pretreatment, the concentration of fermentation inhibitor (acetic acid and furfural) formation in the hydrolyzate obtained from

the acid hydrolysis of pretreated biomass was found to be low compared to earlier reports. Typical composition of the hydrolyzate was glucose (16.58 g/L), xylose (8.21 g/L), arabinose (0.81 g/L), furfural (0.81 g/L) and acetic acid (1.79 g/L) [57]. Recently Fang et al., provided a comprehensive account of the application of ultrasound in promoting a variety of crucial reactions in the conversion of biomass to biofuels. The role of ultrasound for (a) dewaxing and removal of impurities (like silica), (b) particle size reduction of biomass, (c) isolation of chemicals from biomass, (e) delignification, (f) fractionation, (g) reduction of crystallinity and (h) acceleration of saccharification and fermentation are pictorially depicted in Fig. 6.4 [58].

Microwave (0.3–300 GHz or 1–1,000 mm or  $3 \times 10^8$  to  $3 \times 10^{11}$  cycles/s) irradiation is as potential as ultrasound for the acceleration of the vital reactions involved in biomass conversion. Much remains to be unfolded in this area. Localized heating of the lignocellulosic components upon microwave irradiation is responsible for the degradation of the biomass structure. Upon interaction of the microwaves with the organic matter, enormous heat is generated within the material owing to the absorption of microwaves by water, carbohydrates and other components in the biomass. This leads to the disruption of the biomass structure and makes the carbohydrates accessible to the attack by catalytic species resulting in the acceleration of hydrolysis process [59]. Unlike conventional heating (conduction or convection), during microwave heating, there is direct interaction between the target and the electromagnetic field. As a result, the process of heating is rapid

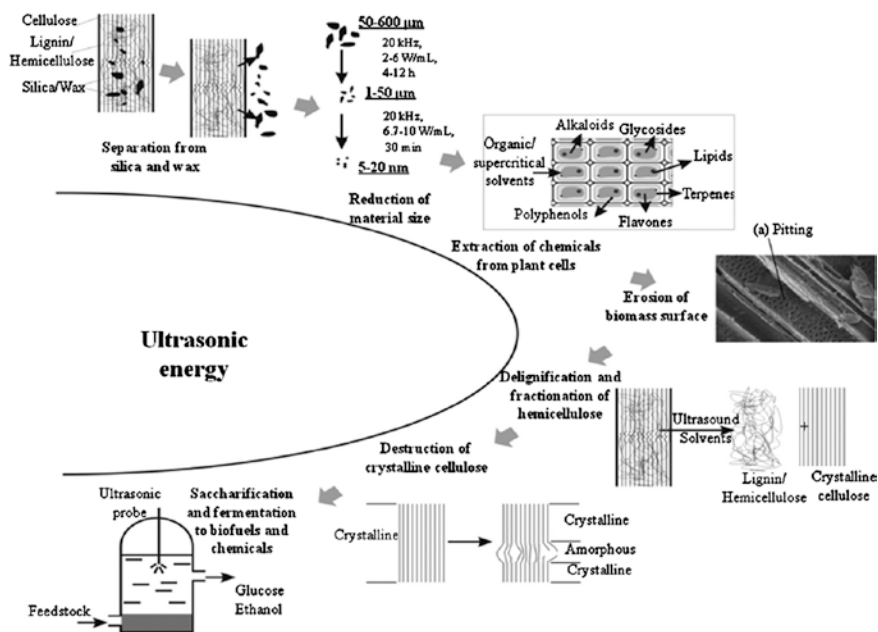


**Fig. 6.4** Role of ultrasonic energy for the conversion of biomass to biofuels. Reprinted with permission from [58], Copyright © 2014, Elsevier

as well as volumetric. Such a rapid heating might cause explosive effect among the target particles resulting in the degradation of the highly recalcitrant structure like lignin. In addition to degrading the lignin and hemicellulose, microwave irradiation alters the cellulosic structure at the nanoscale [48]. Pang et al., made a comparison between the effectiveness of steam explosion (SE) alone and a combination of steam explosion and microwave irradiation (SEMI). Sugar yields were found to be improved upon SEMI pretreatment of corn stover. The yields of glucose, xylose and total sugar in the hydrolyzate from pretreated (SEMI) corn stover were found to be 57.4, 17.8 and 75.2 % respectively. In addition the SEMI (540 W, 200 °C, 5 min) pretreatment lowered the crystallinity of the biomass by 19 % compared to SE treatment alone [60]. Verma et al., demonstrated the microwave sensitizing action of ammonium molybdate—H<sub>2</sub>O<sub>2</sub> system for the selective delignification of beech wood biomass. Compared to hydrothermal method, microwave pretreatment resulted in 17.7 % improvement in the sugar yield in the hydrolyzate. The ammonium counter cation was found to be important in the microwave sensitized action of the molybdate for selective delignification [61]. Effective biomass pretreatment method is a key factor for a sustainable biorefinery. In high probability, microwave and sonication techniques play a key role in practical biorefinery.

### ***6.5.2 Hydrolysis of Biomass Using Microwave Irradiation***

Microwave irradiation technique has been extensively exploited for accelerating biomass hydrolysis process leading to fast release of fermentable sugars from polysaccharides. Gedanken et al., have exploited the potential of microwave irradiation for the conversion of a variety of renewable biopolymers like starch, cellulose, and glycogen to glucose in a fast acid catalyzed process using microwave irradiation [4, 62, 63].

#### **6.5.2.1 Glycogen as a Renewable Feedstock for Glucose Production Using Microwave Irradiation**

Analogous to the storage of sugars in plants as starch and cellulose, glucose is stored in animal cells as glycogen. Animal remains serve as an abundant renewable source for glycogen. Efforts were made to produce glucose from glycogen using microwave irradiation. Under optimal acid hydrolysis conditions (10 min, 1 M HCl), 62 wt% glucose yield from glycogen was achieved [62]. On the contrary, conventional heating in an oil bath takes more than 6 h for the complete conversion of glycogen. The acceleration of glycogen hydrolysis under microwave irradiation was attributed to the generation of localized heating (formation of hot spots) in the reaction medium. The experimental setup used for carrying out the hydrolysis of glycogen under conventional versus microwave heating was shown in Fig. 6.5.

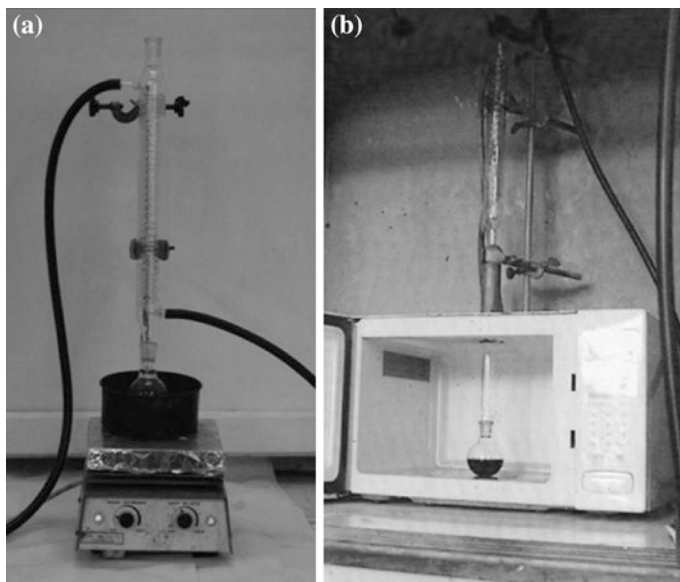


**Fig. 6.5** Pictorial representation of the experimental setup used for glycogen hydrolysis **a** conventional heating and **b** microwave heating. Reprinted with permission from [62], Copyright © 2012, RSC

### 6.5.2.2 Acceleration of Starch and Cellulose Hydrolysis Using Microwave Irradiation

Gedanken et al., successfully converted the renewable kitchen wastes into glucose using microwave irradiation in the presence of a solid acid catalyst. Potato starch was chemically hydrolyzed to glucose using silicotungstic acid (HSiW) as catalyst under microwave irradiation in a short duration (5 min). Potato starch was completely converted to glucose, levulinic acid and formic acid. The methodology was further used for the conversion of potato peel waste (PPW), a zero value waste to glucose. A glucose yield of 79.1 wt% was obtained upon the microwave irradiation (15 min) of PPW. The amount of glucose in the hydrolyzate of potato peel waste as a function of irradiation time is depicted Fig. 6.6.

The amount of glucose in the hydrolyzate of potato peel waste is estimated using the glucose sensor developed by Gedanken et al., based on the in situ generation of carbon nanoparticles from the decomposition of the glucose present in the hydrolyzate [64].

Microwave irradiation was found to depolymerize the starch much faster than sonochemical irradiation. The combined use of solid acid catalyst and microwave irradiation offered a fast and green process for glucose production from starch based waste materials.

The primary motivation for the synthesis of glucose lies in the fact that glucose could be subsequently converted to several fine chemicals and fuels (ethanol in particular) as depicted in Scheme 6.1.

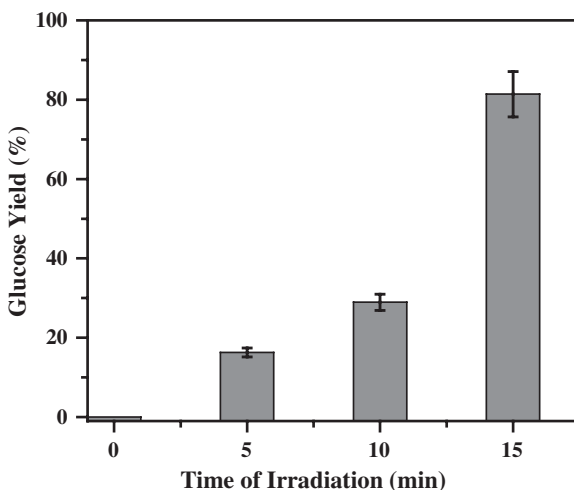
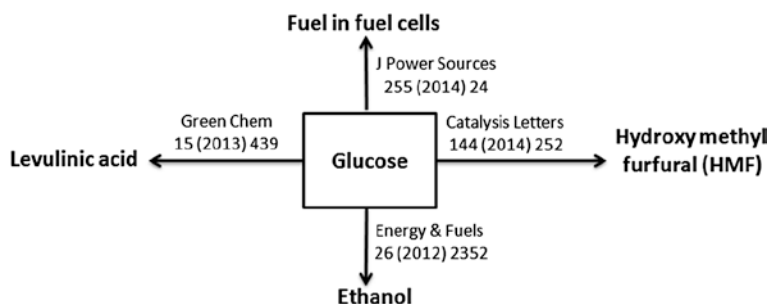


**Fig. 6.6** Histogram depicting the production of glucose from potato peel waste as a function of microwave irradiation time

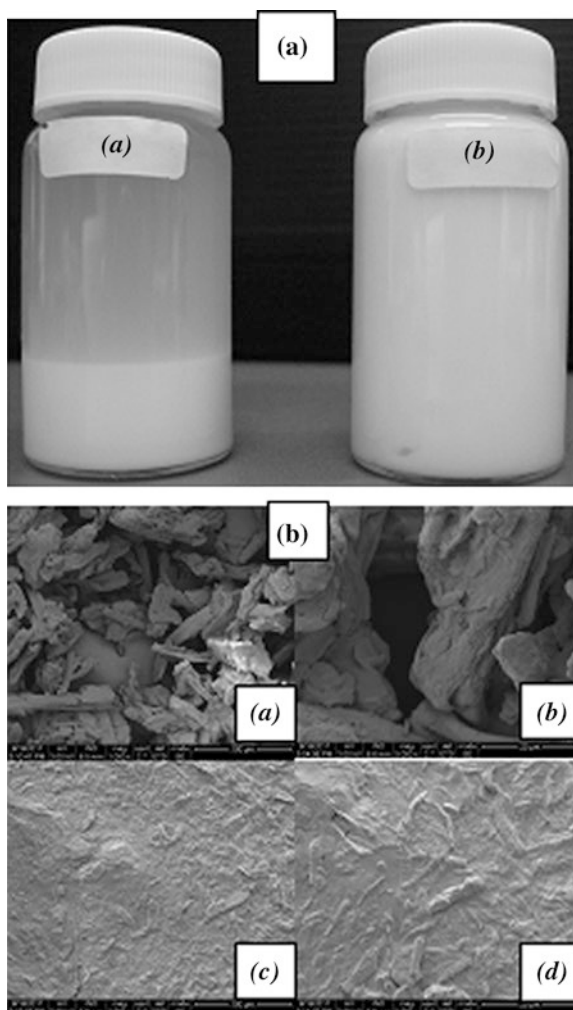


**Scheme 6.1** Schematic representation of potential industrial uses of glucose

The type of bonding that links the glucose units in starch is quite different from that present in cellulose. The presence of extensive inter and intra molecular hydrogen as well as the type of linking of the D-anhydro-glucopyranose bonding present in the cellulose structure makes the hydrolysis of cellulose nearly 100 times tougher than starch hydrolysis [65]. Such a rigid polymer like cellulose could be successfully depolymerized in a fast process with the aid of microwave irradiation and sonication [4, 63]. Under optimal irradiation conditions (7 min, 70 % power, 2.38 M HCl) cellulose could be selectively hydrolyzed to glucose with a glucose yield of 67 wt%. The glucose thus produced from Avicel® PH-101 (commercial cellulose) is demonstrated to be a potential feedstock for bioethanol production [4]. The enhancement in the conversion of cellulose upon microwave irradiation could be due to reduced hydrogen bonding interactions that facilitate easy accessibility of acidic protons to the reaction site ( $\beta$ -(1 $\rightarrow$ 4)-glycosidic bonds).

Dissolution of cellulose in water is a problem that further poses a problem in cellulose transformation. Gedanken et al., solved this problem using ultrasound. Sonication (Sonics and Materials, VC-600, 20 kHz, 100 W/cm<sup>2</sup>, 1 h) was found to have a useful effect in obtaining homogeneous suspensions of cellulose in water even at a cellulose concentration as high as 10 wt%. As depicted in Fig. 6.7a. prior to sonication, the cellulose is insoluble in water and settles down at the bottom of the container (Fig. 6.7a(a)). Upon sonication, the stable and homogeneous dispersion of cellulose in water was generated (Fig. 6.7a(b)). The HRSEM images of cellulose (10 wt%) before and after sonication are shown in Fig. 6.7b. Before sonication the cellulose particles resembled like blocks and logs of wood. After sonication the original identity of the cellulose particles is lost. Thin layers and fibers of cellulose

**Fig. 6.7** **a** Pictorial representation of the 10 wt% cellulose powder in water (a) before and (b) after sonication. **b** SEM images of the 10 wt% cellulose powder in water (a & b) before and (c & d) after sonication (the samples were dried in a vacuum oven prior to SEM analysis)





are generated upon sonication. Such a transformation in the shape and size of the cellulose particles upon sonication will facilitate a better exposure of the surface of the cellulose for the action of catalytic species for its subsequent degradation.

Interestingly, the nanospheres produced from Avicel® PH-101 were found to be more feasible for glucose production from cellulose. Using sonochemical irradiation, nanospheres of cellulose ( $\approx 50$  nm) were produced as depicted in Fig. 6.8d.

The spherical cellulose nanoparticles were then hydrolyzed exclusively to glucose with the aid of microwave irradiation in the presence of solid acid catalyst (HSiW) in a short duration of 3 min with a glucose yield of 30 wt%. The mechanism of formation of nanospherical cellulose containers is depicted schematically in Fig. 6.9 [71].

Free radicals ( $H^\cdot$  and  $OH^\cdot$ ) are formed upon sonochemical irradiation of aqueous solution. Subsequently, the hydroxyl radicals recombine to form  $H_2O_2$ .  $H_2O_2$  formed as well as its sonolytic decomposition products promote the degradation of organic molecules in the presence of ultrasound. A stable radical at the anomeric carbon is formed as  $H^\cdot$  leaves the organic molecule as a result of sonication.

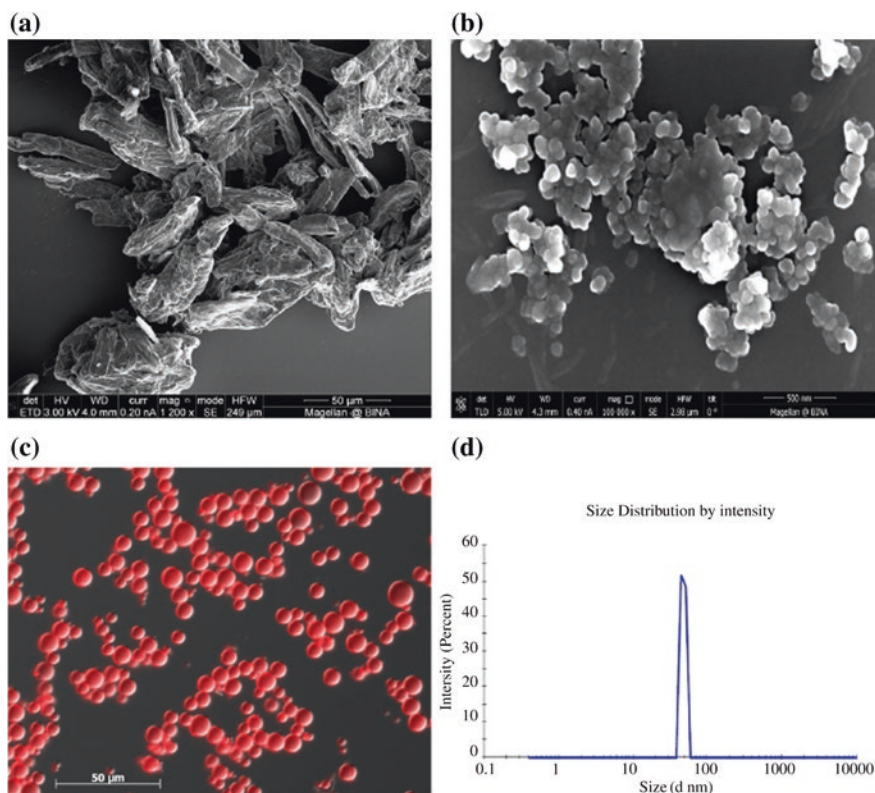


**Fig. 6.8** HRSEM images of **a** Avicel® PH-101, **b** Spherical cellulose containers, **c** fluorescence microscope image of cellulose spheres and **d** DLS graph of size distribution of cellulose spheres from sonication. Reprinted with permission from [63], Copyright © 2014, ACS



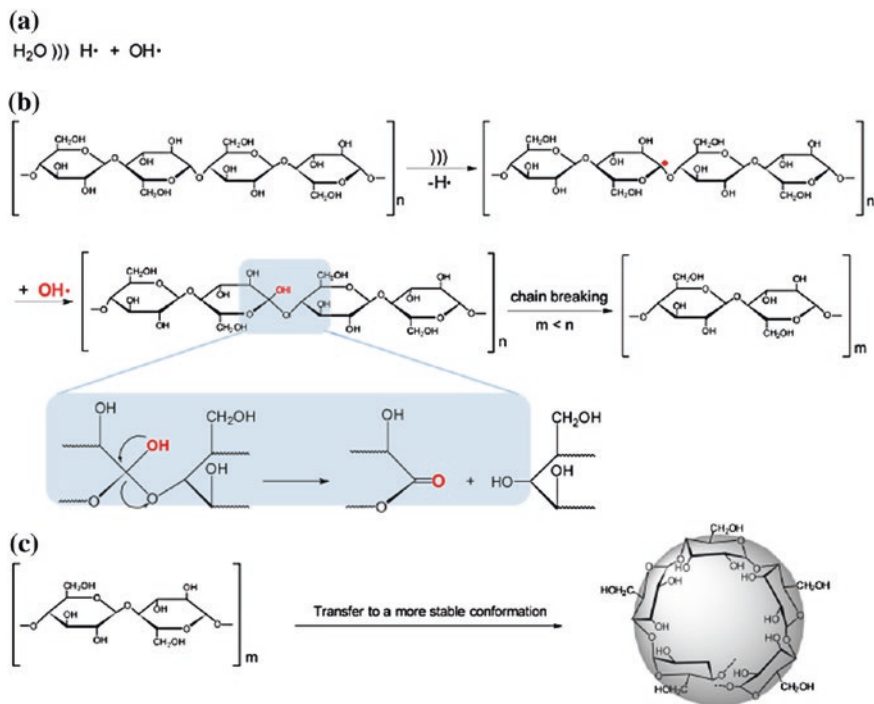
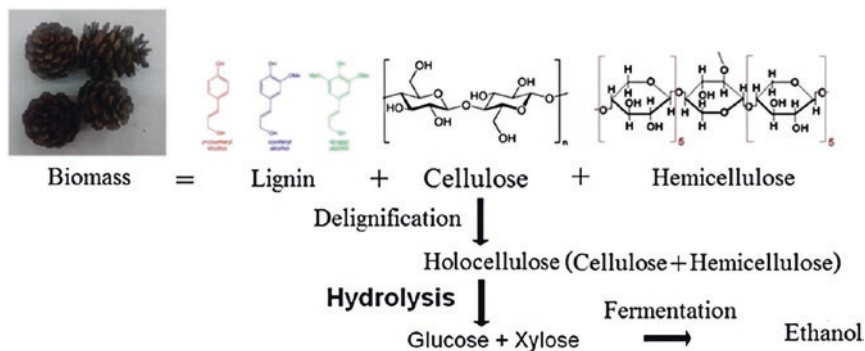


**Fig. 6.9** Schematic representation of formation of nanospherical cellulose containers using sonication. Reprinted with permission from [63], Copyright © 2014, ACS

Subsequently, hydroxyl radical ( $OH\cdot$ ) will replace the  $H\cdot$  at the anomeric carbon. Such a replacement causes the polymer chain to cleave selectively. Later on smaller fragments generated would reorganize to a more thermodynamically stable conformations resulting in the formation of nanospheres of cellulose.

After demonstrating microwave irradiation as a potential technique for the production of fermentable sugars from biopolymers the methodology was further extrapolated for the conversion of renewable and abundant biomass, i.e., pine cones from *pinus radiata*. Various experimental stages involved in their conversion to bioethanol, namely, delignification, hydrolysis of holocellulose and fermentation of holocellulose, in the conversion of pine cones to ethanol are schematically depicted in Scheme 6.2.

Pine cones from *Pinus radiata* were found to be a potential feedstock for the production of bioethanol. Alkaline ( $NaOH$ ) pretreatment was carried out to delignify the lignocellulosic material and generate holocellulose (72 wt% yield). The pretreated biomass was hydrolysed using  $HCl$  as catalyst under microwave irradiation and hydrothermal conditions. Microwave irradiation was found to be better than the hydrothermal process. Microwave irradiation accelerated the hydrolysis of biomass (42 wt% conversion) with the reaction conditions being 3 M  $HCl$  and 5 min of irradiation time. The hydrolyzate was fermented to ethanol using *Saccharomyces cerevisiae*. 8.3 g of ethanol could be produced from 100 g of pine cones.



**Scheme 6.2** Production of ethanol from pine cones

### 6.5.3 Application of Sonochemistry for Bioethanol Production

The objective of this part of the chapter is to present an overview of the potential of ultrasonic waves for the production of bioethanol. Sonication is widely employed for the pretreatment (as discussed in Sect. 6.5.1) as well as for the conversion of biomass to biofuels.

Most of the work in this field was focused on the delignification of lignocellulose assisted by the application of ultrasonic waves, or the pretreatment of the biomass employing ultrasonic waves. However, a few reports describing the direct sonochemical application in the conversion of glucose, or cellulose, or biomass into ethanol also exist. Naturally the focus of this section is on the direct ethanol production. In parallel some attention would also be devoted to the use of sonochemistry in the delignification as well as the pretreatment processes which are major steps in the production of bioethanol from biomass. Bamboo (*Neosinocalamus affinis*) was subjected to successive pretreatments to isolate cellulose rich fractions for further utilization [66]. Ball-milled bamboo underwent ultrasound treatment in ethanol solution at 20 °C for 0, 5, 15, 35, and 50 min, respectively. Then the samples were dissolved with 7 % NaOH/12 % urea solutions at −12 °C, followed by successive extractions with dioxane, ethanol, and dimethyl sulfoxide (DMSO). The yields of the obtained cellulose rich fractions ranged from 75.1 to 77.7 %. The changes of chemical structures and morphology of the treated sample suggested that the cold sodium hydroxide/urea based pretreatments effectively disrupted the recalcitrance of bamboo, generating highly reactive cellulosic materials for enzymatic hydrolysis to produce bioethanol.

A case in which ultrasonic waves were employed in the fermentation process was presented by Sulaiman et al. The authors reported on the [67] production of ethanol from lactose by fermentation with the yeast *Kluyveromyces marxianus* (ATCC 46537) under various sonication regimens. Batch fermentations were carried out at low-intensity sonication (11.8 W cm<sup>−2</sup> sonication

intensity at the sonotrode tip) using 10, 20 and 40 % duty cycles. (A duty cycle of 10 %, for example, was equivalent to sonication for 1 s followed by a rest period (no sonication) of 10 s.) Fermentation reaction was carried out in a 7.5 L (3 L working volume) stirred bioreactor. The sonotrode was mounted in an external chamber and the fermentation broth was continuously recirculated between the bioreactor and the sonication chamber. The flow rate through the sonication loop was  $0.2 \text{ L min}^{-1}$ . All duty cycles tested improved ethanol production relative to control (no sonication). A 20 % duty cycle appeared to be optimal wherein a final ethanol concentration of  $5.20 \pm 0.68 \text{ g L}^{-1}$  was obtained, or nearly 3.5-fold enhancement compared to the control fermentation. Sonication at a controlled temperature was found to substantially enhance productivity of bioethanol fermentation.

Ultrasound radiation was used as a pretreatment tool for the production of sugar monomers from sugar cane bagasse (SCB) in a sonoassisted acid hydrolysis [68]. The SCB was subjected to sonoassisted alkaline pretreatment. The cellulose and hemicellulose recovery were 99 and 78.95 %, respectively, and lignin removal was about 75.44 %. The solid content obtained was subjected to sonoassisted acid hydrolysis. Under optimized conditions, the maximum hexose and pentose yield observed were 69.06 and 81.35 % of theoretical yield, respectively. The hydrolysate obtained was found to contain less inhibitors, which improved the bioethanol production with an yield of 0.17 g/g of pretreated SCB.

Low energy ultrasound irradiation ( $20 \text{ kHz}$ ,  $1.0 \text{ W L}^{-1}$ ) was applied to enhance bioethanol production from whey ultrafiltration permeate by co-immobilized *Saccharomyces cerevisiae* cells and beta-galactosidase enzyme [69]. Sugar utilization and ethanol formation were investigated as a function of hydraulic retention time (HRT) between 12 and 36 h. Maximum ethanol production under HRT of 36 h was 26.30 g/L with ultrasound exposure, and 23.60 g/L without. Maximum ethanol yield was 0.532 g/g lactose in the fermentation process with ultrasound irradiation, and 0.511 g/g lactose without. For the continuously operating bioreactors, the maximum rates of sugar utilization were 98.9 and 92.4 % for the yeast with and without ultrasound exposure, respectively. These results highlight the positive effect of low-intensity ultrasounds in bioethanol fermentation from whey permeates, providing a solution for its disposal. This work is one of the few examples in which the fermentation process was accelerated upon sonication. Ultrasonic pretreatment of the SSF process of triticale meal with ultrasound was conducted at  $60 \text{ }^\circ\text{C}$ . The process time may be reduced from 72 to 48 h with the aid of sonication [70]. At that point of the SSF, maximum bioethanol content of 9.55 % (w/v), bioethanol yield of 0.43 g/g of triticale starch, and percentage of the theoretical bioethanol yield of 84.56 % were achieved.

There is no point in presenting the many similar attempts to pretreat various biomasses for producing bioethanol. The references to the respective biomass are given: sugar beet pulp [71], rice straw residues [72], cassava root [73], *Ziziphus rugosa* and *Albizia lucida* [56], and sugarcane bagasse [74].

Two recent reports have discussed the direct production of ethanol either from glucose or from biomass. The first manuscript reported on a successful attempt

to accelerate the well-known sugar fermentation process by applying soft sonication [75]. Fermentation is a crucial stage involved in the biomass conversion to bioethanol. To accelerate the fermentation reaction, sonication has been successfully employed. Fermentation of glucose was carried out using *Saccharomyces cerevisiae* under continuous mild ultrasonication conditions. Enhancement in the reaction rate constant by a factor of  $2.3 \pm 0.2$  and  $2.5 \pm 0.2$  as a result of sonication at 30 and 20 °C, respectively were observed compared to a conventional stirred reaction. A 10-fold increase in the fermentation reaction rate constant was observed under sonication relative to a non-stirred fermentation. The acceleration in the fermentation of glucose was observed for both 20 and 40 wt% concentrations of the glucose solution. Gedanken et al., further extended the methodology for the conversion of marine biomass (*Ulva regida*) to bioethanol in a single step simultaneous saccharification and fermentation (SSF) process using mixed cultures. The starch and cellulose components of the algae were selectively converted exclusively to glucose by the action of amylase and cellulase respectively. Typical constitution of the broth for SSF process comprise of: 1.68 g of dried *U. regida* in 40 mL of distilled water and 40 mL of 200  $\mu$ M sodium acetate (buffer) (2.1 % w/v) taken in a 100 mL glass media bottles with cap (Fisher band). Into the suspension were added enzymes, 100  $\mu$ L *amyloglucosidase* 300 units/mL, 40  $\mu$ L  $\alpha$ -amylase 250 units/mL, 0.1 g *cellulase* (0.3 units/mg) and 0.5 g of Baker's yeast. The SSF process was carried out in two ways: in the conventional incubator and under mild sonication at 37 °C and at a pH of 7. The glucose released from the algae is simultaneously consumed by the yeast in the broth to yield ethanol. Sonication provided a faster way for the simultaneous release of glucose from *Ulva regida* and its conversion into bioethanol. In a short duration of 30 min the yield of ethanol under sonication ( $4.3 \pm 0.26$  wt% of dry biomass) is significantly high compared to the value ( $1.0 \pm 0.13$  wt% of dry biomass) under incubation. The value increased steadily and reached a saturation at 180 min ( $6.2 \pm 0.13$  wt% vs.  $4.9 \pm 0.1$  wt% under incubation). Even after incubation for 48 h, the ethanol yield under incubation is only  $6.1 \pm 0.13$  wt% which could be achieved in a short duration of 120 min. The salient features of the SSF process include (i) no pre-treatment of algae (ii) unit process (iii) selective production of glucose (iv) fast release of glucose and its conversion to ethanol. The role of sonication in accelerating the fermentation kinetics has also been studied in detail. Briefly, sonication provides a more effective stirring and thus may augment the effects of regular stirring. Relative to a conventional stirred reaction, mild sonication accelerated the glucose fermentation by 2.3 times. To confirm if the acceleration is due to the faster stirring that facilitates removal of ethanol from the yeast surface and well as CO<sub>2</sub> from the broth, fermentation was also evaluated by using an ultraturrax device. With a high mechanical agitation at 20, 000 rpm a 2.3-fold enhancement in the rate of fermentation compared to the reaction under shaking in an incubator at 30 °C is observed. Thus mechanical agitation had an accelerating effect on the fermentation of glucose into ethanol. When applied to regular biomass, sonication enhanced the release of glucose from the algae upon sonication. This is attributed to mechanical and thermal effects. Ultrasound is known to improve the hydrolysis

process by the reduction of the structural rigidity of the lignocellulose and starch components in plant biomass. Moreover, ultrasound-assisted enzymatic hydrolysis was found to reduce the hydrolysis reaction time by improving mixing and phase transfer, and by enhancing the diffusion of enzymes across cell membranes (algea), so that enzymes can easily reach the bulk of the substrate.

In another paper Shaheen et al. [76] explored the application of Low-Intensity Pulsed Ultrasound (LIPUS) technology to improve the metabolic activity of microorganisms. In this study LIPUS was shown to improve bioethanol production from lignocellulosic biomass. The authors determined specific LIPUS conditions to increase the metabolic activity of both the cellulose degrading fungus, *Trichoderma reesei* Rut C-30 and the ethanol producing yeast, *Saccharomyces cerevisiae*. LIPUS conditions of 1.5 MHz, 0 % duty cycle, 80 mW/cm<sup>2</sup> intensity, 5 min exposure and 12 exposures per day were found to improve the activity of the organisms the most. These LIPUS treatment conditions increased cellulase production by *T reesei* by  $16 \pm 6$  %. The same LIPUS treatment conditions induced a  $31 \pm 10$  % increase in ethanol production by *S. cerevisiae* which implies a cumulative improvement of  $52 \pm 16$  % in lignocellulosic bioethanol production with LIPUS. In essence, the sonication is a stirring mode of the reactants and helps a fast removal of the ethanol from the yeast surface.

## 6.6 Conclusions and Future Outlook

For quick industrial adoption of the microwave and sonication based methods for biomass conversion, efforts need to be devoted in designing continuous flow processes for both bioethanol and biodiesel production. The optimized batch process parameters need to be appropriately modified for the flow process. Moreover, efforts should be made in utilizing solar power for running the ultrasound and microwave generators for making the biofuel production processes cost effective.

**Acknowledgement** Gedanken thanks the Ministry of Science and Technology (MOST) for the research grant 3-9802 and the Israel Science Foundation (ISF) for supporting the research via a grant 12/586.

## References

1. Koberg M, Gedanken A (2012) Optimization of bio-diesel production from oils, cooking oils, microalgae, and castor and jatropha seeds: probing various heating sources and catalysts. *Energy Environ Sci* 5:7460–7469
2. Koberg M, Gedanken A (2012) Direct transesterification of castor and jatropha seeds for FAME production by microwave and ultrasound radiation using a SrO catalyst. *Bioenergy Res* 5:958–968
3. Koberg M, Abu-Much R, Gedanken A (2011) Optimization of bio-diesel production from soybean and wastes of cooked oil: combining dielectric microwave irradiation and a SrO catalyst. *Bioresour Technol* 102:1073–1078
4. Pulidindi IN, Kimchi BB, Gedanken A (2014) Can cellulose be a feedstock for bioethanol production? *Renew Energy* 71:77–80

5. Pulidindi IN, Kimchi BB, Gedanken A (2014) Selective chemical reduction of carbon dioxide to formate using microwave irradiation. *J CO<sub>2</sub> Utilization* 7:19–22
6. Kumar VB, Gedanken A, Pradip P (2013) Triangular core-shell ZnO@SiO<sub>2</sub> nanoparticles. *ChemPhysChem* 14:3215–3220
7. Eshed M, Lellouche J, Banin E, Gedanken A (2013) MgF<sub>2</sub> nanoparticle coated teeth inhibit *streptococcus mutans* biofilm formation on the tooth model. *J Mater Chem B* 1:3985–3991
8. Grinberg O, Shimanovich U, Gedanken A (2013) Encapsulating bioactive materials in sonochemically produced micro- and nano-spheres. *J Mater Chem B* 1:595–605
9. Richter F, Fricke T, Wachendorf M (2011) Influence of sward maturity and pre-conditioning temperature on the energy production from grass silage through the integrated generation of solid fuel and biogas from biomass (IFBB): 1. The fate of mineral compounds. *Bioresour Technol* 102:4855–4865
10. Penner SS (2006) Steps toward the hydrogen economy. *Energy* 31:33–43
11. Kruse O, Rupprecht J, Mussgnug JR, Dismukes GC, Hankamer B (2005) Photosynthesis: a blueprint for solar energy capture and biohydrogen production technologies. *Photochem Photobiol Sci* 4:957–969
12. Blackler T, Iqbal MT (2006) Pre-feasibility study of wind power generation in holyrood, newfoundland. *Renew Energy* 31:489–502
13. Lü J, Sheahan C, Fu P (2011) Metabolic engineering of algae for fourth generation biofuels production. *Energy Environ Sci* 4:2451–2466
14. Smith AL, Wood S, Hewitt N, Henriques I, Yan N, Bazely DR (2013) Second generation biofuels and bioinvasions: an evaluation of invasive risks and policy responses in the United States and Canada. *Renew Sustain Energy Rev* 27:30–42
15. McCormick N, Howard G (2013) Beating back biofuel crop invasions: guidelines on managing the invasive risk of biofuel developments. *Renew Energy* 49:263–269
16. Eisen B, Green KP (2010) Environmental policy and the law of unintended consequences: eight case studies from around the world. Frontier Centre for Public Policy, Winnipeg
17. Gupta RB, Demirbas A (2010) Gasoline, diesel and ethanol biofuels from grasses and plants. Cambridge University Press, Cambridge
18. Walburger AM, LeRoy D, Kaushik KK, Klein KK (2006) Policies to stimulate biofuel production in Canada: lessons from Europe and the United States. A BIOCAP research integration program, BIOCAP Canada, Kingston
19. Suslick KS, Choe SB, Cichowlas AA, Grinstaff MW (1991) Sonochemical synthesis of amorphous iron. *Nature* 353:414–416
20. Hiller R, Putterman SJ, Barber BP (1992) Spectrum of synchronous picosecond sonoluminescence. *Phys Rev Lett* 69:1182–1184
21. Barber BP, Putterman SJ (1991) Observation of synchronous picosecond sonoluminescence. *Nature* 352:318–320
22. Gedanken A (2004) Using sonochemistry for the fabrication of nanomaterials. *Ultrason Sonochem* 11:47–55
23. Gedanken A (2008) Preparation and properties of proteinaceous microspheres made sonochemically. *Chem Eur J* 14:3840–3853
24. Mingos DMP, Baghurst DR (1991) Applications of microwave dielectric heating effects to synthetic problems in Chemistry. *Chem Soc Rev* 20:1–47
25. Strauss CR, Trainor RW (1995) Developments in microwave-assisted organic chemistry. *Aust J Chem* 48:1665–1692
26. Galema SA (1997) Microwave chemistry. *Chem Soc Rev* 26:233–238
27. Corsaro A, Chiacchio U, Pistara V, Romeo G (2004) Microwave-assisted chemistry of carbohydrates. *Current Organ Chem* 8:511–538
28. Leonelli C, Mason TJ (2010) Microwave and ultrasonic processing: now a realistic option for industry. *Chem Eng Proc* 49:885–900
29. Rao KJ, Vaidhyanathan B, Ganguli M, Ramakrishnan PA (1999) Synthesis of inorganic solids using microwaves. *Chem Mater* 11:882–895
30. Stavarache C, Vinatoru M, Nishimura R, Maeda Y (2003) Conversion of vegetable oil to biodiesel using ultrasonic irradiation. *Chem Lett* 32:716–717



31. Stavarache C, Vinatoru M, Nishimura R, Maeda Y (2005) Fatty acids methyl esters from vegetable oil by means of ultrasonic energy. *Ultrason Sonochem* 12:367–372
32. Stavarache C, Vinatoru M, Maeda Y (2007) Aspects of ultrasonically assisted transesterification of various vegetable oils with methanol. *Ultrason Sonochem* 14:380–386
33. Stavarache C, Vinatoru M, Maeda Y, Bandow H (2007) Ultrasonically driven continuous process for vegetable oil transesterification. *Ultrason Sonochem* 14:413–417
34. Hanh HD, Nguyen TD, Okitsu K, Nishimura R, Maeda Y (2009) Biodiesel production through transesterification of triolein with various alcohols in an ultrasonic field. *Renew Energy* 34:766–768
35. Hanh HD, Nguyen TD, Okitsu K, Nishimura R, Maeda Y (2009) Biodiesel production by esterification of oleic acid with short-chain alcohols under ultrasonic irradiation condition. *Renew Energy* 34:780–783
36. Rokhina EV, Lens P, Virkutyte J (2009) Low-frequency ultrasound in biotechnology: state of the art. *Trends Biotechnol* 27:298–306
37. Koc AB, Vatandas M (2006) Ultrasonic velocity measurements on some liquids under thermal cycle: ultrasonic velocity hysteresis. *Food Res Int* 39:1076–1083
38. Kelkar MA, Gogate PR, Pandit AB (2008) Intensification of esterification of acids for synthesis of biodiesel using acoustic and hydrodynamic cavitation. *Ultrason Sonochem* 15:188–194
39. Kalva A, Sivasankar T, Moholkar VS (2009) Physical mechanism of ultrasound-assisted synthesis of biodiesel. *Ind Eng Chem Res* 48:534–544
40. Mahamuni NN, Adewuyi YG (2009) Optimization of the synthesis of biodiesel via ultrasound-enhanced base-catalyzed transesterification of soybean oil using a multifrequency ultrasonic reactor. *Energy Fuel* 23:2757–2766
41. Mahamuni NN, Adewuyi YG (2010) Application of Taguchi method to investigate the effects of process parameters on the transesterification of soybean oil using high frequency ultrasound. *Energy Fuel* 24:2120–2126
42. Deshmane VG, Adewuyi YG (2013) Synthesis and kinetics of biodiesel formation via calcium methoxide base catalyzed transesterification reaction in the absence and presence of ultrasound. *Fuel* 107:474–482
43. Koberg M, Cohen M, Ben-Amotz A, Gedanken A (2011) Bio-diesel production directly from the microalgae biomass of *Nannochloropsis* by microwave and ultrasound radiation. *Bioresour Technol* 102:4265–4269
44. Ranjan A, Patil C, Moholkar VS (2010) Mechanistic assessment of microalgal lipid extraction. *Ind Eng Chem Res* 49:2979–2985
45. Parkar PA, Choudhary HA, Moholkar VS (2012) Mechanistic and kinetic investigations in ultrasound assisted acid catalyzed biodiesel synthesis. *Chem Eng J* 187:248–260
46. Choudhury HA, Malani RS, Moholkar VS (2013) Acid catalyzed biodiesel synthesis from jatropha oil: mechanistic aspects of ultrasonic intensification. *Chem Eng J* 231:262–272
47. Hobuss CB, Venzke D, Pacheco BS, Souza AO, Santos MAZ, Moura S, Quina FH, Fiametti KG, Oliveira JV, Pereira CMP (2012) Ultrasound-assisted synthesis of aliphatic acid esters at room temperature. *Ultrason Sonochem* 19:387–389
48. Verma A, Kumar S, Jain PK (2011) Key pretreatment technologies on cellulosic ethanol production. *Ind J Sci Res* 55:57–63
49. Shewale SD, Pandit AB (2009) Enzymatic production of glucose from different qualities of grain sorghum and application of ultrasound to enhance the yield. *Carbohydr Res* 344:52–60
50. Alvira P, Tomas-Pejo E, Ballesteros M, Negro MJ (2010) Pretreatment technologies for an efficient bioethanol production process based on enzymatic hydrolysis: a review. *Bioresour Technol* 101:4851–4861
51. Subhedar PB, Gogate PR (2013) Intensification of enzymatic hydrolysis of lignocellulose using ultrasound for efficient bioethanol production: a review. *Ind Eng Chem Res* 52:11816–11828
52. Nikolic S, Mojovic L, Rakin M, Pejin D, Pejin J (2010) Ultrasound-assisted production of bioethanol by simultaneous saccharification and fermentation of corn meal. *Food Chem* 122:216–222
53. Goshadrou A, Karimi K, Taherzadeh MJ (2011) Bioethanol production from sweet sorghum bagasse by *Mucor hiemalis*. *Ind Crop Prod* 34:1219–1225

54. Bussemaker MJ, Xu F, Zhang DK (2013) Manipulation of ultrasonic effects on lignocellulose by varying the frequency, particle size, loading and stirring. *Bioresour Technol* 148:15–23
55. Sindhu R, Kuttiraja M, Preeti VE, Vani S, Sukumaran RK, Binod PA (2013) Novel surfactant-assisted ultrasound pretreatment of sugarcane tops for improved enzymatic release of sugars. *Bioresour Technol* 135:67–72
56. Sasmal S, Goud VV, Mohanty K (2012) Ultrasound assisted lime pretreatment of lignocellulosic biomass toward bioethanol production. *Energy Fuel* 26:3777–3784
57. Ramadoss G, Muthukumar K (2014) Ultrasound assisted ammonia pretreatment of sugarcane bagasse for fermentable sugar production. *Biochem Eng J* 83:33–41
58. Luo J, Fang Z, Smith RL Jr (2014) Ultrasound-enhanced conversion of biomass to biofuels. *Prog Energy Combust Sci* 41:56–93
59. Chaturvedi V, Verma P (2013) An overview of key pretreatment processes employed for bioconversion of lignocellulosic biomass into biofuels and value added products. 3 *Biotech* 3:415–431
60. Pang F, Xue S, Yu S, Zhang C, Li B, Kang Y (2013) Effects of combination of steam explosion and microwave irradiation (SE–MI) pretreatment on enzymatic hydrolysis, sugar yields and structural properties of corn stover. *Ind Crop Prod* 42:402–408
61. Verma P, Watanabe T, Honda Y, Watanabe T (2011) Microwave-assisted pretreatment of woody biomass with ammonium molybdate activated by H<sub>2</sub>O<sub>2</sub>. *Bioresour Technol* 102:3941–3945
62. Klein M, Pulidindi IN, Perkas N, Meltzer-Mats E, Gruzman AL, Gedanken A (2012) Direct production of glucose from glycogen under microwave irradiation. *RSC Adv* 2:7262–7267
63. Tzhayi O, Pulidindi IN, Gedanken A (2014) forming nanospherical cellulose containers. *Ind Eng Chem Res* 53(36):13871–13880
64. Pulidindi IN, Gedanken A (2014) Carbon nanoparticles based non-enzymatic glucose sensor. *Int J Environ Anal Chem* 94:28–35
65. Victor A, Pulidindi IN, Gedanken A (2014) Levulinic acid production from *Cicer arietinum*, cotton, *Pinus radiata* and sugarcane bagasse. *RSC Adv* 4:44706–44711
66. Li MF, Fan YM, Xu F, Sun RC, Zhang XL (2010) Cold sodium hydroxide/urea based pretreatment of bamboo for bioethanol production: characterization of the cellulose rich fraction. *Ind Crop Prod* 32:551–559
67. Sulaiman AZ, Yunus RM, Chisti Y (2011) Ultrasound-assisted fermentation enhances bioethanol productivity. *Biochem Eng J* 54:141–150
68. Velmurugan R, Muthukumar K (2011) Utilization of sugarcane bagasse for bioethanol production: sono-assisted acid hydrolysis approach. *Bioresour Technol* 102:7119–7123
69. Kisielewska M (2012) Ultrasonic stimulation of co-immobilized *Saccharomyces cerevisiae* cells and beta-galactosidase enzyme for enhanced ethanol production from whey ultrafiltration permeate. *Pol J Environ Stud* 21:387–393
70. Pejin DJ, Mojovic LV, Pejin JD, Grujic OS, Markov SL, Nikolic SB, Markovic MN (2012) Increase in bioethanol production yield from triticale by simultaneous saccharification and fermentation with application of ultrasound. *J Chem Technol Biotechnol* 87:170–176
71. Rezic T, Oros D, Markovic I, Kracher D, Ludwig R, Santek B (2013) Integrated hydrolyzate and fermentation of sugar beet pulp to bioethanol. *J Microbiol Biotechnol* 23:1244–1252
72. Belal ED (2013) Bioethanol production from rice straw residue. *Braz J Microbiol* 44:225–234
73. Eshtiaghi MN, Kuldiloke J, Yoswathana N, Ebadi AG (2012) Application of ultrasound and technical enzymes during bioethanol production from fresh cassava root. *J Food Agric Environ* 10:905–909
74. Velmurugan R, Muthukumar K (2012) Sono-assisted enzymatic saccharification of sugar cane bagasse for bioethanol production. *Biochem Eng J* 63:1–9
75. Pulidindi IN, Gedanken A, Schwarz R, Sendersky E (2012) Mild sonication accelerates ethanol production by yeast fermentation. *Energy Fuel* 26:2352–2356
76. Shaheen M, Choi M, Ang W, Zhao YP, Xing J, Yang R, Xing JD, Zhang J, Chen J (2013) Application of low-intensity pulsed ultrasound to increase bioethanol production. *Renew Energy* 57:462–468



**Part III**  
**Lignocellulose and Industrial Waste:**  
**Pretreatment and Conversions**

# Chapter 7

## Ultrasound as a Green Processing Technology for Pretreatment and Conversion of Biomass into Biofuels

Siah Ying Tang and Manickam Sivakumar

**Abstract** In the past decades, a great deal of attention has been focused on mechanical, thermal or chemical pretreatments of lignocellulosic and algal biomass for the production of biofuel. This chapter is focused on the potential of ultrasound (US) technology in pretreating the biomass to enhance the conversion of cellulose to fermentable sugars and also the disintegration and component extraction of microalgae for the generation of bioethanol or biogas. In addition, US can supplement existing biomass pretreatment methods to greatly enhance their performance and their efficacy. Low frequency ultrasound (LFU, 20–100 kHz) is commonly used in biomass processing, particularly in processes that require intense physical effects such as cell disruption and polymer degradation. High frequency ultrasound (HFU, 400 kHz–2 MHz) recently attracted considerable interest as potential alternative technique for pretreating both the lignocellulosic and algal biomass for sustainable biofuel production. HFU is gaining increasing importance because of its environmentally sound and energy-saving production method since it demands lower energy input for the conversion of biomass. It not only saves time and energy but also lowers the chemical/enzyme dosage and hence novel and considered to be a new sustainable and environmentally-friendly green technique. Although many studies have shown the promise of ultrasound in the cell breakdown for enhanced enzymatic hydrolysis, there is limited information in the application of HFU on biomass pretreatment processes. This chapter provides an overview on the fundamentals of US, the critical parameters that control the conversion of biomass, challenges involved with the application of US in the biomass conversion and its future perspectives.

---

S.Y. Tang

Chemical Engineering Discipline, School of Engineering, Monash University Malaysia, Jalan Lagoon Selatan, 46150 Bandar Sunway, Selangor, Malaysia

M. Sivakumar (✉)

Manufacturing and Industrial Processes Research Division, Faculty of Engineering, University of Nottingham Malaysia Campus, 43500 Semenyih, Selangor, Malaysia  
e-mail: sivakumar.manickam@nottingham.edu.my

**Keywords** Ultrasound · Cavitation · High frequency · Biomass · Biodiesel · Lignocellulose · Microalgae

## 7.1 Introduction

According to the World Energy Council, fossil resources such as petroleum, natural gas and coal provide nearly 82 % of world's total commercial energy needs [1]. Increasing energy demand, especially in developing nations will continue increasing the global energy needs over 50 % by 2025 [2]. Due to the large consumption of fossil-derived fuels and its non-renewability, it has been estimated that both petroleum and natural gas will be depleted in the next 4–6 decades [3, 4]. Furthermore, global warming is becoming increasingly severe due to the large emissions of greenhouse gases such as carbon dioxide resulting from the burning of fossil fuels [5]. The exhaustion of fossil fuels and global warming have forced many countries to find alternative sustainable and green energy sources. Clearly, the need for developing sustainable and clean energy from renewable resources is crucial towards World population growth, increasing demand for energy and concerns over the environmental impact inflicted by the use of fossil-based fuels. In the past decade, various biomasses derived from the carbonaceous waste of human and natural activities have been explored as renewable energy resources. Biofuel, especially ethanol which is made from renewable agricultural or biological sources has gained considerable importance as an alternative energy.

At present, bio-fuel produced from sugarcane/corn crops, lignocellulosic and algal biomass is most widely recognized and has great potential as renewable alternatives to fossil-derived petrol, with the advantage of being compatible with current infrastructures. Bio-ethanol is currently produced mainly from sugarcane or corn, and thus is classified as the first generation bioethanol [6]. However, the major bottleneck of this first generation bioethanol is that it competes with human consumable food sources and also requires arable land. Besides, lignocellulosic biomass is one of the renewable resources for the production of second generation biofuels. Lignocellulose is the most abundant carbohydrate source in nature and a variety of lignocellulosic biomass such as agricultural residues (e.g., wheat straw, sugarcane bagasse, corn stover), forest products (hardwood and softwood), switch grass, etc. have been utilized for the production of biofuels. Although there is an intensive research in the utilization of lignocellulosic feedstock for biofuel production, the major obstacle in biochemical conversion of lignocelluloses to bio-ethanol is the development of an efficient pretreatment method. As lignocelluloses are complex and strongly resistant to enzymatic hydrolysis due to their recalcitrance, a pretreatment process is necessary to disrupt the naturally recalcitrant structure of carbohydrate lignin shields to increase the accessibility of enzymes and microbes to cellulose and hemicelluloses [7]. For the degradation of lignin, various thermal, mechanical and chemical pretreatment techniques have been reported in Ref. [8]. There are different pre-processing methods including the use of alkali, dilute acid,

steam explosion, ionic liquids, ammonia fibre explosion, lime and organo solvent pretreatments to improve the enzymatic saccharification [9–13]. However, most of these methods are not only energy and resource (water) intensive, but also lead to the formation of undesirable by-products and cause loss of carbohydrates [14–16]. Expensive biological and enzymatic processes are required to prepare lignocellulosic materials for hydrolysis to produce fermentable sugars (glucose).

Microalgae is emerging as a promising biomass feedstock for the production of third generation biofuels [17] and chemicals [18]. Many kinds of microalgae such as *Chlorella*, *Dunaliella salina* and diatoms have the ability to accumulate lipids in the range of 20–50 % of dry cell weight, and are therefore appeared to be excellent materials for the synthesis of biodiesel [19, 20]. Other microalgae such as *Scenedesmus*, *Spirulina* possess a high content of carbohydrates (mainly starch, >50 % of the dry cell weight), polysaccharides, oligomers and even hydrocarbons, making them more suitable as feedstocks for the production of valuable chemicals such as sugars, hydrogen and biogas (methane) via thermochemical or biochemical routes [18, 21]. The biogas generated could be used as fuel for the generation of electricity and heating purposes. The carbohydrates from microalgae can be hydrolyzed and converted into glucose which is an important substrate for heterotrophic microorganisms such as yeast, bacteria and fungus to produce bio-ethanol [22]. Apart from high lipid/carbohydrates content, microalgae offers more advantages over other biofuel crops such as fast growth rate, high yield per hectare and CO<sub>2</sub> biofixation capability [23]. More importantly, microalgae can be produced in large scale on non-arable lands and do not need potable water to grow. Consequently, there is no competition with food production for the growing human population, thus overcoming the major drawbacks of first and second generation biofuels to a greater extent [24]. Furthermore, microalgae composition is generally more uniform and consistent than lignocellulosic biomass. This has resulted into an exponential growth of interest in researching the modern biotechnology to explore microalgae for biofuel production.

The use of US to promote the pretreatment of biomass has received wider and wider attention and has been attempted as a promising approach to enhance the bioconversion of a variety of biomass including vegetable oils, carbohydrates, lignocellulosic and algal materials. Compared to microwave, gamma-ray, and electron beam, US is the most studied irradiation method. The application of US in the field of biorenewables is still fairly a new concept, and has demonstrated potential as a facile processing technique to enhance the enzymatic hydrolysis and subsequent ethanol fermentation [25, 26]. The application of US facilitates mass transfer in addition to the turbulent mixing and secondary effects attributed to acoustic cavitation (the formation, growth, and collapse of bubbles) [27]. The implosion of acoustic cavitation bubbles in water leads to extremely high temperatures (ca. 5,000 °C) and pressures (ca. 100 MPa) and heating and cooling rates above 10<sup>10</sup> K/s in the microenvironment. The resulting high concentrated energy can bring about significant modification in the surface morphology and composition at liquid-solid interfaces and fragmentation of friable solids to increase the surface area by shock waves and microjets and also the formation of free radicals

caused by the breakdown of water molecules during asymmetric cavitation bubble collapse [28, 29]. US produces intense cavitation shear forces in an aqueous phase due to the rapid streaming of solvent molecules around the cavitation bubble, as well as the intense shock waves emanated from collapse. The dependence of physical and sonochemical effects of acoustic cavitation as a function of ultrasonic frequency has been observed. US frequency influences the behaviour of bubble cavitation through the change in the duration time of acoustic cycle [30]. Low US frequencies (20–100 kHz) favour the occurrence of active cavitation which induces physical disruption of the materials while the higher US frequencies (>100 kHz) increase the free radical generation which promotes sonochemical oxidation [31]. This chapter aims to summarize US-assisted pretreatments, reactions of biomass materials and applications of US for the conversion of lignocelluloses and microalgae.

## 7.2 Ultrasonic Destruction and Fractionation of Lignocellulosic Biomass

Sonication for pre-processing of lignocellulosic biomass appears to facilitate the solvation and fractionation of raw lignocelluloses and subsequently enhances the degradation of biomass by enzymes. Ultrasonic cavitation can disrupt cell wall structure, increase the specific surface area, and reduce the degree of polymerization, leading to increased biodegradability of lignocellulosic biomass [32]. US generates monolithic cavitation and results in physical and chemical reactions in liquid solutions. Ultrasonic irradiation of various types of biomass including maize [33], cassava chip slurry [26], corn meal [34], switchgrass [35], sugarcane bagasse [36], and waxy rice [37] have shown that US enhances the rate of enzymatic hydrolysis and bioethanol production. Luo et al. [38] critically discussed the application of US technology in the biomass pretreatment intended for biorefinery and biofuel applications and highlighted the process benefits of its application, including shorter treatment time and lower energy requirements, and increased accessibility to enzymatic hydrolysis and delignification. The cavitation shear force facilitates the disintegration and dissociation of coarse particles in the slurry into finer biomass particles thereby exposes more surface area for enzyme and microbial activity. Nitayavardhana et al. [39] reported that a considerable particle size reduction of cassava chips resulted in a significant improvement in the sugar yield by 180 % during enzymatic hydrolysis. Nitayavardhana et al. [26] also found that the US pretreatment of cassava chip slurries enhanced the overall ethanol yield and fermentation rate. The ethanol yield from the sonicated sample increased by 2.7-fold while the fermentation time was reduced by nearly 24 h for sonicated samples to achieve the same ethanol yield as control sample. In fact, Khanal et al. (2007) found that corn particles derived from dry-grind ethanol plant declined nearly 20-fold following US pretreatment at high power settings and the glucose release rate from sonicated samples increased as much as threefold compared to the control group.

Combined strategy of incorporating two or more pretreatment techniques showed a significant improvement in the biofuel yield. For instance, the combination of US and chemicals can cause significant destruction of cell wall structure. Subhedar and Gogate [7] investigated the use of combined approach of alkali with US for the delignification of sustainable biomass in the form of waste newspaper. As compared to alkaline method alone, delignification increases by nearly twofold and the incorporation of US helps to reduce the requirement of alkaline concentration from 1.75 to 1 N. SEM images revealed that the surface structure of newspaper after ultrasound-assisted alkaline pretreatment was not smooth, and had disrupted the surface which might be beneficial to enzymatic attack and its adsorption onto the biomass (Fig. 7.1).

There are several studies reported on the use of US to pretreat lignocellulosic biomass for sustainable production of biogas. A study of rice stalks from Wang et al. [40] using combination of alkaline and US demonstrated 35–48 % higher daily biogas production than the simple alkali technique, and 67–77 % higher than in absence of any preliminary treatment. With this combined approach, 41 % lignin degradation was achieved. Compared with single chemical treatment methods, combined use of chemical and US technologies could be beneficial due to higher methane yield, reduced processing time, and more complete biomass utilization. Elbeshbishy et al. [41] observed that sonication with temperature control (less than 30 °C) resulted in an increase in the volumetric hydrogen production by 120 % over the untreated sludge, and by 40 % over the heat-shock and acid pretreated sludge, with a marginal (~10 %) increase in the hydrogen production rate. This study revealed the superiority of US irradiation with temperature control over conventional means to biological hydrogen production such as heat-shock, acid, and base pretreatment. In comparison to conventional physicochemical methods, anaerobic digester sludge showed enhanced biohydrogen production from glucose in batch reactors after pretreated by ultrasound. In addition, Cesaro et al. [42] reported that US produced a 24 % increase in

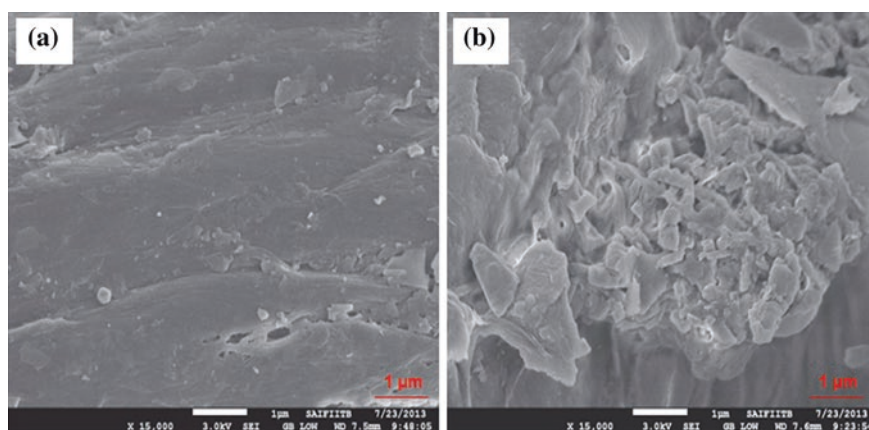


**Fig. 7.1** SEM images of untreated (a) and pretreated (b) newspaper by US. Reprinted with permission from [7]. Copyright © 2014, Elsevier

biogas yield of the pretreated organic fraction of municipal solid waste, compared with untreated feedstock. It has been concluded that US was more efficient than ozonation in terms of enhancement of biogas production from organic solid waste, with a remarkable increment of solubilisation of organic solid waste and improvement of biogas production rate.

Combined use of US and lignolytic enzymes brings about remarkable enhancement in the degradation of lignocellulosic biomass. The application of sequential US exploits the physical and sonochemical effects of ultrasonication as a preliminary treatment to physically disrupt the lignocellulosic matrix of the biomass. In a study conducted by Sabarez et al. [25], wheat chaff were pretreated by US (40 kHz/0.5 W cm<sup>-2</sup>/10 min and 400 kHz/0.5 W cm<sup>-2</sup>/10 min applied sequentially) prior to digestion by enzyme extracts. They found that US combined with subsequent biodegradation by lignolytic enzyme was more effective in improving the susceptibility of lignocellulosic biomass to degradation compared to the use of enzyme only or application of US without using any enzymes. This was evident from the increased amounts of sugar- and phenolic-derived components generated and enhanced in vitro rumen digestibility of treated solid residues. A similar two-step method consisting of a mild ultrasonic treatment step (40 kHz, 250 W) followed by treatment with *Pleurotus ostreatus* was reported for the enzymatic hydrolysis of rice hulls. With similar combination, Yu et al. also observed a significant increase in lignin degradation as compared to any single pretreatment method studied. Besides, combined use of novel bio-derived cholinium ionic liquids (choline acetate) and US irradiation for the pre-processing of lignocellulosic material resulted in a profound improvement in enzymatic saccharification as compared to conventional heating [43]. The study showed that the cellulose saccharification ratio of bamboo powder after ultrasonication in choline acetate (92 %) was significantly higher than the ratio obtained (55 %) for those samples pretreated thermally at 110 °C for 60 min. The SEM analysis indicated that the hybrid pre-processing of bamboo powder in the cholinium ionic liquid with US irradiation could destroy the lignin network and inlaying crystalline cellulose more effectively than the thermal approach (Fig. 7.2).

Apart from the foregoing combined approaches, Sindhu et al. [44] have successfully developed a novel surfactant-assisted US pretreatment that removes hemicelluloses and lignin and improves the reducing sugar yield from sugarcane

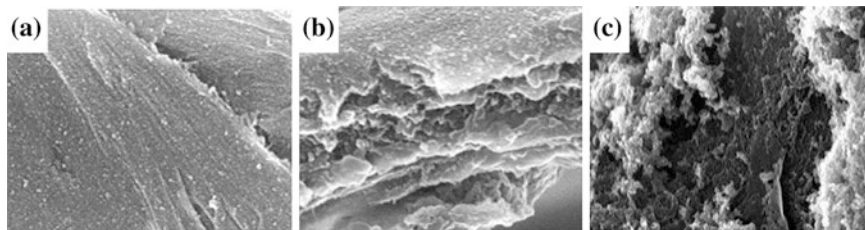


**Fig. 7.2** SEM images of bamboo powder without pretreatment (a), thermal pretreatment in choline acetate (b), and US pretreatment in choline acetate (c). Reprinted with permission from [27]. Copyright © 2013, Elsevier



tops. Under optimal hydrolysis conditions, Tween 80-assisted US treatment of sugarcane tops for 1 min resulted into 0.661 g/g reducing sugar after enzymatic saccharification [44]. In the processing of palm oil fronds for sustainable production of bioethanol, US-assisted simultaneous saccharification and fermentation (SSF) of modified organosolvent pretreatment has been investigated. According to this recent study, the ultrasonic-assisted SSF of pretreated palm oil fronds was found to improve the bioethanol yield (57 %) compared to the SSF processes without US (14 %) at a significantly shorter times. On the other hand, Shaheen et al. [6] investigated the use of low-intensity pulsed US (LIPUS) technology to improve the metabolic activity of cellulose-degrading fungi and ethanol-producing yeasts. The authors showed that LIPUS (1.5 MHz, 80 mW/cm<sup>2</sup>, 20 % duty cycle) resulted in an increase in the cellulase production by *Trichoderma reesei* by 16 % and induced 31 % increase in the ethanol production by *Saccharomyces cerevisiae* [6]. There was a significant difference in terms of morphology between the samples with and without LIPUS treatments as shown in Fig. 7.3. This observation implies that LIPUS could be an efficient technology

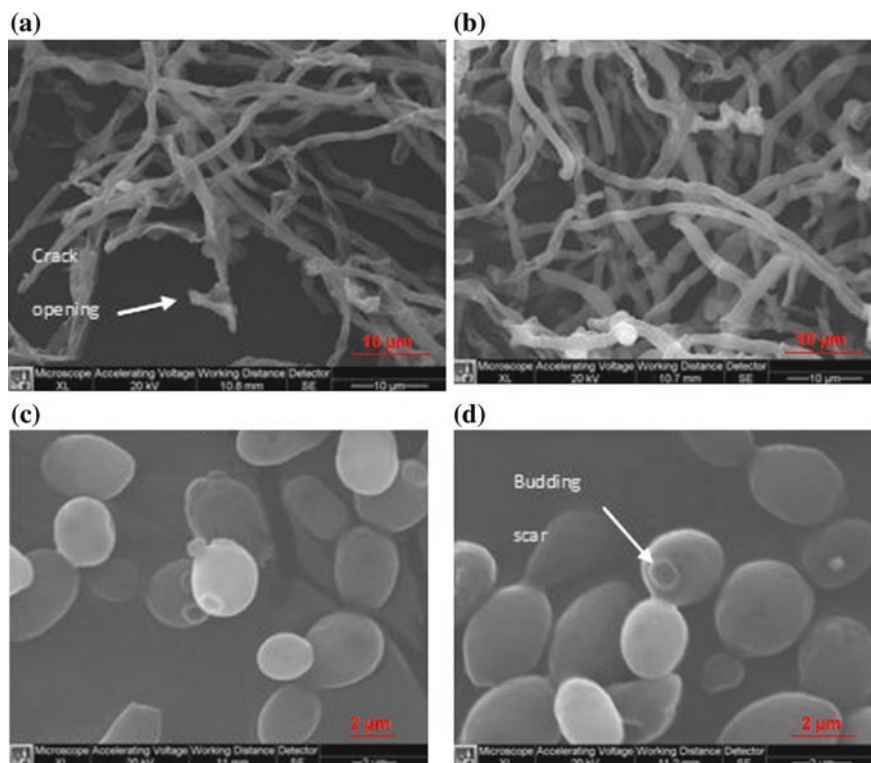


**Fig. 7.3** SEM images of *Trichoderma reesei* (*T. reesei*) treated with low-intensity pulsed US (LIPUS) during fermentations shows shrinking mycelia with crack openings (a). *T. reesei* that received no LIPUS treatment (b), *Saccharomyces cerevisiae* (*S. cerevisiae*) that received LIPUS treatment and one that did not (c) and (d), respectively. It seemed that LIPUS treated cells have more budding scars than the control sample. Reprinted with permission from [6]. Copyright © 2013, Elsevier



**Table 7.1** Types of ultrasound-assisted processes and their process parameters and important findings using different types of lignocellulosic biomass

Ultrasound-assisted processes	Lignocellulosic substrate	Ultrasonic parameters	Key findings	Reference	Year
Combined pretreatment (sequential US + lignolytic enzyme) for the release of sugar	Wheat chaff	Transducer plate (40 kHz/0.5 W cm <sup>-2</sup> /10 min and 400 kHz/0.5 W cm <sup>-2</sup> /10 min, enzyme: white rot fungi ( <i>Phanerochaete chrysosporium</i> or <i>Trametes</i> sp.), biomass loading: 8 % w/v, particle size: 1–2 cm)	Concentration of sugar improved by 2.4-fold at a shorter incubation time of 24 h compared to 48 h for the samples without US pretreatment In vitro digestibility increased to 3–8 % after 72 h of incubation compared to the original raw samples	[25]	2014
Combined pretreatment (surfactant + US) for enzymatic release of sugar	Sugarcane tops	Probe, 20 kHz, 40 % amplitude, pulse 59 s on and 59 s off, surfactant concentration: 0.125–0.2 % w/w, incubation time: 24–60 h, biomass loading: 7.5–15 % w/w, enzyme (cellulose) loading: 20–80 FPU <sup>1</sup> /g of pretreated biomass	Optimization results: A maximum of 0.661 g/g reducing sugar was attained after enzymatic saccharification using the conditions of biomass loading of 11.25 % w/w, enzyme loading of 50 FPU, Tween 40 concentration of 0.2 % w/w, and incubation time of 60 h	[44]	2013
Combined pretreatment (alkaline + US) for cellulose recovery and delignification	Sugarcane bagasse	Probe, 24 kHz, amplitude: 100 %, 400 W, 15–45 min, NaOH concentration: 5, 10 and 15 % v/v, liquid to solid ratio (LSR in mL/g): 10:1, 15:1 and 20:1, biomass loading: 0.01 % w/v, particle size: 0.274, 0.460 and 0.925 mm, temperature: 40, 60 and 80 °C	Optimization results: Maximum cellulose recovery (95.78 %) and delignification (58.14 %) was achieved using the following conditions: particle size of 0.274 mm, sonication time of 45 min, NaOH concentration of 10 %, LSR of 10 mL/g and temperature of 80 °C. A maximum catalytic efficiency of 9.32 and less inhibitors formation (1.59 g/L) was observed	[51]	2014
Combined pretreatment (alkaline + US) for intensification of delignification	Newspaper	Probe, 20 kHz, 100 W, 10–70 min, duty cycle of 80 %, NaOH concentration: 1 N, biomass loading: 0.5 % w/v	With US-assisted alkaline pretreatment delignification improved by twofold as compared to alkaline pretreatment	[12]	2012

(continued)

Table 7.1 (continued)

Ultrasound-assisted processes	Lignocellulosic substrate	Ultrasonic parameters	Key findings	Reference	Year
Combined pretreatment (cholinium IL <sup>b</sup> + US) for enhanced enzymatic saccharification	Bamboo powder	Probe, 24 kHz, 35 W, 0–120 min biomass loading: 1 % w/w	With sonication at 25 °C for 60 min, cellulose saccharification ratio of bamboo powder increased to 92 % in the presence of cholinium IL as compared to 55 % obtained by the thermal pretreated sample in the same IL at 110 °C	[43]	2013

<sup>a</sup>FPU filter paper unit [44]

<sup>b</sup>IL ionic liquid [43]

of pretreating lignocellulosic biomass to obtain fermentable substrates for bioethanol production [45].

The introduction of high-intensity US achieves favourable results in solvation, delignification, fractionation and extraction of raw lignocellulosic biomass at relatively mild conditions and at short treatment time. The strong physical effects of US such as shockwaves, microjets and microstreaming significantly increase the surface area of solid biomass through the reduction of biomass size and cavitation erosion of lignocellulose particles. This resulted in an enhancement in the extraction of chemicals from biomass and the saccharification of cellulosic materials for bioethanol production [46, 47]. In general, delignification and extraction of plant fractions such as polyphenols, flavones, alkaloids, terpenes, glycosides and waxes require a power rating of 1–3 W/mL [48]. US irradiation at an ultrasonic power range of 700–1,000 W can substantially decrease the crystallinity and the polymerization degree of plant-derived cellulose which gives rise to an increase in the hydrophilicity and accessibility of substrates to microbes or enzymes and activation of chemical catalysts [47, 49]. The influence of ultrasonic treatment on the chemical and crystalline structure may depend on the type of treated biomass materials and applied ultrasonic power. High power input benefits the destruction and fractionation of high-strength intermolecular hydrogen-bonding network in cellulose, but excessive power input may produce unwanted degradation of amorphous regions [50]. Hence, the intensity of US should be adapted to different types of lignocellulosic biomass and reactions by changing the acoustic parameters and integrated optimization of ultrasonic parameters should be performed. Table 7.1 summarizes the recent ultrasonic pretreatment methods of lignocellulosic biomass in literature.

### 7.3 Ultrasonic Pretreatment and Conversion of Algal Biomass

As a renewable energy source, algal biomass offers great promise as a third generation biofuel of the future since it produces a much higher oil yield per hectare with good controllability, while the upscaling is easier than with other closed systems. This has given rise to euphoria over the potential of algae for sustainable bioethanol production through microorganism fermentation. Current algal cell disruption methods can be classified as chemical (alkaline, solvents, antibiotics), biological (enzyme), thermal (microwave heating), and mechanical (grinding/milling, high shear processing, high-pressure homogenization) [52, 53]. Among all the techniques, biological pretreatment method (enzymatic degradation) is comparatively effective in terms of organic solubility and cell wall disruption. However, one major constraint to the scalability of this biological system is its high material cost. Mechanical treatments are considered more economical but most of the current mechanical methods are neither effective to treat microalgae cells nor easy to scale-up. Recently, US appears to be as one of the microalgal cell disruption methods and has attracted increasing attention [54, 55]. US is

efficient in the disruption and extraction of algal cells without the addition of beads (for milling) or chemicals such as NaCl (for osmotic shock). US has the advantage of being able to disrupt cells with less energy consumption at relatively lower temperatures as compared to microwave, leading to less thermal protein denaturation [56]. High-pressure methods such as Hughes press or French press, where the power consumption is directly proportional to operating pressure, are applicable for use at laboratory scale only [53]. There are several studies reporting that US helps in the rupture of both microalgae cells and in the reduction of biomass particle size for better release of chemical contents, and thus improves the extraction efficiency with solvents.

There are numerous investigations on the US disruption of algal cells to assist oil extraction and most of these studies have focused on low frequency US (mostly 20–40 kHz) [22, 57]. It is well-known that US increases the efficiency of extraction. For example, in ultrasound-assisted extraction of lipids from *Chlorella vulgaris*, the Bligh and Dyer method assisted by US gave rise to the highest extraction of oil from *C. vulgaris* (52.5 % w/w) as compared to other four extraction methods: Chen, Folch, Hara and Radin, and Soxhlet [58]. The disruption and extraction of algal cells with HUS strongly depends on the type of extraction solvents and the species of microalgae. With US irradiation, oil recovery is possible in the extraction of lipids from fresh *Nannochloropsis oculata* biomass without using any solvent [59]. Gerde et al. [60] studied the breakage of cells of autotrophic and heterotrophic microalgae using US irradiation and monitored the algae cell disruption via intracellular material release. In both types of algae, they observed that increasing the energy input increased the lipid extraction, regardless of the cell concentrations studied. They also claimed that excessive sonication can contribute to the formation of free radicals, which can impair the quality of oil through the formation of lipid hydroperoxides. In addition to this, in an US-assisted extraction (UAE) of carbohydrates/glucose biomass from microalgae as low-cost feedstock for biofuels production by microorganism fermentation, UAE (800 W, 80 min) appears to be a very effective approach with the highest glucose yield approximately 37 g/100 g dry cell weight as compared to other three pretreatment methods [22]. It is apparent that the lipid/glucose extraction from microalgae by low frequency US requires proper control of ultrasonic parameters and optimization endeavour to maximize the extraction yield.

High-intensity ultrasonic energy can locally produce pressure waves, localised heating and free radical production and thus has very interesting prospects in the mechanical alteration of algal cells or tissue. The formation of free radicals at higher frequencies can cause immediate damage on intracellular chlorophyll, leading to a significant loss in photosynthetic cell viability. However, the concept of using high-frequency US for algal cell disruption is currently in the preliminary phase of research. Wang et al. (2012) demonstrated that high-frequency focussed US (HFFU, 3.2 MHz, 40 W) could be as effective as low-frequency non-focused US (LFNFU, 20 kHz, 100 W) in the disruption of two microalgal cells (*Scenedesmus dimorphus* and *Nannochloropsis oculata*) with lower energy consumption [61]. Figure 7.4 shows the experimental set-up used in this study.

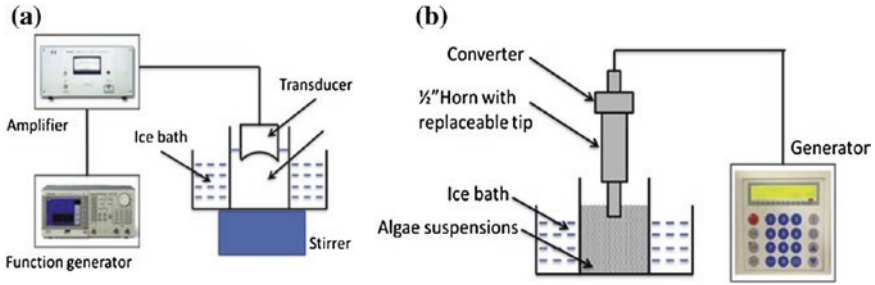
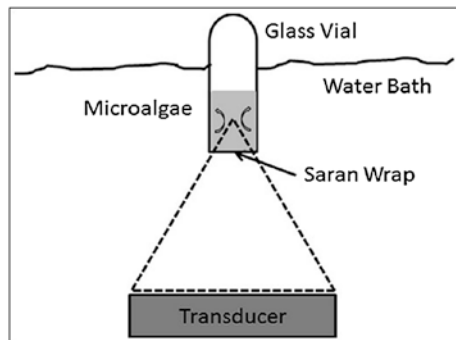


**Fig. 7.4** Experimental set-up: High frequency US (3.2 MHz, 40 W input power) (a) and low frequency US (20 kHz, 100 W input power) (b) treatments. Reprinted with permission from [61]. Copyright © 2014, Elsevier

They also treated *S. dimorphus* strains sequentially using HFFU and LFNFU each for 1 min. They observed that the relative lipid increase rates (RLIR) of combined treatment (102 %) was significantly higher than RLIR obtained using single frequency treatment (64.5 % with HFFU, 78.3 % with LFNFU) for 2 min. It was also reported that high frequency sonication effectively decreased the growth rate of algae and inhibited cell division. Based on the comparison of biomass, chlorophyll and photosynthetic activity, Hao et al. [62] found that the inhibition effectiveness of cyanobacterial proliferation by ultrasound increased in the order: 200 kHz > 1.7 MHz > 20 kHz and became saturated with the increased power. The inhibition mechanism can be mainly attributed to the mechanical damage to the cell structures caused by acoustic cavitation [62]. Using *Chlamydomonas reinhardtii* as a model organism, Bigelow et al. [63] successfully used high-intensity focused US of 1.1 MHz for efficient lysis of microalgae for lipid extraction (Fig. 7.5). The study revealed that longer exposures resulted in a nearly complete cell fragmentation, releasing almost all of the protein and chlorophyll into the supernatant. This further showed that ultrasonic frequency played a critical role in algal cell disruption.

US technology is a powerful tool for breaking down unicellular algal biomass and enhancing production of biogas, for example, up to a 60 % increase in methane

**Fig. 7.5** Schematic diagram of experimental set-up for microalgae lysis (*Chlamydomonas reinhardtii*) using high- frequency US of 1.1 MHz. Reprinted with permission from [63]. Copyright © 2014, Elsevier



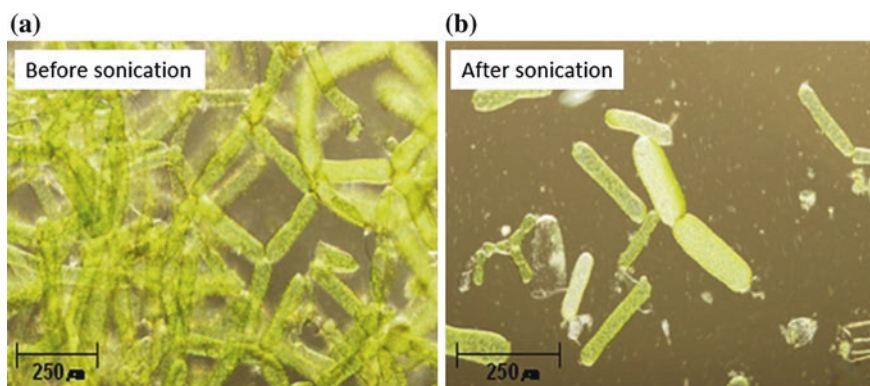


**Fig. 7.6** Microscopic images of filamentous alga *Hydrodictyon reticulatum*. Before (a) and after (b) application of US dose of 5,000 J/mL. Reprinted with permission from [54]. Copyright © 2014, Elsevier

yield has been achieved by researchers [64, 65]. Lee et al. [54] investigated the effects of ultrasonic energy (10–5,000 J/mL) on the pretreatment of filamentous algae, *Hydrodictyon reticulatum* for improved biogas production. The specific methane production at a dose of 40 J/mL increased up to 384 mL/g-VS fed that was 2.3 times higher than the untreated sample after subjecting to US irradiation. Figure 7.6 shows the significant disruption of *H. reticulatum* cells after the application of US. The use of US has also proven to be effective in improving the disintegration and anaerobic biodegradability of waste microalgal biomass, *Chlorella vulgaris* [66]. Park et al. [66] demonstrated that ultrasonic pretreatment using power densities in the range of 5–200 J/mL<sup>-1</sup> significantly improved the solubility of substrate and higher soluble COD was attained at higher applied energy. Compared to the untreated sample, the specific methane production increased by 90 % in the US-treated sample at an energy dose of 200 J/mL<sup>-1</sup>. A microscopic photograph of microalgae *C. vulgaris* is shown in Fig. 7.7. For the conversion of harvested microalgae into biodiesel, one-stage direct transesterification of

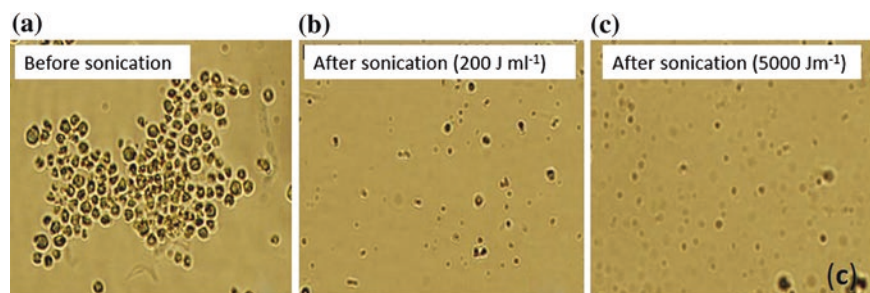


**Fig. 7.7** Microscopic photograph of the microalgae *C. vulgaris*. Before (a) and after (b) sonication. Reprinted with permission from [66]. Copyright © 2013, Elsevier

**Table 7.2** Type of ultrasound-assisted processes and their process parameters and important findings for different types of algal biomass

Ultrasound-assisted processes	Microalgae	Ultrasomic parameters	Key findings	Reference	Year
Release of glucose for fermentation	<i>Chlorella</i> sp.	Probe, 20 kHz, 600–800 W, 20–100 min, microalgal concentration: 0.3, 1.0 and 3.0 g/L	Optimization results: maximum glucose yield of 36.94 g/100 g dcw <sup>a</sup> at an ultrasomic power of 800 W and an extraction time of 80 min	[22]	2013
Lipid extraction for biodiesel production	Mixed microalgae ( <i>Scenedesmus</i> sp., <i>Chlorococcum</i> sp.)	Probe, 30 kHz, 0.1–0.5 W/ mL, 5–60 min, microalgal concentration: 250 mg/L	With sonication at 0.4 kWh/L, lipid extraction yields improved by 1.5–2.0-fold in the presence of solvents	[69]	2014
Pretreatment for methane production	<i>Hydrodictyon reticulatum</i>	Probe, 20 kHz, 150 W, 10–5,000 J/mL, microalgal concentration: 10,000 mg/L	Using US dose of 40 J/mL, methane yield of pre-sonicated samples increased up to 384 mL/g vs <sup>b</sup> fed that was 2.3 times higher than the untreated sample	[54]	2014
Anaerobic digestion for methane production	<i>Chlorella vulgaris</i>	Probe, 20 kHz, 150 W, 5–200 J/mL, microalgal biomass: 100 mL	Specific methane production of pre-sonicated samples increased by 90 % at an energy dose of 200 J/ml. Disintegration reached up to 70 % at 200 J/ml of energy	[66]	2013
Combined pretreatment (acid + US) for hydrogen production	<i>Chlorella vulgaris</i>	Probe, 20 kHz, 150 W, supplied energy of 10,000–100,000 kJ/kg dcw <sup>a</sup> , HCl concentration: 0.1–3 % (v/w), microalgal biomass: 100 mL	Optimization results: maximum yield of 42.1 mL H <sub>2</sub> /g dcw, 0.79 % (v/w) HCl, specific energy input (SEI) of 49,600 kJ/kg dcw	[70]	2013
Combined pretreatment (microwave + US) for hydrogen production with tungstated zirconia as solid acid catalyst	<i>Scenedesmus</i> sp.	Microwave: 1,000 W, 100 °C, 10 min of ultrasound: probe, 22.5 kHz, 100 W, 10 min	Energy efficiency: microwave (65.1 %), US (36.75 %) At lower reaction temperature (50 °C), sonication gave a higher conversion of <i>Scenedesmus</i> sp. to biodiesel amounting to ~71 % as compared to ~52 % with microwave	[71]	2014

<sup>a</sup>d<sub>cw</sub> Dry cell weight; <sup>b</sup>v<sub>S</sub> Volatile solid



*Nannochloropsis* biomass to biodiesel production had also been attempted using US approach with the aid of SrO catalyst [67]. Srisuksomwong et al. [68] studied the feasibility of US technology on *Microcystis* sp. and musty odour degradation of pond water. In this novel study, they treated the water from fish ponds with US at five different frequencies (29, 43, 108, 200 and 1,000 kHz) and they found that ultrasonication at 200 kHz effectively reduced microcystin and musty odors [68]. Intriguingly, scanning electron microscopy (SEM) revealed that US at a frequency of 200 kHz for 240 s did not disintegrate *Microcystis* sp. cells, but easily broke up the sticky mucus layers of scum. Table 7.2 presents a brief comparison of different pretreatment methods reported in the recent literature.

## 7.4 Conclusions and Future Outlook

In summary, the introduction of ultrasonic energy plays a prominent role in treating a broad range of lignocellulosic and algal biomass feedstocks for the production of biofuel. Pre-sonication can disrupt the recalcitrant lignocellulosic structure, decreases the crystallinity of cellulose, increases the accessible surface area, and thus enhances the conversion rate. On the other hand, US irradiation, especially at a high frequency of 1.1–3.2 MHz range benefits the harvesting, component extraction and conversion of microalgae to biofuel. The main mechanisms should be attributed to the effective disruption and thus the lysis of algal cells under high-intensity sonication. Combined intensification of ultrasonic cavitation with other technologies such as microwave, biological enzymes and chemical treatment which give maximum yields and generate minimum inhibitory residues and by-products should be more intensively studied. However, it should be stressed that the efficiency of pretreatment and biochemical conversion of biomass is highly dependent on the types of lignocellulosic and algal biomass feedstock. The selection and optimization of ultrasonic parameters should also consider the mechanism of different chemical reactions and the metabolic pathways of different biological processing. Of the ultrasound-assisted pretreatment and conversion of biomass-to-energy works reviewed in this chapter, biofuel production from biomass using acoustic cavitation approach is relatively a new approach. Although the yield improvement has been observed, there appears to be a lack of stimulus for the development of such concept. The application of ultrasound technology for biofuel production is still in the emerging stage and many types of engineering data are scarce; more development is needed to design full-scale production plants. Nevertheless, the future of ultrasound in industrial development for biofuel production deserves considerable attention.

**Acknowledgment** Authors would like to thank Ministry of Science, Technology and Innovation (MOSTI) for the funding support through eScience (M0058.54.01).



## References

1. Berndes G, Hoogwijk M, van den Broek R (2003) The contribution of biomass in the future global energy supply: a review of 17 studies. *Biomass Bioenergy* 25(1):1–28
2. Ragauskas AJ, Williams CK, Davison BH, Britovsek G, Cairney J, Eckert CA, Frederick WJ Jr, Hallett JP, Leak DJ, Liotta CL, Mielenz JR, Murphy R, Templer R, Tschaplinski T (2006) The path forward for biofuels and biomaterials. *Science* 311(5760):484–489
3. Mills RM (2008) *The myth of the oil crisis: overcoming the challenges of depletion geopolitics, and global warming*. Praeger, California
4. McNerney JC, Cheek M (2011) *Clean energy nation: freeing America from the tyranny of fossil fuels*. Amacom, New York
5. Lam MK, Lee KT (2012) Microalgae biofuels: a critical review of issues, problems and the way forward. *Biotechnol Adv* 30(3):673–690
6. Shaheen M, Choi M, Ang W, Zhao Y, Xing J, Yang R, Xing J, Zhang J, Chen J (2013) Application of low-intensity pulsed ultrasound to increase bio-ethanol production. *Renew Energ* 57:462–468
7. Subhedar PB, Gogate PR (2014) Alkaline and ultrasound assisted alkaline pretreatment for intensification of delignification process from sustainable raw-material. *Ultrason Sonochem* 21(1):216–225
8. Saritha M, Arora A, Lata (2012) Biological pretreatment of lignocellulosic substrates for enhanced delignification and enzymatic digestibility. *Indian J Microbiol* 52(2):122–130
9. Sindhu R, Kuttiraja M, Binod P, Janu KU, Sukumaran RK, Pandey A (2011) Dilute acid pretreatment and enzymatic saccharification of sugarcane tops for bioethanol production. *Bioresour Technol* 102(23):10915–10921
10. Sindhu R, Binod P, Satyanagalakshmi K, Janu KU, Sajna KV, Kurien N, Sukumaran RK, Pandey A (2010) Formic acid as a potential pretreatment agent for the conversion of sugarcane bagasse to bioethanol. *Appl Biochem and Biotechnol* 162(8):2313–2323
11. Sindhu R, Binod P, Janu KU, Sukumaran RK, Pandey A (2012) Organosolvent pretreatment and enzymatic hydrolysis of rice straw for the production of bioethanol. *World J Microbiol Biotechnol* 28(2):473–483
12. Preeti VE, Sandhya SV, Kuttiraja M, Sindhu R, Vani S, Kumar SR, Pandey A, Binod P (2012) An evaluation of chemical pretreatment methods for improving enzymatic saccharification of chili postharvest residue. *Appl Biochem Biotechnol* 167(6):1489–1500
13. Weerachanchai P, Leong SSI, Chang MW, Ching CB, Lee J-M (2012) Improvement of biomass properties by pretreatment with ionic liquids for bioconversion process. *Bioresour Technol* 111:453–459
14. Mosier N, Hendrickson R, Ho N, Sedlak M, Ladisch MR (2005) Optimization of pH controlled liquid hot water pretreatment of corn stover. *Bioresour Technol* 96(18):1986–1993
15. Hendriks ATWM, Zeeman G (2009) Pretreatments to enhance the digestibility of lignocellulosic biomass. *Bioresour Technol* 100(1):10–18
16. Sasmal S, Goud VV, Mohanty K (2012) Ultrasound assisted lime pretreatment of lignocellulosic biomass toward bioethanol production. *Energ Fuel* 26(6):3777–3784
17. Brennan L, Owende P (2010) Biofuels from microalgae—a review of technologies for production, processing, and extractions of biofuels and co-products. *Renew Sust Energ Rev* 14(2):557–577
18. Ferrell J, Sarisky-Reed V (2010) *National algal biofuels technology roadmap*. Office of energy efficiency and renewable energy: biomass program. US Department of Energy, Washington DC
19. Hu Q, Sommerfeld M, Jarvis E, Ghirardi M, Posewitz M, Seibert M, Darzins A (2008) Microalgal triacylglycerols as feedstocks for biofuel production: perspectives and advances. *Plant J* 54(4):621–639
20. Chisti Y (2007) Biodiesel from microalgae. *Biotechnol Adv* 25(3):294–306
21. Ueda R, Hirayama S, Sugata K, Nakayama H (1996) Process for the production of ethanol from microalgae. US patent 5578472, 26 Nov 1996

22. Zhao G, Chen X, Wang L, Zhou S, Feng H, Chen WN, Lau R (2013) Ultrasound assisted extraction of carbohydrates from microalgae as feedstock for yeast fermentation. *Bioresour Technol* 128:337–344
23. Schenk P, Thomas-Hall S, Stephens E, Marx U, Mussgnug J, Posten C, Kruse O, Hankamer B (2008) Second generation biofuels: high-efficiency microalgae for biodiesel production. *Bioenerg Res* 1(1):20–43
24. Singh J, Gu S (2010) Commercialization potential of microalgae for biofuels production. *Renew Sust Energ Rev* 14(9):2596–2610
25. Sabarez H, Oliver CM, Mawson R, Dumsday G, Singh T, Bitto N, McSweeney C, Augustin MA (2014) Synergism between ultrasonic pretreatment and white rot fungal enzymes on biodegradation of wheat chaff. *Ultrason Sonochem* 21(6):2084–2091
26. Nitayavardhana S, Shrestha P, Rasmussen ML, Lamsal BP, van Leeuwen J, Khanal SK (2010) Ultrasound improved ethanol fermentation from cassava chips in cassava-based ethanol plants. *Bioresour Technol* 101(8):2741–2747
27. Ninomiya K, Kamide K, Takahashi K, Shimizu N (2012) Enhanced enzymatic saccharification of kenaf powder after ultrasonic pretreatment in ionic liquids at room temperature. *Bioresour Technol* 103(1):259–265
28. Mason TJ, Cobley AJ, Graves JE, Morgan D (2011) New evidence for the inverse dependence of mechanical and chemical effects on the frequency of ultrasound. *Ultrason Sonochem* 18(1):226–230
29. Suslick KS (1995) Applications of ultrasound to materials chemistry. *MRS Bull* 20(04):29–34
30. Thompson LH, Doraiswamy LK (1999) Sonochemistry: science and engineering. *Ind Eng Chem Res* 38(4):1215–1249
31. Ashokkumar M, Sunartio D, Kentish S, Mawson R, Simons L, Vilku K, Versteeg C (2008) Modification of food ingredients by ultrasound to improve functionality: a preliminary study on a model system. *Innov Food Sci Emerg Technol* 9(2):155–160
32. Zheng Y, Zhao J, Xu F, Li Y (2014) Pretreatment of lignocellulosic biomass for enhanced biogas production. *Prog Energy Combust Sci* 42:35–53
33. Choi JH, Kim SB (1994) Effect of ultrasound on sulfuric acid-catalysed hydrolysis of starch. *Korean J Chem Eng* 11(3):178–184
34. Nikolić S, Mojović L, Rakin M, Pejin D, Pejin J (2010) Ultrasound-assisted production of bioethanol by simultaneous saccharification and fermentation of corn meal. *Food Chem* 122(1):216–222
35. Eason MW, Condon B, Dien BS, Iten L, Slopek R, Yoshioka-Tarver M, Lambert A, Smith J (2011) The application of ultrasound in the enzymatic hydrolysis of switchgrass. *Appl Biochem Biotechnol* 165(5–6):1322–1331
36. Velmurugan R, Muthukumar K (2012) Sono-assisted enzymatic saccharification of sugarcane bagasse for bioethanol production. *Biochem Eng J* 63:1–9
37. Isono Y, Kumagai T, Watanabe T (1994) Ultrasonic degradation of waxy rice starch. *Biosci Biotechnol Biochem* 58(10):1799–1802
38. Luo J, Fang Z, Smith RL Jr (2014) Ultrasound-enhanced conversion of biomass to biofuels. *Prog Energy Combust Sci* 41:56–93
39. Nitayavardhana S, Rakshit SK, Grewell D, Van Leeuwen J, Khanal SK (2008) Ultrasound pretreatment of cassava chip slurry to enhance sugar release for subsequent ethanol production. *Biotechnol Bioeng* 101(3):487–496
40. Wang YZ, Xiong C, Zhi W, Zhao JF, Fan TT, Li DS, Wang JH (2012) Effect of low concentration alkali and ultrasound combination pretreatment on biogas production by stalk. *Adv Mat Res* 383–390:3434–3437
41. Elbeshbishy E, Hafez H, Nakhla G (2010) Enhancement of biohydrogen producing using ultrasonication. *Int J Hydrogen Energ* 35(12):6184–6193
42. Cesaro A, Naddeo V, Amodio V, Belgiorno V (2012) Enhanced biogas production from anaerobic codigestion of solid waste by sonolysis. *Ultrason Sonochem* 19(3):596–600

43. Ninomiya K, Ohta A, Omote S, Ogino C, Takahashi K, Shimizu N (2013) Combined use of completely bio-derived cholinium ionic liquids and ultrasound irradiation for the pretreatment of lignocellulosic material to enhance enzymatic saccharification. *Chem Eng J* 215–216:811–818
44. Sindhu R, Kuttiraja M, Elizabeth Preeti V, Vani S, Sukumaran RK, Binod P (2013) A novel surfactant-assisted ultrasound pretreatment of sugarcane tops for improved enzymatic release of sugars. *Bioresour Technol* 135:67–72
45. Ofori-Boateng C, Lee KT (2014) Ultrasonic-assisted simultaneous saccharification and fermentation of pretreated oil palm fronds for sustainable bioethanol production. *Fuel* 119:285–291
46. Karki B, Lamsal BP, Jung S, van Leeuwen J, Pometto Iii AL, Grewell D, Khanal SK (2010) Enhancing protein and sugar release from defatted soy flakes using ultrasound technology. *J Food Eng* 96(2):270–278
47. Zhang Q, Benoit M, De Oliveira Vigier K, Barrault J, Jégou G, Philippe M, Jérôme F (2013) Pretreatment of microcrystalline cellulose by ultrasounds: effect of particle size in the heterogeneously-catalyzed hydrolysis of cellulose to glucose. *Green Chem* 15(4):963–969
48. Shirsath SR, Sonawane SH, Gogate PR (2012) Intensification of extraction of natural products using ultrasonic irradiations—a review of current status. *Chem Eng Prog* 53:10–23
49. Wang X, Fang G, Hu C, Du T (2008) Application of ultrasonic waves in activation of microcrystalline cellulose. *J Appl Polym Sci* 109(5):2762–2767
50. Chen W, Yu H, Liu Y, Chen P, Zhang M, Hai Y (2011) Individualization of cellulose nanofibers from wood using high-intensity ultrasonication combined with chemical pretreatments. *Carbohydr Polym* 83(4):1804–1811
51. Ramadoss G, Muthukumar K (2014) Ultrasound assisted ammonia pretreatment of sugarcane bagasse for fermentable sugar production. *Biochem Eng J* 83:33–41
52. Chisti Y, Moo-Young M (1986) Disruption of microbial cells for intracellular products. *Enzyme Microb Tech* 8(4):194–204
53. Geciova J, Bury D, Jelen P (2002) Methods for disruption of microbial cells for potential use in the dairy industry—a review. *Int Dairy J* 12(6):541–553
54. Lee K, Chantrasakdakul P, Kim D, Kong M, Park KY (2014) Ultrasound pretreatment of filamentous algal biomass for enhanced biogas production. *Waste Manage* 34(6):1035–1040
55. Wu X, Joyce EM, Mason TJ (2012) Evaluation of the mechanisms of the effect of ultrasound on *Microcystis aeruginosa* at different ultrasonic frequencies. *Water Res* 46(9):2851–2858
56. Bosma R, Van Spronsen WA, Tramper J, Wijffels RH (2003) Ultrasound, a new separation technique to harvest microalgae. *J Appl Phycol* 15(2–3):143–153
57. Wiyarno B, Yunus RM, Mel M (2010) Ultrasound extraction assisted (UEA) of oil from microalgae (*Nannochloropsis* sp.). *Int J Eng Sci* 1(3):65–71
58. Araujo GS, Matos LJBL, Fernandes JO, Cartaxo SJM, Gonçalves LRB, Fernandes FAN, Farias WRL (2013) Extraction of lipids from microalgae by ultrasound application: prospection of the optimal extraction method. *Ultrason Sonochem* 20(1):95–98
59. Adam F, Abert-Vian M, Peltier G, Chemat F (2012) “Solvent-free” ultrasound-assisted extraction of lipids from fresh microalgae cells: a green, clean and scalable process. *Bioresour Technol* 114:457–465
60. Gerde JA, Montalbo-Lomboy M, Yao L, Grewell D, Wang T (2012) Evaluation of microalgae cell disruption by ultrasonic treatment. *Bioresour Technol* 125:175–181
61. Wang M, Yuan W, Jiang X, Jing Y, Wang Z (2014) Disruption of microalgal cells using high-frequency focused ultrasound. *Bioresour Technol* 153:315–321
62. Hao H, Wu M, Chen Y, Tang J, Wu Q (2004) Cavitation mechanism in cyanobacterial growth inhibition by ultrasonic irradiation. *Colloid Surf B* 33(3–4):151–156
63. Bigelow TA, Xu J, Stessman DJ, Yao L, Spalding MH, Wang T (2014) Lysis of *Chlamydomonas reinhardtii* by high-intensity focused ultrasound as a function of exposure time. *Ultrason Sonochem* 21(3):1258–1264
64. González-Fernández C, Sialve B, Bernet N, Steyer JP (2012) Comparison of ultrasound and thermal pretreatment of *Scenedesmus* biomass on methane production. *Bioresour Technol* 110:610–616

65. Alzate ME, Muñoz R, Rogalla F, Fdz-Polanco F, Pérez-Elvira SI (2012) Biochemical methane potential of microalgae: influence of substrate to inoculum ratio, biomass concentration and pretreatment. *Bioresour Technol* 123:488–494
66. Park KY, Kweon J, Chantrasakdakul P, Lee K, Cha HY (2013) Anaerobic digestion of microalgal biomass with ultrasonic disintegration. *Int Biodeter Biodegr* 85:598–602
67. Koberg M, Cohen M, Ben-Amotz A, Gedanken A (2011) Bio-diesel production directly from the microalgae biomass of *Nannochloropsis* by microwave and ultrasound radiation. *Bioresour Technol* 102(5):4265–4269
68. Srisuksomwong P, Whangchai N, Yagita Y, Okada K, Peerapornpisal Y, Nomura N (2011) Effects of ultrasonic irradiation on degradation of microcystin in fish ponds. *Int J Agr Biol* 13(1):67–70
69. Keris-Sen UD, Sen U, Soydemir G, Gurol MD (2014) An investigation of ultrasound effect on microalgal cell integrity and lipid extraction efficiency. *Bioresour Technol* 152:407–413
70. Yun Y-M, Jung K-W, Kim D-H, Oh Y-K, Cho S-K, Shin H-S (2013) Optimization of dark fermentative H<sub>2</sub> production from microalgal biomass by combined (acid + ultrasonic) pretreatment. *Bioresour Technol* 141:220–226
71. Guldhe A, Singh B, Rawat I, Bux F (2014) Synthesis of biodiesel from *Scenedesmus* sp. by microwave and ultrasound assisted in situ transesterification using tungstated zirconia as a solid acid catalyst. *Chem Eng Res Des* 92(8):1503–1511

# Chapter 8

## Ultrasound-Enhanced Biogas Production from Different Substrates

**Cristina Gonzalez-Fernandez, Rudolphus Antonius Timmers, Begoña Ruiz and Beatriz Molinuevo-Salces**

**Abstract** Among the biofuel production processes using different substrates, the biogas generation process is one of the simplest. Compared with bioethanol or biodiesel production processes, anaerobic digestion is a process where all the organic matter (carbohydrates, lipids and proteins) can be biologically degraded for methane production. Biological degradations of those polymeric substrates are carried out by several enzymes during the first stage of hydrolysis. Nevertheless, due to the substrates physical state, microbial degradation is frequently hampered. Substrate pretreatment enhances the performance of anaerobic digestion by improving the bioavailability of the substrate for anaerobic digestion and thus accelerating the hydrolysis step. Appropriate methods are currently under development in order to increase accessibility of the enzymes to the materials and therefore optimise the ultimate methane production. The present chapter is dedicated to providing a review of ultrasound pretreatment applied to different substrates (lignocelulosic materials, manures, sludge and microalgae). The advantages and constraints, that ultrasound pretreatment exhibit towards biogas production, are discussed and compared with other pretreatment methods.

---

C. Gonzalez-Fernandez (✉)

IMDEA Energy, Avda. Ramón de La Sagra 3, 28935 Móstoles, Spain

e-mail: cristina.gonzalez@imdea.org

R.A. Timmers

Department of Chemical and Energy Technology, Rey Juan Carlos University,

28933 Móstoles, Spain

B. Ruiz

ainia Technology Centre, Valencia Technology Park, Benjamin Franklin 5-11,

46980 Paterna, Valencia, Spain

B. Molinuevo-Salces

Section for Sustainable Biotechnology, Aalborg University Copenhagen,

AC Meyers Vænge 15, 2450 København SV, Denmark

**Keywords** Ultrasound · Biogas · Methane · Lignocellulose · Livestock · Sludge · Microalgae

## 8.1 The Anaerobic Digestion Process

Anaerobic digestion processes are defined as the biological degradation of organic materials in the absence of oxygen [1]. Anaerobic conversions occur naturally in a variety of environments, such as marine and fresh water sediments or in the intestinal tract of animals. Mankind has used this process in order to obtain environmental and energy benefits. In this way, the anaerobic digestion process offers several advantages such as organic matter bioconversion into energy (biogas), reduction of greenhouse gas emissions, odor and pathogen reduction and conversion of organic nitrogen into nitrogen available for plant growth (fertilizer capacity). Biogas production renders this technology an important pathway for biomass valorization, thus allowing the production of renewable energy [2].

Several microorganisms are involved in the three phases that can be distinguished in the anaerobic digestion process [3] (Fig. 8.1):

- Hydrolysis and acidogenesis: Undissolved biodegradable organic matter (lipids, proteins and carbohydrates) is converted into simpler compounds (long chain fatty acids, amino acids and monosaccharides). This conversion is carried out by exoenzymes (lipases, proteases and cellulases,) excreted by fermentative bacteria. Then, the dissolved compounds are transformed into fermentation products [volatile fatty acids (VFA), ethanol, lactic acid, hydrogen and carbon dioxide].
- Acetogenesis: Fermentation products are oxidized to acetate, carbon dioxide and hydrogen, which are indeed the substrates for methanogenic microorganisms.
- Methanogenesis: Methane can be produced through two different routes, namely hydrogenotrophic methanogenesis (30 %), where hydrogen and carbon dioxide are converted into methane and acetoclastic methanogenesis (70 %), where acetate is converted into methane and carbon dioxide. Traditionally, the ratio between hydrogenotrophic and acetoclastic microorganisms has been set around 70/30. However, it seems that the proportion of the hydrogenotrophic microorganisms becomes higher when the methane is produced from renewable resources, i.e.. energy crops [4].

Even though anaerobic digestion is a well-known technology, suboptimal performance often occurs due to process instability (nutrients imbalance, inhibitions...) and therefore low methane yields have been reported for some substrates [5, 6]. Many research efforts are devoted to find proper co-substrates that improve the nutrients balance [7], to increase the biodegradability of different feedstocks by applying different pretreatments to the substrates [8] and to study the underlying degradative mechanisms [9], with the ultimate objective of overcoming those drawbacks.

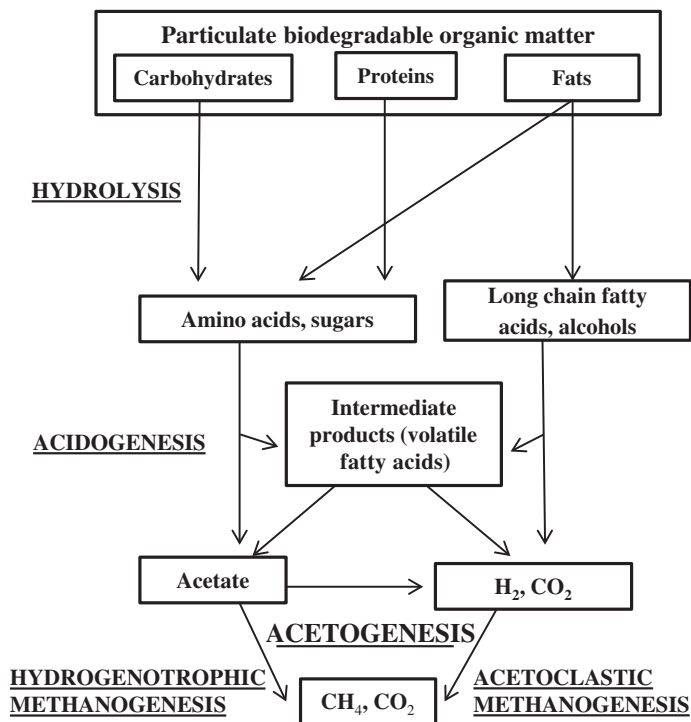


**Fig. 8.1** Anaerobic degradation of complex organic matter. Adapted with permission from [3]. Copyright © 2014, Elsevier

Methane yields ( $\text{L CH}_4 \text{ kg}^{-1}$  chemical oxygen demand (COD) or volatile solids (VS) introduced $^{-1}$ ) are normally linked to substrate composition. In the case of easily degradable substrates, such as molasses and vinasses, the fast conversion of organic matter into volatile fatty acids (VFAs), often results in acids accumulation since the conversion rates of methanogens are lower than those of acidogens [10]. In this manner, inhibition of the anaerobic digestion process arises by VFAs accumulation for easily degradable substrates, and hence methanogenesis is the limiting step. Opposite to that, in particulate complex organic substrates (lignocellulosic material, manure, activated sludge and microalgae biomass), the first phase of the anaerobic digestion (hydrolysis-acidogenesis) is the rate-limiting step. The extent of the hydrolysis of a specific substrate is related to its chemical composition and its bioavailability. One of the possibilities to increase the extent of the hydrolysis step would be the application of a pretreatment, which should be designed in accordance to the chemical composition and structure of the targeted substrate.

Depending on the raw material composition and the operational conditions applied, pretreatments can lead to the formation of non-desired compounds. Those compounds are the result of lignin degradation (phenolic compounds), sugars degradation (furans) and organic nitrogen mineralization (ammonia) [8]. Those

degradation byproducts can inhibit the anaerobic microorganism's activity. More information regarding anaerobic digestion inhibiting compounds can be found elsewhere [5]. The advantage of anaerobic digestion over other biofuel-production technologies is that this technology always uses a mixture of micro-organisms so that they can be adapted to high concentrations of the potential inhibiting compounds. Moreover, those microorganisms can transform some of the inhibitory compounds (i.e. VFAs) into biogas after a period of microbial adaptation [8].

## 8.2 Principles of Ultrasonic Pretreatment

Ultrasound is an elastic wave with a frequency higher than the audible for humans. The frequency of ultrasounds ranges between 20 kHz and 1 GHz. Ultrasonic vibrations can propagate in elastic media such as gases, liquids and solids, with different speed of propagation in each of these environments. The phenomena caused by the ultrasonic waves include variable pressure and flow, radiation pressure, cavitation and friction at the interface [11]. Of these phenomena, cavitation is the most powerful to enhance biogas production. Cavitation occurs inside a liquid when it is subjected to changes in the pressure field over time and distance (in this case, caused by ultrasonic waves of high frequency, 20 kHz to 1 MHz). Under these conditions, bubbles are formed in the liquid, and filled with the liquid's vapor and dissolved gases. Above a critical value of local pressure, the bubbles implode violently, producing powerful hydromechanical shear forces in the liquid surrounding them. At the same time, a dramatic increase in temperature and pressure is occurring in a very small region, leading to thermal destruction of the compounds inside the bubbles and to the formation of radicals that initiate the so called sonochemical reactions. On micro scale, the cavitation process produces temperatures of around 5,000 °C and pressures of 50 MPa for microseconds [12]. The high temperature and pressure subsequently disrupt and break down the fibers (in the case of manure and lignocellulosic materials) and microorganisms' cell walls (in the case of activated sludge and microalgae) by imposing: (i) shear stress, (ii) oxidation stress by formation of strongly oxidizing radicals such as ·OH, ·H, ·O, and ·N, and (iii) thermal stress [13, 14]. These mechanisms result in degradation and depolymerization, which is the reason to use ultrasound as pretreatment to facilitate and enhance anaerobic digestion.

The effect of ultrasonic treatment depends on (i) the substrate characteristics such as total solids (TS) concentration, chemical and structural characteristics of the biomass and (ii) ultrasound treatment parameters such as specific energy input, ultrasonic intensity and ultrasonic density. The most common parameters used to specify the ultrasound pretreatment include:

Specific energy input ( $E_s$ ) can be calculated with the following equation:

$$E_s = \frac{P * t}{V * TS} \quad (8.1)$$



where  $P$  is the power (W),  $t$  is the sonication time (s),  $V$  is the sample volume (L) and TS is the initial total solids concentration (g TS L<sup>-1</sup>). The units of  $E_s$  are kJ kg<sup>-1</sup> TS<sup>-1</sup>, or kW s kg<sup>-1</sup> TS<sup>-1</sup>.

Ultrasound density ( $D$ ) is expressed in W L<sup>-1</sup> and it is calculated with the following equation:

$$D = \frac{P}{V} \quad (8.2)$$

Ultrasound intensity ( $I$ ) is expressed in W cm<sup>-2</sup> and it can be calculated with the following equation:

$$I = \frac{P}{A} \quad (8.3)$$

where  $A$  is surface area of the probe in cm<sup>2</sup>.

As shown in Eq. (8.1), the total solids concentration has a crucial role in performance and overall costs of the ultrasound pretreatment. Several pretreatments have shown their efficiency towards biomass disruption and subsequent methane production, nevertheless the energy and cost assessments have evidenced the need of increasing biomass concentration to attain a feasible operation from an economic and energy point of view [15, 16]. On the other hand, this initial TS concentration should be carefully chosen, since high TS concentration can hinder cavitation due to the viscosity increase [17].

Many ultrasound investigations are performed using equipment operating at 20–40 kHz. Hydro mechanical shear forces responsible for the ultrasound disruption effect occur at frequencies below 40 kHz, while sonochemical processes mediated by radicals' formation are mostly related to frequencies in the range of 200–1,000 kHz [18]. The radius of the bubbles formed during cavitation is inversely proportional to the ultrasound frequency. The application of high frequencies diminishes the occurrence of cavitation and hence the collapse of bubbles is also decreased [19]. Regarding the use of ultrasound for biomass disruption purposes, frequencies around 20–40 kHz have been reported to present the highest efficiency and thus, its effect is mainly attributed to the hydromechanical shear forces [18].

The above mentioned factors influence the overall phenomena and effects resulting from the interaction of the ultrasonic wave with the organic matter: frequency of the ultrasonic wave, intensity, the medium's physical structure and chemical constituents, and its acoustic coupling efficiency [11]. Without a doubt, sonication is one of the most powerful methods of disruption. Although it is a highly efficient pretreatment in terms of biomass disruption, the power consumption can become too high for economical application. Additionally, an effective biomass disruption does not always lead directly to methane production increase, due to either the formation of inhibitors or the mineralization of organic matter. The following sections will review the characteristics, different disruption pretreatments, and methane production yields enhancements achieved by applying ultrasound to the most common substrates anaerobically digested.

### 8.3 Ultrasound Enhanced Biogas Production from Lignocellulosic Materials

#### 8.3.1 Characteristics and Limitations of Lignocellulosic Materials as Substrate for Biogas Production

The term “lignocellulosic materials” comprises a wide range of organic matter, including plant waste material (straw, harvest residues), some energy crops, pulp and paper industry waste, organic fraction of municipal solid waste (OFMSW) and wood. All these materials have lignocellulose as one of the main compounds of their dry matter.

Chemically, lignocellulose is composed of polymeric lignin, cellulose and hemicelluloses (Fig. 8.2). The lignin fraction is responsible for the three-dimensional structure of the lignocellulose fibers. Lignin covers the fibers and binds the cellulose and hemicellulose. While both cellulose and hemicellulose are attacked by the anaerobic microorganisms, the lignin is hardly biodegradable due to its complex molecular structure. Therefore, the higher the lignin content, the lower is the biodegradability of the lignocellulosic materials [21]. Average lignin contents

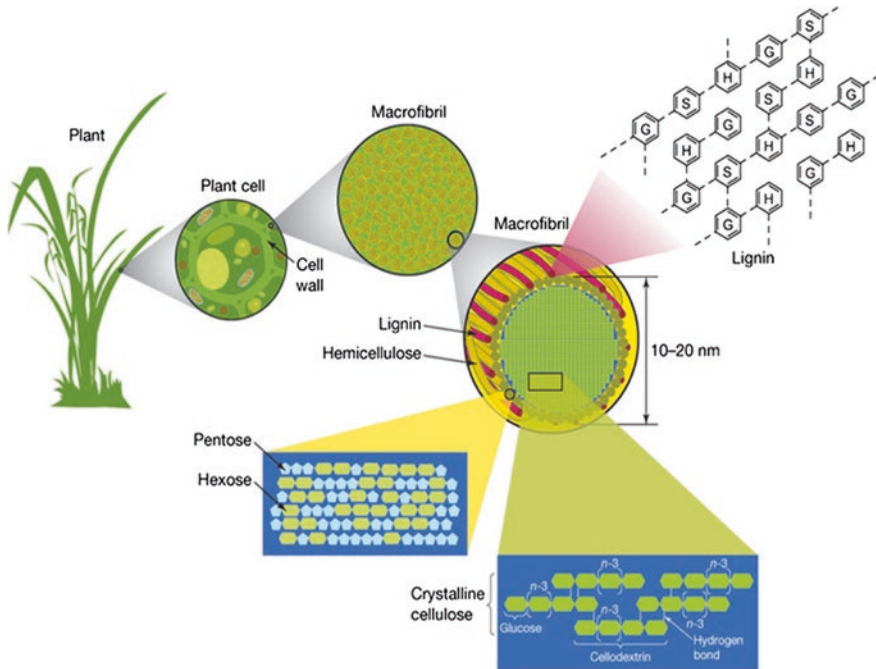


**Fig. 8.2** Lignocellulose structure where *H* is p-coumaryl alcohol, *G* coniferyl alcohol and *S* is sinapyl alcohol. Reprinted with permission from [20]. Copyright © 2008, Nature

may range 13–28 % in different substrates such as rice straw, bagasses, prunings and biomass energy crops (*Paulownia*, *Miscanthus*) [22, 23]. In this manner, even though the fiber fraction is accounting for organic matter content, its low availability decreases the methane yields achievable by digesting these substrates. Lignin content is not the only factor limiting the hydrolysis of lignocellulose. Other factors including cellulose crystallinity, degree of polymerization, moisture content and available surface area for enzymatic attack are also important parameters to take into consideration when digesting lignocellulosic materials [8].

The biochemical methane potential (BMP) for different lignocellulosic materials varies from 80 to 380 L CH<sub>4</sub> kg<sup>-1</sup> VS<sup>-1</sup>. The lowest values (78–100 L CH<sub>4</sub> kg<sup>-1</sup> VS<sup>-1</sup>) correspond to substrates such as grape stalks and wheat straw while the higher ones (317–384 L CH<sub>4</sub> kg<sup>-1</sup> VS<sup>-1</sup>) are reported for rice straw and thickened pulp mill waste [24–30]. The BMP of lignocellulosic substrates is mainly dependent on its chemical composition and structure. Lignocellulosic materials are abundant and they present high energy potential when subjected to anaerobic digestion. However, pretreatment is needed to increase their biodegradability.

### 8.3.2 Current Technologies to Improve Biogas Production of Lignocellulosic Materials

The objective of pretreatment applied to lignocellulosic materials prior to anaerobic digestion is to increase the bioavailability of the cellulose and hemicellulose fractions for the anaerobic microorganisms. Pretreatment aims at increasing the methane production rate and yield. Physical, chemical and biological pretreatment have been proposed with this objective.

Chemical pretreatment consists in the addition of chemical reagents to the substrate at different conditions of temperature and time. The chemicals include alkalis, acids and strong oxidizers. Most of these treatments can double the methane production of lignocellulosic materials such as straw, bagasses, stalks or OFMSW at chemical loadings of 1–10 % (w w<sup>-1</sup> dry matter basis [21]). Nevertheless, the chemical pretreatment exhibits some disadvantages as well. Alkali treatment is carried out frequently by NaOH addition. This addition concomitantly results in high Na<sup>+</sup> concentrations, which may hinder the anaerobic digestion, if the concentration is above 5.6–53 g L<sup>-1</sup> [5]. On the other hand, acid treatment requires neutralization prior to the anaerobic digestion so that the pH of the feed is compatible with the pH required for optimum activity of anaerobic microorganisms (pH 6.5–8.0). Strong oxidizers (peroxides, ozone) can lead to the formation of inhibitors or organic matter mineralization depending on the dose and the chemical composition of the substrate [31]. Although chemical pretreatment improves the methane production, careful selection of the reagents to be added and treatment conditions is required so that the subsequent anaerobic digestion is not negatively affected [21].

Biological pretreatment involves the action of fungi, enzymes and microbial consortia. Compared to other pretreatment technologies, biological approaches require less energy input and no chemical addition. However, the treatment times are usually long (ranging from days to weeks in the case of fungal or microbial treatments), and the treatment itself can consume part of the organic matter that otherwise should be available for biogas production [21].

The key issue in the pretreatment is the selection of the most adequate enzyme, fungi and microbes, as well as the treatment conditions (temperature, time, pH) to enhance the treatment effect. Methane yield increases up to 96 % have been observed for cassava residues when treated with a cellulose-degrading microbial consortium [32]. Likewise, combination of enzymatic activities (cellulase and hemicellulase) has resulted in higher methane yields than using these enzymes individually [33, 34].

Size reduction is the most widespread pretreatment for all kinds of lignocellulosic materials. Depending on the technology used, the particle size is different. Milling and grinding provides particles ranging 0.2–2 mm while chipping results in particles of 10–30 mm [35]. The increase of methane yield can reach 30 % when applying size reduction in the range of 0.003–30 mm to straw, grass or OFMSW. However, this process is very inefficient in terms of energy that is high energy consumption versus energy produced with the pretreated material, and it is not able to remove the lignin, which is the main barrier for the biogas production since it links the biodegradable cellulose and hemicellulose, limiting their bioavailability [21]. An alternative size reduction technology is extrusion. Extrusion is an industrial process that is usually employed for creating products (metals, plastics, food, etc.) with a fixed cross-section. The whole process includes a pre-heating of the material, loading it into the press container and applying the pressure. This technology is more energy efficient with less energy consumption for similar energy production enhancement achieved by other treatments and produces a high methane yield (70 % enhancement for barley straw [36]).

Thermal treatments include several technologies that differ on the methodology employed for heat supply: high pressure saturated steam (steam explosion), or liquid hot water (hydrothermolysis). When using the steam explosion, the hemicellulose is hydrolyzed and the lignin is redistributed [37]. The efficiency of the pretreatment can be further enhanced by the addition of chemicals. The selection of appropriate treatment conditions is critical, since inadequate conditions may result in negative effects on the methane yield. In some cases, degradation of some compounds, that otherwise would be converted to biogas, are transformed in other by-products that can act as inhibitors of the digestion [21]. For example, hydroxymethylfurfural and furfural formation leading to 50 % inhibition of the anaerobic digestion was observed in the steam explosion of *Arundo donax* at 180 °C and 10 min when adding H<sub>2</sub>SO<sub>4</sub> as catalyst [38]. Steam explosion at 180 °C for 15 min can lead to methane yield increases up to 20 % in wheat straw [39]. Hydrothermolysis acts similarly to steam explosion, but uses liquid water instead of steam and the amount of inhibitors generated is low. Using this technology, methane yield enhancement can reach 220 % for rice straw pre-treated at 200 °C for 10 min [26].

Irradiation treatments include mainly microwave and ultrasound. Compared to conventional thermal treatment, microwaves heat the substrates faster and

therefore reduce the treatment cost. However, it can lead to the formation of refractory and/or inhibitory compounds when applied to lignocellulosic materials [21]. Ultrasound treatment increases the biodegradability of lignocellulosic biomass by attacking the fibers cell walls, increasing the specific surface area, and reducing the polymerization degree. At industrial level, physical pretreatments are common before anaerobic digestion, while chemical or enzymatic pretreatments are mostly employed prior to bioethanol production.

### ***8.3.3 Ultrasound Enhanced Biogas Production of Lignocellulosic Materials***

The great majority of investigations have been conducted on sewage sludge, and few studies with lignocellulosic biomasses have been reported (Table 8.1). The ultrasonic treatment applied to lignocellulosic materials has resulted in cellulose and hemicellulose extraction from the fibers [45].

The TS content influences the required energy for the treatment (Eq. 8.1, Sect. 8.2). More specifically, lower energy levels are required at higher TS concentration since cavitation bubbles have more probabilities to find the particles [46]. However, according to Cesaro et al. [43] there is also an upper limit (5–10 % TS) that should not be exceeded for an optimum methane production with sonicated substrates. Low frequency treatment is recommended for sonication as pretreatment to enhance methane production of lignocellulosic materials [45, 46]. All studies reported in Table 8.1 have been carried out at 20–30 kHz. The specific energy input reported in the ultrasound treatment studies ranges 2–600 MJ kg<sup>-1</sup> TS<sup>-1</sup> and the ultrasound densities range 0.37–1 W mL<sup>-1</sup>.

There are several industrial applications of ultrasound pretreatment in industrial scale plants for biogas production. In some German biogas plants operated with energy crops, this pretreatment has been applied with the aim to increase the biogas production of the substrate. Ultrasonic treatment is applied mainly in a bypass system, where part of the digester content (usually 30 %) is pretreated with ultrasound [47].

#### **8.3.3.1 Organic Matter Solubilisation**

Normally, solubilization of organic matter increases with the specific energy applied. However, there is a limit, possibly due to mineralization of the substrate [21, 48]. This mineralization converts the organic matter into inorganic matter, as demonstrated by an increment of ash at high (160 W cm<sup>-2</sup>) ultrasound intensities applied to plant material [48], and hence it is not available for the anaerobic microorganisms. There is no consensus in the literature about this specific energy input threshold, however some authors have suggested this limit is in the range of 15–24 MJ kg<sup>-1</sup> TS<sup>-1</sup> depending on the lignocellulosic materials targeted [42, 43]. The data reported in the literature are not enough to determine if this limit depends

**Table 8.1** Summary of literature review on ultrasound treatment prior to anaerobic digestion of lignocellulosic materials

Substrate	Substrate data			US equipment data				US treatment data			BMP test data			Reference
	TS (g L <sup>-1</sup> )	VS (g L <sup>-1</sup> )	COD (g L <sup>-1</sup> )	Power (W)	Tip diameter (mm)	Frequency (kHz)	US density (W mL <sup>-1</sup> )	T max (°C)	E <sub>s</sub> (kJ kg <sup>-1</sup> TS <sup>-1</sup> )	Time (minutes)	T (°C)	HRT (days)	CH <sub>4</sub> yield untreated material (mL CH <sub>4</sub> g <sup>-1</sup> VS <sup>-1</sup> )	
Paper mill waste (mixed sludge)	-	9	16	400	12.7	20	1	55	-	15	35	43	114	23
	-	-	-	-	-	-	-	-	60	30	35	43	114	27
	-	-	-	-	-	-	-	-	90	60	35	43	114	48
Paper mill waste	-	8.2	15	400	12.7	20	1	55	-	15	55	43	94	5
	-	-	-	-	-	-	-	-	30	30	55	43	94	23
	-	-	-	-	-	-	-	-	60	60	55	43	94	31
Paper mill waste	22	18	34	400	12.7	20	1	55	83,758	60	35	43	123	54
	-	-	-	-	-	-	-	-	117,719	90	55	43	94	43
	-	-	-	-	-	-	-	-	117,719	90	55	43	94	38
Paper mill waste	-	-	-	-	-	-	-	-	15	30	35	43	139	41
	-	-	-	-	-	-	-	-	60	60	35	43	139	33
	-	-	-	-	-	-	-	-	90	90	35	43	139	45
Paper mill waste	-	8.2	15	400	12.7	20	1	55	-	15	55	43	174	51
	-	-	-	-	-	-	-	-	30	30	55	43	174	12
	-	-	-	-	-	-	-	-	60	60	55	43	174	5
Paper mill waste	25	20	40	400	12.7	20	1	55	117,719	90	35	43	150	20
	-	-	-	-	-	-	-	-	117,719	90	55	43	190	28
	-	-	-	-	-	-	-	-	117,719	90	55	43	190	28
Sunflower cake	20	19	25	120	-	20	0.48	20	24,000	16.6	-	-	188	54
	-	-	-	-	-	-	-	-	96,000	60.6	-	-	188	54
	-	-	-	-	-	-	-	-	192,000	133.3	35	7	188	54
OFMSW digestate	50-100	-	-	1,000	-	20	0.37	-	432,000	300	-	-	-	46
	-	-	-	-	-	-	-	-	597,600	331.2	-	-	-	60
	-	-	-	-	-	-	-	-	2,102	5	-	-	-	71
Rice straw + NaOH	263	234	-	750	13	20	-	15,000	4,219	10	35	15	-	16
	-	-	-	400	-	30	-	-	6,291	15	-	-	-	16
	-	-	-	-	-	-	-	-	-	-	-	-	-	41.8

 $E_s$  specific energy input $T$  temperature $HRT$  hydraulic retention time

on the substrate characteristics, the ultrasound equipment specifications or the operating conditions of the treatment. Probably, all these factors affect organic matter solubilization and mineralization.

The solubilization degree depends on the substrate composition and the ultrasound treatment conditions. For instance, Fernández-Cegrí et al. [42] reported 14–21 % chemical oxygen demand (COD) solubilisation when applying  $E_s$  of 24–597 MJ kg<sup>-1</sup> TS<sup>-1</sup> to sunflower cake. Slightly higher values were attained for the organic fraction of municipal waste (OFMSW). In this case, COD solubilisation of 22–53 % was recorded when this substrate was pretreated at specific energy levels of 2.1–6.3 MJ kg<sup>-1</sup> TS<sup>-1</sup> [43].

### 8.3.3.2 Enhanced Methane Production

The solubilisation of organic matter is not directly related to methane yield enhancement. Depending on the substrate's nature, COD solubilization can give a decrease in the methane potential [40, 41]. This is explained by the polymerization reactions initiated by radicals formed during ultrasound treatments under certain conditions that lead to difficult to biodegrade compounds.

Methane production yields increase after ultrasound treatment of lignocellulosic materials range from 5 to 71 %. This variation is due to the composition of the substrates and the ultrasound treatment conditions. The methane production was increased by approximately 50 % at  $E_s$  of 84–118 MJ kg<sup>-1</sup> TS<sup>-1</sup> applied to paper mill waste [41, 42]. For sunflower cake, the methane yield increase was similar (54 %) to that of the paper mill waste, but this value was attained with considerably lower  $E_s$  input (24 MJ kg<sup>-1</sup> TS<sup>-1</sup> [42]). Higher methane production yields increase were achieved (46–71 %) with lower specific energy inputs (2.1–6.3 MJ kg<sup>-1</sup> TS<sup>-1</sup>) in the case of ultrasound pretreatment of digested OFMSW [43]. On the other hand, lower results (only 16 % improvement with regard to the fresh substrate methane yield) were recorded for grounded raw OFMSW after applying 15 MJ kg<sup>-1</sup> TS<sup>-1</sup> [31]. In this manner, these studies clearly showed that despite using similar  $E_s$ , the different substrate targeted for pretreatment is of great importance since some of them may be more amenable towards ultrasound.

## 8.4 Ultrasound Enhanced Biogas Production From Livestock Wastes (Manure)

### 8.4.1 *Characteristics and Limitations of Livestock Wastes (Manure) as Substrate for Biogas Production*

The current intensive and concentrated farming activity in Europe is leading to a large amount of livestock wastes. The high organic matter and nutrient content of those wastes could result in pollution of the environment when not properly



treated. Anaerobic digestion offers several environmental advantages such as the reduction of organic matter, greenhouse gas emissions and odors from manure.

High water content coupled with the recalcitrant nature of the organic matter in manure (fibers) result in low methane yields, rendering this material a poor substrate for anaerobic digestion [49]. However, manure presents some advantages as substrate for anaerobic digestion since it has a high buffer capacity and provides nutrients (i.e. nitrogen and trace elements) for anaerobic microorganisms' growth. Different from other substrates, such as crops, manure is produced during the entire year and thus it is not seasonally dependent. Moreover, anaerobically digested manure results in a digestate that could be easily used for fertilizing purposes [50].

Methane yields of manure are in the range of 130–240 L CH<sub>4</sub> kg<sup>-1</sup> VS<sup>-1</sup> [51, 52]. To obtain a more economically feasible process in manure-based biogas plants, methane yield enhancement is currently a major issue. Methane yield can be increased by co-digesting manure with cheap carbon-rich substrates or by applying pretreatments to the manure. Regarding the second option, a primary mechanical treatment involving solid–liquid separation is considered to be a low-cost technology for increasing manure biogas yield since 90–95 % of the manure is water. The solid fraction may be used for biogas production after that separation. This strategy would reduce transport costs, but still, secondary pretreatment to increase the biodegradability of the lignocellulosic fibers, thus enhancing biogas production from manure, is necessary [53].

#### ***8.4.2 Current Technologies to Improve Biogas Production***

The ultimate effect of pretreatment on manure fibers is to increase the methane yield by increasing the organic matter fraction available to optimise methanogenic microorganism's performance. Most of the research has been focused on studying the effect of thermal and chemical pretreatment applied to manure. Thermal pretreatment results in solubilization of organic matter (hemicellulose) and increases the surface area for enzymatic attack [54, 55]. The positive effects of thermal pretreatment on the anaerobic digestion generally increase when applying temperatures in the range of 60–190 °C [56]. However, the formation of refractory compounds towards anaerobic digestion has been reported when working at temperatures higher than 100 °C [53]. Carrère et al. [56] observed that the solubilization of organic matter was not directly correlated with the biodegradability but with the reduction of hemicellulose fraction of fibers contained in the manure. According to this study, the positive impact of the thermal pretreatment on the methane yield started at 70 °C for the liquid fraction of hog manure, while 130 °C were necessary in the case of the total fraction. These authors reported maximum methane yield improvements of 121 and 64 % when applying 190 °C for 20 min to the liquid and the total fraction of hog manure, respectively. Similarly, wet explosion pretreatment, involving thermophysical effects, has been correlated to the organic composition of the substrate. This technology is more efficient when



treating the recalcitrant fraction left in manure fibers after anaerobic digestion [57]. In this way, methane yield in digested manure fibers was increased by 163 % after wet explosion treatment at 180 °C for 10 min and 1 MPa [58].

Despite the risk of inhibitory compounds generation, the addition of chemicals to the thermal treatment of manure has generally improved the results with regard to methane production. In this manner, methane yield increase of 78 % was obtained when adding an alkali reagent to reach a pH of 10 combined with high temperatures (190 °C and 20 min), while an inhibition of the anaerobic process was reported when working at pH 12 [56]. On the other hand, when working at lower temperatures (32 °C), an increase of 13 % in methane production was obtained treating the solid fraction of hog manure with a strong alkali for 24 h [59].

### ***8.4.3 Ultrasound Enhanced Biogas Production of Livestock Wastes (Manure)***

Few studies have been carried out applying ultrasounds to livestock waste. The effect of ultrasonic pretreatment on manure results in particle size reduction and solubilization of organic matter. The bioavailability of organic matter contained in manure fibers is increased and hence, the hydrolysis rate during the anaerobic digestion is improved. As a consequence of the higher bioavailability of the organic matter after the pretreatment, methane production is enhanced. This approach has been shown to be beneficial for manure digestion by decreasing hydraulic retention times in continuous operation and reducing odor emissions [60, 61]. At this point, it should be stressed out that manure seems to be a good substrate for ultrasound pretreatment prior to anaerobic digestion in terms of energy consumption. In this manner, specific energy inputs in the range of 0.5–7.5 MJ kg<sup>-1</sup> TS<sup>-1</sup> applied to manure were necessary to obtain the same efficiencies than those obtained at 20–30 MJ kg<sup>-1</sup> TS<sup>-1</sup> in sewage sludge [62]. This would mean that manure is around 6–8 times more degradable when pretreated with ultrasound than sewage sludge.

#### **8.4.3.1 Organic Matter Solubilisation**

The effect of ultrasonic pretreatment has been studied for chicken, dairy and hog manure, as well as for different manure-based co-digestions, namely cattle manure and animal by-products (ABP), cattle manure and glycerin or cattle manure supplemented with food waste and sewage sludge (Table 8.2). In all these cases, organic matter solubilisation was observed after the ultrasonic pretreatment. Elbeshbishy et al. [62] studied the effect of different specific energy inputs ( $E_s$ ) on hog manure organic matter solubilization, obtaining the maximum solubilization (27 % when compared to the untreated manure) at the highest  $E_s$  tested (30 MJ kg<sup>-1</sup> TS<sup>-1</sup>). Similar results for organic matter solubilization were

reported by Luste and Loustarinen [51] who worked with cattle manure at lower  $E_s$ . In this case, 22–27 % increase in soluble organic matter was obtained for  $E_s$  inputs of 6 and 9 MJ kg<sup>-1</sup> TS<sup>-1</sup>. However, these authors also observed that higher  $E_s$  (14 MJ kg<sup>-1</sup> TS<sup>-1</sup>) resulted in lower soluble organic matter than the untreated cattle slurry. Due to the long duration of this ultrasound pretreatment, a decrease in soluble organic matter was attributed to the degradation, evaporation or precipitation of soluble materials or pyrolysis reactions inside the cavitation bubbles. In some cases, low organic matter solubilisation was obtained after the ultrasonic pretreatment, but the methane yield increase was enhanced when compared to the raw manure. For those cases, the ultrasound pretreatment was related to an increase in organic matter bioavailability rather than solubilization [63, 64].

#### 8.4.3.2 Enhanced Methane Production

Compared to untreated manures, different types of livestock wastes (chicken, hog and cattle) pretreated with ultrasound have exhibited methane yields improvements ranging 15–41 %. In general, low specific energy inputs (up to 0.76, 0.50 and 6 MJ kg<sup>-1</sup> TS<sup>-1</sup> for chicken, hog and cattle manure, respectively) and low sonication times were necessary to obtain those methane yields improvements (Table 8.2). The increased bioavailability of the substrate after the ultrasonic pretreatment seemed to be responsible for the increased methane yields in most of the cases [51, 62, 63]. More specifically, in the case of cattle manure, the methane yield enhancement was related to the disruption of lignin-cellulose bonds since lignin-related compounds concentration was increased by 32 % during the pretreatment [51].

Likewise, the effect of ultrasonic pretreatment has also been studied on the anaerobic co-digestion of livestock wastes. The addition of animal by-products (ABP) to cattle manure in a ratio 1:3 resulted in methane yield increase of 11–13.3 % after sonication at 1 and 6 MJ kg<sup>-1</sup> TS<sup>-1</sup>, respectively [64]. In this context, it can be observed that increasing  $E_s$  applied by 6-fold did not increase significantly methane yield. The effect of ultrasonic pretreatment on the co-digestion of cattle manure and glycerin (6 % in volume) has been studied under batch and continuous operation. Specific energy in the range of 1.1–1.3 MJ kg<sup>-1</sup> TS<sup>-1</sup> applied to the mixture of cattle manure and glycerin resulted in a maximum methane yield of 174 L CH<sub>4</sub> kg<sup>-1</sup> VS<sup>-1</sup> under batch anaerobic digestion at 55 °C [60]. The same mixture of substrates was tested in continuously fed reactors and the methane yield increased up to 590 L CH<sub>4</sub> kg<sup>-1</sup> VS<sup>-1</sup>, using an induced bed reactor working at 18 days HRT (OLR of 6.4 kg<sup>-1</sup> COD m<sup>-3</sup> day<sup>-1</sup>) [60, 65]. In the case of other co-digestion products such as cattle manure, food waste and sewage sludge, higher energy inputs (7.5 MJ kg<sup>-1</sup> TS<sup>-1</sup>) were required to improve biogas production [61, 66]. Nevertheless, the low methane yield increase (2–4 %) reported for cattle manure with food waste and sewage sludge did not justify the use of ultrasound.

**Table 8.2** Summary of literature review on ultrasound treatment prior to anaerobic digestion of manures

Substrate	Total solids (%)	Volatile solids (%)	Specific energy input (KJ Kg <sup>-1</sup> TS <sup>-1</sup> )	Time (minutes)	Reactor	T (°C)	HRT (days)	OLR (g VS L <sup>-1</sup> d <sup>-1</sup> )	CH <sub>4</sub> yield untreated (mL CH <sub>4</sub> g <sup>-1</sup> VS <sup>-1</sup> )	Increase in CH <sub>4</sub> yield after ultrasound (%)	Reference
Chicken manure	5	4.25	245	1	Batch	37	-	-	278	29	[63]
	5	4.25	306	2	Batch	37	-	-	278	41	
	5	4.25	398	1	Batch	37	-	-	278	27	
	5	4.25	520	2	Batch	37	-	-	278	41	
	5	4.25	612	1	Batch	37	-	-	278	31	
	5	4.25	765	2	Batch	37	-	-	278	36	
Hog manure	9.3	6.7	500	*	Batch	37	-	-	n.f.	28	[62]
	9.3	6.7	30,000	*			-	-	n.f.	21	
Cattle manure	5.8	4.4	6,000	*	Batch	35			210	15	[51]
	5.25	3.51	3,000	1-8	Batch	35			24**	121	[60]
Screened cattle manure	7.2-7.5	5.9-6.2	6,000	*	Batch	35			300	13.3	[64]
	7.4-7.7	6.1-6.3	6,000	*	CSTR	35	21	3	260	12	
	7.2-7.5	5.9-6.2	1,000	*	CSTR	35	21	3	270	11	

(continued)

Table 8.2 (continued)

Substrate	Total solids (%)	Volatile solids (%)	Specific energy input (KJ Kg <sup>-1</sup> TS <sup>-1</sup> )	Time (minutes)	Reactor	T (°C)	HRT (days)	OLR (g VS L <sup>-1</sup> d <sup>-1</sup> )	CH <sub>4</sub> yield untreated (mL CH <sub>4</sub> g <sup>-1</sup> VS <sup>-1</sup> )	Increase in CH <sub>4</sub> yield after ultrasound (%)	Reference
Cattle manure + glycerin (6 %)	7.2	5.8	1,100–1,300	4	CSTR	55	18	3.24	166**	99	[65]
	7.2	5.8	1,100–1,300	4	CSTR	55	20	2.91	166**	261	
	6.9	5.2	1,100–1,300	4	CSTR	55	22	2.35	166**	27	
	9	6.7	1,100–1,300	4	IBR	55	16	4.17	166**	n.f.	
	9	6.7	1,100–1,300	4	IBR	55	18	3.71	166**	255	
	10.9	6.6	1,100–1,300	4	IBR	55	20	2.75	166**	219	
Cattle manure + food waste + sewage sludge (7:2:1 w/w/w)	3.5–4.5	2.2–3.4	7,500	*	CSTR	36	22	1.2	603	2	[66]
	3.5–4.5	2.2–3.4	7,500	*	CSTR	55	22	1.2	424	3.8	
Cattle manure + food waste + Sewage sludge (7:1:2 w/w/w)	3.5–4.5	2.2–3.4	7,500	*	CSTR	36	22	1.2	473	3	

(continued)

Table 8.2 (continued)

Substrate	Total solids (%)	Volatile solids (%)	Specific energy input (KJ Kg <sup>-1</sup> TS <sup>-1</sup> )	Time (minutes)	Reactor	T (°C)	HRT (days)	OLR (g VS L <sup>-1</sup> d <sup>-1</sup> )	CH <sub>4</sub> yield untreated (mL CH <sub>4</sub> g <sup>-1</sup> VS <sup>-1</sup> )	Increase in CH <sub>4</sub> yield after ultrasound (%)	Reference
Cattle manure + food waste + sewage sludge (7:2:1 w/w/w)	1.5–2.4	0.9–1.3	7,500 (manure sonicated)	*	CSTR	36	22	1.5–2.2	603	-38	[61]
	1.9–2.9	1.0–1.4		*	CSTR	36	20	1.9–2.6	546	-29	
	1.5–3.1	0.8–1.2		*	CSTR	36	18	1.7–2.5	431	-2	
	2.1–2.4	1.1–1.4	7,500 (manure and sludge sonicated)	*	CSTR	36	22	1.9–2.4	603	-29	
	1.9–2.4	1.0–1.3		*	CSTR	36	20	1.9–2.4	546	-16	
	1.5–3.1	0.8–1.3		*	CSTR	36	18	1.7–2.7	431	-6	
	1.9–2.8	1.1–1.9	7,500 (manure sonicated)	*	CSTR	55	22	1.9–2.2	424	-1	
	1.7–3.3	1.0–1.8		*	CSTR	55	20	1.9–2.6	423	-7	
	1.8–3.1	1.0–1.4		*	CSTR	55	18	2.1–2.9	329	41	
	2.0–2.8	1.0–1.3	7,500 (manure and sludge sonicated)	*	CSTR	55	22	1.7–2.2	424	-17	
1.7–3.5	1.0–1.8		*	CSTR	55	20	1.9–3.4	423	-10		
1.8–2.7	1.0–1.8		*	CSTR	55	18	2.1–3.8	329	21		

T digestion temperature

HRT hydraulic retention time

OLR organic loading rate

\*Sonication time is dependent on specific energy input and percentage of TS, \*\*Average ref number found literature n.f not found

## 8.5 Ultrasound Enhanced Biogas Production from Sludge

### 8.5.1 Characteristics and Limitations of Activated Sludge Biomass as a Substrate for Biogas Production

Sewage sludge is an undesired by-product of wastewater treatment, which is produced by a solid separation step before biological treatment (primary sludge), and a solid separation step after the biological treatment [secondary sludge or waste activated sludge (WAS)]. The management of WAS becomes more and more important as it makes up to 60 % of the capital costs of wastewater treatment plants [67]. Moreover, due to enforcement of environmental regulations, regarding the disposal and effluent quality, the economic costs of wastewater treatment and especially sewage sludge production are rising [68]. Therefore, adequate management of sewage sludge is required. This management must be focused on mass reduction, reduced disposal costs, and recycling of nutrients and bio-energy production to increase revenue [69]. In wastewater treatment, anaerobic digestion is widely applied on a mixture of primary and waste activated sludge for stabilization, reduction of sludge quantity and production biogas. However, WAS is difficult to digest which results in high economical costs and, therefore, limited feasibility of this technology. The cell wall of aerobic microorganisms contained in WAS limits its anaerobic digestion by reducing the availability of readily biodegradable organic compounds. Biodegradable organic compounds are present in sewage sludge cells but unavailable. To improve the feasibility of anaerobic digestion, intracellular readily biodegradable compounds should be liberated and the hydrolysis stage must be improved [70, 71]. Hydrolysis can be improved by an increase of accessibility of the WAS for the anaerobic bacteria and enzymes performing the hydrolysis (Fig. 8.3). In order to do so, biomass components are rendered more accessible for anaerobic digestion through different pretreatments.

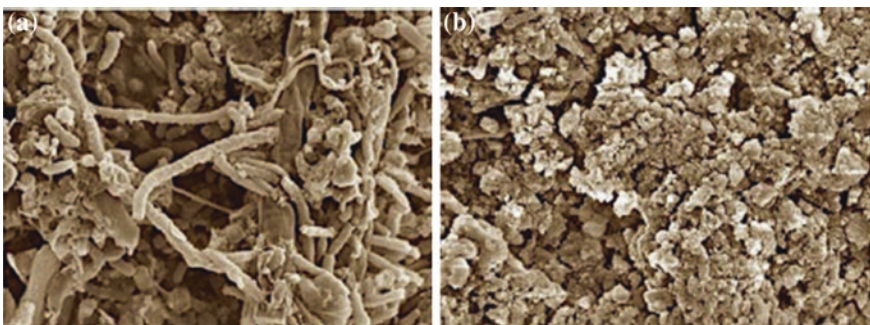


**Fig. 8.3** Scanning electronic microscopic photographs of bacterial WAS cells before (a) and after pretreatment (b). Reprinted with permission from [72]. Copyright © 2013, Elsevier

### ***8.5.2 Current Technologies to Improve Biogas Production of Waste Activated Sludge***

Extensive research has been carried out to establish the best economically feasible pretreatment technology to enhance sludge digestibility. Various pretreatment methods have been tested and reported to enhance the sludge disintegration and solubilization. Thermal hydrolysis and mechanical treatments are the most used ones. Thermal pretreatment offer several advantages including sludge sanitation and easier handling due to the reduced viscosity [73]. Studies regarding thermal pretreatment of WAS have pointed out an optimum temperature range of 160–180 °C and treatment times of 30–60 min [46]. Methane yields of substrates pretreated at those temperatures have exhibited 40–100 % increase of methane production. Higher temperatures have conducted to the formation of melanoids (difficult to digest anaerobically) through Maillard reactions taking place between carbohydrates and aminoacids [74]. Similarly, the addition of chemicals often results in subsequent inhibition of anaerobic digestion due to the formation of inhibitors. Alkali or hydrogen peroxide addition and ozonation are the most common pretreatments encountered in literature. Nevertheless, the oxidative strength of these chemicals may result in destruction of organic matter and thus hinder methane production. An in depth review on this topic can be found elsewhere [46]. Pretreatment of sludge is required to rupture the cell wall and to facilitate the release of intracellular matter into the aqueous phase to increase biodegradability. However, economic constraints of these technologies have limited their scale-up implementation.

### ***8.5.3 Ultrasound Enhanced Biogas Production of Waste Activated Sludge***

The objective of ultrasonic pretreatment is to disrupt and breakdown activated sludge bacterial cell walls to liberate the readily biodegradable intracellular material and thus to increase the availability of non-readily biodegradable material for hydrolysis. When using this substrate, the effect of the ultrasonic pretreatment is evaluated based on parameters relevant for sludge management: (i) physical parameters: particle size distribution, settleability and dewaterability, (ii) chemical parameters: soluble chemical oxygen demand, and total volatile suspended solids, (iii) biological parameters: oxygen uptake and digestibility of the sewage sludge and (iv) energy balance of the sludge management.

#### **8.5.3.1 Ultrasound Can Cause Two Effects: Biocatalysis Stimulation and Organic Matter Solubilisation (Sludge Disintegration)**

Ultrasound applied on activated sludge has two effects, namely stimulation of enzymatic activities and organic matter solubilization. The former effect entails a biological effect that stimulates enzymes release and activity. Anaerobic digestion is a

biological process and therefore the importance of these enzyme activities enhancements may be inferred. It seems that during ultrasound treatment of WAS, two mechanisms can increase enzymes activity. On one hand, the enzymes contained within the sludge flocs can be released to the medium and thus the biological process is improved. On the other hand, the second mechanism involves the weakening of cell wall/membrane of the microorganisms in the sludge, and hence decreasing the permeability and improving enzymes transport [75]. This enzyme activity stimulation is energy dependent. Each enzyme can handle different energy inputs [76]. Enzymatic activities are markedly influenced by sonication time and power density [77]. For instance, protease and lipases are hydrolytic enzymes extracted from waste activated sludge at frequency of 24 kHz and 3.9 W mL<sup>-1</sup> [78]. Some other enzymes released upon ultrasonic energy application from this substrate include  $\beta$ -glucosidase, acid and alkaline phosphatase [79]. Those enzymes are related to the hydrolysis of proteins and carbohydrates. Noteworthy to mention that this approach should be conducted at low temperature in order to avoid denaturalization of enzymes released during the ultrasound pretreatment. Microbial activity is enhanced when sludge disintegration is low and vice versa [76]. In addition to the enzymes released by the activated sludge, which in this case is the substrate, the methanogens (microorganisms involved in biogas production) also have been reported to release or increase the activity of certain enzymes upon ultrasound application [80].

While this biocatalysis stimulation is not so developed, the ultrasound pretreatment to disrupt WAS has been studied in depth. Sludge solubilisation is taking place above a threshold of specific energy ranging 1–16 MJ kg<sup>-1</sup> TS<sup>-1</sup> [46]. Soluble COD increase is often used as a key indicator of WAS disruption. As a matter of fact, some investigations have concluded that there is a direct relationship between the percentage of soluble COD released during the pretreatment and the methane production enhancement. Regarding COD solubilisation, Bougrier et al. [81] observed a concomitant increase of organic matter solubilisation at increasing  $E_s$  supplied in the range of 0–10 MJ kg<sup>-1</sup> TS<sup>-1</sup>. The highest solubilisation (32 %) was recorded at 10 MJ kg TS<sup>-1</sup>. After this energy level, the COD remained mostly constant. Similarly, Tiehm et al. [18] also concluded that the degree of sludge disintegration was directly related to the specific energy applied. This investigation also studied the effect of ultrasound frequency and the results showed that increasing frequencies diminished organic matter solubilisation. This fact was attributed to the formation of large cavitation bubbles that mediated the formation of radicals rather than the hydromechanical shear forces required for an optimum biomass disruption. When compared to other pretreatments, the nature of the organic matter released seemed different. Despite the lower solubilization degree (15–17 %) achieved during ultrasound pretreatment at 6.2 and 9.3 MJ kg<sup>-1</sup> TS<sup>-1</sup>, the organic matter was biodegraded rapidly, whereas higher solubilization percentages (42–48 %) were reached with thermal application of 170–190 °C; this resulted in less biodegradable organic matter [68]. The reason for this behavior was the different effect produced under both scenarios. While the thermal pretreatment solubilized the organic matter (polymers degradation), the main effect of sonication was the disruption of the biomass.



Soluble COD entails the contribution to the organic chemical demand of the different macromolecules present in the bacterial cells. The relationship between biogas production and the different macromolecules (proteins, carbohydrates and lipids) cannot be neglected. According to Angelidaki and Sanders [82], proteins and carbohydrate specific methane yield range 496 and 415 L CH<sub>4</sub> kg<sup>-1</sup> VS<sup>-1</sup>, respectively. Although lipids exhibit the highest energy content (1,014 L CH<sub>4</sub> kg<sup>-1</sup> VS<sup>-1</sup>), these macromolecules represent a small fraction of WAS. Taking a closer look into the macromolecules released by this substrate upon ultrasound pretreatment, proteins solubilization prevailed over carbohydrates. More specifically, proteins and carbohydrates solubilization increased 68.2 and 10-fold with regard to the raw WAS when applying 90 MJ kg<sup>-1</sup> TS<sup>-1</sup> [79]. Lower  $E_s$  provided similar trend. In this context,  $E_s$  of 3 MJ kg<sup>-1</sup> TS<sup>-1</sup> enhanced the solubilization of proteins by 15.9-fold while the effect on carbohydrates was mostly negligible. Overall, this study demonstrated that at the highest  $E_s$  tested 50 and 24 % of the total proteins and carbohydrates contained in the activated sludge were solubilized.

### 8.5.3.2 Enhanced Methane Production

Ultrasonic pretreatment of bacterial cells is a promising technology to improve sludge anaerobic digestion by causing the release of intracellular organic matter and cell lyses [83–85]. This enhances the hydrolysis step of WAS and directly results in an augmented methane generation and a decrease in solid biomass. Ultrasonic sludge disintegration is most effective at low ultrasound frequencies [86]. Tiehm et al. [86] investigated the effect of ultrasound pretreatment on the digestibility of WAS with batch anaerobic digestion tests at different hydraulic retention times (22, 16, 12, and 8 days). The results showed that with ultrasonic pretreatment there was a reduction in the biosolids concentration and an increase in the methane production. At long retention times (HRT of 22 days), the reduction of volatile solids increased from 45.9 % in the raw sludge to 50.3 % with pretreated substrate, while the effect of ultrasound at short retention times (8 days) affected biogas productivity. More specifically, the biogas productivity increased from 36.6 L day<sup>-1</sup> for the raw sludge to 100 L day<sup>-1</sup> for the pretreated sludge. These results are similar to the ones obtained by Bougrier et al. [68]. This study showed methane production increase of 47.1 and 51.1 % when applying  $E_s$  of 6.2 and 9.3 MJ kg<sup>-1</sup> TS<sup>-1</sup>. These results clearly indicated an improvement of the biodegradability of WAS; however, the sludge did not become fully biodegradable.

The treatment time or specific applied energy has a positive effect on the ultrasonic pretreatment [86]. The methane production was respectively 1.84, 1.77, 2.24, 2.57, 2.53 L at pretreatment duration of 0, 7.5, 30, 60 and 150 min, respectively [18]. Regarding the  $E_s$  applied, there is a threshold of 1 MJ kg<sup>-1</sup> VS<sup>-1</sup>, below which the effect of the ultrasound pretreatment is limited to reduce floc size and cell disruption is not observed [81]. This means that below this threshold organic matter is not released into the liquid phase. Hence, the increase in methane

production is only due to the increased superficial bioavailability of organic matter, i.e. floc size reduction.

Methane production is proportional to the net rate of particle solubilization in the anaerobic digester, and thus the importance of working with the optimum inoculum concentration can be inferred [71, 87]. To investigate this, Braguglia et al. [88] evaluated the combined effect of the food/inoculum ratio and ultrasonic pretreatment on the digestibility of WAS. The methane production augmented concomitantly with increasing feed/inoculum ratio. This clearly indicated that the solubilization (hydrolysis stage) limited the methane production. Maximum biogas production enhancement (40 %) was achieved with a feed/inoculum ratio of 0.5 when  $E_s$  of  $45 \text{ MJ kg}^{-1} \text{ TS}^{-1}$  was applied. As a matter of fact, the hydrolysis rate constant increased from  $0.06\text{--}0.17 \text{ day}^{-1}$  for the raw biomass to  $0.13\text{--}0.23 \text{ day}^{-1}$  for the ultrasound pretreated biomass. Interestingly, high frequency ultrasonic pretreatment (200 kHz) is more efficient at low food/inoculum ratios [89, 90]. At low food/inoculum ratios (0.3), the amount of active biomass is large compared to the amount of biodegradable organic compounds. The high frequency resulted in destruction of flocs, which increased the availability of readily biodegradable organic compound and therefore methane production was doubled under this low food/inoculum ratio scenario [90]. At higher ratios ( $>0.5$ ), the availability of readily biodegradable organic compounds is not limiting methane production but the amount of active biomass. Under this food/inoculum ratio, ultrasonic pretreatment was inefficient. Moreover, the pretreatment could increase the volatile organic compound concentration to a level that is toxic for the active biomass. This is supported by the decrease in the biogas production rate at a food/inoculum ratio of 0.9. At this ratio there was an increase in total biogas production of only 9 % [90].

Full-scale application of ultrasonic pretreatment of sewage sludge has resulted in increased biogas production, better solids reduction, improved dewatering characteristics and relatively short payback periods [91]. Sonic Ltd. developed a full-scale ultrasound pretreatment technology. Several wastewater treatment plants in the UK, US, and Australia are using Sonix<sup>TM</sup> technology for sludge management. The performance of this technology resulted in an improvement of TS reduction from 40 % for the untreated biomass to 60 % for the pretreated sludge and VS reduction from 50 to 70 %, respectively [91]. Besides the waste reduction, biogas production was increased by 40–50 %. Similar performance of full-scale systems is reported in Europe [92]. Data provided in this study showed that ultrasound pretreated increased biogas production and VS reduction by 20–50 %. Besides significant improvements of the properties of the sludge (dewaterability) at full-scale operation, the energy balance was positive. In this case, the energy input for the ultrasonic pretreatment was smaller than the extra energy gained by the improved biogas production. More specifically, this investigation reported that for a digester of  $1,200 \text{ m}^3$ , HRT of 20 days, temperature of  $15 \text{ }^\circ\text{C}$ , and a flow rate of  $200 \text{ m}^3 \text{ day}^{-1}$  at 5 % TS fed with pretreated waste activated sludge, 1 KW of ultrasound input will generate 7 KW of electrical energy after losses [92].

## 8.6 Ultrasound Enhanced Biogas Production from Microalgae

### 8.6.1 *Characteristics and Limitations of Microalgae Biomass as Substrates for Biogas Production*

Microalgae are sun-powered microorganisms that can be cultivated with low cost nutrition requirements (CO<sub>2</sub> exhaust gas streams and wastewater). More specifically, this biomass requires a carbon source that can be provided through a flue gas stream or atmospheric carbon dioxide and other nutrients, such as nitrogen and phosphorus that can be provided with wastewater. In this manner, this feedstock is contributing to the greenhouse gases sequestration and wastewater bioremediation. Furthermore, their doubling time is really short and their production rates are much higher when compared to terrestrial plants. For all these reasons, microalgae seem to be the alternative renewable resource to meet societal energy demands.

For energy purposes, microalgae biomass is nowadays mainly exploited for biodiesel production. Nevertheless, until now all studies have concluded that the approaches are economically unaffordable. One of the main reasons for such a negative balance is due to the macromolecular distribution of microalgae. The production of bioethanol and biodiesel uses only the fraction of carbohydrates and lipids, respectively. In this manner, only a small fraction of the microalgae is utilized and hence the spent biomass is still rich on unused organic matter. Opposite to bioethanol and biodiesel, anaerobic digestion uses all the macromolecular components (carbohydrates, lipids and proteins) as substrate. Therefore, the anaerobic digestion advantage of microalgae implies lower process complexity while producing energy together with a mineralized digestate which contains valuable nutrients. Indeed, anaerobic digestion is a more straightforward process of producing energy since intense concentration, drying, and oil extraction are not required.

Coupling microalgae biomass production with anaerobic digestion was already studied in the 60s by Golueke et al. [93]. Their study reported methane production of 170–320 L CH<sub>4</sub> kg VS<sup>-1</sup> when digesting a microalgae ecosystem composed by *Chlorella* sp. and *Scenedesmus* sp. This methane yield is quite low and similar values have been reported repetitively [94, 95]. Possible causes for such a low efficiency could imply ammonia-mediated inhibition or cell wall resistance to anaerobic bacterial attack. Some studies have focused on the ammonium concentration of the digesters' effluents, and the normal concentration reached does not seem to be inhibitory for anaerobic microorganisms [95, 96]. When organic matter conversion to biogas is low due to this cell wall barrier, the organic nitrogen mineralization is low as well. The low methane production is attributed to the cell wall resistance. In this manner, it seems likely that the cell wall breakage is mandatory for an efficient biogas production.

### 8.6.2 Current Technologies to Improve Biogas Production

A high number of microalgae cells are protected by a semi-rigid structure that hinders the hydrolysis of organic matter. To release the intracellular organics and increase the efficiency of the digestion process, microalgae cell walls should be disrupted prior to anaerobic digestion (Fig. 8.4). Biogas production enhancement has been achieved by subjecting microalgae biomass to different pretreatments. Most pretreatments are conducted through thermal, mechanical or chemical means [15, 16, 98, 99].

Thermal pretreatment affects weak hydrogen bonds when mild temperatures (70–100 °C) are applied, while cellulose and hemicellulose solubilize when higher temperatures (>150 °C) are employed [98, 100]. Literature regarding this topic is diverse since thermal pretreatment conditions and algae species studied are quite broad. *Chlorella vulgaris* biomass subjected to three temperatures, namely 140, 160, and 180 °C for 20 min, resulted in increasing carbohydrates solubilization concomitantly with increasing temperatures [101]. In this case, methane production improvement ranged 1.4–1.6 times higher than the raw biomass. These values are higher than the observed by Cho et al. [102]. In this latter study, the pretreatment of a microalgae mixture (*Scenedesmus* sp. and *Chlorella* sp.) at 120 °C for 30 min resulted in 1.2-fold methane yield enhancement. On the contrary, Gonzalez et al. [16] observed an increased methane production of 2.2-fold in the thermally (90 °C, 180 min) pretreated biomass with regard to the untreated *Scenedesmus* sp.

Chemical pretreatment solubilize complex polymers, thus favoring microbial degradation. At this point, it has to be stressed that higher solubilization of organic matter during the pretreatment is not directly linked to enhanced methane production. This is the case for instance of Mendez [99]. Those authors pretreated *Chlorella vulgaris* biomass by adding sulfuric acid and sodium hydroxide combined with mild temperatures (120 °C). Despite the enhanced organic matter solubilisation exhibited by the thermochemically pretreated biomasses with regard to the thermally pretreated biomass, the methane production had unfavorable tendency. More specifically, methane yield for thermally pretreated biomass

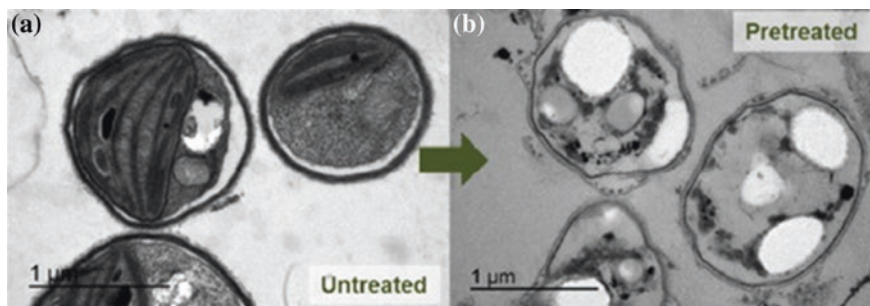


**Fig. 8.4** Scanning electronic microscopic photographs of microalgae *Monoraphidium* sp. cells before (a) and after pretreatment (b). Reprinted with permission from [97]. Copyright © 2014, Elsevier

was 267.7 L CH<sub>4</sub> kg<sup>-1</sup> COD in<sup>-1</sup> while the thermochemically pretreated biomass ranged 228.8–240.6 L CH<sub>4</sub> kg<sup>-1</sup> COD in<sup>-1</sup>. Chemical supplementation combined with mild temperatures may hinder methane production probably mediated by side-product release taking place during pretreatment. Overall, those pretreatments have shown to be beneficial to enhance methane production [99, 103]. However, the drawbacks of using concentrated chemicals include material corrosion and the formation of by-products can result in anaerobic digestion inhibition.

Physical pretreatment involves the reduction of particle size and thus increases the surface/volume ratio of the substrates for further biodegradation. Even though milling is used for other substrates such as lignocellulosic material, in the case of microalgae it does not make sense due to their microscopic size. Microwave pretreatment, on the other hand, has been employed to improve methane production of microalgae substrate. The polarization of macromolecules takes place during microwave irradiation which changes protein structures and disrupts the cell wall. Passos et al. [15] observed a methane production enhancement of 1.6–1.8 fold when pretreating a mixture of *Chlorella* sp. and *Scenedesmus* sp. at 65.4 MJ kg<sup>-1</sup> TS<sup>-1</sup>. Despite the good results obtained on methane production, the energy balance was unfavorable. In this manner, those authors concluded that the application of microwave can only be affordable when working with concentrated biomass.

### 8.6.3 Ultrasound Enhanced Biogas Production of Microalgae Biomass

#### 8.6.3.1 Organic Matter Solubilisation

Similarly to the other pretreatments mentioned above, ultrasound application to microalgae biomass also results in cell wall disruption and therefore organic matter solubilization. In fact, organic matter solubilization is frequently related to methane production enhancement [104, 105]. Studies regarding this subject have shown that ultrasound is a powerful technology to disrupt the cell wall and hence release the organic matter to the soluble phase. The effectiveness of ultrasound has been compared with thermal pretreatment at mild temperatures ranging 70–90 °C [98]. Their results showed that soluble COD may be increased by 2.2–3.1-fold depending on the specific supplied energy (35.5–129 MJ kg<sup>-1</sup> TS<sup>-1</sup> *Scenedesmus* sp. biomass), while thermal application at 80 °C provided an increase of 2-fold soluble COD. At this point, it should be stressed that the cell wall of *Scenedesmus obliquus* is probably one of the most difficult microalgae cell walls to disrupt [106]. Similar results were attained with other microalgae strains. Thermal pretreatment at 170 °C of fresh *Nannochloropsis gaditana* achieved soluble COD of 18 %, while the ultrasound application in the range of 40–57 MJ kg<sup>-1</sup> TS<sup>-1</sup> supported a slightly higher solubilisation reaching 21 % soluble COD [107]. When those ultrasonic dosages were applied to lipid-extracted *N. gaditana* biomass, the COD solubilisation ranged 12–16 %. After chemical extraction, the cell wall of

this microalga is already disrupted, however the ultrasound application resulted in organic matter solubilisation. In this manner, it can be inferred that the ultrasound application resulting in polymer deconstruction than in a merely intracellular organic matter release. In the case of filamentous algae biomass (*Hydrodictyon reticulatum*), ultrasound dose of  $250 \text{ MJ kg}^{-1} \text{ TS}^{-1}$ , increased soluble COD by 3.6-fold [108]. Additionally, those authors observed that a higher ultrasound dosage ( $500 \text{ MJ kg}^{-1} \text{ TS}^{-1}$ ) caused conversion of organic into inorganic matter. This mineralization of the organic matter is considered an issue if the final target is biogas, which is obtained from organic matter.

As stated in the previous section of WAS, biogas production was related to the different macromolecules (proteins, carbohydrates and lipids) in the substrate biomass. Taking a closer look on the effect of ultrasound treatment on determined macromolecules that constitute the biomass organic matter, few studies have followed the extraction of proteins, lipids and carbohydrates. With regard to this latter macromolecule, Zhao et al. [109] studied the effect of operational ultrasound parameters (ultrasonic power, working time, cell concentration and flow rate) on *Chlorella* sp. carbohydrates extraction. The authors concluded that cell breakage rate was significantly affected by power and extraction time, while increasing flow rates had a negative effect on carbohydrates extraction. Ultrasonic power of 800 W for 80 min at flow rate of  $1.52 \text{ L min}^{-1}$  and cell concentration of  $0.3 \text{ g L}^{-1}$  resulted in 100 % carbohydrates extraction, which is much higher than other conventional technologies such as solvent extraction. The lengthy pretreatment together with the high power required at low cell densities is probably not economically feasible, however the authors did not examined that point.

As observed for carbohydrates, proteins were totally released from *Chlamydomonas reinhardtii* during ultrasound application of 5 min with an acoustic power output of 26.2 W [110]. Those authors also observed that even though short exposure time (few seconds) to ultrasound may damage the microalgae cell, the released protein was minimal. This microalgae strain has also been tested for lipids extractability by ultrasound means. Cell wall breakage and hence extractability of lipids was higher at lower ultrasound dosages (up to  $2.5 \text{ MJ kg}^{-1} \text{ TS}^{-1}$  [111]). Similar lipids extractability was achieved regardless the ultrasound energy application at higher dosages ( $100\text{--}500 \text{ J mL}^{-1}$ ) and at different microalgae concentration ( $1.5\text{--}14 \text{ g L}^{-1}$ ). These good results attained for *Chlamydomonas reinhardtii* may be due to the fact that this microalga has a weak cell wall [112, 113] compared to other green microalgae. Nevertheless, some other studies proved the high efficiency of ultrasound to extract lipids as well from *Scenedesmus* sp. For this strain, it has been observed that the combination of ultrasound and solvent addition (chloroform-methanol) for lipid extraction may double the extraction yield [114].

It is worth to note that most of those studies highlighted the existence of a power threshold after which different behavior can take place. In the context of lipids extractability from microalgae biomass, Gerde et al. [111] pointed out that above this threshold (specific for each microalgae strain and ultrasound conditions) the formation of free radicals can damage the quality of the oil by forming lipid hydroperoxides. Likewise, excessive sonication can result in excessive cavitation bubbles that interact among themselves instead of with the cells [115].



### 8.6.3.2 Enhanced Methane Production

As rule of thumb, a higher organic matter solubilisation would result in a higher methane production. Nevertheless, some investigations have shown that this cannot be confirmed unequivocally [16, 107]. To avoid the formation of anaerobic microorganisms' inhibitors, the organic matter released during ultrasound application should be carefully studied. In this context, some investigations have been conducted with microalgae biomass strains through BMP tests. Note worth to mention that the effect that ultrasound has on methane production is strain specific (Table 8.3). *Hydrodictyon reticulatum* subjected to 4 MJ kg TS<sup>-1</sup> increased

**Table 8.3** Summary of literature review on ultrasound treatment prior to anaerobic digestion of microalgae

Substrate micro-algae strain	Frequency (KHz)	Ultrasound energy input (MJ Kg <sup>-1</sup> TS <sup>-1</sup> )	Sonication time (minutes)	CH <sub>4</sub> yield untreated	CH <sub>4</sub> yield after ultrasound	Reference
				(mL CH <sub>4</sub> g VS <sup>-1</sup> in <sup>-1</sup> )		
Scenedesmus obliquus	20	35.5	15	51	40.5 <sup>a</sup>	[16]
		47.2	15	51	38.9 <sup>a</sup>	
		76.5	15	51	51.8 <sup>a</sup>	
		100.7	15	51	79.7 <sup>a</sup>	
		128.9	30	51	85.3 <sup>a</sup>	
Nannochloropsis gaditana	24	10	n.s.	300.1	281	[103]
		27	n.s.	300.1	274	
		40	n.s.	300.1	342	
		57	n.s.	300.1	361	
Nannochloropsis gaditana after lipids extraction	24	10	n.s.	331	318	[103]
		27	n.s.	331	348	
		40	n.s.	331	356	
		57	n.s.	331	382	
Nannochloropsis salina	30	0.03 <sup>b</sup>	3	347 <sup>c</sup>	247	[116]
Hydrodictyon reticulatum	20	5	n.s.	165.9	348.3	[108]
		50	n.s.	165.9	326.2	
		100	n.s.	165.9	318.9	
		250	n.s.	165.9	313.5	
		500	n.s.	165.9	333.2	
Rhizoclonium sp.	20	0.45 <sup>b</sup>	10	153.8	184 <sup>d</sup>	[117]

*n.s.* means not specified in the referenced study

<sup>a</sup>Assuming a COD/VS ratio of 1.8 (Gonzalez-Fernandez et al. 2013)

<sup>b</sup>Correspond to the MJ applied, however no specification regarding the TS concentration was found in the referenced study

<sup>c</sup>No biogas composition with regard to the CH<sub>4</sub> content was found in this work. The value correspond to mL biogas g VS in<sup>-1</sup>

<sup>d</sup>All the digestion presented herein are conducted under mesophilic conditions (35 °C), exception made for this reference where digestion was conducted at thermophilic range (53 °C)

the methane production by 2.3-fold with regard to the raw biomass [108]. As explained above, in this study it can be observed that higher ultrasound doses increased organic matter release during the pretreatment but this solubilisation did not correspond to a methane production enhancement. In the case of *Chlorella vulgaris* and *Scenedesmus obliquus*, two of the most robust microalgae, ultrasound pretreatment has also been proven as an effective pretreatment. When subjecting *Scenedesmus obliquus* to different ultrasound  $E_s$ , the results showed methane production rates 2-fold higher at low ultrasound levels ( $35.5 \text{ MJ kg}^{-1} \text{ TS}^{-1}$ ) and 4-fold when applying a higher range of energy ( $76.5\text{--}130 \text{ MJ kg}^{-1} \text{ TS}^{-1}$  [16]) the first days of digestion. As expected, methane productivity was enhanced due to the cell wall disruption of the ultrasound pretreatment. The first days of digestion, in which hydrolysis of the organic matter is the limiting stage, the methane production rate is enhanced since the hydrolysis is favored during the pretreatment. As it can be seen in Table 8.3, the highest energy supplied ( $100\text{--}130 \text{ MJ kg}^{-1} \text{ TS}^{-1}$ ) almost doubled the methane production with regard to the untreated *S. obliquus*. This study also provided a parallel study in which this biomass was subjected to thermal pretreatment. This latter pretreatment temperature was set at  $80 \text{ }^\circ\text{C}$  since this was the temperature achieved during the sonication pretreatment. The results exhibited a 1.6-fold increase regarding methane production, and thus the ultrasound pretreatment was more efficient. Furthermore, the soluble COD percentage released during this thermal treatment was similar to the soluble COD determined after pretreatment at  $35.5 \text{ MJ kg}^{-1} \text{ TS}^{-1}$ , nevertheless the methane production achieved by thermal pretreatment was double than the one obtained using the sonicated biomass. This clearly shows the importance of determining the nature of the organic matter released upon the different pretreatments. Similar trend was observed for *Chlorella vulgaris*. In this case, low  $E_s$  input ( $5\text{--}20 \text{ J mL}^{-1}$ , unfortunately those authors did not mention the TS concentration of this suspension subjected to ultrasound) exhibited organic matter release, but not methane production improvement [118]. Only high energy dosages in the range of  $50\text{--}200 \text{ J mL}^{-1}$  of *Chlorella vulgaris* suspension enhanced methane production around 1.6–1.95-fold.

Contrary to this beneficial effect of ultrasound on those commonly encountered microalgae, the strain *Nannochloropsis* sp. did not show any significant improvement on methane production. After subjecting *Nannochloropsis salina* to different pretreatments, ultrasound pretreatment of 3 min at 200 W slightly enhanced methane production while thermal pretreatment at  $100 \text{ }^\circ\text{C}$  for 8 h doubled biogas production [116]. This neutral effect of ultrasound on this microalga was attributed to the release of inhibitors within the organic matter solubilisation. Similarly, Alzate et al. [103] pretreated *Nannochloropsis gaditana* at different ultrasound dosages, and the lower dosages ( $10\text{--}27 \text{ MJ kg}^{-1} \text{ TS}^{-1}$ ) provided lower methane production than the raw material. This fact would confirm the formation of inhibitors during the pretreatment at low  $E_s$  dosages. Furthermore, the use of higher dosages ( $40\text{--}57 \text{ MJ kg}^{-1} \text{ TS}^{-1}$ ) only increased the methane production by 1.2-fold.



## 8.7 Conclusions and Future Outlook

The effect of ultrasound application varies among substrates. In the case of lignocellulosic materials and manure, ultrasound pretreatment generally results in two main effects: organic matter solubilization and bioavailability increase by disruption of the lignocellulosic complex surface. In this way, the effect of ultrasound pretreatment on methane yield is not always related to the organic matter solubilization but to the increased bioavailability. The main effect of this mechanical pretreatment on microalgae biomass and activated sludge is organic matter solubilisation at high  $E_s$  and flocs disaggregation at low  $E_s$ . This organic matter can be released in two ways, namely by cells wall disruption and polymers solubilisation/degradation. In this way, mineralization of organic compounds and inhibitory substances production can hamper methane production.

Overall, the ultrasound treatment has been proven efficient for increasing the methane production of lignocellulosic materials, manure, activated sludge and microalgae biomass. The treatment conditions should be to carefully chosen depending on the substrate characteristics and the ultrasound equipment and the parameters applied to obtain maximum efficiency of the pretreatment in terms of methane yield. The results obtained until now for lignocellulosic materials, manure and microalgae biomass are quite recent and broad. Additionally, some information is lacking with regard to the use of those pretreated substrates on semi-continuously fed reactors, as well as some studies concerning economics and energy turnover. Until now, only the research dealing with ultrasonic pretreatment on activated sludge for enhanced methane production has obtained economic benefits and implemented the technology on an industrial scale.

## References

1. Burton CH, Turner C (2003) Manure management: treatment strategies for sustainable agriculture, 2nd edn. Sisloe Research Institute, UK
2. Cantrell KB, Ducey T, Ro KS, Hunt PG (2008) Livestock waste-to-bioenergy generation opportunities. *Bioresour Technol* 99:7941–7953
3. Christy PM, Gopinath LR, Divya D (2014) A review on anaerobic decomposition and enhancement of biogas production through enzymes and microorganisms. *Renew Sust Energy Rev* 34:167–173
4. Bauer C, Korthals M, Gronauer A, Leuhn M (2008) Methanogens in biogas production from renewable resources—a novel molecular population analysis approach. *Water Sci Technol* 58:1433–1439
5. Chen Y, Cheng JJ, Creamer KS (2008) Inhibition of anaerobic digestion process: a review. *Bioresour Technol* 99:4044–4064
6. Rajagopal R, Massé DI, Singh G (2013) A critical review on inhibition of anaerobic digestion process by excess ammonia. *Bioresour Technol* 143:632–641
7. Mata-Alvarez J, Dosta J, Romero-Güiza MS, Fonoll X, Peces M, Astals S (2014) A critical review on anaerobic co-digestion achievements between 2010 and 2013. *Renew Sustain Energy Rev* 36:412–427

8. Hendriks Zeeman G (2009) Pretreatments to enhance the digestibility of lignocellulosic biomass. *Bioresour Technol* 100:10–18
9. Kythreotou N, Florides G, Tassou SA (2014) A review of simple to scientific models for anaerobic digestion. *Renew Energy* 71:701–714
10. Al Seadi T, Rutz D, Prassl H, Köttner M, Finsterwalder T, Volk S, Janssen R (2008) *The biogas handbook*. University of Southern Denmark Esbjerg, Denmark
11. Ozonek J (2012) *Application of hydrodynamic cavitation in environmental engineering*. CRC Press, Boca Raton. ISBN:13:978-0-203-10609-9
12. Suslick KS (1990) Sonochemistry. *Science* 247:1439–1445
13. Khanal SK, Grewell D, Sung S, Van Leeuwen J (2007) Ultrasound applications in wastewater sludge pretreatment: a review. *Crit Rev Environ Sci Technol* 37:277–313
14. Wang F, Wang Y, Ji M (2005) Mechanisms and kinetic models for ultrasonic waste activated sludge disintegration. *J Hazard Mater* 123:145–150
15. Passos F, Solé M, García J, Ferrer I (2013) Biogas production from microalgae grown in wastewater: effect of microwave pretreatment. *Appl Energy* 108:168–175
16. González-Fernández C, Sialve B, Bernet N, Steyer JP (2012) Comparison of ultrasound and thermal pretreatment of *Scenedesmus* biomass on methane production. *Bioresour Technol* 110:610–616
17. Show KY, Mao T, Lee DJ (2007) Optimisation of sludge disruption by sonication. *Water Res* 41:4741–4747
18. Tiehm A, Nickel K, Zellhorn M, Neis U (2001) Ultrasonic waste activated sludge disintegration for improving anaerobic stabilization. *Wat Res* 35:2003–2009
19. Luo J, Fang Z, Smith RL Jr (2014) Ultrasound-enhanced conversion of biomass to biofuels. *Prog Energy Comb Sci* 41:56–93
20. Rubin E (2008) Genomics of cellulosic biofuels. *Nature* 454:841–845
21. Zheng Y, Zhao J, Xu F, Li Y (2014) Pretreatment of lignocellulosic biomass for enhanced biogas production. *Prog Energy Comb Sci* 42:35–53
22. Guo GL, Hsu DC, Chen WH, Chen WH, Hwang WS (2009) Characterization of enzymatic saccharification for acid-pretreated lignocellulosic materials with different lignin composition. *Enzyme Microb Technol* 45:80–87
23. García A, González Alriols M, Labidi J (2014) Evaluation of different lignocellulosic raw materials as potential alternative feedstocks in biorefinery processes. *Ind Crops Prod* 53:102–110
24. Bruni E, Jensen AP, Angelidaki I (2010) Comparative study of mechanical, hydrothermal, chemical and enzymatic treatments of digested biofibers to improve biogas production. *Bioresour Technol* 101:8713–8717
25. Cabbai V, Ballico M, Aneggi E, Goi D (2013) BMP tests of source selected OFMSW to evaluate anaerobic codigestion with sewage sludge. *Waste Manag* 33:1626–1632
26. Chandra R, Takeuchi H, Hasegawa T (2012) Hydrothermal pretreatment of rice straw biomass: a potential and promising method for enhanced biogas production. *Appl Energy* 94:129–140
27. Dinuccio E, Balsari P, Gioelli F, Menardo S (2010) Evaluation of biogas productivity potential of some Italian agro-industrial biomasses. *Bioresour Technol* 101:3780–3783
28. Klimiuk E, Pokój T, Budzyński W, Dubis B (2010) Theoretical and observed biogas production from plant biomass of different fibre contents. *Bioresour Technol* 101:9527–9535
29. Park ND, Helle SS, Thring RW (2012) Combined alkaline and ultrasound pre-treatment of thickened pulp mill waste activated sludge for improved anaerobic digestion. *Biomass Bioenergy* 46:750–756
30. Silvestre G, Gómez P, Pascual A, Ruiz B (2013) Anaerobic co-digestion of cattle manure with rice straw: economic and energy feasibility. *Water Sci Technol* 67:745–755
31. Cesaro A, Belgiorno V (2013) Sonolysis and ozonation as pretreatment for anaerobic digestion of solid organic waste. *Ultrason Sonochem* 20:931–936
32. Zhang Q, He J, Tian M, Mao Z, Tang L et al (2011) Enhancement of methane production from cassava residues by biological pretreatment using a constructed microbial consortium. *Bioresour Technol* 102:8899–8906

33. Pavón-Orozco P, Santiago-Hernández A, Rosengren A, Hidalgo-Lara ME, Stalbrand H (2012) The family II carbohydrate-binding module of xylanase CfxYn11A from *Cellulomonas flavigena* increases the synergy with cellulase TrCel7B from *Trichoderma reesei* during the hydrolysis of sugar cane bagasse. *Bioresour Technol* 104:622–630
34. Ziemniński K, Romanowska I, Kowalska M (2002) Enzymatic pre-treatment of lignocellulosic wastes to improve biogas production. *Waste Manag* 32:1131–1137
35. Sun Y, Cheng JJ (2002) Hydrolysis of lignocellulosic materials for ethanol production: a review. *Bioresour Technol* 83:1–11
36. Hjorth M, Gränitz K, Adamsen APS, Moller HB (2011) Extrusion as a pretreatment to increase biogas production. *Bioresour Technol* 102:4989–4994
37. Wang J, Yue ZB, Chen TH, Peng SC, Yu HQ, Chen HZ (2010) Anaerobic digestibility and fiber composition of bulrush in response to steam explosion. *Bioresour Technol* 101:6610–6614
38. Di Girolamo G, Grigatti M, Barbanti L, Angelidaki I (2013) Effects of hydrothermal pretreatments on Giant reed (*Arundo donax*) methane yield. *Bioresour Technol* 147:152–159
39. Bauer A, Bosch P, Friedl A, Amon T (2009) Analysis of methane potentials of steam-exploded wheat straw and estimation of energy yields of combined ethanol and methane production. *J Biotechnol* 142:50–55
40. Mehdizadeh SN, Eskicioglu C, Milani AS, Saha M (2012) Empirical modelling of the effects of emerging pretreatment methods on anaerobic digestion of pulp mill biosolids. *Biochem Eng J* 68:167–177
41. Saha M, Eskicioglu C, Marin J (2011) Microwave, ultrasonic and chemo-mechanical pretreatments for enhancing methane potential of pulp mill wastewater treatment sludge. *Bioresour Technol* 102:7815–7826
42. Fernández-Cegrí V, de la Rubia MA, Raposo F, Borja R (2012) Impact of ultrasonic pretreatment under different operational conditions on the mesophilic anaerobic digestion of sunflower oil cake in batch mode. *Ultrason Sonochem* 19:1003–1010
43. Cesaro A, Velten S, Belgiorno V, Kuchta K (2014) Enhanced anaerobic digestion by ultrasonic pretreatment of organic residues for energy production. *J Cleaner Prod* 74:119–124
44. Yong-ze W, Xiong C, Zhi W, Jin-fan Z, Ting-ting F, Dong-sheng L, Jinhua W (2012) Effect of low concentration alkali and ultrasound combination pretreatment on biogas production by stalk. *Adv Mat Res* 383–390:3434–3437
45. Iskalieva A, Yimmou BM, Gogate PR, Horvath M, Horvath PG, Csoka L (2012) Cavitation assisted delignification of wheat straw: a review. *Ultrason Sonochem* 19:984–993
46. Carrère H, Dumas C, Battimelli A, Batstone DJ, Delgenès JP, Steyer JP, Ferrer I (2010) Pretreatment methods to improve sludge anaerobic degradability: a review. *J Hazard Mat* 183:1–15
47. Deublein D, Steinhauser A (2008) *Biogas from waste and renewable resources. An introduction*. Wiley-VCH, London. ISBN 978-3-527-31841-4
48. Sul'man EM, Sul'man MG, Prutenskaya EA (2011) Effect of ultrasonic pretreatment on the composition of lignocellulosic material in biotechnological processes. *Catal Ind* 3:28–33
49. Angelidaki I, Ahring BK (1993) Thermophilic anaerobic digestion of livestock waste: the effect of ammonia. *Appl Microbiol Biotechnol* 38:560–564
50. Albuquerque JA, de la Fuente C, Campoy M, Carrasco L, Nájera I, Baixauli C, Caravaca F, Roldán A, Cegarra J, Bernal MP (2012) Agricultural use of digestate for horticultural crop production and improvement of soil properties. *Eur J Agron* 43:119–128
51. Luste S, Luostarinen S (2011) Enhanced methane production from ultrasound pre-treated and hygienized dairy cattle slurry. *Waste Manag* 31:2174–2179
52. Molinuevo-Salces B (2011) *Anaerobic digestion of livestock wastes: vegetable residues as co-substrate and digestate post-treatment*. PhD dissertation
53. Carlsson M, Lagerkvist A, Morgan-Sagastume F (2012) The effects of substrate pre-treatment on anaerobic digestion systems: a review. *Waste Manag* 32:1634–1650
54. Bonmatí A, Flotats X, Mateu L, Campos E (2001) Study of thermal as a pretreatment to mesophilic anaerobic digestion of pig slurry. *Wat Sci Technol* 44:109–116

55. Mladenovska Z, Hartmann H, Kvist T, Sales-Cruz M, Gani R, Ahring BK (2006) Thermal pre-treatment of the solid fraction of manure: impact on the biogas reactor performance and microbial community. *Wat Sci Technol* 53:59–67
56. Carrère H, Sialve B, Bernet N (2009) Improving pig manure conversion into biogas by thermal and thermo-chemical pretreatments. *Bioresour Technol* 100:3690–3694
57. Uellendahl H, Mladenovska Z, Ahring BK (2007) Wet oxidation of crude manure and manure fibers: substrate characteristics influencing the pretreatment efficiency for increasing the biogas yield of manure. In: Proceedings of 11th IWA world congress on anaerobic digestion, Brisbane
58. Biswas R, Ahring BK, Uellendahl H (2012) Improving biogas yields using an innovative concept for conversion of the fiber fraction of manure. *Wat Sci Technol* 66:1751–1758
59. Gonzalez-Fernández C, León-Cofreces C, García-Encina P (2008) Different pretreatments for increasing the anaerobic biodegradability in swine manure. *Bioresour Technol* 99:8710–8714
60. Castrillón L, Fernández-Nava Y, Ormaechea P, Marañón E (2011) Optimization of biogas production from cattle manure by pre-treatment with ultrasound and co-digestion with crude glycerin. *Bioresour Technol* 102:7845–7849
61. Quiroga G, Castrillón L, Fernández-Nava Y, Marañón E, Negral L et al (2014) Effect of ultrasound pre-treatment in the anaerobic co-digestion of cattle manure with food waste and sludge. *Bioresour Technol* 54:74–79
62. Elbeshbishy E, Aldin S, Hafez H, Nakhla G, Ray M (2011) Impact of ultrasonication of hog manure on anaerobic digestability. *Ultrason Sonochem* 18:164–171
63. Braeutigam P, Franke M, Ondruschka B (2014) Effect of ultrasound amplitude and reaction time on the anaerobic fermentation of chicken manure for biogas production. *Biomass Bioenerg* 63:109–113
64. Luste S, Heinonen-Tanski H, Luostarinen S (2012) Co-digestion of dairy cattle slurry and industrial meat-processing by-products- effect of ultrasound and hygienization pre-treatments. *Bioresour Technol* 104:195–201
65. Castrillón L, Fernández-Nava Y, Ormaechea P, Marañón E (2013) Methane production from cattle manure supplemented with crude glycerin from the biodiesel industry in CSTR and IBR. *Bioresour Technol* 127:312–317
66. Marañón E, Castrillón L, Quiroga G, Fernández-Nava Y, Gómez L, García MM (2012) Co-digestion of cattle manure with food waste and sludge to increase biogas production. *Waste Manag* 32:1821–1825
67. Canales A, Pareilleux A, Rols JL, Goma C, Huyard A (1994) Decreased sludge production strategy for domestic wastewater treatment. *Water Sci Technol* 30:96–106
68. Bougrier C, Albasi C, Delgenès JP, Carrère H (2006) Effect of ultrasonic, thermal and ozone pre-treatments on activated sludge solubilisation and anaerobic biodegradability. *Chem En Proc* 45:711–718
69. Apul OG, Sanin FD (2010) Ultrasonic pretreatment and subsequent anaerobic digestion under different operational condition. *Bioresour Technol* 101:8984–8992
70. Eastman JA, Ferguson JF (1981) Solubilization of particulate organic carbon during the acid phase of anaerobic digestion. *J Water Pollut Control Fed* 53:352–366
71. Gujer W, Zehnder AJB (1983) Conversion processes in anaerobic digestion. *Water Sci Technol* 12:127–167
72. Tyagi VK, Lo S-L (2013) Microwave irradiation: a sustainable way for sludge treatment and resource recovery. *Renew Sustain Energ Rev* 18:288–305
73. Kepp U, Machenbach I, Weisz N, Solheim OE (2000) Enhanced stabilisation of sewage sludge through thermal hydrolysis—three years of experience with full scale plant. *Water Sci Technol* 42:89–96
74. Dwyer J, Starenburg D, Tait S, Barr K, Batstone DJ, Lant P (2008) Decreasing activated sludge thermal hydrolysis temperature reduces product colour, without decreasing degradability. *Water Res* 42:4699–4709
75. Xie B, Liu H, Yan Y (2009) Improvement of the activity of anaerobic sludge by low-intensity ultrasound. *J Environ Manage* 90:260–264

76. Kwiatkowska B, Bennett J, Akunna J, Walker GM, Bremner DH (2011) Stimulation of bioprocesses by ultrasound. *Biotechnol Adv* 29:768–780
77. Yu GH, He PJ, Shao LM, Zhu YS (2008) Extracellular proteins, polysaccharides and enzymes impact on sludge aerobic digestion after ultrasonic pretreatment. *Water Res* 42:1925–1934
78. Nabarlätz D, Vondrysova J, Janicek P, Stüber F, Font J, Fortuny A et al (2010) Hydrolytic enzymes in activated sludge: extraction of protease and lipase by stirring and ultrasonication. *Ultrason Sonochem* 17:923–931
79. Yan Y, Feng L, Zhang C, Zhu H, Zhou Q (2010) Effect of ultrasonic specific energy on waste activated sludge solubilization and enzyme activity. *African J Biotechnol* 9:1776–1782
80. Kim Y, Lee J (2005) Effect of ultrasound on methanogenic activity of anaerobic granules. *Jpn J Appl Phys* 44:8259–8261
81. Bougrier C, Carrère H, Delgenès JP (2005) Solubilisation of waste-activated sludge by ultrasonic treatment. *Chem Eng J* 106:163–169
82. Angelidaki I, Sanders W (2004) Assessment of the anaerobic biodegradability of macropollutants. *Rev Environ Sci Biotechnol* 3:117–129
83. Kapucu H, Gulsoy N, Mehmetoglu U (2000) Disruption and protein released kinetics by ultrasonication of *Acetobacter peroxydan* cells. *Biochem Eng J* 5:57–62
84. Sanders RC, McNeil B, Finberg HJ, Hessel SJ, Siegelman SS et al (1983) A prospective study of computed tomography and ultrasound in the detection and staging of pelvic masses. *Radiology* 146:439–442
85. Harrison STL (1991) Bacterial cell disruption: a key unit operation in the recovery of intracellular products. *Biotechnol Adv* 9:217–240
86. Tiehm A, Nickel K, Neis U (1997) The use of ultrasound to accelerate the anaerobic digestion of sewage sludge. *Water Sci Technol* 36:121–128
87. Akin B, Khanal SK, Sung S, Grewell D, Van-Leeuwen J (2006) Ultrasound pre-treatment of waste activated sludge. *Water Sci Technol* 6:35–42
88. Braguglia CM, Mininni GMC, Tomel MC, Rolle E (2006) Effect of feed/inoculum ratio on anaerobic digestion of sonicated sludge. *Water Sci Technol* 54:77–84
89. Braguglia CM, Cagliano MC, Rossetti S (2012) High frequency pretreatment for sludge anaerobic digestion: effect on floc structure and microbial population. *Bioresour Technol* 110:43–49
90. Gallipoli A, Gianico A, Cagliano MC, Braguglia CM (2014) Potential of high frequency ultrasounds to improve sludge anaerobic conversion and surfactants removal at different food/inoculum ratio. *Bioresour Technol* 159:207–214
91. Hogan F, Mormede S, Clark P, Crane M (2004) Ultrasonic sludge treatment for enhanced anaerobic digestion. *Water Sci Technol* 50:25–32
92. Barber WP (2005) The effects of ultrasound on sludge digestion. *J Chart Inst Water Environ Manage* 19:2–7
93. Golueke CG, Oswald WJ, Gotaas HB (1957) Anaerobic digestion of algae. *Appl Microbiol* 5:47–55
94. Ras M, Lardon L, Sialve B, Bernet N, Steyer JP (2011) Experimental study on a coupled process of production and anaerobic digestion of *Chlorella vulgaris*. *Bioresour Technol* 102:200–206
95. González-Fernández C, Molinuevo-Salces B, García-González MC (2011) Evaluation of anaerobic codigestion of microalgal biomass and swine manure via response surface methodology. *Appl Eng* 88:3448–3453
96. Mahdy A, Mendez L, Blanco S, Ballesteros M, González-Fernández C (2014) Protease cell wall degradation of *Chlorella vulgaris*: effect on methane production. *Bioresour Technol* (accepted). doi:[10.1016/j.biortech.2014.08.091](https://doi.org/10.1016/j.biortech.2014.08.091)
97. Passos F, Hernández-Mariné M, García J, Ferrer I (2014) Long-term anaerobic digestion of microalgae grown in HRAP for wastewater treatment. Effect of microwave pretreatment. *Water Res* 49:351–359

98. González-Fernández C, Sialve B, Bernet N, Steyer JP (2012) Thermal pretreatment to improve methane production of *Scenedesmus* biomass. *Biomass Bioenerg* 40:105–111
99. Mendez L, Mahdy A, Timmers RA, Ballesteros M, González-Fernández C (2013) Enhancing methane production of *Chlorella vulgaris* via thermochemical pretreatments. *Bioresour Technol* 149:136–141
100. Garrote G, Domínguez H, Parajo JC (1999) Hydrothermal processing of lignocellulosic materials. *Holz Roh Werkst* 57:191–202
101. Mendez L, Mahdy A, Demuez M, Ballesteros M, González-Fernández C (2014) Effect of high pressure thermal pretreatment on *Chlorella vulgaris* biomass: organic matter solubilisation and biochemical methane potential. *Fuel* 117:674–679
102. Cho S, Park S, Seon J, Yu J, Lee T (2013) Evaluation of thermal, ultrasonic and alkali pretreatments on mixed-microalgal biomass to enhance anaerobic methane production. *Bioresour Technol* 143:330–336
103. Alzate ME, Muñoz R, Rogalla F, Fdz-Polanco F, Perez-Elvira SI (2014) Biochemical methane potential of microalgae after lipid extraction. *Chem Eng J* 243:403–410
104. Passos F, García J, Ferrer I (2013) Impact of low temperature pretreatment on the anaerobic digestion of microalgal biomass. *Bioresour Technol* 138:79–86
105. Carrère H, Bougrier C, Castets D, Delgenès JP (2008) Impact of initial biodegradability on sludge anaerobic digestion enhancement by thermal pretreatment. *J Environ Sci Health A Tox Hazard Subst Environ Eng* 13:1551–1555
106. Mussnug H, Klassen V, Schlüte A, Kruse O (2010) Microalgae as substrates for fermentative biogas production in a combined biorefinery concept. *J Biotechnol* 1:51–56
107. Alzate ME, Muñoz R, Rogalla F, Fdz-Polanco F, Pérez-Elvira SI (2012) Biochemical methane potential of microalgae: influence of substrate to inoculum ratio, biomass concentration and pretreatment. *Bioresour Technol* 123:488–494
108. Lee K, Chantrasakdakul P, Kim D, Kong M, Park KY (2014) Ultrasound pretreatment of filamentous algal biomass for enhanced biogas production. *Waste Manag* 34:1035–1040
109. Zhao G, Chen X, Wang L, Zhou S, Feng H, Chen WN, Lau R (2013) Ultrasound assisted extraction of carbohydrates from microalgae as feedstock for yeast fermentation. *Bioresour Technol* 128:337–344
110. Bigelow TA, Xu J, Stessman DJ, Yao L, Spalding MH, Wang T (2014) Lysis of *Chlamydomonas reinhardtii* by high-intensity focused ultrasound as a function of exposure time. *Ultrason Sonochem* 21:1258–1264
111. Gerde JA, Montalbo-Lombay M, Yao L, Grewell D, Wang T (2012) Evaluation of microalgae cell disruption by ultrasonic treatment. *Bioresour Technol* 125:175–181
112. Adair WS, Snell WJ (1990) The *Chlamydomonas reinhardtii* cell wall: structure, biochemistry, and molecular biology. In: Mecham RP, Adair WS (eds) Organization and assembly of plant and animal extracellular matrix. Academic Press, Orlando, pp 15–84
113. Reichardt LF (1993) Extracellular matrix molecules and their receptors. In: Kreis T, Vale R (eds) Guidebook to extracellular matrix, adhesion proteins. Oxford University Press, Oxford, pp 3–11
114. Keris-Sen UD, Sen U, Soydemir G, Gurol MD (2014) An investigation of ultrasound effect on microalgal cell integrity and lipid extraction efficiency. *Bioresour Technol* 152:407–413
115. Sivakumar M, Pandit AB (2001) Ultrasound enhanced degradation of Rhodamine B: optimization with power density. *Ultrason Sonochem* 8:233–240
116. Schwede S, Kowalczyk A, Gerber M, Span R (2011) Influence of different cell disruption techniques on mono digestion of algal biomass. *World Renewable Energy Congress, Linköping*
117. Ehimen EA, Holm-Nielsen JB, Poulsen M, Boelsmand JE (2013) Influence of different pre-treatment routes on the anaerobic digestion of a filamentous algae. *Renew Energ* 50:476–480
118. Park KY, Kweon J, Chantrasakdakul P, Lee K, Cha HY (2013) Anaerobic digestion of microalgal biomass with ultrasonic disintegration. *Int Biodet Biodeg* 85:598–602



# Chapter 9

## Ultrasonic Vibration-Assisted Pelleting of Cellulosic Biomass for Biofuel Production

Meng Zhang, Xiaoxu Song, Z.J. Pei and Donghai Wang

**Abstract** Cellulosic biofuels have the potential to partially replace petroleum-based liquid transportation fuels. Several technical barriers hinder large-scale and cost-effective production of cellulosic biofuels, such as the low density of cellulosic biomass feedstocks (causing high transportation and storage cost), and the lack of efficient pretreatment technologies for cellulosic biomass. Ultrasonic vibration-assisted (UV-A) pelletizing is a novel biomass feedstock preprocessing technology. UV-A pelletizing is characterized by a combination of pelletizing and ultrasonic treatment into one process. This chapter reports experimental and theoretical investigations on UV-A pelletizing of cellulosic biomass for biofuel production. It covers studies on pellet quality, pellet sugar yield, pelletizing energy consumption, and pelletizing temperature.

**Keywords** Cellulosic biomass · Energy consumption · Pellet density · Pellet durability · Predictive model · Sugar yield · Temperature · Ultrasonic vibration-assisted (UV-A) pelletizing

### Nomenclature

- $C$  Specific heat capacity of cellulosic biomass (J/kg K)
- $K$  Thermal conductivity of cellulosic biomass (W/m K)
- $M$  Mass of cellulosic biomass pellet (kg)
- $P$  Density of cellulosic biomass pellet (kg/m<sup>3</sup>)

---

M. Zhang (✉) · X. Song · Z.J. Pei  
Department of Industrial and Manufacturing Systems Engineering,  
Kansas State University, Manhattan, KS 66506, USA  
e-mail: meng@ksu.edu

D. Wang  
Department of Biological and Agricultural Engineering,  
Kansas State University, Manhattan, KS 66506, USA

- $T$  Temperature of cellulosic biomass pellet (K)  
 $H$  Height of cellulosic biomass pellet (m)  
 $A$  Absorption coefficient of cellulosic biomass ( $\text{m}^{-1}$ )  
 $I$  Ultrasound intensity ( $\text{W}/\text{m}^2$ )  
 $I_0$  Ultrasound intensity at the top surface of a pellet ( $\text{W}/\text{m}^2$ )  
 $Q$  Volumetric heat generation rate ( $\text{W}/\text{m}^3$ )  
 $T$  Pelleting time (s)  
 $T_0$  Room temperature (300 K)  
 $Z$  Distance from the top surface of a pellet (m)

## 9.1 Introduction

### 9.1.1 Significance of Cellulosic Biofuels

Worldwide economies are currently dependent on fossil fuels including petroleum, which are finite, nonrenewable energy resources. Fossil fuels currently provide more than 85 % of all the energy consumed in the U.S. and virtually all of the liquid transportation fuels [1–3]. In 2011, half of the petroleum used in the U.S. was imported [1]. The dependence on foreign petroleum is a real threat to national energy security [3, 4]. Furthermore, the transportation sector is responsible for about 30 % of U.S. greenhouse gas (GHG) emissions [5]. Energy security, economy, and environment sustainability are all driving factors to develop alternative liquid transportation fuels that are domestically produced and environmentally friendly [4]. Promoting biofuels is one of the efforts to reduce the use of petroleum-based fuels in the transportation section [4–6].

First generation biofuels rely largely on cornstarch (in the U.S.) or sugar cane (in Brazil) [7, 8]. The next generation biofuels are expected to be made from cellulosic biomass of non-food resources, such as residues from agricultural and forestry practices, and crops grown only for conversion to fuels (dedicated energy crops such as miscanthus and switchgrass). It was reported that approximately 550 million tons of cellulosic biomass could be sustainably produced annually in the U.S. by 2020 without major impacts on food and feed production [9].

Presently, about 97 % of the biofuels used in the U.S. are derived from cornstarch. The production of biofuels from starch is a mature technology, and it is not likely to see significant reduction in their production costs [10]. Moreover, corn-based biofuels cause a dangerous competition for the limited agricultural farmland and other agricultural resources against food production [11]. However, if cellulosic biomass feedstocks are used instead of corn, there will be much less competition between fuel and food. Cellulosic biomass feedstocks are abundant and diverse [12, 13]. Thus, the ability to produce biofuels from cellulosic biomass will be a key to making biofuels competitive with petroleum-based fuels [12–14].

Biofuels have the potential to reduce GHG emissions by an average of 34 % comparing to gasoline [15]. The carbon dioxide released during fuel combustion is “recycled” by the plant as it grows [16]. Biofuels can also reduce pollutant



emissions. Bioethanol, in particular, can ensure complete combustion, reducing carbon monoxide emissions [17].

Currently, several technical barriers hinder large-scale and cost-effective production of cellulosic biofuels, such as the low density of cellulosic biomass feedstocks (causing high transportation and storage cost), and the lack of efficient pretreatment technologies for cellulosic biomass [12, 13].

### ***9.1.2 Application of Ultrasonic Energy in Biofuel Production***

Ultrasound is a mechanical acoustic wave with the frequency greater than the upper limit of the human hearing range. The frequency of ultrasound ranges from roughly 10 kHz to 20 MHz [18, 19]. Ultrasound waves have certain unique physical properties. When ultrasound waves are applied in a medium such as liquid or slurry, it can accumulate energy by acoustic cavitation, and then release energy instantaneously by the collapse of cavitation bubbles within several microseconds. The intensity of the released energy can provide powerful hydro-mechanical shear forces to break down chemical linkage, destroy the limit in multiphase interface of reactants, and enhance heat and mass transfer during the reaction [19–21].

The introduction of ultrasonic energy in biofuel production can alter the recalcitrance structure features and separate complicated compositions in biofuel feedstock materials. These efforts are helpful to overcome the technical barriers that limit efficient biofuel production [22]. Ultrasonic energy has been applied to many research fields related to biofuel production including pretreatment, hydrolysis, fermentation of cellulosic biomass, and biodiesel synthesis [22–33].

It has been reported that ultrasound energy combined with proper solvents could increase the porosity of cellulose fiber and the cleavage of linkages in lignin [26–28], reduce particle size [29], increase surface area [29], and decrease the crystallinity of cellulosic material [30]. Integration of ultrasound energy with some pretreatment methods such as alkaline pretreatment, fungal pretreatment, and ionic liquid pretreatment could increase sugar yield by 10–300 % in bioethanol production from cellulosic biomass [22–33]. The application of ultrasound energy also improved the efficiency of biodiesel production by reducing reaction time and temperature [22–33]. Progress in the application of ultrasonic energy to biofuel production can be found in an in-depth literature review [33].

## **9.2 Ultrasonic Vibration-Assisted Pelleting of Cellulosic Biomass Overview**

Ultrasound energy combined with proper solvents has been used in various reactions throughout biofuel production. Ultrasonic vibration-assisted (UV-A) pelleting of cellulosic biomass is the first effort to apply ultrasound energy to dry biomass feedstock for the purpose of biofuel production.

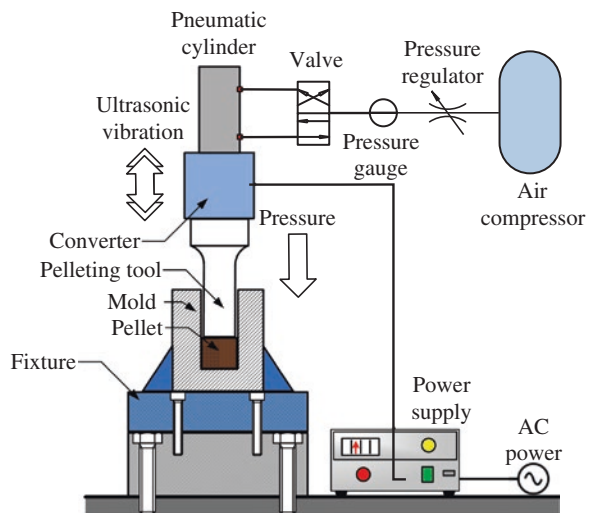
Pelleting is generally described as “the agglomeration of small particles into firm, uniformly shaped granules by means of mechanical processes” [34]. Pelleting of cellulosic biomass can increase the overall efficiency of biofuel production by enabling the use of existing transportation infrastructure and storage systems [35]. Traditionally, biomass pellets are made by ring-die pelleting, flat-die pelleting, screw extrusion, and briquetting press processes [36–40]. Ultrasonic vibration-assisted (UV-A) pelleting is a newly developed pelleting method. UV-A pelleting can produce biomass pellets with density as high as  $1,000 \text{ kg/m}^3$ , which is approximately an increase by a factor of 30 in density compared with the bulk density of cellulosic biomass before pelleting [41, 42].

Figure 9.1 illustrates UV-A pelleting of cellulosic biomass. UV-A pelleting is performed on a modified ultrasonic machine (Model AP-1000, Sonic-Mill, Albuquerque, NM, USA). The machine includes a power supply that converts 60 Hz conventional line electrical power into 20 kHz electrical power, a piezoelectric converter that converts high frequency electrical energy into mechanical vibration, and a titanium pelleting tool. The tip of the pelleting tool is a solid cylinder with a flat end. The ultrasonic motion from the converter is amplified and transmitted to the pelleting tool. This causes the pelleting tool to vibrate perpendicularly to the tool end surface at high frequency.

Before making pellets, biomass particles are loaded into an aluminum mold, which consists of three parts. The upper two parts formed a cylindrical cavity, and the bottom part is a square plate serving as a base. They are assembled together with pins.

Pelleting pressure is applied by a pneumatic cylinder with compressed air from an air compressor. The air pressure in the pneumatic cylinder is controlled by a pressure regulator. A higher air pressure gives a higher pelleting pressure applied to the biomass in the mold by the pelleting tool.

**Fig. 9.1** Schematic illustration of ultrasonic vibration-assisted pelleting (after [41, 42, 49])



## 9.3 Pellet Quality

### 9.3.1 Significance of Pellet Quality

Pelleting plays an important role in the logistic efficiency of cellulosic biomass as the feedstock material for biofuel production. High costs related to cellulosic feedstock production and logistics (e.g. transportation and storage) can constitute 35 % or more of the total costs in manufacturing of cellulosic biofuels [43, 44]. Specifically, the logistics associated with transportation and storage of low-density biomass can make up more than 50 % of the feedstock costs [35]. If cellulosic biomass feedstock is pelleted, its handling efficiency will be greatly improved due to the increase in density and the improvement in flow ability [45, 46]. Pellets share bulk handling properties similar to those of grains, and thus can be handled efficiently using existing grain handling equipment and infrastructures, resulting in a significant reduction in logistics costs [35].

Conventional pelleting methods (e.g. ring-die pelleting, flat-die pelleting, screw extrusion, and briquetting press [47, 48]) generally involve high-temperature steam, high pressure, and often use binder materials, making it difficult to realize cost-effective pelleting on or near the field where cellulosic feedstock is available. UV-A pelleting, without using high-temperature steam or binder materials, can produce biomass pellets whose density is comparable to that processed by conventional pelleting methods [41, 42, 49].

### 9.3.2 Pellet Density

Density of a pellet is calculated by the ratio of its weight over its volume.

First of all, the density of wheat straw pellets produced with ultrasonic vibration was compared with that of pellets produced without ultrasonic vibration while all other process parameters were kept the same. Density measurements were carried out from Day 0, just after pellets were made and taken out of the mold, and were conducted every 24 h for the next 9 days. From each of the two test groups, which were pellets produced with ultrasonic vibration and pellets produced without ultrasonic vibration, five pellets were randomly chosen for density measurement, and the average was used to represent the group density.

The effect of ultrasonic vibration on pellet density is shown in Fig. 9.2. In the test group with ultrasonic vibration, pellet density stayed stable at around 740 kg/m<sup>3</sup> for 10 days. In the test group without ultrasonic vibration, pellet density decreased during the first 5 days. After Day 6, all the pellets produced without ultrasonic vibration fell apart into particles; thus, measurements could not be conducted. Hence, density data were not available for the next few days. It is clearly shown that pellets produced with ultrasonic vibration had much higher density than those produced without ultrasonic vibration [49].

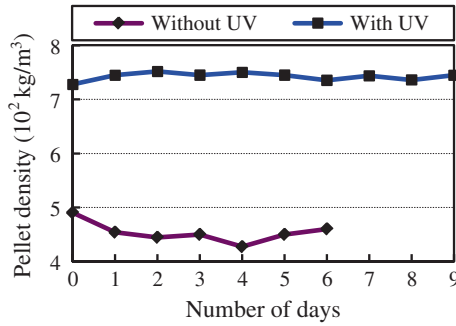


**Fig. 9.2** Effect of ultrasonic vibration on pellet density (after [49])

Figure 9.3a, b show a clear contrast between two pellets right after they were taken out of the mold. The one on the right was produced with ultrasonic vibration, and it was in a solid cylindrical shape with loose particles. The one on the left was processed without ultrasonic vibration, which was loose with many stray particles. From the microscopic pictures of the pellets cylindrical surfaces (Fig. 9.3c, d),

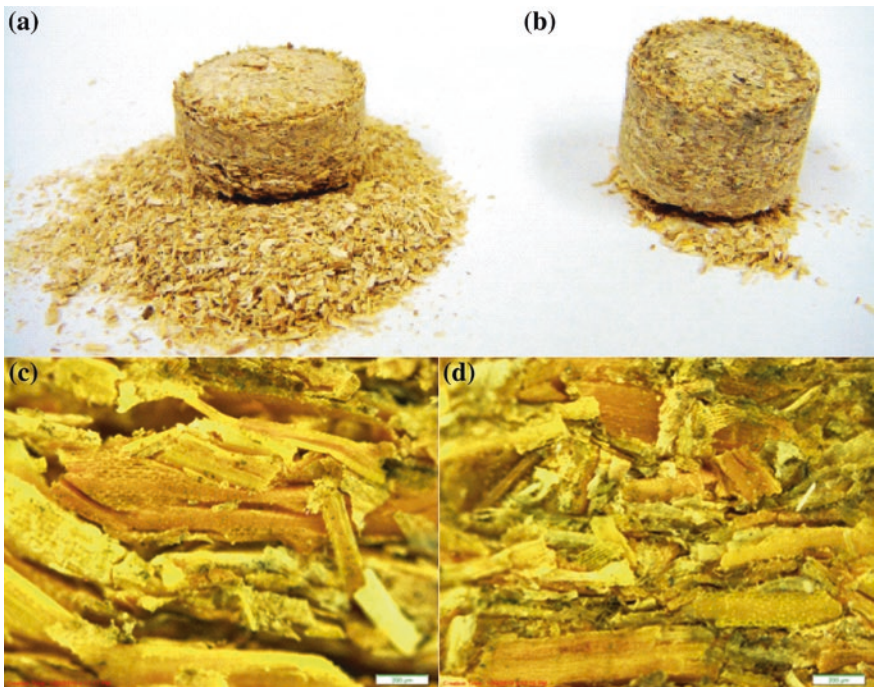


**Fig. 9.3** Pictures of pellets produced **a** without ultrasonic vibration and **b** with ultrasonic vibration; **c** and **d** top view microscopic ( $\times 50$ ) pictures of pellets shown in **a** and **b**

it was obvious that particles of the pellet processed with ultrasonic vibration were much more densely packed than those of the pellet processed without ultrasonic vibration.

It was also observed that, the pelleting force when ultrasonic vibration was used was not higher than that when ultrasonic vibration was not used. When pelleting pressure and time were kept constant as 345 kPa (50 psi) and 120 s, the maximum pelleting force was 2,834 N and the average pelleting force was 2,758 N without ultrasonic vibration; while the maximum pelleting force was 2,835 N and the average pelleting force was 2,760 N with ultrasonic vibration. Although a certain degree of variations could be observed on the pelleting force curve with ultrasonic vibration while the pelleting force curve without ultrasonic vibration was smoother, there was no significant difference in the average pelleting forces with or without vibration.

Similar improvement in pelleting density was observed when UV-A pelleting was applied to several other cellulosic biomass materials, such as sorghum stalks and switchgrass [50]. Compared with the density of pellets made by a conventional pelleting method such as a ring-die pelleting machine, UV-A pelleting produced slightly lower density [51]. However, commercially available ring-die pelleting machine has much higher production capacity and torque than the lab-scale UV-A pelleting machine. In addition, conventional pelleting methods produce pellets as animal feed or direct heating fuels, not as feedstocks for biofuel production. The optimal pellet density suitable for biofuel production has not been determined.

Several process parameters are reported to greatly affect pellet density in UV-A pelleting of cellulosic biomass. These parameters include ultrasonic power, pelleting pressure, moisture content of cellulosic biomass, and particle size of cellulosic biomass.

Ultrasonic power refers to the power provided to the ultrasonic converter by a power supply (as shown in Fig. 9.1). It determines the tool vibration amplitude. A larger ultrasonic power creates higher tool vibration amplitude. The selected ultrasonic power is expressed as a percentage of the maximum ultrasonic power for the machine, ranging from 0 % (no ultrasonic vibration applied) to 100 %. The frequency of the tool vibration is fixed as 20 kHz for this machine. Reported studies revealed that, when pelleting pressure was kept at 275 kPa (40 psi) in UV-A pelleting of wheat straw and sorghum stalk, pellet density increased dramatically as the ultrasonic power increased from 30 to 50 %. However, when the ultrasonic power increased from 50 to 55 %, the produced pellet density remained approximately at the same level [52, 53].

Pelleting pressure represents the air pressure in the pneumatic cylinder driving the pelleting tool. A higher air pressure in the pneumatic cylinder produces a larger compressive force upon cellulosic biomass loaded into the mold. In UV-A pelleting of wheat straw and sorghum stalk, there was a dramatic increase in pellet density as pelleting pressure increased from 138 kPa (20 psi) to 206 kPa (30 psi) and further increased to 275 kPa (40 psi). However, when pelleting pressure was increased to 345 kPa (50 psi), the pellet density did not increase noticeably [52, 54].

Material properties of cellulosic biomass also play an important role in determining pellet density. Moisture content of cellulosic biomass represents the amount of moisture (water) contained in the biomass. Higher moisture content means more water in the material. Moisture content is usually measured by following the American Society of Agricultural and Biological Engineers (ASABE) Standard S358.2 [55] and calculated by the ratio of the weight of water in the material to the total weight of the biomass material. The effect of moisture content of cellulosic biomass on pellet density in UV-A pelleting has been studied using three types of biomass materials: wheat straw, switchgrass, and sorghum. Generally, pellet density increased as moisture content of cellulosic biomass decreased from 25 to 20 %, and to 13 % [41]. It has been suggested that, in UV-A pelleting of wheat straw, moisture content should be lower than 15 %. Similar conclusions were reached when using conventional pelleting methods [40, 56].

Particle size of cellulosic biomass in UV-A pelleting also has a strong impact on pellet density. Before cellulosic biomass is ready to be made into pellets, it needs to be treated through a size reduction process. Size reduction produces small particles from large stems of biomass materials. This process is usually conducted on knife mills or hammer mills [57]. Particle size is often referred to as the opening size on a sieve installed on mills.

A typical knife mill has three or four knives mounted on the rotor inside the milling chamber. Cutting bars are mounted on the inside wall of the chamber. Cellulosic biomass is cut into particles between the knives and the cutting bars. A sieve is installed at the bottom of the chamber. The opening size on the sieve will determine the particles processed through size reduction. During knife milling, cellulosic biomass particles that are smaller than the opening size on the sieve will pass through the sieve, while those larger than the opening size will be recirculated and milled further. Milling cellulosic biomass using a sieve with smaller opening size produces finer particles. However this consumes more specific energy.

Effects of particle size of cellulosic biomass on pellet density in UV-A pelleting of wheat straw have been studied with four levels of particle sizes produced by knife milling: 0.25, 1, 2, and 8 mm. Pellet density increased as particle size decreased [54, 58]. This trend is somewhat different from that observed in ring-die pelleting of wheat straw, corn stover, big bluestem, and sorghum stalk when particles of two levels of particle size (3.2 and 6.5 mm) were used. There, the difference in particle size did not have significant influences on pellet density [59].

### ***9.3.3 Pellet Durability***

After cellulosic biomass pellets leave the pelleting facility, they are exposed to fragmentation and abrasion as they go through handling and transportation. These impacts and forces can degrade biomass pellets. Durability tests are often performed on a pellet durability tester by following the American Society of Agricultural and Biological Engineers (ASABE) Standard S269.4 [60]. First,



pellets are loaded into the chambers of the tester. Then, the chambers are rotated (tumbling) at 50 rpm for 10 min. Results of the test are interpreted as a standard measure of pellet quality referred to as durability index. Durability index is calculated as the ratio between the weight of whole pellets after tumbling and the weight of pellets before tumbling. A higher durability index means that the pellets have a higher ability to survive the impacts and forces through handling and transportation.

When comparing durability indexes of pellets produced with and without ultrasonic vibration, it is found that pellets produced with ultrasonic vibration had a durability index of 80 % after tumbling for 2 min. This means that 80 % of the pellets were still in a solid cylindrical shape. Durability index decreases to 68 % after another 4 min of tumbling. After 10 min of tumbling, durability index of the pellets produced with ultrasonic vibration stayed at 63 %. For pellets processed without ultrasonic vibration, none of them could survive after the first 2 min of tumbling. In another way, none of them could hold their cylindrical shape; therefore they broke down back into particles [49].

Process parameters that affect the durability of pellets in UV-A pelleting include ultrasonic power, pelleting pressure, moisture content of cellulosic biomass, and particle size of cellulosic biomass.

For wheat straw pellets made by UV-A pelleting, it is found that durability index increased as ultrasonic power increased from 30 to 40 % and to 50 %. Ultrasonic power of 50 and 55 % result in approximately the same durability index [52]. It is observed that pellet durability index increased as pelleting pressure increased from 138 kPa (20 psi) to 206 kPa (30 psi) and to 275 kPa (40 psi). However, when pelleting pressure increased to 345 kPa (50 psi), durability index did not change much [52, 54].

Studies also show that, in UV-A pelleting of switchgrass, higher moisture content (>15 %) led to lower durability index. A similar observation was also reported in conventional pelleting of other cellulosic biomass, such as alfalfa and peanut hull. Relative low moisture content (5–10 %) is preferable to achieve high pellet durability [37, 61]. Reported studies also indicate that smaller particle size of cellulosic biomass is preferable as feedstocks in UV-A pelleting to achieve better durability [54, 62].

### **9.3.4 Pellet Stability**

Stability of a biomass pellet is determined by evaluating changes in its dimensions (volumetric basis) with time. The general trend is that the volume of a pellet will increase (spring-back) with time after it is taken out of the mold. The stability of a pellet is measured by the spring-back of the pellet. Pellets having a lower spring-back have higher stability.

When comparing spring-back of pellets produced without and with ultrasonic vibration, it is found that pellets processed with ultrasonic vibration are more stable (i.e. smaller spring-back) [49].

One study shows that, as ultrasonic power increased from 30 to 40 %, spring-back of wheat straw pellets decreased slightly. When ultrasonic power increased to 50 %, there was a dramatic decrease in spring-back. Ultrasonic power of 50 and 55 % did not make much difference in spring-back of the pellets [52]. As pelleting pressure increased from 138 kPa (20 psi) to 345 kPa (50 psi), there was no significant difference in spring-back values of pellets.

For UV-A pelleting, lower moisture content (<15 %) and smaller particle size tend to produce pellets with higher stability [54, 62].

## 9.4 Pellet Sugar Yield

### 9.4.1 Cellulosic Biomass Composition and Structure

The compositions of cellulosic biomass include approximately 40–50 % cellulose, 20–30 % hemicellulose, and 15–20 % lignin [63, 64]. Cellulose, the principal carbohydrate component, is organized into fibrils. A fibril is an aggregate of cellulose chains consisting of many cellobiose units. These sheets of glucan chains stacking on top of each other give cellulose its highly ordered crystalline characteristic [65].

Surrounding cellulose fibrils is hemicellulose that forms a matrix by bonding with cellulose and other hemicellulose molecules. Hemicellulose consists of various sugar units. The dominant carbohydrate components of hemicellulose are xylan and glucomannan [66]. Cellulose and hemicellulose are polysaccharides that can be hydrolyzed to sugars fermentable to ethanol biofuels.

Lignin is considered filler in the spaces between cellulose and hemicellulose. Lignin performs an important role in strengthening cell walls of cellulosic biomass by cross-linking polysaccharides (primarily hemicellulose) and providing support to structural elements in a plant body [67]. This extensive cross-linking of lignin and other polysaccharides limits the accessibility of enzymes to digesting polysaccharides. Lignin contains no sugar components and it cannot be digested by cellulase enzymes [68]. Lignin can be used as a compound for pharmaceutical purposes or can be burned to produce electricity and heat [66, 69].

### 9.4.2 Major Conversion Technologies to Produce Cellulosic Biofuels

Figure 9.4 shows process steps in a biorefinery. After arriving at the biorefinery, biomass pellets are converted into biofuels through either sugar or syngas platform. This section will focus on effects of UV-A pelleting on yield through the sugar platform.



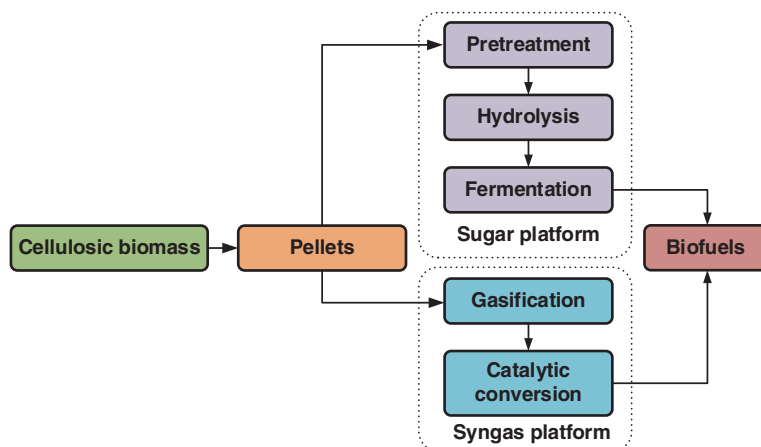


**Fig. 9.4** Two platforms to convert biomass pellets into biofuels (after [10])

Through the sugar platform, pellets are first dissolved in solvents and pretreated. Pretreatment is necessary to break down the crystalline structure of cellulosic biomass, and to isolate the cellulose from lignin and hemicellulose in cell walls. This step makes cellulosic biomass more accessible to hydrolysis; thus, it can speed up the saccharification rate of cellulose to fermentable sugar and increase sugar yield in hydrolysis. Enzymatic hydrolysis is a commonly used technology to obtain fermentable sugars from cellulosic biomass. Cellulase enzymes such as exoglucanase, endoglucanase, and beta-glucosidase are often utilized to break down long chain sugar polymers in cellulosic biomass into fermentable sugars (such as glucose, xylose, arabinose, galactose, and mannose). Afterwards, fermentation will convert sugars into ethanol by using microorganisms such as yeast. An ethanol recovery and distillation process will be added to produce fuel grade bioethanol [64, 66]. Sugar yield through this platform is critical to the cost effectiveness of biofuel production, because it is approximately proportional to the ethanol biofuel yield [70, 71].

In the syngas platform, pellets are taken through a gasification process. In this process, biomass is heated in the presence of air or steam to produce synthesis gas or syngas. Syngas is a mixture of carbon monoxide, hydrogen, and other hydrocarbons. Syngas is more efficient than direct combustion of the original cellulosic biomass feedstocks. Syngas can then be burned directly in internal combustion engines or turbines, or be used to produce methanol or methoxymethane [72].

### 9.4.3 Diluted Acid Pretreatment of Cellulosic Biomass Pellets

Feedstock pretreatment strategies for cellulosic biofuel production have been extensively investigated. There are several review articles presenting comprehensive

overviews on this topic [73, 74]. Generally speaking, pretreatment can be classified into chemical pretreatment, physical pretreatment, and biological pretreatment, depending on what forces or energy forms are consumed in the processes. Also, some pretreatment technologies involve two or more pretreatment methods from the above three categories [73]. However, none of these pretreatment technologies can be declared as an optimal solution, because each pretreatment has its advantages and disadvantages [71, 73, 74].

Dilute acid pretreatment with sulfuric acid has been proven to be a successful choice for a wide range of cellulosic biomass materials due to its low cost and effectiveness [73, 74]. It will solubilize hemicellulose to disrupt the shield formed by hemicelluloses and lignin and keep cellulose and lignin intact so that the enzymatic hydrolysis of cellulose into fermentable sugars is enhanced [75–77]. It is employed to pretreat cellulosic biomass pellets made from wheat straw, switchgrass, sorghum stalk, and corn stover in studies discussed in this chapter.

Dilute acid pretreatment of pellets was carried out in a bench top reactor. Pellets were mixed and dissolved with diluted sulfuric acid (0.8–2 % concentration) to obtain biomass slurry with 5 % solid content. The biomass slurry was then loaded into a reaction vessel. The valve on the cooling loop, motor driving the impeller, and thermocouple and heater were all connected to a controller. The pretreatment conditions were: 120–140 °C pretreatment temperature, 20–30 min pretreatment time, and 100–120 rpm rotation speed of the impeller mixer.

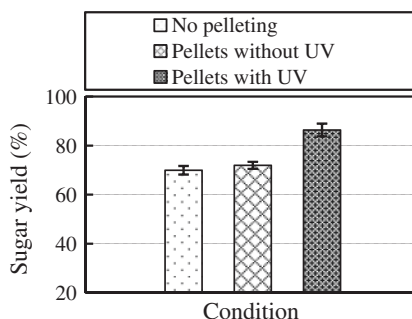
#### 9.4.4 Process Parameters that Affect Sugar Yield

As discussed previously, pretreated cellulosic biomass is hydrolyzed into fermentable sugar (mainly glucose) in enzymatic hydrolysis. Glucose concentration can be detected using high-performance liquid chromatography (HPLC), a chromatographic technique that can identify and quantify individual components of a liquid mixture [78].

Sugar yield is used to evaluate the efficiency of enzymatic hydrolysis. It is expressed in terms of the percentage of cellulose converted to fermentable sugar (glucose).

Figure 9.5 shows effects of ultrasonic vibration on sugar yield. Sugar yield results were compared among three groups of switchgrass biomass: particles

**Fig. 9.5** Effects of ultrasonic vibration on sugar yield (after [50])



(without pelleting), pellets produced without ultrasonic vibration, and pellets produced with ultrasonic vibration. The sugar yield of pellets produced with ultrasonic vibration (86.4 %) was about 24 % higher than those without UV-A pelleting (70 % for non-pelleted switchgrass particles and 71.2 % for switchgrass pellets made without ultrasonic vibration) [50]. Sugar yields of pellets made from different types of cellulosic biomass: wheat straw, corn stover, and sorghum were improved by 10–25 % when ultrasonic vibration was applied compared with sugar yields of those pellets produced without ultrasonic vibration [79].

UV-A pelleting can also reduce solid weight loss during dilute acid pretreatment. Only the solid biomass collected after pretreatment goes into the subsequent enzymatic hydrolysis. This means that, for the same amount of cellulosic biomass; less solid weight loss in pretreatment leads to higher sugar yield. It was reported that, for pellets made from all four types of cellulosic biomass mentioned above, solid weight loss in pretreatment was approximately 25 % lower when ultrasonic vibration was applied [79].

In UV-A pelleting of wheat straw and sorghum stalk, as ultrasonic power increased from 30 to 55 %, sugar yield of produced pellets was increased by about 30 % [52, 54]. Pelleting pressure also affected pellet sugar yield. As pelleting pressure increased from 138 kPa (20 psi) to 345 kPa (50 psi), sugar yield decreased first and then increased. The lowest sugar yield was found when pelleting pressure was 275 kPa (40 psi). There was no significant difference between sugar yields when pelleting pressure was 138 kPa (20 psi) and 345 kPa (50 psi) [52].

A 2<sup>4</sup> (four factors, two levels) full factorial design of experiments revealed that increasing moisture content of wheat straw from 10 to 20 % had little impact on pellet sugar yield [54]. Some researchers believe that cellulosic biomass of smaller particle size has larger surface area for enzymes to access; thus, smaller particle size may result in higher sugar yield in enzymatic hydrolysis [80–83]. However, in UV-A pelleting of 0.2 and 2.4 mm switchgrass particles, sugar yields of the produced pellets had no significant difference [54]. It was also reported that cellulosic biomass particle sizes before and after UV-A pelleting were not significantly different [84].

## 9.5 Pelleting Energy Consumption

### 9.5.1 Significance of Energy Consumption

Cellulosic biofuels have been considered as sustainable substitute for petroleum-based liquid transportation fuels. One major concern over wide adoption of cellulosic biofuels is the energy consumption during biofuel production processes.

Sugar yield through hydrolysis of cellulosic biomass was once regarded as the first research priority in biofuel production [73, 74]. Recently, due to the increase of awareness of sustainable development, the significance of energy consumption in biofuel production has also been recognized. Energy consumption in biofuel

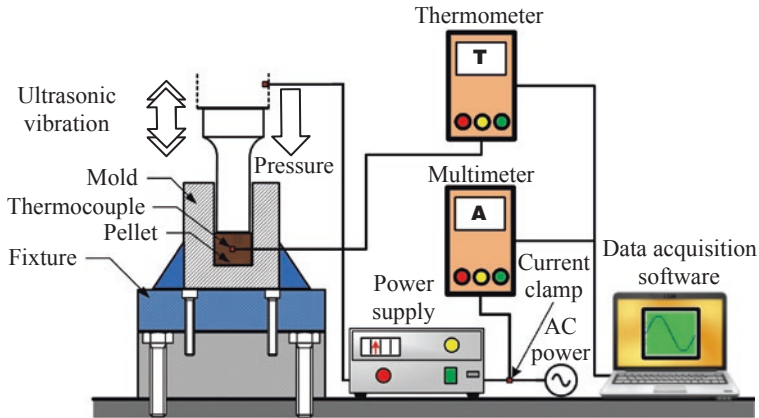


**Fig. 9.6** Illustration of energy consumption and temperature measurement in ultrasonic vibration-assisted pelleting (after [58])

production has a substantial influence in the reduction of production cost and greenhouse gas emission for a successful large scale substitution for petroleum-based liquid transportation fuels.

UV-A pelleting of cellulosic biomass is a newly developed technology. It is imperative to identify critical process parameters that significantly influence energy consumption. Energy consumption in UV-A pelleting is referred to as the electrical energy consumed by the power supply. The power supply had a near constant voltage ( $V$ ) of 120 V. As shown in Fig. 9.6, a current clamp and a multimeter were used to measure the electric current when UV-A pelleting was performed under different conditions. Current data were collected using data acquisition software. After each experiment run, the average current value ( $I_{AVE}$ ) would be used to calculate the total energy consumption ( $E$ ) during the pelleting period ( $t$ ) using Eq. (9.1):

$$E = \frac{V \times I_{AVE} \times t}{3,600} \text{ (Wh)} \quad (9.1)$$

### 9.5.2 Parameters that Affect Pelleting Energy Consumption

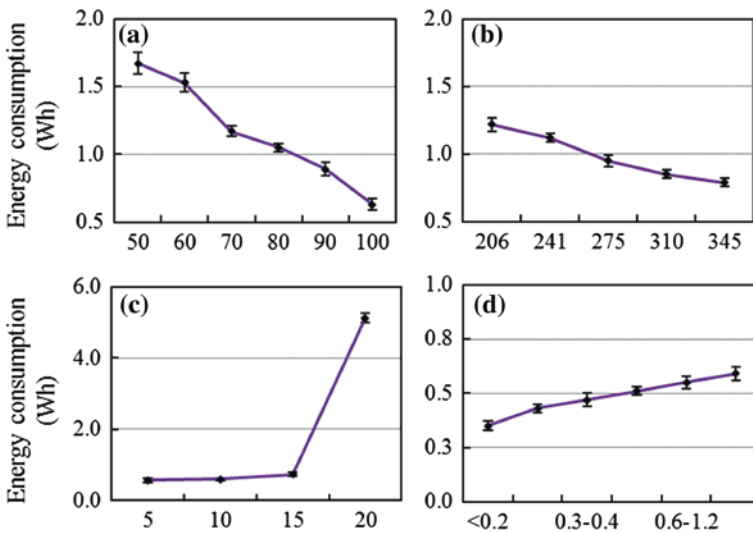
Process parameters that affect energy consumption in UV-A pelleting of cellulosic biomass include ultrasonic power, pelleting pressure, moisture content of cellulosic biomass, and particle size of cellulosic biomass [58, 85]. To investigate their effects on energy consumption, experiments were carried out to measure energy consumption when producing wheat straw pellets with the same target density ( $930 \text{ kg/m}^3$ ) under different parameter settings. Pellet weight (weight of biomass particles loaded into mold to make one pellet) was kept constant at 1 g [85]. This means that, to achieve the desired density, different amounts of time and energy are required under different parameter settings.

As shown in Fig. 9.7a, energy consumption decreased rapidly as ultrasonic power increased from 50 to 100 %. It was also found that the pellet time needed to achieve the target density was shortened greatly as ultrasonic power increased [85]. In a separate study, when pelleting time was fixed, energy consumption increased more than 60 % as ultrasonic power was tuned up from 20 to 40 % [58]. So it was concluded by the first study [85] that high energy consumption for low ultrasonic power was caused by the longer time needed to produce pellets of the desired density. Another observation was that with the same length of pellet time, energy consumption increased almost linearly as pellet weight increased from 0.5 to 3 g [58].

Similar to ultrasonic power, with other parameters remaining at the same settings, higher pelleting pressure needed a shorter period of time to achieve the target density [85]. This can be used to explain the trend plotted in Fig. 9.7b. Alternatively, when pelleting time remained constant, a 25 % drop in energy consumption was noticed when pelleting pressure was increased from 206 kPa (30 psi) to 275 kPa (40 psi). However, there was no significant decline in energy consumption when pelleting pressure was further increased from 275 kPa (40 psi) to 345 kPa (50 psi).

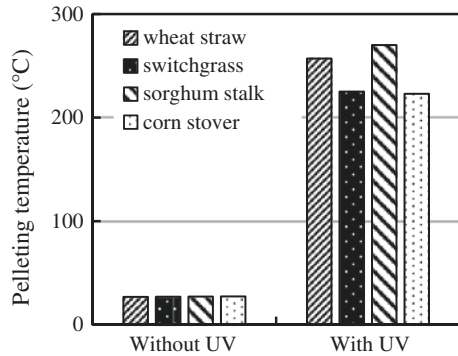
The effect of moisture content of the cellulosic biomass on energy consumption is shown in Fig. 9.7c. As moisture content of cellulosic biomass increased from 15 to 20 %, much higher energy was required to obtain pellets of the desired density. There was only a slight rise in energy consumption when moisture content increased from 5 to 10 % [85].

Figure 9.8d shows the energy consumed to produce pellets of the desired density using 6 groups of particles of different sizes (<0.2, 0.2–0.3, 0.3–0.4, 0.4–0.6,



**Fig. 9.7** Effects of process parameters on energy consumption (after [58, 85]). **a** Ultrasonic power (%), **b** pelleting pressure (kPa), **c** moisture content (%) and **d** particle size range (mm)

**Fig. 9.8** Effect of ultrasonic vibration on pelleting temperature. Reprinted with permission from [79]. Copyright © 2013, Springer



0.6–1.2, and 1.2–2.4 mm). A clear trend was observed that smaller particles consume less energy [85]. The same trend was also found when comparing the energy consumption of pelleting 2, 4, and 8 mm wheat straw particles [58]. Other biomass materials such as corn stover, sorghum stalk, and big bluestem particles of 3.5 mm needed less energy to be made into pellets than their respective 9.6 mm counterparts [51]. Comparing the aforementioned four types of cellulosic biomass, under same UV-A pelleting parameter settings, sorghum stalk consumed the least power, and the other three types did not differ greatly regarding power consumption [86].

Predictive models for energy consumption in UV-A pelleting using the response surface methodology can also be found in the literature [87, 88]. With the current lab-scale setup, the specific energy (energy per unit weight) consumption of UV-A pelleting is higher than that of conventional ring-die pelleting. It is believed that with a production scale setup, the energy efficiency would be greatly improved [51].

## 9.6 Pelleting Temperature

### 9.6.1 Significance of Pelleting Temperature

In conventional pelleting of cellulosic biomass (e.g. ring-die pelleting, flat-die pelleting, screw extrusion, and briquetting press [47, 48]), pelleting temperature has been identified as a key factor affecting pellet quality in terms of density, durability, and stability. In general, cellulosic biomass needs to be preheated by high-temperature steam or heated dies to achieve quality pellets [89]. This benefit can be interpreted as follows. Less thermostable than cellulose, lignin would become soft and melted when heated, exhibiting thermosetting property. This property would cause lignin to become permanently rigid and likely to bond together with other polymers (cellulose and hemicellulose) in the biomass to form pellets [90].

UV-A pelleting can also induce an increase in temperature of cellulosic biomass due to application of high frequency ultrasonic vibration. Ultrasonic vibration causes

biomass particles to vibrate at high frequency, resulting in absorption of ultrasound energy mainly in the form of heat generation. It was found that during UV-A pelleting of wheat straw, temperature of cellulosic biomass could rise as high as 300 °C [91]. However, charring might happen inside a pellet when temperature was too high, which can result in deterioration of pellet quality and a reduction in sugar yield [91–93]. The following hypothesis was also proposed: high temperature generated during UV-A pelleting could decompose lignin. Lignin serves as a protecting shield over cellulose. This effect might help to release more cellulose and make cellulose biomass more amenable to enzymatic hydrolysis towards a higher sugar yield [79].

Figure 9.6 illustrates the temperature measurement in UV-A pelleting. Thermocouples were inserted inside a biomass pellet, and were connected to a thermometer. Temperature measurement data were recorded using data acquisition software.

### ***9.6.2 Parameters that Affect Pelleting Temperature***

For four types of cellulosic biomass shown in Fig. 9.8, with the same pelleting pressure and time, there was a dramatic temperature increase when ultrasonic vibration was applied at the 40 % ultrasonic power level compared with no ultrasonic vibration applied [79].

A 2<sup>3</sup> (three factors, two levels) full factorial design of experiments was used to investigate effects of three parameters (ultrasonic power, pelleting pressure, and pellet weight) on pelleting temperature [85]. Levels of these parameters were: 60 and 20 % for ultrasonic power, 138 kPa (20 psi) and 345 kPa (50 psi) for pelleting pressure, and 2.6 and 1.4 g for pellet weight. Analysis of variance results indicated that pelleting temperature was significantly affected by ultrasonic power and pellet weight. Pelleting pressure did not affect temperature significantly.

Reports on effects of moisture content and particle size of cellulosic biomass on UV-A pelleting temperature are currently not available.

### ***9.6.3 A Physics-Based Temperature Model***

#### **9.6.3.1 Model Development**

A physics-based temperature model has been developed to explain experimentally determined relations between UV-A pelleting parameters and temperature, and provide guidelines to optimize these parameters for producing quality pellets [94].

Assumptions of this model include (1) biomass particles uniformly fill the mold; (2) thermal conductivity of biomass is not dependent on temperature; (3) ultrasound energy absorbed by biomass particles results in heat generation; (4) heat transfer takes place within biomass particles by conduction only; and (5) boundary temperatures are fixed as room temperature.



According to conservation of energy, the rate at which thermal energy enters the volume element across the face at  $x$  is given by the product of the heat flux  $q_x|_x$  and the cross-sectional area  $A$ . Similarly, the rate at which thermal energy leaves the volume element across the face at  $x + \Delta x$  is  $q_x|_{x+\Delta x}$ . The net rate of heat generation is  $QA\Delta x$ . Finally, the rate of accumulation is given by the time derivative of the thermal energy content of the volume element. Thus, the balance equation becomes:

$$(q_x|_x - q_x|_{x+\Delta x})A + QA\Delta x = \rho c \frac{\partial T}{\partial t} A \Delta x \quad (9.2)$$

Taking the limit as  $\Delta x \rightarrow 0$  and using Fourier's law, the balance equation becomes:

$$\frac{\partial}{\partial x} \left( k \frac{\partial T}{\partial x} \right) + Q = \rho c \frac{\partial T}{\partial t} \quad (9.3)$$

According to the assumption that thermal conductivity of biomass  $k$  is not dependent on temperature, the heat conduction differential equation becomes:

$$k \frac{\partial^2 T}{\partial r^2} + \frac{k}{r} \frac{\partial T}{\partial r} + k \frac{\partial^2 T}{\partial z^2} + Q - \rho c \frac{\partial T}{\partial t} = 0 \quad (9.4)$$

When an ultrasonic wave passes through a medium, attenuation occurs due to reflection, scattering, and absorption [95]. As the wave travels through the medium, energy is irreversibly lost to the medium in the form of heat generation at a rate given by [95]:

$$Q = 2\alpha I, \quad I = I_0 e^{-2\alpha z} \quad (9.5)$$

Introducing Eq. (9.5) in Eq. (9.4) gives the heat transfer equation as follows:

$$k \frac{\partial^2 T}{\partial r^2} + \frac{k}{r} \frac{\partial T}{\partial r} + k \frac{\partial^2 T}{\partial z^2} + 2\alpha I_0 e^{-2\alpha z} - \rho c \frac{\partial T}{\partial t} = 0 \quad (9.6)$$

Equation (9.6) and boundary conditions together give finite difference equations where subscripts denote location and superscripts denote time ( $T(x_i, t_j) = T_i^j$ ). Considering a cylindrical shaped pellet of radius  $r$  and height  $h$ , the approximation for the Eq. (9.4) at  $T(x_i, t_j)$  is:

$$T_i^{j+1} = \left[ \frac{k(T_{i+1}^j - 2T_i^j + T_{i-1}^j)}{\Delta x^2} + Q \right] \frac{\Delta t}{\rho c} + T_i^j \quad (9.7)$$

Explicit finite difference method can be used to solve temperatures at all locations within one pellet.

### 9.6.3.2 Predicted Effects of Parameters on Temperature

Using this model, effects of ultrasonic power on temperature in UV-A pelleting of wheat straw can be predicted. In order to implement the computation numerically, constants in the model are given in Table 9.1. Necessary conversions of ultrasonic

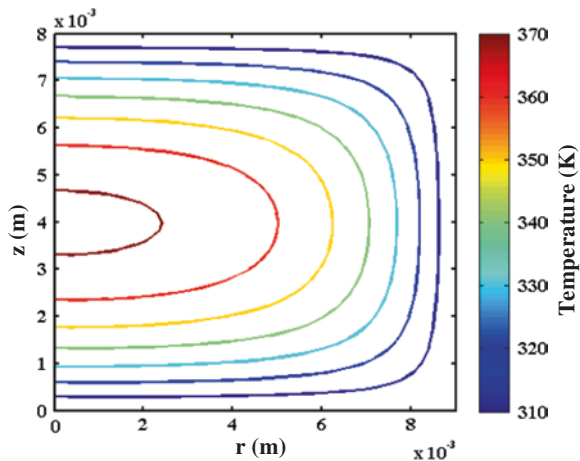
**Table 9.1** Values of variables in the model

Variable	Value
<i>c</i>	1,243 J/kg K
<i>k</i>	0.34 W/m K
<i>m</i>	0.002 kg
<i>h</i>	0.008 m
$\alpha$	3.13 m <sup>-1</sup>
<i>t</i>	400 s

**Table 9.2** Conversion chart of ultrasonic power to ultrasound intensity

Ultrasonic power (%)	Ultrasonic wattage (W)	Ultrasonic intensity (W/m <sup>2</sup> )
10	50	210,379
20	100	420,757
30	150	631,136
40	200	841,515
50	250	1,051,894
60	300	1,262,272
70	350	1,472,651
80	400	1,683,030
90	450	1,893,409
100	500	2,103,787

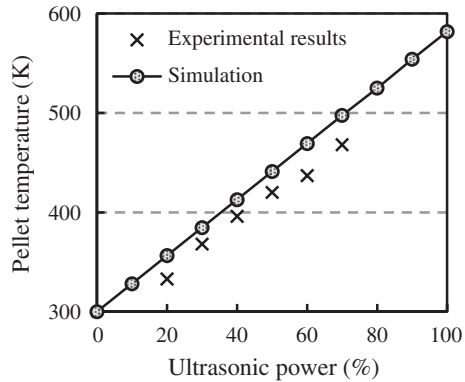
**Fig. 9.9** Predicted temperature distribution (ultrasonic power = 40 %). Reprinted with permission from. Copyright © 2014, Elsevier



power percentage values into ultrasonic wattage and ultrasonic intensity are listed in Table 9.2.

Figure 9.9 shows the predicted temperature distribution in a pellet at 400 s when ultrasonic power is set at 40 %. The temperature distribution is symmetric to the pellet center. For one pellet, the equilibrium temperature (temperature changes

**Fig. 9.10** Comparison of pellet temperature between predicted results and experimental results at pellet center. Reprinted with permission from [94]. Copyright © 2014, Elsevier



with time is less than 0.01 K/s) at different locations are different. As the distance to the pellet center increases, the equilibrium temperature becomes lower. The highest equilibrium temperature locates at the pellet center.

It is also predicted that temperature increases as ultrasonic power and pelleting duration increase.

### 9.6.3.3 Pilot Experimental Validation

To verify the relations predicted by the model, experiments were performed under ultrasonic power of six levels while other parameters were kept constant. Experimental and predicted temperatures at the pellet center are compared in Fig. 9.10. Temperature rise was proportional to the increase of ultrasonic power. It can be seen that the trend of predicted relation between ultrasonic power and temperature agreed well with that determined by experiments.

## 9.7 Conclusions and Future Outlook

Ultrasonic vibration-assisted (UV-A) pelleting of cellulosic biomass is a novel feedstock preprocessing technology for cellulosic biofuel production. UV-A pelleting combines pelletizing and ultrasonic treatment into one process. Major conclusions that can be reached from published studies are: (1) UV-A pelleting can produce dense, durable, and stable biomass pellets. Process parameters (including ultrasonic power, pelleting pressure, moisture content of cellulosic biomass, and particle size of cellulosic biomass) affect density, durability, and stability of pellets produced by UV-A pelleting. (2) Compared with non-pelleted biomass or biomass pelleted without ultrasonic vibration, pellets produced by UV-A pelleting have more than 20 % higher sugar yield. (3) There is a dramatic temperature increase inside the pellet during UV-A pelleting process. Such temperature increase is

hypothesized to be the key factor affecting pellet quality and sugar yield. A physics-based temperature model has been developed to explain experimentally determined relations between UV-A pelleting process parameters and temperature, and provide guidelines to optimize these parameters for producing high-quality pellets.

Many research perspectives of UV-A pelleting remain to explore. Examples are: (1) the underlying mechanism of how UV-A pelleting enhances sugar yield; (2) physics-based models for pellet density, durability, and stability; and (3) energy balance and life-cycle assessment of UV-A pelleting.

## References

1. Energy Information Administration (2012) Annual energy review 2011. <http://www.eia.gov/totalenergy/data/annual/pdf/aer.pdf>
2. Energy Information Administration (2012) U.S. Energy consumption by sector of 1949–2011. <http://www.eia.gov/totalenergy/data/annual/txt/ptb0201a.html>
3. Energy Information Administration (2014) Monthly energy review. <http://www.eia.gov/totalenergy/data/monthly/pdf/mer.pdf>
4. Huber GW (2008) Breaking the chemical and engineering barriers to lignocellulosic bio-fuels: next generation hydrocarbon biorefineries. <http://www.ecs.umass.edu/biofuels/Images/Roadmap2-08.pdf>
5. Environmental Protection Agency (2011) Inventory of U.S. greenhouse gas emissions and sinks: 1990–2009. [http://www.epa.gov/climatechange/Downloads/ghgemissions/US-GHG-Inventory-2011-Complete\\_Report.pdf](http://www.epa.gov/climatechange/Downloads/ghgemissions/US-GHG-Inventory-2011-Complete_Report.pdf)
6. Klass DL (1998) Biomass for renewable energy, fuels, and chemicals. Academic Press, Salt Lake City
7. Parikka M (2004) Global biomass fuel resources. *Biomass Bioenergy* 27(6):613–620
8. Lovins AB (2004) Winning the oil endgame: innovation for profits, jobs and security. Rocky Mountain Institute, Snowmass Village
9. National Academy of Sciences, National Academy of Engineering, and National Research Council (2009) Liquid transportation fuels from coal and biomass: technological status, costs, and environmental impacts. The National Academies Press, Washington, DC
10. Drapcho C, Nghiem J, Walker T (2008) Biofuels engineering process technology. McGraw-Hill Companies Inc, New York City
11. Brown LR (2008) Why ethanol production will drive world food prices even higher in 2008. [http://www.earth-policy.org/plan\\_b\\_updates/2008/update69](http://www.earth-policy.org/plan_b_updates/2008/update69)
12. Perlack RD, Wright LL, Turhollow AF, Graham RL, Stokes BJ, Erbach DC (2005) Biomass as feedstocks for a bioenergy and byproducts industry: the technical feasibility of a billion-ton annual supply, DOE/GO-102005-2135, Oak Ridge National Laboratory. [http://feedstockreview.ornl.gov/pdf/billion\\_ton\\_vision.pdf](http://feedstockreview.ornl.gov/pdf/billion_ton_vision.pdf)
13. Perlack RD, Stokes BJ (2011) U.S. billion-ton update: biomass supply for a bioenergy and bioproducts industry, ORNL/TM-2011/224, Oak Ridge National Laboratory. [http://www1.eere.energy.gov/biomass/pdfs/billion\\_ton\\_update.pdf](http://www1.eere.energy.gov/biomass/pdfs/billion_ton_update.pdf)
14. Department of Energy (2012) The production of ethanol from cellulosic biomass. [http://cta.ornl.gov/bedb/biofuels/ethanol/The\\_Production\\_of\\_Ethanol\\_from\\_Cellulosic\\_Biomass-Figure.xls](http://cta.ornl.gov/bedb/biofuels/ethanol/The_Production_of_Ethanol_from_Cellulosic_Biomass-Figure.xls)
15. Department of Energy (2013) Replacing the whole barrel to reduce U.S. dependence on oil. [http://www.energy.gov/sites/prod/files/2014/04/f14/replacing\\_barrel\\_overview.pdf](http://www.energy.gov/sites/prod/files/2014/04/f14/replacing_barrel_overview.pdf)
16. Renewable Fuels Association (2011) Ethanol facts: environment. <http://www.ethanolrfa.org/pages/ethanol-facts-environment>

17. Environmental Protection Agency (2014) Recalculations and improvements. <http://www.epa.gov/climatechange/Downloads/ghgemissions/US-GHG-Inventory-2014-Chapter-10-Recalculations-and-Improvements.pdf>
18. Corso JF (1963) Bone conduction thresholds for sonic and ultrasonic frequencies. *J Acoust Soc Am* 35(11):1738–1743
19. Suslick KS (1990) Sonochemistry. *Science* 247(4949):1439–1445
20. Suslick KS, McNamara III WB, Didenko Y (1999) Hot spot conditions during multi-bubble cavitation. In: Crum LA, Mason TJ, Reisse J, Suslick KS (eds) *Sonochemistry and sonoluminescence*. Kluwer Publishers, Dordrecht
21. Kuttruff H (1991) *Ultrasonics fundamentals and applications*. Elsevier Science Publishers, New York
22. Rehman MSU, Kim I, Chisti Y, Han J-I (2013) Use of ultrasound in the production of bioethanol from lignocellulosic biomass. *EEST Part A: Energ Sci Res* 30(2):1391–1410
23. Khanal SK, Montalbo M, van Leeuwen J, Srinivasan G, Grewell D (2007) Ultrasound enhanced glucose release from corn in ethanol plants. *Biotechnol Bioeng* 98(5):978–985
24. Tang A, Zhang H, Chen G, Xie G, Liang W (2005) Influence of ultrasound treatment on accessibility and regioselective oxidation reactivity of cellulose. *Ultrason Sonochem* 12(6):467–472
25. Wang N, Ding E, Cheng R (2007) Thermal degradation behaviors of spherical cellulose nanocrystals with sulfate groups. *Polymer* 48(12):3486–3493
26. Wang X, Fang G, Hu C, Du T (2008) Application of ultrasonic waves in activation of microcrystalline cellulose. *J Appl Polym Sci* 109(5):2762–2767
27. Wong SS, Kasapis S, Tan YM (2009) Bacterial and plant cellulose modification using ultrasound irradiation. *Carbohydr Polym* 77(2):280–287
28. Seino T, Yoshioka A, Fujiwara M, Chen K-L, Erata T, Tabata M, Takai M (2001) ESR studies of radicals generated by ultrasonic irradiation of lignin solution: an application of the spin trapping method. *Wood Sci Technol* 35(1–2):97–106
29. Toma M, Bandow H, Vinatoru M, Maeda Y (2006) Ultrasonically assisted conversion of lignocellulosic biomass to ethanol. In: *Proceedings of conference on AIChE annual meeting, San Francisco, 12–17 Nov 2006*
30. Ninomiya K, Kamide K, Takahashi K, Shimizu N (2012) Enhanced enzymatic saccharification of kenaf powder after ultrasonic pretreatment in ionic liquids at room temperature. *Bioresour Technol* 103(1):259–265
31. Velmurugan R, Muthukumar K (2012) Ultrasound-assisted alkaline pretreatment of sugarcane bagasse for fermentable sugar production: optimization through response surface methodology. *Bioresour Technol* 112:293–299
32. Sasmal S, Goud VV, Mohanty K (2012) Ultrasound assisted lime pretreatment of lignocellulosic biomass toward bioethanol production. *Energy Fuels* 26(6):3777–3784
33. Luo J, Fang Z, Smith RL Jr (2014) Ultrasound-enhanced conversion of biomass to biofuels. *Prog Energy Combust Sci* 41:56–93
34. Falk D (1985) *Feed manufacturing technology III*. American Feed Industry Association, Arlington
35. Hess JR, Wright CT, Kenney KL (2007) Cellulosic biomass feedstocks and logistics for ethanol production. *Biofuels, Bioprod Biorefin* 1(3):181–190
36. Sokhansanj S, Turhollow A (2004) Biomass densification-cubing operations and costs for corn stover. *Appl Eng Agric* 20(4):495–502
37. Fasina OO, Sokhansanj S (1996) Storage and handling characteristics of alfalfa pellets. *Powder Handling Process* 8(4):361–365
38. Sokhansanj S, Tabil LG (1999) Characteristics of plant tissue to form pellets: powder handling and processing. *Int J Storing Handling Process Powder* 11(2):149–159
39. Behnke KC (2001) Processing factors influencing pellet quality. *Feed Tech* 5(4):1–7
40. Mani S, Tabil LG, Sokhansanj S (2006) Effects of compressive force, particle size and moisture content on mechanical properties of biomass pellets from grasses. *Biomass Bioenergy* 30(7):648–654

41. Song XX, Zhang M, Pei ZJ, Deines T (2010) Ultrasonic-vibration-assisted pelleting of cellulosic biomass: effects of moisture content. In: Proceedings of the ASME 2010 international manufacturing science and engineering conference (MSEC), Erie, 12–15 Oct 2010
42. Zhang M, Song XX, Deines TW, Zhang PF, Zhang Q, Cong WL, Qin N, Pei ZJ (2010) Vibration-assisted pelleting of switchgrass: effects of binder material. In: Proceedings of the IIE annual conference and expo, Cancun, 5–9 June 2010
43. Aden A, Ruth M, Ibsen K, Jechura J, Neeves K, Sheehan J (2002) Lignocellulosic biomass to ethanol process design and economics utilizing co-current dilute acid prehydrolysis and enzymatic hydrolysis for corn stover. NREL technical paper, TP-510-32438
44. Phillips S, Aden A, Jechura J, Dayton D, Eggeman T (2007) Thermochemical ethanol via indirect gasification and mixed alcohol synthesis of lignocellulosic biomass. NREL technical paper, TP-510-41168
45. Leaver RH (1984) The pelleting process. Sprout-Waldron, Muncy
46. Robinson RA (1975) The pelleting of millfeed. Assoc Operative Millers Bull July 3545–3549
47. Sokhansanj S, Mani S, Bi X, Zaini P, Tabil L (2005) Binderless pelletization of biomass. In: Proceedings of the 2005 ASAE annual international meeting, Tampa, 17–20 July 2005
48. Mani S, Tabil LG, Sokhansanj S (2003) An overview of compaction of biomass grinds. Powder Handling Process 15(3):160–168
49. Zhang M, Song XX, Pei ZJ, Deines TW, Treadwell C (2012) Ultrasonic vibration-assisted pelleting of wheat straw: an experimental investigation. Int J Manuf Res 7(1):59–71
50. Zhang PF, Pei ZJ, Wang D, Wu X, Cong WL, Zhang M, Deines TW (2011) Ultrasonic vibration-assisted pelleting of cellulosic biomass for biofuel manufacturing. J Manufact Sci Eng 133(1):011012-011011–011012-011017
51. Zhang Q, Zhang PF, Pei ZJ, Wilson J, McKinney L, Pritchett G (2011) An experimental comparison of two pelleting methods for cellulosic ethanol manufacturing. In: ASME 2011 international manufacturing science and engineering conference, Corvallis, 13–17 June 2011
52. Zhang Q, Zhang PF, Deines T, Pei ZJ, Wang D, Wu X Pritchett G (2010) Ultrasonic vibration-assisted pelleting of sorghum stalks: effects of pressure and ultrasonic power. In: Proceedings of the ASME 2010 international manufacturing science and engineering conference (MSEC), Erie, 12–15 Oct 2010
53. Zhang PF, Zhang Q, Pei ZJ, Pei L (2011) An experimental investigation on cellulosic biofuel manufacturing: effects of biomass particle size on sugar yield. In: Proceedings of the ASME 2011 international mechanical engineering congress and exposition (IMECE), Denver, 11–17 Nov 2011
54. Zhang PF, Deines TW, Nottingham D, Pei ZJ, Wang D, Wu X (2010) Ultrasonic vibration-assisted pelleting of biomass: a designed experimental investigation on pellet quality and sugar yield. In: Proceedings of the ASME 2010 international manufacturing science and engineering conference (MSEC), Erie, 12–15 Oct 2010
55. ASAE/ASABE (2008) Moisture measurement-forages. <http://asae.frymulti.com/azdez.asp?JID=2&AID=24452&CID=s2000&T=2>
56. Colley Z, Fasina O, Bransby D, Lee Y (2006) Moisture effect on the physical characteristics of switchgrass pellets. Trans ASABE 49(6):1845–1851
57. Zhang M, Song XX, Pei ZJ, Wang DH (2010) Effects of mechanical comminution on enzymatic conversion of cellulosic biomass in biofuel manufacturing: a review. In: Proceedings of the ASME 2010 international manufacturing science and engineering conference (MSEC), Erie, 12–15 Oct 2010
58. Song XX, Zhang M, Deines TW, Zhang PF, Pei ZJ (2012) Energy consumption study in ultrasonic vibration-assisted pelleting of wheat straw for cellulosic biofuel manufacturing. Int J Manuf Res 8(2):135–149
59. Theerarattananon K, Xu F, Wilson J, Staggenborg S, McKinney L, Vadlani P, Pei ZJ, Wang D (2012) Effects of the pelleting conditions on chemical composition and sugar yield of corn stover, big bluestem, wheat straw, and sorghum stalk pellets. Bioprocess Biosyst Eng 35(4):615–623

60. ASABE (2002) Pellets, and crumbles-definitions and methods for determining density, durability, and moisture content, standard S269.4. <http://www.doa.go.th/aeri/files/pht2008/lecture%20slides/mr%20viboon/grain%20drying/aeae-1998/pdfs/section5/506.pdf>
61. Fasina O (2008) Physical properties of peanut hull pellets. *Bioresour Technol* 99(5):1259–1266
62. Zhang Q, Zhang PF, Deines TW, Zhang M, Song XX, Pei ZJ (2010) Ultrasonic vibration-assisted pelleting of wheat straw: effects of particle size. In: Proceedings of the 20th international conference on flexible automation and intelligent manufacturing (FAIM 2010), California State University, 2010
63. Zaldivar J, Nielsen J, Olsson L (2001) Fuel ethanol production from lignocellulosic: a challenge for metabolic engineering and process integration. *Appl Microbiol Biotechnol* 56(1–2):17–34
64. Saha BC (2003) Hemicellulose bioconversion. *J Ind Microbiol Biotechnol* 30(5):279–291
65. Laureano-Perez L, Teymouri F, Alizadeh H, Dale BE (2005) Understanding factors that limit enzymatic hydrolysis of biomass. *Appl Biochem Biotechnol* 124(1–3):1081–1099
66. Kumar R, Singh S, Singh OV (2008) Bioconversion of lignocellulosic biomass: biochemical and molecular perspectives. *J Ind Microbiol Biotechnol* 35(5):377–391
67. Harris PJ, Stone BA (2008) Chemistry and molecular organization of plant cell walls. In: Himmel ME (ed) *Biomass recalcitrance: deconstructing the plant cell wall for bioenergy*. Blackwell Publishing Ltd., Oxford, pp 61–93
68. Sun RC (2008) Detoxification of biomass for bioethanol. *Bioresources* 4(2):452–455
69. Szulczyk KR, McCarl BA, Cornforth G (2010) Market penetration of ethanol. *Renew Sustain Energy Rev* 14(1):394–403
70. Nigam J (2002) Bioconversion of water-yacynth (*Eichhornia crassipes*) hemicellulose acid hydrolysate to motor fuel ethanol by xylose-fermenting yeast. *J Biotechnol* 97(2):107–116
71. Wyman C (1996) *Handbook on bioethanol: production and utilization*. Taylor & Francis, Boca Raton
72. Henstra AM, Sipma J, Rinzema A, Stams AJ (2007) Microbiology of synthesis gas fermentation for biofuel production. *Curr Opin Biotechnol* 18(3):200–206
73. Hu G, Heitmann JA, Rojas OJ (2008) Feedstock pretreatment strategies for producing ethanol from wood, bark, and forest residues. *BioResources* 3(1):270–294
74. Zheng Y, Pan Z, Zhang R (2009) Overview of biomass pretreatment for cellulosic ethanol production. *Int J Agric Biol Eng* 2(3):51–68
75. Grohmann K, Torget R, Himmel M (1986) Dilute acid pretreatment of biomass at high solid concentrations. *Biotechnol Bioeng Symp* 17:135–151
76. Grohmann K, Torget RW (1992) Two-state dilute acid prehydrolysis of biomass. USA patent
77. Torget R, Teh-An H (1994) Two-temperature dilute-acid prehydrolysis of hardwood xylan using a percolation process. *Appl Biochem Biotechnol* 45(1):5–22
78. Snyder LR, Kirkland JJ, Dolan JW (2011) *Introduction to modern liquid chromatography*. Wiley, Hoboken
79. Song X, Zhang M, Pei ZJ (2013) Effects of ultrasonic vibration-assisted pelleting of cellulosic biomass on sugar yield for biofuel manufacturing. *Biomass Convers Biorefinery* 3(3):231–238
80. Mais U, Esteghlalian AR, Saddler JN, Mansfield SD (2002) Enhancing the enzymatic hydrolysis of cellulosic materials using simultaneous ball milling. *Appl Biochem Biotechnol* 815–832
81. Grethlein HE (1985) The effect of pore size distribution on the rate of enzymatic hydrolysis of cellulosic substrates. *Nat Biotechnol* 3(2):155–160
82. Gharpuray MM, Lee YH, Fan LT (1983) Structural modification of lignocellulosics by pretreatments to enhance enzymatic hydrolysis. *Biotechnol Bioeng* 25(1):157–172
83. Chang VS, Holtzapple MT (2000) Fundamental factors affecting biomass enzymatic reactivity. *Appl Biochem Biotechnol* 84–86:5–38
84. Zhang PF, Zhang Q, Pei ZJ, Pei L (2011) Ultrasonic vibration-assisted pelleting in manufacturing of cellulosic biofuels: an investigation on biomass particle size. In: Proceedings of the ASME 2011 international mechanical engineering congress and exposition (IMECE), Denver, 11–17 Nov 2011

85. Zhang Q, Zhang PF, Pei ZJ, Wang D (2013) Ultrasonic vibration-assisted pelleting for cellulosic biofuel manufacturing: investigation on power consumption. *Renew Energy* 55:175–181
86. Zhang Q, Zhang PF, Pei ZJ, Wilson J, McKinney L, Pritchett G (2011) Ultrasonic-vibration assisted pelleting for cellulosic ethanol manufacturing: an experimental investigation of power consumption. In: *Proceedings of the ASME 2011 international mechanical engineering congress and exposition (IMECE)*, Denver, 11–17 Nov 2011
87. Song X, Zhang M, Pei Z, Wang D (2014) Ultrasonic vibration-assisted pelleting of wheat straw: a predictive model for energy consumption using response surface methodology. *Ultrasonics* 54(1):305–311
88. Sun ZY, Li L, Wang DH, Zhang M (2014) Relationship investigation between energy consumption and parameters in size reduction and pelleting process of biofuel manufacturing. Paper presented at the proceedings of the 2014 ASME international manufacturing science and engineering conference, Detroit, 9–13 June
89. Kaliyan N, Morey R, White M, Doering A (2009) Roll press briquetting and pelleting of corn stover and switchgrass. *Trans ASABE* 52(2):543–555
90. Van Dam JEG, van den Oever MJA, Teunissen W, Keijsers ERP, Peralta AG (2004) Process for production of high density/high performance binderless boards from whole coconut husk: part 1: lignin as intrinsic thermosetting binder resin. *Ind Crops Prod* 19(3):207–216
91. Tang YJ, Chen CM, Wang G (2012) Temperature on-line measured in ultrasonic vibration-assisted pelleting cellulosic biomass. *Appl Mech Mater* 151:245–249
92. Feng Q, Cong WL, Zhang M, Pei ZJ, Ren CZ (2010) An experimental study on temperature in ultrasonic vibration-assisted pelleting of cellulosic biomass. In: *Proceedings of the ASME 2010 international manufacturing science and engineering conference (MSEC)*, Erie, 12–15 Oct 2010
93. Feng Q, Cong WL, Zhang M, Pei ZJ (2011) An experimental study on charring of cellulosic biomass in ultrasonic vibration-assisted pelleting. *Int J Manuf Res* 6(1):77–86
94. Song X, Yu X, Zhang M, Pei ZJ, Wang D (2014) A physics-based temperature model for ultrasonic vibration-assisted pelleting of cellulosic biomass. *Ultrasonics* 54(7):2042–2049
95. Love L, Kremkau F (1980) Intracellular temperature distribution produced by ultrasound. *J Acoust Soc Am* 67:1045



# Chapter 10

## Mechanical and Combined Chemical and Mechanical Treatment of Biomass

Richard G. Blair

**Abstract** Mechanical processing is a critical step in the utilization of biomass as a feedstock. It may be applied to reduce the size of the feedstock for ease of handling, to enhance hydrolysis, or to convert the feedstock into a useable product in a single step. Mechanical processing can be energy intensive and a balance needs to be struck between the need for reduced particle size, reduced crystallinity, and low operational costs. By combining mechanical and chemical treatments the operational costs can be greatly reduced and valuable products can be realized that can not be produced through mechanical, chemical, or enzymatic means alone.

**Keywords** Mechanochemistry · Mechanocatalysis · Ball mill · Milling · Attrition · Processing · Hydrolysis · Hammer mill · Cutting mill · Scalability

### 10.1 Introduction

Mechanical processing is an important step in realizing any products from biomass. This processing is used for several reasons:

1. Size reduction
2. Improved handling
3. Fiber and cell wall disruption
4. Reduction of cellulose crystallinity

Two types of force, compressive and shear dominate mechanical processing. These forces are illustrated in Fig. 10.1. Brittle materials are easily fragmented under the application of compressive force, while soft materials are more easily

---

R.G. Blair (✉)

Department of Physics, Mechanical and Aerospace Engineering, University of Central Florida, 4000 Central Florida Blvd., PSB 430, Orlando, FL 32816-2385, USA  
e-mail: richard.blair@ucf.edu

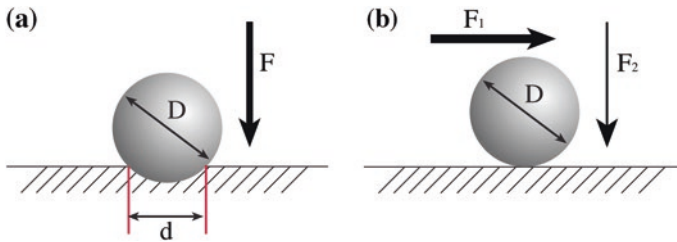


**Fig. 10.1** Compressive forces (a) are best for comminuting hard, brittle feedstocks while shear forces (b) are best for soft feedstocks

processed by the application of shear force. Comminution devices are typically optimized for one type of force.

The resistance of woods to compressive force has been quantified by a value known as the Janka hardness which ranks woods by the force required to embed an 11.28 mm steel ball into the sample to half its diameter [1]. Non-woody biomass has not been so well characterized.

## 10.2 Mechanical Processing

### 10.2.1 Size Reduction and Improved Handling

Conversion of lignocellulosic biomass to sugars in a processing plant presents a materials handling problem. The raw forms of woody and herbaceous biomass do not lend themselves to conveyance. Transport of these materials in either dry or slurry form as well as their hydrolysis is facilitated by size reduction [2]. Although there are many milling technologies available, two technologies have come to the forefront for size reduction: cutting mills and hammer mills. Fundamentally, these mills differ in the type of mechanical force that is applied. Cutting mills use blades to produce high shear forces that slice the material into smaller pieces (Fig. 10.2). Cutting mills optimize the process that generates sawdust when producing lumber. They are essentially saws whose purpose is to produce fine particles.

Cutting mills do not work efficiently when dry hard feedstocks are used (such as grains). Processing of these feedstocks is typically performed using mills that use swinging arms (hammers) that produce large compressive forces upon impact that shatter the material into small pieces (Fig. 10.2b).

Both of these technologies are optimized for attrition alone [3]. Chemical processes are suppressed through short dwell times and rigorous control of the temperature during comminution. Comminution processes can be energy intensive and extensive work has gone into characterizing the optimal configuration for size reduction and energy consumption. Knife (cutting) mills can consume 4–120 kWh/MT [4, 5] depending on the initial particle size and feedstock properties. Work by Schell et al. indicate that other milling modes can be quite energy intensive. An energy consumption of 200–400 kWh/MT was reported for attrition milling and

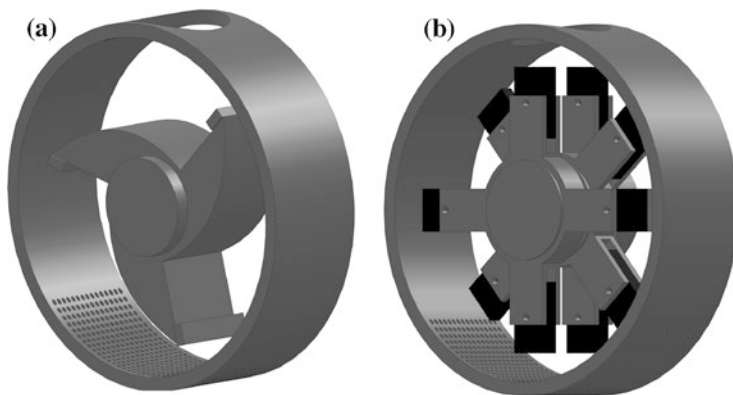


**Fig. 10.2** A cutting mill (a) consists of a rotating blade assembly that applies shear force to the feedstock. Hammer mills (b) utilize fixed or swinging bars to induce attrition through the application of compressive force. A screen allows classification of the particles produced. Material will remain in the impact zone until it is small enough to pass through the screen

90–130 kWh/MT for hammer milling [6]. This initial work may overestimate the processing energy requirements. Subsequent work using hammer mills lowered the energy consumption to 80 kWh/MT [5] and then 35–55 kWh/MT [7]. This variability indicates that the successful implementation of a milling technology both for size reduction and profitability is highly dependent on the nature of the feedstocks interaction with the forces developed in a mill.

### ***10.2.2 Fiber and Cell Wall Disruption***

After bulk mechanical processing, material with particle sizes from a few to tens of millimeters are produced [8]. However, the microstructure of the feedstock is still largely intact. Plant cell walls are composed of crystalline cellulose fibrils, hemicellulose, and lignin. For feedstocks composed mainly of starch or hemicellulose this does not present a problem and the material can be moved onto chemical or enzymatic digestion. However, feedstocks with high cellulose and lignin content require further processing to make them amenable to conversion. The crystallinity of the cellulose makes acid and enzymatic hydrolysis inefficient and the highly cross-linked structure of lignin reduces the efficacy of attrition. Even low cellulose-content feedstock benefit from a disruption step. The most common form of disruption is steam explosion [9] where the feedstock is subjected to steam under pressures of 1–3 MPa and temperatures of 180–240 °C. Steam infiltrates the cell walls of the feedstock and plasticizes the material. A rapid release of pressure separates the cellulose fibrils through internally generated compressive forces as the steam expands. Care must be taken to limit processing time since undesirable side reactions such as humification can occur at the elevated temperatures used.

### 10.2.3 Reduction of Cellulose Crystallinity

Native cellulose is highly crystalline in nature. This crystallinity severely limits its acid and enzymatic hydrolysis rate [10, 11]. The crystallinity of cellulose can be reduced through the application of mechanical force alone [12, 13] or through chemical processing. Acid hydrolysis can eventually reduce the crystallinity of the feedstock through hydrolysis and subsequent reduction in the degree of polymerization of the feedstock. However, extended processing with acid can lead to the formation of inhibitory compounds such as furfural, levoglucosenone, levoglucosan, and 5-hydroxymethylfurfural. These compounds themselves have higher value than the glucose itself and research is being performed to increase their yields [14–18] (Fig. 10.3).

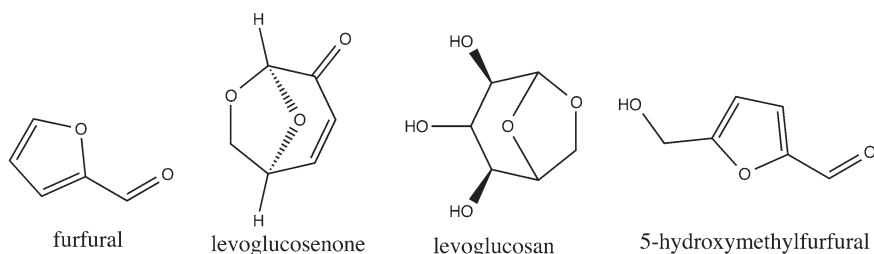


**Fig. 10.3** Acid hydrolysis of cellulose and hemicellulose can produce the dehydration by-products furfural, levoglucosenone, levoglucosan, and 5-hydroxymethylfurfural. These compounds can inhibit fermentation

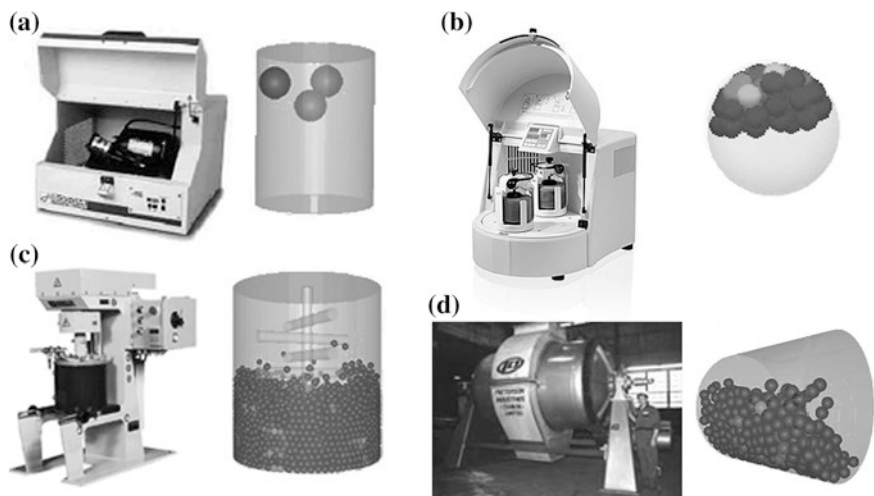


**Fig. 10.4** Some of the milling technologies being used at the laboratory and plant scale for the processing of biomass. The motion of the milling media is indicated in schematics next to each mill. These vary from the small scale **a** SPEX mixer mill (65 mL) [26], to the medium scale, **b** planetary mill (250 mL) [27], **c** attritor (4 l) [28], to the production scale, **d** rolling ball mill (hundreds of liters) [29]

Acid preprocessing must be limited or the by-product must be removed before fermentation as 5-hydroxymethylfurfural as this compound has an inhibitory effect on yeast fermentation [19]. Mechanical processing through steam explosion or high energy ball milling [12] can sufficiently reduce the crystallinity of the parent material to realize improved hydrolysis rates while at the same time limiting the amount of undesirable by-products. When crystallinity reduction is desired, ball mills are often chosen over hammer and cutting mills. Ball mills produce both shear and compressive forces that can disrupt the crystallinity of the feedstock. Highly energetic impacts are needed to break down the crystalline structure of the feedstock.

On a laboratory scale these forces are produced in a mixer-type mill (Fig. 10.4a) or a planetary-type mill (Fig. 10.4b). The equipment and tools used for a combined mechanical and chemical treatment of biomass have been adopted from equipment used by the materials processing community who have exploited these tools for mechanical alloying [20–22] and the synthesis of advanced materials [23–25]. Scalable solutions are realized through the use of attrition milling (Fig. 10.4c) or pebble milling (Fig. 10.4d).

### 10.3 Combined Mechanical and Chemical Treatment of Biomass

Current work in mechanochemical and mechanocatalytic processing of biomass has shown that it can be an effective approach for realizing sugars and chemicals in a single reactor [18, 30–38]. Mechanochemical hydrolysis of biomass can solubilize up to 100 % of the available cellulose and hemicellulose. This approach is not without its challenges as condensation reactions leading to oligomerization of the saccharide monomers are also observed. Through understanding of the thermal and mechanical energies available during processing it is possible to reduce the production of these undesirable products. In addition, application of catalysts and utilization of reagents such as hydrogen in the mechanochemical reactor can effectively produce high value compounds such as sugar alcohols and small platform molecules.

#### 10.3.1 Mechanical Considerations

Simply soaking biomass in a strong acid or base can reduce its crystallinity enough to produce improved hydrolysis rates [11, 39], however, treatment times can be lengthy due to the initial crystallinity of the feedstock. These rates can be improved by milling acid impregnated carbon with the cellulose source in a low-energy ball mill which is a smaller version of that illustrated in Fig. 10.4d [18]. Through the combination of high-energy attrition process, which reduces particle size and crystallinity, and chemical hydrolysis, which reduces crystallinity as well

as decreasing fracture toughness through the disruption of the feedstocks structure, greatly enhanced hydrolysis rates can be achieved [2, 12, 35]. Figure 10.5 illustrates the crystallinity reduction achieved by milling in a SPEX mill with kaolinite.

Acid hydrolysis can be enhanced through pretreatment in a ball mill and using the high shear achieved in screw extruders [40]. Practically, screw extrusion technology is an attractive option since it is truly a continuous approach to processing.

It is often stated that mechanical processing such as ball milling produces high transient pressures and temperatures. However, recent work has shown that high temperatures are not achieved [41]. Computer models have indicated that forces in excess of 3,000 N may be achievable (Fig. 10.6) [42–47]. This correlates to

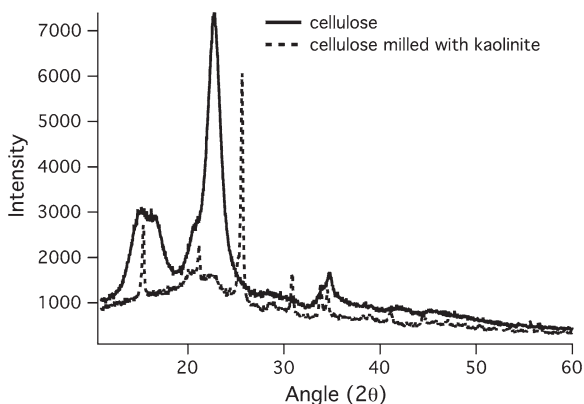


**Fig. 10.5** Milling feedstock (here pure microcrystalline cellulose) with an acid catalyst effectively amorphitizes the feedstock in addition to hydrolyzing it. The peaks in the milled mixture are due to kaolinite

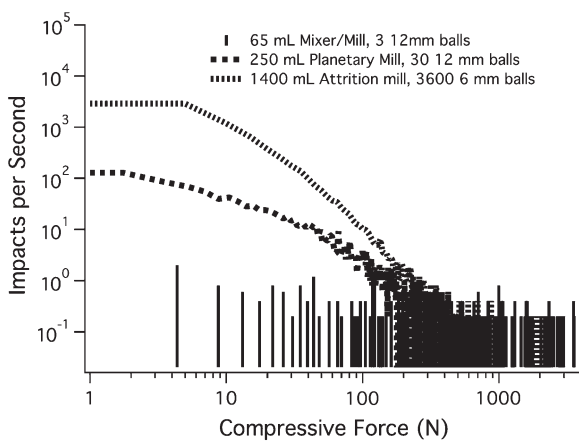


**Fig. 10.6** Discrete element models of commonly used laboratory mills indicate that compressive forces in excess of 1,000 N can be realized in each type

pressure of over 3 GPa when a  $0.1 \text{ mm}^2$  interaction area is assumed. It can be difficult to monitor the reaction condition in a mill in real time, although work has shown that useful powder X-ray diffraction data can be obtained during processing [48]. This approach offers the promise of improving milling efficiencies without excessive trials. The analysis of media motion in a ball mill is particularly suited for models that use discrete element methods. In the discrete element method, particles are treated as classical bodies with the effects of gravity, collisions, and container motion taken into account. Typically, a Hertzian model [49] is used to determine the forces, velocities, and deformations produced during impact events [50]. This model uses the elastic properties of the materials involved in these collisions. DEM solutions produces a software package that simplifies implementation of DEM code [51]. These simulations can be used to characterize the forces and energies and available during milling (Fig. 10.6).

### 10.3.2 Surface Acidity

The acid catalyzed hydrolysis of the glycosidic bond (Fig. 10.7) in cellulose is improved through the application of elevated temperatures and pressures [11]. Current methods use acidic solutions, however, many solids (silicates and oxides) exhibit a phenomenon known as surface acidity. Surface acidity is expressed by the Hammett and Deryups  $H_0$  function [52]. An  $H_0$  of  $-8.2$  corresponds to an acidity of 90 % sulfuric acid while that of  $-3.0$  is equivalent to 48 % sulfuric acid. Acidity equivalent to 48 % sulfuric acid is enough to catalyze the hydrolysis of cellulose at moderate temperatures and pressures. However, the interaction between these surface sites with solids is severely limited by diffusion. This barrier can be overcome by using the force of a ball mill. Additionally, the high transient forces realized in a ball mill can be used to improve the hydrolysis rate through a reduction of the feedstock's crystallinity. Initial work [38] showed that many minerals with surface acid sites can catalyze this hydrolysis (Fig. 10.8). The layered phyllosilicates bentonite and kaolinite were the most efficient due to access to open acid sites and naturally adsorbed water essential for hydrolysis.

Phyllosilicates are layered aluminosilicate minerals with water trapped between the layers. This is in contrast to the zeolite-type structure employed in heterogeneous catalysis (Fig. 10.9). In a zeolite, the catalytically active sites are

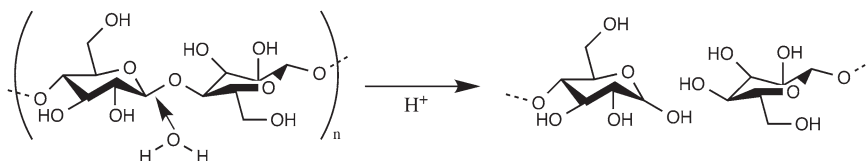


**Fig. 10.7** The hydrolysis of the glycosidic bond in cellulose is catalyzed by the presence of an acid

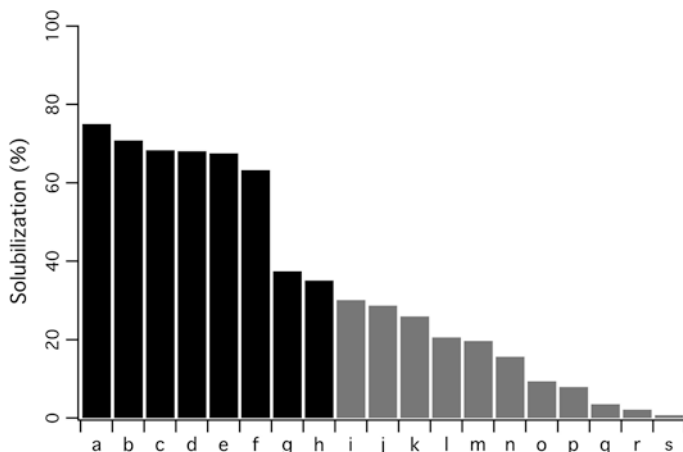


**Fig. 10.8** After mechanically processing biomass for 2 h, with a solid acid, a portion becomes water-soluble. The *black bars* indicate materials with a surface acidity ( $H_0$ )  $< -3$  as determined by dicinnamalacetone. One gram of biomass was processed with 1 g of catalyst in a SPEX 8000D mixer mill. Three 0.5" balls and a vial with an internal volume of 65 mL was used [38]. The acids examined were: (a) physically delaminated kaolinite, acidified, (b) bentonite, acidified, (c) kaolinite, acidified, (d) chemical delaminated kaolinite, (e) kaolinite, (f) physically delaminated kaolinite, (g) kaolinite, anhydrous, (h) alumina super acid, (i) aluminum phosphate, (j) alumina, (k) talc, (l) Y-type zeolite, (m) bentonite, (n) vermiculite, (o) quartz, (p) muscovite mica, (q) silicon carbide, (r) graphite, (s) aluminum sulfate

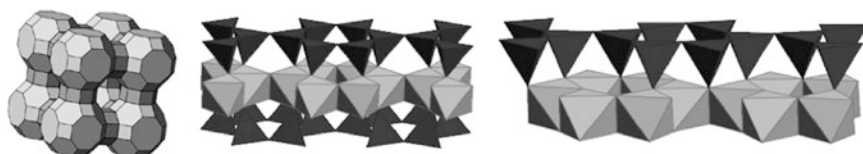


**Fig. 10.9** The polyhedral structures for a typical zeolite (*left*), bentonite (*middle*), and kaolinite (*right*) illustrate the difference in acid site accessibility. The *dark* tetrahedra are  $SiO_4$  structures and the *light* octahedra are  $AlO_6$  structures

accessible in the cavities of the structure while active sites in phyllosilicates are surface aluminum-containing octahedra. These sites have both Lewis and Brønsted acid properties that act as catalysts for the cleavage of the cellulose glycosidic bond or for any acid-catalyzed process. Kaolinite exhibits a higher catalytic activity than untreated bentonite that can be understood by examining the structure of the lattice. Bentonite is a 2:1 layered silicate; there are two silicon-containing layers for every aluminum-containing layer; this structure inhibits interaction with the aluminum sites. In contrast, kaolinite is termed a 1:1 layered silicate in that there is one silicon-containing layer for every aluminum-containing layer; the aluminum sites of kaolinite are free to interact with the chemical process.



Surface acidity is very important. This can be seen in the low catalytic efficacy of talc and micas. Although talc has similar mechanical properties to the clays bentonite and kaolinite and also contains water, it is not as acidic. The micas (muscovite and vermiculite) are also not as acidic as bentonite and kaolinite. In all cases aside from kaolinite, a lower yield of solubilized material is realized; ref. [38] which indicates that a minimum surface acidity is needed for hydrolysis.

It is also important to consider the role of the mechanical properties of the catalyst. A major difficulty in any attrition process is wear, in the form of erosion, on the milling media. Clays and micas (phyllosilicates) have a Moh's hardness ranging from 1 to 3, while zeolites have a Moh's hardness ranging from 3.5 to 5.5. Zeolites with high silica content are on the harder end of this scale. The use of zeolite-type catalysts for mechanochemical processes would result in substantial wear on the steel milling media. A harder milling media, such as alumina or zirconia, could be used to minimize the erosion, but this adds to process costs. Layered structures produce little or no mill wear. In fact, studies have shown that measurable wear on steel containers and balls occurs while milling cellulose systems [53].

The incorporation of acids into the cellulose hydrolysis reaction is not limited to the solids in the study by Hick [38]. It has been known that activated carbons can pick up quantities of acid sites by soaking in strong acids. This approach was used to produce a highly-acidic carbon that can hydrolyze cellulose without aggressive milling, although the stirrer used does impart mechanical energy into any solid–solid interactions [54]. The application of adsorbed acid species was realized in its most basic form by Meine et al. [30] who impregnated cellulose with various acids and subjected it to the mechanical force generated by a

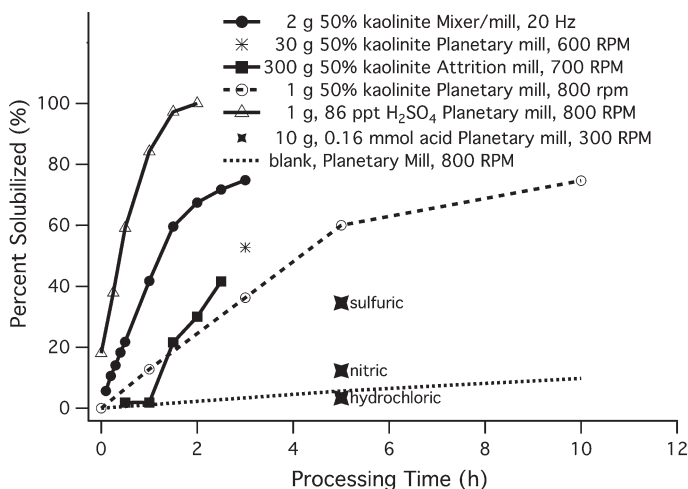


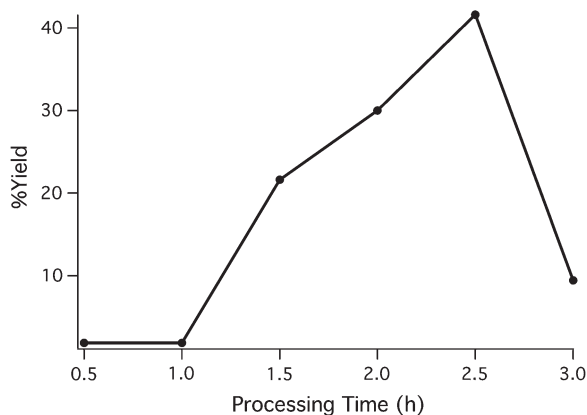
**Fig. 10.10** The solubilization of cellulose in water, when processed mechanochemically, is dependent on the nature of the acid catalyst (kaolinite, hydrochloric acid, nitric acid, or sulfuric acid) and the milling process. The kaolinite conversion rate is much higher in a mixer mill than in a planetary or attrition mill [30, 33, 38, 55]

planetary ball mill. In fact, conversion rates and efficiencies were improved over those achieved using kaolinite (Fig. 10.10). It is interesting to note that quite different conversion profiles are obtained with differing feedstock masses, milling apparatus and milling intensities. A simple scale-up in the application of planetary milling produced a 10 % increase in yield for the same processing time (\* and dashed line in Fig. 10.10) [55].

### 10.3.3 Nature of the Hydrolysis Product

Ideally cellulose and hemicellulose should be cleanly hydrolyzed into their monosaccharide units. However, it is well known that acid hydrolysis can lead to undesirable products such as furfural, levoglucosenone, levoglucosan, and 5-hydroxymethyl furfural. These products mainly arrive from unwanted dehydration reactions and retro-aldol reactions. Ultimately, this process ends with the production of humins and little if any fermentable material is isolable (Fig. 10.11). A reduction in yield is observed when feedstocks are over processed due to formation of insoluble humins. These unwanted reactions can be exacerbated when mechanochemically processing biomass due to the low water content typically used in the reactors. If there is insufficient water in the reaction zone, the water required for cellulose hydrolysis can come from any saccharide products. As the reaction product builds up and covers the feedstock, this process becomes more probable. However, too much water can hinder hydrolysis through modification of the mechanical properties of the feedstock. This was observed in simple attrition experiments and can be seen in mechanochemical treatment where Meine et al. reported quite high conversion rates using non-aqueous acid impregnation methods and Shotri et al. reported much poorer conversion rates using aqueous acid impregnation methods [30, 33]. These researchers utilized similar milling technologies (planetary mills) but different scales (1 and 10 g respectively) and

**Fig. 10.11** Saccharide yield from the kaolinite catalyzed depolymerization of microcrystalline cellulose in an attrition mill



different milling intensities (800 RPM vs. 300 RPM respectively). The nature of the impacts at these scales and speeds may also be a contributing factor.

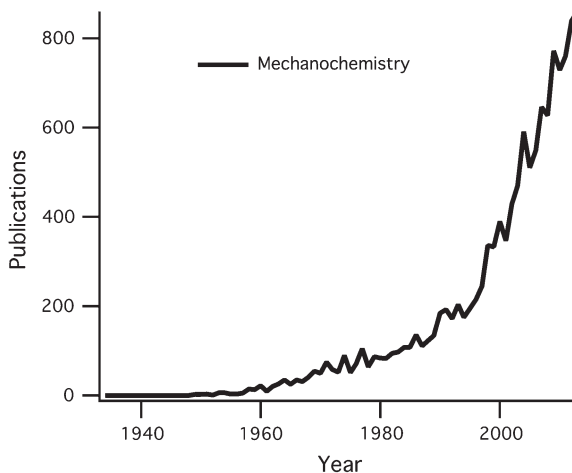
The utilization of strong acids and small amounts of water can produce an interesting problem. Although high solubilizations can be achieved little or no simple saccharides were detected. This discrepancy has been attributed to the repolymerization of saccharides to polysaccharides. In fact, milling pure glucose with an acid leads to a high yield of  $n > 3$  oligomers [30]. Because this is a random process, a variety of glycosidic bonds can be formed. Not only were  $\beta(1-4)$  linkages reformed, but  $\alpha(1-6)$  linkages are also detected [33]. Fortunately, these oligomers are amenable to enzymatic hydrolysis and glucose can be recovered after a final enzyme treatment.

### 10.3.4 Scale-Up

Researchers typically utilize small shaker-type and planetary-type mills. However, moving to a scalable solution can present a challenge. Scalability can be addressed through discrete element models (DEM), thermal monitoring, and reactor design. Impact forces and macroscopic mixing are important factors in implementing a truly scalable process. Many studies have been published on the chemical reactions facilitated by ball-milling (Fig. 10.12) [56–60].

However, most of these studies have been limited to laboratory scale implementation and few have sought to develop routes to scalable implementations [61]. There are well-established pathways to scaling traditional chemical processes. The issues of mixing, heat transfer, and material transport have largely been solved for these processes, but not for mechanochemical approaches. Industry is reluctant to use processes that are not fully understood.

**Fig. 10.12** Number of journal articles published on mechanochemical processes as of mid-2014. SciFinder scholar was queried with the search terms: mechanochemical, mechanochemistry, and mechanocatalysis



Often, industrialists adopt existing tools and knowledge to assess a new process. These assumptions can lead to process failure. Although, efforts have been made to understand the processes occurring during mechanochemical syntheses [62–68], simple conditions are usually assumed. To realize an industrially useful process, routes to multi-ton processes must be developed.

Figure 10.13 shows some commonly used laboratory milling containers and their capacities. Figure 10.14 shows the energies achievable in three commonly used milling technologies. A mixer mill is amendable to small exploratory

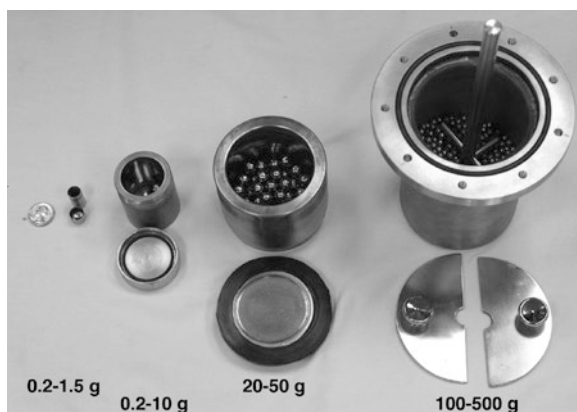


**Fig. 10.13** Reaction scales achievable in a small laboratory. From *left to right*, a microvial for a SPEX 5100 mixer mill, a vial for a SPEX 8000 mixer mill, a vial for a Fritsch Pulverisette 6 planetary mill and a tank for a Union Process 01-HDDM attrition mill. Reprinted with permission from [55]. Copyright © 2014, Royal Society of Chemistry

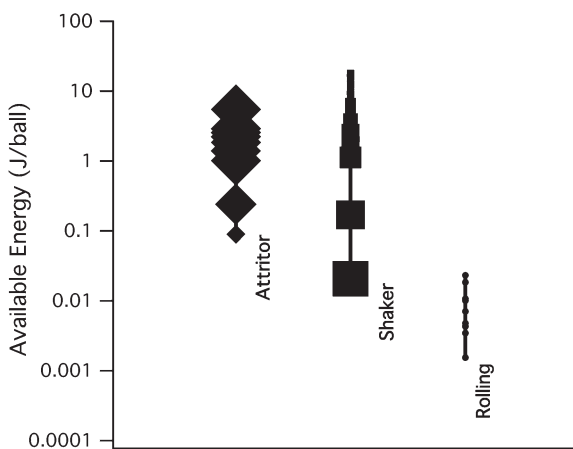


**Fig. 10.14** The energies available in a milling system (J/ball) are dependent on the mill design. Larger markers indicate more variance in the kinetic energies. Large variances indicate good mixing

reactions, but does not scale. Planetary mills can be used for larger batches, but apparatus costs typically limit implementation. Attrition mills represent a linearly scalable technology, but laboratory-scale apparatus typically require at least 100 g for efficient operation.

Mixer mills and planetary mills represent high-energy processing methods; high impact energies translate to shorter chemical processing times. The combined chemical and mechanical processing of biomass is dominated by two phenomena: attrition or particle size reduction, as previously discussed, and chemical hydrolysis. Batch processing of cellulose with a solid acid catalyst [38] shows a significant induction period (of around 4 h, Fig. 10.15) before any appreciable yield is realized. The origin of this induction period was a paradigm difference between the laboratory and the production facility. Attrition technology is typically used in applications where it is undesirable for chemical change to occur during processing. This is exemplified by the construction of the cutting and hammer mills illustrated in Fig. 10.2. These mills are designed to remove heat and separate particles quickly to eliminate side reactions and heating. Mechanocatalytic processes capitalize on the forces generated in a mill to induce chemical reactions. A simple change in process parameters such as higher mill speeds and different media size can effectively eliminate the induction period observed (Fig. 10.15).

The mixer mill induces the fastest conversion of cellulose into sugars due to the high amount of compressive force that rapidly amorphitizes the feedstock (Figs. 10.5 and 10.6). A planetary mill is slightly less efficient and attrition milling has significant induction periods. Several processes are occurring during this treatment. The catalyst

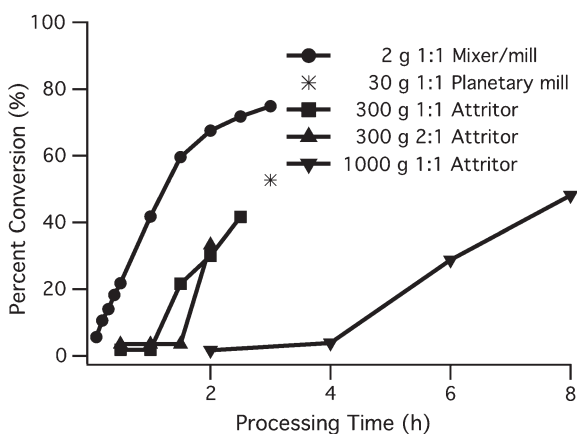
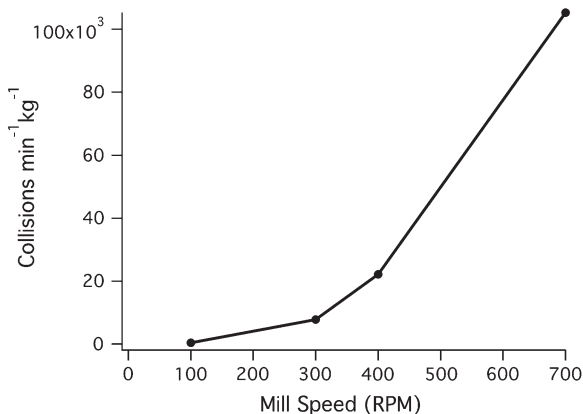


**Fig. 10.15** The fraction of cellulose converted to soluble products illustrates the scalability in the hydrolysis of microcrystalline cellulose at various (cellulose:catalyst) ratios. The SPEX mill was run at 20 Hz with 12 mm media, the planetary mill at 600 RPM with 12 mm media, the small attritor (300 g) at 700 RPM with 6 mm media and the large attritor (1,000 g) mill at 350 RPM with 9 mm media. The higher rotational speeds of the small attritor significantly reduced the induction period. Reprinted with from [55]. Copyright ©2014, Royal Society of Chemistry

**Fig. 10.16** Improved media/feedstock contacts can be achieved by increasing the milling intensity. The plot shows the improvement achievable in a 160 l attrition mill capable of processing 30 kg batches



and cellulose size are being reduced through attrition and the cellulose crystallinity is also being reduced; saccharides are being produced by acid-catalyzed hydrolysis; frictional heating and water loss are promoting dehydration and humification reactions. The undesirable processes can be addressed individually. Ideally, the process should be dominated by hydrolysis. Attrition and amorphitization can be accelerated through applications of a preliminary treatment step (steam explosion, impregnation with acid, milling) followed by catalytic processing. Increasing the number of media/feedstock interactions can increase conversion rates in a mill (Figs. 10.15 and 10.16). By increasing the number of impacts, both chemical and mechanical processing rates can be improved. This is typically described as the ball to powder ratio (BPR) in mechanical alloying experiments. In a mechanochemical process, increasing the BPR produces more collisions. This can be done by increasing the amount of milling media used or adding a powdered material that is harder than cellulose (milling aid), which increases the BPR, by adding a large number of microscale milling media. If the media is free to move then this also keeps the force distribution of the impacts similar. However, if severe confinement is produced through the use of large amounts of reactant or media, then compressive forces will be severely reduced. Increasing the media size or the milling speed also increases the intensity of the collisions produced by the mill. Through the application of discrete element modeling (DEM) it is possible to relate the experimental observations to the compressive forces produced in a mill.

The distribution of compressive forces and the fraction of impacts that produce non-zero compressive forces are both critical to the reaction rate. In general, higher milling intensities and larger media size produce higher collision forces. By producing DEM models, the forces developed in a mill and the macroscopic mixing can be better understood. For example, in all traditional implementations of the attritor a dead zone forms around the shaft of the tree when the media rises up due to the application of rotation energy. DEM models of a tank, rotated 90°, indicated that gravity encourages mixing and the segregation problem would be eliminated. This example (Fig. 10.16) illustrates the need for whole reactor modeling in scaling mechanochemical reactions. Simple force calculations would not predict inadequate mixing or the formation of dead zones. Favorable conversion kinetics are achieved

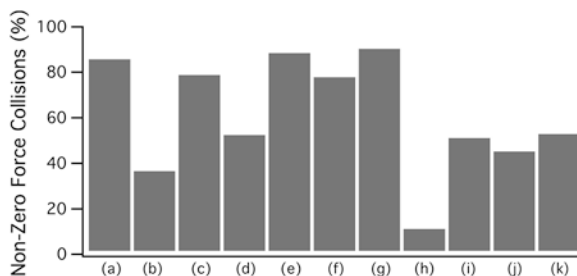


**Fig. 10.17** A comparison of collisions in a planetary mill (a) 0.5 l, 12 mm media, 600 RPM and various attrition mill configurations (b) 1.4 l, 6 mm media, 300 RPM, (c) 1.4 l, 12 mm media, 300 RPM, (d) 1.4 l, 6 mm media, 700 RPM, (e) 1.4 l, 12 mm media, 700 RPM, (f) 4 l, 12 mm media, 500 RPM, (g) 4 l, 12 mm media, 500 RPM, sideways, (h) 28 l, 12 mm media, 500 RPM, (i) 160 l, 6 mm media, 300 RPM, (j) 160 l, 9 mm media, 300 RPM, and (k) 160 l, 9 mm media, 700 RPM

when the fraction of non-zero force collisions is high (Fig. 10.17). This represents a large scale confirmation of similar phenomena observed in microscale reactions [41].

## 10.4 Energy Consumption

Small laboratory mills require significant amounts of energy. Profitability can only be realized through large-scale implementation. Scaling up by 1,000-fold (1 g–1 kg) results in a 24-fold decrease in energy consumption. Further increases in scale will further reduce the energy consumption on a per MT basis

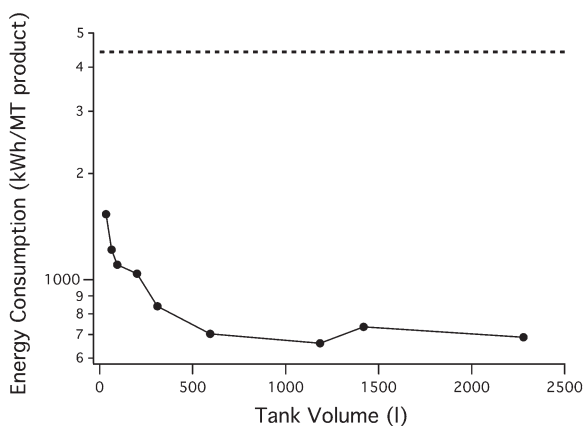


**Fig. 10.18** The energy consumption of commercially available attrition mills for 1 MT of hexose produced in 1 h with 50 % yield. The dotted line represents the energy contained in the ethanol that could be realized from the hexose

(Fig. 10.18). Although these values are 5–10× that required for size reduction alone they represent a combined process that eliminates the acid hydrolysis step in a biorefinery. Cost savings are realized by reduction in process complexity and waste generated. New mill designs such as the IsaMill designed by Netsch and mills designed by the Zoz group offer the promise of lower energy consumption. However, these mills have been optimized for ore processing and work still needs to be done on implementation for biomass processing.

## 10.5 Conclusions and Future Outlook

Saccharides and subsequent fermentation products from cellulose and hemicellulose are often low value products. Conversion of these products into higher-value chemicals would increase the profitability of a biorefinery. The dehydration by-products furfural, levoglucosenone, levoglucosan, and 5-hydroxymethylfurfural represent high value compounds that could be produced in addition to saccharides. Mechanochemical processing offers the potential for increased yields of these compounds and high value sugar alcohols though an added hydrogenation step [31, 32, 69]. This chapter has focused on processing of cellulose and hemicellulose, but the third component, lignin, offers the potential for high profits. The lignin from biomass represents a rich source of aromatic compounds. Lignin is an underutilized resource and lignin extracted from biomass during the production of sugars is currently being burned for fuel instead of being processed into higher value materials. Complete depolymerization of lignin could produce salable products such as syringaldehyde, vanillin, vanillic acid and syringic acid. However, much research has gone into Kraft lignin produced by the paper industry and little value has been obtained. Emerging cellulosic ethanol technologies will provide a new source of pure lignins. These lignins will not have been modified by the harsh processes involved in papermaking and may yet offer the chance for profit. Markets for these materials will expand as demand grows for non-petroleum sourced materials. For example, the current market value of vanillin is ~\$20 U.S.D/kg. Traditional methods for the extraction of vanillin from Kraft liquor produce 160 kg of caustic waste for every kilogram of vanillin produced [70]. This waste reduces the profitability of vanillin realized from lignin. Mechanochemical approaches could increase the profitability of these chemicals by using a reagent-light or catalytic process and reduce the production of this caustic waste. Preliminary work has shown that valuable products can be extracted from this lignin by milling under basic conditions to produce depolymerization products [71]. These products could be extracted from the reaction residue using ethanol produced through fermentation of cellulosic sugars.

As combined mechanical and chemical processing becomes a more mature technology the barriers to its implementation will be overcome. Improved mill designs and a better understanding of the processes occurring during milling



will reduce energy consumption and facilitate even more efficient chemical transformations.

## References

1. ASTM (2012) D1037-12: standard test methods for evaluating properties of wood-base fiber and particle panel materials. ASTM International, West Conshohocken, p 37
2. Zhu JY (2011) Physical pretreatment—woody biomass size reduction—for forest biorefinery. In: Sustainable production of fuels, chemicals, and fibers from forest biomass. American Chemical Society, pp 89–107
3. Bitra VSP, Womac AR, Chevanan N, Miu PI, Igathinathane C, Sokhansanj S, Smith DR (2009) Direct mechanical energy measures of hammer mill comminution of switchgrass, wheat straw, and corn stover and analysis of their particle size distributions. *Powder Technol* 193:32–45
4. Bitra VSP, Womac AR, Igathinathane C, Miu PI, Yang YT, Smith DR, Chevanan N, Sokhansanj S (2009) Direct measures of mechanical energy for knife mill size reduction of switchgrass, wheat straw, and corn stover. *Bioresour Technol* 100:6578–6585
5. Schell D, Harwood C (1994) Milling of lignocellulosic biomass. *Appl Biochem Biotechnol* 45–46:159–168
6. Himmel M, Tucker M, Baker J, Rivard C, Oh K, Grohmann K (1985) Comminution of biomass: hammer and knife mills. *Biotechnol Bioeng Symp* 15:39–58
7. Bitra VSP, Womac AR, Chevanan N, Sokhansanj S (2008) Comminution properties of biomass in hammer mill and its particle size characterization. In: ASABE annual international meeting, 2008, Providence, Rhode Island, p 22
8. Esteban LS, Carrasco JE (2006) Evaluation of different strategies for pulverization of forest biomasses. *Powder Technol* 166:139–151
9. Cara C, Ruiz E, Ballesteros M, Manzanares P, Negro MJ, Castro E (2008) Production of fuel ethanol from steam-explosion pretreated olive tree pruning. *Fuel* 87:692–700
10. Zhang YHP, Lynd LR (2004) Toward an aggregated understanding of enzymatic hydrolysis of cellulose: noncomplexed cellulase systems. *Biotechnol Bioeng* 88:797–824
11. Kitani O, Hall CW (1989) Hydrolysis. In: *Biomass handbook*. Gordon and Breach Science, New York, pp 434–451
12. Yu Y, Wu H (2011) Effect of ball milling on the hydrolysis of microcrystalline cellulose in hot-compressed water. *AIChE J* 57:793–800
13. Stubičar N, Šmit v, Stubičar M, Tonejc A, Jánosi A, Jánosi A, Schurz J, Zipper P (2009) An X-ray diffraction study of the crystalline to amorphous phase change in cellulose during high-energy dry ball milling. *Holzforchung—Int J Biol Chem Phys Technol Wood* 52:455–458
14. Roman-Leshkov Y, Barrett CJ, Liu ZY, Dumesic JA (2007) Production of dimethylfuran for liquid fuels from biomass-derived carbohydrates. *Nature* 447:982–985
15. Zhao H, Holladay JE, Brown H, Zhangn ZC (2007) Metal chlorides in ionic liquid solvents convert sugars to 5-hydroxymethylfurfural. *Science* 316:1597–1600
16. Chidambaram M, Bell AT (2010) A two-step approach for the catalytic conversion of glucose to 2,5-dimethylfuran in ionic liquids. *Green Chem* 12:1253–1262
17. Kudo S, Zhou Z, Norinaga K, Hayashi Ji (2011) Efficient levoglucosenone production by catalytic pyrolysis of cellulose mixed with ionic liquid. *Green Chem* 13:3306–3311
18. Kobayashi H, Yabushita M, Komanoya T, Hara K, Fujita I, Fukuoka A (2013) High-yielding one-pot synthesis of glucose from cellulose using simple activated carbons and trace hydrochloric acid. *ACS Catal* 3:581–587

19. Klinka HB, Thomsen AB, Ahring BK (2004) Inhibition of ethanol-producing yeast and bacteria by degradation products produced during pre-treatment of biomass. *Appl Microbiol Biotechnol* 66:10–26
20. Suryanarayana C (2001) Mechanical alloying and milling. *Prog Mater Sci* 46:1–184
21. Boldyrev VV, Tkacova K (2000) Mechanochemistry of solids: past, present, and prospects. *J Mater Synth Process* 8:121–132
22. Takacs L (1997) Solid state reactions induced by ball milling. *Hyperfine Interact* 111:245–250
23. Balaz P, Achimovicova M, Balaz M, Billik P, Cherkezova-Zheleva Z, Criado JM, Delogu F, Dutkova E, Gaffet E, Gotor FJ, Kumar R, Mitov I, Rojac T, Senna M, Streletskaia A, Wieczorek-Ciurowa K (2013) Hallmarks of mechanochemistry: from nanoparticles to technology. *Chem Soc Rev* 42:7571–7637
24. Barraud E, Begin-Colin S, Le Caer G, Barres O, Villieras F (2008) Mechanically activated solid-state synthesis of hafnium carbide and hafnium nitride nanoparticles. *J Alloys Compd* 456:224–233
25. Rosen BM, Percec V (2007) Mechanochemistry: a reaction to stress. *Nature* 446:381–382 (London, UK)
26. SPEXCertiprep (2008) Products for pulverizing and blending. <http://www.spexcsp.com/sampleprep/catalog/aid4tid8.html>
27. Fritsch (2009) Planetary mills. <http://www.fritsch.de>
28. Process U (2008) Dry grinding attritors: laboratory mills. [http://www.unionprocess.com/dry\\_lab.html](http://www.unionprocess.com/dry_lab.html)
29. Industries P (2008) Ball and pebble mills. [http://www.pattersonindustries.com/7a\\_pics.html](http://www.pattersonindustries.com/7a_pics.html)
30. Meine N, Rinaldi R, Schüth F (2012) Solvent-free catalytic depolymerization of cellulose to water-soluble oligosaccharides. *ChemSusChem* 5:1322–1329
31. Carrasquillo-Flores R, Källdström M, Schüth F, Dumesic JA, Rinaldi R (2013) Mechanocatalytic depolymerization of dry (ligno)cellulose as an entry process for high-yield production of furfurals. *ACS Catal* 3:993–997
32. Hilgert J, Meine N, Rinaldi R, Schuth F (2013) Mechanocatalytic depolymerization of cellulose combined with hydrogenolysis as a highly efficient pathway to sugar alcohols. *Energy Environ Sci* 6:92–96
33. Shrotri A, Lambert LK, Tanksale A, Beltramini J (2013) Mechanical depolymerisation of acidulated cellulose: understanding the solubility of high molecular weight oligomers. *Green Chem* 15:2761–2768
34. Zhang Q, Jérôme F (2013) Mechanocatalytic deconstruction of cellulose: an emerging entry into biorefinery. *ChemSusChem* 6:2042–2044
35. Barakat A, Chuetor S, Monlau F, Solhy A, Rouau X (2014) Eco-friendly dry chemo-mechanical pretreatments of lignocellulosic biomass: impact on energy and yield of the enzymatic hydrolysis. *Appl Energy* 113:97–105
36. Kaldstrom M, Meine N, Fares C, Rinaldi R, Schuth F (2014) Fractionation of ‘water-soluble lignocellulose’ into C5/C6 sugars and sulfur-free lignins. *Green Chem* 16:2454–2462
37. Kaldstrom M, Meine N, Fares C, Schuth F, Rinaldi R (2014) Deciphering ‘water-soluble lignocellulose’ obtained by mechanocatalysis: new insights into the chemical processes leading to deep depolymerization. *Green Chem* 16:3528–3538
38. Hick SM, Griebel C, Restrepo DT, Truitt JH, Buker EJ, Bylda C, Blair RG (2010) Mechanocatalysis for biomass-derived chemicals and fuels. *Green Chem* 12:468–474
39. Kim TH, Lee YY (2007) Pretreatment of corn stover by soaking in aqueous ammonia at moderate temperatures. *Appl Biochem Biotechnol* 136–140:81–92
40. Lin Z, Liu L, Li R, Shi J (2012) Screw extrusion pretreatments to enhance the hydrolysis of lignocellulosic biomass. *Microb Biochem Technol* S12
41. McKissic KS, Caruso JT, Blair RG, Mack J (2014) Comparison of shaking versus baking: further understanding the energetics of a mechanochemical reaction. *Green Chem* 16:1628–1632

42. Blair RG (2011) Oxidative cleavage of unsaturated carboxylic acids. Application, WO (University of Central Florida Research Foundation, Inc., USA), pp 21
43. Watanabe R, Hashimoto H, Lee GG (1995) Computer simulation of milling ball motion in mechanical alloying (overview). *Mater Trans JIM* 36:102–109
44. Cleary PW (1998) Predicting charge motion, power draw, segregation and wear in ball mills using discrete element methods. *Miner Eng* 11:1061–1080
45. Rajamani RK, Mishra BK, Venugopal R, Datta A (2000) Discrete element analysis of tumbling mills. *Powder Technol* 109:105–112
46. Mio H (2005) Estimation of mechanochemical reaction rate and optimum design of planetary ball mill by discrete element method. *Funtai Kogaku Kaishi* 42:134–139
47. Sinnott M, Cleary PW, Morrison R (2006) Analysis of stirred mill performance using DEM simulation: part 1—media motion, energy consumption and collisional environment. *Min Eng* 19:1537–1550
48. Frišćić T, Halasz I, Beldon PJ, Belenguer AM, Adams F, Kimber SAJ, Honkimäki V, Dinnebier RE (2013) Real-time and in situ monitoring of mechanochemical milling reactions. *Nat Chem* 5:66–73
49. Guban D (2000) Inelastic collision and the Hertz theory of impact. *Am F Phys* 68:920–924
50. van Dijk P (2000) Contact spots. In: 20th conference on electrical contacts
51. DEMSolutions (2007) EDEM. <http://www.dem-solutions.com/>
52. Yamanaka T, Tanabe K (1976) A representative parameter, H<sub>0</sub> max, of acid-base strength on solid metal-oxygen compounds. *J Phys Chem* 80:1723–1727
53. Rinaldi R (2012) Media wear. In: Blair RG (ed) Private communication, 3 August 2012
54. Yamaguchi D, Kitano M, Sugauma S, Nakajima K, Kato H, Hara M (2009) Hydrolysis of cellulose by a solid acid catalyst under optimal reaction conditions. *J Phys Chem C* 113:3181–3188
55. Blair RG, Chagoya K, Jackson S, Biltek S, Taraboletti A, Sinclair A, Restrepo DT (2014) Scalability in the mechanochemical syntheses of edge functionalized graphene materials and biomass-derived chemicals. *Faraday Discuss (Advance Article)*
56. James SL, Adams CJ, Bolm C, Braga D, Collier P, Friscic T, Grepioni F, Harris KDM, Hyett G, Jones W, Krebs A, Mack J, Maini L, Orpen AG, Parkin IP, Shearouse WC, Steed JW, Waddell DC (2012) Mechanochemistry: opportunities for new and cleaner synthesis. *Chem Soc Rev* 41:413–447
57. Cincic D, Brekalo I, Kaitner B (2012) Effect of atmosphere on solid-state amine-aldehyde condensations: gas-phase catalysts for solid-state transformations. *Chem Commun* 48:11683–11685
58. Mitsudome T, Mikami Y, Funai H, Mizugaki T, Jitsukawa K, Kaneda K (2008) Oxidant-free alcohol dehydrogenation using a reusable hydrotalcite-supported silver nanoparticle catalyst. *Angew Chem* 120:144–147
59. Schnuerch M, Holzweber M, Mihovilovic MD, Stanetty P (2007) A facile and green synthetic route to boronic acid esters utilizing mechanochemistry. *Green Chem* 9:139–145
60. Rodríguez B, Bruckmann A, Rantanen T, Bolm C (2007) Solvent-free carbon–carbon bond formations in ball mills. *Adv Synth Catal* 349:2213–2233
61. Dushkin AV (2004) Potential of mechanochemical technology in organic synthesis and synthesis of new materials. *Chem. Sust. Dev.* 12:251–273
62. Schaffer GB, McCormick PG (1992) On the kinetics of mechanical alloying. *Metall Trans A* 23A:1285–1290
63. Takacs L (2002) Self-sustaining reactions induced by ball milling. *Prog Mater Sci* 47:355–414
64. Urakaev FK, Boldyrev VV (2000) Mechanism and kinetics of mechanochemical processes in comminuting devices 2. Applications of the theory. *Experiment. Powder Technol* 107:197–206

65. Urakaev FK, Boldyrev VV (2000) Mechanism and kinetics of mechanochemical processes in comminuting devices 1. Theory. *Powder Technol* 107:93–107
66. Maglia F, Milanese C, Anselmi-Tamburini U, Doppiu S, Cocco G, Munir ZA (2004) Combustion synthesis of mechanically activated powders in the Ta-Si system. *J Alloy Compd* 385:269–275
67. Delogu F, Mulas G, Schiffini L, Cocco G (2004) Mechanical work and conversion degree in mechanically induced processes. *Mater Sci Eng A* A382:280–287
68. Manai G, Delogu F, Schiffini L, Cocco G (2004) Mechanically induced self-propagating combustions: experimental findings and numerical simulation results. *J Mater Sci* 39:5319–5324
69. Schüth F, Rinaldi R, Meine N, Käldestrom M, Hilgert J, Rechulski MDK (2014) Mechanocatalytic depolymerization of cellulose and raw biomass and downstream processing of the products. *Catalysis Today* 234:24–30
70. Hocking MB (1997) Vanillin: synthetic flavoring from spent sulfite liquor. *J Chem Educ* 74:1055
71. Kleine T, Buendia J, Bolm C (2013) Mechanochemical degradation of lignin and wood by solvent-free grinding in a reactive medium. *Green Chem* 15:160–166

# Chapter 11

## Production of Glucose from Starch-Based Waste Employing Ultrasound and/or Microwave Irradiation

Audrey Villière, Giancarlo Cravotto, Raphaël Vibert, Arnaud Perrier, Ulla Lassi and Jean-Marc Lévêque

**Abstract** Industrial bio-waste valorization is an alternative approach to reduce residues, waste disposals or landfills, essential to a sustainable development. This chapter deals with the valorization of a starch-based industrial waste into sugars employing ultrasound and microwave technologies. Potato peel is a product-specific waste with high starch content, a macromolecule that can be hydrolyzed into building blocks such as sugars. The combination of ultrasound and microwave technologies for starch degradation to explore synergetic interactions is developed in the second part of this chapter.

**Keywords** Starch · Waste · Valorization · Reducing sugars · Ultrasound · Microwave · Combined technology

---

A. Villière (✉) · U. Lassi

Kokkola University Consortium Chydenius, Talonpojankatu 2B, 67100 Kokkola, Finland  
e-mail: audrey.villiere@gmail.com

A. Villière · J.-M. Lévêque (✉)

Laboratoire de Chimie Moléculaire et Environnement, Université de Savoie,  
73376 Le Bourget du Lac Cedex, France  
e-mail: jm.leveque@petronas.com.my

G. Cravotto

Dipartimento di Scienza e Tecnologia del Farmaco,  
University of Turin, Via Giuria 9, 10125 Turin, Italy

R. Vibert · A. Perrier

Synetude, P.A. de Côte Rousse 180, Rue du Genevois, 73000 Chambéry, France

U. Lassi

Department of Chemistry, University of Oulu, P.O. Box 3000, 90014 Oulu, Finland

J.-M. Lévêque

Department of Fundamental and Applied Sciences, Universiti Teknologi Petronas,  
Bandar Seri Iskandar, 31750 Tronoh, Perak, Malaysia

## 11.1 Introduction

The procedure of traditional waste ‘valorization’ is their use as waste as either animal feed (e.g., spent grains, distiller’s wash) or fertilizer (filtration sludge, carbonation sludge). Agro-residues, industrial waste and non-food crops possess real chemical potential to be treated as feedstock. The main benefit of industrial waste is their quantity and availability, and it can be considered as an alternative source of energy for biofuels due to the medium-term depletion of fossil fuel reserves. Indeed, industrial waste is an opportunity to switch from petroleum-based to renewable resource economy. Considering potato peels as a raw material is challenging due to its high water content, its rapid oxidation as well as its high level of enzymatic activity, leading to a rapid degradation of the organic-based contents. Potato peel is a typical product-specific waste, extracted from the desired products and possessing an undeniable potential for further processes. Industrial food waste is characterized by a high ratio of product specific waste. The generation of waste appears also unavoidable and it is necessary to consider food waste as valuable raw material. This potato peel waste is mainly constituted of starch, a macromolecule that can be hydrolyzed into building blocks and serve as platform chemicals for essential chemicals [1]. Starch can be converted into sugars with conventional heating systems, which are quite demanding in time and energy. Ultrasonic and microwave irradiations are non-conventional technologies able to reduce necessary reaction time and energy consumption while increasing yields. The overall goal of this chapter is to valorize a starch-based industrial waste into sugars employing low- and high-frequency ultrasound or microwave irradiations. The second part is focus on the combination of these two technologies to envisage synergetic interactions.

## 11.2 Starch-Based Waste as a Raw Material

### 11.2.1 *Composition of the Waste*

The industrial waste to be valorized is potato peel slurry, mechanically peeled with rotation peaks. This industrial waste was provided by ready-cooked varieties of vacuum potatoes for professional catering, named Jépuan Peruna Oy. About 15–20 tons are daily generated and mainly transported to cattle and pig farms. The skin and a part of the potato are washed down with water. The high organic contents in potato peels render this feedstock very promising for chemicals and/or biofuels. Physico-chemical analyses of this feedstock confirms that it is composed of two-third of water and of one-third of dry matter, including starch molecules, free sugars, proteins, and fibers. To better characterize this waste, thermo gravimetric analyses and particle size distribution of pure cooking potato starch, and the starch-based industrial waste (potato peel) have been performed (Fig. 11.1). Mostly composed of starch, pure sample of potato starch was also taken as reference to compare results with the industrial potato peel waste.

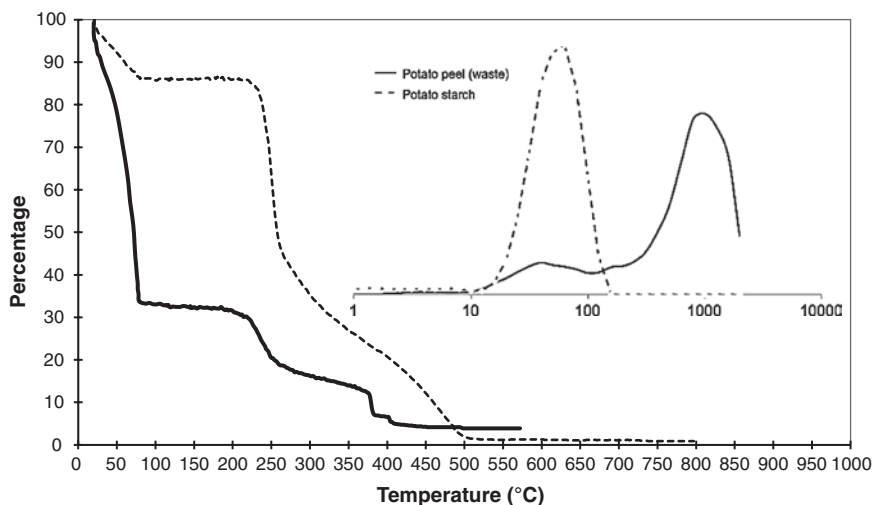


**Fig. 11.1** Thermogravimetric analysis (*left-side*) and particles size distribution (*right-side*) of potato starch (*dashed line*) and potato peel (*filled line*) [2, 3]

Particles size distribution of potato starch displayed a median diameter of 63  $\mu\text{m}$  with a single population, whereas potato peel displayed a bimodal distribution at 40 and 1,000  $\mu\text{m}$  with a median diameter of 656  $\mu\text{m}$ . Field emission scanning electron microscopy (FE-SEM) matched the previous results; single grains are observed in the potato starch with a range of 20–100  $\mu\text{m}$  whereas agglomerated grains corroborate the 1,000  $\mu\text{m}$  distribution of potato peel material (Fig. 11.2a).

The company Jepuan Peruna Oy performed a complete characterization of potato peel, which revealed 23 % of starch, 8 % of crude protein, 7 % of ash, 4 % of crude fiber, <1 % of crude fat, <1 % of free sugars and the remaining of water [4]. Potato tubers contain also non-starch polysaccharides, cellulose and hemicellulose, located in cell wall and potato skin [5]. High water content could be an issue for waste valorization due to transport costs or the high-energy demand of water removing. A possible solution is to keep water as the solvent for the hydrolysis process. A total hydrolysis of the potato peel displayed a sugar potential of 29 %, which corroborates the previous results obtained by the company.

### 11.2.2 Molecular Composition of Starch

Starch is semi-crystalline polysaccharide stored in grains (i.e. corn, rice...), tubers (i.e. potato...) and roots. Botanical sources influence the shape, size, morphology, composition, and molecular structure of starches. Naturally, starches are arranged in granules alternatively in semi-crystalline and amorphous layers. Granule size



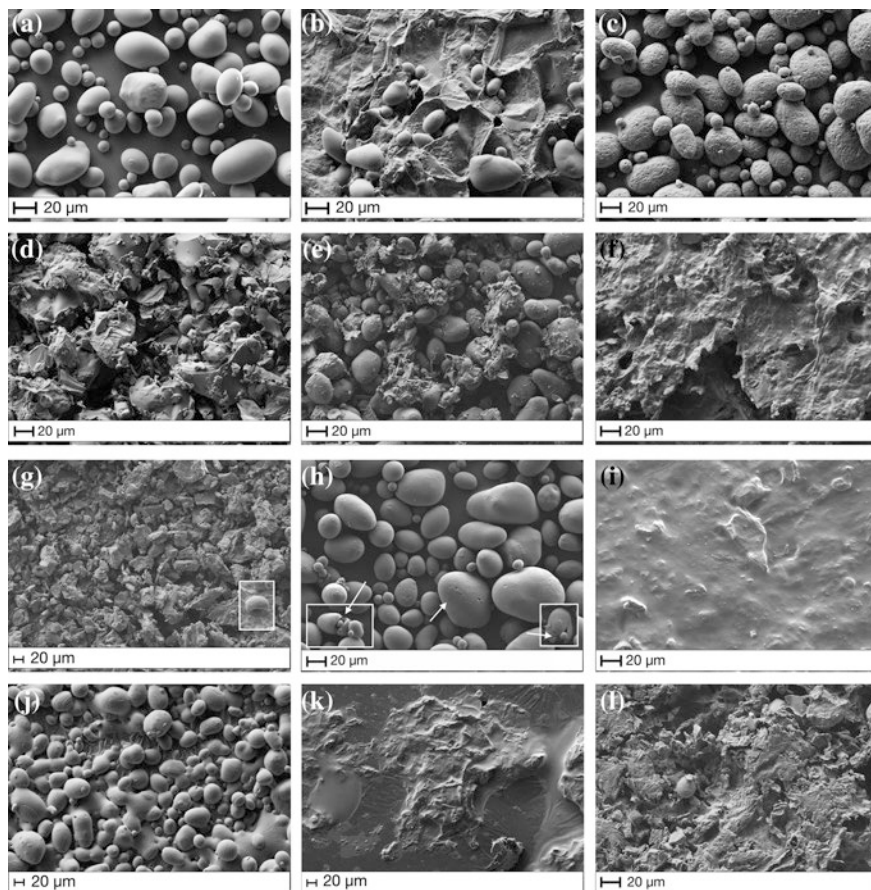


**Fig. 11.2** Field emission scanning electron microscopy (*FE-SEM*) residue images of **a** potato starch no treatment, **b** potato peel (waste) no treatment, **c** potato starch after ultrasound (*US*) 20 kHz Pyrex probe, **d** potato peel after *US* 20 kHz Pyrex probe, **e** potato peel after *US* 24 kHz bath, **f** potato peel after *US* 500 kHz, **g** potato peel after combined *US* 20 kHz Pyrex probe/multimode microwave (*MW*), **h** potato starch after dual *US* 20/500 kHz, **i** potato peel after *US* 20/500 kHz, **j** potato starch after monomode *MW*, **k** potato peel after monomode *MW*, and **l** potato peel after combined *US* 20 kHz Pyrex probe/multimode microwave (13-wt% suspension); conditions: 3-wt%—120 min irradiation— $3 \text{ mol L}^{-1} \text{ H}_2\text{SO}_4$  [2–4]

varies from  $<1 \mu\text{m}$  for rice to  $100 \mu\text{m}$  for potato. Starch, lipids (phospholipids and free fatty acids), phosphate monoesters and proteins/enzymes are stored in granules. Starch is composed of two macromolecules, amylose and amylopectine (Fig. 11.3). Granules are composed of many different compounds; however amylose and amylopectin influence at most functional properties (thermal and rheological properties). Although other components are in minor amount, they may also influence some functional properties. According to botanical sources, normal starches contain 20–30 % of amylose and 70–80 % of amylopectin. Molecular



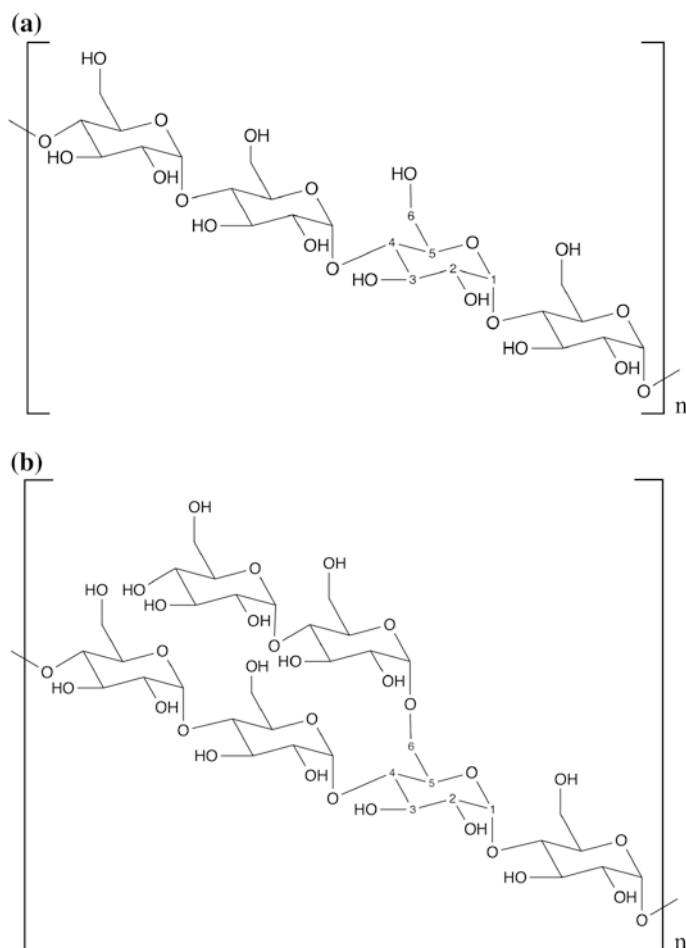


**Fig. 11.3** Structure of amylose (a: top) in a chair conformation—bonded in  $\alpha$ -(1,4) glycosidic linkage, linear molecule with a six glycosidic units double helical shape (sixfold helix) and amylopectin (b: bottom), also in a chair conformation—bonded in  $\alpha$ -(1,4) and  $\alpha$ -(1,6) glycosidic linkage, which gives a highly branched structure [6]

structure of amylose is mainly  $\alpha$ -1,4-glycosidic linkages and some parts appear to be slightly branched in  $\alpha$ -1,6-glycosidic linkages. Geometry of amylose orients the molecule in a helix conformation. Amylopectin is a macromolecule branched in  $\alpha$ -1,4 and  $\alpha$ -1,6-glycosidic bonds. It possesses one reducing sugar end and plenty of non-reducing sugar ends due to the  $\alpha$ -1,6 linkages, whereas amylose possesses one of each as a linear molecule. Reducing sugars are defined as sugars containing aldehyde or ketone group that can be oxidized into carboxylic acids. Reducing sugars possess hemiacetal or hemiketal, which can undergo mutarotation and be reduced in carboxylic acids, whereas it is impossible with non-reducing sugars due to the acetal of ketal carbon.

The starch-based waste is mainly composed of potato peels. Potato starch has the lowest amount of non-carbohydrate component, with less than 0.5 % of proteins and few lipids of phospholipids [7]. However, the presence of phosphorous in potato starch may influence physico-chemical properties. Phosphorous is naturally present in three different forms: phosphate monoesters, phospholipids and inorganic phosphates. Phosphate monoesters are covalently bonded in tubers and roots starches up to 0.09 % (w/w) Phospholipids are present in cereal starches. Starch granules are alternatively formed of semi-crystalline and amorphous layers and the semi-crystalline parts are also formed of crystalline and amorphous layers [2]. Phosphate monoesters are located in the amorphous parts, even in the amorphous parts of semi-crystalline layers [8]. Naturally charged, these monoester groups increase the electrostatic repulsion between molecules [9].

### 11.2.3 Physico-chemical Properties of Starch Granules in Water

When starch granules are heated over 60 °C in aqueous solution, an irreversible process occurs, breaking down inter- and intra-molecular bonds, also called starch gelatinization. This gelatinization process is directly related to the botanical source of starch, the size of the granule and the number of granules per gram of starch (Table 11.1). Polarization crosses start to disappear, granules begin to swell irreversibly increasing viscosity. Hydrogen bondings are broken down leading to disorder in the granule structure [10]. Potato starch has a high swelling power, giving a large gel volume compared to other sources of starch. Swelling power mainly occurs in the amorphous regions [11]. Moreover, this phenomenon increases due to the high presence of phosphate monoesters in potato starch granules. Those phosphates are located in the amorphous part of the semi-crystalline regions, causing an increase of the absorption of water due to the

**Table 11.1** Physico-chemical properties of various sources of starch (potato, maize and wheat) [2, 12, 13]

	Potato starch	Maize starch	Wheat starch
Shape of the granule	Oval/ spherical	Round polygonal	Round lenticular
Diameter range of the granule ( $\mu\text{m}$ )	5–100	2–30	0.5–45
Number of granules per gram starch $\times 10^6$	100	1,300	2,600
Amylose content (%)	20.1–31.0	22.4–32.5	18.0–30.0
Solubility (%) (°C)	82 (95)	22 (95)	1.6 (100)
Swelling power (g/g) (°C)	1,159 (95)	22 (95)	18–26 (100)
T <sub>g</sub> range (°C) <sup>a</sup>	60–65	75–80	80–85
Presence of phosphate, range (w/w)	0.01–0.09	0.003–0.01	0.001–0.06

<sup>a</sup>Approximate values of gelatinization temperature

repulsion of the phosphate groups. This phenomenon renders the crystalline part water-soluble. Afterwards, retrogradation process occurs, while starch has reached its gelatinization point, realigning linear part of starch molecules in a more crystalline structure to form intermolecular hydrogen bonds.

### ***11.2.4 Experimental Conditions for Starch Degradation***

During the industrial process of potato peeling, water is used to gather the peels, and potato peel waste contains up to 70 % of water. On an industrial scale, water is interesting for its cost, availability and 'greenability'; a change of reaction medium would be highly expensive and energy demanding. However, starch is a water insoluble polysaccharide leading to heterogeneous process and the use of catalysts is required to increase efficiency while decreasing reaction time. Potato starch, mainly composed of amylose and amylopectin, was used as a reference for comparison with the degradation of starch-based peel waste. A 3-wt% suspension of potato starch or potato peel (waste) was irradiated for 2 h in acidic aqueous solution (3 mol L<sup>-1</sup> sulfuric acid, pH 0). It was demonstrated [3] that an acidic medium and a temperature of 60 °C appeared both essential for low molecular weight sugar production. Several acids may be suitable for starch depolymerization, and it proved to be difficult to find the most adapted one. Mineral acids appear to be the most attractive catalysts for starch depolymerization notably owing to their relatively low price and availability [14] and several of them have been already compared. Hydrochloric acid can generate toxic fumes while increasing temperature and also large amount of mineral salts during neutralization. It might be necessary to desalinate the solution for further process including high cost and poor efficiency [15]. Phosphoric acid seems to be more efficient on  $\alpha$ -1,6 bonds and lignocellulosic degradation [16]. Nitric acid is a strong oxidizing mineral more appropriated for copolymerization processes [17]. Sulfuric acid is a strong diprotic acid with low volatility, appropriate for the degradation of starch, which occurs around 60 °C [18, 19]. The lower acidic concentration the safer is from an industrial and environmental point of view. After processes, sulfuric acid was neutralized with sodium hydroxide and the quantity of reducing sugars in the liquid phases were determined with the total reducing sugar method (TRS) according to revised Miller technique [20]. Indeed, 2.0 mL of unknown solution was added to 2.0 mL of 1 % dinitrosalicylic acid reagent solution previously prepared. The prepared solution was boiled for exactly 10 min, and afterwards 1.0 mL of a 40 % solution of potassium sodium tartrate was added to maintain the coloration for analysis. The solution was cooled down to room temperature to quench the oxidation, and analyzed at 575 nm against a blank containing 2.0 mL of water instead of unknown solution. TRS was calculated according to a standard curve performed on glucose. Glucose analysis was executed with the glucose oxidase-peroxidase assay reagent from Sigma-Aldrich glucose kit [21]. Experimentally, 1.0 mL of unknown solution, 1.0 mL of glucose reagent and 0.5 mL of distilled water were incubated at 37 ± 1 °C for exactly 30 min. 1.0 mL of sulfuric acid (6 mol L<sup>-1</sup>) was added

to quench the reaction and gave a pink solution. The absorbance was measured against a blank reagent containing 1.0 mL of distilled water instead of unknown solution at a wavelength of 540 nm. Glucose concentration was calculated with the standardization curve performed on glucose standard provided in the kit.

## 11.3 Ultrasound-Assisted Hydrolysis of Starch-Based Waste

### 11.3.1 Previous Related Researches

Ultrasonic irradiations generate two fundamental effects according to the frequency applied, developed in Chap. 1. Several ultrasonic frequencies were utilized to depolymerize the starch-based industrial waste in order to understand their impact on the starch molecule structure. Two areas of frequencies were studied, low frequency irradiation around 20 kHz primarily for mechanical effects, and higher frequency around 500 kHz assimilated to 'chemical' effects, due to the formation of highly reactive compounds, free radicals, during the propagation of the ultrasonic wave in the medium.

The hydrolysis of starch assisted with ultrasound was already referred to in 1933 [22], however, its investigation was only highlighted in the last decades. Various frequencies were employed to convert starch molecules into short-chain carbohydrates till glucose. Several authors explored the use of low concentration acid systems maybe in reason of eventual corrosion and attack of the probe [18, 23]. Corn starch hydrolysis into glucose was investigated with an ultrasonic probe of 24 kHz in 1994 [23]. Maltotriose (three glycosidic units), maltose (two glycosidic units) and glucose (up to 63 %) were obtained under low concentration of sulfuric acid (0.3-wt%), high pressure ( $5 \times 10^5$  Pa) and high temperature (159 °C). Hydroxymethylfurfural (HMF) was additionally produced during the process. Starch was first converted into glucose and the hydrolysis continued to HMF. The conversion of a 3-wt% suspension was almost complete within 2 h at 100 °C in 5-wt% sulfuric acid solution but no aspect of the ultrasonic probe was mentioned in the article; an eventual degradation might occur at such a temperature combined with acid concentration. It is noteworthy that hydrolysis was performed in a closed vessel under relatively high pressure providing a process quite demanding in energy even if acoustically more efficient. A 20 kHz ultrasonic probe was utilized to degrade native dextran into lower molecular weight sugars [24]. Dextrans are branched polysaccharides in  $\alpha$ -1,6 and  $\alpha$ -1,3 glycosidic linkages (3–2,000 kDa). A 2 w/v% solution was irradiated with the ultrasonic probe delivering 60 W acoustic for 4 h at 30 °C. The particles size distribution of dextrans dramatically reduced. Ultrasound is a critical factor for dextran degradation, because 64 h were necessary to reach similar results without ultrasonic irradiation. An increase of the dextran concentration up to 10 w/v% decreases the degradation rate. A comparison of several ultrasonic frequencies (35, 500, 800 and 1,600 kHz) on the degradation of dextrans revealed that low frequency irradiation generated the lowest molecular

weight distribution [25]. It was suggested that low molecular weight compounds were more degraded with high frequencies irradiation due to radicals' formation, whereas low frequencies degraded long chain polymers due to shockwaves. A 360 kHz ultrasonic reactor was employed on starch molecules and decreased the molecular weight of a solution containing  $5 \times 10^{-2} \text{ mol L}^{-1} \text{ NaClO}_4$  [26]. Sodium perchlorate was used as a radical scavenger to demonstrate that free radicals formed were crucial for starch degradation. It is noteworthy that water-soluble carbohydrates can be degraded at 20 and 500 kHz ultrasonic irradiation [27], whereas for non-water-soluble ones, long chains are degraded into shorter ones with 20 kHz due to shear forces and shorter chains with radicals formed at higher frequencies.

### 11.3.2 Comparison of Various Ultrasonic Frequencies on Starch

#### 11.3.2.1 Low Frequencies Ultrasonic Irradiation

First of all, a 5 L 'Kerry Pulsatron' 24 kHz ultrasonic bath was employed (Fig. 11.4d). Ultrasonic baths are widely present in laboratories for cleaning and can be utilized as exploratory campaign. Ultrasonic baths provide indirect irradiation,

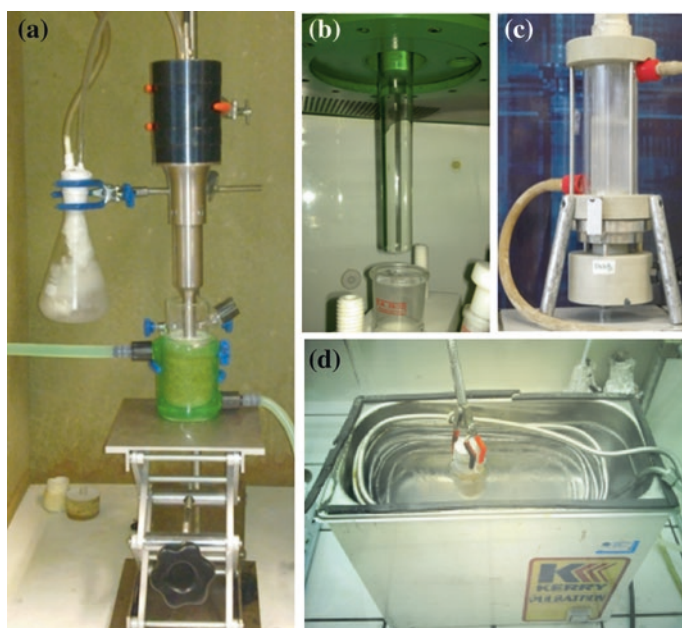


**Fig. 11.4** Ultrasonic devices utilized for the experiments: **a** 20 kHz ultrasonic titanium probe, **b** 20 kHz ultrasonic Pyrex probe, **c** 500 kHz ultrasonic reactor with piezoceramic transducer, and **d** 24 kHz ultrasonic bath

glassware reactors are settled in the bath containing liquid solution (i.e. water, alcohol...). Baths are mainly filled with pure water to avoid wave interferences. However, water in the bath absorbs a part of the ultrasonic wave resulting of a loss of energy inside the glassware reactor. Previously, Choi and Kim [23] irradiated a 3-wt% starch suspension with a low frequency ultrasonic probe at 90 °C for 2 h in 0.5 mol L<sup>-1</sup> sulfuric acid solution and produced only 18 % yield of glucose.

In our experiments, the low frequency ultrasonic irradiation of potato starch in a 1 mol L<sup>-1</sup> sulfuric acid solution at 60 °C did not degrade the starch molecule since no reducing sugars were detected [3]. Low acidic concentration has little effect on  $\alpha$ -1,6-glycosidic bonds due to its strong linkage [28] and the increase of acid concentration up to 3 mol L<sup>-1</sup> led within 2 h to 36 % of reducing sugars under mechanical stirring and 61 % with the ultrasonic bath (Fig. 11.5) [3]. Thanks to these results, identical conditions were applied to the waste potato peel and only 6 % of reducing sugars were produced; starch granules are entrapped in biomass debris, confirmed by SEM imaging (Fig. 11.2b) and may not be reached by the ultrasonic waves. Moreover, the low power density of the ultrasonic bath of 10 W cm<sup>-2</sup>, the attenuated wave due to water bath and the glassware vessel reduced the cavitation efficiency. MALDI TOF analysis (Matrix-assisted laser desorption/ionization Time-of-flight) was performed on the sugar solution obtained and revealed a main intensive peak at 507 g mol<sup>-1</sup> (Fig. 11.6b). No selection was observed under conventional heating (Fig. 11.6a). In order to get the maximal disturbance and minimal loss of intensity, an optimum position of the glassware placed in the water bath were investigated. High disturbances were observed while the interfaces liquid/air in the vessel and in the the water bath were at the same height, where reflection waves reduced are at a minimum level [29]. To increase reducing sugars production, the acoustic power has to be improved.

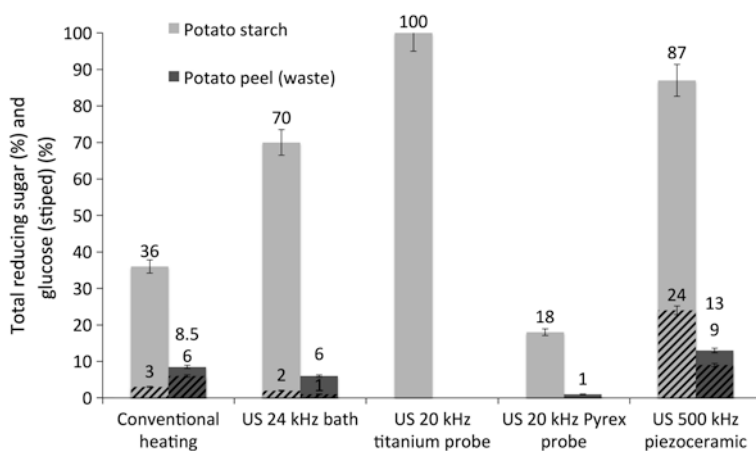


**Fig. 11.5** Total reducing sugar and glucose (*striped*) yields of the experiments performed under conventional heating, and various ultrasonic irradiations; conditions: 2 h process, sulphuric acid 3 mol L<sup>-1</sup>, 60 °C [3]

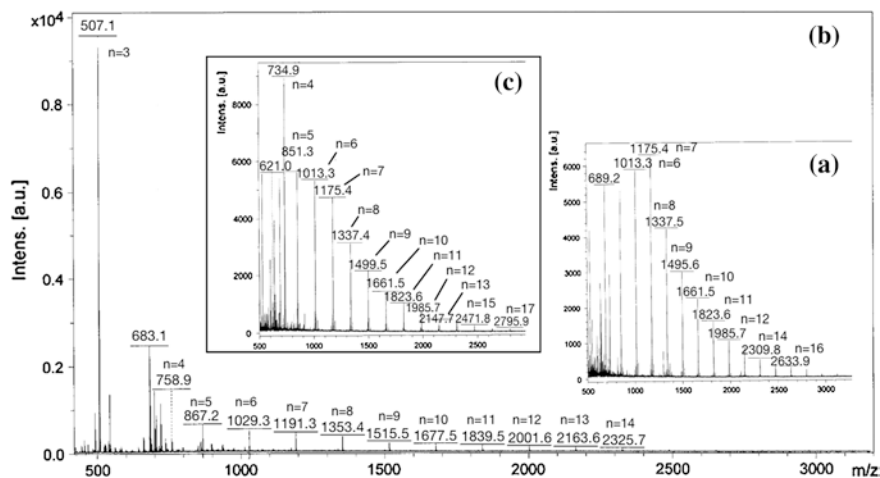


**Fig. 11.6** MALDI TOF analyses of sugars (counter ion  $H^+$ ) after (a) conventional heating process, (b) 24 kHz ultrasonic bath irradiation, and (c) 500 kHz piezoceramic transducer reactor irradiation of potato starch; conditions: 2 h process, sulphuric acid 3 mol  $L^{-1}$ , 60 °C [3]

Ultrasonic probes generate higher acoustic power and are directly immersed into the reaction vessel, removing interferences. An ultrasonic probe made of Pyrex was employed to avoid acidic attack due to the concentration of sulfuric acid (Fig. 11.4b). The acoustic power of 17 W, measured by calorimetry according to standardization [30], attacked only the surface of granules of potato starch (Fig. 11.2c) to produce 18 % of reducing sugars (Fig. 11.5). As expected, the acoustic power was not high enough to disrupt the biomass debris and liberate the starch granules of the potato peel (waste) material (Fig. 11.2d), however SEM images revealed encouraging results as the surface of few granules was attacked. It was shown that ultrasonic probes could degrade amorphous and crystalline regions of cornstarch granules without disrupting the entire structure [31]. Maltose crosses were still visible after ultrasonic irradiation. Maltose crosses reflect the crystalline structure and therefore the presence of granules. It was suggested that channels were formed on granule surface favoring higher reagent reactivity. However, the crystalline structure of cornstarch was broken within 15 min of irradiation with a 24 kHz ultrasonic probe (7 mm titanium tip) [32]. It was suggested that hydrogen bonds were formed between water and hydroxyl groups located in amylose and amylopectin, encouraging granules' agglomeration. The acoustic power is a critical factor and the Pyrex probe was not able to provide higher power due to the limitations of the material. Therefore, a 19 mm tip titanium probe at a frequency of 20 kHz was utilized on potato starch (Fig. 11.4a). The titanium probe provided an acoustic power of 86 W at 75 % amplitude. Astonishing results were obtained; potato starch was totally hydrolyzed into reducing sugars within 2 h (Fig. 11.5). Sulfuric acid was essential to initiate the hydrolysis but unfortunately badly damaged the probe by dissolving the nickel contained in the alloy ultrasonic tip.



The acoustic power of 86 W might be the key to disrupt granules and liberate the starch molecules into the medium. No experiments were performed on potato peel (waste) in order to prevent more damage on the titanium probe. To prevent this, adding a protective coating on the ultrasonic probe might be a good answer against high corrosion. Previously, Jambrak et al. [32] demonstrated that a 24 kHz ultrasonic probe disrupted the crystalline region of starch granules and reduced the turbidity of a 10 wt% suspension solution at low concentration of sulfuric acid (below  $0.5 \text{ mol L}^{-1}$ ). The authors did not mention anything about the aspect of the ultrasonic probe, although the reactions were performed under sulfuric acid at  $100 \text{ }^\circ\text{C}$ . Turbidity is directly related to starch degradation; starch is a non water-soluble molecule and its degradation produced water-soluble sugars.

### 11.3.2.2 Higher Frequencies Ultrasonic Irradiation

To perform potato starch and potato peel degradation at 500 kHz, a 50 mL ultrasonic reactor was designed in our laboratories (Fig. 11.4c) [3]. Electric power of 25 W is provided to the piezoceramic transducer, which delivered an acoustic power of 8 W. The reactor was cooled down with a heat-transfer fluid, such as ethylene glycol, to maintain  $60 \pm 3 \text{ }^\circ\text{C}$  inside the reactor. An air-cooling flow maintained the piezoceramic transducer to a reasonable working temperature. This type of reactor is hardly employed in research laboratories and quite complicated to acquire. At search frequencies, radicals are mainly formed through sonolysis of water molecules. Convection field is produced during the sonolysis; an acoustic fountain is formed in the center of the reactor. A great yield of 87 % of reducing sugars, including one third of glucose, was obtained from a 3-wt% potato starch suspension (experimental conditions: 120 min irradiation at  $60 \text{ }^\circ\text{C}$  in a  $3 \text{ mol L}^{-1}$  sulfuric acid solution) (Fig. 11.5). The use of a radical scavenger showed that free radicals play an important role in carbohydrates depolymerization [26, 27]. A MALDI-TOF analysis showed a peak at  $734 \text{ g mol}^{-1}$ , representing oligosaccharides of four glycosidic units (Fig. 11.6). A kind of selectivity occurred under high frequency ultrasonic irradiation, probably caused by the radical degradation. The irradiation of the potato peel (waste) under identical condition aforementioned generated 13 % of reducing sugars, and 70 % of these sugars is glucose (Fig. 11.5). This result appears quite low compared to potato starch depolymerization, however, it is so far the highest yield of reducing sugars reached. As aforementioned, potato peel is a complex matrix with entrapped granules surrounded by fibers and biomass debris (Fig. 11.2b). SEM images of potato peel ultrasonic degradation showed that starch molecules were liberated from the granules (Fig. 11.2f) due to the disappearance of granules. The low yield of reducing sugars might be interpreted that amylose and amylopectin were entrapped in biomass debris could not undergo hydrolysis. It is important to notice that the highest yields of glucose were obtained under high frequency irradiation. Regarding the results obtained, this technology appears promising for starch molecule depolymerization.



Energy consumption is reduced under ultrasonic irradiation compared to conventional heating; indeed the 0.5 kW electrical power of the ultrasonic generator is lower than the 1.2 kW electrical power delivered with a common magnetic hot-plate. Moreover, in the case of conventional heating, necessary time has to be considered to heat up the oil bath to 60 °C.

## 11.4 Microwave-Assisted Hydrolysis of Starch-Based Waste

### 11.4.1 Principle of Microwave-Assisted Irradiation

Microwaves are electromagnetic waves in frequency range 300–300 GHz, corresponding to the wavelengths between 1 mm and 1 m respectively. Microwave frequencies are mainly used for telecommunications in range of 30–300 GHz. In order to avoid interferences with this frequency range, heating applications have to be in the ISM bands (Industrial Scientific and Medical frequencies). The only ISM frequencies allowed are 27.12, 433.9, 915 MHz and 2.45 GHz. Domestic microwaves as well as commercially available microwave reactors for chemical synthesis operate at a frequency of 2.45 GHz (corresponding to a wavelength of 12.25 cm). Official request is required for the use of other frequencies [33, 34].

Microwave chemistry is based on the heating efficiency, provoked by dielectric heating effects due to two mechanisms: dipolar polarization and ionic conduction. The magnetron imposes an alternative electric field to the system and the microwave field is oscillating. Dipoles in the field align with the oscillating field causing rotation of the polar molecules. These rotations induce a dissipation of energy into heat through intermolecular frictions. This phenomenon is called dipolar polarization. The second phenomenon, ionic conduction, is defined as the back and forth oscillation of charged molecules in microwave field. This oscillation provokes the collision of charged molecules generating heat energy [35]. Microwave reactors generate dielectric heating, where electric energy is converted into kinetic energy and into heat.

Dielectric heating suggests that a material must possess certain dielectric properties in order to be efficiently heated in the microwave field. The materials behavior depends on their ability to absorb, reflect or be transparent to microwaves. Microwave irradiation induces electromagnetic waves consisting of electric and magnetic fields. Electric field is responsible for dielectric heating, while magnetic field induces the structure (direction and strength) in magnetic moments. Interaction between the electromagnetic waves and the matter is connected to two physical phenomena, the dielectric permittivity,  $\epsilon$  and the magnetic susceptibility,  $\mu$ . Actually, the dielectric permittivity is a complex number made up of two parts:

$$\epsilon = \epsilon' + i\epsilon'' \quad \text{and} \quad \tan \delta = \frac{\epsilon''}{\epsilon'} \quad (11.1)$$

where

- $\epsilon'$  is the dielectric constant represents the ability of a molecule to be polarized by an electric field;
- $\epsilon''$  is the dielectric loss is a factor that measures the ability of a material, polarized by a electric field, to convert energy into heat;
- $\tan \delta$  is the dielectric loss tangent is the ratio between the dielectric loss and the dielectric constant [34].

The loss tangent factor reflects the ability of a solvent to be transparent or absorb the microwaves. Solvents possessing a  $\tan \delta > 0.5$  (ethylene glycol 1.350; ethanol 0.941; formic acid 0.722; 1-butanol 0.571) highly absorb microwaves; medium  $\tan \delta$  ( $0.1 < \tan \delta < 0.5$ ) are less absorbing microwaves, whereas solvents with a  $\tan \delta < 0.1$  are almost transparent to microwaves (toluene 0.040; hexane 0.020) [36]. In other words, polar mixtures are required for efficient microwave heating. However, several authors have postulated specific effects of microwaves unrelated to thermal effects. An entire chapter is dedicated to the non-thermal microwave effects [37].

In general, organic syntheses are performed in oil bath as heat source. The main difficulty with conventional heating is the slow speed of heating. The energy heat is first transmitted to the oil bath, then to the surface of the reaction vessel and finally to the reaction medium. Conventional heating is highly demanding in energy and time. In contrast, microwave irradiation results in a powerful internal heating due to the dielectric heating of polar molecules. The high efficiency conversion of electromagnetic energy into heat energy results in extremely fast heating rate, not achievable with conventional heating. Formation of byproducts is reduced due to rapid heating of required temperature. Another benefit of modern professional microwave irradiation is the excellent ability to control temperature and pressure parameters to improve reproducibility.

Microwave instrumentations for synthesis are monomode or multimode. Multimode devices are mainly used in laboratories. Electromagnetic waves are reflected from cavity walls and interact with cavity loads. In multimode microwaves, the vessel is heated from multiple electromagnetic waves. In order to increase the amount of vessels simultaneously irradiated, a multimode cavity is required and is considered as parallel synthesis. Monomode microwaves can be considered as a second generation of microwave reactors. Only one mode is present in monomode reactor, which means a focused electromagnetic wave irradiates a precise-designed vessel settled at a fixed distance, producing a standing wave [36]. The industrial advantage of a monomode reactor is that high throughput can be achieved with sequential processing but this technology remains yet difficult to scale-up and is still related to small-scale lab use.

The utilization of microwave reactors for the degradation of starch molecules has been investigated since the end of the 70s. A 10 % starch suspension irradiated in a multimode microwave sealed reactor for 20 min generated 80, 10 and 3 % of total sugars, reducing sugars and glucose respectively [38]. In this process, the solution reached a temperature of 175 °C and a pressure of 9 bar, while the pH dropped from neutral to 3.9. Whereas a 10 % wheat starch suspension in hydrochloric acid solution ( $\text{pH } 1.85\text{--}0.014 \text{ mol L}^{-1}$ ) required 5 min of irradiation

at identical temperature and pressure to reach 95, 89 and 84 % of total sugars, reducing sugars and glucose respectively [39]. The authors observed that high temperature and pressure generated a dark brown charred residue with a characteristic caramel odor, coming probably for the caramelisation of glucose. A 10 % starch suspension diluted in 0.5 mol L<sup>-1</sup> hydrochloric acid required 5 min microwave irradiation to produce glucose, where 60 min was necessary under conventional heating for the same concentration of glucose [40]. Warrand and Janssen [41] performed a microwave irradiation of pure amylose in acidic condition (0.45 mol L<sup>-1</sup> of HCl); 97 % of malto-oligosaccharides with two degree of polymerization, such as maltose, was generated within 10 min of pretreatment followed by 10 min of irradiation. Microwave irradiation appears to enhance starch degradation into reducing sugars and glucose with the presence of acid.

### 11.4.2 Effect of Microwave Irradiation on Starch

Our experiments were performed with a monomode synthesis microwave Prolabo Synthwave S402 providing electric power of 0.6 kW (lower than the 1.2 kW electrical power provided by common magnetic hot plate). Temperature was measured at the bottom of the vessel with infrared sensor calibrated by an optic-fiber probe. A professional multimode synthesis microwave (Microsynth, Milestone) was also employed for the degradation of potato starch and potato peel (waste). Irradiations of potato starch and potato peel 3-wt% suspensions were performed at 60 °C in sulfuric acid (3 mol L<sup>-1</sup>) for 60 min with the monomode and 120 min for the multimode microwave (Fig. 11.7). Time had to be reduced with the monomode

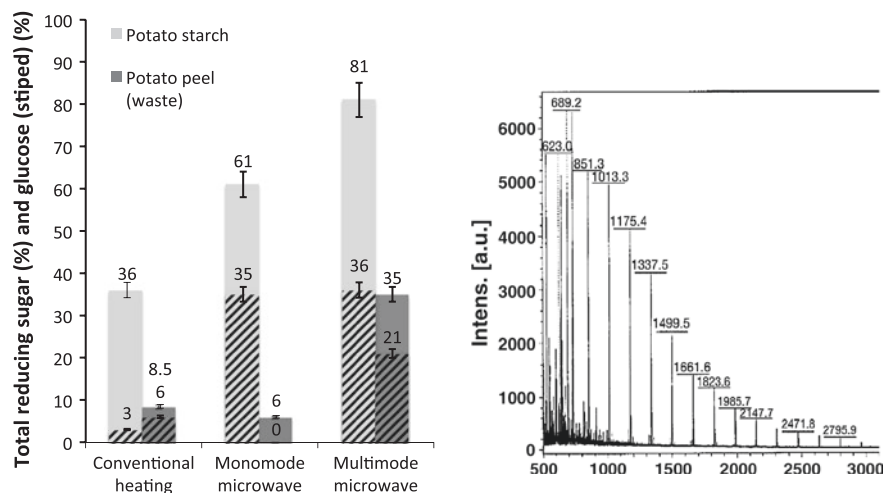


**Fig. 11.7** Total reducing sugar and glucose (*striped*) yields of the experiments performed under conventional heating, and various microwave irradiations (on the *left* side); MALDI-TOF analyses of sugars (counter ion H<sup>+</sup>) after monomode microwave irradiation (1 h process) of potato starch (on the *right* side); conditions: sulphuric acid 3 mol L<sup>-1</sup>, 60 °C

microwave due to the formation of a dark residue after 60 min. This can be explained by the fact that in monomode ovens, as aforementioned, microwave waves are focused and irradiate a precise-designed vessel leading to an enhanced field density, which is particularly high for small cavities such as for Synthrowave S402.

The irradiation of potato starch suspension in the monomode microwave instrument produced 61 % of reducing sugars, including almost two-third of glucose (Fig. 11.7) [3]. The yield of reducing sugars dropped to 6 % (no glucose measured) with the starch-based industrial waste, due to the poor accessibility of the starch granules trapped into biomass debris confirmed by the SEM images (Fig. 11.2j) and also in reason of an inefficient stirring mode even if present with the use of a glass-rod stirrer. A change of structure was solely noticed after microwave irradiation of potato starch leading to swelling lines on the granule surfaces, although some granules merged together without being damaged. This change of structure has been observed previously in literature [42]. Microwave irradiation entirely disrupted the structure of the starch-based waste (Fig. 11.2k), and no granules were observed because debris were trapped in the gel structure. A MALDI-TOF was performed on potato starch after microwave irradiation to determine the degree of polymerization of the oligosaccharides obtained. A similar distribution with conventional heating of three to six degrees of polymerization was revealed with the MALDI-TOF analysis (Fig. 11.6a) [3]. No noticeable selectivity was observed compared to ultrasonic irradiation aforementioned. The irradiation of potato starch and potato peel under multimode microwave instrument generated high yield of reducing sugars of 81 and 35 %, respectively (Fig. 11.7). Almost half of the reducing sugars were glucose from potato starch and two-third from potato peel.

Ultrasonic and microwave irradiations have their advantages (induce shockwaves and efficient stirring for low frequency ultrasound, generate highly reactive radicals for higher frequency ultrasound or shorten overall process time, increase selectivity for microwave) and also some drawbacks (no stirring effect at high frequency ultrasound and microwave) on potato starch and potato peel. Indeed, the real potato waste is a very complex matrix containing biomass debris. The limitations of one technology can be overcome by the advantages of the other one. Therefore, we decided to add efficient stirring to thermal degradation (combined device including low frequency ultrasound and multimode microwave). According to the great yield of reducing sugars obtained from potato starch under high frequency ultrasound, but poor with potato peel, due to lack of stirring, we decided to combine low and high frequencies to get simultaneously shockwaves and radical formation.

## 11.5 Combined Irradiation-Assisted Hydrolysis of Starch-Based Waste

The main objective of combining technologies is to generate a synergism phenomenon. Two different devices were employed; the first one combine multimode syntheses microwave with an ultrasonic Pyrex probe and the second one combine low and high ultrasonic frequencies. Devices employed are represented in Fig. 11.8.

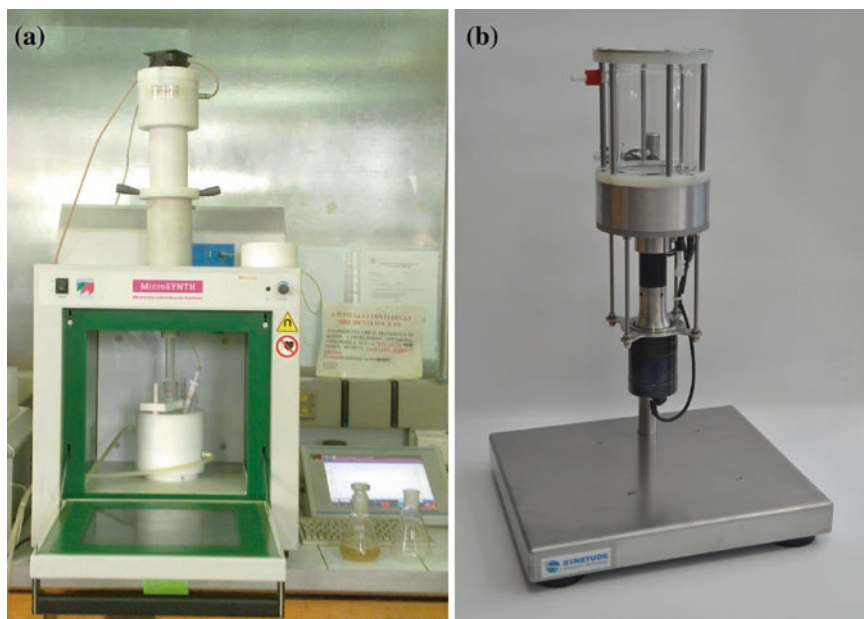


**Fig. 11.8** Combined devices: milestone microwave with low frequency ultrasonic Pyrex probe (a) and ultrasonic low and high frequency in co-axial reactor developed by Syntetude (b)

### ***11.5.1 Combined Technologies: Microwave and Low Frequency Ultrasonic Irradiations***

The combination of microwave with ultrasonic irradiations enhances syntheses by increasing mass transfer, catalysts activity and reducing reaction time. The main principle of this combination of technologies is that microwaves induce dielectric and selective heating, while low frequency ultrasonic waves generate shockwaves resulting in surface erosion. Indeed, microwave irradiation is a rapid heating method of polar components that enhances selectivity, reaction rates and decreases reaction time and side products. Ultrasonic irradiation at low frequencies of aqueous medium generates cavitation bubbles that collapse under high temperature and pressure, inducing shockwaves in the medium, generating molecule fragmentations. Energy saving is another benefit of the combination of these technologies. Microwave heating reduces energy consumption by bringing the required temperature in few seconds and ultrasonic irradiation decreases reaction time and increases the yield. It is noteworthy that molecule vibration frequencies range from  $10^{12}$  to  $10^{14}$  Hz, unable to interfere with ultrasonic frequencies ( $10^3$ – $10^6$  Hz). Metallic probe is the main hurdle engendered in this combination. Indeed, metallic or conductive objects interfere with microwaves and create electric arc. Although metallic probes are highly efficient delivering high acoustic power, it appears inconceivable to introduce this type of probe in

a microwave cavity. Thus, appropriate materials microwave-inert and enable to transmit ultrasonic waves replaced the metallic probe inside the reactor, such as Polyether ether ketone (PEEK), Polytetrafluoroethylene (PTFE) and Pyrex.

This dual technology has been utilized in the field of nanotechnologies for nanowire syntheses [43], in organic syntheses [44–47], extraction technologies [48, 49], anaerobic digestion [50] and also biodiesel synthesis [51]. Maeda and Amemiya [52] are known as the inventors of this dual technology, however Chemat has widely developed it for the urea pyrolysis, propanol [53], digestion and dissolution of biological and chemical products [54] and also Kjeldahl determination in digestion process [55]. The type of reactors, synthesis and catalysis applications of this combined technology was discussed in a short review [56].

Two distinctive features are emerged from the various publications on combined devices: simultaneous irradiation and sequential irradiation. In simultaneous irradiation, microwaves and ultrasonic waves are irradiating the reaction medium at the same time. Several reactor designs were described in literature. The first device described is a cup-horn ultrasonic reactor underneath a digestive microwave in order to utilize a metallic probe for its efficiency [53–55]. A coaxial microwave emitter added to a glassware reactor with an ultrasonic metallic probe was recently developed [57]. With these designs, metallic probes are not placed inside the microwave cavity and therefore no interferences occur. Another kind of reactor can be designed for simultaneous irradiation. Metallic probes could not be used in microwave reactors, microwave-inert material can replace them, as aforementioned. An ultrasonic probe featuring a Pyrex horn with a tip diameter of 17 mm and a frequency of 20.1 kHz introduced in a professional multimode microwave synthesis (Microsynth, Milestone) was utilized for several types of syntheses [46, 58, 59] and also starch-based waste depolymerization [4]. The acoustic power of 17 W for an electric power of 40 W was reached with the ultrasonic Pyrex probe, indicating an energy efficiency of 42.5 %. Acoustic power delivered is quite low compared to metallic horn (86 W with an ultrasonic probe [3]). The device described is on Fig. 11.8a. The second type of design referred to as sequential irradiation. In this case, ultrasonic and microwave device are used alternatively [51, 60], and are often placed in serial.

### ***11.5.2 Multimode Microwave Combined with an Ultrasonic Pyrex Tip***

For our research, potato starch and potato peel (waste) were irradiated simultaneously with microwave and ultrasonic Pyrex probe in the reactor previously described (Fig. 11.8a). In order to compare the results, the raw materials were simply irradiated with the ultrasonic Pyrex probe or only with the microwaves, under identical conditions. A microscopic imaging analysis performed on before and after hydrolyses revealed granule disruptions (Fig. 11.2). Potato starch is a simple matrix containing essentially starch trapped in granules (Fig. 11.2a),

which is considered as a reference. It is used in comparison with potato peel, containing granules entrapped in biomass debris (Fig. 11.2b). The simple ultrasonic irradiation eroded the surface of potato starch (Fig. 11.2c), forming pits and holes on the granule surface. However, irradiation intensity was not enough to disrupt the granule and release starch molecules. This type of surface alteration has been widely observed in literature [31, 61]. Ultrasonic irradiation of potato peel disrupted the biomass debris and released a part of the starch granules, which underwent the irradiation (Fig. 11.2d). Granule similarities are observed with ultrasonic irradiation of potato starch. Once again, sonication intensity might not be strong enough. Some of the granules seemed to have merged without any disruptions (Fig. 11.2j). This phenomenon has been previously observed in the literature of a conventional thermal reaction of potato starch with linoleic acid [62]. A total change of structure was observed with the microwave irradiation of potato peel, starch granules lost their entire granularity, previously observed in literature [42]. Combined irradiation of potato starch generated a dark oil residue probably caused by a complicated control of temperature and too high power, and no solid could be analyzed. However, liquid was extracted from the residue and 79 % of reducing sugars were measured (Fig. 11.9). Finally, combined irradiation of potato peel disrupted the massive starch granules, but the smallest revealed intact (Fig. 11.2g). Some granules underwent the initialization step of gelatinization, with a ‘collapse’ of the granule. Ultrasonic irradiation released the granules entrapped in biomass debris, while microwave energy disrupted water molecules present in the crystalline regions. These imaging results were confirmed with a total reducing sugar analysis

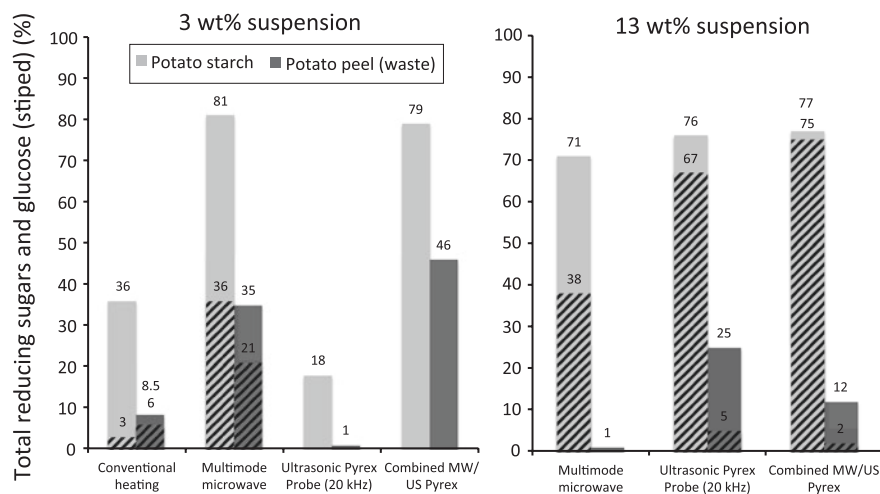


**Fig. 11.9** Total reducing sugars and glucose (*striped*) yields of the experiments performed under conventional heating, microwave, ultrasonic Pyrex probe, and combined; conditions: 2 h process, sulphuric acid  $3 \text{ mol L}^{-1}$ ,  $60 \text{ }^\circ\text{C}$ , 3 wt% suspension on the *left side* and 13 wt% suspension on the *right side*



of the liquid phase. Combined irradiation of a 3 wt% potato peel (waste) suspension for 120 min at 60 °C in 3 mol L<sup>-1</sup> of H<sub>2</sub>SO<sub>4</sub> generated 46 % of reducing sugars (Fig. 11.9) [4]. Owing to the great results obtained, the increase of weight percentage to 13-wt% appeared necessary; potato starch and potato peel (waste) were irradiated with the microwave/ultrasonic device under the identical conditions. Surprisingly, the 13-wt% of potato starch generated 77 % of reducing sugars, including 97 % of glucose (Fig. 11.9). Some specific effects may be observed with combined irradiation. The increase of weight percentage of potato peel generated only 12 % of reducing sugars with few percent of glucose. Ultrasonic wave was not enough intense to stir the suspension for hydrolysis. However, an increase of the weight percentage conducted to a surprising result of glucose selectivity from potato starch (Fig. 11.9).

Combined technology allows a rapid heat transfer of energy into the bulk in a short time with microwave irradiation and an increase of mass transfer due to low frequency ultrasonic irradiation. A depolymerization rate of 46 % of reducing sugars originated from the starch-based industrial waste was the highest yield obtained without any separation pretreatments. However, due to the TRS error analysis of ±5 %, no synergetic effects were observed.

### ***11.5.3 Dual Frequency Ultrasonic Irradiation***

#### **11.5.3.1 Benefits of the Combined Technology**

Efficient stirring are mainly produced at low frequency, while cavitation bubbles have enough time to accumulate energy. At higher frequency, radicals are formed due to more local and also more violent bubbles' implosion. The combination of these two phenomena might generate a highly concentrated area of mass and energy transfer.

The ultrasonic irradiation at 500 kHz of starch-based industrial waste—potato peel—generated only 13 % of reducing sugars, so far the greatest yield obtained with simple irradiation. Unfortunately, the individual 20 kHz metallic probe was not employed on potato peel, due to ineluctable corrosion in sulfuric acid. The protection of the 20 kHz tip of the dual reactor appeared essential to us for further experimentations. The screwable tip was made with high resistance to corrosion Inconel© alloy to resist to acidic attack during the process. Higher frequency irradiations are mainly dominated by local phenomenon of radicals' formation with poor stirring of the medium. Therefore, a combined irradiation reactor might improve radical reactions due to efficient stirring. Moreover, the investigation of dextran degradation under low and higher ultrasonic frequencies indicated that low molecular weight compounds were more degraded with high frequencies irradiation due to radicals' formation, whereas low frequencies degraded long chain polymers due to shockwaves [25].



### 11.5.3.2 Notable Previous Dual Frequency Ultrasonic Reactors

Multi-frequencies ultrasonic irradiation reactors have been developed for degradation [63, 64], sonoluminescence [65, 66], ozonation [67] or even hydrogen peroxide production [66]. Design of the device and frequencies are essential for specific irradiations. Low frequencies simultaneous irradiation [63, 64, 67, 68] as well as combination of low and high frequencies [64, 69–71] have been notably developed in opposite [63, 64] and orthogonal [67, 70, 71] arrangements. It is noteworthy that two different frequencies' emission can form a destructive or constructive interferences based on waves' superposition. Destructive interferences should reduce or even suppress the overall ultrasonic effect. Constructive interferences generate resultant waves displaying at various frequencies in harmonic and sub-harmonic range. These resultant waves possess higher amplitude than the accumulation of two waves due to their reverberations provided by several sources [63]. Several authors postulated that new cavitation nuclei are formed during combined irradiation, increasing the cavitation yield and stirring heterogeneous systems [67, 70].

### 11.5.3.3 Dual Frequency Ultrasonic Irradiation of Starch-Based Potato Peels

A dual frequency reactor irradiated in a coaxial and same direction has never been reported in the literature. Therefore, our prototype allows irradiations in the same direction in order to have waves in phase and avoid destructive interferences. A double-jacket cylindrical glassware reactor with a capacity of 1 L is represented in Fig. 11.8b. This ultrasonic device employs two different ranges of frequencies simultaneously. Thus, a 19 mm ultrasonic probe of 20 kHz was installed underneath the reactor to obtain a cup-horn system (Fig. 11.10). The thin layer of Teflon can be identified in the center of the Fig. 11.10a, b. At 75 % amplitude, the ultrasonic probe delivered a power density of  $39.6 \text{ W cm}^{-2}$ . The bottom of the cavity is made of polypropylene, and three piezoceramic transducers at 500 kHz were equilaterally inserted from below protected with Pyrex to avoid acidic attack.

The reactor was designed to concentrate energy transfer in a locate area. Indeed, the piezoceramic transducers are oriented in phase for constructive interferences to obtain a highly reactive zone of radicals' production. Underneath, an ultrasonic probe generates an efficient stirring due to a geyser in the identical zone. An increase of 10–15 °C in the geyser's core was measured with a thermocouple. A hexagonal pattern in a shape of honeycomb appeared on the interface liquid/air during the irradiation of the three piezoceramic transducers (Fig. 11.10b). Thus, this dual irradiation generates chemical and mechanical effects in an extremely reactive zone. This approach differs from the orthogonal or opposite irradiation arrangement observed in literature [72].

Potato starch and potato peel (waste) suspensions were irradiated with the dual ultrasonic device and compared with previous results (Table 11.2). The

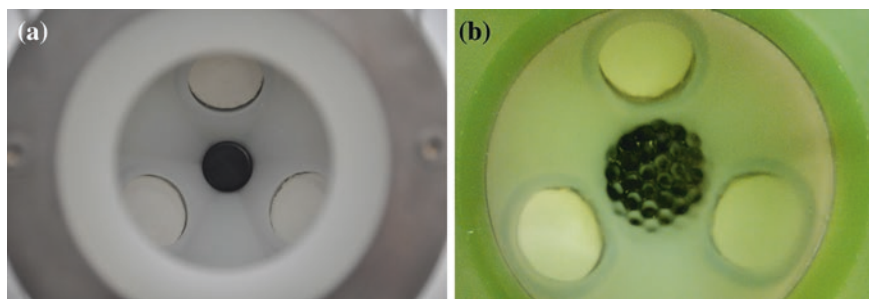


**Fig. 11.10** View from above the reactor, containing three piezoceramic transducers tuned at 500 kHz each and the tip of the 20 kHz ultrasonic probe coated with teflon (a); formation of the hexagonal pattern on the surface during the irradiation with the three transducers (b)

**Table 11.2** Yields of total reducing sugars (TRS) of potato starch and potato peel (waste), irradiated at various frequencies (experiments were performed in triplicate)

Experiment <sup>a</sup>	Device employed	TRS (%) potato starch	TRS (%) potato peels	Power density <sup>b</sup> (W cm <sup>-2</sup> )
1	Conventional heating <sup>c</sup> (reference)	36	9	n.a. <sup>d</sup>
2	20 kHz pyrex <sup>®</sup> probe	18	1	7.5
3	24 kHz bath (indirect mode)	70	6	n.a. <sup>e</sup>
4	Piezoceramic 500 kHz reactor	80	35	15.9
5	Dual frequency reactor	0 <sup>f</sup>	48	87.3 <sup>g</sup>

<sup>a</sup>Experiments performed for 2 h, at 60 ± 3 °C, 3-wt% dry matter in sulfuric acid 3 mol L<sup>-1</sup>—the volume of the reaction were 50 mL except for the dual frequency, which was 300 mL

<sup>b</sup>Acoustic power was measured by calorimetry according to the standardization performed by Kimura et al. [30] and the power density is expressed in watts per unit area of the emitting surface (W cm<sup>-2</sup>)

<sup>c</sup>Oil bath at 65 °C to reach 60 °C in the reactor

<sup>d</sup>None applicable

<sup>e</sup>None applicable—the volume of the ultrasonic bath rendered the accuracy of the measurement inappropriate

<sup>f</sup>Reaction performed at 37 ± 4 °C due to gelatinization issues

<sup>g</sup>Acoustic power density provided by the 20 kHz ultrasonic was 39.6 W cm<sup>-2</sup> while the three piezoceramic transducers provided 3 × 15.9 W cm<sup>-2</sup>

first experiment performed on potato starch at 60 °C in sulfuric acid 3 mol L<sup>-1</sup> produced a thick gel within few minutes. High intensity (87.3 W cm<sup>-2</sup>) occurred in the suspension, and might have produced local hot spot with harsh mixing. In order to avoid any gelatinization process, temperature was decreased to 37 ± 4 °C, and no reducing sugars were measured. This result was confirmed

with FESEM images performed on the solid content, granules surface were poorly attacked and only few granules were disrupted compared to untreated sample (Figs. 11.2a and 11.4h). Temperature appeared to be a significant parameter in potato starch depolymerization. The dual irradiation of potato peel (waste) produced a promising result of 48 % of reducing sugars within 2 h (Table 11.2). In comparison with a previous research in the literature [19], 86 % of dextrose equivalent was obtained within 60 min hydrolysis of potato tuber mash under harsh conditions of boiling sulfuric acid  $1 \text{ mol L}^{-1}$ . Indeed, boiling sulfuric acid generates hazardous vapors and products. FESEM images of the remaining solid displayed an entire gelatinized surface compared to the untreated potato peel (Fig. 11.2b, i). Starch granules were trapped in the biomass debris before irradiation, and no granule were observed after the process, ensuring a release of starch molecules into the medium. A geyser could be observed in the center of the reactor confirming the efficient mixing provided by the 20 kHz probe. Synergetic effects were observed in dual (low and higher frequencies) ultrasonic irradiation with a device in opposition arrangement [64]. A 700 kHz ultrasonic reactor enhanced with 20 kHz steady field ultrasonic probe produced new cavitation bubbles due to the low frequency field [69]. High ultrasonic frequencies reach a cavitation threshold that was reduced while the amount of cavitation bubbles increased in the rarefaction cycle thanks to the low frequency field [69, 70].

This original dual frequency irradiation possesses a large potential for simultaneous irradiation at various frequencies for efficient stirring and radicals formation.

A continuous system might be more appropriate for an industrial point of view. Currently, a continuous low frequency apparatus so-called Sonitube from Synetude is under investigation (Fig. 11.11). This continuous mode ultrasonic device can allow flow up to a few hundred liters per hour with low electric

**Fig. 11.11** Continuous flow ultrasonic device Sonitube from Synetude (low frequency ultrasonic irradiation)



consumption (1.5 kW) compared to batch-type ultrasonic probes with a volume of 50 mL. However, some coating modifications have to be performed on the apparatus to prevent corrosion.

## 11.6 Conclusions and Future Outlook

The major goal of this chapter was to demonstrate the potential of a starch-based industrial waste and its ability to be converted into platform molecules employing non-conventional technologies. Single ultrasonic and microwave irradiations determined the potential of potato peel with the production of reducing sugars. Several selectivities resulted from these single irradiations; three and four glycosidic units selectivity was observed with ultrasonic irradiation and glucose selectivity was revealed under microwave irradiation. Simultaneous irradiations combining ultrasound (20 kHz) and microwave or dual ultrasonic frequencies (20/500 kHz) of potato peel entrapped granules from biomass debris and generated up to 50 % of reducing sugars without preliminary separation process. Glucose selectivity was also revealed with combined ultrasonic and microwave irradiation of potato starch. The results obtained with the dual frequency reactor proved its potential and an eventual scaling up might be considered, even a continuous flow more appropriate to an industrial scale.

## References

1. Serrano-Ruiz JC, Perez JMC, Francavilla M, Menendez C, Garcia AB, Reyes AAR, Luque R, Garcia-Suarez EJ (2012) Efficient microwave-assisted production of furfural from C5 sugars in aqueous media catalysed by Brønsted acidic ionic liquids. *Catal Sci Technol* 2:1828–1832
2. Hernoux-Villière A (2013) Catalytic depolymerisation of starch-based industrial waste: use of non-conventional activation methods and novel reaction media. Thesis, University of Oulu, Université de Savoie
3. Hernoux A, Lévêque J-M, Lassi U, Molina-Boisseau S, Marais M-F (2013) Conversion of a non-water soluble potato starch waste into reducing sugars under non-conventional technologies. *Carbohydr Polym* 92:2065–2074
4. Hernoux-Villière A, Lassi U, Hu T, Paquet A, Rinaldi L, Cravotto G, Molina-Boisseau S, Marais M-F, Lévêque J-M (2013) Simultaneous microwave/ultrasound-assisted hydrolysis of starch-based industrial waste into reducing sugars. *ACS Sustain Chem Eng* 1:995–1002
5. Torres MDÁ, Parreño WC (2009) Thermal processing and quality optimization. In: Singh J, Kaur L (eds) *Advances in potato chemistry and technology*. Academic Press, San Diego, pp 163–219
6. BeMiller JN, Whistler RL (2009) *Starch—chemistry and technology*, 3rd edn. Academic Press, San Diego
7. Jane J (2009) Structural features of starch granules II. In: BeMiller J, Whistler R (eds) *Starch*, 3rd edn. Academic Press, San Diego, pp 193–236
8. Buléon A, Colonna P, Planchot V, Ball S (1998) Starch granules: structure and biosynthesis. *Int J Biol Macromol* 23:85–112

9. Liu Q, Donner E, Tarn R, Singh J, Chung H-J (2009) Advanced analytical techniques to evaluate the quality of potato and potato starch. In: Singh J, Kaur L (eds) *Advances in potato chemistry and technology*. Academic Press, San Diego, pp 221–248
10. Biliaderis CG (2009) Structural transitions and related physical properties of starch. In: BeMiller J, Whistler R (eds) *Starch*, 3rd edn. Academic Press, San Diego, pp 293–372
11. Jenkins PJ, Donald AM (1998) Gelatinisation of starch: a combined SAXS/WAXS/DSC and SANS study. *Carbohydr Res* 308:133–147
12. Grommers HE, van der Krogt DA (2009) Potato starch: production, modifications and uses. In: BeMiller J, Whistler R (eds) *Starch*, 3rd edn. Academic Press, San Diego, pp 511–539
13. Singh J, Kaur L, McCarthy OJ (2009) Potato starch and its modification. In: Singh J, Kaur L (eds) *Advances in potato chemistry and technology*. Academic Press, San Diego, pp 273–318
14. Morehouse AL, Malzahn RC, Day JT (1972) Hydrolysis of starch. US patent 3663369 A
15. Fontana JD, Mitchell DA, Molina OE, Gaitan A, Bonfim TMB, Adelman J, Grzybowski A, Passos M (2008) Starch depolymerization with diluted phosphoric acid and application of the hydrolysate in Astaxanthin fermentation. *Food Technol Biotechnol* 46:305–310
16. Lenihan P, Orozco A, O'Neill E, Ahmad MNM, Rooney DW, Walker GM (2010) Dilute acid hydrolysis of lignocellulosic biomass. *Chem Eng J* 156:395–403
17. Patil DR, Fanta GF (1993) Graft copolymerization of starch with methyl acrylate: an examination of reaction variables. *J Appl Polym Sci* 47:1765–1772
18. Singh V, Ali SZ (2000) Acid degradation of starch. The effect of acid and starch type. *Carbohydr Polym* 41:191–195
19. Tasić MB, Konstantinović BV, Lazić ML, Veljković VB (2009) The acid hydrolysis of potato tuber mash in bioethanol production. *Biochem Eng J* 43:208–211
20. Miller GL (1959) Use of dinitrosalicylic acid reagent for determination of reducing sugar. *Anal Chem* 31:426–428
21. Sigma-Aldrich (2011) Glucose (GO) assay kit product code GAGO-20
22. Szalay A (1933) The destruction of highly polymerized molecules by ultrasonic waves. *Z Phys Chem A* 164:234–240
23. Choi JH, Kim SB (1994) Effect of ultrasound on sulfuric acid-catalysed hydrolysis of starch. *Korean J Chem Eng* 11:178–184
24. Lorimer JP, Mason TJ, Cuthbert TC, Brookfield EA (1995) Effect of ultrasound on the degradation of aqueous native dextran. *Ultrason Sonochem* 2:S55–S57
25. Portenlänger G, Heusinger H (1997) The influence of frequency on the mechanical and radical effects for the ultrasonic degradation of dextrans. *Ultrason Sonochem* 4:127–130
26. Czechowska-Biskup R, Rokita B, Lotfy S, Ulanski P, Rosiak JM (2005) Degradation of chitosan and starch by 360-kHz ultrasound. *Carbohydr Polym* 60:175–184
27. Koda S, Taguchi K, Futamura K (2011) Effects of frequency and a radical scavenger on ultrasonic degradation of water-soluble polymers. *Ultrason Sonochem* 18:276–281
28. Wang Y-J, Truong V-D, Wang L (2003) Structures and rheological properties of corn starch as affected by acid hydrolysis. *Carbohydr Polym* 52:327–333
29. Mason TJ, Cintas P (2002) Sonochemistry. In: Clark JH, Macquarrie D (eds) *Handbook of green chemistry and technology*. Blackwell Science Ltd, Oxford, pp 372–396
30. Kimura T, Sakamoto T, Leveque J-M, Sohmiya H, Fujita M, Ikeda S, Ando T (1996) Standardization of ultrasonic power for sonochemical reaction. *Ultrason Sonochem* 3:S157–S161
31. Huang Q, Li L, Fu X (2007) Ultrasound effects on the structure and chemical reactivity of cornstarch granules. *Starch-Stärke* 59:371–378
32. Jamrak AR, Herceg Z, Subaric D, Babic J, Brncic M, Brncic SR, Bosiljkov T, Cvek D, Tripalo B, Gelo J (2010) Ultrasound effect on physical properties of corn starch. *Carbohydr Polym* 79:91–100
33. Metaxas AC, Meredith RJ (1983) Industrial microwave heating. IET
34. Stuerger D (2006) Microwave-material interactions and dielectric properties, key ingredients for mastery of chemical microwave processes. In: Loupy A (ed) *Microwaves in organic synthesis*. Wiley-VCH Verlag GmbH, London, pp 1–61

35. Loupy (2006) *Microwaves in organic synthesis—second, completely revised and enlarged edition*. Wiley-CH, London
36. Kappe CO, Dallinger D, Murphree SS (2008) *Practical microwave synthesis for organic chemists*. Wiley, London
37. Perreux L, Loupy A (2006) Nonthermal effects of microwaves in organic synthesis. In: Loupy A (ed) *Microwaves in organic synthesis*. Wiley-VCH Verlag GmbH, London, pp 134–218
38. Khan AR, Johnson JA, Robinson RJ (1979) Degradation of starch polymers by microwave energy. *Cereal Chem* 56:303–304
39. Khan AR, Robinson RJ, Johnson JA (1980) Starch hydrolysis by acid and microwave energy. *J Food Sci* 45:1449
40. Yu H-M, Chen S-T, Suree P, Nuansri R, Wang K-T (1996) Effect of microwave irradiation on acid-catalyzed hydrolysis of starch. *J Org Chem* 61:9608–9609
41. Warrand J, Janssen H-G (2007) Controlled production of oligosaccharides from amylose by acid-hydrolysis under microwave treatment: comparison with conventional heating. *Carbohydr Polym* 69:353–362
42. Palav T, Seetharaman K (2007) Impact of microwave heating on the physico-chemical properties of a starch–water model system. *Carbohydr Polym* 67:596–604
43. Shen X-F (2009) Combining microwave and ultrasound irradiation for rapid synthesis of nanowires: a case study on Pb(OH)Br. *J Chem Technol Biotechnol* 84:1811–1817
44. Peng Y, Song G (2002) Combined microwave and ultrasound assisted Williamson ether synthesis in the absence of phase-transfer catalysts. *Green Chem* 4:349–351
45. Cravotto G, Beggiato M, Penoni A, Palmisano G, Tollari S, Lévêque J-M, Bonrath W (2005) High-intensity ultrasound and microwave, alone or combined, promote Pd/C-catalyzed aryl–aryl couplings. *Tetrahedron Lett* 46:2267–2271
46. Cravotto G, Boffa L, Lévêque J, Estager J, Draye M, Bonrath W (2007) A speedy one-pot synthesis of second-generation ionic liquids under ultrasound and/or microwave irradiation. *Aust J Chem* 60:946–950
47. Čížová A, Sroková I, Sasínková V, Malovíková A, Ebringerová A (2008) Carboxymethyl starch octenylsuccinate: microwave- and ultrasound-assisted synthesis and properties. *Starch–Stärke* 60:389–397
48. Lianfu Z, Zelong L (2008) Optimization and comparison of ultrasound/microwave assisted extraction (UMAE) and ultrasonic assisted extraction (UAE) of lycopene from tomatoes. *Ultrason Sonochem* 15:731–737
49. Hu Y, Wang T, Mingxiao Wang, Han S, Wan P, Fan M (2008) Extraction of isoflavonoids from *Pueraria* by combining ultrasound with microwave vacuum. *Chem Eng Process Process Intensif* 47:2256–2261
50. Yeneneh AM, Chong S, Sen TK, Ang HM, Kayaalp A (2013) Effect of ultrasonic, microwave and combined microwave-ultrasonic pretreatment of municipal sludge on anaerobic digester performance. *Water Air Soil Pollut* 224:1–9
51. Gole VL, Gogate PR (2013) Intensification of synthesis of biodiesel from non-edible oil using sequential combination of microwave and ultrasound. *Fuel Process Technol* 106:62–69
52. Maeda M, Amemiya H (1995) Chemical effects under simultaneous irradiation by microwaves and ultrasound. *New J Chem* 19:1023–1028
53. Chemat F, Poux M, Di Martino JL, Berlan J (1996) An original microwave-ultrasound combined reactor suitable for organic synthesis: application to pyrolysis and esterification. *J Microw Power Electromagn Energy* 31:19–22
54. Lagha A, Chemat S, Bartels PV, Chemat F (1999) Microwave-ultrasound combined reactor suitable for atmospheric sample preparation procedure of biological and chemical products. *Analisis* 27:452–457
55. Chemat S, Lagha A, Amar H Ait, Chemat F (2004) Ultrasound assisted microwave digestion. *Ultrason Sonochem* 11:5–8
56. Cravotto G, Cintas P (2007) The combined use of microwaves and ultrasound: improved tools in process chemistry and organic synthesis. *Chem Eur J* 13:1902–1909

57. Ragaini V, Pirola C, Borrelli S, Ferrari C, Longo I (2012) Simultaneous ultrasound and microwave new reactor: detailed description and energetic considerations. *Ultrason Sonochem* 19:872–876
58. Domini C, Vidal L, Cravotto G, Canals A (2009) A simultaneous, direct microwave/ultrasound-assisted digestion procedure for the determination of total Kjeldahl nitrogen. *Ultrason Sonochem* 16:564–569
59. Cravotto G, Boffa L, Mantegna S, Perego P, Avogadro M, Cintas P (2008) Improved extraction of vegetable oils under high-intensity ultrasound and/or microwaves. *Ultrason Sonochem* 15:898–902
60. Wu Z-L, Ondruschka B, Cravotto G (2008) Degradation of phenol under combined irradiation of microwaves and ultrasound. *Environ Sci Technol* 42:8083–8087
61. Luo Z, Fu X, He X, Luo F, Gao Q, Yu S (2008) Effect of ultrasonic treatment on the physicochemical properties of maize starches differing in amylose content. *Starch–Stärke* 60:646–653
62. Kapusniak J, Siemion P (2007) Thermal reactions of starch with long-chain unsaturated fatty acids. Part 2. Linoleic acid. *J Food Eng* 78:323–332
63. Sivakumar M, Tataka PA, Pandit AB (2002) Kinetics of p-nitrophenol degradation: effect of reaction conditions and cavitation parameters for a multiple frequency system. *Chem Eng J* 85:327–338
64. Wang S, Huang B, Wang Y, Liao L (2006) Comparison of enhancement of pentachlorophenol sonolysis at 20 kHz by dual-frequency sonication. *Ultrason Sonochem* 13:506–510
65. Brotchie A, Ashokkumar M, Grieser F (2007) Effect of water-soluble solutes on sonoluminescence under dual-frequency sonication. *J Phys Chem C* 111:3066–3070
66. Lee M, Oh J (2011) Synergistic effect of hydrogen peroxide production and sonochemiluminescence under dual frequency ultrasound irradiation. *Ultrason Sonochem* 18:781–788
67. Zhao L, Ma J, Zhai X (2010) Enhanced mechanism of catalytic ozonation by ultrasound with orthogonal dual frequencies for the degradation of nitrobenzene in aqueous solution. *Ultrason Sonochem* 17:84–91
68. Tataka PA, Pandit AB (2002) Modelling and experimental investigation into cavity dynamics and cavitation yield: influence of dual frequency ultrasound sources. *Chem Eng Sci* 57:4987–4995
69. Iermetti G, Ciuti P, Dezhkunov NV, Reali M, Francescutto A, Johri GK (1997) Enhancement of high-frequency acoustic cavitation effects by a low-frequency stimulation. *Ultrason Sonochem* 4:263–268
70. Feng R, Zhao Y, Zhu C, Mason T (2002) Enhancement of ultrasonic cavitation yield by multi-frequency sonication. *Ultrason Sonochem* 9:231–236
71. Moholkar VS (2009) Mechanistic optimization of a dual frequency sonochemical reactor. *Chem Eng Sci* 64:5255–5267
72. Gogate PR, Tataka PA, Kanthale PM, Pandit AB (2002) Mapping of sonochemical reactors: review, analysis, and experimental verification. *AIChE J* 48:1542–1560



## Chapter 12

# Techno-economic Assessment Methodology for Ultrasonic Production of Biofuels

Miet Van Dael, Tom Kuppens, Sebastien Lizin and Steven Van Passel

**Abstract** Many market introductions fail due to economic reasons and not because of process performance. A techno-economic assessment (TEA) tool can help in making good choices during process development and raise the success rate of market introduction. In this chapter, the advantages of performing a TEA in early development stage of an innovative technology are highlighted. Seeing the current state of ultrasound technology, a TEA can help to steer further research into the most interesting pathway. The chapter, therefore, elaborates on the methodology that can be used to perform such a TEA and on the specific components which should be taken into account when applying a TEA on the ultrasonic production of biofuels and chemicals. Finally, a review is provided on the existing scientific literature concerning the economic performance of ultrasound technology.

**Keywords** Techno-economic assessment · Cost-benefit analysis · Mass balance · Energy balance · Biofuels · Ultrasound

---

M. Van Dael (✉) · T. Kuppens · S. Lizin · S. Van Passel  
Centre for Environmental Sciences, Hasselt University,  
Martelarenlaan 42, 3500 Hasselt, Belgium  
e-mail: miet.vandael@uhasselt.be; miet.vandael@vito.be

T. Kuppens  
e-mail: tom.kuppens@uhasselt.be

S. Lizin  
e-mail: sebastien.lizin@uhasselt.be

S. Van Passel  
e-mail: steven.vanpassel@uhasselt.be

M. Van Dael  
VITO, Boeretang 200, 2400 Mol, Belgium

## List of Abbreviations

BCR	Benefit cost ratio
Capex	Capital cost
CBA	Cost-benefit analysis
CEENE	Cumulative exergy extraction from the natural environment
CEPCI	Chemical engineering plant cost index
$CF_n$	Cash flow in year $n$
DPBP	Discounted payback period
FCI	Fixed capital investment
$i$	Discount rate
$I_0$	Initial investment in year 0
IRR	Internal rate of return
LCA	Life cycle analysis
LCC	Life cycle costing
LCSA	Life cycle sustainability assessment
M&S Index	Marshall and Swift equipment cost index
MFD	Mass flow diagram
NPV	Net present value
Opex	Operational cost
PBP	Payback period
PFD	Process flow diagram
SLCA	Social life cycle analysis
$T$	Life span
TCI	Total capital investment
TEA	Techno-economic assessment
$TS_{in}$	Total solids in
TSS	Total suspended solids

## 12.1 Introduction

When developing innovative technologies, it is important to have a clear idea on the economic performance of the technology or the process. Proving economic viability will increase private companies' interest. It is also important to know which parameters one should focus on during the development of the technology or the process. A parameter which only has a minor influence on the economic performance of the whole process may not be worth the effort of further improvement. A systematic economic analysis tool that integrates both technical and economic calculations is lacking. Often the economic calculations are added ex-post to get a first idea of the economic feasibility of developed concepts. However, detailed information on the parameters used is in many cases not provided. Moreover, an insight into the parameters that influence the economic

feasibility is most often not given. Models that do provide this kind of analysis are in many cases not integrated with technical calculations. This implies that it cannot be determined whether technical or economic parameters are most important for the economic feasibility. Researchers are driven to perform a technical optimization first, that is followed by an economic optimization. As a consequence, researchers cannot determine which technical parameters that they should focus on to enhance the chances of actual implementation. Therefore, the likely possibility exists that technical optimizations are executed on parameters that have a negligible influence on the economic feasibility. As such, R&D costs can become substantial. Moreover, by doing so, no evaluation is made yet of the sustainability of the process. However, in case of bioenergy in Europe this is important since subsidies are best provided to technologies that allow for producing energy products that may be taken into account for attaining the 20-20-20 EU targets. Therefore, the use of (extended) techno-economic assessment (TEA) tools can help in solving this problem.

A techno-economic assessment, also called techno-economic evaluation or techno-economic analysis, is a rather new term which that is being used frequently since 2010. A literature search was performed on EBSCOHOST to examine how many scientific papers mention ‘techno-economic assessment’, ‘techno-economic analysis’ or ‘techno-economic evaluation’ in the title since 1995. The results of this search are provided in Fig. 12.1. The number of papers that mention one of the three terms in the text is almost double the number of papers which mention the term in the title as well.

If the same search is repeated on Google Scholar, the number of hits is significantly higher (Table 12.1). This can be explained by the fact that Google Scholar has a wider searching scope than EBSCOHOST. However, the number of hits is still rather small in comparison to papers that only use ‘economic analysis’ or ‘technical analysis’. If a search is performed using Google Scholar on papers that mention ‘economic analysis’ in the text 96,300 hits are found in 2013 only, whereas 5,170 hits can be found for 2013 when searching for papers mentioning ‘technical analysis’ in the text. Furthermore, it is found that almost half the papers that mention TEA or one of the other synonyms can be linked to biomass. This is because biomass processes lend themselves perfectly for this kind of analysis

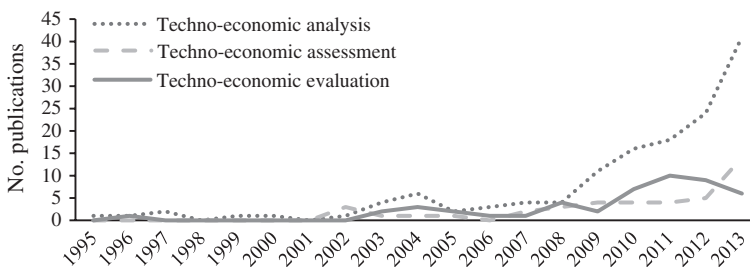


**Fig. 12.1** Number of papers mentioning TEA in title (EBSCOHOST, date of search 2014)

**Table 12.1** Number of papers mentioning TEA in text (google scholar, date of search 2014)

Keyword search/year	1995	2000	2005	2010	2013
Techno-economic analysis	26	84	165	612	1,120
Techno-economic assessment	9	39	58	176	396
Techno-economic evaluation	43	50	147	389	581
Techno-economic analysis AND (biofuel OR biomass)	6	20	28	212	605
Techno-economic assessment AND (biofuel OR biomass)	4	18	27	113	210
Techno-economic evaluation AND (biofuel OR biomass)	2	8	37	179	361

in which technical and economic calculations are combined. The number of papers that mention ‘techno-economic assessment’, ‘techno-economic analysis’ or ‘techno-economic evaluation’ combined with ‘biomass’ or ‘biofuel’ in the text, is represented in Table 12.1.

Although the use of techno-economic assessments is significantly increasing, no clear accepted definition exists of what constitutes a TEA. However, some efforts have been made to provide a definition of the TEA methodology. Kantor et al. [1] describe TEA as an analysis that integrates investment analysis with a performance analysis that takes into account some technical calculations. Smura et al. (2008) provide the following definition: “Techno-economic modeling methods are typically used to evaluate the economic feasibility of new technologies and services. Techno-economic modeling combines forecasting, network design, and investment analysis methods, typically utilizing spreadsheet-based tool” [2]. The National Advance Biofuels Consortium of the United States describes the goal of TEA as follows: “TEA combines process modeling and engineering design with economic evaluation to qualitatively understand the impact that technology and research breakthroughs have on the financial viability of a conversion strategy” [3]. However, in this chapter, we will use the definition provided by Kuppens [4] in which a TEA is defined as ‘*The evaluation of the technic performance or potential and the economic feasibility of a new technology that aims to improve the social or environmental impact of a technology currently in practice, and which helps decision makers in directing research and development or investments*’. We have chosen this definition as we feel that it fits the goal of TEA for ultrasound technologies best.

According to Kuppens [4] a TEA has to answer three important questions: (1) How does the technology work? (2) Is the technology profitable? and (3) Is the technology desirable? However, strictly following the provided definition, a TEA consists of an integrated technological (i.e. mass and energy balance) and economic evaluation (i.e. investment analysis) only. Adding a sustainability analysis (i.e. answering the third question) can be seen as an extended form of a TEA. In short, TEA can help to optimize the development of a process and to determine the most important parameters. Consistently applying the methodology will enhance chances of success when introducing (innovative) processes on the market. For that reason, the development process will be divided in different steps or stages after which a go/no-go decision has to be taken. The TEA can help in

taking this decision and as such diminishes chances of missed opportunities or failed market introductions. Focus needs to be lying on the dynamics of a TEA and the integration of technical (e.g. mass and energy balance) and economic calculations. Too often both calculations are done separately which keeps researchers from identifying the technical parameters that have the highest impact on the economic performance. Although researchers may have a good idea of these parameters, when applying a dynamic TEA it can help to convince potential investors of the success of the technology, especially since TEA allows for risk analysis that is essential when dealing with innovative technologies.

Although the definition provided by Kuppens [4] can be used, clear methodological guidelines are still lacking. There are even no textbooks on TEA, unlike cost-benefit analysis (CBA). Furthermore, many scholars incorrectly call their analysis a techno-economic analysis whereas they perform a technical and an economic analysis separately [5, 6]. Still, from the number of articles it can be concluded that there is a large interest in TEAs. Moreover, the terminology is used in many different research areas, such as innovations in communication networks [7, 8], logistics [9], and on energy related topics [10]. However, the methodology is mainly used for the evaluation of new technologies designed for environmental purposes, e.g. recycling practices [11], CO<sub>2</sub> capture [12], renewable energy [13–16], biofuel production [17, 18], or fast pyrolysis [19]. Also in the field of ultrasound technology the term TEA has already been used [20].

Although, TEAs or economic evaluations have already been performed for ultrasound technology, many questions remain unanswered. To commercialize the technology, a more thorough evaluation is needed [21]. Sonication is a physico-chemical treatment process that provides energy in the form of sound waves [22]. It can be used to improve e.g. biomass pretreatment processes or chemical reactions under mild conditions such as the conversion of cellulose to fermentable sugars, and results in increased reaction efficiency and higher catalytic activity over thermochemical methods. Moreover, it accelerates the reaction rate or changes the kinetics [23]. Ultrasound are acoustic waves with a frequency between 10 kHz and 20 MHz [24, 25] that create micro-bubbles in a liquid, which, when they collapse, result in a physical and chemical effect [26, 27]. Depending on the frequency levels, ultrasound can be divided into different regions: (1) 20–100 kHz or conventional power ultrasound, (2) 100 kHz to 2 MHz or extended frequency range for sonochemistry, and (3) 2–10 MHz low power high frequency ultrasound [25]. The physical effect implies that micro-convection is created which results in extremely strong shear forces that are able to scatter liquids into tiny droplets or crush solid particles into fine powders and may result in emulsification or dispersion of fluids and particles. The chemical effect comes from a release of a huge amount of energy creating local hotspots able to destroy crystalline structures, melt or fuse solid particles, and create short-lived free reactive radicals from reactants or solvents [23]. From the review of Luo et al. [23] and Rehman et al. [21] it is clear that questions remain concerning the economic feasibility and market maturity. Therefore, it is important to know how to perform a proper TEA. For that reason, in this chapter we will first provide a clear explanation of what a TEA is and how

to perform a TEA in every step of the development process. Also, we will provide more details on how to apply the different steps specifically to the further development of ultrasound-enhanced production of biofuels or chemicals. A literature review is given on the economic performance of ultrasound technology.

## **12.2 General Methodology Description**

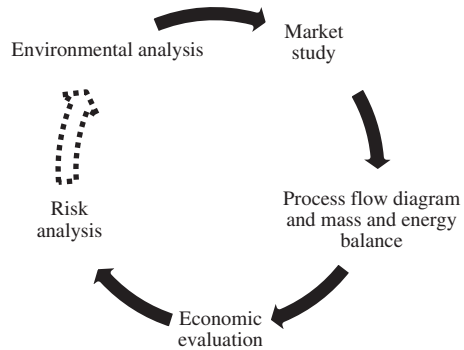
### ***12.2.1 General Framework of the Methodology***

A TEA can be applied to both a project that is still in its development-stage (ex-ante) and to one that has been already implemented and is either expanding or re-evaluating its conditions (ex-post). It is nevertheless advised to perform a TEA from the early development of innovative processes. In that case, a TEA can provide: (1) an initial assessment on the overall technical and operational barriers to overcome, (2) an optimal sizing for the project in terms of feedstock availability or plant capacity, (3) desirable product yields and waste management and (4) an indication of the (preliminary) economic feasibility or the main technical or financial factors that limit its feasibility. Furthermore, one should keep in mind that finding data for evaluating projects, costs a lot of time and money. Searching for this kind of information concerning parameters that do not have a large impact on the economic feasibility might be a waste of resources. Furthermore, a broader market study needs to be done to be sure that the process' end products do have market potential. Also, one should investigate whether all input streams are available on the market and under which conditions. Input streams might not be available in the amount needed, or they might be or become expensive when solutions are found for the stream, or they might be polluted requiring additional treatment (and costs) that need to be integrated. Often in development stages homogeneous systems are used for testing and for the resulting economic analysis. However, in reality such input streams are often unavailable, causing additional costs to be incurred. Alternatively, it might be that the research does not have sufficient potential.

### ***12.2.2 Phases in a TEA***

A TEA can be divided into four different phases. As information gathering is expensive, a TEA is performed in an iterative way with a go/no-go decision after every iteration. First, a market study is performed. Second, a preliminary process design is defined and translated into a simplified process flow diagram (PFD) and mass and energy balance. Third, this information is directly integrated into a dynamic CBA (i.e. economic evaluation). From this analysis, the profitability is identified. Fourth, a risk analysis is performed to identify the potential barriers. Optionally, an environmental analysis can be added as a fifth phase to produce an

**Fig. 12.2** Schematic overview of iterative (extended) techno-economic assessment methodology



extended TEA. Note that both technological, as well as economic barriers can be identified thanks to the direct integration. Based on the results of this cycle, risk reduction strategies can be formulated and steps can be repeated when the results sound promising. These four phases are also mentioned by Verbrugge et al. [28], Barbiroli [29] and Van Dael et al. [16]. A schematic overview of the TEA phases can be found in Fig. 12.2.

### 12.2.3 TEA Tool Overview

In the paper of Van Dael et al. [16] a translation of the different phases is made into a tool or model. A clear distinction has been made between the different methodological aspects of a TEA. The description of the TEA tool in this chapter is based on the work of Van Dael et al. [16].

The TEA model/tool is preferably excel-based as many innovative processes are not yet integrated into existing software packages. Moreover, using existing software packages often requires dedicated training. Furthermore, an advanced level of knowledge is needed to change the assumptions made within packages. Excel-based tools enhance user friendliness and transparency, as most scientists are familiar with working in Excel. Also, it allows the design a model that is very specific to the researcher's process and allows for an increasing level of detail throughout the different TEA iterations.

The Excel-based model consists of two data input sheets, one with data regarding the mass and energy balance and one with information concerning the economic parameters. Consequently, both the second and third phase are directly integrated in the model. The first phase (i.e. market study) is used to define the broader scope of the technology development and to gather data that will be used as input in the other phases. The fourth phase (i.e. risk analysis) can be performed on the integrated model in Excel. Especially for this last phase it is interesting to use input sheets since this allows the quick selection of the parameters that have to be varied in this analysis. Furthermore, the model contains one output sheet for



every concept that is evaluated. In other words, different alternative processes can be gathered in one model, which is interesting for comparison afterwards. The sheet that is provided for every alternative, consists of a process flow diagram (PFD) of the concept, the mass and energy balance calculations and a cost benefit analysis (CBA) with calculation of the most frequently used investment criteria, i.e. net present value (NPV), internal rate of return (IRR) and discounted payback period (DPBP) [30–34]. The investment criteria mentioned above will be explained in more detail in Sect. 12.2.2. An overview of the Excel-based model can be found in Fig. 12.3. In the first iteration, not all technical or economic details are taken into account as a detailed analysis takes too much time and effort that may result in missing the goal of the methodology. Therefore, in a first iteration, a model is made in which an overview is provided from the input streams, the main conversion parameters and the output products and waste streams. The process itself is more or less treated as a black box in which a certain conversion takes place. All parameters from the technical calculation are directly integrated with the economic part in which scale advantages are preferably taken into account when calculating NPV, IRR and DPBP. Furthermore, the model allows the user to alter the different input parameters and visualize the impact on both the mass and energy balance and financial viability of each concept. Finally, a summary sheet is included to allow the user to easily check the impact on the economic feasibility and compare different concepts, without consulting all the underlying details.

As the values used for the calculations are uncertain, a sensitivity analysis or risk analysis is performed. The prediction of the values is often based on literature

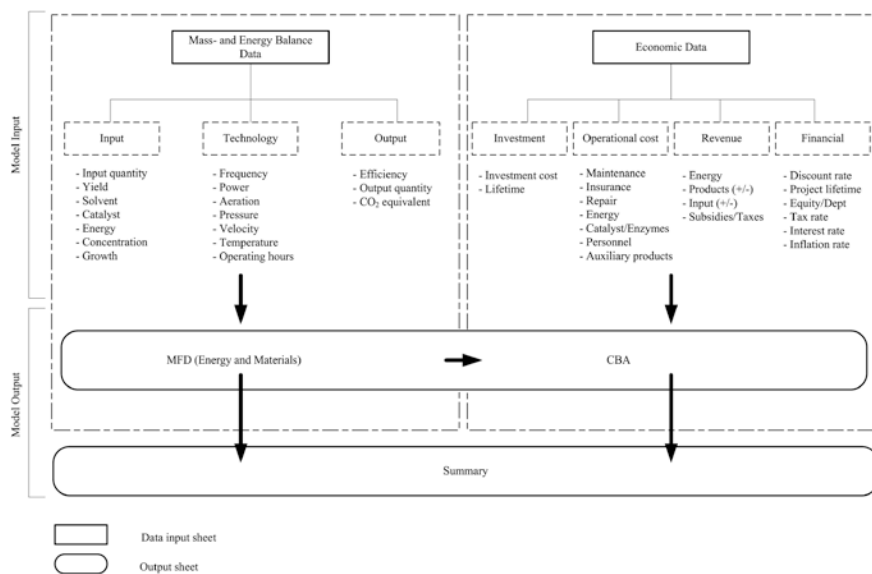


**Fig. 12.3** Parameters input for techno-economic assessment applied on the ultrasound technology (based on [16], copyright © 2013, Elsevier). *MFD* mass flow diagram; *CBA* cost benefit analysis

and checked with expert opinion. The values are therefore deterministic rather than stochastic. In the paper of Van Dael et al. [16] a Monte Carlo simulation (50,000 trials) is performed for each model, varying the variables (technical as well as economic) following a triangular distribution with a positive and negative change of maximum 10 %. The goal of this quick scan is to determine the parameters that have the highest impact on the variance of e.g. the NPV. The analysis searches for the parameters that should be investigated into more detail. For this reason, the chosen distribution and ranges can be justified. Based on the results, more analyses have to follow on those parameters with the highest impact by varying them over realistic ranges, as most of the times a range of values can be found in literature or by expert opinion. When only literature data or expert judgments and no large datasets or historical data are available, only the lowest value, the highest value and the most likely value of the input variables can be assessed with large certainty, whereas the distribution is unknown. The triangular distribution is an adequate solution when literature is insufficient for deriving probabilities [35]. It is also the most commonly used distribution for modeling expert opinion [36]. Results of these analyses provide some insight into the risk potential investors take. Based on the results of this first iteration, a decision can be made concerning the potential of this technology. In case the results are promising, a second iteration can follow with more detailed information on the critical success factors that were identified in the sensitivity analysis. However, when the results do not show the expected outcomes, it can either be decided to stop with the research or the results can help to refocus the research on the most critical parameters that have the highest influence on the economic feasibility.

Finally, it is clear that different phases within a TEA require multidisciplinary teams to execute the different phases of the analysis. However, too often the performers of the TEA are the technological developers of the process, who carry out the assessment without the help of economists. Only rarely one of the authors can be explicitly identified as a fellow worker of an economic department of a university, a research institution or a government agency. This might be a disadvantage and raises questions concerning the accuracy of the analysis. It is advisable to carry out the evaluation with a multidisciplinary team, which provides more insight since different members of the team will ask different questions, have divergent interests and as such help to attain a broad picture of the innovation process.

#### ***12.2.4 TEA and Ultrasound Technology***

The TEA approach described in the previous section can be of high added value in the future development of ultrasound-enhanced production of biofuels and chemicals. The amount of literature that can be found on the economic evaluation of ultrasound technology for the production of biofuels or chemicals is rather limited. Papers concerning the ultrasound technology that mention economic evaluation or TEA in

the title are almost non-existent. However, scientific research describing the use of ultrasound technology is available for more than 15 years. Still, commercialization seems to still be difficult. Therefore, a TEA can help in determining where scientists should put focus on, i.e. which are the applications with the highest potential for market uptake and which conditions have to be met. Furthermore, the methodology allows finding out to what extent the improvement of the critical success factors translates into economic feasibility. The critical success factors are already determined in the review of Luo et al. [23] and Rehman et al. [21]. However, it is not yet investigated whether improvements to the technical optimum will translate into economic feasibility, nor is it explored, which reactor design will be most optimal. It is not too late for ultrasound to enter the market seeing that Alvira et al. [37] indicate that no preferred pretreatment method is yet established. The critical success factors determined in these reviews can be interesting input for a TEA. From the reviews, it is clear that energy consumption should be reduced and that an optimization of the design and parameters should be searched for. In other words, the following parameters are indicated as the most likely ones for the current failure in market uptake:

- Energy intensity of active micro-bubbles:
  - Ultrasonic mode: continuous or pulse;
  - Frequency;
  - Power;
  - Processing temperature;
  - Solvent;
  - Aeration;
  - Design of reactor.
- Population of active micro-bubbles.

Based on the above overview, Fig. 12.3 provides an overview of the parameters that minimally need to be taken into account when performing a TEA for ultrasound processes. It is for example important that a TEA can provide more information on whether the efficacy of ultrasound as a pretreatment process can compensate for the extra costs that result from it. A TEA can indicate how the process parameters, that are taken into account, have to be optimized in order to come to the most economically viable design.

In the following section, more details are provided on how to perform a TEA for ultrasound processes.

### ***12.2.5 Detailed Explanation of TEA Phases***

When a researcher begins with the research, it is important to know why the research is started and why it is of interest to someone. Based on this information, a problem statement is formulated and the researcher tries to find a solution. However, knowing why the research is started is not sufficient. One also needs to

know who exactly might be interested in the results, who will use the end-products or who will be interested in the process technology itself, where do the products come from and which conditions have to be met. To obtain this kind of information, a market research is performed. If a researcher wants to commercialize the process or findings, this phase is crucial. An interesting tool to help asking the right questions and developing or improving business models, is the business model canvas<sup>1</sup> proposed by Alexander Osterwalder in 2008.

### ***12.2.6 Market Study***

The market study allows the researcher to identify the competitors and customers. It also provides information concerning the size of the market, the needs of the market, and the alternatives on the market. Furthermore, it will also provide information concerning the costs and revenues. Moreover, a market study contains a study of the legislation that is in place. Finally, a market research provides insight into market trends. However, the latter is more difficult to estimate when working with innovative technologies. A suitable proxy to determine the technological development state of ultrasound technology can be found in combining patent analysis with diffusion theory as shown in Ref. [38].

Some examples illustrating the importance of a market study are provided next. If your customers are for example situated in the pharmaceuticals or food market, conditions will be stricter than in e.g. water recycling. A good knowledge of the norms and legislation in this case is important. Another example is the size of your installation that has to be adjusted to the availability of input products (i.e. market supply) and market demand of end-products. It is of no use to make a large installation to reduce cost due to scale advantages, if this exceeds the demand for the products produced. A third and last example concerns customer preferences. If the researcher has an idea of what the customer values most, more money can be spent on the parameters that customers want to pay for. An interesting example of the latter is the study performed by Lizin et al. [39] in which the preferences of customers for attributes of organic photovoltaic solar cells are investigated using choice modelling. The study served as an input for technical researchers and indicated that efficiency and lifetime are most important for customers in their decision to buy consumer electronics.

When a market research is performed well, it provides a lot of information that will be of interest in the following phases of the TEA. Furthermore, the information can be used to convince investors, policy makers or customers as useful background information can help them to understand the potential of the product or process better.

---

<sup>1</sup> [http://www.businessmodelgeneration.com/downloads/business\\_model\\_canvas\\_poster.pdf](http://www.businessmodelgeneration.com/downloads/business_model_canvas_poster.pdf).

### ***12.2.7 Process Flow Diagram and Mass and Energy Balance***

This section discusses the process flow diagram (PFD) and energy balance.

In Sect. 12.2.3, we already mentioned that it is advisable to work in multi-disciplinary teams. This is an advantage as many different points of view can be taken into account. However, it is also important that everyone understands each other. Often economists use different words than people working in the laboratory. Especially for the technical processes, it is important that everyone is talking about the same idea and that everyone understands the big picture. This can be taken literally by making a PFD. The PFD provides a schematic overview of the main parts in the process and its inputs and outputs. In the first iteration it can even be a block scheme that only shows what goes in and what comes out of the process. Later on, more details can be added when moving through the different development phases. However, keep in mind that a PFD shows only major parts of the process and not details such as piping. Some examples of general PFD (i.e. first iteration) and more detailed ones are provided in the literature [16, 23].

The numbers shown in the PFD are the result of the mass and energy balance calculations. In the mass balance, how much mass that goes into the process is calculated, how much is divided over the different steps and how much comes out of the process are given. Important here is to keep in mind that there is no mass that can disappear. This means that one can easily check whether the calculations are right. Within the energy balance an overview is made of the energy that is used within the different parts of the process and the amount of energy that might be produced. When making the mass and energy balance calculations, one should try to make them dependent on each other as much as possible. In other words, the less fixed values that one needs to fill in when calculating your balances, the better. This is important for the fourth phase (i.e. the sensitivity analysis) in which you want to check what the influence is of a change in a technical parameter on the economic feasibility. One might want to check, for example, how an increase in the process efficiency by 2 % affects the economics. If this influence is known, then it is possible to estimate what the cost might be for increasing the efficiency further.

### ***12.2.8 Economic Evaluation***

To check whether a technology is worthy of investigation, the economic feasibility of the technology under investigation has to be analyzed. The economic analysis should give a clear picture of the capital and operational costs of the technology, and ideally also contains a calculation of the benefits. Sometimes, when the goal of the technology is limited to improving cost effectiveness (e.g. [14]) or the reduction of capital expenditure (sometimes labelled as “capex”) and operational

expenditure (sometimes labelled as “opex”), studying the costs suffices to answer the second question. A full economic picture, however, also requires estimates of the economic benefits of a new technology for the prediction the incoming and outgoing cash flows, which are then discounted to take into account the opportunity cost of money. Finally, a discounted cash flow analysis yields the NPV of cash flows as an indicator of the technology’s profitability. Furthermore, a distinction has to be made on the goal of the analysis one wants to perform. In case the goal is to check the economic feasibility of an innovative process, all costs and revenues of that process have to be taken into account. This also allows the comparison of the feasibility of different process configurations, e.g. the comparison of different enzymes. However, one might also be interested in checking whether an innovative technology is more interesting than a reference scenario. For example, one might be interested in whether sonication can supplement a conventional pretreatment process. In that case, only additional or avoided costs and revenues have to be taken into account. However, note that the latter is often more difficult to execute as also a clear picture of the costs and revenues of the reference scenario is needed.

To calculate a net present value (NPV) the total capital investment of the technology is needed. A description of the total capital investment and its different parts, are described in Kuppens [4]. “Capital investment is the total amount of money needed to supply the necessary plant and manufacturing facilities plus the amount of money required as working capital for operation of the facilities”. The total capital investment (TCI) of a technology thus comprises the fixed capital investment in the plant and equipment (fixed assets), as well as the working capital with which expenses can be paid before sales revenues become available (current assets). The fixed capital investment (FCI) includes both direct and indirect costs. Direct costs consist of the capital required for the purchase of construction items for the plant, i.e. property, all process equipment and materials. Indirect costs include construction services such as overhead, supervision and engineering expenses, legal expenses (e.g. for permits), contractor’s fees and contingencies (i.e. provisions for possible future events or problems) [40]. The fixed capital investment should include land costs. Working capital is required to cope with the irregular, non-coinciding time character of incoming cash from sales and outgoing cash for the payment of operational costs. It is the difference between current assets and current liabilities [41–43]. At the end of the project lifetime, the working capital and the land costs can be recovered. It is generally assumed that the amount in euros spent on working capital and land at the beginning of the project can be fully recovered at the end of the project lifetime [43]. However, land costs are often excluded because they are site specific. Although fully recoverable, the amount of working capital has an important negative influence on the NPV of the investment project due to the time cost of money and should not be neglected [42]. Though, it is not always clear whether and how much of the total capital investment other authors have dedicated to working capital.

### *Total capital investment estimation methods*

Central in a TEA is thus the determination of the total capital investment. It is not always straightforward to get the exact economic data needed for the analysis: one might even say that the scope of a TEA is limited only by the quality and availability of data for the project. Therefore, some methodologies are provided that can be used to estimate the total capital investment.

First, note that capital cost estimates can be classified according to the project detail or completeness of engineering which determines the amount of information available for estimation purposes and the expected accuracy of the capital cost estimation. Logically, the accuracy range can be narrowed by increasing the level of engineering detail [43]. During the first iterations, the level of detail is relatively small due to the availability of information. By moving across the development phases, the level of detail increases. Eventually offers might be asked from technology suppliers, however, this still implies accuracy ranges between 10 and 20 %. Note that in a research environment these are already very interesting ranges. Only when moving to real implementation, accuracy ranges will lower further. Various organisations, such as the Association of Cost Engineers in the United Kingdom and the Norwegian Project Management Association, have been classifying capital cost estimates into comparable categories. Here, the Cost Estimate Classification System developed by the Association for the Advancement of Cost Engineering (AACE International, i.e. the former American Association of Cost Engineering) is briefly presented, consisting of five classes of cost estimates, based on the degree of project definition. The classes are distinguished from another by five characteristics: degree of project definition (primary characteristic), end use of the estimate, estimating methodology, accuracy and effort required to prepare the estimate (secondary characteristics) [44, 45]. The five classes of cost estimates can be summarised as [43, 45]:

- *Class 5—Order of magnitude estimate:*  
based on very limited general information of project data and previous cost data with typical accuracy ranges of  $-20$  to  $-50$  % on the low side and  $+30$  to  $+100$  % on the high side.
- *Class 4—Study estimate:*  
based on knowledge of the major equipment; accuracy ranges between  $-15$  to  $-30$  % (low side) and  $+20$  to  $+30$  % (high side).
- *Class 3—Preliminary estimate:*  
prepared for budget authorisation which requires that most of the process data are defined and that at least some preliminary work has been done on engineering deliverables; accuracy ranges between  $-10$  to  $-20$  % and  $+10$  to  $+30$  %.
- *Class 2—Definitive estimate:*  
based on almost complete data but before full completion of engineering drawings and specifications; accuracy between  $-5$  to  $-15$  % and  $+5$  to  $+20$  %.
- *Class 1—Detailed estimate:*  
based on complete drawings and specifications; accuracy between  $-3$  to  $-10$  % and  $+3$  to  $+15$  %.



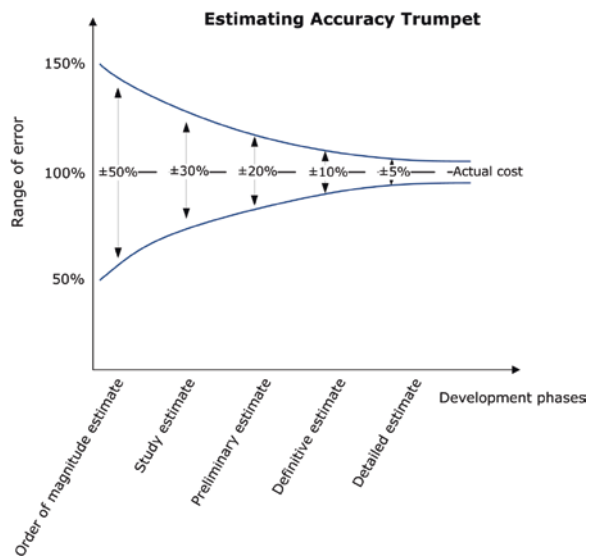
These classes can also be graphically represented by the estimating accuracy trumpet (see Fig. 12.4).

The choice for a capital cost estimation method depends on the adequacy of product and process definition, the disposable information, the desired level of accuracy and detail and time constraints [43, 44, 46]. A summary of the methods described by Peters et al. [43] and Dysert [44] is provided below.

For the case where a detailed item capital cost estimate is needed, a list of the specific equipment items, materials and personnel for construction and installation required by the process is necessary along with information about the size or capacity of the items. Equipment and material needs are determined by complete engineering drawings and specifications. In early stages of a process or product development, this information is often difficult to obtain or incomplete because some needs or specific requirements only become apparent later in the development process. Note that capital cost estimation methods which require less information are indispensable at early stages of process and product development [47].

The method called ‘percentage of delivered equipment cost’ is typically applied during the feasibility stage of a project. The first step is to estimate the cost of each piece of process equipment. All other costs are calculated as a percentage of the delivered equipment cost. This method has been introduced by Lang [48, 49] and sometimes the applied percentages are referred to as Lang factors. At the time of preliminary and study estimates, one might not have an exhaustive list of all equipment items, because some requirements become only visible at the moment of construction. Therefore, it is important to assume a cost percentage for auxiliary equipment that has not yet been identified [44]. Peters et al. [43] give a general overview of factors when one wants to calculate the cost of total direct plant cost if the delivered equipment cost is known.

**Fig. 12.4** Estimating accuracy trumpet



Another methodology is called ‘capacity factored estimates’ or ‘six-tenth rule’. It is a relatively quick method that is often applied for feasibility or order-of-magnitude estimates and can be used to estimate the cost of a whole processing unit or battery of units, but also for estimating the cost of individual equipment items. Williams was the first to mention the rule of six-tenths in 1947 in his article “Six-tenths Factor Aids in Approximating Costs” in the Chemical Engineering magazine of December 1947. It relates the FCI of a new process plant to the FCI of similar previously constructed plants with a known capacity by an exponential ratio relying on the nonlinear relationship between plant capacity and plant cost. The formula can be found in Eq. (12.1).

$$\text{Cost plant A} = \text{Cost plant B} \times \left( \frac{\text{Capacity plant A}}{\text{Capacity plant B}} \right)^y \quad (12.1)$$

The exponent  $y$  typically is on average between 0.6 and 0.7—hence the name six-tenth rule—for many process facilities [43], but can be as low as 0.5 or as high as 0.85 for some specific types of plants or equipment [44]. An exponent smaller than 1, indicates the presence of economies of scales so that plant costs increase with a smaller percentage than the plant’s capacity increase. Strictly speaking the exponent  $y$  is not constant, i.e. the exponent tends to increase with increasing plant capacity because there are limits to technology. When the exponent reaches the value of 1, it becomes more economic interesting to build two smaller plants than one large plant [44].

One problem that might arise with the previous method is that predesign estimates are mainly based on historical cost data from the past. These cost data should be updated to current prices and economic conditions. This can be done by multiplying the past cost item with the ratio of the present value of the cost index to the value of the index at the time that the previous cost estimate has been made [43, 50]. Equation (12.2) provides the formula for the cost update.

$$\text{Cost in year A} = \text{Cost in year B} \times \left( \frac{\text{Cost index in year A}}{\text{Cost index in year B}} \right) \quad (12.2)$$

One can get fairly accurate cost estimates if the bridged period is no longer than 10 years [43]. The two most cited indices are the Chemical Engineering Plant Cost Index (CEPCI) and the Marshall and Swift equipment cost index (M&S Index). The annual values of the CEPCI and the M&S Index are published monthly in the Chemical Engineering magazine (see [www.che.com](http://www.che.com)). The CEPCI provides values for overall plants on the basis of various types of equipment, building, construction labour and engineering fees whereas the M&S Index only provides equipment cost indices in accordance to process industry (e.g. cement, chemicals, glass, petroleum products, electrical power).

Finally, a parametric cost estimation is defined as “a mathematical representation of cost relationships that provide a logical and predictable correlation between the physical or functional characteristics of a plant and its resultant cost” [44]. It relates cost as a dependent variable to one or more independent variables or cost

drivers [51]. The resultant cost equation typically depends of the amount of output and is of the functional form as described in Eq. (12.3) [52, 53]:

$$C = aQ^d \quad (12.3)$$

with:

$C$  the total plant cost in function of scale  $Q$ ;

$Q$  indicator of the plant's scale;

$a$  the theoretical cost of the smallest scale;

$d$  a constant reflecting economies of scale.

This implies that the cost per unit declines by some constant percentage as the plant's scale doubles. This method is the preferred method to use within a TEA as a clear link is made between the capacity of the plant and the investment cost.

#### *Investment criteria*

After the total capital investment is estimated, the investment criteria such as NPV, IRR and DPBP can be calculated. A description on how to calculate the criteria is provided below.

$$NPV = \sum_{n=1}^T \frac{CF_n}{(1+i)^n} - I_0 \quad (12.4)$$

The NPV gives an indication of the profitability of the technology using Eq. (12.4), where  $T$  is the life span of the investment,  $CF_n$  the difference between revenues and costs in year  $n$ ,  $I_0$  the initial investment in year 0, and  $i$  the discount rate. A technology is considered interesting when the NPV is positive [31, 54]. The NPV compares the amount of money invested in a project today to the present value of the future cash receipts from the investment. In other words, the amount invested is compared to the future cash amounts after they are discounted by a specified rate of return (i.e. discount rate). The NPV considers the investment today and the revenues and expenses from each year of the lifetime of a project. The more risky an investment, the higher the estimated discount rate has to be. Typical discount rates are (i) 10 % for cost improvement of conventional technologies, (ii) 15 % for the expansion of conventional technologies, (iii) 20 % for product development, and (iv) 30 % for speculative venture [42]. However, in most articles a discount rate of 10–15 % is opted in combination with a life span of 10–15 years.

Other popular measures for evaluating whether an investment is financially worthwhile are the DPBP and the internal rate of return IRR. The payback period (PBP) is defined as the point in time when the initial investment is paid back by the net incoming cash flows, but it has the disadvantage of not taking into account the time value of money. Therefore, one can use the discounted PBP (or DPBP) that does take into account the time value of money. The shorter the DPBP the more attractive the investment is. The IRR is the discount rate at which the NPV is zero. It thus equates the present value of the future cash flows of an investment with the initial investment and provides the effective interest rate being earned on

a project after taking into consideration the time periods when the various cash amounts are flowing in or out. For an IRR to be attractive for an investor it must be higher than the return rate that can be generated in lower risk markets or investments than the project, e.g. saving the investment money in a bank or investing in safe, low-risk bonds. Because the IRR is a percentage, it can only be used as a decision rule for selecting projects when there is only one alternative to a status quo and should certainly not be used to select one project from a group of mutually exclusive projects that differ in size [55]. Therefore, when one has to choose between more than one technology or process (i.e. alternatives), the NPV ranking is mostly preferred over the IRR ranking [33].

### ***12.2.9 Risk Analysis***

In Sect. 12.2.1, a Monte Carlo simulation is proposed as a risk assessment methodology, however, also other techniques can be used to provide insight into the risk of the process for investors. We will briefly explain some of these alternative methodologies, based on Kuppens [4].

One option that is often applied in a TEA or economic evaluation in general, is the investigation to which extent the key technologic or economic indicators change when a single assumption has been changed. This is called one-factor-at-a-time or partial sensitivity analysis which implies varying the value of one variable and checking the impact on the economic indicator under investigation (often the NPV of the cash flows) without taking into account whether the change in the value of the variable is realistic, sometimes resulting in many useless calculations because of a lack of practical relevance. One can partly counter this disadvantage by using a dynamic TEA in which as many parameters as possible are dependent on each other and leave unrealistic combinations out.

Another option is that authors take into account real possible outcomes by determining several scenarios for the uncertain variables during scenario analysis, though these scenarios are often only limited to a pessimistic, an optimistic and a most expected scenario, also called best case/worst case scenario analysis [42, 55]. In this kind of analysis, the worst case scenario provides information on the maximal economic loss. Note that when the worst case yields a positive NPV, an investment is worthwhile taking the risk, whereas in the other case, i.e. when the best case yields a negative NPV it is wise to conclude that an investment should not be carried out. However, values near the base case assumptions (i.e. most expected scenario) are often more likely to occur than values near the extremes (i.e. pessimistic and optimistic scenario), so that these are actually not very likely to occur because they require the joint occurrence of low probability events. When one is able to assign probabilities of occurrence to each of these states, one can calculate the expected value of the project's net benefits, though it is often difficult to assign accurate probabilities, especially for innovative technologies. As a consequence the probabilities attached to the events are often subjective assessments that cannot

be made with great confidence [55]. Another problem with expected value analysis is that risk sometimes can only be pooled across several individuals or policies, so that the actually realized values of costs and benefits are very far from its expected value.

Finally, it can, in some cases, be useful to delay a decision, especially with regard to irreversible investments for which relevant information can become available in the future. The specific conditions and prices under which these kind of decisions, i.e. investments under uncertainty, will be taken, can be analyzed using the theory of real options which is based on dynamic programming [56]. The expected value of the information gained in the future is called a quasi-option value [57]. Given the uncertainty with respect to the costs of innovative technologies, it might be interesting to incorporate this kind of analysis in future research.

### ***12.2.10 Environmental Analysis***

When performing an extended TEA, also an environmental analysis is performed. This kind of evaluation addresses whether the technology indeed solves the social or environmental issues for its design. Methods that are useful in providing an answer to this part of an extended TEA are discussed next.

Probably the most used method for assessing the environmental impact is life cycle analysis (LCA). This is an environmental assessment methodology which analyses all resource requirements (e.g. water and energy) and material flows (inputs and outputs, emissions, etc.) of a product system [58]. LCA methodology has been standardized in ISO standards (ISO-14040 to ISO-14043). An LCA can be divided into different steps: (1) goal and scope definition, (2) inventory analysis, (3) impact analysis and (4) interpretation [58, 59]. In the first step, i.e. goal and scope definition, the functional unit is defined. During the second step, i.e. inventory analysis, all inputs and outputs are first quantified and then expressed in terms of this functional unit. Also all resources and emissions linked to the material flows are quantified. During the third step, i.e. impact assessment, the inventoried quantities are aggregated into several impact categories that correspond to an environmental problem [58]. In the last step, i.e. interpretation, conclusions are drawn. Life cycle analysis can be complemented by (environmental) life cycle costing (LCC). The latter envisages to calculate all costs associated with the life cycle of a product, regardless of the agent who bears the costs [60]. Together with a social LCA (or SLCA), LCA and LCC can be integrated in what is called a life cycle sustainability assessment or LCSA [61]. Such an LCSA analyses a product, service or technology for each of the three pillars of sustainability, i.e. environment (LCA), economy (LCC) and social equity (SLCA). Particularly when coping with technologies that are developed for environmental purposes, a traditional CBA will provide incomplete information for the evaluation of the new technology. Also, when environmental externalities are present, it can be advised to value these externalities and extend the traditional CBA in what is called an

“extended CBA” or “environmental CBA”. Seeing that many different sustainability assessment tools related to LCA exist and that conflicting outcomes result, this can create confusion for many policy and business decisions, thus, a framework is provided by Hoogmartens et al. [62] that clarifies the connections and coherence between the included assessment methodologies.

Another methodology that can be used to assess the environmental impact, is the CEENE (Cumulative exergy extraction from the natural environment) methodology that follows the cumulative use of exergy during the life cycle of a product. Exergy or ‘available energy’ has been defined as “*The maximum amount of useful work that can be obtained from a system or resource when it is brought to equilibrium with the surroundings through reversible processes in which the system is allowed to interact only with the environment*” [63]. Compared with energy, the exergy concept is much more precisely defined, and applicable to both energy flows and flows of matter. Note that exergy provides a mutual basis for all energy forms: mechanical, chemical, electrical, thermal or potential. This is especially interesting when one thinks of applying ultrasound technologies in the field of biorefineries where energy as well as materials are produced. Moreover, the cumulative use of exergy building up during the life cycle allows including both direct energy use and ‘grey energy’ (i.e. energy being used for mineral resources, the manufacturing of intermediate products, or resources used up in the production) [64].

### 12.2.11 Recommendation for Ultrasound Technology

Using the information above, one should be able to perform a TEA for ultrasound technology. A more detailed schematic overview is provided in Fig. 12.5. Rehman et al. [21] and Luo et al. [23] both made an interesting list of recommendations for further research in their review of ultrasound technology. They indicated some major drawbacks and potentials for improvement which shows the need to perform TEAs on the topic. The suggestions for improvement can be summarized as follows. Firstly, it should be verified whether the chosen input is suitable. It has

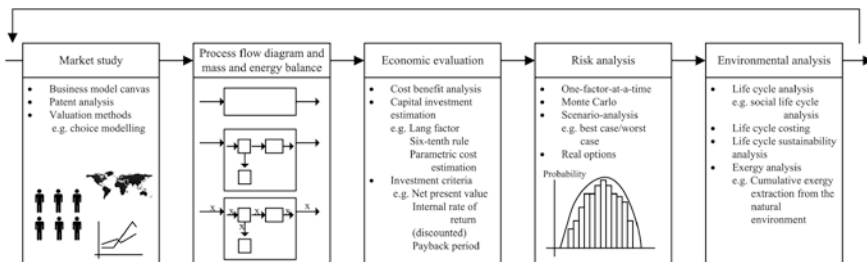


Fig. 12.5 Schematic overview of extended techno-economic assessment methodology

to fulfill two conditions simultaneously. On the one hand, it has to respond well to the ultrasound treatment. On the other hand, even if it responds well, market study has to show that there is (significant) demand for the end product being made. Secondly, the process parameters and reactor design should be optimized. An iterative approach has been suggested to achieve these goals. According to this milestone planning, the first step is reaching proper cavitation intensity, the second step is obtaining a uniform distribution of that cavitation energy in the reactor, and finally in the optimal scenario the same result should be repeated with less energy input. A dynamic techno-economic analysis is a perfect match to steer such technical optimization in an economically viable direction. Thirdly, as already mentioned, in reality biomass is a heterogeneous system causing extra costs to be incurred in comparison to calculations made from pilot lines using homogenous input material. In case no synergy exists between both pretreatment techniques which increases productivity with an amount equal to the extra investment cost, economic viability will be affected. Finally, in case by-products of added value are manufactured, these additional streams of revenue should be grasped at minimal cost. The use of a flow reactor to separate by-products from the main product in-line is one way to achieve this goal.

As already indicated, although not numerous, some economic feasibility studies have already been performed concerning ultrasound technology. In the following section a review is given of the available literature. Information from these sources can be used as input for new, optimized TEAs.

### **12.3 Economic Feasibility Studies for Ultrasound Technology**

While searching for economic articles related to ultrasound technology, our first finding was that there is little literature available. Only a few articles mention economic analysis in their title, which indicates that economic feasibility studies are not the main concern of researchers at this moment. Furthermore, we could conclude that no economists were involved in the studies found based on the authors' affiliation. Below, we will provide a short description of the scientific literature that we have found in chronological order and discuss the economic approach in short.

Salsabil et al. [20] compared the dynamic, technical and economic performance of aerobic and anaerobic digestions with different sludge reduction processes, one of which was ultrasonic. The goal was to provide information concerning the selection of the best digestion and pretreatment type for sludge reduction and cost saving. They concluded that the ultrasound process led to the best total suspended solids (TSS) reduction. Furthermore, they concluded that ultrasonic pretreatment led to a cost reduction in comparison to a control sample, based on the energetic balance. In the title of their article, they claim to perform a TEA, but actually they assess the cost effectiveness of sonication on the reduction of wastewater biomass



volume before aerobic or anaerobic digestion. Though cost effectiveness is shown to be the highest for ultrasound compared to ozonation and thermal treatment, this result's merit is limited as the study only takes energy expenses into account. They point out themselves that also other parameters may interfere with economic efficiency, such as investment costs, personnel costs, maintenance costs and dewatering.

Elbeshbishy et al. [65] evaluated the efficiency of ultrasonication as a pretreatment method for hog manure with high solid content prior to anaerobic digestion. More specifically they studied the impact on solubilisation and anaerobic degradability, with emphasis on the effect on bound proteins solubilisation. They found that a specific energy of 500 kJ/kg TS (Total solids) can be considered to be the optimum energy input to be economically viable, as the value of the energy output exceeds that of the energy input by \$4.1/ton of dry solids. However, the economic analysis does not contain many details about the calculations. Also, the story is incomplete as no investment costs have been taken into account. Without a full overview of costs and benefits that are timely discounted, no conclusions can be reached about economic viability.

Montalbo-Lombo et al. [66] compare the economic viability of simultaneous saccharification and fermentation of corn slurry which was pretreated either by ultrasound or jet cooking. In previous work the promise of the use of ultrasonication has already been shown, however, no comparison was yet made with the large-scale jet cooking systems. In this study, the reference approach has been adopted, leading to the conclusion that ultrasound is more viable than jet cooking given that it has a lower manufacturing cost. Care should be taken in the interpretation as this does not entail being economically viable on its own. Although the economic study in this paper is well performed and a clear overview is made of the assumptions, a linkage with the technical parameters seems to be missing. The model could be improved by translating it into a dynamic TEA. This would also allow checking for the influence of changes in technical parameters when performing the sensitivity analysis.

Similarly Deenu et al. [67] compare the economic viability of ultrasound extraction of lutein from *Chlorella vulgaris* to that of conventional treatment and ultrasound with enzymatic pretreatment. It is shown that ultrasound has the lowest manufacturing cost of the three alternatives. Again, this does not entail being economically viable.

Chen et al. [68] used the cost-benefit analysis to determine the minimal cost that a person or investor was willing to accept for pyrolysis oil from the ultrasound-assisted oxidative desulfurization (UAOD) technology as an indication of the level of payment required to achieve resource recycling and economic objectives. The authors compared three different strategies (1) one set of UAOD units, (2) two sets of UAOD units connected in series, and (3) pyrolysis oil without any desulfurization strategy. From the study it is concluded that using one set of UAOD continuous-flow units (i.e. first strategy) provides full benefits and has few environmental or health impacts. The authors performed a cost benefit analysis to provide economic information on the market and nonmarket values resulting from

the continuous flow UAOD technology in processing pyrolysis oil, however, they did not account for the time value of money.

Franchetti [69] studied the cost, energy and global warming implications of the use of several emerging food waste to energy technologies using the internal rate of return (IRR), payback period and LCA method. The author found that a two-stage anaerobic digestion system using ultrasound pre-treatment was the most profitable investment option for waste digestion among (1) landfilling, (2) two-stage anaerobic digestion system using ultrasound pre-treating, (3) two-stage continuous combined thermophilic acidogenic hydrogenesis and mesophilic with recirculation of the digested sludge, (4) long term anaerobic digestion of food waste stabilized by trace elements, and (5) single stage anaerobic digestion. However, for reaching this conclusion it was claimed that a positive IRR was sufficient for economic viability. Unfortunately, this is incorrect, since the IRR has to be higher than the discount rate, which mirrors the time value of money, used for appraising the project's viability. Moreover, it was noted that the IRR is the preferred criteria when comparing projects, however, this is not the case as mentioned in Sect. 12.2.8.

Vieira et al. [70] aimed to provide an answer to three research topics: (1) investigate the efficacy of ultrasound on antioxidant compound extraction from jussara and compare the results from conventional solvent extraction using an agitated bed, (2) evaluate the influence of extraction conditions on phenolic and anthocyanin yield, and (3) estimate the manufacturing cost of the crude extracts. The authors used SuperPro Designer 6.0 software to economically evaluate the extraction of natural antioxidant obtained by ultrasound-assisted and agitated bed extraction from jussara pulp. However, the reader is left here with no clue of whether costs (and benefits) have been discounted.

An overview of the used economic metrics in each of the above mentioned studies is provided in Table 12.2.

Other studies do not provide an economic analysis, however, they conclude that ultrasound technology had an interesting impact on technical results. These studies lend themselves perfectly to techno-economic evaluation.

Velmurugan and Muthukumar [71] concluded from their study that the hydrolysate from sono-assisted acid hydrolysis of sugarcane bagasse was more susceptible for bioethanol production as it contained very few inhibitors. In another study of Velmurugan and Muthukumar [72] the authors indicated that the ultrasound-assisted alkaline pretreatment process resulted in a decreased pretreatment time and lower temperature with improved efficiency in comparison to commercial alkaline pretreatment. It would be interesting to show what the economic impact is of this change in order to convince industry to adopt the ultrasound technology in their existing processes. Furthermore, the authors indicated that upscaling still has to be proven. In that study, the authors concluded that the sono-assisted pretreatment is an interesting alternative method for the structured modification of sugarcane bagasse [73]. However, how much better is the technology in economic terms and in case that the costs are higher and the performance better, are customers willing to pay this extra cost?

**Table 12.2** Review of used economic metrics

Author	Year	Economic indicator	Details	Source
Salsabil et al.	2010	Energetic cost		[20]
Elbeshbishy et al.	2011	Cost energy in versus cost energy out	\$/ton $TS_{in}$	[65]
Montalbo-Lomboy et al.	2011	NPV, BCR	$i = 15\%$ ; $T = 10$ year	[66]
Deenu et al.	2013			[67]
Chen et al.	2013	CBA, risk monetarisation		[68]
Franchetti	2013	IRR, PBP	$T = 10$ year	[69]
Vieira et al.	2013	Manufacturing cost	$i = 10\%$ ; $T = 15$ year	[70]

*BCR* Benefit cost ratio

*CBA* Cost benefit analysis

*IRR* Internal rate of return

*NPV* Net present value

*PBP* Payback period

$i$  Discount rate

$T$  Life span

$TS_{in}$  Total solids in

Nitayavardhana et al. [74] investigated the effect of different sonication conditions on reducing the sugar yield from cassava chip slurry. The results of these analyses are very interesting to couple directly to economic calculations in a TEA. The authors also indicated in their article that energy balance calculations should be based on continuous sonication tests in order to get more accurate analysis. These kinds of calculations (i.e. more details) would then be added in a next iteration of a TEA. Bussemaker and Zhang [75] indicated in their review that challenges exist in scaling-up the technology due to additional energy use. They also indicated that a CBA has to be performed before scale-up. We agree that a CBA has to be performed, however, the CBA has not only to be done prior to scale-up, but during the whole development phase of the technology.

Kapilan and Baykov [76] made a review of innovative technologies (i.e. microwave, ultrasonic and pyrolysis) to produce biodiesel. The authors concluded that these innovative technologies have the potential to improve the economic feasibility by reducing production time and cost, however, the authors did not provide an economic analysis.

## 12.4 Conclusions and Future Outlook

In this chapter, clear guidelines are provided to perform a reliable extended techno-economic analysis. Although the term TEA has become very popular, the guidelines are not well documented. An extended TEA consists of five different

steps that are iteratively performed: (i) the first step is a market study, (ii) followed by a process flow diagram and mass and energy balance calculation, (iii) in the next step an economic analysis is integrated, (iv) after which a risk analysis is performed, and (v) in the last step an environmental analysis is added. As such an extended TEA can be framed within the wider concept of sustainability assessment tools. In general, a sustainability assessment should integrate economic, environmental as well as social aspects. However, many scholars focus on only one dimension of sustainability. This so called reductionism is compatible with the question raised by stakeholders and policy makers to keep it simple. However, Gasparatos and Scolobig [77] conclude that a combination of different tools might be more appropriate to represent sustainability than using a single tool (i.e. reductionism). An extended TEA is an example of such a combination of monetary tools and biophysical tools. From the different papers it could be concluded that ultrasound seems to be an interesting technology from an economic point of view, however, without taking all costs into account and provide a clear overview of the assumptions made, no final conclusion can be made. Moreover, technological results sound promising based on lab scale tests. However, to convince investors, upscaling has to be realized and the economic benefits have to be proven. Therefore, from the review it is clear that more thorough economic analyses are needed, preferably in the form of TEAs. TEAs are especially interesting for ultrasound technology as also technological optimization still has to be performed. Within this chapter, some recommendations are made to perform a TEA for ultrasound technology. It is highly recommended to use a TEA to help in defining the prior tests that have to be performed in order to result in the largest economic gain. Moreover, we hope to have provided ample evidence to allow repeating our claim of the need for multi-disciplinary teams in performing TEAs.

In this chapter we have provided general guidelines to perform an extended TEA and have provided specific recommendations to perform the assessment for ultrasound technologies. However, the general methodological guidelines are suitable for different kinds of processes such as microwave or pyrolysis. Moreover, the methodology is applicable on mature, as well as innovative technologies and can be adopted in different phases of development. TEA is a decision support tool that researchers can use when deciding on the pathways to take when developing their processes.

## References

1. Kantor M, Wajda K, Lannoo B, Casier K, Verbrugge S, Pickavet M, Wosinska L, Chen J, Mitsenkov A (2010) General framework for techno-economic analysis of next generation access networks. In: 12th international conference on transparent optical networks (ICTON). IEEE
2. Smura T, Kiiski A, Hämmäinen H (2007) Virtual operators in the mobile industry: a techno-economic analysis. *NETNOMICS: Econ Res Electron Netw* 8:25–48
3. NABC (2011) Techno-economic analysis: evaluating the economic viability and potential of the nabc process strategies (cited 19 Nov 2012). Available from: [http://www.nabcprojects.org/pdfs/techno-economic\\_analysis\\_evaluating\\_economic\\_viability.pdf](http://www.nabcprojects.org/pdfs/techno-economic_analysis_evaluating_economic_viability.pdf)

4. Kuppens T (2012) Techno-economic assessment of fast pyrolysis for the valorisation of short rotation coppice cultivated for phytoextraction
5. Njomo D (1995) Techno-economic analysis of a plastic cover solar air heater. *Energy Convers Manage* 36:1023–1029
6. Petit PJ, Meyer JP (1998) Techno-economic analysis between the performances of heat source air conditioners in South Africa. *Energy Convers Manage* 39:661–669
7. Staessens D, Angelou M, De Groote M, Azodolmolky S, Klonidis D, Verbrugge S, Colle D, Pickavet M, Tomkos L (2011) Techno-economic analysis of a dynamic impairment-aware optical network. In: *Optical fiber communication conference and exposition, Los Angeles*
8. Jerman-Blazic B (2007) Comparative study and techno-economic analysis of broadband backbone upgrading: a case study. *Informatica* 31:279–284
9. Lannoo B, Naudts B, Van Hauwaert E, Ruckebusch P, Hoebeke J, Moerman I (2012) Techno-economic evaluation of a cost-efficient standard container monitoring system. In: *Key developments in the port and maritime sector, Antwerp*
10. Didden M (2003) Techno-economic analysis of methods to reduce damage due to voltage dips. Doctoral thesis, Faculty of applied science, Catholic University of Louvain, Leuven
11. Athanassiou M, Zabaniotou A (2008) Techno-economic assessment of recycling practices of municipal solid wastes in Cyprus. *J Clean Prod* 16:1474–1483
12. Myles P, Herron SE, Grol E, Le P, Kuehn N (2012) Techno-economic analysis of CO<sub>2</sub> capture-ready coal-fired power plants (DOE/NETL-2012/1581). Report prepared for the U.S. Department of Energy, National Energy Technology Laboratory
13. Chong WT, Naghavi MS, Poh SC, Mahlia TMI, Pan KC (2011) Techno-economic analysis of a wind–solar hybrid renewable energy system with rainwater collection feature for urban high-rise application. *Appl Energy* 88:4067–4077
14. Hernández H, Tübke A (2011) Techno-economic analysis of key renewable energy technologies (PV, CSP and wind). EUR 24904 EN. Publications Office of the European Union, Luxembourg
15. Bakos GC, Soursos M (2002) Techno-economic assessment of a stand-alone PV/hybrid installation for low-cost electrification of a tourist resort in Greece. *Appl Energy* 73:183–193
16. Van Dael M, Van Passel S, Pelkmans L, Guisson R, Reumermann P, Luzardo NM, Witters N, Broeze J (2013) A techno-economic evaluation of a biomass energy conversion park. *Appl Energy* 104:611–622
17. Enguídanos M, Soria A, Kavalov B, Jensen P (2002) Techno-economic analysis of bio-diesel production in the EU: a short summary for decision-makers. Report EUR 20279 EN, Institute for prospective technological studies, report for the European Commission, Joint Research Centre
18. Klein-Marcuschamer D, Oleskowicz-Popiel P, Simmons BA, Blanch HW (2010) Technoeconomic analysis of biofuels: a wiki-based platform for lignocellulosic biorefineries. *Biomass Bioenergy* 34:1914–1921
19. Wright MM, Daugaard DE, Satrio JA, Brown RC (2010) Techno-economic analysis of biomass fast pyrolysis to transportation fuels. *Fuel* 89(Supplement 1):S2–S10
20. Salsabil MR, Laurent J, Casellas M, Dagot C (2010) Techno-economic evaluation of thermal treatment, ozonation and sonication for the reduction of wastewater biomass volume before aerobic or anaerobic digestion. *J Hazard Mater* 174:323–333
21. Rehman MSU, Kim I, Chisti Y, Han J-I (2013) Use of ultrasound in the production of bioethanol from lignocellulosic biomass. *EEST Part A: Energ Sci Res* 30:1391–1410
22. Ensminger D, Bond LJ (2011) *Ultrasonics: fundamentals, technologies, and applications*. CRC Press, Boca Raton
23. Luo J, Fang Z, Smith RL Jr (2014) Ultrasound-enhanced conversion of biomass to biofuels. *Prog Energy Combust Sci* 41:56–93
24. Suslick KS (1990) Sonochemistry. *Science* 247:1439–1445
25. Mason TJ, Peters D (2002) *Practical sonochemistry: power ultrasound uses and applications*. Woodhead Publishing, Cambridge

26. Ashokkumar M (2011) The characterization of acoustic cavitation bubbles—an overview. *Ultrason Sonochem* 18:864–872
27. Capelo-Martínez J-L (2008) *Ultrasound in chemistry: analytical applications*. Wiley, New York
28. Verbrugge S, Casier K, Van Ooteghem J, Lannoo B (2008) Practical steps in techno-economic evaluation of network deployment planning part 1: methodology overview. In: 13th international telecommunications network strategy and planning symposium (networks 2008). IEEE
29. Barbiroli G (1997) *The dynamics of technology: a methodological framework for techno-economic analyses*. Kluwer Academic, Berlin
30. Biezma MV, Cristóbal JRS (2006) Investment criteria for the selection of cogeneration plants—a state of the art review. *Appl Therm Eng* 26:583–588
31. Levy H, Sarnat M (1994) *Capital investment and financial decisions*. Prentice Hall, New Jersey
32. Karellas S, Boukis I, Kontopoulos G (2010) Development of an investment decision tool for biogas production from agricultural waste. *Renew Sust Energy Rev* 14:1273–1282
33. Lorie JH, Savage LJ (1955) Three problems in rationing capital. *J Bus* 28(4):229–239
34. Carpaneto E, Chicco G, Mancarella P, Russo A (2011) Cogeneration planning under uncertainty. Part II: decision theory-based assessment of planning alternatives. *Appl Energy* 88:1075–1083
35. Haimes YY (2005) *Risk modeling, assessment, and management*, vol 40. Wiley, New York
36. Vose D (1996) *Quantitative risk analysis: a guide to monte carlo simulation modelling*. Wiley, New York
37. Alvira P, Tomás-Pejó E, Ballesteros M, Negro MJ (2010) Pretreatment technologies for an efficient bioethanol production process based on enzymatic hydrolysis: a review. *Bioresour Technol* 101:4851–4861
38. Lizin S, Leroy J, Delvenne C, Dijk M, De Schepper E, Van Passel S (2013) A patent landscape analysis for organic photovoltaic solar cells: identifying the technology's development phase. *Renew Energy* 57:5–11
39. Lizin S, Van Passel S, De Schepper E, Vranken L (2012) The future of organic photovoltaic solar cells as a direct power source for consumer electronics. *Sol Energy Mater Sol Cells* 103:1–10
40. Whitesides RW (2007) Process equipment cost estimating by ratio and proportion. In: PDH Course G127, Fairfax
41. Horngren CT, Bhimani A, Datar SM, Foster G (2005) *Management and cost accounting*, 3rd edn. Pearson Education Limited, Harlow
42. Mercken R (2004) *De investeringsbeslissing. Een beleidsgerichte analyse*. Garant, Antwerpen
43. Peters MS, Timmerhaus KD, West RE (2004) *Plant design and economics for chemical engineers*, 5th edn. McGraw-Hill, New York
44. Dysert LR (2003) Sharpen your cost estimating skills. *Cost Eng* 45(6):22–30
45. Christensen P, Dysert L (2005) Cost estimate classification system—as applied in engineering, procurement, and construction for the process industries in recommended practice no. 18R-97. In: International A (ed). *AACE international*
46. Long JA (2000) Parametric cost estimating in the new millennium. *PRICE Systems White Papers*
47. Anderson J (2009) Determining manufacturing costs. *Chem Eng Prog (CEP)* 105
48. Lang HJ (1947) Cost relationships in preliminary cost estimation. *Chem Eng Mag* 54:117–121
49. Lang HJ (1948) Simplified approach to preliminary cost estimates. *Chem Eng Mag* 55:112
50. Sinnott RK (2005) *Chemical engineering design*, 4th edn. In: Coulson and Richardson's chemical engineering series, vol 6. Elsevier Butterworth-Heinemann, Oxford
51. Dysert LR (2008) An introduction to parametric estimating. In: *AACE international transactions of the annual meeting 2008, EST.03*

52. Dysert LR (2005) So you think you're an estimator? In: AACE international transactions of the annual meeting 2005, EST.01
53. Caputo AC, Palumbo M, Pelagagge PM, Scacchia F (2005) Economics of biomass energy utilization in combustion and gasification plants: effects of logistic variables. *Biomass Bioenergy* 28:35–51
54. Fiala M, Pellizzi G, Riva G (1997) A model for the optimal dimensioning of biomass-fuelled electric power plants. *J Agr Eng Res* 67:17–25
55. Boardman AE, Greenberg DH, Vining AR (2006) Cost benefit analysis. Concepts and practice. Pearson Education, New Jersey
56. Dixit AK, Pindyck RS (1994) Investment under uncertainty. Princeton University Press, New Jersey, p 468
57. Arrow KJ, Fisher AC (1974) Environmental preservation, uncertainty, and irreversibility. *Q J Econ* 88:312–319
58. Jungk NC, Patyck A, Reinhardt GA, Calzoni J, Caspersen N, Dercas N, Gaillard G, Gosse G, Hanegraaf M, Heinzer L, Kool A, Korsuize G, Lechner M, Leviel B, Neumayr R, Nielsen AM, Nielsen PH, Nikolaou A, Panoutsou P, Panvini A, Rathbauer J, Riva G, Smedile E, Stettler C, Pedersen Weidema B, Wörgetter M, van Zeijts H (2000) Bioenergy for Europe: which one fits best—a comparative analysis for the community. Final report (contract CT 98 3832), Institute for Energy and Environmental Research Heidelberg, Heidelberg
59. Klöpffer W (1997) Life cycle assessment: from the beginning to the current state. *Environ Sci Pollut R* 4:223–228
60. Ciroth A, Hunkeler D, Lichtenvort K (2008) Environmental life cycle costing. SETAC, Pensacola
61. Swarr TE, Hunkeler D, Klöpffer W, Personen H-L, Ciroth A, Brent AC, Pagan R (2011) Environmental life-cycle costing: a code of practice. *Int J Life Cycle Ass* 16:389–391
62. Hoogmartens R, Van Passel S, Van Acker K, Dubois M (2014) Bridging the gap between LCA, LCC and CBA as sustainability assessment tools. *Environ Impact Assess Rev* 48:27–33
63. Dewulf J, Van Langenhove H, Muys B, Bruers S, Bakshi BR, Grubb GF, Paulus DM, Sciubba E (2008) Exergy: its potential and limitations in environmental science and technology. *Environ Sci Technol* 42:2221–2232
64. Maes D, Van Dael M, Vanheusden B, Goovaerts L, Reumerman P, Márquez Luzardo N, Van Passel S (2014) Assessment of the RED sustainability guidelines: the case of biorefineries. *J Clean Prod.* doi:10.1016/j.jclepro.2014.04.051
65. Elbeshbishy E, Aldin S, Hafez H, Nakhla G, Ray M (2011) Impact of ultrasonication of hog manure on anaerobic digestability. *Ultrason Sonochem* 18:164–171
66. Montalbo-Lomboy M, Khanal SK, van Leeuwen J, Raj Raman D, Grewell D (2011) Simultaneous saccharification and fermentation and economic evaluation of ultrasonic and jet cooking pretreatment of corn slurry. *Biotechnol Prog* 27:1561–1569
67. Deenu A, Naruenartwongsakul S, Kim SM (2013) Optimization and economic evaluation of ultrasound extraction of lutein from *Chlorella vulgaris*. *Biotechnol Bioproc E* 18:1151–1162
68. Chen T-C, Shen Y-H, Lee W-J, Lin C-C, Wan M-W (2013) An economic analysis of the continuous ultrasound-assisted oxidative desulfurization process applied to oil recovered from waste tires. *J Clean Prod* 39:129–136
69. Franchetti M (2013) Economic and environmental analysis of four different configurations of anaerobic digestion for food waste to energy conversion using LCA for: a food service provider case study. *J Environ Manage* 123:42–48
70. Vieira GS, Cavalcanti RN, Meireles MAA, Hubinger MD (2013) Chemical and economic evaluation of natural antioxidant extracts obtained by ultrasound-assisted and agitated bed extraction from jussara pulp (*Euterpe edulis*). *J Food Eng* 119:196–204
71. Velmurugan R, Muthukumar K (2011) Utilization of sugarcane bagasse for bioethanol production: sono-assisted acid hydrolysis approach. *Bioresour Technol* 102:7119–7123
72. Velmurugan R, Muthukumar K (2012) Ultrasound-assisted alkaline pretreatment of sugarcane bagasse for fermentable sugar production: optimization through response surface methodology. *Bioresour Technol* 112:293–299



73. Velmurugan R, Muthukumar K (2012) Sono-assisted enzymatic saccharification of sugarcane bagasse for bioethanol production. *Biochem Eng J* 63:1–9
74. Nitayavardhana S, Rakshit SK, Grewell D, van Leeuwen JH, Khanal SK (2008) Ultrasound pretreatment of cassava chip slurry to enhance sugar release for subsequent ethanol production. *Biotechnol Bioeng* 101:487–496
75. Bussemaker MJ, Zhang D (2013) Effect of ultrasound on lignocellulosic biomass as a pretreatment for biorefinery and biofuel applications. *Ind Eng Chem Res* 52:3563–3580
76. Kapilan N, Baykov BD (2014) A review on new methods used for the production of biodiesel. *Pet Coal* 56:62–73
77. Gasparatos A, Scolobig A (2012) Choosing the most appropriate sustainability assessment tool. *Ecolog Econ* 80:1–7

# Index

## A

- Absorption coefficient of cellulosic biomass, 261
- Acceleration, 12, 15, 42, 164, 172–174, 181
- Acetogenesis, 210, 211
- Acid hydrolysis, 37, 75, 78, 82, 172, 173, 180, 272, 274, 278, 284, 339
- Acidogenesis, 210, 211
- Acids
- activated carbons, 277
  - adsorbed acid, 277
  - alumina, 276, 277
  - alumina super acid, 276
  - aluminum phosphate, 276
  - aluminum sulfate, 276
  - bentonite, 275, 276
  - graphite, 276
  - hydrochloric acid, 277, 295, 302
  - kaolinite, 274–278
  - muscovite mica, 276
  - nitric acid, 277, 295
  - phyllosilicates, 275
  - quartz, 276
  - silicon carbide, 276
  - sulfuric acid, 9, 90, 232, 254, 275, 277, 298, 300, 308
  - talc, 276
  - vermiculite, 276
  - Y-type zeolite, 276
  - zeolite, 275, 277
- Acoustic
- amplitude, 4, 6, 7, 20, 24, 38, 39, 45, 51, 71, 76, 169, 249, 309
  - attenuation, 11, 18, 24, 27, 28, 39, 260
  - cavitation, 4–7, 9, 14, 15, 18–21, 24–30, 37, 38–41, 45, 47–49, 51, 52, 55–57, 63, 69, 70, 72, 78, 79, 82, 89, 92, 97, 103, 110, 125, 127, 135, 146, 154, 164, 168–170, 191, 198, 212, 245, 305, 337
  - cavitation structure, 21
  - characteristic impedance, 4
  - cycle, 8, 10, 14, 15, 23, 26, 27, 42, 51, 55, 192
  - emitting surface, 23
  - energy, 4, 8, 10, 14, 19, 20, 27, 28, 36, 44, 51, 55, 61, 103, 117, 120, 121, 125, 142, 156, 166, 190, 202, 210, 215, 219, 226, 231, 237, 244, 256, 270, 283, 290, 309, 320, 326, 328, 338, 340
  - frequency, 4, 5, 8, 18, 19, 26, 28, 38, 48, 76, 99, 107, 126, 127, 166, 199, 200, 212, 217, 246, 298, 301, 304, 311
  - frequency spectroscopy (AFS), 17
  - intensity, 4, 5, 9, 14, 18, 19, 22, 23, 26–28, 168, 213, 244, 307
  - interference, 298, 306
  - Lichtenberg figure, 21
  - microstreaming, 4
  - power, 4, 5, 48, 127, 142, 162, 175, 198, 213, 234, 246, 251, 257, 261, 294, 299, 303, 310, 332
  - power density, 9, 102, 105, 110, 309, 310
  - pressure, 4, 6, 7, 9, 11, 14, 16, 20, 24, 27, 37, 40, 45, 48, 71, 74, 82, 130, 145, 148, 199, 216, 249, 255, 259, 296
  - speed, 5, 23
  - streaming, 6, 14, 25, 39, 76
  - velocity, 5

- wave, 4, 5, 14, 39, 48
  - wavelength, 5
- Activation energy, 57, 60, 104
- Active zone, 9, 10, 24
- Activity, 23, 60, 167, 182, 192, 200, 212, 215, 228, 276, 290, 305
- Adiabatic, 8, 24, 37, 47
- Adsorption, 16, 57, 61, 95, 96, 193
- Agglomeration, 164, 170, 246, 299
- Alcohol-oil molar ratio, 163
- Algae, 122, 124, 142, 143, 145, 152, 154, 167, 199
- Algae production, 234
- Algal biomass, 49, 189, 203
- Algal cell, 50, 198–200
- Alkaline pretreatment, 77, 196, 245
- Alkyl ester, 36, 142
- Alternative fuels, 160
- Aluminum foil erosion, 18
- Amberlyst<sup>®</sup>, 91
- Ammonium, 74, 173
- Amorphous, 198, 291, 294
- Amylopectin, 292, 293, 299
- Amylose, 169, 294, 299
- Anaerobic, 118, 122, 123, 193, 210, 211, 214, 215, 221, 222, 223, 230, 235
- Anaerobic digestion, 122, 202, 209–212, 215–217, 220–221, 225–227, 229, 231–233, 235, 306, 337–339
- Analysis of variance, 57, 166, 259
- Anova, 57, 166
- Antinodes of ultrasonic wave, 17
- Attrition, 80, 270, 271, 273, 277, 278, 280–283
- Audible sound, 4
- Autoclaving, 75, 76, 80
- Autotrophic, 199
- Avicel<sup>®</sup>, 175, 177
  
- B**
- Ball to powder ratio, 282
- Ball-milled, 179
- Ball-milling, 279
- Bamboo, 179
- Bamboo powder, 194, 197
- Base, 52, 55, 56, 59, 165, 193, 246, 273, 334
- Base-catalysis, 162
- Batch esterification, 91
- Batch fermentations, 179
- Bath-type reactor, 19
- Beer-Lambert law, 18
- BET, 167
- Beta-galactosidase, 180
- Beta-glucosidase, 253
- Bioavailability, 209, 211, 215, 216, 221, 222, 230, 237
- Biocatalysis, 227, 228
- Biochemical, 5, 190, 191
- Biochemical methane potential, 215
- Bioconversion, 38, 62, 66, 70, 191, 210
- Biodegradability, 122, 192, 201, 210, 214, 215, 217, 220, 227, 229
- Biodegradable, 164
- Biodegradation, 194, 233
- Biodiesel
  - production, 9, 37, 69, 89, 119, 137, 142, 189–191, 202, 203, 209, 231, 245
  - yield, 15, 36, 58, 66, 101, 108, 128, 166, 171, 175, 191, 193, 252, 253
- Bioenergy, 4, 319
- Bioethanol, 38, 118, 160, 178, 181, 189, 190, 192, 195, 198, 209, 217, 231, 245, 253, 339
- Biofuels, 35, 38, 75, 142, 160, 190, 191, 199, 243–245, 247, 252, 253, 255, 290, 317, 320, 322, 325
- Biogas, 36, 118, 189, 191, 193, 200, 209, 210, 212, 214–217, 219–222, 226–234, 236
- Biogas plants, 217
- Biohydrogen, 142, 193
- Biological, 4, 5, 160, 190, 191, 193, 198, 203, 209, 210, 215, 216, 226, 227, 250, 254, 306
- Biological pretreatment, 198
- Biomass
  - debris, 129, 130, 298–300, 304, 307, 311, 312
  - pellets, 132, 246, 247, 250, 252–254, 262
- Bioreactor, 180
- Biorefinery, 173, 192, 252, 284
- Biorenewables, 191
- Biotechnology, 167, 191
- Blake threshold, 6, 14
- Bligh and Dyer method, 49, 199
- Boltzmann constant, 13
- Booster, 107
- Boundary layer approximation, 10
- Box–Behnken, 168
- Box–Behnken method, 59
- Breaking, 9, 200, 294
- Bubble
  - cloud, 16, 20, 26
  - coalescence, 14–17, 24, 26
  - collapse, 4, 8, 12, 22, 24, 27, 41, 43, 72, 191, 213, 305
  - density, 5, 13, 22, 52
  - dynamics, 4, 7, 28, 40, 57, 117

- dynamics model, 48
- expansion, 8, 15, 47
- interior, 12, 13, 15, 24, 170
- shrinkage, 15
- Bubble/liquid interface, 16, 24
- Building blocks, 24, 290
- Butanol, 36, 63, 302
- By-products, 165, 191, 203, 216, 233, 273, 337
  
- C**
- Calcium methoxide, 59, 167
- Capacity factored estimates, 332
- Capillary wave action, 24
- Capital investment
  - fixed, 17, 96, 329
  - total, 11, 12, 107, 109, 134, 329, 330, 333
- Carbohydrate, 77, 143, 190, 191, 199, 209, 210, 227–229, 231, 232, 234, 252, 300
- Carbonyl carbon, 56
- Cash flow, 329, 333, 334
- Cassava chip slurry, 192, 340
- Cassava root, 180
- Catalyst
  - concentration, 12, 18, 27, 42, 53, 59, 66, 71, 95, 97, 101, 129, 148, 171
  - Hammett and Deyrups  $H_0$  function, 275
  - homogeneous catalyst, 90
  - loading, 57, 166
  - storage, 118, 135
  - surface acidity, 275, 277
- Cavitation
  - acoustic, 4, 9, 19, 191, 192, 200, 203
  - bubble, 4, 8, 14, 22, 39, 40, 43, 46–48, 52, 191, 192, 213, 217, 221, 228, 234, 308, 311
  - bubble dynamics, 3, 27, 40, 48, 56, 63, 79
  - efficiency, 19, 25, 26, 30, 118, 125, 128, 130, 135, 144, 152
  - energy, 308, 337
  - hydrodynamic, 39, 104
  - nuclei, 309
  - number, 19, 20
  - yield, 19
- Cavitation energy, 337
- Cell disruption, 117, 121, 127, 130, 135, 143, 168, 189, 198–200, 229
- Cell wall, 122, 128, 143, 152, 168, 192, 193, 198, 212, 217, 226, 227, 231, 233, 234, 252, 253, 271, 291
- Cellobiose, 76, 252
- Cellulase, 125, 181, 182, 195, 210, 216, 252, 253
- Cellulose
  - crystallinity, 79, 171, 198, 203, 215, 245, 271, 272, 282
  - glycosidic bond, 79, 275, 276
- Cellulosic biofuel, 243–245, 247, 252, 253, 255, 262
- Cellulosic biomass, 37, 38, 75, 182, 243–247, 249–259, 262
- Central composite design, 80
- Chapman–Enskog theory, 41, 43
- Chemical
  - activation, 6, 198
  - effects, 4, 22, 48, 79, 164, 296
  - engineering plant cost index, 332
  - oxygen demand (COD), 211, 219
  - pretreatment, 27
  - reactivity, 26, 27
  - species, 4, 24, 42, 43, 71
- Chilton relation, 57
- Chlorella, 117, 128, 130, 133, 191, 231
- Chlorophyll, 143, 199, 200
- Chlorosulfonic acid, 61
- Choice modelling, 26, 135, 327
- Choline acetate, 194
- Climate change, 36, 160
- Clostridium pasteurianum, 63, 69
- CO<sub>2</sub> capture, 321
- Collapse, 6, 8, 13, 14, 16, 22, 26, 71, 125, 164, 170, 191, 213, 245, 307, 321
- Collisions, 66, 79, 161, 275, 282, 283
- Combined technologies, 305
- Commercial cellulase, 80
- Comminution, 270
- Communication networks, 321
- Competitors, 327
- Compositions, 124, 141, 152, 156, 245, 252
- Compressed zone, 5
- Compression ratio of bubble radius, 14
- Concerted collapse, 3, 17, 21
- Conducting ions, 161
- Conical bubble structure, 21
- Contact angle, 7
- Continuous
  - flow system, 163
  - flow ultrasonic device, 311
  - reactor, 237
  - stirred tank reactor (CSTR), 90
  - ultrasound, 15, 117
- Conversion
  - micro-, 203
- Conversion rates, 110, 211, 278, 282
- Cooked oils, 100, 106
- Corn meal, 192
- Corn starch granules, 296

- Co-solvent, 89
- Cost
  - capital, 226, 328, 330, 331
  - effectiveness, 173, 253, 254, 328, 337
  - operational, 328, 329
- Cost-benefit analysis
  - environmental, 335
  - extended, 336
- Crevice, 6, 28, 39
- Critical size of cavitating bubble, 4, 15, 24
- Crude glycerol, 35, 38, 62
- Crystalline cellulose, 79, 194, 271
- Crystallinity, 77, 171, 198, 269, 271, 273
- Cumulative exergy extraction from the natural environment, 336
- Customers, 327, 339
  
- D**
- Decanol, 163
- Degassing pretreatment, 27
- Degree of polymerization, 77, 272, 304
- Dehydration products
  - furfural, 76, 216, 284
  - humins, 278
  - hydroxymethylfurfural, 76, 216
  - levoglucosan, 284
  - levoglucosenone, 284
- Delignification, 37, 77, 78, 82, 171, 173, 192, 193, 198
- Denaturation, 199
- Density gradient, 8
- Denucleation, 20, 28
- Depolymerization, 78, 79, 83, 212, 284, 295, 300, 308
- Design of experiments, 57, 59, 255, 259
- Destruction, 4, 193, 198, 227, 230
- Desulfurization, 35, 70, 338
- Dibenzothiophene, 70, 74
- Dielectric
  - heating, 160, 161, 301, 305
  - loss, 302
  - loss tangent, 302
  - permittivity, 301
- Diffusion
  - coefficient, 11, 43
  - limited process, 42
  - theory, 327
- Diffusive penetration depth, 12, 43
- Digester, 230, 231
- Digestibility, 77, 227, 229, 230
- Digestion
  - aerobic, 338
  - anaerobic, 118, 122, 202, 209, 210, 215
- Diluted acid pretreatment, 76, 77, 253
- Dimethyl sulfoxide, 70, 179
- Dioxane, 179
- Dipolar polarization, 301
- Discrete element methods (DEM), 275, 279, 282
- Disruption, 49, 117, 121, 125, 132, 135, 136, 199, 222, 228, 237, 271, 307
- Dissociation equilibrium, 65
- Downstream processing, 70, 121, 122, 125
- Dual irradiation, 309
- Durability index, 251
- Dynamic
  - programming, 335
  - viscosity, 11
  
- E**
- Economic
  - analysis tool, 318
- Economies of scale, 332
- Economy, 36, 63, 244, 290, 335
- Efficiencies, 118, 130, 221, 275, 278
- Efficiency, 3, 24, 118, 132, 134, 142, 146, 164, 199, 203, 213, 216, 231, 232, 234, 245, 254, 295, 306, 327, 338, 339
- Electromagnetic radiation, 161, 302
- Emissive shell, 9, 23
- Emulsification, 25, 53, 59, 74, 165, 168, 321
- Emulsifying, 87, 164
- Emulsion, 24, 92, 105, 148, 164
- Endothermic reaction, 14
- Energy
  - absorption, 4, 259
  - balance, 13, 43
  - barrier, 6, 7, 231, 245
  - consumption, 26, 127, 130, 131, 134, 142, 199, 216, 221, 255–257, 270, 283, 305, 326
  - cost, 4, 213, 291
  - crops, 142
  - density, 9, 110, 146, 256, 257
  - dissipation, 39, 166, 171, 301
  - efficiency, 25, 258, 302, 306
  - security, 36, 160, 244
- Engine, 36, 88, 142, 164, 253
- Enthalpy, 13
- Environmental analysis, 137, 322, 335, 341
- Enzymatic
  - hydrolysis, 37, 75, 170, 179, 190–192, 253–255, 259, 272, 279
  - pretreatment, 37, 190
  - processes, 38, 191
  - saccharification, 37, 191

- Enzyme  
  accessibility, 190, 192, 209, 252  
  consumption, 216  
  kinetics, 63, 66, 69, 282  
Equilibrium constant, 56, 95–97  
Ester linkage, 78  
Esterification, 36, 52, 59, 90, 91, 99, 104, 105  
Estimating accuracy trumpet, 331  
Ethanol, 36, 63, 70, 121, 122, 146, 169, 179,  
  190, 192, 210, 253  
Ethanol productivity, 36  
Evaporation heat, 15  
Excel, 323, 324  
Exergy, 336  
Extraction  
  lipid extraction mechanism, 49, 199, 200  
  solvent, 121, 199, 234, 339  
  ultrasound, 117, 199, 234  
Extraction of lipids, 49, 50, 52, 82, 125, 128,  
  135, 168, 199
- F**  
Fabrication, 119  
Far-field zone, 23  
Fast pyrolysis, 154, 321  
Fatty acid methyl esters (FAME), 150, 152,  
  153  
Fatty acids  
  methyl esters, 89, 91, 105, 143, 152  
Feedstock, 36, 57, 60, 70, 89, 117, 118, 142,  
  175, 190, 191, 199, 203, 231, 243, 245,  
  247, 251, 262, 269–274, 278, 281, 290,  
  322  
Fenton reaction, 52, 73  
Fermentable, 75, 169, 173, 189, 254, 321  
Fermentation, 36, 37, 63, 118, 159, 180, 181,  
  191, 192, 198, 253, 272, 338  
Fermentation reaction, 180, 181  
Fibers, 176, 212, 214, 220, 221, 300  
Field Emission Scanning Electron Microscopy  
  (FE-SEM), 81, 291  
Filamentous algae, 201  
Fish ponds, 203  
Flow cytometry, 63, 66  
Flue gas, 119, 167, 231  
Fluorescence spectroscopy, 18  
Force  
  compressive, 269, 270, 271, 273, 274, 281,  
  282  
  shear, 135, 148, 152  
  non-zero compressive, 282  
Forward integration, 36, 63  
Fossil fuels, 160, 190, 244  
Fractionation, 171, 192, 198  
Free fatty acids, 36, 59, 61, 110, 292  
Fricke method, 18  
Frictional heating, 282  
Full-scale implementations, 203, 230  
Functional groups, 77, 78, 162  
Fundamental frequency, 296  
Fungus, 182, 191
- G**  
Gas solubility, 27  
Gasoline, 36, 37, 118, 160, 244  
Gelatinization, 294, 307, 310  
Geyser, 309, 311  
Glactose, 180  
Glycerol, 36, 62–66, 69  
Glycosidic bonds, 175, 279, 293, 298  
Glycosidic linkage, 293, 296  
Green house gases, 36, 119, 142, 160, 164,  
  190, 210, 220, 231, 244, 256  
Greenhouse gas emissions, 160, 210, 220
- H**  
Harmonic frequency, 18, 19  
Heat transfer, 8–10, 13, 22, 27, 162, 259, 260,  
  279, 308  
Heterogeneously catalyzed, 91, 167  
Heterotrophic, 191, 199  
Hexanol, 163  
Hexose, 75, 76, 180, 283  
High energy ball milling, 273  
High frequency ultrasound, 171, 189, 304, 321  
High performance liquid chromatography  
  (HPLC), 18, 254  
Higher throughput, 166  
High-frequency focused ultrasound, 199  
High-intensity ultrasound, 199, 203  
High-speed stirring, 166  
Horn-type reactor, 19  
Hotspot, 8, 321  
Hot spot mechanism, 161  
Humification, 271, 282  
Hydraulic retention time, 180, 221, 229  
Hydrodynamic cavitation, 39, 89, 103, 164  
Hydrogen, 36, 70, 128, 154, 175, 191, 193, 202,  
  210, 227, 232, 253, 273, 295, 299, 309  
Hydrogen cells, 160  
Hydrolysate, 180, 339  
Hydrolysis  
  acid, 190, 215  
  enzymatic, 37, 75, 80, 182, 189, 192, 194,  
  254, 255, 271

mechanochemical, 273, 284  
 rate, 7, 192  
 Hydrophobic surface, 7  
 Hydrophobe, 18, 19  
 Hydrostatic pressure of fluid, 4  
 Hydrothermolysis, 216

## I

Immobilized cells, 69  
 Impacts, 24, 244, 250, 273, 279, 282, 338  
 Impeller, 109, 254  
 Impurity, 58  
 Incident wave, 18  
 Induction period, 15, 281  
 Induction period of bubble formation, 6, 7, 94  
 Industrial waste, 290, 296, 308, 312  
 Infrasonic sound, 4  
 Inhibition, 61, 65, 69, 70, 200, 211, 216, 221, 227, 231, 233  
 Inhibitors, 180, 196, 213, 215, 216, 227, 235, 236, 339  
 Inhibitory compounds, 212, 217, 221, 272  
 Integral multiples of quarter-wavelength, 17  
 Intensification, 4, 6, 17, 25, 29, 37, 39, 53, 63, 164, 196, 203  
 Interfacial area, 53, 56, 59, 71, 83, 164, 168  
 Intermolecular interaction, 4, 198, 295  
 Internal rate of return, 324, 333, 339  
 Interphase mass transfer, 71, 74  
 Intrinsic  
   behavior, 168  
   kinetics, 56, 58, 62, 168  
 Invasive weed, 37  
 Investment  
   analysis, 320  
   criteria, 324, 333  
 Iodine method, 18, 20  
 Ionic conduction, 301  
 Ionic liquids, 26, 30, 191, 194  
 Irradiation  
   pretreatment, 169, 216  
*Isochrysis galbana*, 141, 150, 152–155

## J

Janka hardness, 270  
*Jatropha curcas*, 36  
*Jatropha* seeds, 36, 58, 59  
 Jet cooking, 338  
 Jet-induced bubble structure, 21, 191

## K

*Karanja*, 36  
 Keller-Miksis equation, 11

Kinematic viscosity, 11, 45  
 Kinetic, 35–37, 43, 53, 57, 59, 61, 63, 65, 66, 69, 74, 81, 82, 95, 166–168, 181, 321  
   constants, 56, 63, 69, 168  
   control, 63, 66, 69, 168  
   model, 282, 323  
   eley Rideal, 87  
*Kluyveromyces marxianus*, 179

## L

Lactose, 179, 180, 253  
 Lang factors, 331  
 Large-scale, 156, 243, 245, 283, 338  
 Laser phase-Doppler method, 18, 20  
 Laser scattering method, 18, 20  
 Legislation, 327  
 Life cycle  
   analysis, 117, 121, 128, 137, 335  
   costing, 335  
   social, 335  
   sustainability assessment, 335  
 Life cycle analysis  
   cultivation, 119  
   harvesting, 119, 120  
   conversion to biodiesel, 120  
   coproduction and recycling, 121  
   global warming potential, 118  
   energy depletion potential, 118  
   cell disruption, 117  
 Lignin  
   syringaldehyde  
     syringic acid, 284  
     vanillic acid, 284  
     vanillin, 284  
 Lignocellulose, 29, 142, 170, 179, 182, 190, 192, 198, 214  
 Lignocellulosic  
   biomass, 37, 38, 75, 182, 190–194, 198, 217, 270  
   materials, 191, 212, 214, 215, 217, 237  
 Lineweaver—Burk plot, 81  
 Lipase, 91, 100, 210, 228  
 Lipid extraction methods  
   accelerated solvent extraction, 141  
   automatic Soxhlet extraction, 149  
   cell explosion, 149  
   high-pressure homogenizer, 143, 148  
   microwave-assisted extraction, 141  
   osmotic shock extraction, 147  
   solvent extraction, 147  
   Soxhlet extraction (SE), 145  
   supercritical fluid extraction (SFE), 144  
   ultrasound-assisted extraction, 150, 152



- Lipidic phase, 6, 14, 89, 95, 127, 144, 149, 161, 229, 295, 308
- Lipids, 35, 36, 49, 52, 94, 117, 118, 121–125, 127–131, 133, 135, 142, 144–146, 149, 151, 152, 154, 155, 160, 191, 199, 209, 229, 231, 234, 292, 294
- LIPUS (low frequency ultrasound), 162, 182, 189, 195, 304
- Liquid compressibility, 40
- Liquid density, 8, 11
- Livestock waste, 219, 221, 222
- Logistics, 247, 321
- Loop reactor, 105
- Low frequency ultrasound, 162, 304
- Lower residence time, 166
- Low-Intensity Pulsed Ultrasound (LIPUS), 182
- Luminol (3-Aminophthalhydrazide), 18
- Lysis, 121
- M**
- Macromolecules, 78, 229, 233, 234, 292
- Maize, 192, 294
- Malto-oligosaccharides, 303
- Maltose, 296, 303
- Manure, 209, 211, 212, 220–222, 237, 338
- Market
- demand, 327
  - potential, 322
  - research, 327
  - size, 327
  - study, 322, 323, 327, 337, 341
  - supply, 327
  - trends, 327
- Marshall and Swift equipment cost index, 332
- Mass
- balance, 95, 96, 328
  - diffusion, 11, 12, 41
  - diffusion length, 12
  - transfer, 10, 12, 15, 25, 35, 37, 43, 56, 58, 59, 61, 74, 77, 79, 81, 82, 89, 90, 94, 95, 97, 99, 105, 146, 164, 168, 170, 171, 191, 245, 305, 308
- Mass transfer
- transfer constant, 56, 81, 95–97, 99
  - transfer limited, 12
  - transfer resistances, 57, 61, 87, 90, 94, 95, 168
- Matrix, 12, 76–78, 128, 169, 194, 252, 300, 304, 306
- Matrix-assisted laser desorption/ionization—Time-of-flight (MALDI-TOF), 298
- Mechanical
- processing, 269, 271, 274, 281, 282
  - properties, 277, 278
  - stirring, 78, 90, 93, 94, 110, 162, 163, 298
  - treatment, 198, 220, 227
- Mechanism, 3, 4, 7, 25, 30, 39, 41, 42, 50, 56, 59, 61, 71, 77, 78, 83, 95, 117, 128, 135, 136, 161, 164, 167, 168, 177, 200, 203, 210, 228, 263, 301
- Mechanocatalytic, 273, 281
- Mechanochemical, 273, 277, 279, 282, 284
- Media, 94, 181, 212, 272, 275, 277, 281, 282
- Metabolic
- activity, 182, 195
  - pathway, 63–66, 69, 203
- Methane, 36, 50, 122, 191, 193, 200, 202, 209, 210, 213, 215–217, 219, 220, 222, 227, 229–231, 232, 233, 235–237
- Methane yield, 202, 211, 216, 219, 220, 222, 229, 231, 232, 237
- Methanogenesis, 210, 211
- Methanol, 15, 16, 36, 49, 52, 53, 56, 57, 59, 61, 70, 82, 89, 90, 92, 94, 95, 102–105, 109, 110, 118, 121, 127, 129, 134, 143, 145, 156, 162–164, 166–168, 253
- Methoxenium, 61
- Methoxide, 52, 53, 59, 105, 166
- Methoxide anions, 166
- Methyl esters, 90, 93, 104, 109, 144, 150, 153, 156
- Methyl radical recombination, 20
- Michaelis Menten constant, 66, 69
- Microalgae
- harvesting techniques, 149
  - filtration, 149
  - high-speed centrifugation, 149
  - pH precipitation, 149, 150
- Microbes, 190, 198, 216
- Microbubble, 7, 20, 22, 28, 125, 321, 326
- Micro-convection, 168, 321
- Microjet, 22, 23, 25, 48, 169, 191, 198
- Micromixing, 168
- Microscopic analysis, 49, 66, 168
- Microstreaming, 4, 6, 27, 198
- Microstructure, 271
- Microturbulence, 7, 22, 25, 27, 47, 50, 52, 53, 57, 71, 76, 78, 82, 164
- Microwave
- irradiation, 167, 169, 172–175, 177, 178, 233, 290, 301–305, 307, 308, 312
  - oven, 162, 167
  - pretreatment, 173, 233
- Migration, 21
- Milling
- apparatus, 278
  - attrition mill, 270, 273, 281
  - cutting mill, 270

- hammer mill, 270, 271
- mixer mill, 276, 280
- pebble mill, 273
- planetary mill, 272, 278
- screw extrusion, 246
- intensities, 278, 282
- modes, 270
- Minimum support price, 37
- Mixing power, 109
- Mobile electric charges, 161
- Moh's hardness, 277
- Moisture content, 120, 215, 249–251, 255–257, 259, 262
- Molar ratio, 53, 56, 57–59, 61, 72, 104, 162–164, 166, 168
- Molecular hot spots, 162
- Monomode synthesis microwave, 303
- Monosaccharide, 77, 210, 278
- Monte Carlo, 325, 334
- Morphology, 24, 66, 179, 191, 195, 291
- Mucor hiemalis*, 171
- Multibubble cavitation, 3, 14, 15, 20
- Multibubble sonoluminescence (MBSL), 20, 30
- Multimode synthesis microwave, 303
- Municipal solid waste, 194, 214
  
- N**
- Nannochloropsis, 117, 126, 127, 130, 131, 167, 199, 203, 233, 236
- Nanomaterials, 160
- Near-surface zone, 23
- Negative acoustic pressure, 6, 7
- Neighboring bubble, 3, 14, 16, 22
- Neosinocalamus affinis*, 179
- Net present value, 324, 329
- Newspaper, 193, 196
- Nodes of ultrasonic wave, 17
- Non-catalytic site, 65, 69
- Non-condensable gas, 7
- Non-equilibrium phase change, 10, 11
- Nonlinear radial motion, 15
- Nucleation, 6, 7, 27, 29, 37, 39
- Nucleation rate, 7
- Nucleophile, 59, 83, 166
- Nucleophilic attack, 56, 59, 83
- Numerical simulation, 11, 14, 47, 56
  
- O**
- Octanol, 163
- Oil
  - canola oil, 93, 94, 95, 97
  - cooking oil, 100
  - nagchampa oil, 91, 100
  - nile Tilapia oil, 90
  - palm oil, 105, 142, 195
  - soybean, 57, 60, 100, 103, 142, 166, 168
  - tobacco oil, 91, 97, 99
- Oil/methanol, 166
- Oleic acid, 91, 92, 94, 97, 163, 307
- Optically opaque plasma, 9
- Optimization, 25, 26, 30, 57–59, 63, 78, 80, 166, 196, 199, 319, 337, 341
- Organic
  - fraction of municipal solid waste (OFMSW), 194, 214
  - matter solubilisation, 217, 221, 227, 228, 232–237
  - solid waste, 194
  - solvents, 137, 143–146, 150, 152, 153, 155
- Oxidative desulfurization, 70, 72–74, 82, 83, 338
- Ozonation, 194, 227, 309, 338
  
- P**
- Palm oil fronds, 195
- Parent bubble, 8
- Parthenium hysterophorus*, 78
- Particle
  - size, 169, 172, 192, 199, 216, 221, 227, 233, 245, 249–251, 255, 256, 259, 262, 270, 273, 281, 290
  - size distribution, 29, 227, 290
- Partition coefficient, 52
- Payback period
  - discounted, 324
- Peak temperature of sonoluminescence, 20, 22–24
- Pellet
  - density, 247, 249, 250
  - durability, 250
  - quality, 247, 251, 258, 263
  - stability, 251
  - sugar yield, 252, 255
  - weight, 256, 259
- Pelleting
  - energy consumption, 256
  - pressure, 257, 259, 262
  - temperature, 258, 259
  - time, 257
- Pentose, 75, 169, 171
- Peracetic acid, 71, 72, 74
- Percentage of delivered equipment cost, 331
- Peroxyorganic acid, 70

- Petroleum, 37, 70, 160, 164, 165, 190, 244, 255, 290, 332
- Phase displacement, 18, 20
- Phosphate monoesters, 292, 294
- Phosphoric acid, 295
- Photography, 15, 20, 30
- Physical
- effects, 35, 46, 51, 56, 168, 189, 198, 220
  - mechanism, 25, 38, 70, 83, 168
  - pretreatment, 217, 233, 254
- Physicochemical, 22, 24, 25, 193, 321
- Piezoceramic transducer, 300
- Piezoelectric transducer, 107, 246
- Pilot plant, 106
- Pinus radiata, 178
- Plasma ionization, 9
- Polar molecules, 161
- Polymer degradation, 189
- Polymerization, 77, 79, 192, 198, 215, 217, 218, 272, 303, 304
- Polysaccharides, 125, 173, 191, 252, 279, 291, 296
- Pond water, 203
- Positive acoustic pressure, 6, 8, 14
- Potassium hydroxide (KOH), 100, 105, 166
- Potato peel, 174, 289–292, 295, 298–300, 303, 304, 306–309, 312
- Potato starch, 174, 291, 292, 294, 295, 298–300, 303, 304, 306, 307, 309, 312
- Power
- density, 9, 102, 105, 107, 110, 228, 298
  - stations, 167
  - ultrasound, 5, 48, 321
- Preprocessing, 243, 262, 273
- Pressure, 4–10, 13, 15, 16, 18–20, 22, 24, 29, 35, 38–40, 46–49, 51, 53, 63, 70–72, 74, 76, 78, 79, 103, 118, 144–146, 148, 164, 191, 199, 216, 246, 249, 251, 255, 257, 259, 271, 274, 296, 302, 303, 305
- Pressure gradient, 8, 47
- Pretreatment
- size reduction, 216
  - steam explosion, 75
- Primary Bjerknes force, 20
- Probe, 107, 196, 202, 296, 299, 303, 305, 306, 308, 309, 312
- Process
- flow diagram, 322, 324, 328, 341
  - intensification, 29, 88, 89, 103, 164
  - parameters, 167, 182, 196, 202, 247, 249, 251, 254, 256, 262, 281, 326, 337
- Processing time, 89, 120, 193, 271, 278, 281
- Profitability, 271, 283, 284, 322, 329, 333
- Propanol, 141, 163, 306
- Protein, 118, 121, 143, 144, 199, 200, 210, 228, 229, 233, 234, 290, 292, 338
- Protonation, 56, 59
- Pseudo first order reaction, 167
- Pulp and paper waste, 214
- Pulse ultrasound, 15
- Push-pull reactor, 101
- Pyrolysis oil, 338
- Q**
- Quadratic model, 57
- Quasi-option value, 335
- R**
- Radical, 20, 22–26, 37, 52, 53, 57, 71, 73, 74, 79, 82, 103, 125, 135, 164, 191, 212, 213, 219, 228, 234, 297, 300, 304, 308, 321
- Radical species, 42, 59, 73
- Rarefacted zone, 5, 6
- Rate constant, 55, 96, 97, 168, 181, 230
- Rate of the ester formation, 163
- Rayleigh-Plesset equation, 7, 10
- Reaction volume, 163
- Reactor configuration, 87, 90, 99
- Real option theory, 335
- Recalcitrance, 179, 190, 245
- Recalcitrant, 171, 173, 190, 203, 220, 221
- Recalcitrant fraction, 221
- Rectified diffusion, 3, 14, 16, 17, 26, 42
- Reducing sugars, 171, 293, 295, 298, 300, 304, 307, 308, 312
- Reflected wave, 18
- Refractory compounds, 220
- Renewable, 36, 120, 159, 160, 164, 173, 174, 178, 190, 198, 210, 231, 244, 290
- Renewable energy, 190, 321
- Repolymerization, 279
- Re-precipitation, 77
- Residence time, 105, 162
- Resonant frequency, 8
- Response surface methodology, 57, 59, 128, 258
- Revenue, 63, 226, 337
- Reynolds number, 11
- Rice
- hulls, 194
  - stalks, 193
  - straw, 76, 215, 216
- Risk analysis, 321, 322, 324, 334, 341
- Rosett cell, 88, 100, 101, 103, 108, 110
- Rupture, 79, 149, 199, 227

- S**
- Saccharification, 38, 169, 172, 181, 194, 196–198, 253, 338
- Saccharomyces cerevisiae*, 178, 180, 182, 195
- Salicylic acid method, 18
- Saponification, 77, 165
- Scale advantages, 324, 327
- Scale-up, 109, 198, 227, 278, 302, 340
- Scattering wave, 18, 20
- Scavenging (of radicals), 73, 74
- Scenario analysis, 334
- Schmidt number, 11
- Secondary effect, 4, 20, 22–27, 29, 35, 191
- Selectivity, 52, 66, 70, 83, 125, 128, 148, 168, 300, 304, 305, 308, 312
- SEM studies, 130, 131, 193, 194, 299, 300
- Semi-continuous reactor, 88, 106, 237
- Semi-crystalline, 291, 294
- Sensitivity analysis  
partial, 334
- Separation, 24, 78, 88, 120, 128, 137, 144, 150, 166, 220, 226, 308, 312
- Sewage sludge, 217, 221, 222, 227, 230
- Shockwaves, 16, 22, 49, 198, 297, 304, 305, 308
- Short-chain alcohols, 162, 163
- Simultaneous saccharification and fermentation (SSF), 195
- Single bubble cavitation, 3, 14, 15
- Six-tenth rule, 332
- Size reduction, 47, 216, 230, 250, 270
- Sludge, 193, 209, 211, 212, 221, 222, 227, 229, 230, 290, 337, 339
- Smoker bubble structure, 21
- Soap, 89, 166
- Sodium hydroxide (NaOH), 78, 79, 162, 171, 178, 179, 196, 215, 232, 295
- Sodium methoxide, 105
- Solar energy, 160
- Solid base catalyst, 59, 166
- Solubility, 77, 125, 144, 148, 198, 201, 294
- Soluble COD, 201, 228, 229, 233, 236
- Solvation, 61, 192, 198
- Solvent selectivity, 52
- Sonication, 3, 4, 9–11, 16, 19, 22–24, 29, 37, 50, 52, 59, 66, 69, 76–79, 81, 101, 108, 164, 168, 171, 173, 175–182, 192, 193, 196, 199–201, 203, 213, 217, 222, 228, 234, 236, 307, 321, 329, 337, 340
- Sonication loop, 180
- Sonitube<sup>®</sup>, 88, 106, 107, 110, 311
- Sonochemical  
immobilization, 161  
reactor, 9, 14, 17, 20, 23, 25, 28, 30, 99, 110, 164
- Sonochemiluminescence, 18, 20
- Sonochemistry, 3, 5, 9, 10, 23, 30, 159, 160, 162, 167, 179, 321
- Sonoluminescence, 16, 18–20, 22–24, 30, 309
- Sonotrode, 21, 22, 129, 180
- Sound wave, 4, 6, 11, 17, 19, 38, 125, 321
- Soxhlet apparatus, 50
- Soxhlet extraction, 49, 50, 127, 128, 141, 145, 146, 149, 167
- Soybean oil, 57, 60, 103, 142, 166
- Spatial distribution, 17, 20, 21, 25, 27, 30
- Specific  
energy input, 202, 212, 217, 219, 221, 222  
heat, 8, 13, 27  
heat capacity, 261  
heat ratio, 8  
rate constant, 57, 168
- SrO catalyst, 126, 167, 203
- Standing wave, 24, 302
- Starch, 169, 171, 173–175, 180, 182, 244, 271, 289–291, 294–296, 298–300, 302, 304, 306, 307, 310, 311
- Static mixer, 105, 108
- Statistical tool, 166
- Steady cavitation, 6–8, 15
- Steam explosion, 75, 173, 191, 216, 273, 282
- Steric hindrance, 163
- Stoichiometry, 162
- Straw, 214–216
- Streaming zone, 23
- Structural rigidity, 169–171, 182
- Subcritical fluid, 29, 121
- Subharmonic frequency, 18, 19
- Substrate binding, 65
- Substrate inhibition, 63, 65, 66, 69
- Sugar  
beet pulp, 180  
cane bagasse, 142, 169, 180, 190, 192, 339  
monomers, 76, 77, 180  
utilization, 180  
yield, 77, 78, 173, 192, 194, 245, 253, 255, 340
- Sugarcane bagasse, 142, 180, 192, 196, 339
- Sugarcane tops, 194, 196
- Sulfuric acid, 9, 163, 168, 254, 275, 295, 299
- Superheating, 162
- Supermarket oils, 142, 338
- Superpro Designer 6.0, 339
- Surface area, 15, 77, 171, 192, 198, 213, 217, 255
- Surface defect, 6, 7
- Surface tension, 6, 8, 11, 26, 27, 49, 148
- Surfactant, 15, 16, 26, 194
- Surrounding liquid, 9, 22, 24

- Sustainability analysis, 320  
Sustainable, 120, 122, 159, 189, 193, 255  
Sweet sorghum bagasse, 171  
Swelling power, 294  
Switchgrass, 192, 244, 249–251, 254, 255  
Synergism, 304
- T**  
Taguchi method, 166  
Taguchi technique, 166  
Tailing bubble structure, 21  
Tait equation, 40  
Tap water, 29  
TAPPI protocol, 78  
Techno-economic analysis  
    assessment, 317, 319–323, 325, 326, 334, 340, 341  
    evaluation, 320, 321, 325, 339  
    extended, 322, 323, 335, 336, 340, 341  
Temperature, 7–9, 11–14, 22, 25, 43, 275, 295, 300, 303, 307, 311  
Temperature gradient, 8  
Terephthalic acid method, 18  
TGA–DSC, 167  
Theoretical studies, 30  
Thermal  
    conductivity, 13, 27, 243, 259  
    diffusion, 13, 43  
    diffusion length, 13, 44  
    diffusivity, 13, 27, 45  
    dissociation, 42, 53, 71  
    energy, 162, 260  
    hydrolysis, 227  
    pretreatment, 194, 220, 227, 228, 233, 236  
Thermochemical, 5, 191, 321  
Thermocouples, 259  
Thermogravimetric analysis (TGA), 291  
Thermometer, 259  
Time scale, 11, 13, 41, 42  
Toluene, 72–74, 302  
Total reducing sugars (TRS), 308, 310  
Transesterification, 36, 52, 53, 55, 56, 59, 61, 62, 87, 89, 99, 101, 104–106, 110, 118, 128, 134, 150, 162–164, 166–168  
Transient cavitation, 8, 37, 48, 52, 59, 61, 66, 79, 82, 168  
Transient cavitation threshold, 48  
Transportation sector, 244  
Trichoderma reesei Rut C-30, 182  
Triglyceride, 36, 56, 59, 60, 142, 166  
Triolein, 163  
Triticale meal, 180
- U**  
Ultraharmonic frequency, 18  
Ultrasonic  
    bath, 17, 90, 91, 297, 298, 310  
    cleaning, 25  
    effects, 309  
    field, 4, 5, 8, 14, 16, 22  
    frequency, 26, 107, 192, 200, 296, 297, 305, 311, 312  
    irradiation, 106, 110, 162, 163, 192, 296, 297, 298, 300, 305, 307, 308, 311, 312  
    power, 102, 106, 166, 198, 234, 249, 251, 257, 259, 261, 262  
    power and frequency, 166  
    pretreatment, 180, 198, 201, 221, 222, 227, 229, 230, 337  
    probe, 103, 296, 298–300, 306, 311  
    Pyrex probe, 299, 304, 306, 307  
    systems, 49, 60, 74, 82, 90, 164  
    theory, 30, 118, 243  
    transducer, 101  
    treatment, 79, 80, 106, 194, 198, 217  
    vibration-assisted (UV-A) pelleting, 243, 245, 249–251, 255, 256, 258–260, 263  
    wave, 17, 143, 146, 147, 179, 212, 213, 296, 305, 306  
Ultrasound, 261  
    density, 213, 217  
    frequency, 127, 171, 228, 229  
    intensity, 213, 217, 244  
    low frequency ultrasound, 162, 182, 195, 304  
    operating parameters, 117, 127, 164  
    pressure amplitude, 11, 21, 35, 39, 41, 48  
    ultrasound homogenizer, 91, 100, 108  
    ultrasound pulses, 16, 101, 107, 109  
Ultraviolet-visible (UV-Vis), 9, 18  
Ulva rigida, 181  
Unicellular, 200  
Urea, 179, 306
- V**  
Vapor pressure, 6, 12, 26, 27, 82  
Vapor transport, 41, 42  
Vaporization, 149, 164  
Vegetable oil, 36, 49, 88, 142, 162, 164, 191  
Velocity potential, 48  
Viable cells, 118, 137, 338  
Viscosity, 4, 8, 26, 40, 47, 144, 213, 294  
Viscous stress, 8  
Volumetric  
    heat generation rate, 244  
    productivity, 15, 37, 173  
    work, 15

**W**

Walne's medium, 150  
Waste, 37, 78, 88, 89, 106, 120, 122, 143, 174,  
190, 193, 201, 214, 215, 219, 221, 222,  
228, 284, 289–291, 298, 304, 322, 324  
Waste activated sludge (WAS), 226  
Water, 11–13, 16, 19, 23, 24, 26, 29, 38, 41,  
61, 75, 77, 82, 94, 96, 97, 105, 117,  
118, 120, 121, 124, 127–129, 134,  
146–148, 150, 151, 172, 176, 181, 191,  
203, 210, 216, 220, 226, 250, 275–278,  
282, 290, 291, 294, 295, 297, 298, 300,  
307  
Water content, 120, 290, 291  
Wavenumber, 6  
Waxy rice, 192  
Wear, 277  
Wheat chaff, 194, 196

Wind power, 160

Work, 8, 13, 15, 26, 47, 53, 72, 82, 101, 120,  
144, 162, 164, 167, 179, 180, 270, 274,  
275, 284, 328, 336, 338

**Y**

Yeast  
growth, 171